UNICA

UNIVERSITÀ
DEGLI STUDI
DI CAGLIARI

Ph.D. DEGREE IN
Electronic and Computer Engineering

Cycle XXXVIII

TITLE OF THE Ph.D. THESIS

Spectroscopic Technologies and Computational Approaches for Real-Time Detection of FMN as Biomarker during Machine Perfusion

Scientific Disciplinary Sector(s)

ING-INF/01

Ph.D. Student:	Lorenzo Agostino Cadinu
Supervisor	Prof. Massimo Barbaro
Co-Supervisor	Prof. Pier Carlo Ricci

Final exam. Academic Year 2024/2025
Thesis defense session: February 2026

University of Cagliari

Faculty of Engineering
PhD Program in Electronic and Computer Engineering

Spectroscopic Technologies and Computational Approaches for Real-Time Detection of FMN as Biomarker during Machine Perfusion

Ph.D. Student
Lorenzo Agostino Cadinu

Supervisor: Prof. Massimo Barbaro
Co-Supervisor: Prof. Pier Carlo Ricci

Finanziato dall'Unione europea
NextGenerationEU

To my friend Francesco

And I will give you a new heart, and a new spirit I will put within you.
And I will remove the heart of stone from your flesh and give you a heart of flesh.
Ezekiel 36:26-29

Abstract

Organ transplant waiting lists are progressively lengthening worldwide due to the shortage of suitable organs, resulting in a high mortality rate among patients. The traditional preservation method is static cold storage, but in recent years a new technique has emerged: machine perfusion. This approach consists of perfusing the organ with an oxygenated solution, either acellular or blood-based, with the aim of reactivating aerobic metabolism prior to transplantation and enabling the assessment of organ viability through the analysis of metabolites released into the perfusion fluid.

This doctoral thesis focuses on the use of technologies for the real-time detection of Flavin Mononucleotide (FMN), considered a biomarker of ischemia-reperfusion injury, during organ perfusion. The methodologies employed are based on spectrophotometric measurements, UV-visible absorption, and fluorescence, using both standard laboratory instruments, such as benchtop spectrophotometers, and an innovative stand-alone device, specifically developed by the company funding the doctoral research, capable of detecting fluorescence signals directly within the perfusion circuit.

A measurement protocol was proposed for the real-time monitoring of FMN and NADH concentrations using benchtop spectrophotometers, with potential clinical application. The stand-alone device was calibrated to detect FMN in the range of 12–237 ng mL^{-1} according to the developed protocol. Furthermore, dedicated software was implemented to identify the FMN spectrum and distinguish it from potential interferents, while a machine learning algorithm allows automatic, real-time quantification of FMN concentration during organ perfusion.

The prototype was validated in preclinical settings, both on animal and human organs, demonstrating excellent performance in biomarker detection. This thesis demonstrates the high potential of this technology for large-scale application in clinical settings.

Preface

This thesis was produced while attending the PhD programme in Electronic and Computer Engineering at the University of Cagliari, Cycle XXXVIII, with the support of a scholarship co-financed by the Ministerial Decree no. 352 of 9th April 2022, based on the NRRP - funded by the European Union - NextGenerationEU - Mission 4 "Education and Research", Component 2 "From Research to Business", Investment 3.3, and by the company Sarmed Srl. Sarmed Srl is a company part of Medica Group Spa.

The preclinical experiments described in this doctoral thesis were conducted on animal organs in full compliance with Italian and European regulations on animal welfare, ethics, and hygiene. The organs were sourced from animals intended for human consumption, already slaughtered according to the applicable food hygiene regulations, thus ensuring their safety.

During the PhD program, the candidate undertook a research period at the Lerner Research Institute of the Cleveland Clinic, serving as a Predoctoral Fellow in the Department of Inflammation & Immunity within Dr. Andrea Schlegel's Laboratory, where the prototype was tested on human organs provided by the institution. Although the related experimental data cannot be disclosed due to the absence of formal authorization, this experience significantly contributed to the development of the project.

The content of the chapter III is largely based on the article Cadinu et al., **Optical Spectroscopic Detection of Mitochondrial Biomarkers (FMN and NADH) for Hypothermic Oxygenated Machine Perfusion: A Comparative Study in Different Perfusion Media**, published in Sensors (MDPI), 2025, 25 pp. 4031. https://doi.org/10.3390/s25134031. The article is distributed under the Creative Commons Attribution (CC BY 4.0) license, which permits use, distribution, and adaptation, provided that the original source is properly cited. Some sections have been reorganized and supplemented with additional material and further insights.

In Chapter IV, which is dedicated to the description of the prototype, no technical details or construction diagrams concerning the hardware, light source, spectrometer, or optical configuration are disclosed. Likewise, no complete software implementations are presented, except for a few short Python code excerpts included for illustrative purposes. The focus is instead placed on the experimental use of the device and on the analysis of its performance. This confidentiality is motivated by the fact that the prototype is protected by industrial secrecy: disclosing its technical or design features could allow potential competitors to replicate the system or benefit from its engineering solutions.

This doctoral dissertation has been carried out within the field of Electronic and Computer Engineering. Since the research is applied in a medical context, it is essential to emphasize that the information presented herein is intended solely for scientific purposes and must not, under any circumstances, be interpreted as medical or clinical advice. The author assumes no responsibility for any improper or inappropriate use of the information contained in this dissertation.

List of Publications

1. **Cadinu, L.A**.; Sun, K.; Jiao, C.; Panconesi, R.; Satish, S.; Yildirim, F.S.; Karakaya, O.F.; Wehrle, C.J.; Crasta, G.S.; Fernandes, F.W.; et al. Optical Spectroscopic Detection of Mitochondrial Biomarkers (FMN and NADH) for Hypothermic Oxygenated Machine Perfusion: A Comparative Study in Different Perfusion Media. Sensors 2025, 25, 4031, https://doi.org/10.3390/s25134031.

2. Sun, K., Jiao, C., Panconesi, R., Satish, S., Karakaya, O. F., De Goeijc, F. H. C.,·Diwan, T., Ali, K., **Cadinu, L. A.**, Cazzaniga, B., Liu, Q.,·Miyazaki, Y., Pita, A., Khalil, M., Kim, J. K., Hussein, A., Müller, P. C.,·Aucejo, F.,·Kwon, D. H. C., Fernandes, E., Esfeh, J. M., Cywinski, J., Fujiki, M., Sun, L.,·Pinna, A., Dutkowski, P., Wehrle, C. J., Fairchild, R. L., Meierhofer, D., De Jonge, J., Miller, C., Hashimoto, K.,·Schlegel, A. Quantifying Flavin mononucleotide: an internationally validated methodological approach for enhanced decision making in organ transplantation. eBiomedicine, 116, 105761, 2025. https://doi.org/10.1016/j.ebiom.2025.105761.

3. Satish S., **Cadinu L.**, Nadeem M., Sun K., Jiao C., Ali K., Karakaya O., Crasta G., Yildirim S., Walsh F., Aucejo F., Kwon D., Kim J., Pita A., Khalil M., Fujiki M., Wehrle C., Miller C., Hashimoto K., Schlegel A. A Novel Risk Score Using Flavin Mononucleotide (FMN) for Predicting Graft Loss After Liver Transplantation with Normothermic Machine Perfusion. American Journal of Transplantation. Volume 25, Issue 8, Supplement 1, S215, August 2025. 10.1016/j.ajt.2025.07.472.

4. Karakaya O., Jiao C., Sun K., Satish S., Yoval-Sanchez B., Panconesi R., Crasta G., Fernandes F., Yildirim S., **Cadinu L**., Wehrle C., Fairchild R., Miller C., Hashimoto K., Galkin A., Schlegel A. Mitochondrial Injury and Function Comparing Hypothermic and Normothermic Machine Perfusion of Human Livers. American Journal of Transplantation, Volume 25, Issue 8, Supplement 1, S801, August 2025. 10.1016/j.ajt.2025.07.1893.

Publications not related to this work

1. Collu, R., Salis, C., Ferrazzano, E., **Cadinu, L.A**., Makni, N., Barbaro, M. (2025). An EEG Based Platform for Emotion Recognition. In: Ruo Roch, M., Bellotti, F., Berta, R., Martina, M., Motto Ros, P. (eds) Applications in Electronics Pervading Industry, Environment and Society. ApplePies

2024. Lecture Notes in Electrical Engineering, vol 1369. Springer, Cham. https://doi.org/10.1007/978-3-031-84100-2_49.

Contents

List of Figures

Chapter I

Chapter II

Chapter III

Chapter IV

Chapter V

List of Tables

Chapter I

Chapter II

Chapter III

Chapter IV

Chapter V

"Non est ad astra mollis e terris via"
Lucio Anneo Seneca, Hercules Furens, verse 437.

Chapter I

1. Introduction

1.1. From Myth to Clinical Reality: The Evolution of Organ Transplantation until Machine Perfusion

Since the dawn of time, the human body has aroused wonder and fascination in the perception that human beings have of themselves, a map of profound meanings and mysteries that each civilization has interpreted in its own way. A journey through cultures and millennia, discovering how the heart, liver, skin, intestine, and other tissues have been much more than mere organs: symbols of life, sacrifice, and regeneration.

In ancient Egypt, the heart – called *ib* – was considered the seat of intellect, feelings, will, and memory. Not by chance, during the solemn ceremony of psychostasia, the heart of the deceased was placed on the scale of the god Thoth, ready to be weighed for judgment in the afterlife. A sacred instant, in which a heartbeat decided eternal destinies.

Across the ocean, among the Aztec temples, the same heart – seen as a casket of will and knowledge – was offered to the Sun in sacred rituals. Torn from the chest, it gave vital energy to the divine star, while the skin, delicately removed, became an offering to the god Xipe Topec. Two gifts, a single sacrifice: the flesh for the light, the skin for rebirth.

And then there was Greece, where the liver – ἧπαρ, hépar – throbbed as the center of emotions and passions [1]. The myth of the titan Prometheus tells us of its power: he stole fire from the gods to give it to men. As punishment, Zeus chained him to a rock in the Caucasus, condemning him to have his liver devoured by a giant eagle, day after day. But each night the organ regenerated, ready to be wounded again. In that eternal tale lies a surprising anatomical truth, perhaps already known to

the ancient Greeks: the liver is the only organ capable of almost completely rebuilding itself. Even today, if part of it is removed, within a few months it reforms itself.

It is not surprising, then, that Hippocrates wisely stated: “if we are able to live a good life, it is thanks to the health of our liver” [2]. Because every organ, every story, every myth reminds us that the human body is not only matter. But a living organism that interacts with the surrounding world.

In ancient medical doctrines, the intestine was often seen as a second brain, a dark and mysterious place where the most hidden humors were born. Hippocratic and Arab physicians read in it a tangle of feelings and intuitions, a visceral labyrinth capable of influencing the soul. It was not just a digestive tube, but a passageway between the external world and the innermost self, where food was transformed into energy and thought. A kingdom of shadows and lights, where it was believed premonitions and those “butterflies” of anxiety or joy – that we still feel fluttering within us today – originated.

And high above, toward the sky, the lungs were the divine breath, the sacred wind of life. For philosophers and alchemists, they represented the bridge between man and the universe. In ancient China, the lung was associated with the Metal element and with the virtue of courage, the breath that gathers the pure energy of the sky (*Qi*) to distribute it throughout the whole body.

For Native American cultures, breath was the sound of the soul conversing with the wind, with the spirits of the ancestors. Each inhalation was an act of receiving the world, each exhalation a gift of oneself to the air. It is no coincidence that when one faces a stressful or anxious situation, taking a deep breath helps to calm stress and relax both body and mind.

The human body functions as an integrated and wonderfully complex network, where every single component is interconnected and interdependent. There are no elements that act in isolation, but all cooperate in a dynamic and harmonious balance, as in a perfect mechanism whose gears, although sometimes mysterious, move in unison to sustain life.

Unfortunately, for various reasons, a gear can break, and the machine, life, begins to falter, making survival a challenge. The most emblematic case is when internal organs are damaged and unable to perform their functions correctly. In the most serious cases, to ensure survival and an acceptable quality of life, it even becomes necessary to replace the organ with a healthier one. From this arises the need for transplantation.

The transplantation of organs and tissues has fascinated humans since the most ancient times. There are numerous legends in mythology that refer to the replacement of damaged tissues with new

ones. An example is the mythical Chimera, an animal whose body was made up of the body of a lion, a serpent's tail, and a goat's head on its back, which was slain by the Greek hero Bellerophon with the help of the mythical winged horse Pegasus, itself an ancient example of fusion between parts of different organisms into a single being. In fact, with transplantation, an individual receives an organ from another donor, thus resulting in a fusion of different parts.

In the same way, the myth of the Lernaean Hydra recalls a concept strikingly close to modern medicine: this monstrous creature, similar to a serpent with many heads, had the ability to regenerate each severed head, multiplying endlessly. Only thanks to the ingenuity of Heracles, who cauterized the wounds with fire to prevent regrowth, was it possible to defeat her. In that legend of infinite regeneration, one can glimpse the observational ability of the ancient Greeks regarding the capacity of tissues to rebuild themselves, an idea that today finds a direct parallel in regenerative medicine and modern transplantation techniques.

The concept of the fusion of different beings into a single entity is not confined to Greek mythology but recurs throughout the myths, legends, and creative expressions of many cultures and eras. This archetype — the union of diverse elements to form a new, hybrid whole — has continued to inspire the human imagination across centuries. It appears in modern science fiction films such as *The Fly* (1986), where human and insect DNA merge into a single organism, as well as in video games like *Return to Castle Wolfenstein* (2001), which depict humans transformed into cybernetic beings. In literature, Mary Shelley's *Frankenstein* (1818) stands as one of the earliest and most powerful reflections on the boundaries between life, science, and the reconstruction of the human body through external components. Even in contemporary popular culture, such as in the Japanese anime *Dragon Ball Z* (1992), the character "Cell" embodies this very idea — a creature born from the cellular synthesis and fusion of multiple beings.

Although these fictional representations serve the purpose of entertainment, they symbolically mirror a process that, in a scientific and biological sense, occurs in organ transplantation. When an organ or tissue is transplanted from a donor to a recipient, a profound cellular dialogue takes place. The donor's cells begin to interact with those of the host, leading to a process of integration that, at the microscopic level, can be seen as a form of biological fusion. In this union — part biological, part symbolic — the boundary between two individuals becomes blurred, giving rise to a new composite entity that embodies both life and continuity.

Even in Christian culture there are references to the possibility of replacing organs, as testified by the words of the prophet Ezekiel (Ezekiel 36:26–29): "I will give you a new heart and put a new

spirit within you; I will remove from your body the heart of stone and give you a heart of flesh…". This verse must be interpreted within the theological and symbolic context in which it is placed. Nevertheless, it is interesting to observe the parallel that can be drawn with the contemporary experience of organ transplantation. In particular, in the case of heart transplantation, cultural narratives and personal testimonies have often referred to the idea that the recipient acquires not only an organ but also a deeper dimension, sometimes described as the "soul" of the donor. Some transplant patients have reported subjective experiences, such as dreams or perceptions related to the donor, although such phenomena currently lack scientific validation. Nonetheless, the biblical verse provides a suggestive perspective for reflecting on the symbolic and anthropological meaning of transplantation, as well as on the connection between body, identity, and spirituality.

From an historic point of view, the oldest mention of tissue transplantation is found in the Ebers Papyrus, written around 1550 BC, which mentioned skin grafting for the treatment of burns [3].

Of note from the Renaissance period is the Bolognese Gaspare Tagliacozzi and his studies collected in *De curtorum chirurgia per insitionem* (1597), where he laid the foundations of plastic and reconstructive surgery thanks to his experience in reconstructing the structure of arms, ears, noses, and lips damaged by disease and mutilation.

In modern times, the first verifiably documented skin transplantation took place in 1869 thanks to the work of the Swiss surgeon Jacques-Louis Reverdin, who demonstrated the success of epidermal grafting [4]. At the beginning of the 20th century, experimental studies on animals began. The Viennese surgeon Emerich Ulmann, a student of Theodor Billroth, one of the masters of modern surgery, defined the technique of transplantation in dogs. In 1909, the breakthrough came with Karl Landsteiner, who provided the basis for understanding and controlling the immune response of organ rejection, also called the "graft" [4].

With the progress of medicine and surgery, organ transplantation passed from myth and symbol to clinical reality. After the first experiments on animals in the 19th century and the first pioneering operations of the early 20th century, the real revolution occurred in the mid-20th century. In 1954, in Boston, the first kidney transplant between two monozygotic twins was performed, a success that demonstrated the concrete possibility of replacing a diseased organ with a healthy one [4]. In the following years, advances in anesthesia, surgical techniques, and especially in the understanding of the immunological mechanisms of rejection made it possible to extend the approach to other vital organs such as the liver, heart, and lungs.

A fundamental turning point was the introduction of cyclosporine in the 1980s, an immunosuppressive drug that greatly improved the survival of patients and grafts, opening a new era for transplants. From that moment, organ transplantation became established as one of the most important life-saving therapies and a symbol of medical progress. Today, transplantation is a widespread clinical practice worldwide and often represents the only option for patients with end-stage organ failure. According to the most recent data, hundreds of thousands of transplants are performed worldwide each year, with the kidney ranking first as the most frequently transplanted organ, followed by liver, heart, lungs, and pancreas.

However, demand far exceeds supply: waiting lists continue to grow, and many patients die without ever having access to a suitable organ [5 – 10]. Despite the difficulties linked to the scarcity of donors, clinical results are extraordinary: survival rates at 1, 5, and 10 years have progressively improved thanks to better surgical techniques, more effective immunosuppressive therapies, and increasingly sophisticated preoperative management.

Furthermore, in recent years there has been a technological revolution with the introduction of new methods of organ preservation, such as machine perfusion, which make it possible to evaluate and keep organs alive in controlled conditions, offering new transplantation opportunities even for organs initially considered marginal [11–20].

Organ transplantation, associated with machine perfusion, is not only a life-saving therapy but also represents an ethical, social, and scientific issue of enormous relevance. It is the result of a unique alliance between donor, recipient, physicians, surgeons, and researchers, and it continues to be a rapidly evolving field, where engineering, biology, and medicine intertwine to give new life to those who would otherwise have no hope.

It is within the field of machine perfusion that the development of this doctoral thesis is situated. We will therefore examine this technique in detail, whose origin is not recent: for several decades, systems of artificial organ perfusion have already been tested. What is innovative today is not so much the principle itself, but rather the new philosophy of use, which transforms it from a simple method of preservation into a dynamic tool for functional evaluation and even regeneration of the organ before transplantation.

Machine perfusion of organs for transplantation is an advanced technique designed to preserve and enhance the viability of donor organs before transplantation [21 – 25]. This method involves the continuous perfusion of organs with a preservation solution, which can be either cold (hypothermic machine perfusion) or at body temperature (normothermic machine perfusion), aimed at sustaining

organ function and assessing viability outside the body [26 – 30]. Unlike of the current preservation method traditionally used in clinical context, the static cold storage (SCS), which has been the gold standard in organ preservation, machine perfusion facilitates the maintenance of physiological conditions, thus potentially improving post-transplant outcomes [31 – 35].

Machine perfusion may appear to be a futuristic technique, almost as if it were taken from science fiction, yet its origins go much further back in time than one might expect. In the next paragraph, we will briefly retrace its beginnings and historical development, leading up to its modern applications.

1.2. A Brief History of Machine Perfusion

Perfusion is a technique that progressively evolved from 19th-century experiments on extracorporeal circulation and blood pumping [36 – 39]. As early as 1812, Cesar Julien Jean Le Gallois suggested that the vitality of a body part could be preserved through artificial circulation.

The first description of organ perfusion dates back to 1849, when Carl Eduard Loebell, in his *Dissertation Inaugurals*, conducted experiments on isolated pig kidneys perfused with defibrinated blood, measuring urine production [40, 41]. He observed that bright red arterial blood, upon exiting the renal vein, appeared darker and richer in solids, while the ureter released a clear liquid containing considerable amounts of proteins [40, 42]. In Loebell's and Bidder's experiments, the reservoirs containing the perfusion fluid were pressurized with columns of water or mercury [43, 44].

In 1850, Claude Bernard was the first to describe an ex vivo liver perfusion model [45]. Shortly after, in 1855, Porter and Bradley patented the first hand-cranked roller pump [38, 39, 46]. Interestingly, the patent listed unconventional applications, such as cleaning cesspools, pumping gastric contents, or enabling injections [39]. However, with subsequent modifications, this invention proved efficient for cardiopulmonary bypass, allowing open-heart surgery to be performed in a relatively bloodless and dry surgical field [39]. Before this advancement, physiologists and pharmacologists had relied on primitive gravity-driven pumps, with the perfusate reservoir simply suspended from the laboratory ceiling [39].

In 1858, Eduard Brown-Séquard carried out striking experiments: he injected blood into the arms of executed criminals, showing that oxygenated blood perfusion could restore reflex nervous activity [46]. He also attempted the first artificial oxygenation of blood by agitating it, transforming it from "black" to "red" [37, 46].

In the following years, several researchers refined oxygenation techniques. In 1867, Alexander Schmidt, together with Carl Friedrich Wilhelm Ludwig, experimented with adding oxygen to venous blood, improving the method of artificial perfusion and perfusing dog kidneys with defibrinated, oxygenated, and linen-filtered blood [37, 46, 47]. In 1876, Bunge and Schmiedeberg achieved similar results by agitating venous blood in atmospheric air until it acquired the bright red color of arterial blood [37, 48].

In 1882, Waldemar von Schröder developed a device capable of oxygenating blood by passing an air stream through it, a process considered the first form of bubble oxygenation [37, 49]. The following year, M. Abeles refined this approach by using pure oxygen instead of air [50].

A decisive step toward modern systems came in 1885, when Max von Frey and Max Gruber built the first prototype of a closed artificial circulation system [40, 37, 42]. This apparatus included an oxygenator (artificial lung) and a pulsatile pump, making it comparable to the first true heart-lung machine [41, 46]. The invention of the closed perfusion circuit launched the challenge of improving pumping systems to deliver oxygenated blood effectively to perfused organs [38, 39].

Later, pulsatile pumping devices were developed and employed by Gustav Hammel [51] and other researchers [52 – 54], laying the foundations for the advances in artificial perfusion that marked the 20th century.

According to the scientist Carl Jacobj, the device built by Max von Frey and Gruber was bulky, expensive, and overly complicated to use. To address these limitations, Jacobj designed a new perfusion apparatus, which he called the “hematisator” [37]. Gas exchange in this device occurred in a manner similar to von Schröder’s technique and, for the first time, the principle of the bubble oxygenator was incorporated into a closed perfusion system [37].

Presented in 1890, this instrument was conceived both for the quantitative analysis of blood and blood gases and for recreating circulation conditions similar to natural ones, while remaining easy to handle [55]. With its use, it became possible to maintain a continuous blood flow through an isolated pig kidney [37]. In 1895, Jacobj further advanced the field by employing dog lungs or pulmonary lobes from pigs and calves as oxygenators [46, 56]. Moreover, he was the first to inhibit coagulation pharmacologically—previously avoided through defibrinated blood—by using an anticoagulant extracted from leeches [37].

The pumping mechanism devised by Jacobj, based on a rubber balloon compressed rhythmically, was later adopted and refined by other researchers [38, 55], including Neubauer et al. [57] and Embley [58]. As early as 1887, E.E. Allen patented a slightly modified pump, which he

named “blood transfusion instrument” [38, 39]. In 1899, Charles Truax introduced the first double-roller pump, improving the system for adjusting pressure and force on the delivery tubing [38, 39].

Further contributions came in 1903 from T.G. Brodie, who developed a device using an alternative pump in which defibrinated blood was mixed with air in the pump chamber [53]. In 1907, Johannes Bock designed one of the first electrically powered syringe pumps, later refined by E. Friedmann [59, 60], while in 1913 Fröhlich described for the first time the use of an electrically driven roller pump for continuous organ perfusion [61].

In the following decades, researchers such as Beck [62], Van Allen [63], Bayliss and Müller [64], as well as Henry and Jouvelet [65], further improved blood pumping systems, recommending the use of roller pumps for transfusions and clinical applications [37]. At the same time, other scientists contributed to the development of extracorporeal circulation, including Neubauer and Groß [57], Friedmann [60], Zeller [66], Bornstein [67], Hooker [68], von Issekutz [69], Richards and Drinker [70], Kermack [71], and others [72].

By the beginning of the 20th century, three oxygenation systems were already in use: bubble, film, and membrane oxygenators [46]. By the late 1920s, several extracorporeal circulation pumps had been described, and successful experimental perfusion of isolated organs had been achieved. These advances enabled a deeper understanding of organ physiology [72].

Additional technical improvements focused on pumping systems, such as the pulsatile membrane pump introduced by Dale and Schuster in 1928 [73], which gained wide popularity in subsequent decades [37]. In 1951, Clarence Dennis used the Dale–Schuster pump in combination with cardiopulmonary bypass to perform the first open-heart surgery [74].

The first major breakthroughs in perfusion and extracorporeal circulation came with the experiments of Sergei Brukhonenko in the 1920s. A military physician during World War I, Brukhonenko had witnessed numerous cases of traumatic shock and severe injuries to the heart, lungs, and major vessels, which led him to envision a method of temporary extracorporeal circulation to keep patients alive during treatment [75].

In 1926, together with Dr. Tchechulin, he developed the “autojector,” a device for the “artificial circulation of blood in warm-blooded animals” [76 – 79]. With this machine, he succeeded in keeping a dog alive for two hours with the heart stopped, solely through artificial circulation [37, 46, 78]. This experiment demonstrated for the first time the feasibility of performing surgery on a temporarily arrested heart while maintaining life through artificial perfusion. Despite the pioneering

nature of his work, Brukhonenko's contribution to the development of the heart-lung machine was rarely mentioned in English-language surgical literature until the 2000s [46].

In parallel, further studies on kidney perfusion were carried out in 1922 by Ernest Verney [80] and in 1924 by Fritz Eichholtz [81]. The technique of perfusion reached a turning point in 1935 with the work of Charles Lindbergh and Alexis Carrel. To demonstrate that isolated organs could continue to live if perfused with a nutrient solution, the two researchers developed a system for perfusate oxygenation [37]. Carrel and Lindbergh described their model, which allowed an organ to live outside the body, "thus realizing for the first time Le Gallois' concept" [37]. This apparatus maintained a sterile pulsating circulation with a medium composed of blood serum and growth-stimulating solutions [37].

The concept of hypothermic perfusion for ex vivo organ preservation was first developed by Carrel himself [82]. With this system, hearts, ovaries, and kidneys could be perfused [83, 84]. Lindbergh also designed a glass perfusion pump capable of sustaining kidneys with an adequate oxygen supply [82]. Later, they conducted experiments with hypothermia, and their work was revisited and republished by Lindbergh in 1966 after Carrel's death [85].

In those same years, specifically in 1937, J. Gibbon proposed the concept of extracorporeal circulation as an aid to cardiac surgery in his classic publication on the artificial maintenance of circulation during temporary occlusion of the pulmonary artery [86]. He argued that using a machine capable of performing the functions of the heart and lungs would allow the surgeon to operate on an "open heart" in a relatively bloodless and dry field, while the other organs of the body continued to receive regular perfusion [39]. Gibbon succeeded in artificially replacing heart and lung functions for 25 minutes during pulmonary artery occlusion [86]. For these results, Gibbon Jr. is considered the father of modern extracorporeal circulation [41].

Other scientists and physicians, such as Crafoord [87], Björk [88], and Jongbloed [89], refined bubble, film, and isolated-lung oxygenation methods for use in the first clinical procedures of cardiopulmonary bypass in humans. In particular, J. Jongbloed developed an oxygenator capable of handling an extracorporeal blood flow comparable to the basal human cardiac output while still ensuring the protection of vital organs [89].

Further contributions to the improvement of blood oxygenation techniques came from Leland Clark, Frank Gollan, and Vishwa B. Gupta, who managed to avoid the drawback of foam formation during bubble oxygenation [72, 73]. Improved bubble and film oxygenators, together with modern blood pumps in closed circulation systems, were assembled into pump oxygenators and later termed

heart-lung machines [37]. Research into different oxygenation techniques continued in the following years [74 – 77].

Parallel to the advances in extracorporeal circulation and in the refinement of pumping systems, research into isolated organ perfusion continued. In the earliest experiments, blood itself served as the perfusion fluid [40]; however, the blood volume of a single animal was insufficient to sustain complete perfusion, since early devices required large amounts of blood. Because mixing blood from different animal species proved harmful, diluted blood with simple saline solutions or Ringer's solution was increasingly used as a perfusate [53].

The use of blood–saline mixtures, however, led to problems such as the development of organ edema, though these attempts provided valuable insights into the physiology of organ function [40]. At the same time, efforts were made to formulate synthetic perfusate solutions containing electrolytes, solutes, vitamins, and other components, capable of at least partially replacing blood [85].

Another critical issue concerned the temperature of organ perfusion [40]. In the earliest attempts, organs were perfused at room temperature; for example, Bunge and Schmiedeberg carried out their experiments at physiological temperatures [42]. However, the protective effects of hypothermia had been known since the time of Hippocrates [90]. Napoleon's surgeon, Baron Larrey, observed that wounded soldiers survived longer when left in the snow compared to those warmed with blankets and hot drinks [91]. For these reasons, scientists began perfusing organs at reduced temperatures, thereby mitigating tissue damage by lowering cellular metabolism [40, 72, 92, 93 – 95].

Carrel and Lindbergh also developed a prototype of normothermic machine perfusion (NMP), which over time was adapted to clinical practice [72]. The two researchers additionally experimented with closed-circuit low-temperature perfusion on organs retrieved from different animals [96]. Studies by Carrel and Lindbergh [96, 97] and Hou et al. [98] demonstrated that organs and tissues could survive ex vivo for several days under normothermic conditions in culture media.

In 1951, investigations into the role of the liver in plasma protein synthesis were carried out using an isolated liver perfused with blood [99]. Later, experiments using cooled diluted serum or heparinized blood extended kidney perfusion from a few hours to as long as 3–5 days [100, 101]. In 1963, Calne et al. [102] showed that vascular flush perfusion was a more efficient method for cooling donor organs than simple surface cooling [72, 103]. However, the use of cold blood also revealed significant drawbacks, including vascular spasm in kidney transplants [102, 104 – 106].

Further evidence of the effectiveness of low-temperature perfusion came from Lapchinsky, who in 1960 successfully reimplanted a canine kidney after 24 hours of preservation in hypothermic

blood [107, 108]. Other studies focused on the protective role of hypothermia in the preservation of abdominal organs [109, 110]. A major breakthrough came with Belzer et al. [111], who refined the hypothermic perfusion machine and reported the successful transplantation of a cadaveric kidney after 17 hours of preservation using a perfusate composed of human plasma at 10 °C enriched with hydrocortisone, magnesium sulfate, dextrose, and penicillin [72].

In 1968, Humphries et al. [101] achieved a milestone by maintaining a kidney in cold perfusion with oxygenated blood for 5 days [40]. Around the same time, other researchers obtained similar results with hypothermic perfusion preservation of animal organs [112 – 114]. Pioneering studies by Brettschneider et al. [115, 116] showed that hypothermic machine perfusion (HMP) applied to the liver yielded outcomes comparable to or even superior to static cold storage (SCS) [117]. In subsequent years, high-quality canine livers were successfully transplanted after 72 hours of cold perfusion preservation [118, 119].

The limitations observed by Calne et al. [102] highlighted the need to develop new synthetic, acellular preservation solutions to improve organ storage at low temperatures [72, 103, 106]. By the late 1960s, mechanical perfusion technology was well established: in 1968, Norman provided a detailed description of a liver perfusion machine [120], with a circuit similar to modern designs. In 1970, Starzl identified the potential benefits of hypothermic oxygenated ex vivo machine perfusion [121], noting that an organ maintained under low-flow, hypothermic oxygenated perfusion could remain viable for up to 8 hours [122].

However, continuous perfusion required expensive and complex equipment that was difficult to transport and available only in limited supply [1, 40, 72, 126]. These logistical and economic barriers hindered widespread adoption [11]. Moreover, transporting organs over long distances to transplant centers compromised function due to hypoxia caused by cessation of blood flow [72, 108].

The key challenge, therefore, was to develop a simple and cost-effective method that could reduce cellular metabolism through cooling without damaging the organ, thus preserving functionality. This problem was solved in 1969 by Collins et al. [123, 124], who developed a low-temperature preservation solution that enabled static cold storage (SCS) of organs [125].

Collins' pioneering work was based on formulating an acellular solution that could closely reproduce the intracellular electrolyte balance of mammalian cells. This represented the first significant attempt to preserve organs with an approach grounded in the understanding of cellular changes induced by hypothermia and hypoxia [94, 103]. The so-called Collins solutions marked a

substantial improvement in organ preservation and were adopted for nearly two decades in transplant centers worldwide [72].

Collins initially succeeded in keeping canine kidneys viable for 12 hours in an iced saline solution, later extending the cold preservation time to 30 hours [123, 124]. This method, known as static cold storage (SCS), proved to be more cost-effective, simple, and practical for organ transportation compared to dynamic perfusion, and it rapidly became the standard preservation modality [11, 40, 103, 125]. SCS involved flushing the explanted organ with a preservation solution at 0–4 °C, followed by immersion in the same solution until transplantation. The hypothermic environment reduced cellular metabolism, while the solution provided cytoprotection [40].

Although limited to about 24–36 hours of preservation, this approach was sufficient to maintain tissue viability and to enable organ sharing between transplant centers even at great distances [94, 103, 108, 125]. Moreover, the technical and logistical challenges of transporting organs perfused with dynamic methods (particularly between the 1950s and 1990s) made Collins' method the most effective choice [127]. His solution proved suitable for liver, kidney, heart, and lung preservation [125].

In the following years, several improvements were introduced to the static cold storage method [108]. In 1980, the Euro-Collins (EC) solution was developed, characterized by high potassium and sodium concentrations (intracellular composition) and glucose as an osmotic agent [94, 103, 108, 125]. Since glucose has low permeability to renal cells, this solution was particularly suited for short-term kidney preservation or in cases of donation after circulatory death (DCD) [132].

In 1987, Belzer et al. [128] at the University of Wisconsin formulated a new solution for abdominal organ preservation, the so-called University of Wisconsin (UW solution). This solution, still widely used today [129, 130], proved superior to Euro-Collins [131]. The UW solution addressed the issue of glucose permeability in hepatic and pancreatic cells, which resulted in loss of osmotic effect and subsequent anaerobic metabolism with intracellular acidosis [132]. To overcome this limitation, glucose was replaced with larger sugars such as lactobionate and raffinose, which remained in the extracellular space, ensuring longer-lasting protection (6–16 hours) [132, 133].

The UW solution also combined impermeant components (raffinose, lactobionate), ATP precursors (adenosine), and antioxidant agents (allopurinol, reduced glutathione), providing more comprehensive protection against edema and oxidative stress [132]. However, it also presented limitations: the presence of hydroxyethyl starch (HES) as an oncotic support resulted in high solution viscosity, with the risk of tissue saturation and reduced blood flow upon reperfusion [134, 135].

Moreover, the high K+ concentration could cause cellular depolarization and unwanted activation of voltage-dependent channels [136].

These drawbacks stimulated the development of new solutions free of HES and featuring different oncotic agents. Alternatives included Celsior and HTK (Custodiol), which lacked oncotic agents, as well as PEG-based formulations as osmotic supports, such as the Institut Georges Lopez (IGL-1) solution and SCOT (Solution for the Conservation of Organs and Tissues) [132]. Later, other solutions enriched with amino acids and protective molecules were introduced [137, 138]. Among these, the Histidine-Tryptophan-Ketoglutarate (HTK solution), developed by Hans Jürgen Bretschneider at the University of Göttingen in 1975 [139], represented one of the most significant innovations thanks to its ability to reduce cold ischemia injury.

1.3. The Dawn of Machine Perfusion

The title of this paragraph, *"The Dawn of Machine Perfusion"*, is inspired by two seminal publications: *"Ex situ liver machine perfusion as an emerging graft protective strategy in clinical liver transplantation: the dawn of a new era"* by Nickkholgh et al. (2019) [140] and *"The dawn of liver perfusion machines"* by Detelich et al. (2018) [141]. Indeed, a new era has already emerged in the field of transplantation: that of organ preservation and treatment through machine perfusion, which stands as a valuable alternative to traditional static cold storage.

The technique of static cold storage (SCS) has been progressively refined and tested in numerous studies from the 1980s to the present, both for abdominal and thoracic organs [142 – 153]. However, the growing demand for transplants has far exceeded the availability of suitable grafts, leading many countries to introduce the concept of Expanded Criteria Donors (ECD), including Donation after Circulatory Death (DCD), in an attempt to address this shortage [11, 12, 35, 154 – 156].

While SCS offers practicality, low costs, and favorable outcomes for high-quality organs, it proves less suitable for preserving high-risk grafts [11, 72]. These include organs from DCD donors, elderly donors (>80 years), fatty livers and pancreas, grafts with prolonged cold ischemia times (CIT > 8–10 h) or warm ischemia times (WIT > 30 min), and organs from donors with significant comorbidities (e.g., diabetes, cardiovascular disease) [11, 12, 72, 140, 157 – 160].

One of the main limitations of DCD livers compared with those from brain-dead donors (DBD) is the inevitable warm ischemia period occurring between withdrawal of life support and

circulatory arrest [161]. This interval, combined with the subsequent cold ischemia during transport, leads to depletion of intracellular energy reserves such as ATP and to metabolic disturbances that compromise cellular viability [162, 163]. Since SCS does not provide active oxygen or nutrient supply, graft survival depends solely on residual energy reserves, which are depleted within 24–48 hours [159], while anaerobic glycolysis becomes the predominant metabolic pathway [164].

The most frequent complications after DCD liver transplantation are biliary complications [165, 166], including several forms of cholangiopathy leading to cholestasis, jaundice, and cholangitis, which may ultimately cause graft loss or patient death [161]. Overall, ECD grafts are particularly vulnerable to hypoxia and anaerobic metabolism during SCS [11, 72, 127, 167 – 175], with consequences such as primary non-function, ischemic cholangiopathy (non-anastomotic strictures, NAS [176]), and recipient mortality [167, 165, 173, 175, 177, 178].

Static preservation further impairs endothelial cell function due to the absence of oxygen and biomechanical stimulation [179]. During cold ischemia, metabolites such as reactive oxygen species and lactic acid accumulate, which upon reperfusion trigger ischemia-reperfusion injury (IRI) [94, 108, 180 – 186]. This process affects all major hepatic cell populations, including hepatocytes, liver sinusoidal endothelial cells (LSEC), and cholangiocytes [187, 188].

The continuous rise in organ demand, long waiting lists, and the high mortality rate among patients awaiting transplantation (estimated at 20–30% due to clinical deterioration or death [8 – 10]) have driven the clinical community to reassess preservation strategies [8, 177, 189, - 192]. At the same time, political and social efforts are growing to raise awareness about donation: in Italy, for instance, in 2020 about 33% of citizens renewing their identity card refused post-mortem organ donation [193].

Although SCS provides partial protection against ischemia-reperfusion injury [151, 203], the need for more advanced preservation methods has become evident, particularly for DCD livers, where biliary strictures remain a major challenge [165, 194]. In this context, machine perfusion (MP) techniques have shown the ability to limit ischemic damage, improve preservation, and allow functional assessment of the organ prior to transplantation [11, 12, 32, 195 – 199].

These advantages have led to renewed interest in the use and optimization of MP strategies for organ preservation [11, 12]. Current trends in liver transplantation are increasingly directed toward the integration of machine perfusion, in its different modalities: hypothermic (HMP), normothermic (NMP), subnormothermic (SNMP), and controlled oxygenated rewarming (COR) [11, 200].

2. The Scientific Problem

We have seen that machine perfusion is not merely a preservation technique, but rather introduces an entirely new dimension in the field of transplantation: the ability to assess, in real time, the viability and functionality of the organ prior to implantation. This opportunity, which represents a substantial improvement over static cold storage, allows clinicians to make more informed decisions regarding graft suitability, thereby reducing the risk of post-transplant complications and increasing the number of organs that can be successfully utilized.

To achieve this, several clinical evaluation protocols and criteria have been developed, based on the monitoring of functional, biochemical, and metabolic parameters during perfusion. Among the most widely used are bile production, lactate clearance, blood flow dynamics, and vascular resistance. In recent years, however, increasing attention has been directed toward molecular biomarkers, which can provide more direct and early insights into cellular vitality. In this context, two molecules have gained particular relevance: Flavin Mononucleotide (FMN) and Nicotinamide Adenine Dinucleotide (NADH).

The intuition to use Flavin Mononucleotide (FMN) as a biomarker of organ viability during machine perfusion did not arise suddenly; rather, it is the result of a scientific path rooted in the study of mitochondrial metabolism and the mechanisms of ischemia–reperfusion injury [201 – 204].

As early as the 1960s and 1970s, with the growing practice of organ transplantation and the study of ex situ preservation methods, research began to focus on the role of mitochondria as the "powerhouses" of the cell [205 – 210]. It soon became evident that the loss of cellular viability after prolonged periods of cold ischemia was closely linked to the collapse of mitochondrial capacity to produce energy in the form of adenosine triphosphate (ATP) [211 – 220]. At the same time, the expanding knowledge of flavoproteins and their cofactors, including FMN, paved the way for the idea that these metabolites could serve as sentinels of the cell's bioenergetic state [32, 202, 221 – 225]. The role of FMN, a molecule part of the family of flavins, as a biomarker of ischemic damage was first characterized in models of stroke and myocardial infarction [226 – 230]; however, its translation into the field of transplantation only occurred alongside the adoption of machine perfusion for graft assessment [221].

Flavins, derived from the Latin term *flavin* meaning "yellow," comprise a group of yellow pigments that are water-soluble, among which riboflavin—also known as vitamin B2—stands out. Riboflavin gives rise to fundamental molecules such as flavin mononucleotide (FMN) and flavin

adenine dinucleotide (FAD). In the cytoplasm of various tissues, such as the small intestine, liver, heart, and kidneys, riboflavin is converted into its coenzymatic forms, FAD and FMN. These coenzymes, essential as cofactors of flavoprotein enzymes, participate in numerous reactions by acting as proton carriers in redox processes involved in energy metabolism, metabolic pathways, and the synthesis of certain vitamins and coenzymes [231].

From riboflavin, the primary hydroxyl group (–OH) is converted into its dihydrogen phosphate ester (PO_4H_2) [232]. FMN plays an active role in the oxidative phosphorylation process and is found in Complex I (**Figure 2.1**), one of the largest protein complexes in mitochondria, which is fundamental for cellular energy production. Complex I acts as a crucial hub in the respiratory chain, the primary mechanism through which cells generate energy. It performs two main functions: transferring electrons from NADH to Coenzyme Q (ubiquinone) and pumping protons across the inner mitochondrial membrane, thereby generating a proton gradient that drives ATP synthesis [233 – 235].

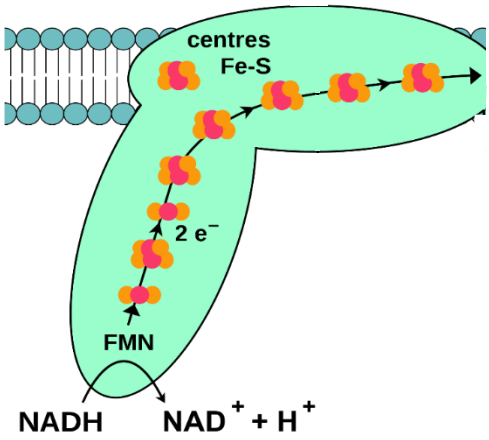

Figure 2.1. Structure of the Complex I of mammalian mitochondria and location of the Flavine Mononucleotide (FMN) and its redox reactions. Image of public domain.

Its structure includes 8 or 9 iron-sulfur (Fe-S) clusters and a noncovalently bound FMN molecule [236]. Seven of the Fe-S clusters form a linear chain for electron transfer between the flavin and quinone [233]. Complex I represents the main site of reactive oxygen species (ROS) production in mitochondria, which are involved in ischemia–reperfusion (I/R) injury. When FMN dissociates, ROS production decreases [236].

FMN, composed of a tricyclic aromatic ring known as the isoalloxazine group, contains carbon, nitrogen, and oxygen atoms (**Figure 2.2**). This group acts as a catalyst in the redox reactions of the molecule, providing an important platform for electron transfer and oxidation–reduction reactions that are vital to cellular metabolism.

FMN, in fact, is a derivative of riboflavin (vitamin B2) and represents an essential cofactor for complex I of the mitochondrial respiratory chain, NADH dehydrogenase [237 – 239].

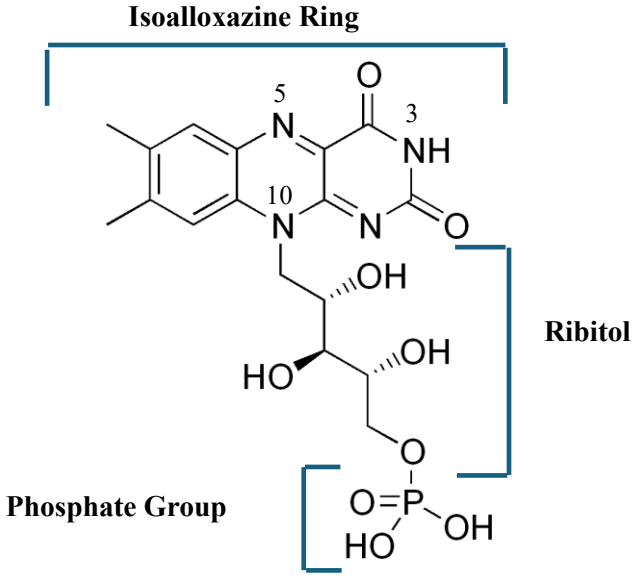

Figure 2.2. Structure of the Flavine Mononucleotide (FMN).

Its molecular architecture consists of three distinct structures:

- The **Isoalloxazine Ring**: this is a tricyclic aromatic heterocyclic ring that serves as the redox-active site of the molecule. The nitrogen atoms at positions N1, N5, and N10 of the isoalloxazine ring are the primary centers for reduction and protonation processes, determining the cofactor's redox versatility.
- The **Ribitol**: this five-carbon polyalcohol, covalently linked to the isoalloxazine, acts primarily as a structural arm, mediating the anchoring of the molecule to the active site of flavoproteins through hydrogen bonding and dipolar interactions.
- The **Phosphate Group**: esterified to the 5' carbon of the ribitol, the phosphate group confers greater hydrophilicity to the molecule and favors specific electrostatic interactions with basic amino acid residues within the enzymatic binding pockets.

The complete structure can therefore be described as Isoalloxazine-Ribitol-Phosphate. Let's go into more detail in the description of the chemical structure.

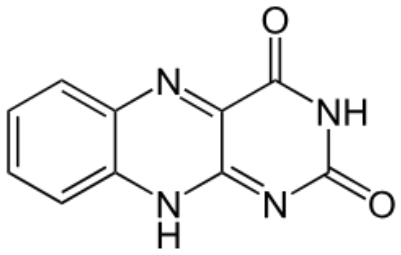

Figure 2.3. Structure of the Isoalloxazine.

The isoalloxazine (**Figure 2.3**) contains π bonds that can shift between bonding and antibonding orbitals. These double bonds, known as chromophores, are significant when the energy difference between the two orbitals falls within the visible spectrum. Conversely, molecules such as benzene, although they possess π bonds, are not chromophoric and absorb wavelengths in the ultraviolet range. For instance, an isolated C=C double bond requires an energy corresponding to about 170 nm (in the UV range) to promote an electron from a π orbital to a π* orbital, a transition invisible to the human eye. More complex molecules, with alternating single and double bonds, can absorb light in the visible range. The conjugation of multiple chromophores shifts absorption toward longer wavelengths, allowing the absorption and re-emission of different wavelengths and thereby giving the substance its characteristic color. The perceived color does not correspond to the absorbed wavelength but rather to those that are reflected.

In general, when FMN is bound to a protein, its fluorescence is quenched—a phenomenon that can also be observed in Complex I [236]. Denaturation of the complex, either due to thermal or chemical alterations, leads to the release of FMN. In this free form, FMN can emit fluorescence, producing light when excited by an energy source such as ultraviolet radiation [236]. Oxidation (loss of electrons) and reduction (gain of electrons) reactions can disrupt the π bonds, resulting in the loss of fluorescence.

Redox Mechanism of the Isoalloxazine Nucleus

The distinctive property of FMN lies in the redox plasticity of its isoalloxazine ring, which allows it to exist in three distinct oxidation states:

- Quinoid Form (FMN): The fully oxidized form.
- Semiquinone (FMNH•): A semi-reduced radical state, stabilized by resonance, resulting from the acquisition of a single electron and a proton.

- Hydroquinone Form ($FMNH_2$): The fully reduced form, obtained from the acquisition of two electrons and two protons.

This ability to participate in both one- and two-electron transfer processes allows FMN to function as an obligatory intermediary between two-electron transfer cofactors (e.g., NADH) and one-electron acceptors (e.g., Iron-Sulfur centers and cytochromes).

A schematic of the reactions is reported in **Figure 2.4**.

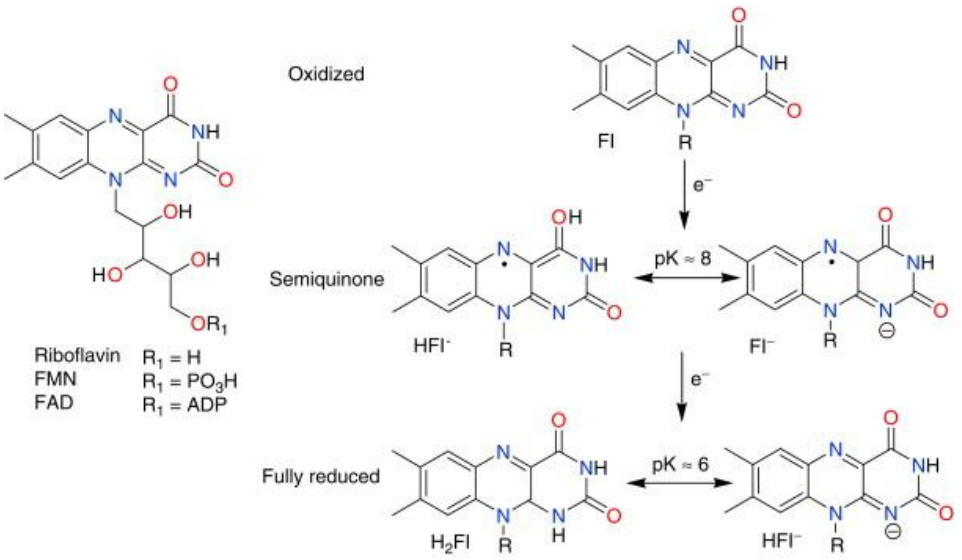

Figure 2.4. Schematic of reactions of FMN. From [240, 241].

The isoalloxazine ring of riboflavin is bound to ribitol (**Figure 2.5**), a pentose sugar derived from the reduction of ribose.

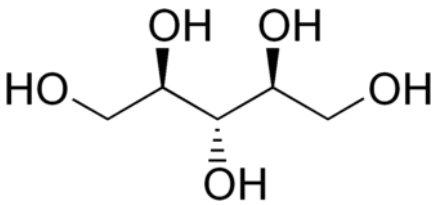

Figure 2.5. Structure of the Ribitol.

The phosphate group (**Figure 2.6**) is bound to ribitol and comes from the phosphorylation reaction of the molecule with ATP, which releases a phosphate group and thus forms FMN.

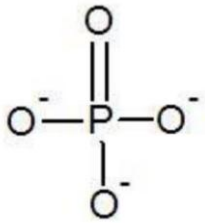

Figure 2.6. Structure of the Phosphate group.

Under normal oxidative conditions, FMN participates in electron transfer processes, enabling the transformation of chemical energy into biologically usable energy [242 – 245]. However, under conditions of oxidative stress and ischemia, when the respiratory chain is compromised, FMN dissociates from complex I and leaks out of the mitochondria, accumulating in the extracellular environment due to its hydrophilic nature of the free molecule [246 – 251].

This phenomenon was first observed in cellular biochemistry studies [252], but its clinical application only became evident later, when machine perfusion techniques allowed organs to be maintained in a controlled and dynamic environment [253], in addition to improvement of understanding of ischemia-reperfusion injury processes [254 – 258]. Unlike static cold storage, ex situ perfusion makes it possible to continuously sample the perfusate and analyze metabolic markers in real time [201, 259, 260]. This feature provided the opportunity to exploit FMN release as a direct and early indicator of mitochondrial injury [32, 202, 203, 261].

The intuition to monitor FMN marked a fundamental turning point. Until 2019, despite considerable interest in various indicators and markers of graft quality, few are routinely used in clinical practice, and no single biomarker or parameter has proven definitive [196, 262]. While traditional parameters (such as bile production, glucose, lactate clearance, transaminases like ALT, AST, total bilirubin, pH, Po_2, Pco_2, bicarbonate, and hemoglobin concentration) provide indirect or delayed information about organ functionality [32, 167, 263 – 265], FMN offers a privileged window into the status of mitochondria, which form the very foundation of cellular vitality [202, 266, 267]. Several preclinical and clinical studies have demonstrated that elevated FMN levels in the perfusate correlate with an increased risk of post-transplant dysfunction, whereas low or stable concentrations are associated with better outcomes [32, 268, 269].

This discovery carries significant practical implications. For the first time, clinicians have access to a quantitative, specific biomarker, measurable in real time, that allows not only the prediction of post-transplant outcomes but also supports clinical decision-making during perfusion

Source	Organ	Perfusion solution; temperature	Metric of organ quality by FMN release	Outcomes prediction
[201]	Liver	Belzer; 10 °C and 37 °C	Study of correlation of perfusate FMN with parameters of liver function and post-transplant parameters of liver function, such as mitochondrial FMN, NAD, ALT, AST	Satisficing: after 30 min of HOPE, FMN was predictive of graft loss
[225]	Kidney	Belzer; 4-12°C	Correlation between FMN quantification and pre-existing kidney graft injury. Correlation of perfusate and mitochondrial FMN content after 2 hours of HOPE	Not explicitly investigated, but confirm the quality of prediction
[261]	Liver	Blood based solution; 37 °C	Comparison of release of FMN in perfusate between DCD-45 min and DCD-5 min	Not explicitly investigated, but suggested good prediction
[272]	Lung	Perfluorocarbon-based oxygen carrier (PFCOC) emulsion; 37 °C	Comparison of FMN release between PFCOC perfused lungs and free PFCOC perfused lungs	Not explicitly investigated, but suggested
[273]	Kidney	Belzer; 2-8°C	Comparison of FMN release between kidneys group perfused with oxygenated HMP and with not oxygenated HMP	Not explicitly investigated, but suggested good prediction
[274]	Heart	St. Thomas No 2 cardioplegic solution at 12 °C/ Krebs-Henseleit buffer at 37 °C	FMN release in perfusate	Not explicitly investigated, but suggested good prediction
[275]	Liver	Vasosol perfusion solution	Comparison of release of FMN measured in SCS livers and perfused liver with oxygenated cold perfusion	Information not available yet
[276]	Liver	Belzer/Celsior; 4 – 12 °C	Comparison of release of FMN levels in perfusate and microdialysate. Correlation of FMN with L-GrAFT score, 2nd-hour MD glucose and lactate, and with clinical outcome measures	Not explicitly investigated, but suggested good prediction
[277]	Liver	Custodiol; 21 °C	Release of FMN in perfusate	Not explicitly investigated, but suggested good prediction

Table 2.1. Detection of FMN in clinical studies.

[32, 201, 203]. The methodology for this real-time monitoring, based on the distinct fluorescence and absorbance properties of FMN, has been systematically refined to ensure reliable detection in clinical perfusion media [203, 270].

For example, an organ showing excessively high FMN levels may be discarded to reduce risk, while one with acceptable values can be selected with greater confidence [32, 221, 271]. This approach is supported by robust clinical validation; a 2025 study validated specific FMN cut-offs measured during Hypothermic Oxygenated Perfusion (HOPE), where concentrations above 23.5 ng

mL^{-1} at 5 minutes of perfusion were strongly predictive of a 62% rate of Early Allograft Dysfunction (EAD) and a 62% one-year mortality, enabling effective risk stratification [202].

Furthermore, the ability to monitor FMN opens new perspectives for the optimization of perfusion protocols, introducing therapeutic strategies aimed at reducing mitochondrial injury and stabilizing cellular bioenergetics. The quantification of FMN, which is released from mitochondrial

Source	Organ	Perfusion solution; temperature	Metric of organ quality by FMN release	Outcomes prediction
[32]	Liver	Belzer; 4 – 12 °C	Study of correlation of perfusate FMN with post-transplant parameters of liver function and injury, such as arterial lactate, INR, and factor V, peak ALT	Satisficing: after 30 min of HOPE, FMN was predictive of 90-day graft loss
[259]	Liver, kidney, lung	Blood based solution; 35 °C–36 °C	Release of FMN and correlation with parameters of renal, liver and lung functionality such as QAS, levels of creatinine, lactate, MEAF score and mortality posttransplant, recipients' hospital stay,	Satisficing for kidney liver: FMN at 30 minutes of normothermic perfusion the suitability for transplantation. Low release of FMN was observed for lungs
[279]	Liver	Blood based solution; 37 °C	Comparison of release of FMN levels in perfusate and of liver function and injury, such as AST, ALT	Not explicitly investigated, but suggested good prediction
[280]	Liver	Belzer; 10 °C	FMN release in perfusate	Not explicitly investigated, but suggested good prediction
[281]	Kidney	Belzer; 4 °C	FMN release in perfusate	No correlation observed between FMN and post-transplant outcomes, including day 5 or 7 serum creatinine, immediate graft function, creatinine clearance and biopsy-proven rejection at one year

Table 2.2. Detection of FMN in clinical studies.

Complex I as an initial sign of ischemia-reperfusion injury, provides a direct window into the mitochondrial functional state, paving the way for tailored perfusion therapies. **Tables 2.1** and **2.2**

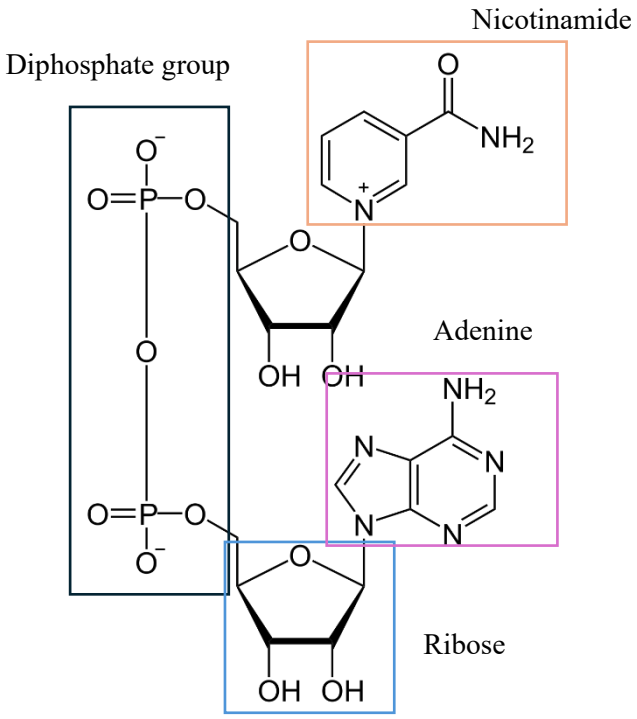

Figure 2.7. Structure of the Nicotinamide Adenine Dinucleotide.

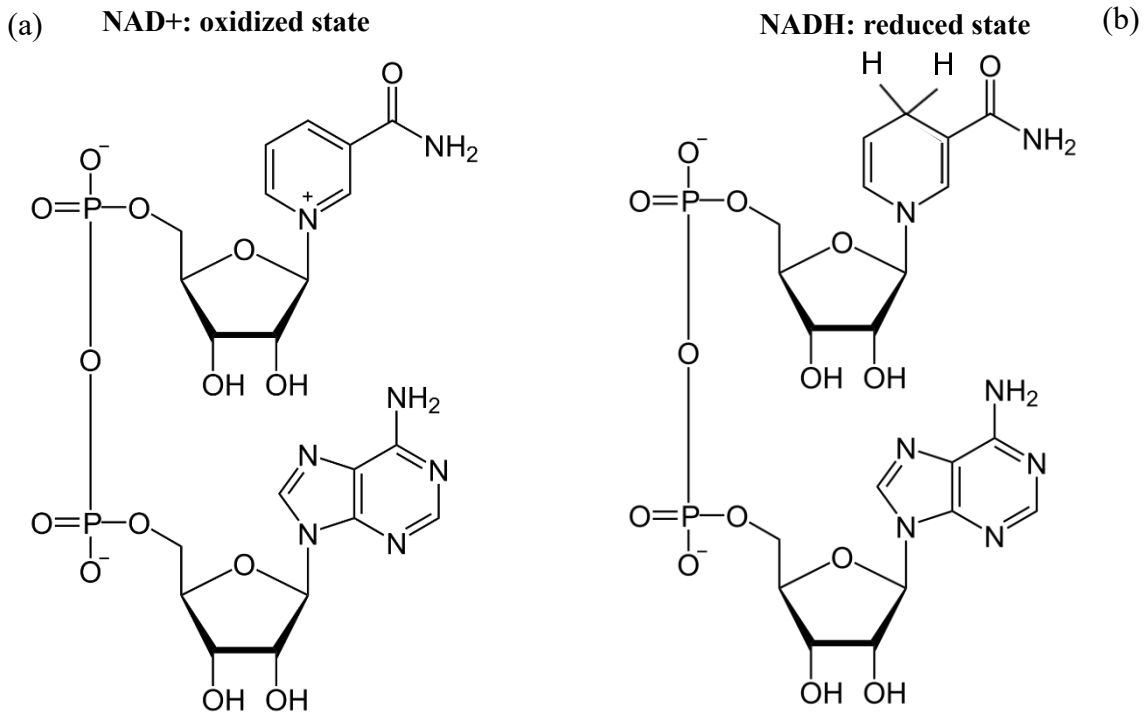

$$NAD^+ + H^+ \leftrightarrow NADH$$

Figure 2.8. NAD+ and NADH.

show the preclinical and clinical studies that detected FMN during machine perfusion.

In this sense, FMN is not merely a passive marker of damage but rather a conceptual bridge between cellular biochemistry and clinical practice, between basic research and transplantation medicine. The idea of “listening to the voice of the mitochondria” through FMN monitoring has contributed to enriching the very philosophy of machine perfusion: no longer only a preservation technique, but a dynamic physiological laboratory capable of providing valuable insights into organ quality and even guiding ex situ therapeutic interventions. However, FMN is not the only biomarker of clinical interest; there is also NADH, Nicotinamide Adenine Dinucleotide, shown in **Figure 2.7** and in **Figure 2.8** is depicted its oxidized and reduced state.

NADH is a molecule composed of two nucleotides—nicotinamide adenine dinucleotide (NAD) and a phosphate group—linked to an adenine residue and a ribose molecule [282]. The term “reduced” indicates that this molecule has gained electrons and is, therefore, involved in electron transfer during biochemical processes.

Nicotinamide, **Figure 2.9**, also known as vitamin B3 or vitamin PP, plays a key role in the metabolism of lipids, carbohydrates, and proteins, making it essential for the proper functioning of the human body [282]. Beyond its involvement in food metabolism, nicotinamide also contributes to oxygen transport within cells, regulates hormonal functions, and supports neurotransmitter synthesis [283].

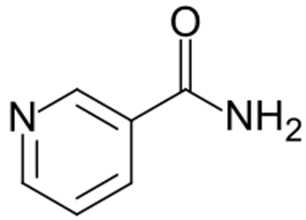

Figure 2.9. Structure of the Nicotinamide.

Adenine, **Figure 2.10**, is one of the two purine nitrogenous bases (together with guanine) that form the nucleotides of the nucleic acids DNA and RNA. As a purine, its structure is characterized by a pyrimidine ring fused with an imidazole ring. Adenine carries an amino group in the 6-position and can thus also be referred to as 6-aminopurine. Through two relatively weak hydrogen bonds, adenine pairs with thymine (T) in DNA and with uracil (U) in RNA. When linked to ribose through a glycosidic bond between the 9-position of the base and the 1'-position of the sugar, it forms the

nucleoside adenosine, which, with the addition of three phosphate groups, becomes the nucleotide adenosine triphosphate (ATP)—the fundamental compound responsible for transferring chemical energy between the reactions that compose cellular metabolism [284].

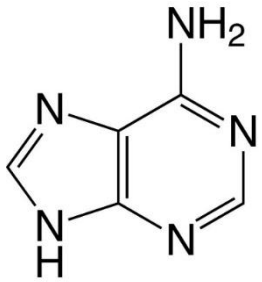

Figure 2.10. Structure of the Adenine.

Purine, **Figure 2.11**, is an aromatic heterocyclic organic molecule characterized by the fusion of a pyrimidine ring with an imidazole ring. The term "purine" is often used generically to indicate specific molecular forms bearing distinct substituents. Among these are two essential nitrogenous bases of nucleic acids: adenine and guanine. Within the DNA structure, these purine bases form hydrogen bonds with their complementary pyrimidine bases—thymine and cytosine. This complementarity is essential to the formation of the DNA double helix. In RNA, adenine pairs with uracil instead. The complementarity between purine and pyrimidine bases is crucial for the structural stability and functional integrity of nucleic acid molecules [285].

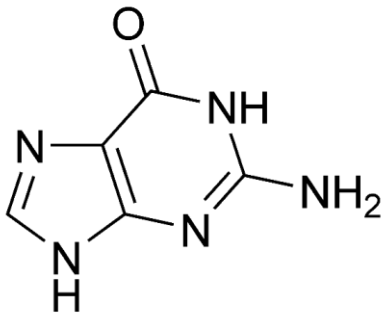

Figure 2.11. Structure of the Purine.

Ribose, **Figure 2.12**, is a five-carbon sugar (a monosaccharide, or aldopentose) with the molecular formula $C_5H_{10}O_5$, a molar mass of 150.13 g/mol, and a melting point of approximately 90 °C. It appears as a white solid that is highly soluble in water. Ribose is widespread in both animal and

plant organisms, as it constitutes the backbone of ribonucleic acid (RNA) and is a component of several important biomolecules such as ATP, NAD, and NADP.

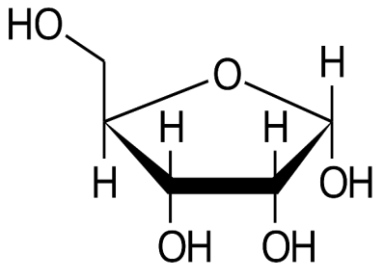

Figure 2.12. Structure of the D-Ribose.

Beyond its role in ribonucleic acid and its related nucleosides and nucleotides, D-ribose is also a molecular constituent of adenosine diphosphate (ADP), adenosine triphosphate (ATP), diphosphopyridine nucleotide (NAD), triphosphopyridine nucleotide (NADP), various natural nucleotides, riboflavin, coenzyme A, and the coenzyme of galactowaldenase. Therefore, it is part of several molecules of major biological significance.

Pyrophosphate, **Figure 2.13**, is the anion, salt, or ester of pyrophosphoric acid. Originally prepared by heating phosphates (hence the Greek prefix *pyro*-, meaning "fire"), pyrophosphates are effective complexing agents for metal ions (such as calcium and many transition metals) and are widely used in the chemical industry. A pyrophosphate group (also called diphosphate) consists of two phosphate (PO_4^{3-}) units linked together by an energy-rich phosphoanhydride bond. This bond is similar to the high-energy bonds found in ATP (adenosine triphosphate). When it breaks (for example, during hydrolysis), it releases a significant amount of energy. In NADH (nicotinamide adenine dinucleotide, reduced form), the pyrophosphate group plays a structural and connecting role. The NADH contains adenine and joined together by a pyrophosphate linkage. In other words, the pyrophosphate group acts as a chemical bridge that links the ribose–phosphate of one nucleotide to the ribose–phosphate of the other. Furthermore, the pyrophosphate bond provides structural stability and contributes to the molecule's overall conformation, allowing the nicotinamide ring (the reactive site) to be correctly positioned for redox reactions. While the pyrophosphate group itself does not participate directly in the redox reaction (the oxidation/reduction occurs on the nicotinamide ring), it is essential for the integrity and recognition of NADH by enzymes. Many dehydrogenases and oxidoreductases recognize NADH through interactions with the phosphate and pyrophosphate regions of the molecule.

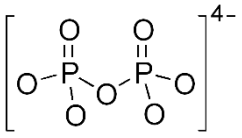

Figure 2.13. Structure of the Diphosphate group.

The NADH/NAD^+ system plays an essential role as an oxidoreductive coenzyme in redox reactions, which include both oxidation and reduction processes within the cell [282]. In oxidation reactions, NAD^+ acts as an electron and proton acceptor, being reduced to NADH. During this process, NAD^+ receives two electrons and two protons (corresponding to two hydrogen atoms) from the substrate molecule [286]. The correct representation of the reduced form of the coenzyme is NADH + H^+, since it can carry only two electrons and one proton; the additional proton is released into the cytosol during the reaction, contributing to the cellular ionic balance.

Conversely, in reduction reactions, NADH is oxidized back to NAD^+, donating two protons and two electrons. Although both reactions are possible, the oxidation reaction is thermodynamically favored, as the NAD^+/NADH system has a redox potential of –0.32 volts. It is noteworthy that during the reduction process, the nicotinamide ring in NAD^+ loses its aromaticity, whereas during oxidation, aromaticity is restored. This gain and loss of aromaticity contributes to the spontaneity of the oxidation reaction within the NAD^+/NADH system [286].

NADH is primarily involved in the electron transport chain, a key phase of cellular respiration [282]. During glycolysis and the Krebs cycle, NADH molecules are produced as a result of glucose oxidation and the breakdown of other organic substrates [286]. Subsequently, these NADH molecules transfer electrons and protons to a series of proteins in the inner mitochondrial membrane, helping to establish a proton gradient across the membrane [282].

Nicotinamide adenine dinucleotide (NAD) participates in a wide range of redox reactions catalyzed by enzymes generally known as oxidoreductases, often referred to as dehydrogenases [286]. These enzymes facilitate the transfer of electrons between substrates, and in many of these reactions, NAD^+ acts as the acceptor of a hydride ion (H^-), a hydrogen atom carrying an extra electron.

Nicotinamide Adenine Dinucleotide in its reduced form (NADH) is a central coenzyme in cellular metabolism, acting as an essential electron carrier in numerous biochemical reactions. Together with its oxidized counterpart (NAD^+), NADH constitutes a fundamental redox couple that regulates the balance between catabolic and anabolic processes within cells [287]. In the

mitochondrial matrix, NADH is primarily generated through oxidative pathways such as glycolysis, the tricarboxylic acid (TCA) cycle, and β-oxidation of fatty acids [288]. It donates high-energy electrons to the electron transport chain (ETC), where they are sequentially transferred through complexes I–IV, ultimately leading to the generation of ATP via oxidative phosphorylation [289, 290].

The redox balance between NAD^+ and NADH is a key determinant of mitochondrial function and overall cellular viability. Disruption of this equilibrium, for instance due to hypoxia or ischemia, leads to impaired oxidative phosphorylation and an accumulation of NADH, reflecting a shift toward anaerobic metabolism and reduced ATP production [201]. Thus, NADH serves as a sensitive marker of the energetic and oxidative state of the cell.

In the context of machine perfusion, the detection and quantification of NADH provide critical insights into the metabolic activity and mitochondrial integrity of the perfused organ. During hypothermic or normothermic perfusion, continuous monitoring of NADH fluorescence enables the identification of mitochondrial dysfunction in real time. An increase in NADH fluorescence intensity typically indicates a compromised electron transport chain, suggesting that oxygen delivery is insufficient or that mitochondrial respiration is impaired. Conversely, stable or decreasing NADH levels are indicative of preserved oxidative metabolism and adequate oxygenation [203].

The capacity to monitor NADH dynamically offers a complementary approach to FMN measurement, as both biomarkers are tightly linked to mitochondrial redox reactions. Whereas FMN release reflects structural damage to Complex I, variations in NADH fluorescence primarily indicate functional alterations in mitochondrial respiration. Together, these two parameters provide a powerful and non-invasive means to assess organ viability during ex situ perfusion, contributing to a more accurate prediction of post-transplant outcomes and potentially guiding the decision to accept or discard a graft.

3. Objectives of the PhD Thesis

The fundamental importance of FMN and NADH in organ transplantation has been highlighted, particularly as markers of mitochondrial integrity and cellular viability. It is therefore essential to develop reliable approaches for detecting these metabolites in the perfusion medium during machine perfusion.

The scientific literature from 2019 to 2025 reports several examples of FMN and NADH detection in various perfusion contexts. However, each clinical center has adopted different analytical

methods and measurement protocols, making it difficult to compare results or establish standardized procedures. Moreover, with only a few exceptions where FMN was monitored in real time, no system currently exists that can automatically calculate the concentration of FMN or NADH dissolved in the circulating perfusate during perfusion.

This PhD thesis aims to fill this gap by proposing an innovative approach for the real-time detection and quantification of FMN and NADH in the context of machine perfusion.

3.1. Main Objectives

The research work is structured around three main objectives:

1. **Development of a standardized measurement method:**
    - To design and validate a rigorous, robust, cost-effective, and easily implementable method that can potentially be applied in the clinical setting for the detection of FMN and NADH through perfusate sampling.
2. **Design and implementation of a stand-alone automatic detection device:**
    - To develop an autonomous system capable of detecting FMN through fluorescence signals, automatically identifying its characteristic emission spectrum, and calculating its real-time concentration in the perfusion medium.
    - This represents the core innovation of the thesis and a significant advancement over the current state of the art.
    - For this purpose, a scientifically rigorous calibration protocol was designed, and spectral recognition algorithms as well as machine learning models were implemented for real-time quantitative analysis.
3. **Experimental validation of the device:**
    - To validate the performance of the proposed system through tests on animal and human organs, assessing its robustness under real perfusion conditions and its potential applicability in the clinical transplantation setting.

3.2. Additional Objectives

In addition to the main research goals, the thesis also addresses two complementary topics:

- **Modeling of FMN release:**

A deterministic model, inspired by chemical engineering principles, was developed to describe the dynamics of FMN release during perfusion. This represents the first known attempt to quantitatively model the phenomenon, with partial validation based on the experimental data collected. Although a complete validation was not achievable, this modeling approach serves as a valuable starting point to stimulate further research in this area.

- **Statistical modeling and prediction of post-transplant outcomes:**

A predictive statistical model was also proposed to estimate post-transplant outcomes based on donor–recipient parameters, including FMN concentration levels. This analysis aims to explore the potential role of FMN as a prognostic biomarker for graft quality assessment and as a tool to refine organ selection criteria in clinical practice.

4. Thesis Structure

This doctoral thesis is organized into five chapters, each addressing a specific aspect of the research work, from theoretical background to experimental validation.

Chapter 1 introduces the research topic, outlining the scientific context in which it is framed. It presents the main problem addressed, the motivations underlying the study, and the specific objectives of the thesis.

Chapter 2 provides an in-depth review of *machine perfusion* from an engineering perspective, without delving into clinical details. This section is crucial for understanding the operating principles of machine perfusion, the key technical parameters that govern it, and the technologies upon which it relies.

Chapter 3 represents the first experimental phase of the research and focuses on the spectroscopic analysis of the coenzymes FMN and NADH. This section explores their spectrophotometric properties when dissolved in different types of organ perfusion solutions prepared in the laboratory.

Chapter 4 describes the development of the prototype designed for automatic FMN detection. Both the scientifically rigorous calibration methodology and the computational aspects of data analysis are detailed, including the implementation of *machine learning* algorithms for real-time and fully automated FMN concentration quantification.

Chapter 5 presents the experimental results obtained from tests performed on both animal and human organs. The temporal trends of FMN concentration in the perfusate are analyzed, and their biological implications are discussed. This chapter also introduces two additional original contributions: the deterministic modeling of FMN release based on chemical engineering principles, and the development of a predictive model for post-transplant outcomes derived from donor–recipient parameters and FMN concentration levels.

The Conclusions summarize the main findings of the research and discuss their scientific and practical implications. In particular, they highlight the original contribution of this work to the field of organ perfusion, with reference to the development of an innovative method and a stand-alone device for real-time FMN monitoring. Finally, future research perspectives are outlined, including technological optimization of the system and the potential extension of its application to clinical transplantation practice.

References

[1] Dina G. Tiniakos, Apostolos Kandilis, Stephen A. Geller, Tityus: A forgotten myth of liver regeneration, Journal of Hepatology, Volume 53, Issue 2, 2010, 357-361, https://doi.org/10.1016/j.jhep.2010.02.032

[2] Safadi R. The liver in Greco-Arabic and Islamic medicine. Clin Liver Dis (Hoboken). 2024 Apr 4;23(1):e0137. doi: 10.1097/CLD.0000000000000137.

[3] Nordham KD, Ninokawa S. The history of organ transplantation. Proc (Bayl Univ Med Cent). 2021 Oct 19;35(1):124-128. doi: 10.1080/08998280.2021.1985889.

[4] Risaliti A. I trapianti d'organo tra mito, storia e realtà. Forum Edizioni; 2016. 48 p.

[5] Punjala SR, Logan AJ, Brock GM, Kenawy DM, Chotai PN, Alebrahim M, Pawlik TM, Washburn WK, Schenk AD. Determinants of Long Waiting Time to Kidney Transplantation. Transplant Proc. 2024 Oct;56(8):1740-1751. doi: 10.1016/j.transproceed.2024.08.010.

[6] Atchade E, Bunel-Gourdy V, Zappella N, Jean-Baptiste S, Tran-Dinh A, Tanaka S, Lortat-Jacob B, Roussel A, Mordant P, Castier Y, Mal H, De Tymowski C, Montravers P. Time on the waiting list is an independent risk factor for day-90

mortality after lung transplantation. Anaesth Crit Care Pain Med. 2025 Apr;44(2):101499. doi: 10.1016/j.accpm.2025.101499.

[7] Vitale A, Trapani S, Russo FP, Miele L, Svegliati Baroni G, et al. Waiting list mortality and 5-year transplant survival benefit of patients with MASLD: An Italian liver transplant registry study. JHEP Rep. 2024 Jun 22;6(9):101147. doi: 10.1016/j.jhepr.2024.101147.

[8] Neuberger J. Liver transplantation in the United Kingdom. Liver Transpl. 2016 Aug;22(8):1129-35. doi: 10.1002/lt.24462.

[9] Handley TJ, Arnow KD, Melcher ML. Despite Increasing Costs, Perfusion Machines Expand the Donor Pool of Livers and Could Save Lives. J Surg Res. 2023 Mar;283:42-51. doi: 10.1016/j.jss.2022.10.002.

[10] Kwong AJ, Kim WR, Lake JR, Smith JM, Schladt DP, Skeans MA, Noreen SM, Foutz J, Booker SE, Cafarella M, Snyder JJ, Israni AK, Kasiske BL. OPTN/SRTR 2019 Annual Data Report: Liver. Am J Transplant. 2021 Feb;21 Suppl 2:208-315. doi: 10.1111/ajt.16494.

[11] Banker A, Bhatt N, Rao PS, Agrawal P, Shah M, Nayak M, Mohanka R. A Review of Machine Perfusion Strategies in Liver Transplantation. J Clin Exp Hepatol. 2023 Mar-Apr;13(2):335-349. doi: 10.1016/j.jceh.2022.08.001. Epub 2022 Aug 10.

[12] Jochmans I, Akhtar MZ, Nasralla D, Kocabayoglu P, Boffa C, Kaisar M, Brat A, O'Callaghan J, Pengel LH, Knight S, Ploeg RJ. Past, Present, and Future of Dynamic Kidney and Liver Preservation and Resuscitation. Am J Transplant. 2016 Sep;16(9):2545-55. doi: 10.1111/ajt.13778. Epub 2016 Apr 1.

[13] Watson CJE, Kosmoliaptsis V, Pley C, Randle L, Fear C, Crick K, Gimson AE, Allison M, Upponi S, Brais R, Jochmans I, Butler AJ. Observations on the ex situ perfusion of livers for transplantation. Am J Transplant. 2018 Aug;18(8):2005-2020. doi: 10.1111/ajt.14687.

[14] Dutkowski P, Schlegel A, de Oliveira M, Müllhaupt B, Neff F, Clavien PA. HOPE for human liver grafts obtained from donors after cardiac death. J Hepatol. 2014 Apr;60(4):765-72. doi: 10.1016/j.jhep.2013.11.023.

[15] Ravikumar R, Jassem W, Mergental H, Heaton N, Mirza D, Perera MT, Quaglia A, Holroyd D, Vogel T, Coussios CC, Friend PJ. Liver Transplantation After Ex Vivo Normothermic Machine Preservation: A Phase 1 (First-in-Man) Clinical Trial. Am J Transplant. 2016 Jun;16(6):1779-87. doi: 10.1111/ajt.13708.

[16] Nasralla D, Coussios CC, Mergental H, Akhtar MZ, Butler AJ, Ceresa CDL, Chiocchia V, Dutton SJ, García-Valdecasas JC, Heaton N, Imber C, Jassem W, Jochmans I, Karani J, Knight SR, Kocabayoglu P, Malagò M, Mirza D, Morris PJ, Pallan A, Paul A, Pavel M, Perera MTPR, Pirenne J, Ravikumar R, Russell L, Upponi S, Watson CJE, Weissenbacher A, Ploeg RJ, Friend PJ; Consortium for Organ Preservation in Europe. A randomized trial of normothermic preservation in liver transplantation. Nature. 2018 May;557(7703):50-56. doi: 10.1038/s41586-018-0047-9.

[17] Scalera I, De Carlis R, Patrono D, Gringeri E, Olivieri T, Pagano D, Lai Q, Rossi M, Gruttadauria S, Di Benedetto F, Cillo U, Romagnoli R, Lupo LG, De Carlis L. How useful is the machine perfusion in liver transplantation? An answer from a national survey. Front Surg. 2022 Sep 22;9:975150. doi: 10.3389/fsurg.2022.975150.

[18] Calleja Lozano R, Hervás Martínez C, Briceño Delgado FJ. Crossroads in Liver Transplantation: Is Artificial Intelligence the Key to Donor-Recipient Matching? Medicina (Kaunas). 2022 Nov 28;58(12):1743. doi: 10.3390/medicina58121743.

[19] Hann, A.; Lembach, H.; Nutu, A.; Dassanayake, B.; Tillakaratne, S.; McKay, S.C.; Boteon, A.P.C.S.; Boteon, Y.L.; Mergental, H.; Murphy, N.; et al. Outcomes of normothermic machine perfusion of liver grafts in repeat liver transplantation (NAPLES initiative). Br. J. Surg. 2022, 109, 372–380.

[20] Knaak JM, Spetzler VN, Goldaracena N, Louis KS, Selzner N, Selzner M. Technique of subnormothermic ex vivo liver perfusion for the storage, assessment, and repair of marginal liver grafts. J Vis Exp. 2014 Aug 13;(90):e51419. doi: 10.3791/51419.

[21] Mergental H, Perera MT, Laing RW, Muiesan P, Isaac JR, Smith A, Stephenson BT, Cilliers H, Neil DA, Hübscher SG, Afford SC, Mirza DF. Transplantation of Declined Liver Allografts Following Normothermic Ex-Situ Evaluation. Am J Transplant. 2016 Nov;16(11):3235-3245. doi: 10.1111/ajt.13875.

[22] op den Dries S, Karimian N, Sutton ME, Westerkamp AC, Nijsten MW, Gouw AS, Wiersema-Buist J, Lisman T, Leuvenink HG, Porte RJ. Ex vivo normothermic machine perfusion and viability testing of discarded human donor livers. Am J Transplant. 2013 May;13(5):1327-35. doi: 10.1111/ajt.12187.

[23] Bessems M, Doorschodt BM, Kolkert JL, Vetelainen RL, van Vliet AK, Vreeling H, van Marle J, van Gulik TM. Preservation of steatotic livers: a comparison between cold storage and machine perfusion preservation. Liver Transpl. 2007 Apr;13(4):497-504. doi: 10.1002/lt.21039.

[24] Rijkse E, IJzermans JN, Minnee RC. Machine perfusion in abdominal organ transplantation: Current use in the Netherlands. World J Transplant. 2020 Jan 18;10(1):15-28. doi: 10.5500/wjt.v10.i1.15.

[25] Tingle SJ, Figueiredo RS, Moir JA, Goodfellow M, Talbot D, Wilson CH. Machine perfusion preservation versus static cold storage for deceased donor kidney transplantation. Cochrane Database Syst Rev. 2019 Mar 15;3(3):CD011671. doi: 10.1002/14651858.CD011671.pub2.

[26] Hosgood SA, Callaghan CJ, Wilson CH, Smith L, Mullings J, Mehew J, Oniscu GC, Phillips BL, Bates L, Nicholson ML. Normothermic machine perfusion versus static cold storage in donation after circulatory death kidney transplantation: a randomized controlled trial. Nat Med. 2023 Jun;29(6):1511-1519. doi: 10.1038/s41591-023-02376-7.

[27] Plūme P, Losevs I, Loseva EA, Maļcevs A, Suhorukovs V, Jegorova O, Ševeļovs V, Jušinskis J. Hypothermic Machine Perfusion vs. Static Cold Storage in Kidney Transplantation: A Retrospective Paired-Kidney Study from Latvia. Medicina (Kaunas). 2025 Sep 10;61(9):1641. doi: 10.3390/medicina61091641.

[28] Hou J, Liavåg OMI, Færden IH, Martinsen ØG, Tønnessen TI, Line PD, Hagness M, Høgetveit JO, Pischke SE, Strand-Amundsen R. Utilization of dielectric properties for assessment of liver ischemia-reperfusion injury in vivo and during machine perfusion. Sci Rep. 2022 Jul 1;12(1):11183. doi: 10.1038/s41598-022-14817-3.

[29] van Leeuwen OB, de Vries Y, de Meijer VE, et al. Hypothermic machine perfusion before viability testing of previously discarded human livers. Nat Commun 2021;12(1):1008. doi: 10.1038/s41467-021-21182-8.

[30] Patrono D, Surra A, Catalano G, Rizza G, Berchialla P, Martini S, Tandoi F, Lupo F, Mirabella S, Stratta C, Salizzoni M, Romagnoli R. Hypothermic Oxygenated Machine Perfusion of Liver Grafts from Brain-Dead Donors. Sci Rep. 2019 Jun 27;9(1):9337. doi: 10.1038/s41598-019-45843-3.

[31] Nguyen MC, Zhang C, Chang YH, Li X, Ohara SY, Kumm KR, Cosentino CP, Aqel BA, Lizaola-Mayo BC, Frasco PE, Nunez-Nateras R, Hewitt WR, Harbell JW, Katariya NN, Singer AL, Moss AA, Reddy KS, Jadlowiec C, Mathur AK. Improved Outcomes and Resource Use With Normothermic Machine Perfusion in Liver Transplantation. JAMA Surg. 2025 Mar 1;160(3):322-330. doi: 10.1001/jamasurg.2024.6520.

[32] Muller X, Schlegel A, Kron P, Eshmuminov D, Würdinger M, Meierhofer D, Clavien PA, Dutkowski P. Novel Real-time Prediction of Liver Graft Function During Hypothermic Oxygenated Machine Perfusion Before Liver Transplantation. Ann Surg. 2019 Nov;270(5):783-790. doi: 10.1097/SLA.0000000000003513.

[33] Del Prete L, Franchi E, Lonati C, et al. Hypothermic machine per-fusion of the liver. The reasons for success. EJT 2023;1:35-4

[34] Markmann JF, Abouljoud MS, Ghobrial RM, Bhati CS, Pelletier SJ, Lu AD, Ottmann S, Klair T, Eymard C, Roll GR, Magliocca J, Pruett TL, Reyes J, Black SM, Marsh CL, Schnickel G, Kinkhabwala M, Florman SS, Merani S, Demetris AJ, Kimura S, Rizzari M, Saharia A, Levy M, Agarwal A, Cigarroa FG, Eason JD, Syed S, Washburn WK, Parekh J, Moon J, Maskin A, Yeh H, Vagefi PA, MacConmara MP. Impact of Portable Normothermic Blood-Based Machine Perfusion on Outcomes of Liver Transplant: The OCS Liver PROTECT Randomized Clinical Trial. JAMA Surg. 2022 Mar 1;157(3):189-198. doi: 10.1001/jamasurg.2021.6781.

[35] Boteon YL, Boteon AP, Attard J, Wallace L, Bhogal RH, Afford SC. Impact of machine perfusion of the liver on post-transplant biliary complications: A systematic review. World J Transplant. 2018 Oct 22;8(6):220-231. doi: 10.5500/wjt.v8.i6.220.

[36] David Hamilton, Transplantation Ancient Legends to Modern Practice, University of Pittsburgh Press, Pittsburgh, (2012), 978-0-8229-4413-3.

[37] Boettcher W, Merkle F, Weitkemper HH. History of extracorporeal circulation: the conceptional and developmental period. J Extra Corpor Technol. 2003 Sep;35(3):172-83.

[38] Holman WL, Timpa J, Kirklin JK. Origins and Evolution of Extracorporeal Circulation: JACC Historical Breakthroughs in Perspective. J Am Coll Cardiol. 2022;79(16):1606–22. doi:10.1016/j.jacc.2022.02.027.

[39] Cooley DA. Development of the roller pump for use in the cardiopulmonary bypass circuit. Tex Heart Inst J. 1987 Jun;14(2):112-8.

[40] Jing L, Yao L, Zhao M, Peng LP, Liu M. Organ preservation: from the past to the future. Acta Pharmacol Sin. 2018 May;39(5):845-857. doi: 10.1038/aps.2017.182.

[41] Šušak S, Redžek A, Rosić M, Velicki L, Okiljević B. Development of cardiopulmonary bypass – A historical review. Srp Arh Celok Lek. 2016 Nov-Dec;144(11-12):670-5

[42] Schurek HJ, Neumann KH, Schweda F, Czogalla J. A Laboratory Manual of Kidney Perfusion Techniques [Internet]. Münster (Germany): University of Münster; 2017. PMID: 33369897. doi: 10.17879/61219766654.

[43] Loebell CE. De conditionibus quibus secretiones in glandulis perficiuntur. Dissertatio Inauguralis Marburg, 1849.

[44] Bidder E. Beiträge zur Lehre von der Function der Niere. Inaugural Dissertation Dorpat, 1862.

[45] Martins PN, Buchwald JE, Mergental H, Vargas L, Quintini C. The role of normothermic machine perfusion in liver transplantation. Int J Surg. 2020 Oct;82S:52-60. doi: 10.1016/j.ijsu.2020.05.026.

[46] Konstantinov IE, Alexi-Meskishvili VV. Sergei S. Brukhonenko: the development of the first heart-lung machine for total body perfusion. Ann Thorac Surg. 2000 Mar;69(3):962-6. doi: 10.1016/s0003-4975(00)01091-2.

[47] Schmidt A. Die Athmung innerhalb des Blutes. Zweite Abhand-lung.—Aus dem physiologischen Institute zu Leipzig. Vorgelegt vondem wirkl. Mitgliede C. Ludwig. Berichte über die Verhandlungender Königlich Sächsischen Gesellschaft der Wissenschaften zuLeipzig. Mathematisch–physische Classe. 1867;19:99–130.

[48] Bunge G, Schmiedeberg O. Über die Bildung der Hippursäure.Archiv für experimentelle Pathologie und Pharmakologie. 1877;6:233–45.

[49] von Schröder W. Ueber die Bildungsstätte des Harnstoffs. Archiv fürexperimentelle Pathologie und Pharmakologie. 1882;15:364–400.

[50] Abeles M. Über Secretion aus der überlebenden durchblutetenNiere. Sitzungsberichte der mathematisch-naturwissenschaftlichenClasse der kaiserlichen Akademie der Wissenschaften. Wien. 1883;87:187–98.

[51] Hamel G. Die Bedeutung des Pulses für den Blutstrom. Zeitschrift für Biologie. 1889;25:474–95.

[52] Hooker DR. A study of the isolated kidney: The influence of pulse pressure upon renal function. Am J Physiol. 1910;27:24–45.

[53] Brodie TG. The perfusion of surviving organs. J Physiol. 1903;29: 266–72.

[54] Gesell RA. On the relation of pulse pressure to renal secretion. Am J Physiol. 1913;32:70–93.

[55] Jacobj C. Apparat zur Durchblutung isolirter überlebender Organe. Archiv für experimentelle Pathologie und Pharmakologie (Naunyn/ Schmiedeberg) 1890;26:388–397.

[56] Jacobj C., Ein Beitrag zur technik der kunstlichen durchblutung uberlebender organe. Arch Exp Pathol Pharmacol. 1895; 36: 330-348.

[57] Neubauer O, Groß W. Zur Kenntnis des Tyrosinabbaus in der künstlich durchbluteten Leber. Hoppe-Seyler's Zeitschrift für Physiologische Chemie. 1910;67:219–29.

[58] Embley EH, Martin CJ. The action of anesthetic quantities of chloroform upon the blood vessels of the bowel and kidney; with an account of an artificial circulation apparatus. J Physiol. 1905;32:147– 58.

[59] Bock J. Ein Apparat zu Infusionsversuchen. Naunyn u. Schmiedebergs Archiv für experimentelle Pathologie und Pharmakologie. 1907;57:177–82.

[60] Friedmann E. Zur Technik der Durchströmung überlebender Organe. Biochemische Zeitschrift. 1910;27:87–96.

[61] Fröhlich A. Eine Vorrichtung für Dauerdurchströmungen von Kaltblüterorganen mit kleinen Flüssigkeitsmengen. Zentralblatt für Physiologie. 1913;27:1011–3.

[62] Beck A. Zur Technik der bluttransfusion. Klin Wschr 1924; 2:1,999.

[63] Van Allen CM. A pump for clinical and laboratory purposes which employs the milking principle. JAMA. 1932;98:1805–6.

[64] Bayliss WM, Muller EA. A simple, high speed rotary pump. J Scient Instrum 1928; 5:278.

[65] Henry L, Jouvelet P. Appareil à transfusion du sang. Bulletin de l'Académie de Médecine. 1934;111: 312–9.

[66] Zeller O. Versuche zur Wiederbelebung von Tieren mittels arterieller Durchströmung des Herzens und der nervösen Zentralorgane. Deutsche Zeitschrift für Chirurgie. 1908;25:488–559.

[67] Bornstein A. Über Durchblutungsversuche an der überlebenden Hundeextremität. Naunyn-Schmiedeberg's Archiv für experimentelle Pathologie und Pharmakologie. 1926;115:367–74.

[68] Hooker DR. A study of the isolated kidney: The influence of pulse pressure upon renal function. Am J Physiol. 1910;27:24–45.

[69] von Issekutz B. Beiträge zur Wirkung des Insulins. II. Mitteilung: Insulin-Adrenalin-Antagonismus. Biochemische Zeitschrift. 1927; 183:283–97.

[70] Richards AN, Drinker CK. An apparatus for the perfusion of isolated organs. J Pharmacol Experiment Therapeu. 1915;7:467–83.

[71] Kermack WO, Lambie CG. An automatic perfusion apparatus. J Physiol. 1925;60:24–5.

[72] Abbas SH and Friend PJ, Principles and current status of abdominal organ preservation for transplantation, Surgery in Practice and Science 3, 2020. 10.1016/j.sipas.2020.100020.

[73] Dale HH, Schuster EHJ. A double perfusion-pump. J Physiol. 1928; 64:356–64.

[74] Dennis C, Spring DS, Nelson GE, et al. Development of a pump oxygenator to replace the heart and lungs: An apparatus applicable to human patients and application in one case. Ann Surg. 1951;134: 709–21.

[75] Brukhonenko S.S., Struggling for life. Tekhnika Molodezi. 1955; 6: 25-29.

[76] Brukhonenko S.S., Tchetchuline S., Experiences avec la tete isolee du chien. J Physiol Path Gen. 1929; 27: 31-45.

[77] Brukhonenko S.S., Tchechulin S.I., Experiments on isolation of dog's head., Trudi Nauchnogo Khimiko-Pharm Inst. 1928; 20: 7-43.

[78] Brukhonenko S.S., Artificial circulation of the whole body of a dog with arrested heart. Trudi Nauchnogo Khimiko-Pharm Inst. 1928; 20: 44-72.

[79] Krementsov N. Off with your heads: isolated organs in early Soviet science and fiction. Stud Hist Philos Biol Biomed Sci. 2009 Jun;40(2):87-100. doi: 10.1016/j.shpsc.2009.03.001.

[80] Verney EB, Starling EH. On secretion by the isolated kidney. J Physiol-London. 1922;56(5):353–8.

[81] Eichholtz F, Starling EH. The action of inorganic salts on the secretion of the isolated kidney. Proc R Soc Lond B Biol Char. 1925;98(687):93–112.

[82] Lee CY, Mangino MJ. Preservation methods for kidney and liver. Organogenesis. 2009 Jul;5(3):105-12. doi: 10.4161/org.5.3.9582.

[83] Carrel A, Lindbergh CA. The culture of whole organs. Science. 1935; 81:621–3.

[84] Lindbergh CA. An apparatus for the culture of whole organs. J Experiment Med. 1935;62:409–33.

[85] Lindbergh CA, Perry VP, Malinin TI, Mouer GH. An apparatus for the pulsating perfusion of whole organs. Cryobiology 1966; 3:252-60.

[86] Gibbon JH. Artificial maintenance of circulation during experimental occlusion of pulmonary artery. Arch Surg 1937; 34:1105-1131.

[87] Crafoord C. Some aspects of the development of intrathoracic surgery. Surg, Gynecol Obstet. 1949;89:629–37.

[88] Björk VO. Brain perfusions in dogs with artificially oxygenated blood. Acta Chirurgica Scand. 1948;96(Suppl. 137):1–122.

[89] Jongbloed J. The mechanical heart–lung system. Surg Gynecol Obstet. 1949;89:684–91.

[90] Shaikh N, Malmstrom MF. Protective hypothermia: An old therapy with a new prospective. Qatar Med J. 2013 Nov 1;2012(2):81-4. doi: 10.5339/qmj.2012.2.19.

[91] Crumplin MKH. The Myles Gibson military lecture: surgery in the Napoleonic Wars. J R Coll Surg Edinb. 2002;47:566–78.

[92] Fuller B, Guibert E, Rodriguez J: Lessons from natural cold-induced dormancy to organ preservation in medicine and biotechnology : from the ‘backwoods to the bedside’; in E Lubens, J Cerda, M Clark (eds): Dormancy and Resistance to Harsh Environments, Topics in Current Genetics. Berlin, Springer, 2010, pp253–278.

[93] R.G. Bickford, F.R. Winton, The influence of temperature on the isolated kidney of the dog, J Physiol, 89 (2) (1937), pp. 198-219.

[94] Petrenko A, Carnevale M, Somov A, Osorio J, Rodríguez J, Guibert E, Fuller B, Froghi F. Organ Preservation into the 2020s: The Era of Dynamic Intervention. Transfus Med Hemother. 2019 Jun;46(3):151-172. doi: 10.1159/000499610.

[95] Voigt MR, DeLario GT. Perspectives on abdominal organ preservation solutions: a comparative literature review. Prog Transplant. 2013 Dec;23(4):383-91. doi: 10.7182/pit2013100.

[96] Carrel A, Lindbergh CA. The culture of whole organs. Science. 1935; 81:621–3.

[97] Carrel A. The culture of whole organs: I. technique of the culture of the thyroid gland. J Exp Med 1937; 65: 515–26.

[98] Hou LT, Ewen SW, Beck JS. Histological, metabolic and histochemical studies on normal human placenta in organ culture. Br J Exp Pathol 1968; 49: 648–57.

[99] MILLER LL, BLY CG, WATSON ML, BALE WF. The dominant role of the liver in plasma protein synthesis; a direct study of the isolated perfused rat liver with the aid of lysine-epsilon-C14. J Exp Med. 1951 Nov;94(5):431-53. doi: 10.1084/jem.94.5.431.

[100] Belzer FO, Ashby BS, Dunphy JE. 24-hour and 72-hour preservation of canine kidneys. Lancet. 1967 Sep 9;2(7515):536-8. doi: 10.1016/s0140-6736(67)90498-9.

[101] Humphries AL Jr, Russell R, Stoddard LD, Moretz WH. Successful five-day kidney preservation. Perfusion with hypothermic, diluted plasma. Invest Urol. 1968 May;5(6):609-18.

[102] Calne RY, Pegg DE, Pryse-Davies J, Brown FL. Renal preservation by ice-cooling: an experimental study relating to kidney transplantation from cadavers. Br Med J 1963; 2: 651–5.

[103] Edgardo E. Guibert, Alexander Y. Petrenkob, Cecilia L. Balabana, Alexander Y. Somovb, Joaquín V. Rodrigueza, Barry J. Fuller, Organ Preservation: Current Concepts and New Strategies for the Next Decade, Transfus Med Hemother 2011;38:125–142.

[104] Schuldt HH, Dauberschmidt R, Seibt F, Althaus P. Hämodynamische, Hemodynamic effects of an alpha-adrenergic blockade following experimental kidney transplantation. Z Urol Nephrol. 1984 Mar;77(3):151-60.

[105] Fanourios Georgiades, Sarah A. Hosgood, Andrew J. Butler, Michael L. Nicholson, Use of ex vivo normothermic machine perfusion after normothermic regional perfusion to salvage a poorly perfused DCD kidney, Am J Transplant. 2019;19:3415–3419.

[106] Pegg DE. An approach to hypothermic renal preservation. Cryobiology. 1978 Feb;15(1):1–17.

[107] Lapchinsky AG. Recent results of experimental transplantation of preserved limbs and kidneys and possible use of this technique in clinical practice. Ann N Y Acad Sci 1960; 46:539–569.

[108] Andrew M. Cameron and Jose F. Barandiaran Cornejo, Organ preservation review: history of organ preservation, Curr Opin Organ Transplant 2015, 20:146–151.

[109] Manax, W. G., Bloch, J. H., Longerbeam, J. K. and Lillehei, R. C.: Successful 24 hour in vitro preservation of canine kidneys by the combined use of hyperbaric oxygenation and hypothermia, Surgery 56: 275–282, 1964.

[110] Hoffman A, Burger C, Persky L. Extracorporeal renal storage. Invest Urol 1965; 2:567-73.

[111] F.O. Belzer, B.S. Ashby, P.F. Gulyassy, M. Powell, Successful seventeen-hour preservation and transplantation of human-cadaver kidney, N. Engl. J. Med., 278 (11) (1968), pp. 608-610.

[112] Matsubara, J. Successful 24 to 48 hour canine kidney preservation. The Japanese Journal of Surgery 2, 30–36 (1972).

[113] Manax, W. G., Bloch, J. H., Longerbeam, J. K. and Lillehei, R. C.: Successful 24 hour in vitro preservation of canine kidneys by the combined use of hyperbaric oxygenation and hypothermia, Surgery 56: 275–282, 1964.

[114] Matsubara, J., Oiwa, S., Kondo, M., Takeuchi, T., Kamiya, K. and Nakata, Y.: Experimental studies on canine kidney preservation, Nihon Gekagakkai Zasshi (J. Jap. Surg. Soc.) 71: 1627–1633, 1970 (in Japanese).

[115] Brettschneider L., Bell P. R. F., Martin A. J., Tarr J. S., Taylor P. D., Starzl T. E. (1969) Conservation of the liver. Transplant. Proc. 1 (1):132–137

[116] Slapak M., Wigmore R. A., MacLean L. D. (1967) Twenty-four hour liver preservation by the use of continuous pulsatile perfusion and hyperbaric oxygen. Transplantation 5 (4):1154–1158

[117] Van Der Plaats A, Maathuis M. H., T. Hart N.A. et al. The Groningen hypothermic liver perfusion pump: Functional evaluation of a new machine perfusion system. Ann Biomed Eng 2006; 34: 1924–1934.

[118] D'Alessandro A. M., Hoffmann R. M., Knechtle S. J., Eckhoff D. E., Love R. B., Kalayoglu M., Sollinger H. W., Belzer F. O. (1995) Successful extrarenal transplantation from non-heart-beating donors. Transplantation 59 (7):977–982.

[119] Pienaar B. H., Lindell S. L., van Gulik T., Southard J. H., Belzer F. O. (1990) Seventy-two-hour preservation of the canine liver by machine perfusion. Transplantation 49 (2):258–260

[120] J.C. Norman, Organ Perfusion and Preservation, Appleton-Century-Crofts (1968) ISBN-10: 0838575161.

[121] Czigany Z, Lurje I, Tolba RH, et al. Machine perfusion for liver transplantation in the era of marginal organs—new kids on the block. Liver Int 2019; 39:228–249.

[122] Penn I, Halgrimson CG, Starzl TE. Liver transplantation in man. Ann N Y Acad Sci. 1970;170:251-258.

[123] Collins GM, Bravo-Shugarman M, Terasaki PI. Kidney preservation for transportation. Initial perfusion and 30 hours' ice storage. Lancet. 1969 Dec 6;2(7632):1219-22. doi: 10.1016/s0140-6736(69)90753-3.

[124] Collins GM, Bravo-Shugarman M, Terasaki PI, Braf Z, Sheil AG, Williams G. Kidney preservation for transportation. IV. Eight-thousand-mile international air transport. Aust N Z J Surg. 1970 Nov;40(2):195-7. doi: 10.1111/j.1445-2197.1970.tb04058.x.

[125] Voigt MR, DeLario GT. Perspectives on abdominal organ preservation solutions: a comparative literature review. Prog Transplant 2013; 23:383–391.

[126] Bae C, Henry SD, Guarrera JV. Is extracorporeal hypothermic machine perfusion of the liver better than the 'good old icebox'? Curr Opin Organ Transplant 2012; 17:137–142.

[127] Ina Jochmans and Jacques Pirenne, Machine Perfusion of Kidneys Donated After Circulatory Death: The Carrel and Lindbergh Legacy, Chapter 16, Part II, Regenerative Medicine Applications in Organ Transplantation, 2014 Elsevier Inc.

[128] Aydin G, Okiye SE, Zincke H. Successful 24-hour preservation of the ischemic canine kidney with Euro-Collins solution. J Urol 1982; 128: 1401–3.

[129] Jamieson RW, Friend PJ. Organ reperfusion and preservation. Front Biosci 2008; 13: 221–35.

[130] Izamis ML, Perk S, Calhoun C, Uygun K, Yarmush ML, Berthiaume F. Machine perfusion enhances hepatocyte isolation yields from ischemic livers. Cryobiology. 2015 Oct;71(2):244-55.

[131] H. Gibelin, M. Eugene, W. Hebrard, et al. Comparison of Euro-Collins and University of Wisconsin solutions in the isolated perfused rat liver model: evaluation by proton nuclear magnetic resonance spectroscopy. Transplant Proc, 32 (2000), p. 2792

[132] Bejaoui M, Pantazi E, Folch-Puy E, Baptista PM, García-Gil A, Adam R, Roselló-Catafau J. Emerging concepts in liver graft preservation. World J Gastroenterol. 2015 Jan 14;21(2):396-407.

[133] Southard JH, Belzer FO. Organ preservation. Annu Rev Med. 1995;46:235–247.

[134] Morariu, A.M.; Van der Plaats, A.; Oeveren, W.V.; Hart, N.A.T.; Leuvenik, H.G.D.; Graaff, R.; Ploegh, R.J.; Rakhorst, G. Hyperaggregating effect of hydroxyethyl starch components and University of Wisconsin solution on human red blood cells:a risk of impaired graft perfusion in organ procurement? Transplantation 2003, 76, 37–43.

[135] Zaouali MA, Ben Abdennebi H, Padrissa-Altés S, Mahfoudh-Boussaid A, Roselló-Catafau J. Pharmacological strategies against cold ischemia reperfusion injury. Expert Opin Pharmacother. 2010;11:537–555. doi: 10.1517/14656560903547836.

[136] Ben Abdennebi H, Steghens JP, Margonari J, Ramella-Virieux S, Barbieux A, Boillot O. High-Na+ low-K+ UW cold storage solution reduces reperfusion injuries of the rat liver graft. Transpl Int. 1998;11:223–230.

[137] Schneeberger S, Biebl M, Steurer W, Hesse UJ, Troisi R, Langrehr JM, et al. A prospective randomized multicenter trial comparing histidine-tryptophane-ketoglutarate versus University of Wisconsin perfusion solution in clinical pancreas transplantation. Transpl Int 2009; 22: 217–24.

[138] Moray G, Sevmis S, Karakayali FY, Gorur SK, Haberal M. Comparison of histidine-tryptophan-ketoglutarate and University of Wisconsin in living-donor liver transplantation. Transplant Proc 2006; 38: 3572–5.

[139] Bretschneider HJ, Hübner G, Knoll D, et al. Myocardial resistance and tolerance to ischemia: physiological and biochemical basis. J Cardiovasc Surg (Torino) 1975;16:241-60.

[140] Nickkholgh A, Nikdad M, Shafie S, et al. Ex situ liver machine perfusion as an emerging graft protective strategy in clinical liver transplantation: the dawn of a new era. Transplantation. 2019;103:2003–2011.

[141] Detelich D, Markmann JF. The dawn of liver perfusion machines. Curr Opin Organ Transplant. 2018;23:151–161.

[142] Aydin G, Okiye SE, Zincke H. Successful 24-hour preservation of the ischemic canine kidney with Euro-Collins solution. J Urol 1982; 128: 1401–3.

[143] Wahlberg JA, Southard JH, Belzer FO. Development of a cold storage solution for pancreas preservation. Cryobiology 1986; 23: 477–82.

[144] Okada Y, Kondo T. Preservation solution for lung transplantation. Gen Thorac Cardiovasc Surg 2009; 57: 635–9.

[145] Pizanis N, Petrov A, Heckmann J, Wiswedel I, Wohlschläger J, de Groot H, et al. A new preservation solution for lung transplantation: evaluation in a porcine transplantation model. J Hear Lung Transplant 2012; 31: 310–7.

[146] Karam G, Compagnon P, Hourmant M, Despins P, Duveau D, Noury D, et al. A single solution for multiple organ procurement and preservation. Transpl Int 2005; 18: 657–63.

[147] Handa M, Fujimura S, Kondo T, Ichinose T, Shiraishi Y, Nakada T. A study of preservation solution for 48- and 96-hour simple hypothermic storage of canine lung transplants. Tohoku J Exp Med 1989; 159: 205–14.

[148] Keshavjee SH, Yamazaki F, Cardoso PF, McRitchie DI, Patterson GA, Cooper JD. A method for safe twelve-hour pulmonary preservation. J Thorac Cardiovasc Surg 1989; 98: 529–34.

[149] Date H, Matsumura A, Manchester JK, Obo H, Lima O, Cooper JM, et al. Evaluation of lung metabolism during successful twenty-four-hour canine lung preservation. J Thorac Cardiovasc Surg 1993; 105: 480–91.

[150] Ikeda M, Bando T, Yamada T, Sato M, Menjyu T, Aoyama A, et al. Clinical application of ET-Kyoto solution for lung transplantation. Surg Today 2015; 45: 439–43.

[151] Okada Y, Matsumura Y, Date H, Bando T, Oto T, Sado T, et al. Clinical application of an extracellular phosphate-buffered solution (EP-TU) for lung preservation: preliminary results of a Japanese series. Surg Today 2012; 42: 152–6.

[152] Omasa M, Hasegawa S, Bando T, Hanaoka N, Yoshimura T, Nakamura T, et al. Application of ET-Kyoto solution in clinical lung transplantation. Ann Thorac Surg 2004; 77: 338–9.

[153] Thomas G. Cotter, Matthew A. Odenwald, Angelica Perez-Gutierrez, Kumar Jayant, Diego DiSabato, Michael Charlton, John Fung, Preservation solutions for static cold storage in donation after circulatory death and donation after brain death liver transplantation in the United States, Liver Transplantation. 2022;28:1454–1462.

[154] Orman ES, Mayorga ME, Wheeler SB, Townsley RM, Toro-Diaz HH, Hayashi PH, et al. Declining liver graft quality threatens the future of liver transplantation in the United States. Liver Transpl. 2015;21(8):1040–50.

[155] .C.o.C.C.M.S.o.C.C.M. Ethics Committee, Recommendations for nonheartbeating organ donation. A position paper by the Ethics Committee, American College of Critical Care Medicine, Society of Critical Care Medicine, Crit. Care Med. 29 (2001) 1826–1831.

[156] R. Adam, P. Mcmaster, J.G. O'Grady, D. Castaing, J.L. Klempnauer, N. Jamieson, P. Neuhaus, J. Lerut, M. Salizzoni, S. Pollard, F. Muhlbacher, X. Rogiers, J.C. Garcia Valdecasas, J. Berenguer, D. Jaeck, G.E. Moreno Evolution of liver transplantation in Europe: report of the European Liver Transplant Registry Liver Transplant., 9 (2003), pp. 1231-1243

[157] Bardallo RG, Da Silva RT, Carbonell T, Palmeira C, Folch-Puy E, Roselló-Catafau J, Adam R, Panisello-Rosello A. Liver Graft Hypothermic Static and Oxygenated Perfusion (HOPE) Strategies: A Mitochondrial Crossroads. Int J Mol Sci. 2022 May 20;23(10):5742.

[158] Ravikumar R, Leuvenink H, Friend PJ. Normothermic liver preservation: a new paradigm? Transpl Int. 2015;28(6):690–9.

[159] Schlegel, A., Muller, X. & Dutkowski, P. Hypothermic Machine Preservation of the Liver: State of the Art. Curr Transplant Rep. 5, 93–102 (2018).

[160] Zamboni F, Franchello A, David E, et al. Effect of macrovescicular steatosis and other donor and recipient characteristics on the outcome of liver transplantation. Clin Transplant. 2001; 15: 53- 57.

[161] van Rijn R, Karimian N, Matton APM, et al. Dual hypothermic oxygenated machine perfusion in liver transplants donated after circulatory death. Br J Surg 2017;104:907-917.

[162] de Rougemont O, Breitenstein S, Leskosek B, et al. One hour hypothermic oxygenated perfusion (HOPE) protects nonviable liver allografts donated after cardiac death. Ann Surg 2009;250:674-683.

[163] Xu H, Berendsen T, Kim K, Soto-Gutierrez A, Bertheium F, Yarmush ML et al Excorporeal normothermic machine perfusion resuscitates pig DCD livers with extended warm ischemia. J Surg Res 2012; 173: e83–e88.

[164] Lockett CJ, Fuller BJ, Busza AL, Proctor E. Hypothermic perfusion preservation of liver: the role of phosphate in stimulating ATP synthesis studied by 31P NMR. Transpl Int. 1995;8(6):440–445.

[165] Foley DP, Fernandez LA, Leverson G, et al. Biliary complications after liver transplantation from donation after cardiac death donors: an analysis of risk factors and long-term outcomes from a single center. Ann Surg 2011;253:817-825.

[166] O'Neill S, Roebuck A, Khoo E, Wigmore SJ, Harrison EM. A meta-analysis and meta-regression of outcomes including biliary complications in donation after cardiac death liver transplantation. Transpl Int 2014;27:1159-1174

[167] Bral M, Gala-Lopez B, Bigam D, et al. Preliminary single-center canadian experience of human normothermic ex vivo liver perfusion: results of a clinical trial. Am J Transplant. 2017;17:1071–1080.

[168] Dutkowski P, Guarrera JV, de Jonge J, Martins PN, Porte RJ, Clavien PA. Evolving trends in machine perfusion for liver transplantation. Gastroenterology 2019;156:1542-1547.

[169] Schlegel A, Muller X, Dutkowski P. Machine perfusion strategies in liver transplantation. Hepatobiliary Surg Nutr. 2019;8:490.

[170] Detelich D, Markmann JF. The dawn of liver perfusion machines. Curr Opin Organ Transplant. 2018;23:151–161.

[171] van Beekum CJ, Vilz TO, Glowka TR, von Websky MW, Kalff JC, Manekeller S. Normothermic machine perfusion (NMP) of the liver – current status and future perspectives. Ann Transplant. 2021;26e931664-1.

[172] Reich DJ, Mulligan DC, Abt PL, et al. ASTS recommended practice guidelines for controlled donation after cardiac death organ procurement and transplantation. Am J Transplant. 2009;9:2004– 2011.

[173] Cursio R, Gugenheim J, Ischemia-reperfusion injury and ischemic-type biliary lesions following liver transplantation. J Transplant. 2012; 2012: 164329

[174] Grewal HP, Willingham DL, Nguyen J et al. Liver transplantation using controlled donation after cardiac death donors: An analysis of a large single-center experience Liver Transpl. 2009; 15: 1028-1035

[175] de Vera ME, Lopez-Solis R, Dvorchik I et al. Liver transplantation using donation after cardiac death donors: Long-term follow-up from a single center. Am J Transplant. 2009; 9: 773-781.

[176] Westerkamp AC, Karimian N, Matton AP, Mahboub P, van Rijn R, Wiersema-Buist J, de Boer MT, Leuvenink HG, Gouw AS, Lisman T, Porte RJ. Oxygenated Hypothermic Machine Perfusion After Static Cold Storage Improves Hepatobiliary Function of Extended Criteria Donor Livers. Transplantation. 2016 Apr;100(4):825-35. doi: 10.1097/TP.0000000000001081.

[177] Boteon Y, Afford S, Mergental H. Pushing the limits: machine preservation of the liver as a tool to recondition high-risk grafts. Curr Transplant reports. 2018;5:113–120

[178] Schlegel A, Kalisvaart M, Scalera I, et al. The UK DCD risk score: a new proposal to define futility in donation-after-circulatory-death liver transplantation. J Hepatol. 2018;Mar:456–464.

[179] Burlage LC, Karimian N, Westerkamp AC, Visser N, Matton APM, van Rijn R, et al. Oxygenated hypothermic machine perfusion after static cold storage improves endothelial function of extended criteria donor livers. Hpb. (2017) 19:538–46.

[180] C.D. Collard, S. Gelman, Pathophysiology, clinical manifestations, and prevention of ischemia-reperfusion injury Anesthesiology, 94 (6) (2001), pp. 1133-1138.

[181] E.T. Chouchani, V.R. Pell, E. Gaude, D. Aksentijević, S.Y. Sundier, E.L. Robb, et al. Ischaemic accumulation of succinate controls reperfusion injury through mitochondrial ROS Nature, 515 (7527) (2014), pp. 431-435.

[182] Fodor M, Cardini B, Peter W, Weissenbacher A, Oberhuber R, Hautz T, Otarashvili G, Margreiter C, Maglione M, Resch T, Krendl F, Meszaros AT, Bogensperger C, Gasteiger S, Messner F, Henninger B, Zoller H, Tilg H, Öfner D, Schneeberger S. Static cold storage compared with normothermic machine perfusion of the liver and effect on ischaemic-type biliary lesions after transplantation: a propensity score-matched study. Br J Surg. 2021 Sep 27;108(9):1082-1089.

[183] Tingle SJ, Figueiredo RS, Moir JA, Goodfellow M, Talbot D, Wilson CH. Machine perfusion preservation versus static cold storage for deceased donor kidney transplantation. Cochrane Database Syst Rev. 2019 Mar 15;3(3):CD011671.

[184] Taylor MJ, Baicu SC. Current state of hypothermic machine perfusion preservation of organs: The clinical perspective. Cryobiology. 2010 Jul;60(3 Suppl):S20-35.

[185] Serifis N, Matheson R, Cloonan D, Rickert CG, Markmann JF and Coe TM (2021) Machine Perfusion of the Liver: A Review of Clinical Trials. Front. Surg. 8:625394.

[186] Kvietkauskas M, Leber B, Strupas K, Stiegler P and Schemmer P (2020) Machine Perfusion of Extended Criteria Donor Organs: Immunological Aspects. Front. Immunol. 11:192.

[187] Bhogal RH, Mirza DF, Afford SC, Mergental H. Biomarkers of Liver Injury during Transplantation in an Era of Machine Perfusion. International Journal of Molecular Sciences. 2020; 21(5):1578.

[188] Konishi, T.; Lentsch, A.B. Hepatic Ischemia/Reperfusion: Mechanisms of Tissue Injury, Repair, and Regeneration. Gene Expr. 2017, 17, 277–287.

[189] Stegemann J, Minor T. Energy charge restoration, mitochondrial protection and reversal of preservation induced liver injury by hypothermic oxygenation prior to reperfusion. Cryobiology. 2009;58:331–336.

[190] Schlegel A, Muller X, Kalisvaart M, Muellhaupt B, Perera MTPR, Isaac JR, et al. Outcomes of DCD liver transplantation using organs treated by hypothermic oxygenated perfusion before implantation. J Hepatol. (2019) 70:50–7.

[191] Parente A, Osei-Bordom DC, Ronca V, Perera MTPR, Mirza D. Organ Restoration With Normothermic Machine Perfusion and Immune Reaction. Front Immunol. 2020 Oct 19;11:565616. doi: 10.3389/fimmu.2020.565616.

[192] D. Monbaliu, J. Pirenne, D. Talbot. Liver transplantation using donation after cardiac death donors J Hepatol, 56 (2) (2012), pp. 474-485

[193]https://www.trapianti.salute.gov.it/trapianti/dettaglioComunicatiNotizieCnt.jsp?lingua=italiano&area=cnt&menu=media&sottomenu=news&id=636 (Accesso 10/01/2023)

[194] de Vries Y, von Meijenfeldt FA, Porte RJ. Post-transplant cholangiopathy: classification, pathogenesis, and preventive strategies. Biochim Biophys Acta Mol Basis Dis 2018;1864:1507-1515.

[195] Watson CJE, Jochmans I. From "gut feeling" to objectivity: machine preservation of the liver as a tool to assess organ viability. Curr Transplant reports. 2018;5:72–81.

[196] Guy AJ, Nath J, Cobbold M, et al. Metabolomic analysis of perfusate during hypothermic machine perfusion of human cadaveric kidneys. Transplantation. 2015;99:754–759

[197] Faitot F, Besch C, Battini S, et al. Impact of real-time metabolomics in liver transplantation: Graft evaluation and donor-recipient matching. J Hepatol. 2018;68:699–706.

[198] Liu Q, Vekemans K, van Pelt J, et al. Discriminate liver warm ischemic injury during hypothermic machine perfusion by proton magnetic resonance spectroscopy: a study in a porcine model. Transplant Proc. 2009;41:3383–3386.

[199] Guarrera JV, Henry SD, Samstein B, Odeh-Ramadan R, Kinkhabwala M, Goldstein MJ, Ratner LE, Renz JF, Lee HT, Brown RS Jr, Emond JC. Hypothermic machine preservation in human liver transplantation: the first clinical series. Am J Transplant. 2010 Feb;10(2):372-81. doi: 10.1111/j.1600-6143.2009.02932.x.

[200] Bellini MI, Nozdrin M, Yiu J, Papalois V. Machine Perfusion for Abdominal Organ Preservation: A Systematic Review of Kidney and Liver Human Grafts. J Clin Med. 2019 Aug 15;8(8):1221.

[201] Schlegel A, Muller X, Mueller M, Stepanova A, Kron P, de Rougemont O, Muiesan P, Clavien PA, Galkin A, Meierhofer D, Dutkowski P. Hypothermic oxygenated perfusion protects from mitochondrial injury before liver transplantation. EBioMedicine. 2020 Oct;60:103014. doi: 10.1016/j.ebiom.2020.103014.

[202] Sousa Da Silva RX, Darius T, Mancina L, Eden J, Wernlé K, Ghoneima AS, Barlow AD, Clavien P-A, Dutkowski P, Kron P. Real-time assessment of kidney allografts during HOPE using flavin mononucleotide (FMN)—A preclinical study. Front Transplant. 2023;2:1132673.

[203] Sun K, Jiao C, Panconesi R, Satish S, Karakaya OF, De Goeij FHC, Diwan T, Ali K, Cadinu LA, Cazzaniga B, Liu Q, Miyazaki Y, Pita A, Khalil M, Kim J, Hussein A, Müller PC, Aucejo F, Kwon DHC, Fernandes E, Esfeh JM, Cywinski J, Fujiki M, Sun L, Pinna A, Dutkowski P, Wehrle CJ, Fairchild RL, Meierhofer D, De Jonge J, Miller C, Hashimoto K, Schlegel A. Quantifying Flavin mononucleotide: an internationally validated methodological approach for enhanced decision making in organ transplantation. EBioMedicine. 2025 Jun;116:105761. doi: 10.1016/j.ebiom.2025.105761.

[204] Panconesi R, Flores Carvalho M, Mueller M, Dutkowski P, Muiesan P, Schlegel A. Mitochondrial Reprogramming—What Is the Benefit of Hypothermic Oxygenated Perfusion in Liver Transplantation? Transplantology. 2021; 2(2):149-161. https://doi.org/10.3390/transplantology2020015.

[205] Wen H, Deng H, Li B, Chen J, Zhu J, Zhang X, Yoshida S, Zhou Y. Mitochondrial diseases: from molecular mechanisms to therapeutic advances. Signal Transduct Target Ther. 2025 Jan 10;10(1):9. doi: 10.1038/s41392-024-02044-3.

[206] Tenchov R, Sasso JM, Wang X, Zhou QA. Aging Hallmarks and Progression and Age-Related Diseases: A Landscape View of Research Advancement. ACS Chem Neurosci. 2024 Jan 3;15(1):1-30. doi: 10.1021/acschemneuro.3c00531.

[207] Riou A, Broeglin A, Grimm A. Mitochondrial transplantation in brain disorders: Achievements, methods, and challenges. Neurosci Biobehav Rev. 2025 Feb;169:105971. doi: 10.1016/j.neubiorev.2024.105971.

[208] Rouslin W, Ranganathan S. Impaired function of mitochondrial electron transfer complex I in canine myocardial ischemia: loss of flavin mononucleotide. J Mol Cell Cardiol. 1983;15:537-542. doi:https://doi.org/10.1016/0022-2828(83)90329-2

[209] Horváth T, Jász DK, Baráth B, Poles MZ, Boros M, Hartmann P. Mitochondrial Consequences of Organ Preservation Techniques during Liver Transplantation. Int J Mol Sci. 2021 Mar 10;22(6):2816. doi: 10.3390/ijms22062816.

[210] Wen, H., Deng, H., Li, B. et al. Mitochondrial diseases: from molecular mechanisms to therapeutic advances. Sig Transduct Target Ther 10, 9 (2025). https://doi.org/10.1038/s41392-024-02044-3.

[211] Wang L, Zhou X, Lu T. Role of mitochondria in physiological activities, diseases, and therapy. Mol Biomed. 2025 Jun 19;6(1):42. doi: 10.1186/s43556-025-00284-5.

[212] Zhang HL, Sandai D, Zhang ZW, Song ZJ, Babu D, Tabana Y, Dahham SS, Adam Ahmed Adam M, Wang Y, Wang W, Zhang HL, Zhao R, Barakat K, Harun MSR, Shapudin SNM, Lok B. Adenosine triphosphate induced cell death: Mechanisms and implications in cancer biology and therapy. World J Clin Oncol. 2023 Dec 24;14(12):549-569. doi: 10.5306/wjco.v14.i12.549.

[213] Li, X., Jiang, O., Chen, M. et al. Mitochondrial homeostasis: shaping health and disease. Curr Med 3, 5 (2024). https://doi.org/10.1007/s44194-024-00032-x

[214] Nikolaou PE, Lambrinidis G, Georgiou M, Karagiannis D, Efentakis P, Bessis-Lazarou P, Founta K, Kampoukos S, Konstantin V, Palmeira CM, Davidson SM, Lougiakis N, Marakos P, Pouli N, Mikros E, Andreadou I. Hydrolytic Activity of Mitochondrial F1FO-ATP Synthase as a Target for Myocardial Ischemia-Reperfusion Injury: Discovery and In Vitro and In Vivo Evaluation of Novel Inhibitors. J Med Chem. 2023 Nov 23;66(22):15115-15140. doi: 10.1021/acs.jmedchem.3c01048.

[215] Huang J, Chen L, Yao ZM, Sun XR, Tong XH, Dong SY. The role of mitochondrial dynamics in cerebral ischemia-reperfusion injury. Biomed Pharmacother. 2023 Jun;162:114671. doi: 10.1016/j.biopha.2023.114671.

[216] Moskowitzova K, Shin B, Liu K, Ramirez-Barbieri G, Guariento A, Blitzer D, Thedsanamoorthy JK, Yao R, Snay ER, Inkster JAH, Orfany A, Zurakowski D, Cowan DB, Packard AB, Visner GA, Del Nido PJ, McCully JD. Mitochondrial transplantation prolongs cold ischemia time in murine heart transplantation. J Heart Lung Transplant. 2019 Jan;38(1):92-99. doi: 10.1016/j.healun.2018.09.025.

[217] Wiedemann D, Schachner T, Bonaros N, Dorn M, Andreas M, Kocher A, Kuznetsov AV. Impact of Cold Ischemia on Mitochondrial Function in Porcine Hearts and Blood Vessels. International Journal of Molecular Sciences. 2013; 14(11):22042-22051. https://doi.org/10.3390/ijms141122042

[218] Jassem W, Fuggle SV, Rela M, Koo DD, Heaton ND. The role of mitochondria in ischemia/reperfusion injury. Transplantation. 2002 Feb 27;73(4):493-9. doi: 10.1097/00007890-200202270-00001.

[219] Moskowitzova K, Shin B, Liu K, Ramirez-Barbieri G, Guariento A, Blitzer D, Thedsanamoorthy JK, Yao R, Snay ER, Inkster JAH, Orfany A, Zurakowski D, Cowan DB, Packard AB, Visner GA, Del Nido PJ, McCully JD. Mitochondrial transplantation prolongs cold ischemia time in murine heart transplantation. J Heart Lung Transplant. 2019 Jan;38(1):92-99. doi: 10.1016/j.healun.2018.09.025.

[220] Saeb-Parsy K, Martin JL, Summers DM, Watson CJE, Krieg T, Murphy MP. Mitochondria as Therapeutic Targets in Transplantation. Trends Mol Med. 2021 Feb;27(2):185-198. doi: 10.1016/j.molmed.2020.08.001. Epub 2020 Sep 17. Erratum in: Trends Mol Med. 2021 May;27(5):512. doi: 10.1016/j.molmed.2021.02.001.

[221] Wehrle CJ, Satish S, Dewey E, Nadeem MA, Sun K, Jiao C, Khalil M, Pita A, Kim J, Aucejo F, Kwon DCH, Fujiki M, Pinna AD, Udeh B, Miller C, Hashimoto K, Schlegel A; Cleveland Clinic Perfusion Group. A New Era of Decision-making in Liver Transplantation: A Prospective Validation and Cost-effectiveness Analysis of FMN-guided Liver Viability Assessment During Normothermic Machine Perfusion. Ann Surg. 2025 Sep 1;282(3):479-493. doi: 10.1097/SLA.0000000000006822.

[222] Eden J, Thorne AM, Bodewes SB, et al. Assessment of liver graft quality during hypothermic oxygenated perfusion: the first international validation study. J Hepatol. 2025;82:523–534.

[223] Eden J, Breuer E, Birrer D, et al. Screening for mitochondrial function before use-routine liver assessment during hypothermic oxygenated perfusion impacts liver utilization. EBioMedicine. 2023;98:104857.

[224] Xynogala, A., Amin, A., Lunsford, K.E. et al. Hypothermic Machine Perfusion Of Liver Allografts: State Of The Art. Curr Transpl Rep 12, 10 (2025). https://doi.org/10.1007/s40472-025-00467-7

[225] Sousa Da Silva RX, Darius T, Mancina L, Eden J, Wernlé K, Ghoneima AS, Barlow AD, Clavien P-A, Dutkowski P, Kron P. Real-time assessment of kidney allografts during HOPE using flavin mononucleotide (FMN)—A preclinical study. Front Transplant. 2023;2:1132673.

[226] McCormick DB, Russell M. Hydrolysis of flavin mononucleotide by acid phosphatases from animal tissues. Comp Biochem Physiol. 1962;5:113–121.

[227] Nagatsu-Ishibashi I, Nagatsu T, Yagi K. Changes of quantity of flavin in the brain after peripheral administration of flavins. Nature. 1961;190:728.

[228] Chance B, Legallais V, Schoener B. Metabolically linked changes in fluorescence emission spectra of cortex of rat brain, kidney and adrenal gland. Nature. 1962;195:1073–1075.

[229] Chance B, Schoener B, Oshino R, et al. Oxidation-reduction ratio studies of mitochondria in freeze-trapped samples. NADH and flavoprotein fluorescence signals. J Biol Chem. 1979;254:4764–4771.

[230] Chance B, Williams GR, Hollunger G. Inhibition of electron and energy transfer in mitochondria. I. Effects of Amytal, thiopental, rotenone, progesterone, and methylene glycol. J Biol Chem. 1963;238:418–431.

[231] EFSA NDA Panel (EFSA Panel on Dietetic Products, Nutrition and Allergies), Turck D, Bresson J-L, Burlingame B, Dean T, Fairweather-Tait S, Heinonen M, Hirsch-Ernst KI, Mangelsdorf I, McArdle HJ, Naska A, Nowicka G, Pentieva

K, Sanz Y, Siani A, Sjödin A, Stern M, Tomé D, Van Loveren H, Vinceti M, Willatts P, Lamberg-Allardt C, Przyrembel H, Tetens I, Dumas C, Fabiani L, Forss AC, Ioannidou S, Neuhäuser-Berthold M. Scientific Opinion on Dietary Reference Values for riboflavin. EFSA J 2017;15(8):4919. doi: 10.2903/j.efsa.2017.4919.

[232] "Flavin mononucleotide | C17H21N4O9P | CID 643976 -PubChem." Accessed: Mar. 29, 2024. [Online]. Available: https://pubchem.ncbi.nlm.nih.gov/compound/Flavin-mononucleotide

[233] Brandt U. Energy converting NADH:quinone oxidoreductase (complex I). Annu Rev Biochem. 2006;75:69-92. doi: 10.1146/annurev.biochem.75.103004.142539.

[234] Efremov RG, Baradaran R, Sazanov LA. The architecture of respiratory complex I. **Nature** 2010 May;465(7297):441-5. doi: 10.1038/nature09066.

[235] Wirth C, Brandt U, Hunte C, Zickermann V. Structure and function of mitochondrial complex I. Biochim Biophys Acta. 2016 Jul;1857(7):902-14. doi: 10.1016/j.bbabio.2016.02.013.

[236] Holt PJ, Efremov RG, Nakamaru-Ogiso E, Sazanov LA. Reversible FMN dissociation from Escherichiacoli respiratory complex I. Biochim Biophys Acta. 2016; 1857(11):1777–85. https://doi.org/10.1016/j.bbabio.2016.08.008

[237] Gutiérrez-Fernández J, Kaszuba K, Minhas GS, Baradaran R, Tambalo M, Gallagher DT, Sazanov LA. Key role of quinone in the mechanism of respiratory complex I. Nat Commun. 2020 Aug 18;11(1):4135. doi: 10.1038/s41467-020-17957-0.

[238] Curtabbi A, Guarás A, Cabrera-Alarcón JL, Rivero M, Calvo E, Rosa-Moreno M, Vázquez J, Medina M, Enríquez JA. Regulation of respiratory complex I assembly by FMN cofactor targeting. Redox Biol. 2024 Feb;69:103001. doi: 10.1016/j.redox.2023.103001.

[239] Curtabbi A, Enríquez JA. The ins and outs of the flavin mononucleotide cofactor of respiratory complex I. IUBMB Life. 2022 Jul;74(7):629-644. doi: 10.1002/iub.2600.

[240] Palmer T, Bonner PL. The chemical nature of enzyme catalysis. In: Palmer T, Bonner PL, editors. Enzymes. Second Edition. Woodhead Publishing; 2011. p. 189-221. doi:10.1533/9780857099921.2.189.

[241] Rich PR, Maréchal A. Electron Transfer Chains: Structures, Mechanisms and Energy Coupling. In: Egelman EH, editor. Comprehensive Biophysics. Oxford: Elsevier; 2012. p. 72-93. https://doi.org/10.1016/B978-0-12-374920-8.00806-7.[242] Zhang L, Xu H, Chen CL, Green-Church KB, Freitas MA, Chen YR. Mass spectrometry profiles superoxide-induced intramolecular disulfide in the FMN-binding subunit of mitochondrial Complex I. J Am Soc Mass Spectrom. 2008 Dec;19(12):1875-86. doi: 10.1016/j.jasms.2008.08.004.

[243] Hall M. Flavoenzymes for biocatalysis. In: Chaiyen P, Tamanoi F, editors. The Enzymes. Vol. 47. Academic Press; 2020. p. 37-62.

[244] Marques HM. Electron transfer in biological systems. J Biol Inorg Chem. 2024 Dec;29(7-8):641-683. doi: 10.1007/s00775-024-02076-8.

[245] Toogood HS, Scrutton NS. Thermal, electrochemical and photochemical reactions involving catalytically versatile ene reductase enzymes. In: Chaiyen P, Tamanoi F, editors. The Enzymes. Vol. 47. Academic Press; 2020. p. 491-515.

[246] Stepanova A, Kahl A, Konrad C, Ten V, Starkov AS, Galkin A. Reverse electron transfer results in a loss of flavin from mitochondrial complex I: Potential mechanism for brain ischemia reperfusion injury. J Cereb Blood Flow Metab. 2017 Dec;37(12):3649-3658. doi: 10.1177/0271678X17730242.

[247] Stepanova A, Sosunov S, Niatsetskaya Z, Konrad C, Starkov AA, Manfredi G, Wittig I, Ten V, Galkin A. Redox-Dependent Loss of Flavin by Mitochondrial Complex I in Brain Ischemia/Reperfusion Injury. Antioxid Redox Signal. 2019 Sep 20;31(9):608-622. doi: 10.1089/ars.2018.7693.

[248] Yoval-Sánchez B, Ansari F, James J, Niatsetskaya Z, Sosunov S, Filipenko P, Tikhonova IG, Ten V, Wittig I, Rafikov R, Galkin A. Redox-dependent loss of flavin by mitochondria complex I is different in brain and heart. Redox Biol. 2022 May;51:102258. doi: 10.1016/j.redox.2022.102258.

[249] Kahl A, Stepanova A, Konrad C, et al. Critical role of flavin and glutathione in complex i-mediated bioenergetic failure in brain ischemia/reperfusion injury. Stroke. 2018; 49:1223–1231.

[250] Zhang M, Liu Q, Meng H. et al. Ischemia-reperfusion injury: molecular mechanisms and therapeutic targets. Sig Transduct Target Ther 2024. 9, 12. https://doi.org/10.1038/s41392-023-01688-x

[251] Garcia KB, Hussein A, Satish S, Wehrle CJ, Karakaya O, Panconesi R, Sun K, Jiao C, Fernandes E, Pinna A, et al. Machine Perfusion as a Strategy to Decrease Ischemia-Reperfusion Injury and Lower Cancer Recurrence Following Liver Transplantation. Cancers. 2024; 16(23):3959.

[252] Ten V, Galkin A. Mechanism of mitochondrial complex I damage in brain ischemia/reperfusion injury. A hypothesis. Mol Cell Neurosci. 2019;100:103408. doi:10.1016/j.mcn.2019.103408.

[253] Bruinsma BG, Sridharan GV, Weeder PD, Avruch JH, Saeidi N, Özer S, Geerts S, Porte RJ, Heger M, van Gulik TM, Martins PN, Markmann JF, Yeh H, Uygun K. Metabolic profiling during ex vivo machine perfusion of the human liver. Sci Rep. 2016 Mar 3;6:22415. doi: 10.1038/srep22415.

[254] Panconesi R, Widmer J, Carvalho MF, Eden J, Dondossola D, Dutkowski P, Schlegel A. Mitochondria and ischemia reperfusion injury. Curr Opin Organ Transplant. 2022 Oct 1;27(5):434-445. doi: 10.1097/MOT.0000000000001015.

[255] Hertz L. Bioenergetics of cerebral ischemia: A cellular perspective. Neuropharmacology. 2008;55(3):289-309. doi:10.1016/j.neuropharm.2008.05.023.

[256] Sims NR, Muyderman H. Mitochondria, oxidative metabolism and cell death in stroke. Biochim Biophys Acta Mol Basis Dis. 2010;1802(1):80-91. doi:10.1016/j.bbadis.2009.09.003.

[257] Ten VS, Starkov A. Hypoxic-ischemic injury in the developing brain: the role of reactive oxygen species originating in mitochondria. Neurol Res Int. 2012;2012:542976.

[258] Vannucci RC, Towfighi J, Vannucci SJ. Secondary energy failure after cerebral hypoxia-ischemia in the immature rat. J Cereb Blood Flow Metab. 2004;24:1090-7.

[259] Wang L, Thompson E, Bates L, Pither TL, Hosgood SA, Nicholson ML, Watson CJE, Wilson C, Fisher AJ, Ali S, et al. Flavin mononucleotide as a biomarker of organ quality—A pilot study. Transplant Direct. 2020;6:e600.

[260] Dingfelder J, Kollmann D, Rauter L, Poumpouridou E, Pereyra D, Kacar S, et al. Mitochondrial flavin mononucleotide measured at beginning of hypothermic machine perfusion predicts patient survival after liver transplantation. Transplantation. 2024 Sep;108(9S):. doi:10.1097/01.tp.0001064804.52586.c6.

[261] Kesseli SJ, Gloria JN, Abraham N, Halpern SE, Cywinska GN, Zhang M, Moris D, Schmitz R, Shaw BI, Fitch ZW, Song M, Guy CD, Hartwig MG, Knechtle S, Barbas AS. Point-of-Care Assessment of DCD Livers During Normothermic Machine Perfusion in a Nonhuman Primate Model. Hepatol Commun. 2021 Sep;5(9):1527-1542. doi: 10.1002/hep4.1734.

[262] Gubernatis G, Pichlmayr R, Lamesch P, et al. HTK-solution (Bretschneider) for human liver transplantation. First clinical experiences. Langenbecks Arch Chir 1990; 375(2):66.

[263] Gilbo N, Wylin T, Heedfeld V, Jochmans I, Pirenne J, Friend P, Monbaliu D. Porcine Liver Normothermic Machine Perfusion: Methodological Framework and Potential Pitfalls. Transplant Direct. 2021 Dec 13;8(1):e1276. doi: 10.1097/TXD.0000000000001276.

[264] Ravikumar R, Jassem W, Mergental H, Heaton N, Mirza D, Perera MT, Quaglia A, Holroyd D, Vogel T, Coussios CC, Friend PJ. Liver Transplantation After Ex Vivo Normothermic Machine Preservation: A Phase 1 (First-in-Man) Clinical Trial. Am J Transplant. 2016 Jun;16(6):1779-87. doi: 10.1111/ajt.13708.

[265] Bruinsma BG, Yeh H, Ozer S, Martins PN, Farmer A, Wu W, Saeidi N, Op den Dries S, Berendsen TA, Smith RN, Markmann JF, Porte RJ, Yarmush ML, Uygun K, Izamis ML. Subnormothermic machine perfusion for ex vivo preservation and recovery of the human liver for transplantation. Am J Transplant. 2014 Jun;14(6):1400-9. doi: 10.1111/ajt.12727.

[266] Nwaduru C, Baker E, Buff M, Selim M, Ovalle LA, Baker TB, Zimmerman MA. Assessing Liver Viability: Insights From Mitochondrial Bioenergetics in Ischemia-Reperfusion Injury. Transplant Proc. 2024 Jan-Feb;56(1):228-235. doi: 10.1016/j.transproceed.2023.11.019.

[267] Hofmann J, Kofler A, Schartner M, Buch ML, Hermann M, Zelger B, Öfner D, Oberhuber R, Hautz T, Schneeberger S and Meszaros AT (2024) Assessment of Mitochondrial Respiration During Hypothermic Storage of Liver Biopsies Following Normothermic Machine Perfusion. Transpl Int 37:12787. doi: 10.3389/ti.2024.12787.

[268] Melandro F, De Carlis R, Torri F, Lauterio A, De Simone P, De Carlis L, Ghinolfi D. Viability Criteria during Liver Ex-Situ Normothermic and Hypothermic Perfusion. Medicina. 2022; 58(10):1434. https://doi.org/10.3390/medicina58101434.

[269] Verstraeten L and Jochmans I (2022) Sense and Sensibilities of Organ Perfusion as a Kidney and Liver Viability Assessment Platform. Transpl Int 35:10312. doi: 10.3389/ti.2022.10312.

[270] Cadinu LA, Sun K, Jiao C, Panconesi R, Satish S, Yildirim FS, Karakaya OF, Wehrle CJ, Crasta GS, Fernandes FW, Eshraghi N, Takase K, Horie H, Ricci PC, Bagnoli D, Carvalho MF, Schlegel A, Barbaro M. Optical Spectroscopic Detection of Mitochondrial Biomarkers (FMN and NADH) for Hypothermic Oxygenated Machine Perfusion: A Comparative Study in Different Perfusion Media. Sensors (Basel). 2025 Jun 28;25(13):4031. doi: 10.3390/s25134031.

[271] Schlegel A, Porte R, Dutkowski P. Protective mechanisms and current clinical evidence of hypothermic oxygenated machine perfusion (HOPE) in preventing post-transplant cholangiopathy. J Hepatol. 2022 Jun;76(6):1330-1347. doi: 10.1016/j.jhep.2022.01.024.

[272] Inci I, Arni S, Iskender I, Citak N, Rodriguez JM, Weisskopf M, et al. unctional, Metabolic and Morphologic Results of Ex Vivo Donor Lung Perfusion with a Perfluorocarbon-Based Oxygen Carrier Nanoemulsion in a Large Animal Transplantation Model. Cells. 2020 Nov; 9: 2501.

[273] Darius T, Vergauwen M, Smith T, Gerin I, Joris V, Mueller M, et al. Brief O(2) uploading during continuous hypothermic machine perfusion is simple yet effective oxygenation method to improve initial kidney function in a porcine autotransplant model. Am J Transplant. 2020 Aug; 20(8): 2030-2043.

[274] Wyss RK, Carmona NM, Arnold M, Segiser A, Mueller M, Dutkowski P, et al. Hypothermic, oxygenated perfusion (HOPE) provides cardioprotection via succinate oxidation prior to normothermic perfusion in a rat model of donation after circulatory death (DCD). Am J Transplant. 2021 Mar; 21(3): 1003-1011.

[275] Panayotova G, Paterno F, Galan M, Simonishvili S, Qin Y, McCarty M, et al. Hypothermic Oxygenated Machine Perfusion Preserves Cholangiocyte Homeostasis and Protects Against Biliary Complications Post Liver Transplantation: Preliminary Results From a Single Center. J Am Coll Surg. 2021 Nov; 233(5): S267-S268.

[276] Patrono D, Roggio D, Mazzeo A, Catalano G, Mazza E, Rizza G, et al. Clinical assessment of liver metabolism during hypothermic oxygenated machine perfusion using microdialysis. Artif Organs. 2022 Feb; 46(2): 281–295.

[277] Leber B, Weber J, Rohrhofer L, Aigelsreiter A, Niedrist T, Stiegler , et al. Real-Time Assessment of Liver Function During Sub-Normothermic Machine Perfusion by a Non-Invasive 13C Based Test. Res Sq. 2022 Mar. https://doi.org/10.21203/rs.3.rs-1450501/v1.

[278] Darius T, Vergauwen M, Maistriaux L, Evrard R, Schlegel A, Mueller M, et al. Intermittent Surface Oxygenation Results in Similar Mitochondrial Protection and Maintenance of Aerobic Metabolism as Compared to Continuous Oxygenation during Hypothermic Machine Kidney Machine Perfusion. J Clin Med. 2023 May; 12(11): 3731.

[279] Schurink IJ, de Haan JE, Willemse J, al. e. A proof of concept study on real-time LiMAx CYP1A2 liver function assessment of donor grafts during normothermic machine perfusion. Sci Rep. 2021 Dec; 11: 23444.

[280] Boteon A, Lima M, Guardia B, Carvalho M, Schlegel A, Boteon Y. Eleven hours of hypothermic oxygenated machine perfusion (HOPE) for complex liver retransplantation: A case report. Artif Organs. 2023 Aug; 47(8): 1413–1415.

[281] van de Leemkolk F, Lo Faro M, Shaheed S, Mulvey J, Huurman V, Alwayn I, et al. The role of flavin mononucleotide (FMN) as a potentially clinically relevant biomarker to predict the quality of kidney grafts during hypothermic (oxygenated) machine perfusion. PLoS One. 2023 Jun; 18(6): e0287713.

[282] National Center for Biotechnology Information. PubChem Compound Summary for CID 439153, Nadh. https://pubchem.ncbi.nlm.nih.gov/compound/Nadh. Accessed Oct. 5, 2025.

[283] Maiese K, Chong ZZ, Hou J, Shang YC. The Vitamin Nicotinamide: Translating Nutrition into Clinical Care. Molecules. 2009; 14(9):3446-3485. https://doi.org/10.3390/molecules14093446

[284] Honikel KO. CONVERSION OF MUSCLE TO MEAT | Glycolysis. In: Dikeman M, Devine C, editors. Encyclopedia of Meat Sciences. 2nd ed. Academic Press; 2014. p. 353-7. doi:10.1016/B978-0-12-384731-7.00095-7.

[285] Magni G and Ceruti S (2021) Purines in Pain as a Gliopathy. Front. Pharmacol. 12:649807. doi: 10.3389/fphar.2021.649807.

[286] Ying W. NAD+ and NADH in cellular functions and cell death. Front Biosci. 2006 Sep 1;11:3129-48. doi: 10.2741/2038.

[287] Xie N, Zhang L, Gao W, et al. NAD+ metabolism: pathophysiologic mechanisms and therapeutic potential. Sig Transduct Target Ther. 2020;5(1):227. doi:10.1038/s41392-020-00311-7.

[288] Luo M, Ma X, Ye J. Reductive stress—a common metabolic feature of obesity and cancer. Acta Pharm Sin B. 2024;14(12):5181-5. doi:10.1016/j.apsb.2024.08.034.

[289] Deshpande OA, Mohiuddin SS. Biochemistry, Oxidative Phosphorylation. 2023 Jul 31. In: StatPearls [Internet]. Treasure Island (FL): StatPearls Publishing; 2025 Jan–. PMID: 31985985.

[290] Luo J, Hu Y, Qiao Y, Li H, Huang J, Xu K, Jiang L, Wu H, Hu X, Jia J, Zhou L, Xie H, Li J, Zheng S. Hypothermic Oxygenated Machine Perfusion Promotes Mitophagy Flux against Hypoxia-Ischemic Injury in Rat DCD Liver. Int J Mol Sci. 2023 Mar 11;24(6):5403. doi: 10.3390/ijms24065403.

"Nihil est in intellectu quod non sit prius in sensu"

Thomas Aquinas, De Veritate (q. 2 a. 3 arg. 19)

Chapter II

Fundamentals of Modern Technology of Machine Perfusion. A Review of Liver Perfusion

1. Introduction

A beating heart isolated from a body, in a transparent sterile chamber, pumping blood through an artificial circulation system. The light-brown color of a liver stored in a cold solution turns into a bright red color when connected to cannulas in which a blood-based solution is flowing. A kidney is secured by a sterile drape to maintain aseptic conditions and fed by the perfusion circuit of a transportable device. Machines made up of cannulas, vessels for collecting oxygenated and nutrient perfusate, roller and centrifugal pumps, sterilized chambers for organ allocation, and electrical and mechanical components controlled by a computer working in an automatic or semiautomatic manner to preserve isolated organs from the human or animal body. A computer capable of keeping alive an organ.

A promise of a new life…

These seem like things from science fiction movies, but it is all real. A constantly changing reality. Researchers from various branches of Science and Engineering are fine-tuning and improving machine perfusion for a worthy goal: saving human lives. Human lives afflicted by acute and chronic end-stage diseases of a vital organ like the liver or kidney, for which transplantation is the only curative treatment [1 – 15]. Although the total number of annual transplantations increased in the last years [16 – 21], there are still not enough donors to meet the demand for organs by all patients on the long waiting lists [7, 17, 18, 20, 22, 23, 24 – 27]. The demand for vital organs includes livers too, making the liver a scarce resource [5, 28 – 31]. The mortality on waiting lists is remarkably high [5,

7, 16, 21, 22, 24, 32 – 36]. It is estimated that up to 23% of patients die or become too sick while waiting [5, 15, 17, 37 – 39]. Additionally, some people will never receive a liver transplant. Many others, especially the poorest people, are at risk of not even being registered on the waiting list [40 – 45]. Increasing the number of transplantable livers should be a priority in the policymakers' agenda [46]. There should be an awareness campaign for organ donation after death to increase the number of available grafts. Just taking an example: in Italy, approximately 33% of the people declared to oppose post-mortem organ donation during the renewal of identity cards in 2020 [47]. To provide for organs shortage and to reduce the waiting lists mortality clinicians at transplant centres in many countries have extended the criteria for donor selection, introducing the so-called Extended Criteria Donors (ECDs) category [6, 23, 32, 48 – 55]; a category of marginal organs believed not transplantable previously [56 – 59]. There is still no global agreement on the definition of an ECD graft [54, 55, 60]. In general, the ECD category includes marginal organs coming from elderly donors (age > 60 or 80), donation after circulatory death, from donors with morbidity (e.g., diabetes, cardiovascular diseases) or organs with cold ischemia times (CITs) of >8–10 h, warm ischemia times (WITs) of > 30 min, organs with graft macrosteatosis >30% (fatty graft), hypernatremia, hemodynamic instability and living donor liver transplants (LDLT) [5, 8, 32, 48, 51, 62 – 71].

Currently, the standard method of liver preservation is static cold storage (SCS) [6, 48, 72 – 78]. SCS procedure involves a flush and immersion of the graft into a cold preservation solution at 4 °C with ice [73, 79 – 81]. The solution most used is the University Wisconsin (UW) solution, but also others as the Histidine-Tryptophan-Ketoglutarate (HTK named also Custodiol) and Celsior solutions are used [72, 73, 79, 82 – 86]. Firstly, the hypothermic environment reduces the liver's cellular metabolism [73, 76, 85, 87, 88], indeed at 4 °C the metabolic rate of the organ is limited approximately to 5 – 10% of the rate at normothermic temperatures [74, 61, 89 – 94]. This means explaining the lower demand for oxygen and other useful metabolites [95 – 97]. Secondly, the preservation solution provides cytoprotection, reduces cellular swelling and removes blood clots from the liver's vasculature [73, 76, 85, 89, 98]. It is possible to store a liver with SCS for a maximum of 12 hours [99]. However, a marginal liver stored through SCS is more vulnerable to the harmful effects of prolonged cold ischemia and anaerobic metabolism due to the absence of oxygen and biomechanical stimulation [6, 13, 49, 61, 62, 79, 100 – 113]. The consequence is a high–risk failure after transplantation due to the increased susceptibility to ischemia-reperfusion injury (IRI), primary nonfunction (PNF), early allograft dysfunction (EAD) and biliary complications [8, 32, 48, 68, 102, 104 – 107, 111, 114 – 119]. These complications may be deadly for the recipient [32, 120, 100, 107, 114, 116]. The weak effectiveness of the standard method SCS to preserve in a manner safe marginal organs have forced researchers to look at another organ preservation method: the machine perfusion

MP ex-situ [3, 12, 62, 89, 101, 121 – 125]. Here, is chosen the terminology presented by Karangwa et al [126]. These authors proposed a terminology to homogenize definitions and terms concerning MP technology. In particular, the term ex-situ refers to "outside the original site/location" and is proposed as a more representative description of what happens during MP [126].

Machine perfusion is a medical technique involving the afflux of blood, a blood–based solution or other fluid through the blood vessels or other natural channels of an isolated organ or tissue from the body of a warm blood animal carried out by an electromechanical device. Machine perfusion of the liver is made up of at least seven main components: an oxygenator, a vessel of perfusate solution, a pumping system, a heat exchanger, perfusion filters, a sterile chamber to house the organ and display control of perfusion parameters [127]. In some machines for normothermic perfusion is integrated a leucocyte filter like the LeukoGuard, Pall Corporation (Portsmouth, UK) used by Watson et al. [128] and Bral et al. [100]. A continuous and/or pulsatile flow of perfusate is pumped in the vascular system of the liver through the portal vein and/or hepatic artery [34, 50, 58, 72, 97, 129 – 139]. In this way, it is possible to supply oxygen, metabolic substrates essential to hold up metabolism, antioxidants, the drug for therapeutic interventions and to flush cytokines, proteins, and toxins from the liver [6, 56, 91, 123, 127, 140 – 146]. Furthermore, the circulating perfusate through the vascular system helps to preserve the microvascular relaxation stimulating the functionality's endothelial cells and to avoid high vascular resistance [88, 111, 132, 143, 147 – 150]. A resistance too high is a risk factor seeing as may impede complete perfusion of the graft and causes organ impairment [150, 151]. Machine perfusion is a technique that currently permits the evaluation of viability, functionality, and degree of injury of the graft before transplantation and potentially can help to predict the viability after transplantation to provide more confidence when accepting an organ [3, 33, 49, 72, 88, 136, 137, 141, 144, 150, 152 – 160]. A representative idea of preservation techniques is shown in **Figure 1.1**.

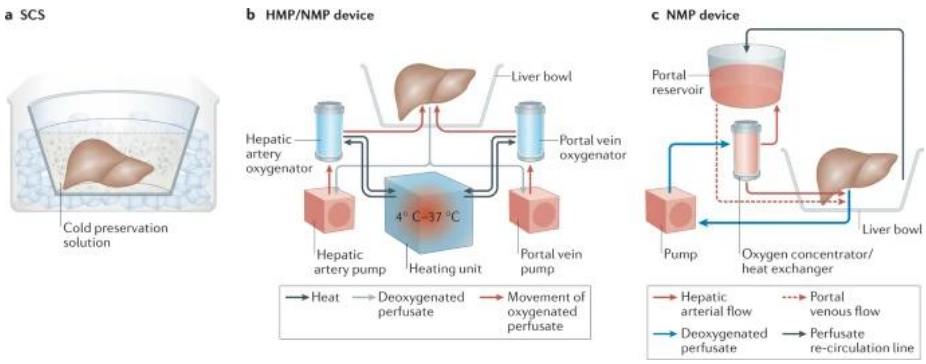

Figure 1.1. Working scheme of current organ preservation [155]. Reproduced from [155] with Creative Commons CC BY license.

Nowadays, there are two types of perfusion techniques depending on temperature: hypothermic perfusion (4 – 12 °C) oxygenated (HOPE) or not oxygenated (HMP) [6, 34, 50, 58, 72, 75, 83, 111, 130 – 132, 134 – 136, 156, 161 – 166] and normothermic perfusion (NMP) (35 – 37 °C) [4, 7, 57, 60, 155, 167 – 170]. A distinction between the two methods is shown in the **Figure 1.2**. First modern clinical trials on hypothermic perfusion were experienced by Guarrera et al [75] in 2010, whereas normothermic perfusion for human applications was conducted in Birmingham (UK) as documented by some authors [7, 33, 168, 169]. At the start of clinical use of hypothermic machine perfusion (HMP), Guarrera et al. [75, 140] used a solution without active oxygenation (i.e. no oxygenator). Initially, researchers wondered about the real need to oxygenate cold solution perfusion [171, 123, 172, 173], since a circulating hypothermic solution can carry far more oxygen than a warm solution [123], or whether simple oxygen diffusion is sufficient to maintain viable oxygen levels [123, 172]. Later, a lot of studies demonstrated that active oxygenation of the perfusate with an oxygenator (generally a hollow fibre oxygenator) enhances liver function, attenuates ischemia injury, and limits post-transplantation complications [83, 95, 97, 130, 131, 172, 175 – 178]. Indeed, hypothermic oxygenated perfusion combines the protective and preservative effects of the cold with the health effects of continuous oxygenation and supply of metabolites that, on one side cause a considerable reduction of the biochemical process of the ischemic injury, and on the other permit the mitochondrial "resuscitation" and complete reinstatement of ATP levels [65, 72, 88, 91, 123, 131, 141, 143, 146, 163, 172, 176, 179 – 185]. It has been demonstrated that cells continue to consume energy at a rate reduced during HOPE, in spite of the hypothermic conditions [97, 130, 131, 175, 186, 187]. Therefore, the regenerative capacity of the liver at low temperatures can be preserved [22, 188]. The cellular energy level restoration and oxygenation of the graft mitigate the deleterious effects of ischemia-reperfusion injury (IRI) occurring during the warm reperfusion after transplantation [22, 72, 83, 131, 136, 172, 176, 177, 189]. The HOPE can increase the ATP levels up to 15 times compared to cellular energy levels at the end of SCS [183]. It was shown that 1 o 2 hours of HOPE are sufficient to restore cellular energy and give protection to IRI [22, 34, 50, 97, 83, 115, 131, 172, 176, 177, 182 – 185, 188, 190, 191]. Currently, two types of hypothermic oxygenated perfusion are employed based on how liquid solution flows in the liver: the first one is single hypothermic oxygenated perfusion, HOPE, which means that perfusate flows into the liver through the only cannula connected to the portal vein [72, 50, 6, 34, 54, 135, 136], the second one is the dual HOPE (DHOPE) which means that solution, like UW solution, perfuse the liver through both cannulas connected to the portal vein and hepatic artery [58, 83, 131, 132, 134, 135, 141, 165, 183, 178, 192]. In both methods, perfusate drains from the inferior cava vein [51, 75, 104, 193 – 198].

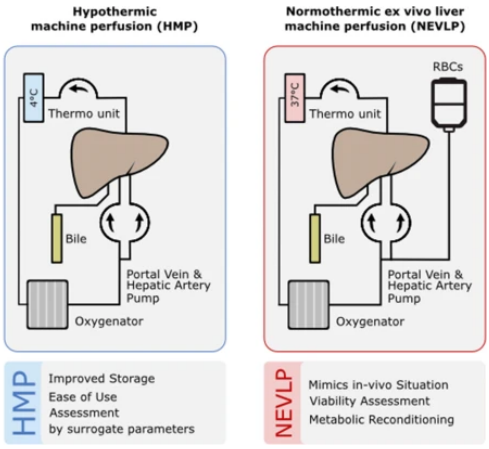

Figure 1.2. A schematic of a simple and general circuit of a liver machine perfusion [8]. Image from [8] reproduced with Creative Commons Attribution 4.0 International License.

Machine perfusion has been developed to minimize injuries caused by storage outside of the body. Clinical experiences have demonstrated its higher performance than the SCS method and its health and protective effects on marginal grafts [2 – 5, 33, 57, 97, 98, 74, 61, 62, 83, 136, 161, 168, 171, 199, 200, 201]. Therefore, at a global level, liver transplantation is introducing MP strategies for organ preservation, albeit with several technical variations based on different machine perfusion methods [48]. On the one hand, liver perfusion offers a unique opportunity to control graft metabolic activity [72, 158, 202]. On the other hand, it is essential to involve further graft criteria selection before, during, and after perfusion to predict post-transplantation outcomes. Currently, there is no universal agreement yet about the criteria selection that allows for an objective evaluation of graft viability and outcome prediction before and during perfusion [203]. Each transplant centre adopts its criteria based on its experience [85, 204]. Based on these criteria, often different for each transplant center, clinicians select organs to perfuse [158, 202, 205]. Moreover, in the scientific community, the debate about the identification of more effective biomarkers in perfusate that can predict outcomes post-transplantation is still ongoing [203, 206]. A combination of various and different biomarkers in perfusate and bile may be the better way [207]. Nowadays, the main methods used to estimate the metabolic activity of the liver include laboratory analysis and investigations of hemodynamic and morphological characteristics [105, 158, 208, 209]. In general, researchers analyze perfusates with discontinuity during time perfusion, typically every 30 minutes [210]. The Zurich Research Group was the first to conduct perfusion with real-time measurement of the biomarker flavin mononucleotide (FMN) using a spectrometric instrument [72]. They postulated that FMN could provide a reliable indication of liver functionality in the recipient. Biomarkers collected by

spectrometric devices during perfusion can be transformed into data and used as input for algorithms implemented in computers to model and study cellular processes without any impact on the graft [158, 211 – 214]. Mathematical models that estimate the current and future conditions of the graft are helpful in understanding the correct actions that must be adopted to preserve the graft from injury and enhance its conditions during perfusion [104, 158, 205, 215 – 219]. The modern technology of machine learning may be crucial in meeting this challenge [220] since it can manage and elaborate a large amount of data [144, 221]. Starting from the first work on the application of neural networks in liver transplantation by Doyle et al. [222] in 1994, today the implementation of artificial intelligence in medicine is widely employed to predict clinical outcomes [221, 223]. The use of machine learning algorithms and mathematical models in machine perfusion is a new area of investigation. This short review aims to provide a practical guide for experts, beginning researchers and even lay readers who may be interested in the modern technology of liver machine perfusion. We begin with the historical background and a simple explanation of ischemia-reperfusion injury. We analyze the technical features of currently used machine perfusion and propose a simple comparison of their performance, based on the information available in the literature. We discuss perfusion parameters such as pressure, temperature, flow rate, resistance, biomarkers, liquid perfusion features, oxygenation, perfusion time, and instrumentation used to analyse the perfusate, and we also briefly touch upon the costs associated with employing this technology. Finally, we explore the application of machine learning tools in machine perfusion based on current published research. The available literature already includes comprehensive and detailed reviews on various aspects of machine perfusion. This chapter can be regarded as a brief introduction to the vast literature characterizing this field of study.

2. Ischemia Reperfusion Injury

Hypoxia is a condition that occurs when the rate of oxygen consumption in tissue exceeds the rate of oxygen supply [224]. In other words, there is a deficit of oxygen in the blood flow rate to the tissue. If the blood flow is stopped, it is not possible to support aerobic metabolism, which can result in a serious shortage of oxygen and essential metabolites. This condition is called ischemia [224]. When tissue is deprived of oxygen, the cells cannot produce ATP (adenosine triphosphate) through aerobic metabolism, instead, they produce it through anaerobic metabolism [61, 90, 225]. However, anaerobic metabolism produces a lesser quantity of ATP [226, 227]. In anaerobic conditions, cells continue to produce and utilize energy, but one of the metabolic by-products is lactate (lactic acid). Thus, lactate could be an optimal indicator of the degree of ischemia [228]. However, the main problem with this indicator is that measuring lactic acidosis (caused by an accumulation of lactate) indicates that

ischemic or hypoxic status has already been reached, and at this point, cellular injuries are occurring [228]. Therefore, lactate cannot be used for real-time monitoring [228]. The final step of cellular respiration is mitochondrial oxidative phosphorylation. When ischemia occurs, oxidative phosphorylation is halted [176, 227]. During ischemia, numerous biochemical and biological reactions are activated, such as mitochondrial dysfunction, alteration of intracellular and extracellular pH, changes in intracellular electrolytic equilibria, lactate accumulation, and production of damaging free radicals [63, 72, 164, 201, 225, 226, 229].

One of the main mechanisms of ischemic injury is free radicals, which damage cells [229]. If the flow of oxygenated blood is rapidly restored to the tissue, ischemic injury can be healed reversibly. However, if cells are exposed to prolonged ischemic time, they will be damaged irreversibly, and the tissue will die [229]. When the oxygenated flow is restored to a tissue that has suffered prolonged ischemia, there are no beneficial effects; instead, the free oxygen reacts with free radicals, generating Reactive Oxygen Species (ROS) and unstable species of nitrogen, such as the hydroxyl radical (•OH) and the superoxide anion (O2•-), among others [229]. These highly unstable and reactive chemical species induce harmful oxidative injury to cellular structures and provoke a local inflammatory response [225 – 227, 131].

Simultaneously, the depletion of ATP reserves causes metabolic and mitochondrial failure, leading to cellular death [131, 189, 181, 230]. Therefore, the restoration of oxygen supply, instead of healing injury due to its absence, intensifies the injury in a tissue suffering prolonged ischemia [231]. This complex phenomenon is called ischemia-reperfusion injury (IRI). Indeed, the most important damage in the tissue occurs during the reperfusion, that is, after the restoration of oxygenated flow [131, 231, 232]. In clinical observations, IRI increases the risk of failure and loss of functionality of the graft after transplantation [132, 233].

IRI is an inconvenient but unfortunately inevitable phenomenon in grafts for transplantation, as grafts are exposed to warm ischemia in deceased donors and cold ischemia during SCS [234]. Many studies have investigated the effects and mechanisms of IRI in liver grafts previously [108, 200, 226, 235 – 246]. In a nutshell, after reperfusion in the liver, the production of ROS, cytokine secretion, and endangerment of hepatic microcirculation provoke inflammation, loss of parenchyma, and injuries to the extended epithelial biliary and peribiliary vascular plexus [230, 241, 242, 247, 248]. These mechanisms are responsible for the development of non-anastomotic biliary stenosis (NAS), a troublesome complication characterized by multiple stenoses of the bile ducts [230]. Moreover, the histological features of IRI include swelling of hepatocytes, apoptosis, necrosis, detachment of sinusoidal endothelial cells, and infiltration of polymorphonucleates [230, 243]. Ischemia-reperfusion

injury is a critical condition for which physicians must verify the extent of cellular damage and preserve organ function [226]. Clinical manifestations of IRI can vary from immediate and minimal damage to early allograft dysfunction (EAD), primary non-functionality (PNF), and NAS [230]. EAD is the result of hepatocellular necrosis and is biochemically evident by elevated transaminases and/or altered synthesis function (elevated total bilirubin, prolonged coagulation) within the first-week post-LT [230].

3. Techniques of liver perfusion

3.1. Typology of hypothermic perfusion: single HOPE or dual DHOPE

Few research groups have investigated whether to carry out liver perfusion through the only portal vein (HOPE) or portal vein and hepatic artery (DHOPE) [129, 249]. An example is reported in **Figure 3.1**. Schlegel et al. [129] conducted an investigation on the livers of rats, pigs, and humans from a donor DCD, observing that perfusion only through the portal vein is capable of achieving complete graft perfusion. They reported that the parenchyma and epithelial cells of the biliary system were well-oxygenated. The supply of oxygen to biliary cells plays an essential role in hepatic regeneration and protection against the development of cholangiopathy after transplantation [250]. It is indisputable that single perfusion simplifies the liver machine perfusion procedure, avoids arterial wounds during graft handling, and does not jeopardize protective and preservative effects against IRI [249, 135]. Additional studies suggest that perfusion-only portal vein may be more favorable than perfusion through the hepatic artery during HMP based on injury biomarkers in the perfusate [147]. Furthermore, de Vries et al. [137], based on the analysis of pig livers undergoing sequence HOPE or DHOPE – NMP, concluded that there were no considerable differences in terms of functionality or endothelial and hepatobiliary injury. Brüggenwirth et al. [251] reported that the dual or single perfusion approach during end-ischemic sub-normothermic liver machine preservation of rats showed comparable outcomes. Nevertheless, the main question is whether HOPE could be the better perfusion practice [132, 249]. Brüggenwirth et al. [249] concluded that it is still not possible to establish whether HOPE is the better method to prevent long-term ischemic cholangiopathy after liver transplantation (LT), but further randomized studies on HOPE and DHOPE are needed. The Groningen Research Group, headed by van Rijn, demonstrated that dual hypothermic machine perfusion (DHOPE) minimizes the IRI in the biliary system in DCD livers [131]. DHOPE involves perfusion through the portal vein and hepatic artery, and this entails better oxygenation of biliary ducts [183]. Indeed, in physiological conditions, the blood supply to the bile ducts depends largely on the hepatic artery

[252]. The occlusion of the hepatic artery may be deleterious for the biliary system [252, 253]; instead, parenchyma is supplied by both the portal vein and the hepatic artery [239, 253, 254]. Moreover, in physiological conditions, the biliary tract is fed with arterial blood via the peribiliary vascular plexus (PVP); therefore, a lesion in the PVP, caused by occlusion of the hepatic artery, the system may bring about ischemic death of the epithelia biliary cells after LT [249, 255]. It was suggested that DHOPE can preserve successfully the PVP system in livers' pig DCD [182]. In light of the above, preservation of the biliary system is strictly necessary and for these reasons, single perfusion through only the portal vein couldn't be sufficient to protect biliary ducts, especially for livers from DCD donors [132]. Nevertheless, still today the question, of whether DHOPE is better than HOPE, remains without a definitive answer [132, 94, 111, 147, 137].

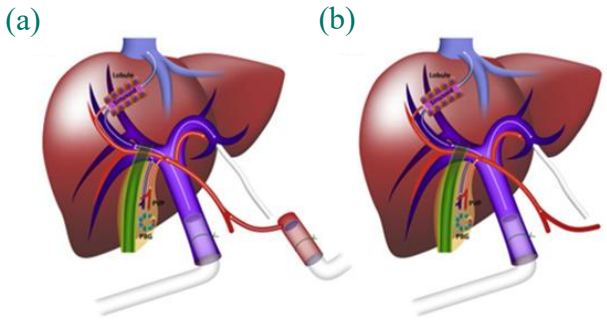

Figure 3.1. Cannulation of liver in machine perfusion. (a) Dual Hypothermic perfusion through both portal vein and hepatic arteria. (b) Single Hypothermic perfusion through only portal vein. From [193]. Reprinted with License number: 6126010828274.

4. Pumping systems: pulsatile or continuous

The debate over the best method of perfusion includes the choice of whether to perfuse the liver through the hepatic artery with pulsatile or continuous flow [129, 249, 111, 138]. The **Figures 4.1** and **4.2** show the possible setting in perfusion pumping and their components. Brüggenwirth et al. [251] observed that pulsatile or continuous perfusion through the hepatic artery did not result in different outcomes. On the contrary, Sezai et al. [256] demonstrated that pulsatile flow support provided better microcirculation in both the kidney and liver compared to continuous flow support [257]. It is worth noting that, some scientists [258, 259] reported that pulsatility is present at the capillary level, and that microcirculatory flow patterns are therefore different between pulsatile flow and continuous flow support [257]. Moreover, some studies suggested that pulsatile perfusion is superior to continuous perfusion for kidneys [133, 260, 261]. In studies on liver pigs, Tawa et al. [138] suggested that pulsatile flow through the hepatic artery may provide superior preservation of

vascularized composite allografts when perfused for 24 hours at subnormothermic temperatures, with the potential for improvement in endothelial function and decreased ischemic injury. Nevertheless, further investigations are still needed to definitively clarify the role of pulsatile arterial perfusion during liver machine perfusion [206, 249, 262, 263]. Many studies report brand names of roller and centrifugal pumps used for perfusion. Nassar et al. [264] used the centrifugal pump Medtronic Inc. (Minneapolis, MN), and the roller pump TERUMO Sarns 8000. Both the roller and centrifugal pump used by Gilbo et al. [265] were produced by Medtronic Inc. Bruinsma et al [266] used the roller pump Masterflex L/S, Cole Palmer. The roller pump of Liver Assist can supply pulsatile flow at 60 bpm with an amplitude of ± 20% of mean pressure [193]. Magbagbeola et al. [267] used a single centrifugal pump PuraLev 1200 MU, Levitronix GmbH, 8005 Zurich, Switzerland. Imber et al. [268] operated with a centrifugal pump Medtronic BP50 Centrifugal Pump.

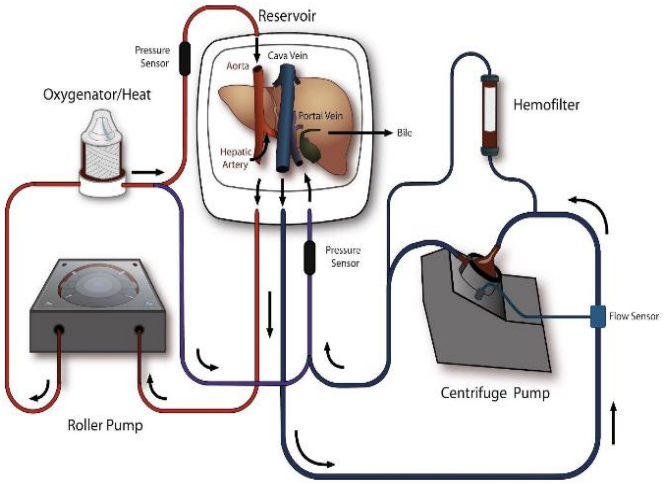

Figure 4.1. Schematic of pumping system of perfusion. The machine perfusion integrates three main structures; a self-design common reservoir (cava reservoir), a centrifugal pump for a low-pressure system (portal branch) interposed with a hemofilter and flow sensor, and a roller pump for a high-pressure system (arterial branch) interposed with an oxygenator a heat exchange [269]. Image from [269] reprinted with License number 6126010170933.

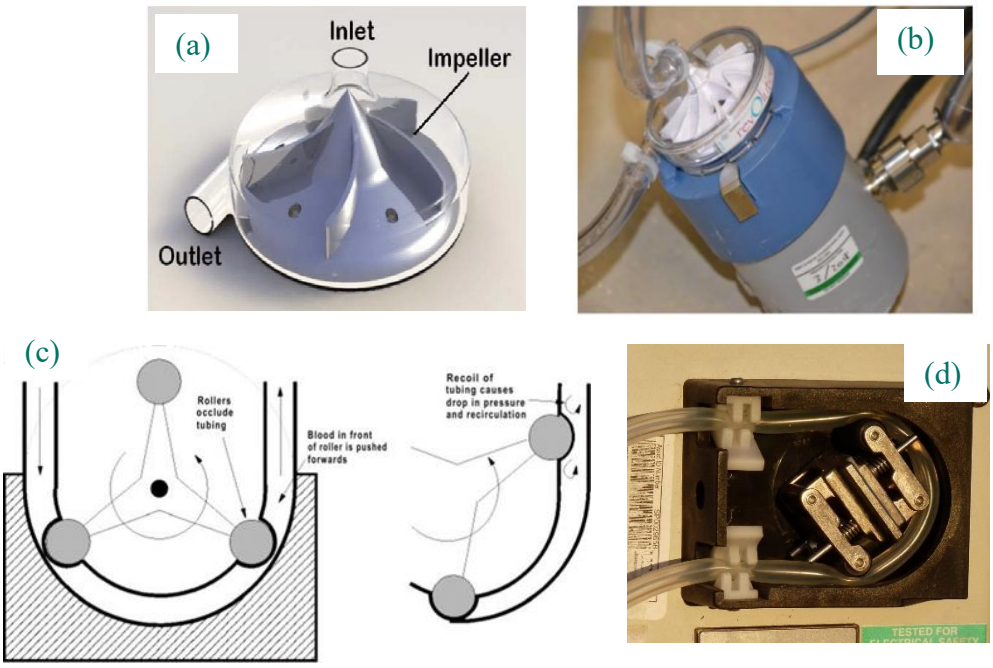

Figure 4.2. Roller and centrifugal pumps. (a) - (b) Details of a centrifugal pump for blood [263, 270]. (c) - (d) Schematic diagram and photo of a roller pump. In reference [271] is reported another photo of a roller pump. License number to use the Figure 4.2a,b from [263]: 502021336. Permission obtained to reproduce Figure 4.2c from [270] from Editor. Figure 4.2d, from [Andy Dingley - https://en.wikipedia.org/wiki/Peristaltic_pump#/media/File:Peristaltic_pump_head.jpg], Wikimedia Commons, is reprinted under License CC BY-SA 3.0.

5. Liquid solutions for hypothermic and normothermic perfusion

Normothermic perfusion has been has been carried out using various of liquid perfusion. Some studies [33, 157, 169, 210, 272 – 274] have used solutions based on human red blood cells (RBCs). However, de Vries et al. [275] pointed out that these types of liquids may exhibit problems related to the scarcity of human blood and the possibility of inducing an infection or immunological response [276, 277]. To overcome these challenges, de Vries et al. [275] and van Leeuwen et al. [141] perfused livers with haemoglobin-based fluid as an oxygen carrier (HBOC, HBO2 Therapeutics, Souderton, PA), using bovine-derived HBOC-201 (Hemopure) along with gelofusine, albumin, metronidazole, cefazolin, nutrients, glutathione, insulin, heparin, and NaHCO3. These authors suggested that this solution has the technical advantage of conducting hypothermic and normothermic perfusion in sequence without the need to change the fluid in the transition from cold to warm perfusion. Lifor is a patented solution (U.S. Patent #7,220,538) containing nutrients such as amino acids, growth factors, salts, sugars, buffers, colloids, and lipid nanoparticles [278 – 280]. A detailed description of the perfusate used during normothermic perfusion was provided by op den Dries et al. [157], Ghinolfi et al. [273], and Mergental et al. [281]. Lifor was first employed by Stowe et al. in 2007 for heart

perfusion [280]. Lifor has been used for static cold storage [279], hypothermic perfusion, sub-normothermic perfusion [282], and normothermic perfusion (Lifeblood Medical) [278]. Some studies have demonstrated that Lifor performs well for organ preservation [283, 284] and is probably better than University of Wisconsin (UW) solution in protecting against warm or cold ischemia–reperfusion injury [280]. In studies conducted through the device Metra OrganOx for normothermic perfusion by Ravikumar et al. [168], Nasralla et al. [57], Ghinolfi et al. [273], and Gilbo et al. [170], livers were initially flushed with 500 ml of a heparinized, plasma-free colloid solution, autologous red blood cell-based perfusate (hematocrit 30%), called Gelofusine (Gelofusine®, B Braun, South Yorkshire, UK). The livers were then perfused with a mixture of substances such as antibiotics, bile salts (sodium taurocholate, New Zealand Pharmaceuticals, Palmerston North, New Zealand), insulin (Actrapid®, Novo Nordisk, West Sussex, UK), heparin (CP Pharmaceuticals, Wrexham, UK), prostacyclin 0.5 mg (Flolan®, Glaxo, Middlesex, UK), sodium taurocholate 5.6 g, 10 mL of calcium gluconate 10%, cefuroxime 1000 mg, and 5–10 mL of sodium bicarbonate 8.4%, along with a variable rate infusion of glucose and amino acids (Nutriflex, B Braun, Sheffield, UK) [57, 168, 170]. On the other hand, Mergental et al. in 2016 [33] used a perfusion fluid based on 3 units of the donor liver-specific blood group, Rhesus-negative, packed red blood cells, supplemented with 1000 mL human albumin solution 5%, 30 mL sodium bicarbonate 8.4%-, and 10-mL calcium gluconate 10%. In this trial, the authors loaded the perfusion circuit with 10 000 IU heparin, 500 mg vancomycin, and 60 mg gentamicin before connecting the liver, with the continuous infusion of epoprostenol (8 μg/h). Perera et al. [169] also conducted NMP with third-party type-specific or O Rh-negative leukocyte-depleted red cell–based fluid at 37 °C using the Liver Assist and Portable Organ Care System (OCS) Liver devices. Watson et al. [272, 274] perfused livers with red cells added to a litre of either succinylated gelatine or Steen solution (Xvivo Perfusion, Göteborg, Sweden) and supplemented with 30 mmol sodium bicarbonate, 25 000 units (50 mg) heparin, antibiotics, calcium chloride, magnesium sulphate, and amino acids (Aminoven-25, Fresenius Kabi Ltd, UK).

In most clinical cases during hypothermic perfusion, researchers have used 3 – 4 liters of UW solution (Bridge to Life® , KPS® Organ Recovery Systems) as perfusate in the machine perfusion [6, 34, 50, 58, 63, 72, 83, 97, 130, 131, 132, 134, 136, 156, 166, 178, 285, 286]. Clinicians have used solutions to perfuse or only to flush livers like Vasosol [75, 140, 161] (Vasosol® Organ Recovery Systems; Preservation Solutions Inc.), HTK (Custodiol-N®, Köhler Chemie, Germany) [63, 285, 286, 287], Celsior (Genzyme-Sanofi, Milan, Italy) [273, 165], IGL-1 and IGL-2 [63]. UW solution was created by Belzer et al. [288] in 1987 at the University of Wisconsin. His better performance convinced clinicians to use it in the place of Euro–Collins solutions for abdominal organ preservation [156, 289 – 293]. UW is a water–based intracellular preservation solution with low sodium and high

potassium concentrations to mimic an intracellular environment [294, 295]. In the solution UW are dissolved some chemicals which conduct a preservative action as adenosine, hydroxyethyl starch (HES), lactobionate, raffinose and antioxidant component (allopurinol and reduced glutathione) [292, 295 – 297]. Adenosine, a precursor of ATP, provides substrates for the regeneration of energy levels during the reperfusion period following cold storage [296, 297], and hydroxyethyl starch (HES) serves as the colloid carrier to minimize interstitial edema during perfusion [295, 296], lactobionate and raffinose, metabolic inert substrates, serve as osmotic membrane – impermeable agents that prevent hypothermia-induced cell swelling [295 – 299], allopurinol and reduced glutathione take the role of antioxidant defence to prevent the formation of ROS [296, 295, 300]. Despite the wide use of UW solution, the main disadvantages of UW solution are due to the presence of HES, high potassium concentration and elevated costs than other solutions [286, 295, 301 – 303]. HES confers a high viscosity (~ 4.5 – 6 cp at 1 – 5 °C depending on HES concentration – **Table 5.1**) to UW solution, which is five–six times higher than water approximately (1.51 cp at 5 °C and 1 cp at 20 °C) [121, 299, 304 – 309]. The high viscosity is a problem because it may be necessary to take more time to flush accurately the organ before and after perfusion [310, 311]. A high viscosity tends to obstruct complete organ perfusion [311]. An ineffective flushing and washout of UW from the liver before transplantation may bring a hemodynamic instability and a possible cardiac arrest induced by post-transplantation hyperkalemia which is caused by high potassium concentration [286, 299, 312 – 316]. In the following table kinematic viscosity values are reported:

Condition	Perfusion Temperature (°C)	Viscosity (m^2/s)
3 WE+O_2 (MP)	20	$4.5x10^{-6}$
4 Lifor+O_2 (MP)	20	$9.4x10^{-6}$
5 Lifor (MP)	20	$9.4x10^{-6}$
6 Vasosol (MP)	5	$1.5x10^{-5}$
7 UW (MP)	5	$1.4x10^{-5}$

Table 5.1. Kinematic viscosity at certain temperatures of some preservation liquids [156]. These viscosities were calculated using Poiseuille's law and assuming the solutions behave as a Newtonian fluid, in which water is the predominant component.

Another not negligible disadvantages are the market prices of UW solution [317]. Some authors reported that the cost of UW starts from 282 $/l which could reach 300 – 400 $/l if additives are added [295, 317, 318]. For these reasons, researchers developed later other solutions for hypothermic

perfusion [292, 319, 320]. Alternative solutions most used are Histidine-Tryptophan-Ketoglutarate, HTK, (named also Custodiol or Custodiol HTK) and Celsior, but in literature are mentioned others solutions as Vasosol, IGL – 1 (Institute George Lopez), IGL – 2, HTK – N (a modified and improved version of HTK) Polysol, Leeds solution, Kyoto University solution, ECOSOL, Williams Medium E and many others [74, 76, 121, 156, 86, 296, 295, 320, 322 – 327]. HTK solution was developed by Hans Jürgen Bretschneider at Göttingen University in 1980 [328]. Initially, HTK has been used for heart preservation [84, 299, 329, 330], and later for abdominal organs [299, 331 – 334]. In 2002 Food and Drug Administration (FDA) in the USA approved the use of HTK solution for organ preservation [299]. Celsior solution was developed by Menasché et al. [326] in 1994 initially for cold storage preservation of cardiac grafts and approved by FDA in the USA in 1999 [299]. Later, it was used for other organs [295]. Potential advantages related to the HTK and Celsior are smaller prices than UW and low viscosity and low potassium content [299, 285, 286, 335 – 337]. At 5 °C HTK's viscosity is 1.68 – 1.8 cp [121, 307] and the at same temperature Celsior has a viscosity of 1.3 cp [307]. The base cost of HTK is 181 $/l [295, 326], whereas the base costs of Celsior and IGL – 1 are 228 and 184 $/l [295, 318, 338]. For these reasons in many transplantation centers HTK and Celsior are used as an alternative to UW solution [299, 334, 335]. In literature, there are many publications about the use of HTK and Celsior solutions vs. UW for human and animal liver storage or hypothermic perfusion [262, 285, 286, 311, 312, 314, 334, 335, 340, 341, 342, 343, 344, 345]. Despite the wide employment of these two solutions, there are no decisive and definitive proofs that HTK and Celsior are better and high – performance than UW [302, 75, 340, 312, 285, 335, 286, 342, 118, 76, 341, 346 – 348]. Effects of the use of UW, HTK and Celsior solutions on liver functionality and biliary complications have created ample and inconclusive debates [286]. Indeed, several studies have reported discordant results [334, 340, 285, 262, 335, 286, 314, 342, 343, 344, 311, 312, 345, 349 – 355]. Many studies by researchers such as Erhard et al [334], Garcia-Gil et al. [340], Meine et al. [312], Feng et al. [341], Karakoyun et al. [285], Rayya et al. [342], Jia et al. [262], Szilágyi et al. [86], Mangus et al. in 2006 [335] and 2008 [314] suggested that HTK may be regarded as an alternative to UW and may be the potentially an optimal perfusate for HMP inasmuch both solutions are equally effective for the preservation of the hepatic graft statistically significant differences of effects in biliary tract flush, prevention of biliary complications. Moreover, these authors have highlighted the relevance of the economic aspects of HTK. Quite the opposite, other researchers as Gulsen et al. [343] and Janßen et al. [353] reported that livers by DCD donors treated with HTK were associated with more post-LT complications, and they demonstrated the superiority of UW than HTK and Celsior. Bessems et al. [356] compared the performance of Celsior and Polysol in the preservation of a pig liver, concluding that Polysol performance is better than Celsior inasmuch were revelated lower AST/ALT levels and

lesser resistance. In the composition of Polysol, there is Polyethylene Glycol 35 (PEG35), a low-weight molecular colloid that confers a reduced viscosity to the solution [356, 357]. Some studies confirmed that the addition of PEG35 in preservation solution as IGL – 1 and IGL – 2 produces healthy effects for the organ [63, 231, 358]. For this reason, it was proposed that PEG35 may be an optimal alternative to HES to prevent oxidative stress during storage and to minimize damage related to IRI [63, 359, 360]. Boer et al. [344] based on other studies [311, 345] concluded that the results explained above may be due to regional differences in donor and recipient features. They suggested that liquid preservation could be chosen based on the clinical experiences of transplantation centers. Guidelines of the Liver Transplantation Society recommend avoiding the use of HTK for the liver which has suffered an ischemic time of a minimum of 8 h [82, 361]. Nardo et al. [354] and Adam et al [345] reported a comparison between HTK and Celsior suggesting a lower survival with the use of HTK. All preservation solutions are used successfully in clinical cases, and although some of these solutions are characterized by an improvement in chemical composition related to UW, the performance of HTK and Celsior has not totally convinced the scientific community, so the debate about the ideal solution is still open [76, 82].

6. Hypothermic and normothermic perfusion: two non – competitive distinct methods with different objectives

Recent studies conducted by Zurigo's Research Group headed by Dutkowski suggest HOPE may serve as a prediction as tool for early graft function in the recipient [72, 152, 180, 365]. Nevertheless, not all researchers consider HOPE a tool for viability testing before transplantation [83]; seeing as the low temperatures decrease drastically liver metabolism rate, it is not possible to complete the evaluation of all clinical data about transplantability and liver functionality [32, 148, 366]. For example, the liver can't produce bile [83]. These reasons may limit the validity of assessment for classic parameters [93, 122, 367, 368]. At present, hypothermic liver perfusion is a technique especially employed to minimise the effects of ischemia injuries [32, 72, 83, 174, 178]. Quite the opposite, hepatic normothermic perfusion is a technique that permits the perfusion in a quasi–physiological condition supporting the metabolism and revitalising capacity of the liver with a continuous supply of oxygen and nutrients [6, 33, 56, 127, 141, 292]. The normothermic perfusion ex-situ NMP is a tool helping clinicians to evaluate hepatobiliary functions since the graft is completely operative from a metabolic point of view [32, 141, 157, 253, 369, 198, 274]. In this way, it is possible to make a complete evaluation of clinical parameters before transplantation and prevent any quality graft deterioration from the perfusion starting [136]. The high temperatures allow rapid

restoration of ATP levels [155]. The superior performance of NMP about SCS has been demonstrated initially by Ravikumar et al. and Mergental et al. in 2016 [33, 168] and later by Nasralla et al in 2018 [57]. Although normothermic oxygenated perfusion confers protection for DCD grafts, it has been postulated that this protection is realised only in the presence of short periods of warm ischemia before the donor's liver removal [180]. Moreover, an extended static cold storage might neutralise the protective effect of NMP on IRI [2, 370]. Reddy et al [371] reported that NMP may significantly be deleterious to the function of porcine liver grafts after a SCS time. Indeed, a rapid rewarming of the graft may accelerate the metabolism rate causing an increment of metabolic demand for oxygen and nutrients that outstrip available metabolic resources supplied by perfusion: this causes further injury [2, 287, 372 – 374]. In these normothermic conditions, the graft might suffer immediate warm ischemia with a high likelihood of graft loss [60, 372, 373, 374]. For this reason, it has been introduced the Controlled Oxygenated Rewarming. Controlled oxygenated rewarming (COR) serves as a gradual and gentle transition between cold preservation and warm reperfusion aiming to minimise organ damage [2, 374]. In this manner, COR can be viewed as a safe bridge between hypothermia and normothermia [275, 373]. Indeed, Groningen's Research Group [275, 373] have established the DHOPE – COR – NMP protocol to permit both mitochondrial activity restoration during hypothermia (DHOPE) and to minimise reperfusion injury by rewarming gradually the graft (COR) and, in the end, to evaluate hepatic function during normothermia (NMP) [22, 275, 141, 253, 369].

The machine perfusion protocol, **Figure 6.1**, included 1 hour of DHOPE, 1 hour of COR, and subsequent NMP for at least 150 minutes. Each phase of machine perfusion served a different purpose as described in the upper part of the figure. Machine perfusion settings were adjusted according to the perfusion temperature. The temperature was kept at 10 °C during DHOPE and was gradually increased to 37 °C during the COR phase, after which the liver was functionally tested during NMP. PV (portal vein) and mean HA (hepatic artery) pressure was set at 5 and 25 mmHg, respectively, during DHOPE and were gradually increased during COR to 10 and 70 mmHg, respectively, at the start of NMP. DHOPE, dual hypothermic oxygenated machine perfusion.

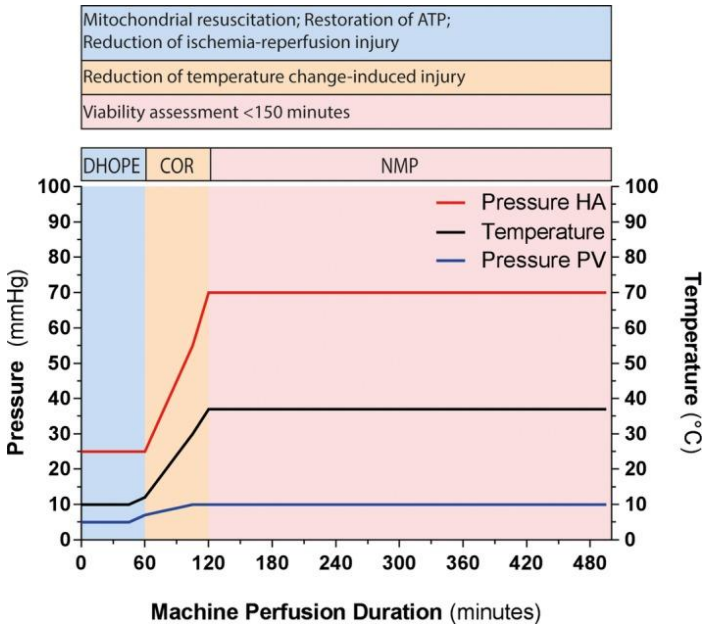

Figure 6.1. Overview of the machine perfusion protocol DHOPE – COR – NMP [275]. Reprinted with License Number: 6126030215024

Numerous studies have reported that livers subjected to hypothermic and normothermic perfusion in sequence exhibit improved endothelial and early functionality, along with reduced injury caused by ischemia-reperfusion [183, 275, 165, 111, 136]. The combination of the preservative effects of HOPE/DHOPE with the protection given by COR and the regenerative effects of NPM could accentuate the potential of MP [22, 176, 186, 2, 141, 34, 111, 375]. Therefore, it has been proposed that hypothermic perfusion should be performed as a preconditioning step before subsequent normothermic or sub-normothermic perfusion, as this sequential approach has been shown to promote superior liver preservation outcomes in terms of endothelial and early functional improvement and reduced injury from ischemia-reperfusion [130, 132, 274, 376]. HOPE/DHOPE and NMP strategies have been seen in the past as different methods, even in competition with each other, each with advantages and disadvantages [180, 136]. The effects of the transition from hypothermic to normothermic perfusion are shown in **Figure 6.2**. Nevertheless, is not still possible at present to carry out a direct comparison between NMP and HOPE/DHOPE [60]. In light of the above, hypothermic

and normothermic machine perfusion serve different goals and are not competing techniques [83]. The two techniques can be applied sequentially with complementary benefits [275, 141, 377].

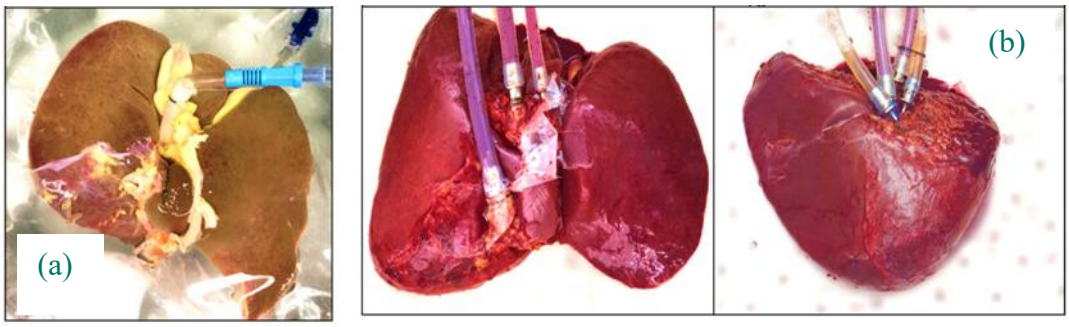

Figure 6.2. Hypothermic vs Normothermic perfusion effects. The first difference between normothermic and hypothermic perfusion is the colour of the liver: on the left (a), the liver perfused at 10 °C with an acellular solution, on the right (b) liver perfused at 37 °C with blood [3]. These Figure from [3] are reprinted with License Number 6126030444428.

7. Perfusion Parameters

7.1 Oxygenation levels

Numerous studies, focused on the role of oxygen to support mitochondrial metabolism to avoid succinate accumulation and release of ROS [83, 378], have allowed a better understanding of biological mechanisms at the base of IRI [174]. During the HOPE/DHOPE hepatic graft is preserved through a cold solution with pulsatile/continuous flow to supply metabolic substrates and oxygen, to restore the microcirculation and to remove toxic substances [123, 91, 143, 145, 146]. Perfusion fluid is usually oxygenated through one (two) hollow-fibre membrane oxygenator(s) depending on the circuit of perfusion. The working principle of a hollow-fibre membrane oxygenator is the diffusion of oxygen and carbon dioxide across a microporous hollow fibre bundle [263, 379]. Oxygen moves from the interior of the hollow fibre into the perfusate, and carbon dioxide diffuses from the perfusion liquid and crosses into the interior of the fibre and is swept away by the regulated gas flow through the hollow fibre [263]. In the following image, **Figure 7.1.1**, there is an explanation of a hollow-fibre membrane oxygenator.

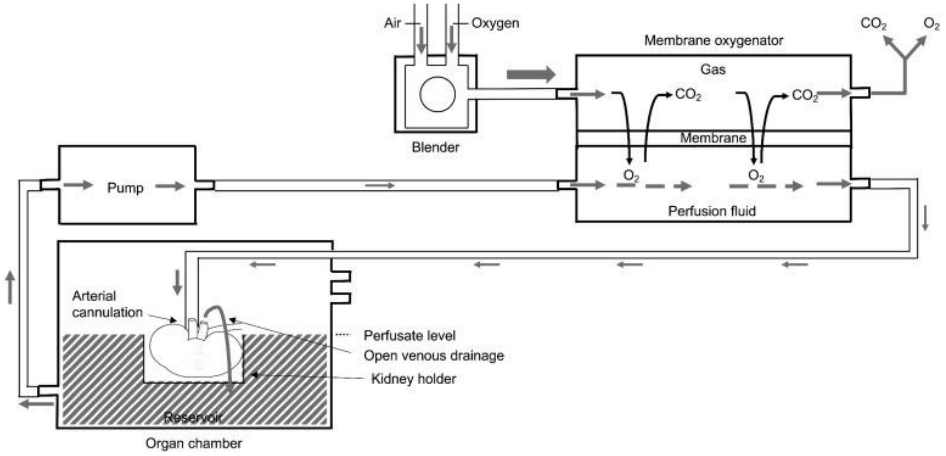

Figure 7.1.1. Basic principles of membrane oxygenation during organ perfusion [91]. Oxygen diffuses from the gas into the perfusion fluid, and carbon dioxide diffuses from the perfusion fluid into the gas for disposal. The oxygenated perfusion fluid is pumped into the organ by arterial and/or venous cannulation. The perfusion fluid drains from the organ and is collected into the reservoir of the organ chamber and again pumped towards the membrane oxygenator to reoxygenate the perfusion fluid. Creative Commons CC BY 4.0 license.

The first membrane oxygenator was developed by Clowes et al. [380] using sheets of polyethylene and Teflon as a membrane but required large surface areas for adequate oxygenation [381]. In 1957, Kammermeyer et al. [382] first reported the excellent gas transfer properties of a polymer of dimethylsiloxane, commonly known as silicone [381]. The following studies have enhanced the efficiency of gas exchange and hemocompatibility, as described by Melchior et al. [383]. From the beginning of the 1980s, hollow fibre membrane oxygenators replaced bubble and classical membrane oxygenators as extracorporeal oxygenators in most clinical applications (e.g., cardiac surgery) [383]. Hollow fibre membrane oxygenator, **Figure 7.1.2**, has reduced haemolysis and superior gas exchange, compared with classical membrane oxygenators and bubble oxygenation [384, 385]. Moreover, hollow fibre polymethyl pentene (PMP) oxygenators, compared to the conventional silicone membrane oxygenators, have significantly less priming volume, and set-up time along with 5- to 10-fold reduced pressure drops [279, 386].

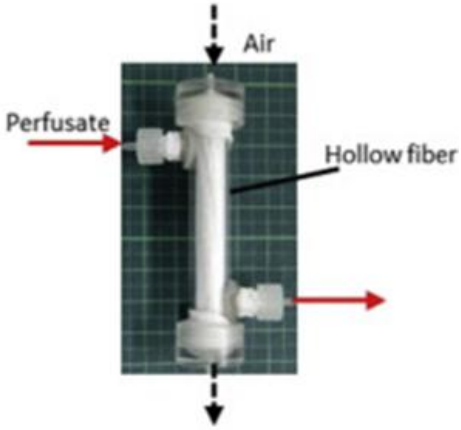

Figure 7.1.2 Working principle of a hollow fiber oxygenator [387]. Figure form [387] reprinted with License Number: 6126030767223.

The oxygenator consisted of housing polycarbonate pipe (inner diameter: 90 mm, outer diameter: 130 mm, and length: 5.5 cm) which was 40% filled with the multi-layered composite hollow-fibre membrane (Mitsubishi Rayon Co. Ltd., Tokyo, Japan), shown in **Figure 7.1.3**, and the total surface area of the hollow-fibres was 200 cm^2. Air was flowed into the hollow fibre at 84 mL/min using the air pump (Marukan Co., Ltd., Osaka, Japan) [387].

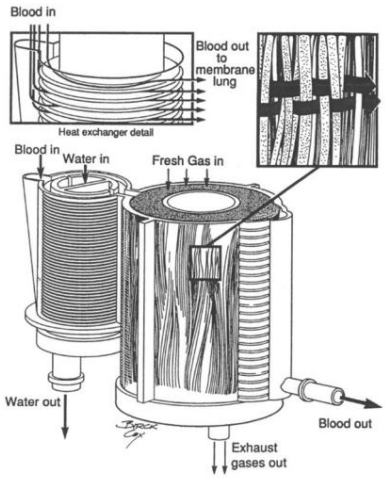

Figure 7.1.3. Details of Hollow fibre membrane oxygenator [388]. Figure from [388] reprinted with License Number: 6126030968830.

Commercially, several hollow fibre membrane oxygenators are available and different based on module structures and hollow fibre arrangements [389]. Some of these types are reported here in the following images, **Figure 7.1.4** and **7.1.5**.

Moreover, another significant feature of hollow fibre membrane oxygenator is the self-mechanical support, good flexibility, and easy handling during module fabrication, membrane preparation, and system operation as explained by Teber et al. [390].

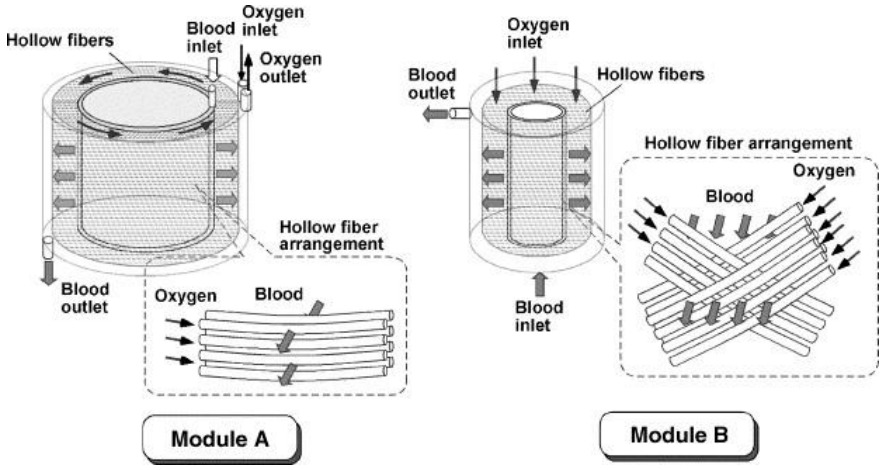

Figure 7.1.4. Hollow fibre arrangement and blood flow direction in coiled construction design membrane oxygenators [389].

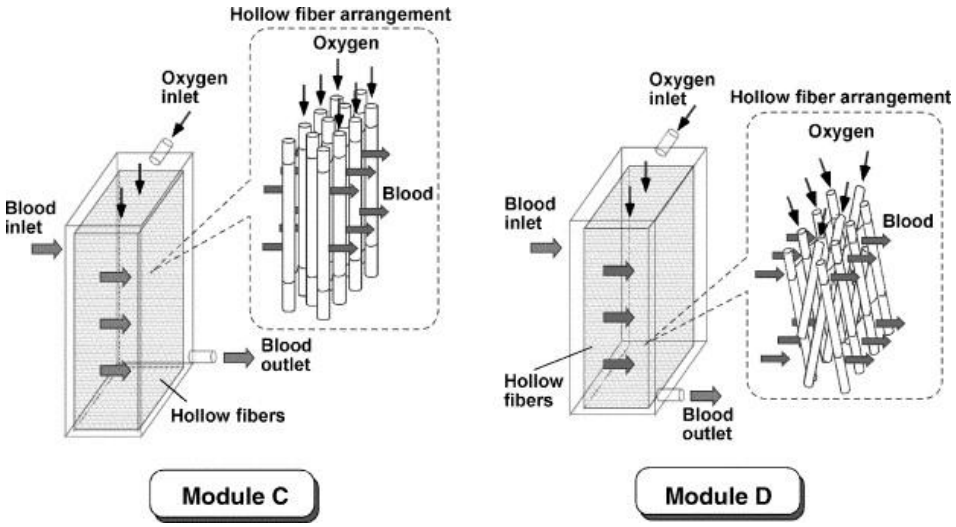

Figure 7.1.5. Hollow fibre arrangement and blood flow direction in rectangular solid design membrane oxygenators [389]. Figures from [389] reprinted with License Number: 6126031101528.

One or two hollow fibre membrane oxygenators were incorporated in the machine perfusion: Kidney Assist Transporter (Organ Assist BV, Groningen, The Netherlands), the VitaSmart (Bridge to Life, Northbrook, IL, USA) [91], two in non-transportable devices as Liver Assist (Organ Assist, Groningen, The Netherlands) [157], in the machine used by Ravaioli et al. [163], one in OrganOx® metra NMP and in Cleveland NMP circuit (Cleveland Clinic, Cleveland, OH, USA) [57, 195].

In the following image is reported an oxygenator assembled in the Liver Assist (Organ Assist, The Netherlands). In this device, a membrane oxygenator is connected to an external oxygen source [391]. There is no information available in the literature about the brand name of the oxygenator used in the Liver Assist device, shown in **Figure 7.1.6**.

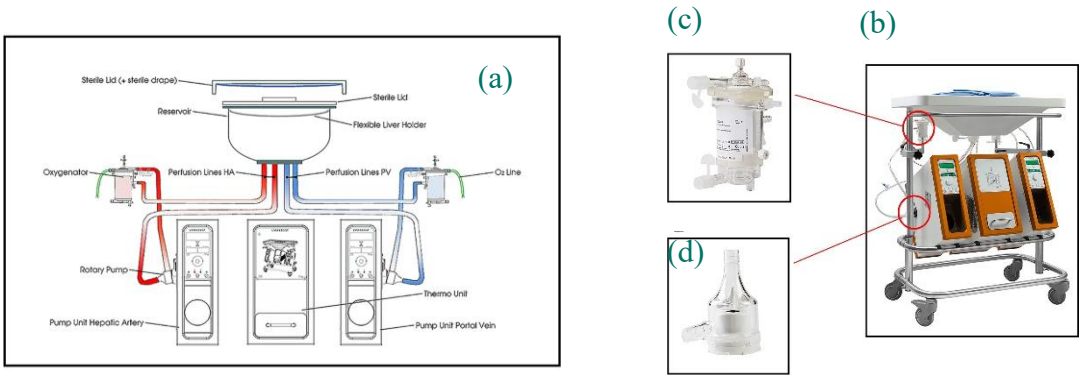

Figure 7.1.6. (a) Schematic of the device Liver Assist . (b) full representation of the device, (c) centrifugal pump used for normothermic machine perfusion, (d) oxygenator. This device has been used in different studies: [83, 132]. Figure 7.16a, from [83] reprinted with permission from Copyright Massachusetts Medical Society. Figure 7.1.6b,c,d is adapted from Karimian, N., Matton, A. P., Westerkamp, A. C., Burlage, L. C., op den Dries, S., Leuvenink, H. G., Lisman, T., Uygun, K., Markmann, J. F., Porte, R. J. *Ex Situ* Normothermic Machine Perfusion of Donor Livers. *J. Vis. Exp.* (99), e52688, doi:10.3791/52688 (2015) with authorization by the publisher.

Some researchers have provided the brand names of the majority of components utilized in the perfusion circuit. For example, many authors operated with an oxygenator by Medtronic (Medtronic Affinity NT) [264, 100], whereas in the device presented by van Der Plaats et al. [392], there was a hollow fibre membrane oxygenator (HILITE 800LT, MEDOS Medizintechnik AG, Stolberg, Germany). Gilbo et al. used a hollow fibre oxygenator (Stockert; Sorin Group, Munich, Germany). Minor et al. [287] oxygenated the perfusate with Hilite LT 2400, Medos, Stolberg, Germany. Instead, Banan et al. [393] used a membrane oxygenator/heat exchanger (CB3381 Carmeda pediatric Minimax Plus; Medtronic Inc. Abudhaise et al. [147] operated with the oxygenator (Dideco Kids D100, Sorin Group Italia, Mirandola, Italy). Zurigo's Research Group [3, 197] employed the Wyss Machine which was integrated with the membrane oxygenator Medos Hilite 2400 LT. Tingle et al. [394] reported that the OrganOx® Metra has been integrated with a Medtronic™ oxygenator without other specifications. There is no specific information about the type of integrated oxygenator in the (OCS™) Liver System (TransMedics® Organ Care System™). Imber et al [268] used a 1500 ECMO Oxygenator Medtronic.

The review of perfusion protocols, by Eshmuminov et al. [395], are reported data on gas mixtures supplied through the oxygenator for human liver perfusion: many authors supplied a mixture of O_2 and CO_2,with a gas composition of 95% O_2 and 5% of CO_2 [183, 111, 274, 393, 395]. Groningen's Research Group [83, 131, 132] oxygenated liquid perfusion with two oxygenators, fed with 500 ml/min of O_2 pure, integrated into Liver Assist device observing measurement of oxygen in liquid perfusion was 80 – 100 kPa (600 – 750 mmHg). The same oxygenation levels were reached by other clinicians [72, 97, 130, 175, 91, 163, 136]. The elevated partial pressure of oxygen (100 kPa) is necessary for ATP restoration [91]. Other clinicians [97, 183, 50, 6, 165, 134, 322, 166, 111] oxygenated actively the perfusate up to measuring a P_{O2} from 40 to 80 kPa in the perfusate (300 – 600 mmHg).

Izamis et al. [156] showed a simple way to calculate the quantity of oxygen adsorbed to liver: Oxygen Delivery Rate, ODR, is the quantity of oxygen dissolved in the perfusate entering in the liver, it is calculated by the product among the volumetric flow rate Q (ml/min), partial pressure of oxygen (mmHg) dissolved in the perfusate (at equilibrium), $P_{O_2}^{in}$, and Henry's constant, H, of oxygen dissolved in water at 5 °C, $k_{5°C}$=6.4x10^{-5} ml_{O2} / (mmHg ml $_{perfusate}$) and at 20°C, $k_{20°C}$=4.1x10^{-5} ml_{O2} / (mmHg ml $_{perfusate}$): $ODR\left[{ml_{O_2}}/{min}\right] = H * P_{O_2}^{in} * Q$. The quantity $H * P_{O_2}^{in}\left[{ml_{O_2}}/{ml_{perfusate}}\right]$ is the volumetric fraction of oxygen in equilibrium with the oxygen in gas phase. The quantity of oxygen exiting from the liver dissolved in the perfusate, Oxygen Exiting Rate, OER, is calculated in the same manner as explained above, but $P_{O_2}^{out}$, in the partial pressure in the outlet from the liver. So, it obtained $OER\left[{ml_{O_2}}/{min}\right] = H * P_{O_2}^{out} * Q$. Where, $H * P_{O_2}^{out}$ is the fraction of oxygen dissolved in perfusate in outlet from the liver. The quantity of oxygen absorbed by the liver is obtained simply by the difference ODR – OER [156]. This difference is greater than zero inasmuch organ in during hypothermic machine perfusion consumes ATP and oxygen [396]. Xu et al. [397] proposed a similar manner to calculate OUR for normothermic perfusion (oxygen uptake rate): $OUR = \frac{\left[Q*\left(C_{O_2}^{inflow} - C_{O_2}^{outflow}\right)\right]}{liver\ weight}$ where Q is the perfusion flow rate (mL/min), C_{O2} is the oxygen concentration (nM) calculated as C_{O2} = 0.0031 PO_2, where PO_2 is the oxygen partial pressure (mmHg), and 0.0031 (mL O_2/(mmHg dL)) is the solubility of oxygen in aqueous solutions.

7.2 Pressures in machine perfusion

In the last decade, researchers have discussed the optimal values of pressure for hypothermic and normothermic perfusion [95]. Schlegel et al. [95] reported that pressure in the portal vein should not exceed 8 mmHg to avoid damage to the hepatic structure. In hypothermic conditions, a strategy to reduce shear stress could be to use perfusion with the lowest possible pressure, which is safer for endothelial sinusoidal liver cells but may be inconvenient if incomplete perfusion occurs [95]. Endothelial sinusoidal liver cells are indeed susceptible to cold shear stress [398]. Van Rijn et al. [132] suggested carrying out DHOPE with a hepatic artery of 25 mmHg and portal vein of 5 mmHg. The values are based on previous studies which suggest that pressures lower than physiological values would help to protect endothelial cells and hepatic micro vascularisation by cold shear stress [172, 182, 399]. Debbaut et al. [399] demonstrated that if the pressure in the hepatic artery and portal vein is lower than 25 mmHg and 3 mmHg, respectively, viscosity has no effect on shear stress, and no deleterious effects can occur in hepatic structures. Moreover, machine perfusion can be controlled by either pressure-controlled or flow-controlled methods [150, 400]. Since flow depends on vascular resistance, high resistance reduces the flow. Therefore, Lascaris et al. [400] suggest operating with a machine pressure-controlled method that permits protection against endothelial cell damage. However, as explained by Gryaznov et al. [150] in the next paragraph, this solution needs some adjustments. In most clinical cases, in DHOPE, arterial pressure is 25 mmHg [83, 132, 163, 141, 58, 178, 134, 166, 111, 183], even though some researchers applied a pressure of 30-40 mmHg in the hepatic artery [182, 103, 147]. Instead, the literature reports that, in DHOPE, portal pressure is often 5 mmHg [83, 75, 132, 182, 163, 141, 58, 134, 111], but other authors employed lower pressures of 3-4 mmHg [164, 178, 166] or higher pressures of 6-7 mmHg [103, 147]. In HOPE, portal vein was 3 – 4 mmHg [72, 97, 75, 130, 50, 6, 34, 135, 136]. In the normothermic perfusion conducted by Westerkamp et al. [183] and van Leeuwen et al. [141] portal vein and hepatic artery were of 11 mmHg and 70 mmHg respectively. Ravikumar et al. [168] during the NMP hepatic artery pressure was set to 60 – 75 mmHg, and the inferior vena cava pressure was set to 1 – 2 mmHg. In clinical cases, researchers monitored pressure in different manners. Furthermore, these authors said that portal pressure was not monitored inasmuch it is effectively fixed by the height of the portal venous reservoir. Nassar et al. [264] report that pressure was monitored with the device Dash 3000 (General Electric, Waukesha, WI). In the study by Post et al. [401] pressure was controlled by a pressure transducer (El-Press P-502C-350R; Bronkhorst High-Tech, Ruurlo, the Netherlands). In the Wyss Machine flow and pressure are measured with Sonoflow CO.56 and PendoTECH [197]. Moreover, Eshmuminov et al. [197] operated with a feedback loop for automatic injection of vasoactive medication to guarantee a certain value of pressure and flow. Another pressure transducer used in

machine perfusion is the Edwards Lifesciences Co., Ltd., USA [402]. In the novel machine perfusion created by Magbagbeola et al. [267] was integrated a single pressure sensor PendoTECH, Princeton NJ 08540, USA. Imber et al. [268] operated with pressure transducers Baxter, Triple Pressure Transducers.

7.3 Flow rates and resistance through the graft

Flow rates are regulated based on the weight of the graft [161, 156, 75]. Guarrera et al. [161, 75] perfused liver with 0,667 ml / (min g liver). Other perfused with 0.1 ml / (min g liver) [50, 6, 136]. Dutkowski et al. [97] perfused the liver through the portal vein with 100 a 150 ml/min (0.13 ml/min g liver) to which corresponding 2.5 – 3 mmHg [9]. In other studies, Dutkowski et al. [72, 130] perfused liver with 120 – 300 ml/min. Dondossola et al [178] applied DHOPE measuring in hepatic artery 84 ml/min and 365 ml/min in portal vein after 2 hours. van Rijn and colleagues [83] during the DHOPE measured 220 ml/min through portal vein, PV, and 100 ml/min for hepatic artery, HA. Burlage et al., [111] and Boteon et al. [136] compared flows rate in livers undergone to SCS + HOPE + NMP (first group) and SCS + NMP (second group). They observed that volumetric flow rates perfusing livers of the first group were double those of the second group. They demonstrate that HOPE is essential for micro vascular preservation [111, 136]. In the studies by Abudhaise et al. [147] has been measured in hepatic artery at 33 ml/min and 92 ml/min in the portal vein in the liver undergoing to SCS + 4 hours of hypothermic perfusion. Moreover, they reported resistance values for HA 0.83 (mmHg min)/ml and PV 0.07 (mmHg min)/ml. In the review by Eshmuminov et al. [395] is reported that in most studies graft weight is missing. Furthermore, they assert that in most clinical cases perfusion was controlled by setting a certain value of pressure both for HA and PV. Vogel et al. [624] during NMP fixed the high of the reservoir to maintain hydrostatic pressure through PV without any control, which lead to a mean portal pressure of approximately 18 mmHg whereas pressure HA varied from 40 to 100 mmHg. During the dual hypothermic machine perfusion has been observed that in a few hours HA and PV resistance decrease, consequently, volumetric flow rates increase. This

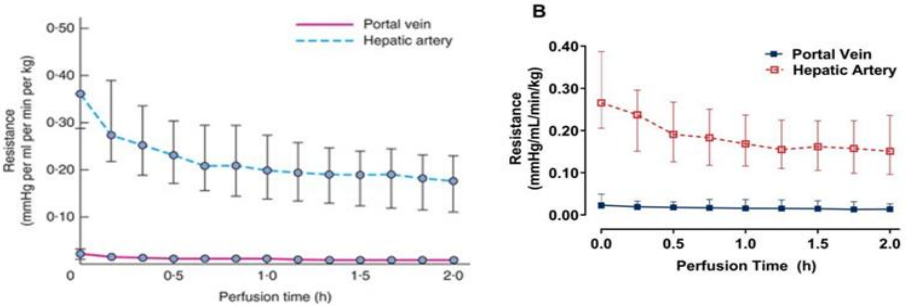

Figure 7.3.1. Time variation of vascular resistance showed in the studies by Groningen's Group [83, 132]. Figure 7.3.1b from [83] reprinted with permission from Copyright Massachusetts Medical Society. Figure 7.3.1from [132] reproduced with License Number 6126390423463

behaviour could be explained by the relaxation of arterial and venous structures and involving micro circulation [132, 143, 147, 148, 149]. Pattern and trends are reported in **Figures 7.3.1 – 4**.

How is explained above, livers undergone HMP before NMP have lower vascular resistance than ones undergone only SCS.

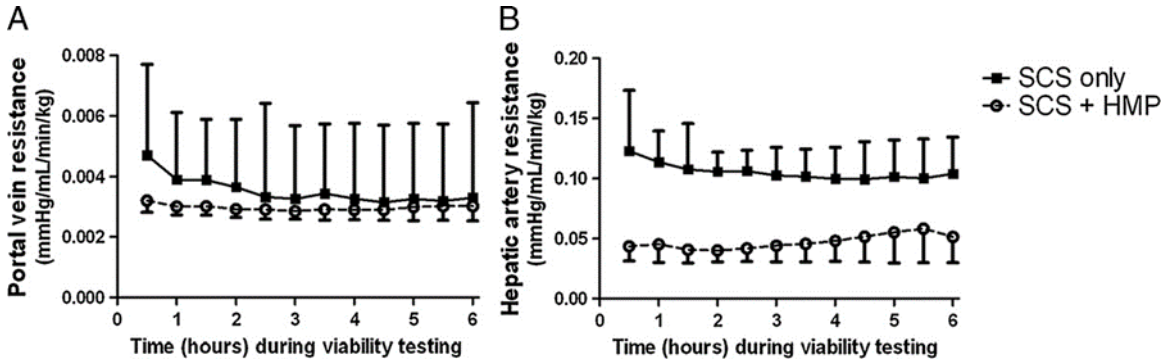

Figure 7.3.2. Vascular resistance patterns in the portal vein and hepatic artery during 6 hours of normothermic machine perfusion (NMP) [183]. During NMP, the vascular resistance in the portal vein and hepatic artery was lower in livers subjected to hypothermic oxygenated machine perfusion (HMP) for the first time than in livers subjected only to static cold storage (SCS); however, these differences were not statistically significant. Reproduced from [183] with License Number 6126391426960.

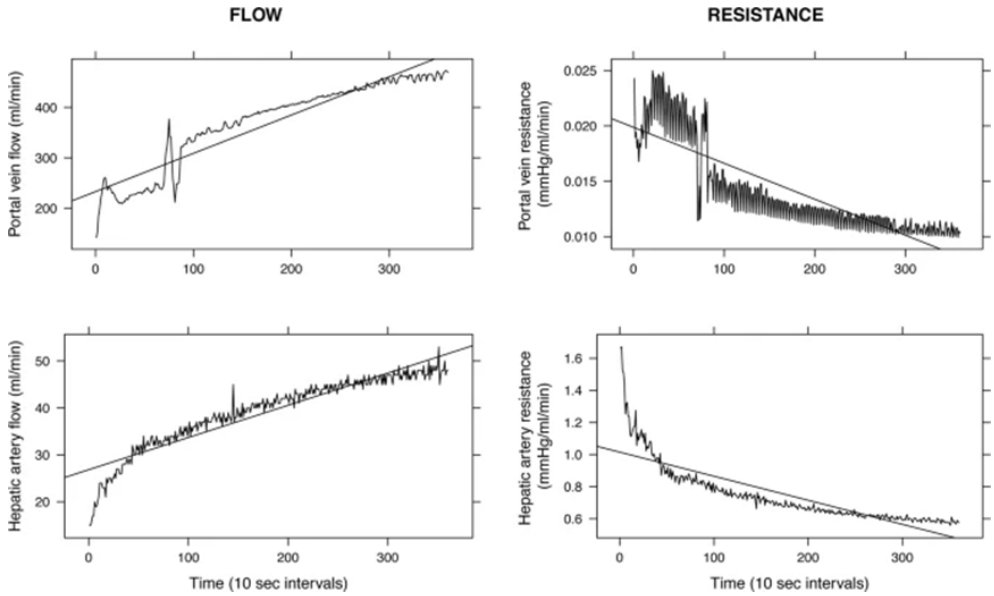

Figure 7.3.3. Time variation of resistances and flows I. Image from [134] reprinted with Creative Commons Attribution 4.0 International License

To evaluate the potential of HOPE in assessing the quality or viability of the graft, Patrono et al. [134] analysed the vascular resistances of the graft during the first hour of perfusion. They measured pressure and flow ml/min and from these obtained the resistance (mmHg min) / ml at the end of the first hour of HOPE [134].

Generally, in literature has been reported that vascular resistance in the hepatic artery and portal vein decrease during perfusion. Moreover, resistance has been calculated simply with an analogy to the Ohm formula expressing resistance in (mmHg min)/(ml) or normalising to liver weight (mmHg min) / (ml kg liver).

Other clinical evidence has been shown by van Rijn et al. [132] and Ravikumar et al [168].

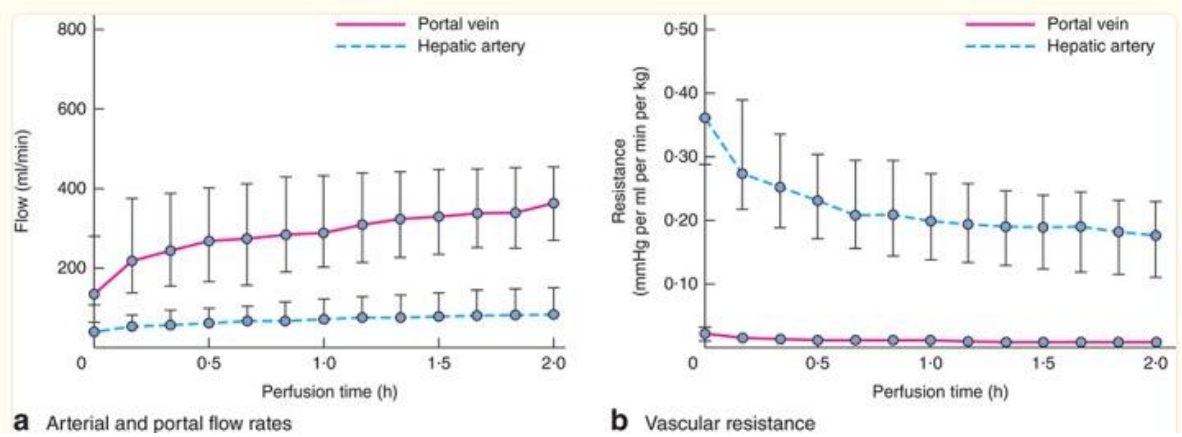

Figure 7.3.4. Time variation of resistances and flows II. Image from [132] reproduced with License Number 6126400707063.

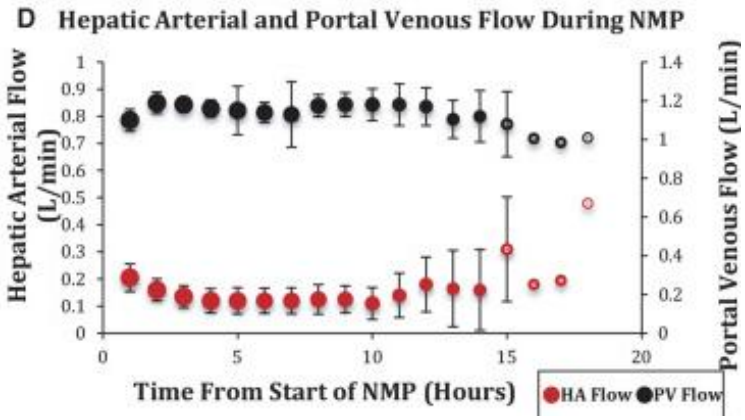

Figure 7.3.5. HA and PV flow during NMP. This image from [168] is reproduced with the Creative Commons Attribution-NonCommercial-No Derivatives License.

Patrono et al. [134] investigated the effects of resistance on AST, ALT, and the onset of EAD. However, their analysis did not confirm any correlation. In contrast, in kidney transplantation, increased renal vascular resistance at the end of hypothermic machine perfusion is a risk factor for delayed transplant function and transplant loss at 1 year, but its predictive value is low [403, 404].

The authors [134] note that patients who did not develop EAD had a significantly greater decline in arterial graft resistance during mechanical perfusion, which suggests that this parameter could potentially play a role in the assessment of graft quality. However, this result should be interpreted with caution and the value of arterial resistance should be evaluated against other well-known parameters of post-LT graft function. Regarding the devices used to measure the flow rate, Imber et al. [268] operated with 2 flow probes Medtronic DP 38P.

7.4 Temperatures

Hypothermic perfusion is carried out in the range of temperatures 4 – 12 °C [48, 93, 181]. Most clinical studies were conducted at 10 °C [97, 130, 83, 131, 132, 50, 6, 58, 164, 165, 34, 134, 166, 135, 111, 136]. In others, studies of hypothermic perfusion are conducted at 4 – 8 °C [161, 156, 75, 163]. Normothermic perfusion is executed at 35 – 37 °C [2, 48]. In machines perfusion there are temperature probes and heat exchangers for temperature control. Post et al. [401] reported that temperature is controlled by a water bath (HMT-200; HETO, Holten, the Netherlands) and thermocouple (C8.B Licox; Integra, Vilvoorde, Belgium). Abudhaise et al. [147] said that hypothermia was maintained between 4 – 8° C using a heat exchanger (Polystat temperature controller, Cole – Parmer UK). Magbagbeola et al. [267] controlled temperature with a thermocouple (Pt100, PreSens Precision Sensing GmbH, 93053 Regensburg, Germany). Nassar et al. [264] used a heat exchanger BioMedicus BioCal 370, Medtronic. Lastly, Imber et al. [268] used a heat exchanger Ecmotherm II HE, Medtronic. In the studies about COR applied in animal liver and kidney perfusion, some researchers [404] started the warming from 10 °C elevating temperatures slowly during ongoing perfusion to, 17 °C, 30 °C and 35 °C after 30, 60, 75 and 90 min, respectively. Other researchers [287] carried out COR starting from 8°C during the first period of perfusion and gradually increasing to 12, 16 and 20°C after 30, 45 and 60 min, respectively. There is no information available about the heat exchanger integrated into commercial devices used in clinical case studies.

7.5 Perfusion Time

The hypothermic perfusion of the liver in some studies lasted for 1 hour [72, 141, 134, 34]. Most clinical studies have been conducted for two hours [97, 83, 130, 131, 132, 183, 50, 178, 135, 111, 136], a duration considered enough to restore mitochondrial activity and ATP levels and to preserve the organs by IRI [97, 83, 172, 177, 183, 184, 188, 185]. Moreover, is shown that after two hours metabolites biomarkers of liver viability such as AST, ALT and LDH reach a steady state after 2 hours [75]. Other researchers conducted hypothermic perfusion for 3 hours [165] or 4 hours [147]. Some research groups carried out perfusion for 4 – 7 hours observing an optimal recovery of hepatic functionality [10, 97, 161, 83, 75, 140, 166]. Generally, hypothermic perfusion has been performed

after some hours of SCS, typically 4 – 6 hours [97, 83, 131, 132], even if De Carlis et al. [166] conducted perfusion after 12 hours of SCS. Likewise, normothermic perfusion has been conducted for more time, from 2.5 up to 22 hours, to evaluate hepatic functionality [37, 100, 101, 275, 141, 57, 60, 168, 165]. In the protocol DHOPE – COR – NMP adopted by van Leeuwen et al. [141] DHOPE was conducted for 1 hour, and COR was operated gradually warming the perfusate of 1 °C every two minutes up to 37°C starting from 8 – 12 °C. Groningen Research Group suggest that 2.5 hours of NMP are enough to determine whether a liver is potentially transplantable [275, 157].

7.6 Metabolites as biomarkers in the perfusate

Machine perfusion is a technique that permits the establishment of a correlation between the biomarkers measured during the perfusion and clinical post-transplantation outcomes parameters [404]. Metabolites generated by the liver are part of the biomarkers. Over the last decade, many metabolites have been studied and measured in the perfusate during perfusion in clinical practice. However, until 2019, no single metabolite had been universally recognized as a definitive parameter for predicting the outcomes of liver transplantation with high accuracy, although several cut-off values were proposed [140, 147, 153, 148, 405]. Generally, clinicians analyse a series of metabolites released in the perfusate as biomarkers for liver damage. Some of these metabolites include lactate, aspartate aminotransferase (AST), alanine aminotransferase (ALT), and lactate dehydrogenase (LDH), γ-glutamyl transferase (GGT), Flavin Mononucleotide (FMN, also known as Mitochondrial Flavin), Nicotine Adenine Dinucleotide reduced (NADH), alpha-glutathione S-transferase (GST), perfusate pH, biliary pH, glucose, bile production and composition, biliary bicarbonate, alkaline phosphatase (ALP), potassium and sodium concentration, and total bilirubin [72, 75, 132, 141, 58, 164, 168, 204, 274, 281]. During NMP hepatobiliary function is tested using the following criteria: lactate <1.7 mmol/L, perfusate pH 7.35 to 7.45, bile production >10 mL, and biliary pH > 7.45 [275, 141]. More specifically, viability criteria for donor liver assessment during the NMP phase are: bile production ≥ 4 mL (or 4 g) by the first hour of NMP and ≥ 10 mL (or 10 g) by 150 minutes of NMP [157, 373], lactate concentration in perfusate is within “normal” values (0.5 – 1.7 mmol/L) by 150 minutes of NMP [275], perfusion fluid pH is within normal values (7.35-7.45) within 150 min of NMP, without the need for repeated addition of NaHCO3 [275], finally biliary pH of > 7.45 within 150 min of NMP [275, 274]. As a result, Groningen Research Group [275, 157, 373, 204] suggested that bile production may be a criterion to identify potentially transplantable ECD livers whereas bile pH, bicarbonate, and glucose as biomarkers of severe bile duct injury. Similar criteria were established by Mergental et al. [33]: perfusate lactate <2.5 mmol/L and sufficient bile production in combination with pH of perfusate >7.3, stable arterial and portal flow and homogeneous graft

perfusion with soft consistency of the parenchyma. In the analysis by de Vries et al. [373] has been pointed out that the criteria used in the study VITTAL (Viability testing and transplantation of marginal livers) on discarded livers in the UK [37, 85] are like the criteria shown above but this one does not include a minimal amount of bile production.

The viability of the liver is considered acceptable for transplantation if all criteria previously listed meet within the first 2.5 h of NMP [183, 275]. If this condition is verified machine perfusion continues and the recipient is brought to the operating room. Quite the opposite, if the liver does not satisfy the predefined viability criteria, machine perfusion is stopped [275]. In most clinical trials metabolites like AST, ALT, LDH, and lactate are measured by collecting every 30 minutes a sample of perfusate [75, 140, 132, 58, 147,]. Guarrera et al. [75, 140] measured them with an Olympus AU 2700 R analyser (Olympus America Inc, Center Valley, PA). Biochemical parameters such as glucose, calcium, lactate, potassium, and sodium have been measured, in a sample of perfusate and blood extracted by perfusion circuit every 30 minutes, with the device as ABL 90 Flex analyser (Radiometer, Brønhøj, Denmark) and Roche P Module (Roche Diagnostics Limited, UK) by many researchers [72, 132, 183, 275, 58, 157, 147]. Xu et al. [397] used a Piccolo blood chemistry analyser (Abaxis, Union City, CA) for the analysis of liver enzymes (AST, ALT, ALP).

Bruinsma et al. [404] determined ALT concentration in the perfusate by assessing the enzymatic conversion of L – alanine by ALT and LDH in a kinetic assay (Infinity Reagent; Thermo Fisher Scientific). Muller, Dutkowski et al. [72] measured in real-time ALT, AST and LDH with the device FujiFilm Dri-CHEm 4000i [72]. Using standard biochemical methods was measured blood gas parameters as pO2, pCO2, sO2, $HCO3^-$ and pH [157]. Watson et al. [274] reported that bile and perfusate gases were analysed using a Cobas b221 benchtop analyser (Roche). Ceresa et al. [406] and Bral et al. [407] rejected livers performing in the perfusate a poor lactate clearance, AST > 2600, ALT > 9000 U/L and shortage or no bile production. Guarrera et al. [140], and Henry and Guarrera [408] proposed to consider that values of AST or ALT > 1000 IU/L in donor serum at the time of organ offer is evidence of important ischemic injury. In the NMP conducted by Ghinolfi et al. [273] the perfusate glucose, transaminases, lactate, interleukin (IL) 6, IL10, tumour necrosis factor α (TNF-α) concentration, and bile production were collected every hour. Moreover, cytokine concentrations were tested after the procedure by enzyme-linked immunosorbent assay sandwich assay and are reported as pg/mL (R&D Systems, Minneapolis, MN). Lastly, Ghinolfi et al. reported that bile pH was measured using a GEM4000 analyser (Instrumentation Laboratory, Bedford, MA). Based upon previous experiences, Watson et al. [128] suggested that an ALT over 200 iu/L would result in the

liver being declined, but latterly perfusion ALTs up to 500 iu/L have been accepted, providing there was no continued rise in ALT between the first and second hour of NMP.

Although lactate, ALT, LDH and AST and other parameters were considered good predictors of hepatic functionality [75, 392], Zurigo's Research Group headed by Philip Dutkowski and Andrea Schlegel suggested that FMN and NADH are more effective to predict outcomes post-LT [72, 164]. Moreover, Xavier et al. [72] and Schlegel et al. [164] carried out the first clinical experience of HOPE monitoring FMN and NADH in real-time with a spectrophotometer along the perfusion circuit. FMN and NADH were determined spectroscopically also by fluorescence in perfusates samples (for NADH there was an excitation at a wavelength of 360 nm, the emission peak of 460 nm whereas for FMN light emission was at a wavelength of 450 nm, with an emission peak at 560 nm (emission between 500 and 600 nm) [72, 164]). Muller, Dutkowski et al. [72] suggested that FMN, in addition to other markers such as nicotine adenine dinucleotide (NAD), succinic acid, inosine monophosphate (IMP), lactate and glucose [72], should be considered as a marker of cellular damage. FMN release serves as a surrogate marker for impaired cellular energy production, as elevated FMN release correlates with ATP breakdown, detectable by increased purine metabolites in the perfusate fluid [72]. The Zurich Research Group points out that the results contrast with the poor predictive value of conventional perfusate parameters such as transaminases or lactate levels that failed to recognise impaired liver function after implantation [72]. Indeed, Guarrera et al [75] observed that lactate levels and LDH increased during perfusion; although this increase is often correlated with increased liver damage, they saw no indication that the levels produced due to mechanical perfusion affected liver function after transplantation [75]. The group led by Xavier and colleagues [72] reported that a high concentration of FMN in the perfusate was correlated with graft loss within 3 months after liver transplantation. The threshold for maximum accuracy in terms of early graft loss was identified at 10000 A.U, i.e., 100 ng FMN/mL perfusate [72]. In conclusion, the Zurich Research Group emphasises the main advantage of measuring the concentration of molecules such as FMN in real-time during mechanical perfusion (MP) allows the opportunity to take advantage of the development of tools for the objective assessment of the metabolic status and degree of injury of an organ before transplantation into the recipient [72, 153, 154]. In this way, an estimate of the future outcome of liver transplantation can be obtained [72]. The technique developed by Muller and Dutkowski in 2019 of estimating the outcome of transplantation may allow the use of liver grafts with greater patient safety.

In the following images, **Figure 7.6.1** and **7.6.2**, are reported ALT, glucose, and lactate measurements by van Rijn et al. [132] and Dutkowski et al. [97].

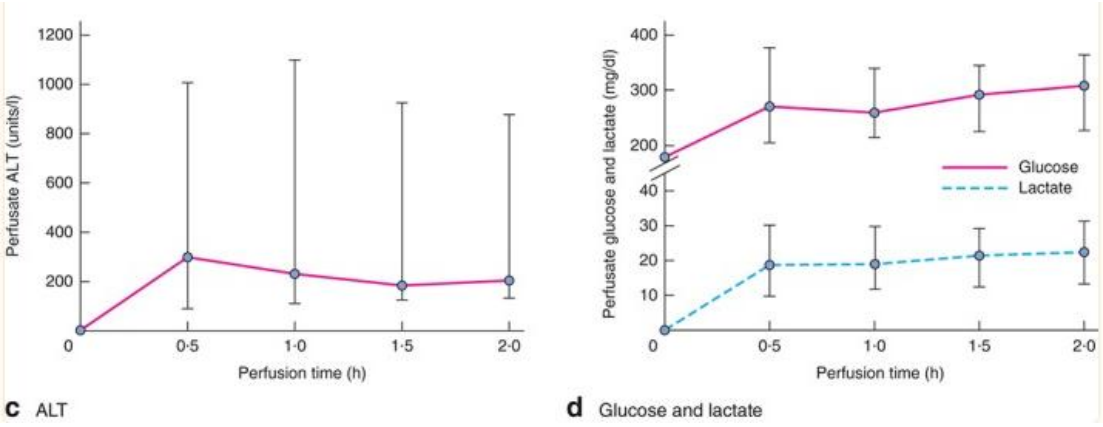

Figure 7.6.1. Perfusion parameters during DHOPE [132]. Image from [132] reproduced with License Number 6126400707063.

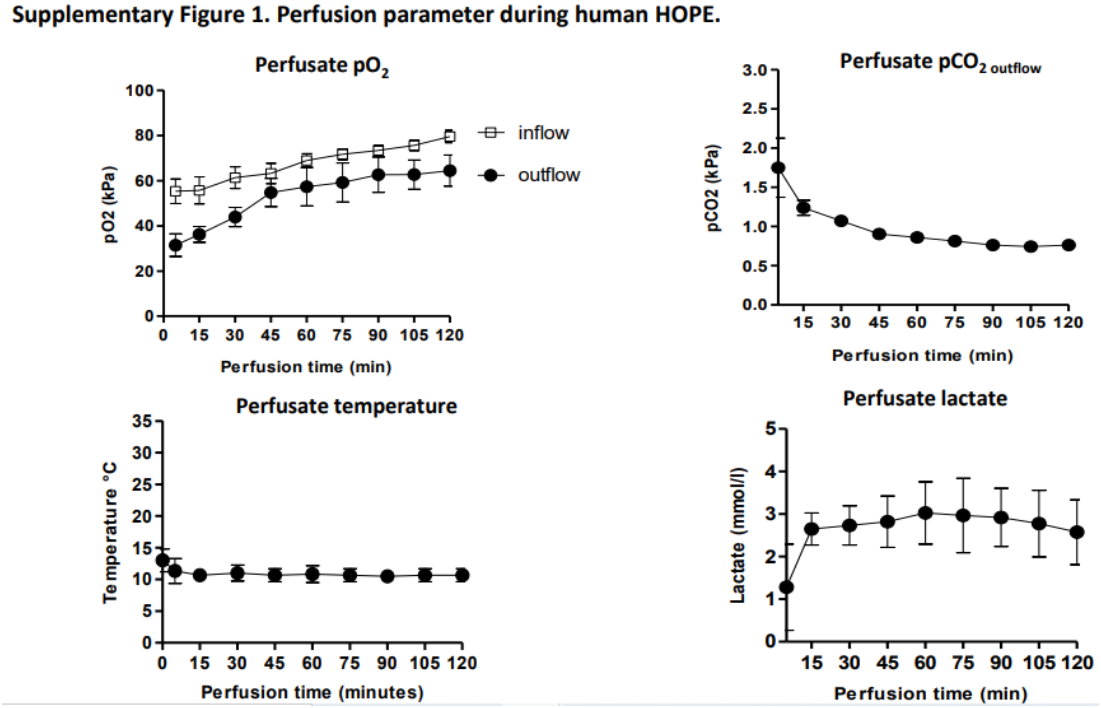

Figure 7.6.2. Perfusion parameters during HOPE [97]. Image from [97] reproduced with License Number 6126410652767.

Bardallo et al. [63] focused on the effect of ischaemic reperfusion injury during HOPE by concentrating on the effects on mitochondrial respiration. They performed perfusion with UW, HTK and IGL-2 solutions and proposed the following as markers for HOPE, i.e., indicators of successful cold oxygenated HOPE perfusion: glutamate dehydrogenase (GLDH) and mitochondrial aldehyde dehydrogenase-2 (ALDH2) best known for its detoxifying role in hepatic alcohol metabolism. Bardallo et al. also chose ALDH2 as there is growing evidence that it also plays a role in IRI through the prevention of oxidative stress processes caused by oxygen-free radicals [231]. In the same study, they suggested that itaconic acid, succinate and FMN should also be considered as markers as they

play a significant role in determining graft viability after revascularisation [63]. Although the release of mitochondrial flavin mononucleotide in perfusate has been correlated with liver function after transplantation [72], it is not known whether this also predicts the risk of cholangiopathy [83].

Guy et al. [153] for the first time employed proto-nuclear magnetic resonance spectroscopy to analyse kidney perfusate fluid to detect, and identify metabolites that may have prognostic or therapeutic value [409]. A study conducted by Liu et al. [409] on pig livers under hypothermic perfusion focused on what markers could be used to establish organ viability before transplantation by analysing the composition of the perfusate. The authors took perfusate samples during the 4-hour hypothermic perfusion. AST in the perfusate was measured using a standard spectrophotometric technique. Using proton magnetic resonance spectroscopy (1H MRS) they measured the amounts of lactate, alanine, and histidine. The authors reported that AST, alanine, and histidine were sensitive discriminators of warm ischaemic damage after 4 hours of HMP, while lactate showed only a trend but no significant difference. Several studies used proton magnetic resonance spectroscopy (1H MRS) to identify the biochemical composition of different biological fluids to assess graft function during reperfusion after HMP by analysing compounds in perfusate in isolated perfused pig kidneys and rat livers [398].

The search for and definition of clinically relevant biomarkers to quantify hepatic IRI, EAD and biliary complications during MP is continuously evolving [207]. The perfusion process allows the assessment of biomarkers in real-time, which further increases their relevance and impact in clinical use [207]. It is likely that a combination of perfusate and bile biomarkers will allow a superior assessment of the overall function of the donor’s livers. The challenge in the field of transplantation is to interpret the significance of biomarkers for a particular donor’s liver use and how they might predict immediate and long-term post-transplant outcomes of the graft [207]. Dutkowski's and Schlegel's experience suggests that soon, spectrophotometers will be installed in perfusion machines, which will allow to obtaining measurements of concentration of key biomarkers in real-time. This information will be invaluable and will guide physicians to a more detailed assessment with a reduced margin of error.

7.7 Perfusion Machines

Today, there are many machines available in the market or used in clinical experiments for liver preservation and transplantation. Currently, the most used devices are the Liver Assist (Organ Assist, Groningen, the Netherlands) [33, 83, 131, 132, 183, 141, 6, 58, 273, 165, 34, 134, 54, 72, 166,

135, 136, 179, 274], followed by OrganOx *metra* (OrganOx Ltd., Oxford, UK) [57, 168, 210, 406], OCS™ Liver System (Transmedics, Andover, Massachusetts) [117], Cleveland NMP circuit (Cleveland Clinic, Cleveland, Ohio) [410, 411] (not commercialised yet), modified Medtronic Portable Bypass System (PBS) [161, 75, 140], VitaSmart Liver Machine Perfusion System (Bridge to Life) and other devices not commercialised [163, 397, 267]. Principle of working of modern machines perfusion is keeping a liver metabolically active for several hours, so the machine has mimic the human body to maintain a physiologic environment for the liver [5]. A representation is in **Figure 7.7.1**.

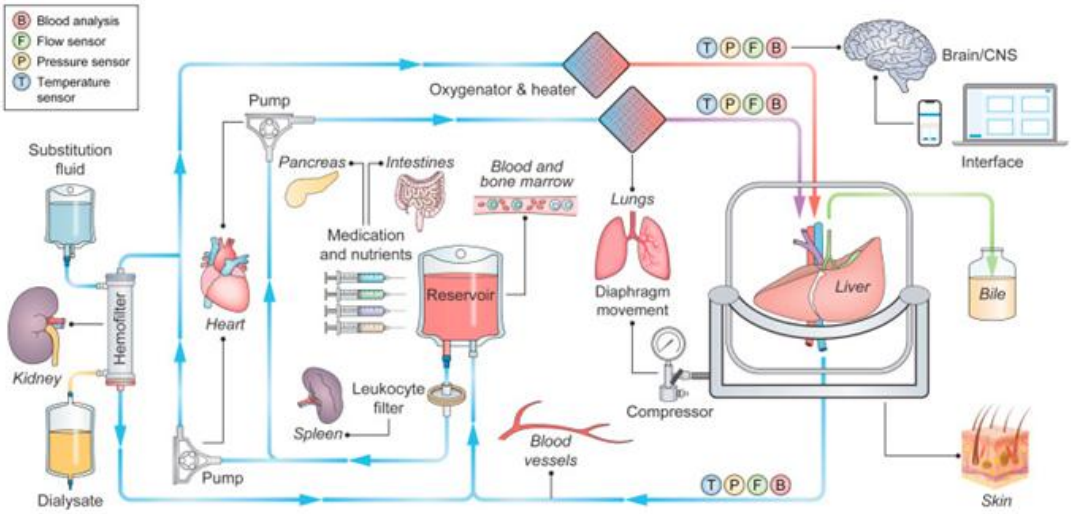

Figure 7.7.1. Schematic and intuitive representation of how machine perfusion may potentially recreate a physiological–human environment to preserve alive a liver or another organ [5]. Image from [5] reproduced with Creative Commons CC-BY license.

The first modern clinical series of liver hypothermic perfusion was carried out by Guarrera et al. in 2010 [75]. In this trial, researchers perfused livers with the device Medtronic Portable Bypass System (PBS) for ex vivo circulation (**Figure 7.7.2)**. Henry et al. [123] in 2012 and Guarrera et al. in 2015 [140] later used and described by other [161, 193]. This perfusion device consists of a stainless-steel tank, a centrifugal pump (non-pulsatile), a heat exchanger and is not equipped with an oxygenator [161, 75, 140, 193]. Vasosol® solution (Preservation Solutions Inc., Elkhorn, WI) was used, with the addition of antioxidants, metabolic substrates, and vasodilators without providing active oxygenation through the portal vein and hepatic artery. The intrahepatic vena cava was blocked with a small vascular clamp to direct the effluent from the liver out of the suprahepatic vena cava [75]. The fluid collected in the basin that housed the organ keeps it at a low temperature. Indeed, he organ cassette does not require cooling, and hypothermia is maintained endothermically with partial

submersion in the basin of cold effluent. A tube connected to the basin collected the perfused fluid to send it back to the circulation pump and heat exchanger.

Later, Dutkowski et al. [97, 130] conducted HOPE using the ECOPS device (Organ Assist®). Limited information is available in the papers written by Zurigo's Research Group about the electro – mechanical components of this machine. The ECOPS device was the first device used to perform HOPE oxygen perfusion [273]. Dutkowski et al. [97] perfused the liver only through the portal vein. The device has a single pump that allows recirculation of the cooled and oxygenated perfusion solution by means of a membrane oxygenator.

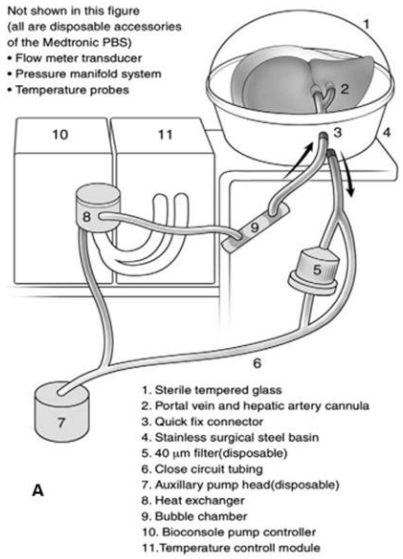

Figure 7.7.2. The Medtronic PBS® used by Guarrera et al. [75] to perform clinical hypothermic machine perfusion.This image from [193] is reproduced with the License Number 6126421073568.

The first studies employing dual mechanical oxygenated DHOPE perfusion with the Liver Assist device (Organ Assist, Groningen, The Netherlands)) are by De Carlis et al. [165] and van Rijn et al. [132]. It was later successfully employed by the Groningen group for liver perfusion [83, 131, 132, 183, 141, 58, 192], the Zurich group [34, 72, 179] and other researchers [50, 6, 165, 134, 54, 166, 136]. The Liver Assist device has also been used to do single perfusion, as done by Dutkowski and his research group [34, 72], Czigany et al. [50], Patrono et al. [134] and others [135, 136]. The device consists of a hepatic artery perfusion unit, a portal vein perfusion unit, and a thermal unit. The hepatic artery and portal vein perfusion circuits are independent, and each is equipped with a centrifugal pump, oxygenator/heat exchanger and antibacterial filter (32 μm) [193]. The donor's liver

is placed in the protective box on the meshwork above the perfusate reservoir. Pumps on each circuit pump the perfusate from the collection reservoir; the hepatic artery pump generates a pulsatile flow of 60 bpm (beats per minute or 1Hz) [83, 132, 51, 58], while the portal vein pump generates a continuous flow. The Liver Assist pump is pressure-controlled. The delivery from each pump is sent into a hollow-fibre membrane oxygenator where the perfusion fluid is oxygenated and its temperature is regulated in the hollow-fibre oxygenator/heat exchanger, after which it passes through the bacterial filter to flow back into the hepatic artery and portal vein. The liver is perfused through the celiac artery or hepatic artery and portal vein, particularly during normothermic perfusion [274, 275, 57, 137]. The inferior vena cava is left open and drains into the reservoir. Thus, the perfused fluid enters through the portal vein and hepatic artery and exits through the inferior vena cava [104, 51, 193, 196]. The cystic duct is ligated, and the common bile duct is catheterised. Target pressures in the hepatic artery and portal vein are 60 mmHg and 8 mmHg, respectively [195]. The thermal unit detects and controls the temperature of the perfusate in the oxygenator-heat exchanger units, allowing perfusion in hypothermic, sub-normothermic or normothermic mode. The temperature settings are not fixed and can be changed manually by the user via the control display [51]. Temperatures, flow rates and pressures are shown in the display in real-time [51]. Since the device is not transportable, like the ECOPS, the livers are stored statically cold from the procurement centre for transport to the transplant centre before being placed on the device. The manufacturer's manual recommends a maximum perfusion duration of 6 hours [136]. Further information and details on Liver Assist can be found on the manufacturer's website [412]. Some recent pioneering studies [413, 414] conducted at the dissertation level evaluated the use of non-invasive imaging techniques, such as computed tomography (CT) or magnetic resonance imaging (MRI), during Liver Assist perfusion as an additional tool for assessing the general state of the liver before transplantation.

Both the Liver Assist device and the Metra device (OrganOx, Oxford, UK), shown in **Figure 7.7.3a** and **7.7.3b**, have been widely used for normothermic perfusion, although other machines have also been used in recent years. Metra (OrganOx, Oxford, UK) is a perfusion device developed to perform only normothermic perfusion. This device, unlike Liver Assist, can be used to transport grafts from a donor hospital to a transplant centre while continuously performing mechanical perfusion [51, 193]. Metra performs double perfusion and active drainage using a normothermic suspension of red blood cells in a colloid to perfuse the liver [155]: basically, the device performs perfusion at physiological temperatures and pressures using oxygenated blood to which drugs and nutrients are added [413]. In addition to cannulation of the portal vein, the celiac trunk and the bile duct, closure of the suprahepatic inferior vena cava with a linear suture and cannulation of the intrahepatic inferior vena cava [51, 193] are also performed on the back table. The perfusate is pumped directly from the

inferior vena cava by a single centrifugal pump and then passes through an oxygenator/heat exchanger. Part of the perfusate is sent to the soft-shell reservoir for perfusion of the portal vein and part of the perfusate is directed directly to the hepatic artery. This device allows perfusion at physiological pressures [51]. The system is designed to perfuse a liver for up to 24 hours [51]. The hepatic artery is perfused by the driving force of the pump, while the portal vein is perfused at constant pressure from the reservoir. Continuous infusions ensure sufficient vasodilatation, protection against coagulation and the provision of an environment that allows metabolic and synthetic liver function under almost physiological conditions [155, 413]. The OrganOx Metra assesses donor liver function by allowing surgeons to monitor markers such as lactate clearance in the perfusate, perfusate pH, transaminase levels, glucose metabolism and bile pH [413]. In addition, the machine automatically monitors the temperature, perfusion pressure, and perfusion rate [51, 193]. Finally, it constantly performs haemogasanalysis to monitor and control pO2 and pCO2 levels, facilitating the maintenance of acid-base homeostasis [155]. Hepatic artery pressure can vary from 60 to 75 mmHg, and inferior vena cava pressure from 1 to 2 mmHg [195]. Portal flow is measured continuously, but portal pressure is not [195]. The operating conditions of the perfusate are 37 degrees centigrade, a pO2 of 12 kPa (partial pressure of oxygen in a hypothetical gas phase in equilibrium with dissolved oxygen in the blood, my interpretation), a pCO2 of 5 kPa and a pH of 7.35 [195]. Watson et al. [274] reports that the oxygen pressure in the perfusate varies between 90 and 150 mmHg (12 and 20 kPa). Compared to static cold storage, Metra was associated with a 50% reduction in transplant damage, as measured by a 50% reduction in peak AST during the 7 days following liver transplantation. This was despite a 54% increase in storage time [413]. Metra can be used in two modes: transport mode (continuous NMP) or back-to-base mode (NMP following static cold storage) offering transplant centres maximum flexibility of use [413]. In a randomised trial, compared to static cold storage, Metra reduced early allograft dysfunction by 74%, while peak serum levels of AST, a predictive biomarker for transplant and patient survival, were 49% and 73% lower during the first 7 days post-transplant for all transplanted livers and transplanted DCD (donation after circulatory death) livers, respectively [413]. Recent studies [46] have evaluated the cost-benefit or cost-effectiveness (translated from cost-utility) associated with the use of normothermic perfusion devices, such as the OrganOx metra, compared to the cost-benefit associated with those who received an organ preserved by static cold storage SCS, concluding that although the use of perfusion machines increases costs, benefits in terms of lives saved are far greater [46, 101].

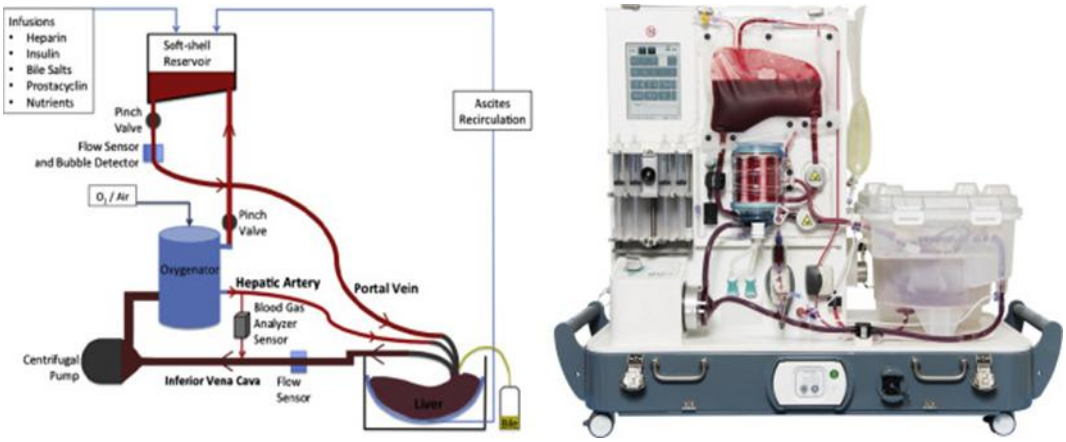

Figure 7.7.3a. A photograph (on right) and schematic drawing (on left) of the OrganOx Metra mobile perfusion device reported by [51]. Figure 7.7.3a (left), from [155] is reproduced with Creative Commons Attribution 4.0 International License. Figure 7.7.3b from [193] is reproduced with License Number 6126430959909.

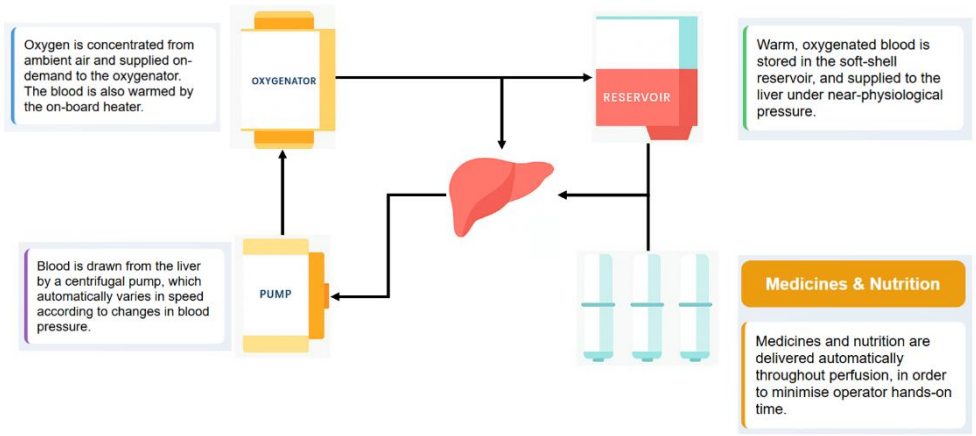

Figure 7.7.3b. The map of OrganOx Metra. Image adapted by [413] and original source: https://hitconsultant.net/2023/07/17/organox-liver-transplantation-device-funding/.

Another device used for liver perfusion is the OCS™ Liver System (Transmedics, Andover, Massachusetts), depicted in **Figure 7.7.4**, used by Markmann et al. in 2022 [117] and 2021 [415]. This device is transportable, like the Metra device, and enables normothermic perfusion of the liver. The OCS Liver consists of an integrated system of 3 components: the OCS Liver console, the OCS Liver perfusion set and the OCS bile salt solution for infusion (Figure xx). The Liver Console is the reusable, non-sterile portable base unit for the OCS Liver System that includes the Wireless Monitor, fluid pumping subsystems (SDS and Circulatory (Pulsatile) Pump), probes, gas cylinder, power

subsystem (including batteries), SD Data Card, Mobile Base, and electronics and software. The Wireless Monitor displays perfusion parameters and system status and allows the user to adjust specific system settings during the transport of the donor's liver. The Liver Console provides a rigid compartment to house and protects the Liver Perfusion Module (LvPM) during transport [416]. The LvPS consists of the Liver Perfusion Module (LvPM) and the disposable LvPS Accessories. The LvPM is a sterile, single-use device that holds, protects, maintains, and supports the liver during preservation and transport. The LvPM encompasses the perfusate and organ-contacting components and interfaces with the Liver Console. The LvPM contains the organ chamber and the perfusion circuit, provides a physical conduit to circulate and oxygenate perfusate, incorporates various sensors, pumps for the perfusate, and provides mechanical and electrical interconnects with the Liver Console. The Wireless Monitor allows the user to observe measurements made within the LvPM. The LvPS also includes the sterile, disposable accessories necessary to instrument the liver and manage the addition and removal of perfusate [416]. The Liver OCS device maintains the donor liver in a non-ischaemic and metabolically active state by allowing perfusion of both the portal venous and hepatic arterial circulation with a warm, oxygenated and nutrient-enriched blood perfusate. The OCS Liver can deliver a pulsatile high-pressure flow rate to the hepatic arterial circulation and simultaneously deliver a high flow rate at low pressure to the portal circulation with a single perfusion pump, giving the user full control over perfusion parameters.

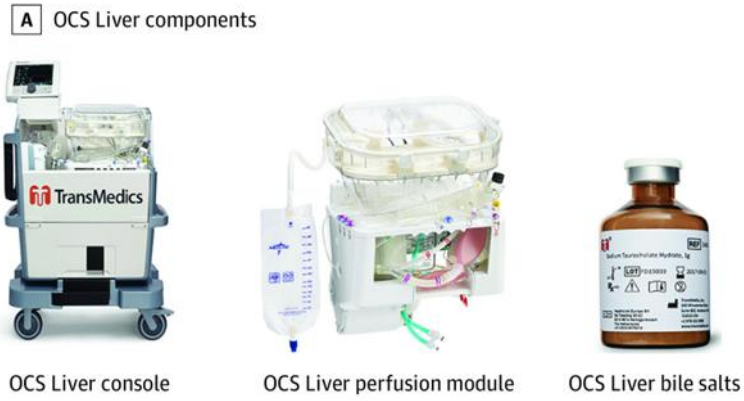

Figure 7.7.4. The Liver OCS device is loaded with an electrolyte solution containing albumin, concentrated red blood cells, and antibiotics and supplemented with a continuous infusion of a 4% amino acid and 10% dextrose nutrient solution, supplemented with insulin and multivitamins. Perfusion is gradually increased to a total flow of 2.0 to 2.5 L and the temperature was set at 34 °C. Haemodynamic parameters of liver perfusion are continuously monitored and recorded during storage. Serial blood gas and lactate levels were measured during storage and changes in lactate level were used to measure the adequacy of perfusion [117]. This figure from [117] is reproduced with the CC-BY license.

More information on OCS™ Liver System Transmedics is available at the company's website [416].

Another normothermic perfusion machine will be marketed by the Cleveland Clinic (Cleveland, Ohio), shown in **Figure 7.7.5**, called the Cleveland NMP circuit used in clinical trials [410]. The liver perfusion circuit consists of a Maquet centrifugal pump, a hard-shell venous reservoir, a heater, an oxygenator, and an organ receptacle [195, 410]. The circuit has a bifurcation at the outlet of the oxygenator for the infusion of the portal vein and the hepatic artery [410]. There is a C-clamp in both the venous and arterial circulation tubes to adjust the flow rates [195]. The Cleveland NMP circuit is a transportable device that has been used in clinical studies [410] but is not yet commercially available [195].

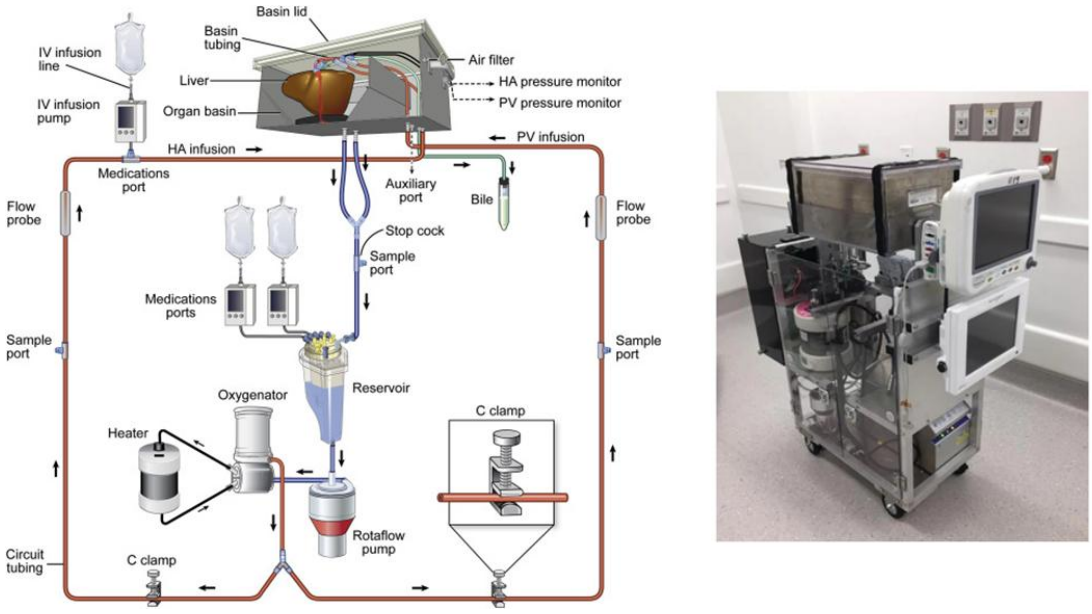

Figure 7.7.5. Diagram of the perfusion device of the Cleveland Clinic's normothermic machine [195, 410]. Figure 7.7.5 (left), from [410], is reprinted with License Number 6126510871874. Figure 7.7.5 (right), from [195], is reprinted with License Number 6126511143696.

In 2006, the Groningen group [392] presented a prototype for hypothermic liver perfusion that they called the Groningen Hypothermic Liver Perfusion Pump, **Figure 7.7.6**. The study focused on the perfusion of pig livers. The device consists of a reservoir in which the liver is placed, two miniaturised centrifugal pumps (Deltastream DPII, MEDOS Medizintechnik AG, Stolberg, Germany)

that deliver continuous and pulsatile flow respectively, a miniaturised hollow-fibre membrane oxygenator (HILITE 800LT, MEDOS Medizintechnik AG, Stolberg, Germany), an oxygen cylinder, a battery pack and a measurement and control unit connected to an interface [392]. The pulsatile pump directs the storage solution (UW - MP) from the reservoir through the oxygenator and into the hepatic artery; the continuous pump perfuses the portal vein without oxygenation. Both pumps are pressure-controlled and recirculate the storage solution with a constant perfusion pressure [392]. The sterile disposable unit of the Groningen Hypothermic Liver Perfusion Pump, comprising the reservoir, pump heads, oxygenator, cannulas and tubing, is located inside a polystyrene cooling box (Wolters kunststoffen, Enter, The Netherlands) filled with melting ice to ensure a hypothermic temperature of 0-4°C for more than 24 hours [392]. To illustrate the process, a schematic representation is shown below. This machine [392] is similar to the previously presented configurations.

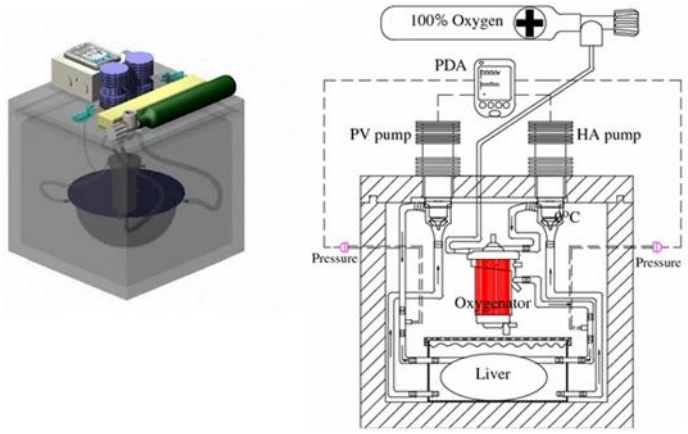

Figure 7.7.6. Diagram of the Groningen Hypothermic Liver Perfusion Pump [392]. This Figure, from [392], is reproduced with License Number 6126511248585.

In 2018, Ravaioli and collaborators [417] and again in 2020 [163] successfully conducted the perfusion of livers and kidneys using a new perfusion machine developed by the company Medica S.p.A. and Centro Iperbarico srl under the guidance of the Italian research group [417]. The device allows perfusion using a pulsatile flow of the perfusate using three peristaltic pumps, each driven by a single motor with the dual purpose of perfusing the organ with the preservation solution and, at the same time, maintaining the constant circulation of the liquid around the organ inside the hyperbaric chamber. The first pump, used only in hyperbaric treatments, breaks the gas-liquid interface, facilitating the diffusion of the compressed gaseous mixture into the preservation solution. The second and third peristaltic pumps are used to perfuse the organ through suction and discharge tubes connected to the organ's blood vessels. The organ is connected via cannulated vascular access with sterile tubing (PVC and silicone) to the machine. The flow and pressure values during perfusion are

evaluated via special sensors, self-regulated and displayed on the device's screen in real-time. To oxygenate organs during perfusion, a membrane oxygenator integrated into the perfusion circuit can be used to supply oxygen to the storage fluid (normobaric oxygenation) or a pressurised chamber where the graft is placed during treatment (hyperbaric oxygenation). To perform normobaric oxygenation, a tube system is used that supplies oxygen to the organ's preservation fluid. This is a hollow-fibre microporous membrane oxygenator consisting of a gas exchange module with an integrated heat exchanger. The device, supplied as disposable and sterile with ethylene oxide, is intended for use in an extracorporeal perfusion circuit to oxygenate and remove carbon dioxide from the fluid during routine perfusion procedures for up to six hours. In addition, the device consists of a pressurisable ('hyperbaric') chamber designed to accommodate the organ completely submerged in the preservation solution. The chamber is compressed with a mixture of medical oxygen (95 per cent) and carbon dioxide (5 per cent) to a pressure above atmospheric pressure. The minimum partial pressure of oxygen (pO2) was inversely proportional to the normalised flow (mL/ (min gorgon)); the device allows pressurisation of up to 200 kilopascals by a certified medical gas cylinder. A special reducer, certified for use with medical oxygen, reduces the gas pressure. The mixture is dissolved in the storage solution at a concentration directly proportional to the pressure exerted by the gas at the gas-liquid interface (Henry's law). The hyperbaric chamber is placed inside a thermal conditioning unit, which can be powered from 12 up to 220 volts [417]. Previously in 2012 Giannone and co-workers [418], in collaboration with the same "Centro Iperbarico srl" (Ravenna, Italy) performed rat liver perfusion using an innovative Hyperbaric Hypothermic Perfusion Machine (HHMP). The HHMP was designed to be easily transported by two people allowing the possibility to start the procedure immediately after procurement and not only in the recipient's transplant centre [418]: this is an important strength compared to the use of other more complicated HMP devices.

The use of the portable Organ Recovery Systems LifePort Liver Transporter device, **Figure 7.7.7**, that enables dual hypothermic perfusion of the liver has also been mentioned in the literature [414], although no clinical trials on the use of this device have been recorded until 2022 [419], but only in animal organs [143] or on discarded human livers [147]. The manufacturer's website states that its use on a clinical level in Europe and the United States has not yet been approved although some preliminary studies have been carried out [420]. More information on the functionality of this machine is available in the study [421].

Figure 7.7.7. Image of the Organ Recovery Systems LifePort Liver Transporter. This Figure, from [414], is reprinted with License Number 6126520137864.

Debbaut et al. [399] developed an electrical model that mimicked blood flow in the human liver. Subsequently, Debbaut et al. [421] validated and calibrated the electrical model of the human liver using data from a human liver subjected to HMP using the Organ Recovery Systems perfusion machine, in Zaventem, Belgium.

Recently, the Zurich group [3, 197] reported that they tested a new normothermic liver perfusion machine, which is not yet commercially available, the Wyss Machine for the Liver4Life project developed by the Wyss Zurich Translational Center (Wyss Zurich), **Figure 7.7.8**, (https://www.wysszurich.ch/).

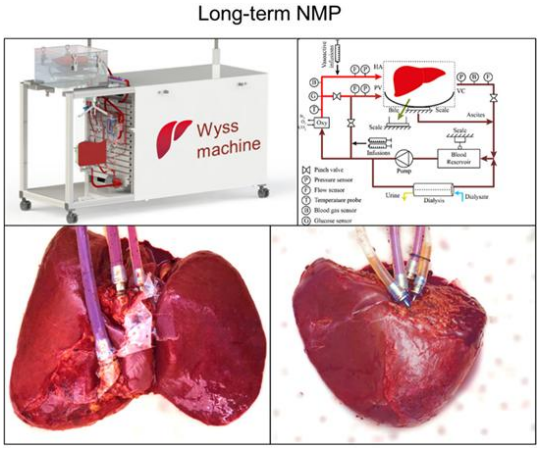

Figure 7.7.8. The long-term normothermic (NMP) liver perfusion machine is shown in the left panel. The top left image illustrates the Wyss machine with the perfusion diagram on the right. The whole and partially perfused human liver are shown below [3]. This Figure is reprinted with License Number 6126520449436.

The Zurich group has used it to achieve long-term normothermic perfusion, reaching up to 10 days so far [197]. Long-term normothermic perfusion thus provides a platform not only for extended

viability assessment but also for the application of several new therapeutic options, in particular ex-situ liver regeneration [3].

To ensure trouble-free physiological operation, the equipment had to be monitored and controlled by elaborate software [3]. This machine, which is significantly more complex than standard devices available on the market, is the first to enable the most successful long-term normothermic perfusion of human livers to date due to its ability to mimic the physiological conditions of the human body [3, 197], automatically controlling glucose levels by injecting insulin and glucagon, removing waste products using a dialysis membrane, and regulating oxygenation and movement of the liver to prevent pressure necrosis [197]. In general, normothermic perfusion requires cannulation of all vessels and the bile duct, while pressure and flow control are provided by standard sensors. In contrast, long-term perfusion requires additional individual and automated control of flow and pressure for each connected vessel to prevent hypo- or hyperperfusion with local ischaemia or perivascular bleeding, respectively [3]. However, not only the flow parameters but also the quality of the perfusate, in this case, the blood-based perfusate, must be constantly monitored and adjusted [3].

The Zurich group reports that liver cannulation takes place via the portal vein and hepatic artery for incoming flow, and via the vena cava for outgoing flow: the hepatic artery receives oxygen-rich blood at high pressure (mean arterial pressure (MAP) $\geq$ 65 mmHg) in a pulsatile manner, whereas the portal vein receives low-pressure blood (approximately 5-10 mmHg) with reduced oxygen content (venous blood, non-pulsatile) [197]. The system maintains the oxygen saturation of 65% in the vena cava by continuously adjusting the oxygen content in the portal vein. The device mimics the physiological transport of nutrients and bile salts in the liver through the portal vein using a nutrient injection of ursodeoxycholic acid conducted through the portal vein during perfusion [197]. The haemodynamic of the hepatic artery is tightly controlled by the automated infusion of vasoconstrictors and vasodilators into the hepatic artery line. The pressure in the vena cava is continuously maintained at physiological levels close to 0 mmHg (0-2 mmHg) to prevent hepatic congestion. An oxygenator supplies oxygen to the hepatic artery and portal vein while removing CO2 from the perfusate. The oxygen tension in the hepatic artery is continuously monitored and controlled to remain within predefined limits, i.e., 10-12 kPa. The CO_2 tension is adjusted via the oxygenator to maintain the blood pH between 7.25 and 7.45. There is an integrated dialysis unit for physiological electrolyte balance and removal of metabolic waste products from the blood. An algorithm automatically regulates the flow of the dialysate by monitoring the red blood cell concentration (haematocrit) based on continuous measurements. Automated insulin and glucagon are administered automatically to maintain physiological blood glucose levels (targeted range of 3.5-6.5 mmol/l) in response to

continuous glucose measurements. The continuous movement of the liver, in an attempt to mimic the oscillations of the diaphragm, is also integrated into the system. The perfusion machine is fully automated, obviating the need for constant staff presence [197]. Finally, the researchers list the performance differences of the Wyss machine compared to other commercially available machines. Additional information are reported in **Figure 7.7.9**.

	Commercial perfusion machines	LIVER4LIFE Long term perfusion machine	
Liver chamber	X	X	Safe liver storage
Pump Continuous flow in PV Pulsatile flow in HA	 X X	 X X	Wave and pulse shape of flow and pressure of commercial machines not reported
Pressure/flow sensors HA PV Vena cava	 X X X	 X X X	Continuous pressure and flow monitoring
Oxygenator Gas supply Heat exchange Individual gas-supply for pH control in blood	 X X	 X X X	pH control with individual O_2, N_2, and CO_2 gas supply to oxygenator
Blood gas analysis HA PV Vena cava	X	 X X X	Monitoring of blood gases and other critical parameters during long term perfusion
Physiologic PV saturation with one oxygenator		X	Prevention of hyperoxygenation Reduction of vasoconstriction
Online glucose sensor		X	Real-time glucose monitoring
Feedback controlled infusions Insulin/glucagon		X	Automated correction of blood glucose level within predefined limits
Feedback controlled dialysis system		X	Metabolic waste removal Acid-base balance Control of sodium & electrolytes Hematocrit control
Liver movement		X	Prevention of pressure necrosis
Continuous response evaluation to vasoactiva, insulin and glucagon		X	Continuous viability assessment

Figure 7.7.9. Performance of the Wyss machine [197].
This Figure is reprinted with License Number 6126520593698.

Shen and Yan [88] presented a paper in which they designed an economical hypothermic perfusion system, shown in **Figure 7.7.10**. The main design strategy consists of the washout of metabolic waste and replenishment of metabolic substrates using mechanical devices, such as compressors and peristaltic pumps. To maintain an adequate organ environment, the necessary physiological parameters in the designed HMP system are monitored in real-time, including storage space temperature, solution pH level, perfusion pressure and flow resistance. Compared to classical HMP devices, several significant advantages can be achieved: automation, monitoring of multiple parameters and low cost of the application. In particular, the flow of the artery solution is pulsed with a human heart rate, which mimics the law of blood flow and provides a more human-like living

environment, to prolong the survival time of the removed organs. In addition, modified Bayes estimation and Fuzzy-PID improve the accuracy of thermal control of current HMP devices. The designed device allows for the perfusion of several organs. The device they created is a hypothermic machine perfusion system to prolong the survival of isolated organs. Four elements are involved in this system, including a machine perfusion system, sensor monitoring, thermostatic control and an oxygenation apparatus. The result demonstrates the satisfactory performance of real-time monitoring of the viability of isolated organs. In addition, a modified two-order Bayes estimation is realised, which introduces the concept of an enhancement factor to mitigate possible errors resulting from sensor faults and noise interference. Compared to the conventional PID controller, the accuracy is improved and the calculation cost is reduced. Experiments have also shown that dynamic properties are related to external temperature, while static properties are mainly dependent to some extent on flow conditions.

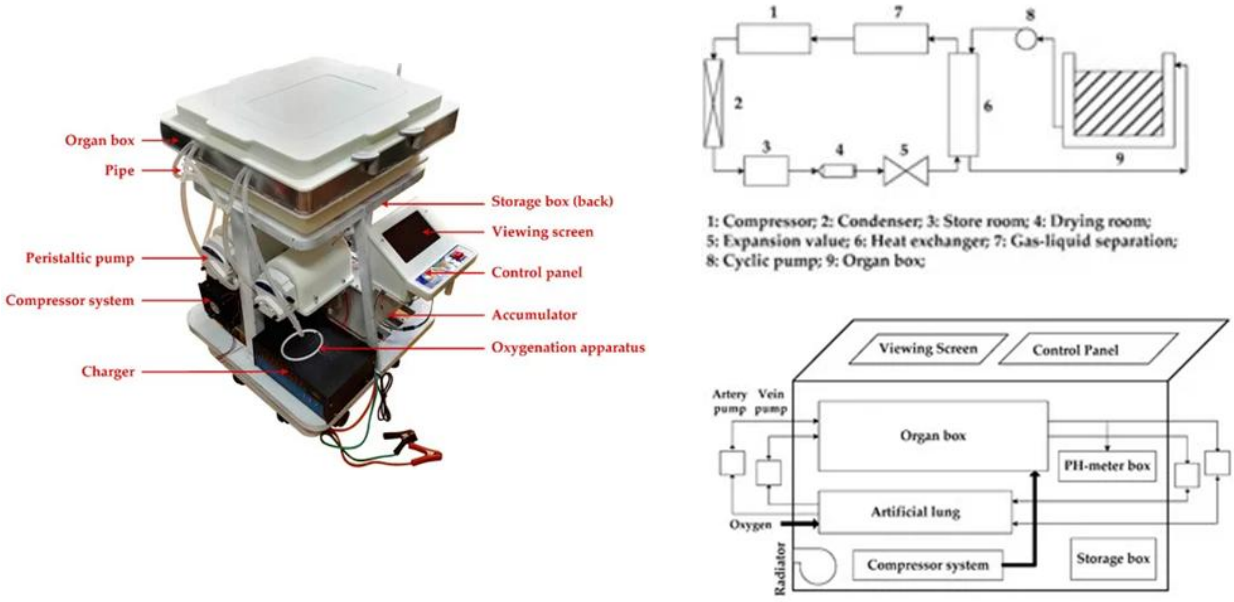

Figure 7.7.10. Diagram and schematic of machine presented by Shen and Yan [88].
These images are used under Creative Commons CC BY 4.0 license.

In literature, there are many other schemes of perfusion circuits, but these are mostly inexpensive home-built machines for the perfusion of animal organs [194, 264]. Magbagbeola et al. [267] present a novel, low-cost, organ perfusion machine designed for use in research, especially for porcine liver perfusion. In **Figure 7.7.11**, is reported a detailed description of this machine made by Magbagbeola et al. [267].

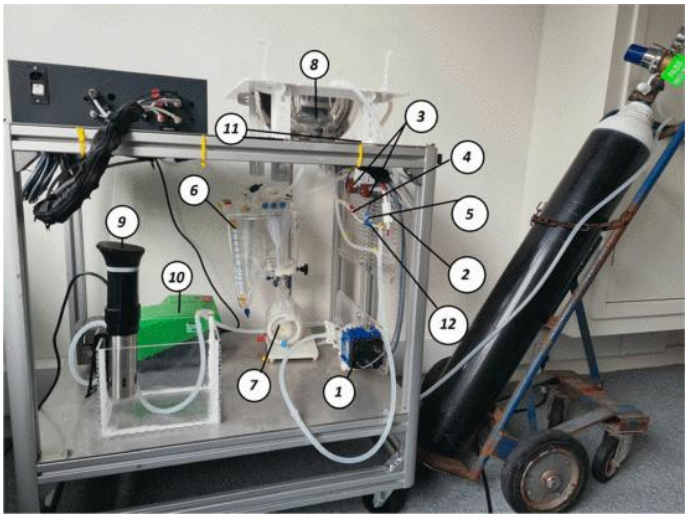

Figure 7.7.11. An overview of a research-orientated perfusion system [267]. (1) Centrifugal pump, (2) Pressure sensor, (3) Flow sensors, (4) Temperature Sensor, (5) Oxygen Sensor, (6) Reservoir (7), Oxygenator (8), Organ chamber (9), Heat exchanger, (10) Peristaltic pump, (11) Load cells, (12) pH sensor. Reprinting this figure from [267] does not require individuals working on a thesis to obtain a formal reuse license according IEEE instructions.

The organ perfusion machine is designed to be inexpensive, robust, modular, and adaptable to various experimental purposes. A single centrifugal pump (PuraLev 1200 MU, Levitronix GmbH, 8005 Zurich, Switzerland) was used to circulate the perfusate through all elements of the system flow circuit. Pressure (Single Use Pressure Sensors, PendoTECH, Princeton NJ 08540, USA) and flow (SONOFLOW co.55/100, SONOTEC, 06112 Halle, Germany) sensors were used to monitor both the input and the output pressure and flow rates of the perfusate while single oxygen (EOM-(t)-FOM, PreSens Precision Sensing GmbH, 93053 Regensburg, Germany), and temperature (Pt100, PreSens Precision Sensing GmbH, 93053 Regensburg, Germany) sensor was used to monitor the input stream only. The organ was suspended via perforated plastic film over the organ chamber. Any runoff perfusate from the liver was collected and, along with the liver output flow, was returned to the 4 L reservoir, where it was filtered. The oxygenator, re-oxygenated blood from the reservoir before it was pumped back through the system. Four load cells, placed directly beneath the four supports of the organ chamber in a square formation, monitored the weight of the liver throughout the perfusion. Fig. 2 shows the circuit diagram of the organ perfusion system and how each sensor of the system integrates with the Raspberry Pi. All peripherals were controlled via a single-board computer (Raspberry Pi 4, Raspberry Pi Foundation, Cambridge CB2 1NF, UK), and were communicated with using a combination of MODBUS (pumps, flow, and pressure sensors), RS-232 (oxygen sensor), and RS-485 (pH sensors) communication protocols. An analogic to digital converter (Waveshare 32-bit

AD/DA board, Waveshare Electronics, Shenzhen, China) was used to interface between the Raspberry Pi and the pressure sensors. The software architecture was implemented using ROS2 to ensure the modularity of system components. All sensor data was displayed in real-time via a laptop interface and the output was recorded for further analysis. The system is designed to enable fine control of all peripherals but was primarily used in this study to control and maintain pressure through either of the two input vessels, the portal vein (PV) and hepatic artery (HA). Pressure could be controlled by directly adjusting the duty cycle of the centrifugal pump or using a closed-loop proportional-integral-derivative (PID) controller. The gain parameters of the PID controller were tuned using the Ziegler-Nichols tuning method and the following parameters were obtained: Kp=5, Ki=2, and Kd=−0.5. These parameters were chosen based on achieving the shortest settling time while minimising potential overshoots.

Xu et al. [397] proposed a simple normothermic pig liver machine perfusion, hereafter explained in detail. A schematic is in **Figure 7.7.12**. The perfusion setup used by Xu et al. is a dual re-circulating circuit that consists of a centrifugal pump (BP50; Medtronic Inc., Minneapolis, MN), heat exchanger, membrane oxygenator (Affinity NT; Medtronic Inc., Minneapolis, MN), bubble trap, venous reservoir, and organ chamber. To maximize sterility, the researchers executed the procedures were performed in a laminar flow hood. Inflow perfusate was oxygenated, warmed to 39°C and divided into two lines: The arterial branch was perfused actively using the centrifugal pump, while the portal branch was fed passively by the gravity of the venous reservoir. Both lines are perfused in a constant flow fashion. After placement into the organ chamber, the liver was immersed in perfusate, which flowed freely from the supra- and infra-hepatic vena cava. Perfusion was conducted for 4 h for each group. flow rates and hydrostatic pressures in the arterial and venous branches were continuously monitored via flow and pressure transducers (TX50 Flow Bio-Probe; Medtronic Inc., Minneapolis, MN; TSD104A Pressure; Biopac System Inc., Goleta, CA) connected to a data acquisition system (MP100; Biopac System Inc.). The total volume of perfusate was 2000mL and comprised 1.5 L whole blood, 0.5 L sterile porcine plasma (Sigma-Aldrich, St. Louis, MO), hydrocortisone (10 mg/L), insulin (2 u/L), penicillin (40,000 U/L), streptomycin (40 mg/L), and heparin (5000 U/L).

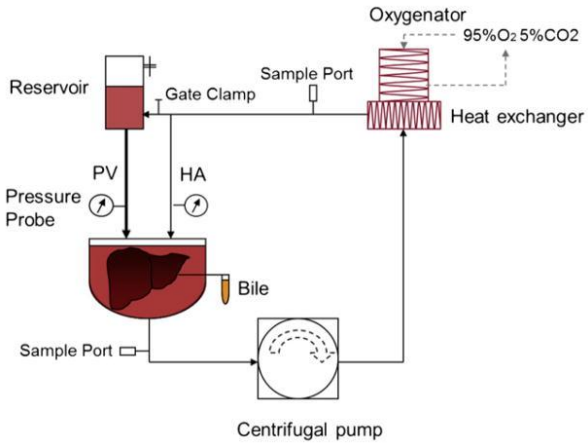

Figure 7.7.12. Schematic of machine presented by Xu et al. [397]. This Figure is reprinted with License Number 6126521032472.

Another machine used in clinical trials is the VitaSmart Machine Perfusion System, distributed by Bridge to Life, shown in **Figure 7.7.13**. This machine is expressly designed for ex vivo perfusion of abdominal organs such liver and kidney [417, 422]. This machine system consists of two roller pumps, one heat exchanger, and three flow and pressure probes. The sterile disposable perfusion set is composed of a membrane oxygenator, tubing for vessel cannulation, and surgical cannulas [422].

Figure 7.7.13. VitaSmart Perfusion System. This Figure is from Panconesi R, Flores Carvalho M, Mueller M, Dutkowski P, Muiesan P, Schlegel A. Mitochondrial Reprogramming—What Is the Benefit of Hypothermic Oxygenated Perfusion in Liver Transplantation? Transplantology. 2021; 2(2):149-161. https://doi.org/10.3390/transplantology2020015. This Figure is used with Creative Commons CC BY 4.0 license.

7.8 Additional observations about Machines Perfusion

There is no information in the literature as to which machine may be better from a performance point of view. One cannot yet speak of the advantages of using one machine or the other from a clinical point of view. Furthermore, it is not possible to determine from the data in the literature which machine may be more cost-effective; in the coming years, the market will provide indications as to what the trends are. In the study by Mergental et al. [33], they employed both the Liver Assist and the OrganOx metra, but the authors' stated aim was not to compare the performance of each machine. All machines have been used successfully from a clinical point of view for normothermic or hypothermic perfusion; therefore, hypothermic and normothermic perfusion are not competitive techniques but are adopted according to the objective to be achieved; in fact, some studies [183, 275, 165, 111, 136] have conducted both hypothermic and normothermic perfusion in sequence [141, 275], the choice of one machine or the other also changes depending on the economic availability, the type of perfusion to be performed and the current logistic conditions. While some machines, such as the Metra OrganOx, Transmedics' Liver OCS and the Cleveland NMP have the advantage of being transportable, allowing perfusion to be performed even while the organ is being transported to the transplant centre, but cannot conduct hypothermic perfusion. The Liver Assist and VitaSmart are not transportable during operation but have the advantage of performing perfusion at any temperature. Other comparisons can be made based on the degree of automation and ease of use of the machine. For example, during HOPE after connecting the liver to the machine the surgeon, perfusion only requires monitoring of the liver graft by the organ perfusionist [317]. In addition, Liver Assist allows the perfusate flow rates to be adjusted via the console, whereas the in the Cleveland Machine Perfusion flow rates are changed manually via clamps. One of the goals of perfusion machine manufacturers such as Medica S.p.A. is to put less expensive machines on the market than the current sub-normothermic or normothermic perfusion machines [163]. The main differences between these devices are in arterial inflow (pulsatile vs. continuous), venous outflow through the inferior vena cava (closed vs. open system) and oxygenator characteristics (integrated vs. external) [198]. The most used device in the UK is the OrganOx metra [198]. To go into more detail, Ceresa et al. [155] report that the volumetric flow rate through the hepatic artery is continuous in the OrganOx metra (OrganOx, Ltd., Oxford, UK) and the Cleveland NMP Device (Cleveland Clinic, OH); in contrast, in the Liver Assist (Organ Assist, Groningen, the Netherlands) and the OCS Liver System (Transmedics, Andover, MA) the arterial flow rate is pulsatile. The OrganOx metra device and the OCS Liver System automatically control the portal and arterial pressure, while in the other two devices, the pressure is

set by the doctor via a control display. Another difference between Liver Assist (Organ Assist, Groningen, the Netherlands) and OrganOx Metra device (OrganOx, Oxford, UK) is in the pumping system: in Liver Assist there are two pumps: first one supplies a continuous flow rate through the portal vein, and the second one, a roller pump supplies a pulsatile flow rate through hepatic artery [423]. Quite the opposite, in OrganOx Metra there is only a centrifuge (continuous and non-pulsatile) pump both for the hepatic artery and portal vein [423]. The cannulation performed in the OrganOx metra and the Cleveland NMP Device and OCS Liver System is the same: the hepatic artery, portal vein and inferior vena cava are cannulated. In the Liver Assist, on the other hand, the inferior vena cava is left open. The battery life of the OCS Liver is 4 hours. The battery life of the OrganOx metra is 2 - 4 hours. The Liver Assist about 20 minutes of the Cleveland NMP Device, is 30 to 4 hours. The oxygenator in the OrganOx metra and OCS Liver device is incorporated, whereas, in the Liver Assist, it is not. A crucial point to note is that when using a closed-loop device, such as the OrganOx metra®, great care must be taken to ensure that all small branches of the IVC, portal vein and hepatic artery are adequately channelled to avoid bleeding at the start of perfusion [198]. Obtaining adequate access to a bleeding vessel once connected to the device can be difficult [198].

An essential aspect of machine perfusion is related to the costs and benefits of the employment of this technology. Few studies have performed an economic evaluation of the use of perfusion machines. HOPE is performed by requiring only a sterile perfusion line kit, including an oxygenator [163]. In Italy, for example, a disposable kit from the Liver Assist Machine (Organ Assist, The Netherlands) for the perfusion of a graft costs approximately 8000 - 12000 euros [103]. Similar data were reported in another study conducted in the UK, which noted that the base cost for liver transplantation using the OrganOx device is £7337.21 while that of the Liver Assist is £4508.11 [425]. Not only that, but red blood cell solutions, drugs, and various nutrients, including multivitamins, sodium bicarbonate, heparin, antibiotics, prostacyclin and creatinine are required to perform normothermic perfusion [103, 163, 198]. However, the problems do not end there as all devices must be handled by qualified and on-call personnel [103]. The convenience of using a normothermic or hypothermic technique can also be influenced by economic factors. The exact cost of NMP is difficult to quantify and the exact health and economic implications are even more so [198]. These have been studied by several previous authors [317]. Consumables for this technology generally include a disposable perfusion circuit, priming fluid (such as gelofusine), human red blood cells and drugs. These are understandably associated with significant expenses compared to cold storage. In addition, NMP requires large personnel for a prolonged period [198]. Raigani et al. in 2020 [425] estimated the average cost to apply the normothermic perfusion technique to an already discarded graft to be $15454 (US), while the cost to identify a viable discarded graft with NMP was $28,099 USD in the

US. The authors considered direct and indirect costs to calculate these figures: direct costs included the cost of the disposable perfusion device, perfusate components (including infusions) and point-of-care equipment. The device costs were based on the three commercial liver perfusion devices currently available for clinical use in Europe or North America (Liver Assist, Groningen, The Netherlands; OrganOx Metra, Oxford, UK; TransMedics, Andover, USA) and the hourly operating cost was calculated using the reported life expectancy of each device (each period of use defined as 12 hours) [425]. Indirect costs included personnel and facility costs, depreciation of the perfusion device and an additional 5% for unforeseen costs [425]. Operating room costs for the time required to prepare the liver for perfusion were included in the facility fees [425]. For personnel costs, the transplant surgeons and nurse's fee was included for the time needed to prepare the liver for perfusion, while the perfusionist's fee was calculated for the entire duration of the perfusion [425]. Benefits, employer fees and training costs were also included [425]. Another study [426] evaluated the additional costs related to the use of the OrganOx device in the UK and showed higher costs per patient compared to SCS (£ 46711 vs. £ 37370). The costs of materials and disposable solutions were around $8160 (US), personnel costs around $680 (US) and a device rental fee of $40800 (US) per year per hospital [426]. The costs of follow-up care, immunosuppressants and visits to specialists and general practitioners for follow-up after transplantation were also considered [317]. Liver transplantation with OrganOx metra for NMP was found to be more expensive than the SCS technique, but more effective: $63527(US) using NMP versus SCS at $50,823(US). The standards committee of the American Society of Transplant Surgeons predicts that the addition of mechanical perfusion will add $25 000 – $50 000 to the overall cost of a liver transplant [427]. Another study conducted in Canada reported that the use of OrganOX has an average public health cost of $15,358 to $16,720 [428]. This initial cost must be considered in the context of the entire liver transplantation process, the patient's health-related quality of life (utility) and clinical outcomes [429]. In the study [429] they stated that the average cost of transplantation by NMP with OrganOX The cost of transplantation by NMP was $118 563 and by SCS was $93 762. [429], of which the cost of supplying and using OrganOX ranged from $15 358.53 to $16 720.11 [429]. In recent years, studies analysing the costs of using organ perfusion are beginning to emerge [54, 317]. So far, the clinical benefits have paved the way for the implementation of liver perfusion programmes; however, liver transplantation professionals are increasingly realising that the full implementation of these programmes passes through hospital administrative staff and local health authorities [317]. Financial constraints force these professionals to make difficult choices and evaluate the return on investment of healthcare interventions more critically than ever before [317]. The most commonly used perfusion solution for HOPE (i.e., the University of Wisconsin's mechanical perfusion solution) costs about USD 400 per

litre, which in most countries is less than human blood products or other solutions with an oxygen carrier [317]. Approximately 3 - 4 litres of mechanical perfusion solution are required to enable dynamic preservation of HOPE, including washing the graft before connection, and no additional perfusion additives such as electrolytes, antibiotics, nutrients or albumin are required [317]. Considering the composition of the perfusate, personnel and duration of perfusion, the costs for HOPE are likely to be much lower than for NMP, but a direct comparison has not yet been made [317]. The cost-efficiency of HMP compared to NMP could have an influence on which method will be more commonly used in the future [365]. Indeed, HMP is a simple method of organ preservation that can be easily performed by junior medical personnel. Furthermore, the solutions used for hypothermic perfusion are commercially available and ready for use after static cold storage [365]. Only one study [54] conducted in France on the use of HOPE reported that the total cost for the perfusion device, including maintenance, was estimated at € 765 per patient based on a payback time of 7 years with 25 procedures per year [54]. The costs for disposable kits and perfusion solution were estimated at € 4195 and € 338 per patient, respectively. Therefore, the total additional costs with the HOPE treatment were estimated at € 5298 (US $ 6323) per patient. The Histidine-Tryptophan-Ketoglutarate (HTK) solution for the kidneys costs approximately $100/150 per litre while UW cost $310/315 per litre [335]. In the study [335], it was shown that it is possible to conduct organ perfusion with 4 litres of HTK solution instead of the 10 to 20 litres used in the initial studies [334]. Furthermore, as there is no evidence of the superiority of HTK over UW [285], but both are valid solutions for liver preservation and conservation [335, 286, 342], the use of HTK would result in considerable cost savings [335, 286]. Based on the data used in the study [335], the savings from using HTK would be around $422 per donor. The LifePort Liver machine has not yet been used in a clinical setting; however, clinical use of the LifePort Kidney device has been approved and clinical studies are reported. One study estimated the cost-benefit in kidney perfusion and reported that the purchase cost of such machines is in the range of $20196 [430].

In conclusion, economic arguments, in addition to altruistic reasons, are needed to convince regional healthcare organizations to adopt this new technology [317]. Not only that, but the current very high costs could hinder the use of the dynamic perfusion technique in poorer countries or countries with a weaker healthcare system than in richer countries.

References

[1] Muller X, Marcon F, Sapisochin G, et al. Defining benchmarks in liver transplantation: a multicenter outcome analysis determining best achievable results. Ann Surg. 2018;267(4):419-425.

[2] Serifis N, Matheson R, Cloonan D, Rickert CG, Markmann JF, Coe TM. Machine perfusion of the liver: a review of clinical trials. Front Surg. 2021;8:625394.

[3] Sousa Da Silva RX, Weber A, Dutkowski P, Clavien PA. Machine perfusion in liver transplantation. Hepatology. 2022;76(5):1531-1549.

[4] Moein M, Capelin J, Toth JF, Tylor D, Weiss ZM, Murugesan BG, et al. Role of normothermic machine perfusion in liver transplantation: current trends and outcomes. Surg Pract Sci. 2022;9:100077.

[5] Lascaris B, de Meijer VE, Porte RJ. Normothermic liver machine perfusion as a dynamic platform for regenerative purposes: what does the future have in store for us? J Hepatol. 2022;77(4):825-836.

[6] Czigany Z, Pratschke J, Froněk J, et al. Hypothermic oxygenated machine perfusion reduces early allograft injury and improves post-transplant outcomes in extended criteria donation liver transplantation from donation after brain death: results from a multicenter randomized controlled trial (HOPE ECD-DBD). Ann Surg. 2021;274(5):705-712.

[7] Parente A, Osei-Bordom DC, Ronca V, Perera MTPR, Mirza D. Organ restoration with normothermic machine perfusion and immune reaction. Front Immunol. 2020;11:565616.

[8] Michelotto J, Gassner JMGV, Moosburner S, Muth V, Patel MS, Selzner M, et al. Ex vivo machine perfusion: current applications and future directions in liver transplantation. Langenbecks Arch Surg. 2021;406(1):39-54.

[9] Mahmud N. Selection for liver transplantation: indications and evaluation. Curr Hepatol Rep. 2020;19(3):203-212.

[10] Siciliano M, Parlati L, Maldarelli F, Rossi M, Ginanni Corradini S. Liver transplantation in adults: choosing the appropriate timing. World J Gastrointest Pharmacol Ther. 2012;3(4):49-61.

[11] Prince MI, Hudson M. Liver transplantation for chronic liver disease: advances and controversies in an era of organ shortages. Postgrad Med J. 2002;78(918):135-141.

[12] Horné F, Drefs M, Schirren MJ, Koch DT, Cepele G, Jacobi SJ, et al. Hypothermic oxygenated machine perfusion (HOPE) prior to liver transplantation mitigates post-reperfusion syndrome and perioperative electrolyte shifts. J Clin Med. 2022;11(24):7381.

[13] Boteon Y, Flores Carvalho MA, Panconesi R, Muiesan P, Schlegel A. Preventing tumour recurrence after liver transplantation: the role of machine perfusion. Int J Mol Sci. 2020;21(16):5791.

[14] Ozturk NB, Muhammad H, Gurakar M, Aslan A, Gurakar A, Dao D. Liver transplantation in developing countries. Hepatol Forum. 2022;3(3):103-107.

[15] Hansen L, Yan Y, Rosenkranz SJ. The power of the liver transplant waiting list: a case presentation. Am J Crit Care. 2014;23(6):510-515.

[16] Neuberger J. Liver transplantation in the United Kingdom. Liver Transpl. 2016;22(8):1129-1135.

[17] Kwong AJ, Kim WR, Lake JR, et al. OPTN/SRTR 2019 annual data report: liver. Am J Transplant. 2021;21(Suppl 2):208-315.

[18] Kupiec-Weglinski JW. Grand challenges in organ transplantation. Front Transplant. 2022;1:897679.

[19] Vanholder R, Domínguez-Gil B, Busic M, et al. Organ donation and transplantation: a multi-stakeholder call to action. Nat Rev Nephrol. 2021;17(8):554-568.

[20] Wynn JJ, Alexander CE. Increasing organ donation and transplantation: the U.S. experience over the past decade. Transpl Int. 2011;24(4):324-332.

[21] Chen CL, Kabiling CS, Concejero AM. Why does living donor liver transplantation flourish in Asia? Nat Rev Gastroenterol Hepatol. 2013;10(12):746-751.

[22] Stegemann J, Minor T. Energy charge restoration, mitochondrial protection and reversal of preservation-induced liver injury by hypothermic oxygenation prior to reperfusion. Cryobiology. 2009;58(3):331-336.

[23] Adam R, McMaster P, O'Grady JG, Castaing D, Klempnauer JL, Jamieson N, et al. Evolution of liver transplantation in Europe: report of the European Liver Transplant Registry. Liver Transpl. 2003;9(12):1231-1243.

[24] Monbaliu D, Pirenne J, Talbot D. Liver transplantation using donation after cardiac death donors. J Hepatol. 2012;56(2):474-485.

[25] Abouna GM. Organ shortage crisis: problems and possible solutions. Transplant Proc. 2008;40(1):34-38.

[26] Chen Z, Wang T, Chen C, Zhao Q, Ma Y, Guo Y, et al. Transplantation of extended criteria donor livers following continuous normothermic machine perfusion without recooling. Transplantation. 2022;106(6):1193-1200.

[27] DeRoos LJ, Marrero WJ, Tapper EB, Sonnenday CJ, Lavieri MS, Hutton DW, et al. Estimated association between organ availability and presumed consent in solid organ transplant. JAMA Netw Open. 2019;2(10):e1912431.

[28] Meyer CH, Grant AA, Enofe N, Matey A, Frankinburger E, Sola R Jr, et al. Organ donation after self-inflicted injury: a single institution analysis. Clin Transplant. 2022;36(7):e14679.

[29] Sandhu S, Goldberg D. Update on organ allocation and liver transplantation. Gastroenterol Hepatol (N Y). 2025;21(7):424-430.

[30] Olawade DB, Marinze S, Qureshi N, Weerasinghe K, Teke J. Transforming organ donation and transplantation: strategies for increasing donor participation and system efficiency. Eur J Intern Med. 2025;133:14-24.

[31] Shukla A, Vadeyar H, Rela M, Shah S. Liver transplantation: East versus West. J Clin Exp Hepatol. 2013;3(3):243-53.

[32] Boteon Y, Afford S, Mergental H. Pushing the limits: machine preservation of the liver as a tool to recondition high-risk grafts. Curr Transplant Rep. 2018;5:113-20.

[33] Mergental H, Perera MTPR, Laing RW, Muiesan P, Nicholson ML, Neil DA, et al. Transplantation of declined liver allografts following normothermic ex-situ evaluation. Am J Transplant. 2016;16:3235-45.

[34] Schlegel A, Muller X, Kalisvaart M, Muellhaupt B, Perera MTPR, Isaac JR, et al. Outcomes of DCD liver transplantation using organs treated by hypothermic oxygenated perfusion before implantation. J Hepatol. 2019;70:50-7.

[35] Lai JC. Defining the threshold for too sick for transplant. Curr Opin Organ Transplant. 2016;21:127-32.

[36] Husen P, Hornung J, Benko T, Klein C, Willuweit K, Buechter M, et al. Risk factors for high mortality on the liver transplant waiting list in times of organ shortage: a single-center analysis. Ann Transplant. 2019;24:242-51.

[37] Mergental H., Laing R.W., Kirkham A.J. et al. Transplantation of discarded livers following viability testing with normothermic machine perfusion. Nat Commun. 2020; 11, 2939.

[38] Jochmans I, van Rosmalen M, Pirenne J, Samuel U. Adult liver allocation in Eurotransplant. Transplantation. 2017;101(7):1542-50.

[39] Lai JC, Feng S, Terrault NA, Lizaola B, Hayssen H, Covinsky K. Frailty predicts waitlist mortality in liver transplant candidates. Am J Transplant. 2014;14(8):1870-9.

[40] Mohamed KA, Ghabril M, Desai A, Orman E, Patidar KR, Holden J, et al. Neighborhood poverty is associated with failure to be waitlisted and death during liver transplantation evaluation. Liver Transpl. 2022;28:1441-53.

[41] Patzer RE, Amaral S, Wasse H, Volkova N, Kleinbaum D, McClellan WM. Neighborhood poverty and racial disparities in kidney transplant waitlisting. J Am Soc Nephrol. 2009;20(6):1333-40.

[42] Patzer RE, Perryman JP, Schrager JD, Pastan S, Amaral S, Gazmararian JA, et al. The role of race and poverty on steps to kidney transplantation in the Southeastern United States. Am J Transplant. 2012;12(2):358-68.

[43] Mohan S, Mutell R, Patzer RE, Holt J, Cohen D, McClellan W. Kidney transplantation and the intensity of poverty in the contiguous United States. Transplantation. 2014;98(6):640-5.

[44] Ozminkowski RJ, White AJ, Hassol A, Murphy M. What if socioeconomics made no difference? Access to a cadaver kidney transplant as an example. Med Care. 1998;36(9):1398-406.

[45] Park C, Jones MM, Kaplan S, et al. A scoping review of inequities in access to organ transplant in the United States. Int J Equity Health. 2022;21:22.

[46] Handley TJ, Arnow KD, Melcher ML. Despite increasing costs, perfusion machines expand the donor pool of livers and could save lives. J Surg Res. 2023;283:42-51.

[47] Centro Nazionale Trapianti. Comunicato stampa. Disponibile su: https://www.trapianti.salute.gov.it/trapianti/dettaglioComunicatiNotizieCnt.jsp?lingua=italiano&area=cnt&menu=media&sottomenu=news&id=636. Accessed on Jan 10 2023.

[48] Banker A, Bhatt N, Rao PS, Agrawal P, Shah M, Nayak M, et al. A review of machine perfusion strategies in liver transplantation. J Clin Exp Hepatol. 2023;13(2):335-49.

[49] Jochmans I, Akhtar MZ, Nasralla D, et al. Past, present, and future of dynamic kidney and liver preservation and resuscitation. Am J Transplant. 2016;16:2545-55.

[50] Czigany Z, Schöning W, Ulmer TF, Bednarsch J, Amygdalos I, Cramer T, et al. Hypothermic oxygenated machine perfusion (HOPE) for orthotopic liver transplantation of human liver allografts from extended criteria donors (ECD) in donation after brain death (DBD): a prospective multicentre randomised controlled trial (HOPE ECD-DBD). BMJ Open. 2017;7(10):e017558.

[51] Ravikumar R, Leuvenink H, Friend PJ. Normothermic liver preservation: a new paradigm? Transpl Int. 2015;28(6):690–9.

[52] Orman ES, Mayorga ME, Wheeler SB, Townsley RM, Toro-Diaz HH, Hayashi PH, et al. Declining liver graft quality threatens the future of liver transplantation in the United States. Liver Transpl. 2015;21(8):1040–50.

[53] Ethics Committee, American College of Critical Care Medicine; Society of Critical Care Medicine. Recommendations for non-heart beating organ donation. A position paper by the Ethics Committee, American College of Critical Care Medicine, Society of Critical Care Medicine. Crit Care Med. 2001;29(9):1826–31. doi:10.1097/00003246-200109000-00029.

[54] Rayar M, Beaurepaire J, Bajeux E, Hamonic S, Renard T, Locher C, et al. Hypothermic oxygenated perfusion (HOPE) improves ECD liver graft function and reduces duration of hospitalisation without extra cost: the PERPHO Study. Liver Transpl. 2021;27(3):349–62.

[55] Vodkin I, Kuo A. Extended Criteria Donors in Liver Transplantation. Clin Liver Dis. 2017;21(2):289–301.

[56] Czigany Z, Lurje I, Tolba RH, et al. Machine perfusion for liver transplantation in the era of marginal organs—new kids on the block. Liver Int. 2019;39:228–49.

[57] Nasralla D, Coussios CC, Mergental H, et al. A randomized trial of normothermic preservation in liver transplantation. Nature. 2018;557:50–6.

[58] van Rijn R, van den Berg AP, Erdmann JI, Heaton N, van Hoek B, de Jonge J, Leuvenink HGD, Mahesh SVK, Mertens S, Monbaliu D, Muiesan P, Perera MTPR, Polak WG, Rogiers X, Troisi RI, de Vries Y, Porte RJ. Study protocol for a multicenter randomized controlled trial to compare the efficacy of end-ischemic dual hypothermic oxygenated machine perfusion with static cold storage in preventing non-anastomotic biliary strictures after transplantation of liver grafts donated after circulatory death: DHOPE-DCD trial. BMC Gastroenterol. 2019;19(1):40.

[59] Wertheim JA. Major challenges limiting liver transplantation in the United States. Am J Transplant. 2011;11:1773–84.

[60] van Beekum CJ, Vilz TO, Glowka TR, von Websky MW, Kalff JC, Manekeller S. Normothermic machine perfusion (NMP) of the liver – current status and future perspectives. Ann Transplant. 2021;26:e931664-1.

[61] Abbas SH, Friend PJ. Principles and current status of abdominal organ preservation for transplantation. Surgery in Practice and Science. 2020;3: 100020.

[62] Widmer J, Eden J, Carvalho MF, Dutkowski P, Schlegel A. Machine perfusion for extended criteria donor livers: what challenges remain? J Clin Med. 2022;11:5218.

[63] Bardallo RG, Da Silva RT, Carbonell T, Palmeira C, Folch-Puy E, Roselló-Catafau J, Adam R, Panisello-Rosello A. Liver graft hypothermic static and oxygenated perfusion (HOPE) strategies: a mitochondrial crossroads. Int J Mol Sci. 2022;23(10):5742.

[64] Nickkholgh A, Nikdad M, Shafie S, et al. Ex situ liver machine perfusion as an emerging graft protective strategy in clinical liver transplantation: the Dawn of a New Era. Transplantation. 2019;103:2003–11.

[65] Schlegel A, Muller X, Dutkowski P. Hypothermic machine preservation of the liver: state of the art. Curr Transplant Rep. 2018;5:93–102.

[66] Zamboni F, Franchello A, David E, et al. Effect of macrovesicular steatosis and other donor and recipient characteristics on the outcome of liver transplantation. Clin Transplant. 2001;15:53–57.

[67] Pezzati D, Ghinolfi D, De Simone P, Balzano E, Filipponi F. Strategies to optimize the use of marginal donors in liver transplantation. World J Hepatol. 2015;7(26):2636–47.

[68] Busuttil RW, Tanaka K. The utility of marginal donors in liver transplantation. Liver Transpl. 2003;9:651–63.

[69] Ghinolfi D, Marti J, De Simone P, Lai Q, Pezzati D, Coletti L, Tartaglia D, Catalano G, Tincani G, Carrai P, et al. Use of octogenarian donors for liver transplantation: a survival analysis. Am J Transplant. 2014;14:2062–71.

[70] Attia M, Silva MA, Mirza DF. The marginal liver donor—an update. Transpl Int. 2008;21:713–24.

[71] de Meijer VE, Fujiyoshi M, Porte RJ. Ex situ machine perfusion strategies in liver transplantation. J Hepatol. 2019;70(1):203–5.

[72] Muller X, Schlegel A, Kron P, Eshmuminov D, Wurdinger M, Meierhofer D, Clavien PA, Dutkowski P. Novel real-time prediction of liver graft function during hypothermic oxygenated machine perfusion before liver transplantation. Ann Surg. 2019; 270(5): 783-790.

[73] Jing L, Yao L, Zhao M, Peng LP, Liu M. Organ preservation: from the past to the future. Acta Pharmacol Sin. 2018;39(5):845–57. doi:10.1038/aps.2017.182.

[74] Guibert EE, Petrenko AY, Balaban CL, Somov AY, Rodriguez JV, Fuller BJ. Organ preservation: current concepts and new strategies for the next decade. Transfus Med Hemother. 2011;38:125–42.

[75] Guarrera JV, Henry SD, Samstein B, Odeh-Ramadan R, Kinkhabwala M, Goldstein MJ, Ratner LE, Renz JF, Lee HT, Brown RS Jr, Emond JC. Hypothermic machine preservation in human liver transplantation: the first clinical series. Am J Transplant. 2010;10:372–81.

[76] Jia JJ, Li JH, Jiang L, Lin BY, Wang L, Su R, Zhou L, Zheng SS. Liver protection strategies in liver transplantation. Hepatobiliary Pancreat Dis Int. 2015;14(1):34–42.

[77] Mergental H, Roll GR. Normothermic machine perfusion of the liver. Clin Liver Dis (Hoboken). 2017;10(4):97–99.

[78] Roll GR. An update on machine preservation of the liver. Clin Liver Dis (Hoboken). 2019;14(5):180–2.

[79] Horváth T, Jász DK, Baráth B, Poles MZ, Boros M, Hartmann P. Mitochondrial consequences of organ preservation techniques during liver transplantation. Int J Mol Sci. 2021;22(6):2816.

[80] Asong-Fontem N, Panisello-Rosello A, Sebagh M, Gonin M, Rosello-Catafau J, Adam R. The role of IGL-2 preservation solution on rat livers during SCS and HOPE. Int J Mol Sci. 2022;23(20):12615.

[81] Bellini MI, Yiu J, Nozdrin M, Papalois V. The effect of preservation temperature on liver, kidney, and pancreas tissue ATP in animal and preclinical human models. J Clin Med. 2019;8(9):1421.

[82] Cotter TG, Odenwald MA, Perez-Gutierrez A, Jayant K, DiSabato D, Charlton M, Fung J. Preservation solutions for static cold storage in donation after circulatory death and donation after brain death liver transplantation in the United States. Liver Transpl. 2022;28:1454–1462.

[83] van Rijn R, Schurink IJ, de Vries Y, van den Berg AP, Cortes Cerisuelo M, Darwish Murad S, Erdmann JI, Gilbo N, de Haas RJ, Heaton N, van Hoek B, Huurman VAL, Jochmans I, van Leeuwen OB, de Meijer VE, Monbaliu D, Polak WG, Slangen JJG, Troisi RI, Vanlander A, de Jonge J, Porte RJ. Hypothermic machine perfusion in liver transplantation — a randomized trial. N Engl J Med. 2021;384:1391–1401.

[84] Edelman JJ, Seco M, Dunne B, Matzelle SJ, Murphy M, Joshi P, Yan TD, Wilson MK, Bannon PG, Vallely MP, Passage J. Custodiol for myocardial protection and preservation. A systematic review. Ann Cardiothorac Surg. 2013;2(6):717–728.

[85] Laing RW, Mergental H, Yap C, Kirkham A, Whilku M, Barton D, et al. Viability testing and transplantation of marginal livers (VITTAL) using normothermic machine perfusion: study protocol for an open-label, non-randomised, prospective, single-arm trial. BMJ Open. 2017;7:e017733.

[86] Szilágyi ÁL, Mátrai P, Hegyi P, Tuboly E, Pécz D, Garami A, Solymár M, Pétervári E, Balaskó M, Veres G, Czopf L, Wobbe B, Szabó D, Wagner J, Hartmann P. Compared efficacy of preservation solutions on the outcome of liver transplantation: meta-analysis. World J Gastroenterol. 2018;24(16):1812–1824.

[87] Taylor MJ, Baicu SC. Current state of hypothermic machine perfusion preservation of organs: the clinical perspective. Cryobiology. 2010;60(3 Suppl):S20–35.

[88] Shen F, Yan R. Design and implementation of a hypothermic machine perfusion device for clinical preservation of isolated organs. Sensors. 2017;17:1256.

[89] Tingle SJ, Figueiredo RS, Moir JA, Goodfellow M, Talbot D, Wilson CH. Machine perfusion preservation versus static cold storage for deceased donor kidney transplantation. Cochrane Database Syst Rev. 2019;3(3):CD011671.

[90] Clatworthy M, Watson C, Allison M, Dark J. Transplantation at a glance. Chichester: Wiley-Blackwell; 2012.

[91] Darius T, Nath J, Mourad M. Simply adding oxygen during hypothermic machine perfusion to combat the negative effects of ischemia-reperfusion injury: fundamentals and current evidence for kidneys. Biomedicines. 2021;9(8):993.

[92] Gillooly JF, Brown JH, West GB, Savage VM, Charnov EL. Effects of size and temperature on metabolic rate. Science. 2001;293:2248–2251.

[93] Fuller BJ, Lee CY. Hypothermic perfusion preservation: the future of organ preservation revisited? Cryobiology. 2007;54:129–145.

[94] Michel SG, Madsen JC. Current perspectives in transplant medicine: hypothermic oxygenated perfusion. Transplant Res Risk Manag. 2016;8:25–30.

[95] Schlegel A, de Rougemont O, Graf R, et al. Protective mechanisms of end-ischemic cold machine perfusion in DCD liver grafts. J Hepatol. 2013;58:278–286.

[96] Stegemann J, Minor T. Energy charge restoration, mitochondrial protection and reversal of preservation induced liver injury by hypothermic oxygenation prior to reperfusion. Cryobiology. 2009;58:331–336.

[97] Dutkowski P, Schlegel A, De Oliveira M, et al. HOPE for human liver grafts obtained from donors after cardiac death. J Hepatol. 2014;60:765–772.

[98] Bae C, Henry SD, Guarrera JV. Is extracorporeal hypothermic machine perfusion of the liver better than the 'good old icebox'? Curr Opin Organ Transplant. 2012;17:137–142.

[99] de Vries R, Tessier SN, Banik PD, Ozer S, Crorin SEJ, Nagpal S, Yeh H, Uygun K. Extending the human liver preservation time for transplantation by supercooling. Transplantation. 2018;102:S396.

[100] Bral M, Gala-Lopez B, Bigam D, et al. Preliminary single-center Canadian experience of human normothermic ex vivo liver perfusion: results of a clinical trial. Am J Transplant. 2017;17:1071–1080.

[101] Fodor M, Cardini B, Peter W, Weissenbacher A, Oberhuber R, Hautz T, Otarashvili G, Margreiter C, Maglione M, Resch T, Krendl F, Meszaros AT, Bogensperger C, Gasteiger S, Messner F, Henninger B, Zoller H, Tilg H, Öfner D, Schneeberger S. Static cold storage compared with normothermic machine perfusion of the liver and effect on ischaemic-type biliary lesions after transplantation: a propensity score-matched study. Br J Surg. 2021;108(9):1082–1089.

[102] Dutkowski P, Guarrera JV, de Jonge J, Martins PN, Porte RJ, Clavien PA. Evolving trends in machine perfusion for liver transplantation. Gastroenterology. 2019;156:1542–1547.

[103] Scalera I, De Carlis R, Patrono D, Gringeri E, Olivieri T, Pagano D, Lai Q, Rossi M, Gruttadauria S, Di Benedetto F, Cillo U, Romagnoli R, Lupo LG, De Carlis L. How useful is the machine perfusion in liver transplantation? An answer from a national survey. Front Surg. 2022;9:975150.

[104] Schlegel A, Muller X, Dutkowski P. Machine perfusion strategies in liver transplantation. Hepatobiliary Surg Nutr. 2019;8:490.

[105] Detelich D, Markmann JF. The dawn of liver perfusion machines. Curr Opin Organ Transplant. 2018;23:151–161.

[106] van Beekum CJ, Vilz TO, Glowka TR, von Websky MW, Kalff JC, Manekeller S. Normothermic machine perfusion (NMP) of the liver – current status and future perspectives. Ann Transplant. 2021;26:e931664-1.

[107] Reich DJ, Mulligan DC, Abt PL, et al. ASTS recommended practice guidelines for controlled donation after cardiac death organ procurement and transplantation. Am J Transplant. 2009;9:2004–2011.

[108] Cursio R, Gugenheim J. Ischemia-reperfusion injury and ischemic-type biliary lesions following liver transplantation. J Transplant. 2012;2012:164329.

[109] Grewal HP, Willingham DL, Nguyen J, et al. Liver transplantation using controlled donation after cardiac death donors: an analysis of a large single-center experience. Liver Transpl. 2009;15:1028–1035.

[110] de Vera ME, Lopez-Solis R, Dvorchik I, et al. Liver transplantation using donation after cardiac death donors: long-term follow-up from a single center. Am J Transplant. 2009;9:773–781.

[111] Burlage LC, Karimian N, Westerkamp AC, Visser N, Matton APM, van Rijn R, et al. Oxygenated hypothermic machine perfusion after static cold storage improves endothelial function of extended criteria donor livers. HPB. 2017;19:538–546.

[112] Brüggenwirth IMA. Prolonged preservation of donor livers: the benefits of hypothermic machine perfusion [Thesis fully internal (DIV), University of Groningen]. University of Groningen; 2022. https://doi.org/10.33612/diss.214594430

[113] Asong-Fontem N, Panisello-Rosello A, Sebagh M, Gonin M, Rosello-Catafau J, Adam R. The role of IGL-2 preservation solution on rat livers during SCS and HOPE. Int J Mol Sci. 2022;23(20):12615.

[114] Foley DP, Fernandez LA, Leverson G, et al. Biliary complications after liver transplantation from donation after cardiac death donors: an analysis of risk factors and long-term outcomes from a single center. Ann Surg. 2011;253:817–825.

[115] O'Neill S, Roebuck A, Khoo E, Wigmore SJ, Harrison EM. A meta-analysis and meta-regression of outcomes including biliary complications in donation after cardiac death liver transplantation. Transpl Int. 2014;27:1159–1174.

[116] Ploeg RJ, D'Alessandro AM, Knechtle SJ, Stegall MD, Pirsch JD, Hoffmann RM, et al. Risk factors for primary dysfunction after liver transplantation—a multivariate analysis. Transplantation. 1993;55(4):807–813.

[117] Markmann JF, Abouljoud MS, Ghobrial RM, Bhati CS, Pelletier SJ, Lu AD, et al. Impact of portable normothermic blood-based machine perfusion on outcomes of liver transplant: the OCS Liver PROTECT randomized clinical trial. JAMA Surg. 2022;157(3):189–198.

[118] Howden BO, Jablonski P. Liver preservation: a comparison of Celsior to colloid-free University of Wisconsin solution. Transplantation. 2000;70(8):1140-2.

[119] Nemes B, Gámán G, Polak WG, Gelley F, Hara T, Ono S, Baimakhanov Z, Piros L, Eguchi S. Extended-criteria donors in liver transplantation part II: reviewing the impact of extended-criteria donors on the complications and outcomes of liver transplantation. Expert Rev Gastroenterol Hepatol. 2016;10(7):841–859.

[120] Schlegel A, Kalisvaart M, Scalera I, et al. The UK DCD risk score: a new proposal to define futility in donation-after-circulatory-death liver transplantation. J Hepatol. 2018; 68(3):456-464.

[121] Petrenko A, Carnevale M, Somov A, Osorio J, Rodríguez J, Guibert E, Fuller B, Froghi F. Organ preservation into the 2020s: the era of dynamic intervention. Transfus Med Hemother. 2019;46:151–172.

[122] Jochmans I, Pirenne J. Chapter 16 - Machine perfusion of kidneys donated after circulatory death: the Carrel and Lindbergh legacy. In: Orlando G, Lerut J, Soker S, Stratta RJ, editors. Regenerative medicine applications in organ transplantation. Academic Press; 2014. p. 211–226. https://doi.org/10.1016/B978-0-12-398523-1.00016-1

[123] Henry SD, Nachber E, Tulipan J, Stone J, Bae C, Reznik L, Kato T, Samstein B, Emond JC, Guarrera JV. Hypothermic machine preservation reduces molecular markers of ischemia/reperfusion injury in human liver transplantation. Am J Transplant. 2012;12:2477–2486.

[124] Xu J, Buchwald JE, Martins PN. Review of current machine perfusion therapeutics for organ preservation. Transplantation. 2020;104:1792–1803.

[125] Monbaliu D, Brassil J. Machine perfusion of the liver: past, present and future. Curr Opin Organ Transplant. 2010;15:160–166.

[126] Karangwa SA, Dutkowski P, Fontes P, Friend PJ, Guarrera JV, Markmann JF, Mergental H, Minor T, Quintini C, Selzner M, Uygun K, Watson CJ, Porte RJ. Machine perfusion of donor livers for transplantation: a proposal for standardized nomenclature and reporting guidelines. Am J Transplant. 2016;16(10):2932–2942.

[127] Gao J, He K, Xia Q, Zhang J. Research progress on hepatic machine perfusion. Int J Med Sci. 2021;18(9):1953–1959.

[128] Watson CJE, Hunt F, Messer S, Currie I, Large S, Sutherland A, Crick K, Wigmore SJ, Fear C, Cornateanu S, Randle LV, Terrace JD, Upponi S, Taylor R, Allen E, Butler AJ, Oniscu GC. In situ normothermic perfusion of livers in controlled circulatory death donation may prevent ischemic cholangiopathy and improve graft survival. Am J Transplant. 2019;19(6):1745–1758.

[129] Schlegel A, Kron P, De Oliveira ML, et al. Is single portal vein approach sufficient for hypothermic machine perfusion of DCD liver grafts? J Hepatol. 2016;64:239–241.

[130] Dutkowski P, Polak WG, Muiesan P, Schlegel A, Verhoeven CJ, Scalera I, et al. First comparison of hypothermic oxygenated perfusion versus static cold storage of human donation after cardiac death liver transplants. Ann Surg. 2015;262(5):764–771.

[131] van Rijn R, van Leeuwen OB, Matton APM, Burlage LC, Wiersema-Buist J, van den Heuvel MC, et al. Hypothermic oxygenated machine perfusion reduces bile duct reperfusion injury after transplantation of donation after circulatory death livers. Liver Transpl. 2018;24(5):655–664.

[132] van Rijn R, Karimian N, Matton APM, et al. Dual hypothermic oxygenated machine perfusion in liver transplants donated after circulatory death. Br J Surg. 2017;104:907–917.

[133] Gallinat A, Fox M, Lüer B, Efferz P, Paul A, Minor T. Role of pulsatility in hypothermic reconditioning of porcine kidney grafts by machine perfusion after cold storage. Transplantation. 2013;96:538–542.

[134] Patrono D, Surra A, Catalano G, et al. Hypothermic oxygenated machine perfusion of liver grafts from brain-dead donors. Sci Rep. 2019;9(1):9337.

[135] Mabrut JY, Lesurtel M, Muller X, Dubois R, Ducerf C, Rossignol G, Mohkam K. Ex vivo liver splitting and hypothermic oxygenated machine perfusion: technical refinements of a promising preservation strategy in split liver transplantation. Transplantation. 2021;105(8):e89–e90.

[136] Boteon Y, Laing R, Schlegel A, Wallace L, Smith A, Attard J, et al. Combined hypothermic and normothermic machine perfusion improves functional recovery of extended criteria donor livers. Liver Transpl. 2018;24:1699–1715.

[137] de Vries Y, Brüggenwirth IMA, Karangwa SA, von Meijenfeldt FA, van Leeuwen OB, Burlage LC, et al. Dual versus single oxygenated hypothermic machine perfusion of porcine livers: impact on hepatobiliary and endothelial cell injury. Transplant Direct. 2021;7(9):e741.

[138] Tawa P, Goutard M, Andrews AR, de Vries RJ, Rosales IA, Yeh H, Uygun B, Randolph MA, Lellouch AG, Uygun K, Cetrulo CL. Continuous versus pulsatile flow in 24-hour vascularized composite allograft machine perfusion in swine: a pilot study. J Surg Res. 2023;283:1145–1153.

[139] Kueckelhaus M, Puscz F, Dermietzel A, et al. Extracorporeal perfusion in vascularized composite allotransplantation: current concepts and future prospects. Ann Plast Surg. 2018;80:669–678.

[140] Guarrera JV, Henry SD, Samstein B, Reznik E, Musat C, Lukose TI, et al. Hypothermic machine preservation facilitates successful transplantation of “orphan” extended criteria donor livers. Am J Transplant. 2015;15:161–169.

[141] van Leeuwen OB, de Vries Y, Fujiyoshi M, et al. Transplantation of high-risk donor livers after ex situ resuscitation and assessment using combined hypo- and normothermic machine perfusion: a prospective clinical trial. Ann Surg. 2019;270:906–914.

[142] Martins PN, Buchwald JE, Mergental H, Varga L, Quintini C. The role of normothermic machine perfusion in liver transplantation. Int J Surg. 2020;82(Suppl):52–60.

[143] Monbaliu D, Vekemans K, De Vos R, Brassil J, Heedfeld V, Qiang L, D’hollander M, Roskams T, Pirenne J. Hemodynamic, biochemical, and morphological characteristics during preservation of normal porcine livers by hypothermic machine perfusion. Transplant Proc. 2007;39(8):2652–2658.

[144] Bishara AM, Lituiev DS, Adelmann D, Kothari RP, Malinoski DJ, Nudel JD, Sally MB, Hirose R, Hadley DD, Niemann CU. Machine learning prediction of liver allograft utilization from deceased organ donors using the National Donor Management Goals Registry. Transplant Direct. 2021;7(10):e771.

[145] Taylor MJ. Biology of cell survival in the cold: the basis for biopreservation of tissues and organs. In: Advances in Biopreservation. Abingdon, UK: Taylor & Francis; 2007. p. 15–62.

[146] Taylor MJ. Hypothermic blood substitution: special considerations for protection of cells during ex vivo and in vivo preservation. Transfus Med Hemother. 2007;34:226–244.

[147] Abudhaise H, Davidson BR, DeMuylder P, Luong TV, Fuller B. Evolution of dynamic, biochemical, and morphological parameters in hypothermic machine perfusion of human livers: a proof-of-concept study. PLoS One. 2018;13(9):e0203803.

[148] Monbaliu D, Liu Q, Libbrecht L, De Vos R, Vekemans K, Debbaut C, et al. Preserving the morphology and evaluating the quality of liver grafts by hypothermic machine perfusion: a proof-of-concept study using discarded human livers. Liver Transpl. 2012;18(12):1495–1507.

[149] Derveaux K, Monbaliu D, Crabbe T, Schein D, Brassil J, Kravitz D, et al. Does ex vivo vascular resistance reflect viability of non-heart-beating donor livers? Transplant Proc. 2005;37(1):338–339.

[150] Gryaznov NA, Kharlamov VV, Gataulin YA, et al. An adaptive algorithm for machine perfusion of isolated donor liver. Biomed Eng. 2018;51:401–406.

[151] Li J, Lu H, Zhang J, Li Y, Zhao Q. Comprehensive approach to assessment of liver viability during normothermic machine perfusion. J Clin Transl Hepatol. 2023;11(2):466–479. doi:10.14218/JCTH.2022.00130

[152] Watson CJE, Jochmans I. From "gut feeling" to objectivity: machine preservation of the liver as a tool to assess organ viability. Curr Transplant Rep. 2018;5:72–81.

[153] Guy AJ, Nath J, Cobbold M, et al. Metabolomic analysis of perfusate during hypothermic machine perfusion of human cadaveric kidneys. Transplantation. 2015;99:754–759.

[154] Faitot F, Besch C, Battini S, et al. Impact of real-time metabolomics in liver transplantation: graft evaluation and donor-recipient matching. J Hepatol. 2018;68:699–706.

[155] Ceresa CDL, Nasralla D, Jassem W. Normothermic Machine Preservation of the Liver: State of the Art. Curr Transplant Rep. 2018;5(1):104-110. doi: 10.1007/s40472-018-0186-9.

[156] Izamis ML, Perk S, Calhoun C, Uygun K, Yarmush ML, Berthiaume F. Machine perfusion enhances hepatocyte isolation yields from ischemic livers. Cryobiology. 2015;71(2):244–255.

[157] op den Dries S, Karimian N, Sutton ME, et al. Ex vivo normothermic machine perfusion and viability testing of discarded human donor livers. Am J Transplant. 2013;13:1327–1335.

[158] Shadrin KV, Pakhomova VG, Yakovleva YA, Kryukova OV, Rupenko AP. Algorithm for analysis of the metabolic activity of the ex vivo perfused liver. In: 2022 IEEE 23rd International Conference of Young Professionals in Electron Devices and Materials (EDM). Altai, Russian Federation; 2022. p. 481–485.

[159] Markgraf W, Malberg H. Preoperative function assessment of ex vivo kidneys with supervised machine learning based on blood and urine markers measured during normothermic machine perfusion. Biomedicines. 2022;10(12):3055.

[160] Panconesi R, Flores Carvalho M, Mueller M, Dutkowski P, Muiesan P, Schlegel A. Mitochondrial reprogramming—what is the benefit of hypothermic oxygenated perfusion in liver transplantation? Transplantology. 2021;2:149–161.

[161] Guarrera JV, Henry SD, Chen SW, Brown T, Nachber E, Arrington B, Boykin J, Samstein B, Brown RS Jr, Emond JC, Lee HT. Hypothermic machine preservation attenuates ischemia/reperfusion markers after liver transplantation: preliminary results. J Surg Res. 2011;167(2):e365–e373.

[162] Petrenko A, Carnevale M, Somov A, Osorio J, Rodríguez J, Guibert E, Fuller B, Froghi F. Organ preservation into the 2020s: the era of dynamic intervention. Transfus Med Hemother. 2019;46:151–172.

[163] Ravaioli M, De Pace V, Angeletti A, et al. Hypothermic oxygenated new machine perfusion system in liver and kidney transplantation of extended criteria donors: first Italian clinical trial. Sci Rep. 2020;10:6063.

[164] Schlegel A, Muller X, Mueller M, Stepanova A, Kron P, de Rougemont O, Muiesan P, Clavien PA, Galkin A, Meierhofer D, Dutkowski P. Hypothermic oxygenated perfusion protects from mitochondrial injury before liver transplantation. EBioMedicine. 2020;60:103014.

[165] De Carlis L, De Carlis R, Lauterio A, Di Sandro S, Ferla F, Zanierato M. Sequential use of normothermic regional perfusion and hypothermic machine perfusion in donation after cardiac death liver transplantation with extended warm ischemia time. Transplantation. 2016;100(10):e101–e102.

[166] De Carlis R, Lauterio A, Ferla F, Di Sandro S, Sguinzi R, De Carlis L. Hypothermic machine perfusion of liver grafts can safely extend cold ischemia for up to 20 hours in cases of necessity. Transplantation. 2017;101(7):e223–e224.

[167] Georgiades F, Hosgood SA, Butler AJ, Nicholson ML. Use of ex vivo normothermic machine perfusion after normothermic regional perfusion to salvage a poorly perfused DCD kidney. Am J Transplant. 2019;19:3415–3419.

[168] Ravikumar R, Jassem W, Mergental H, Heaton N, Mirza D, Perera MT, et al. Liver transplantation after ex vivo normothermic machine preservation: a phase 1 (first-in-man) clinical trial. Am J Transplant. 2016;16(6):1779–1787. Perera T, Mergental H, Stephenson B, Roll GR, Cilliers H, Liang R, et al. First human liver transplantation using a marginal allograft resuscitated by normothermic machine perfusion. Liver Transpl. 2016;22(1):120–124.

[169] Gilbo N, Jacquemin M, Nasralla D, Libbrecht L, Lavend'homme R, Peerlinck K, Ploeg RJ, Friend PJ, Pirenne J, Monbaliu D, Jochmans I. Coagulation factors accumulate during normothermic liver machine perfusion regardless of donor type and severity of ischemic injury. Transplantation. 2022;106(3):510–518. doi:10.1097/TP.0000000000003763

[170] Henry SD, Guarrera JV. Protective effects of hypothermic ex vivo perfusion on ischemia/reperfusion injury and transplant outcomes. Transplant Rev (Orlando). 2012;26(2):163–175.

[171] Henry SD, Guarrera JV. Protective effects of hypothermic ex vivo perfusion on ischemia/reperfusion injury and transplant outcomes. Transplant Rev (Orlando). 2012;26(2):163–175.

[172] Dutkowski P, Furrer K, Tian Y, Graf R, Clavien PA. Novel short-term hypothermic oxygenated perfusion (HOPE) system prevents injury in rat liver graft from non-heart beating donor. Ann Surg. 2006;244:968–976.

[173] Fujita S, Hamamoto I, Nakamura K, Tanaka K, Ozawa K. Evaluation of oxygen requirements during hypothermic liver perfusion. Geka Hokan. 1993;62:228–240.

[174] Friend P, Pollok JM. Hypothermic machine perfusion in liver transplantation—a randomised trial and beyond. Transpl Int. 2022;35:10257.

[175] Jochmans I, Brat A, Davies L, Hofker HS, van de Leemkolk FEM, Leuvenink HGD, et al. Oxygenated versus standard cold perfusion preservation in kidney transplantation (COMPARE): a randomised, double-blind, paired, phase 3 trial. Lancet. 2020;396(10263):1653–1662.

[176] Schlegel A, Graf R, Clavien PA, Dutkowski P. Hypothermic oxygenated perfusion (HOPE) protects from biliary injury in a rodent model of DCD liver transplantation. J Hepatol. 2013;59:984–991.

[177] de Rougemont O, Breitenstein S, Leskosek B, et al. One hour hypothermic oxygenated perfusion (HOPE) protects nonviable liver allografts donated after cardiac death. Ann Surg. 2009;250:674–683.

[178] Dondossola D, Ravaioli M, Lonati C, Maroni L, Pini A, Accardo C, Germinario G, Antonelli B, Odaldi F, Zanella A, Siniscalchi A, Cescon M, Rossi G. The role of ex situ hypothermic oxygenated machine perfusion and cold preservation time in extended criteria donation after circulatory death and donation after brain death. Liver Transpl. 2021;27(8):1130–1143. doi:10.1002/lt.26067

[179] Kron P, Schlegel A, Mancina L, et al. Hypothermic oxygenated perfusion (HOPE) for fatty liver grafts in rats and humans. J Hepatol. 2017. Epub ahead of print. doi:10.1016/j.jhep.2017.08.028

[180] Schlegel A, Kron P, Graf R, et al. Warm vs. cold perfusion techniques to rescue rodent liver grafts. J Hepatol. 2014;61:1267–1275.

[181] Schlegel A, Kron P, Dutkowski P. Hypothermic oxygenated liver perfusion: basic mechanisms and clinical application. Curr Transplant Rep. 2015;2:52–62.

[182] op den Dries S, Sutton ME, Karimian N, de Boer MT, Wiersema-Buist J, et al. Hypothermic oxygenated machine perfusion prevents arteriolonecrosis of the peribiliary plexus in pig livers donated after circulatory death. PLoS One. 2014;9(2):e88521.

[183] Westerkamp AC, Karimian N, Matton APM, Mahboub P, van Rijn R, Wiersema-Buist J, de Boer MT, Leuvenink HGD, Gouw ASH, Lisman T, Porte RJ. Oxygenated hypothermic machine perfusion after static cold storage improves hepatobiliary function of extended criteria donor livers. Transplantation. 2016;100(4):825–835.

[184] Fujita S. Isolated perfusion of rat livers: effect of temperature on O2 consumption, enzyme release, energy store, and morphology. Nihon Geka Hokan. 1993;62:58–70.

[185] Westerkamp AC, Mahboub P, Meyer SL, et al. End-ischemic machine perfusion reduces bile duct injury in donation after circulatory death rat donor livers independent of the machine perfusion temperature. Liver Transpl. 2015;21:1300–1311.

[186] Lüer B, Koetting M, Efferz P, Minor T. Role of oxygen during hypothermic machine perfusion preservation of the liver. Transpl Int. 2010;23:944–950.

[187] Pegg DE, Foreman J, Hunt CJ, Diaper MP. The mechanism of action of retrograde oxygen persufflation in renal preservation. Transplantation. 1989;48:210–217.

[188] van der Plaats A, 'T Hart NA, Verkerke GJ, et al. Hypothermic machine preservation in liver transplantation revisited: concepts and criteria in the new millennium. Ann Biomed Eng. 2004;32:623–631.

[189] van Golen RF, van Gulik TM, Heger M. The sterile immune response during hepatic ischemia/reperfusion. Cytokine Growth Factor Rev. 2012;23:69–84.

[190] Clavien PA, Dutkowski P. Advances in hypothermic perfusion. Liver Transpl. 2017;23(Suppl 1):S52–S55.

[191] Vajdová K, Graf R, Clavien PA. ATP-supplies in the cold-preserved liver: a long-neglected factor of organ viability. Hepatology. 2002;36(6):1543–1552.

[192] Werner MJM, van Leeuwen OB, de Jong IEM, et al. First report of successful transplantation of a pediatric donor liver graft after hypothermic machine perfusion. Pediatr Transplant. 2019;23(3):e13443.

[193] Fujiyoshi M, de Meijer VE, Porte RJ. Machine perfusion for donor organ repair: from vision to everyday clinical practice. In: Orlando G, Keshavjee S, editors. Organ Repair and Regeneration. Amsterdam: Elsevier; 2021. p. 43–73.

[194] Andria B, Bracco A, Attanasio C, Castaldo S, Cerrito MG, Cozzolino S, Di Napoli D, Giovannoni R, Mancini A, Musumeci A, Mezza E, Nasti M, Scuderi V, Staibano S, Lavitrano M, Otterbein LE, Calise F. Biliverdin protects against liver ischemia reperfusion injury in swine. PLoS One. 2013;8(7):e69972.

[195] Pezzati D, Liu Q, Quintini C. Ex vivo normothermic machine perfusion. In: Croome K, Muiesan P, Taner C, editors. Donation after Circulatory Death (DCD) Liver Transplantation. Cham: Springer; 2020. p. 43–73. doi:10.1007/978-3-030-46470-7_15

[196] de Vries RJ, Pendexter CA, Cronin SEJ, Marques B, Hafiz EOA, Muzikansky A, van Gulik TM, Markmann JF, Stott SL, Yeh H, Toner M, Uygun K, Tessier SN. Cell release during perfusion reflects cold ischemic injury in rat livers. Sci Rep. 2020;10:1102.

[197] Eshmuminov D, Becker D, Bautista Borrego L, Hefti M, Schuler MJ, Hagedorn C, et al. An integrated perfusion machine preserves injured human livers for 1 week. Nat Biotechnol. 2020;38(2):189–198.

[198] Durán M, Hann A, Lembach H, Nutu A, Clarke G, Patel I, Sneiders D, Hartog H, Mirza DF, Perera MTPR. Normothermic machine perfusion as a tool for safe transplantation of high-risk recipients. Transplantology. 2022;2:45–56.

[199] Vogel T, Brockmann JG, Friend PJ. Ex-vivo normothermic liver perfusion: an update. Curr Opin Organ Transplant. 2010;15(2):167–172.

[200] Le Moine O, Louis H, Demols A, Desalle F, Demoor F, Quertinmont E, Goldman M, Devière J. Cold liver ischemia-reperfusion injury critically depends on liver T cells and is improved by donor pretreatment with interleukin 10 in mice. Hepatology. 2000;31(6):1266–1274.

[201] Polyak MMR, Grosche A. Comparison of Vasosol and University of Wisconsin solutions on early kidney function after 24 hours of cold ischemia in a canine autotransplantation model. J Surg Res. 2008;150:255–260.

[202] Nostedt JJ, Skubleny DT, Shapiro AMJ, Campbell S, Freed DH, Bigam DL. Normothermic ex vivo machine perfusion for liver grafts recovered from donors after circulatory death: a systematic review and meta-analysis. HPB Surg. 2018;2018:9156473.

[203] Raigani S, de Vries RJ, Uygun K, Yeh H. Pumping new life into old ideas: preservation and rehabilitation of the liver using ex situ machine perfusion. Artif Organs. 2020;44:123–128.

[204] Matton A, de Vries Y, Burlage LC, van Rijn R, Fujiyoshi M, de Meijer VE, et al. Biliary bicarbonate, pH, and glucose are suitable biomarkers of biliary viability during ex situ normothermic machine perfusion of human donor livers. Transplantation. 2019;103:1405–1413.

[205] Iyer A, Gao L, Doyle A, Rao P, Cropper JR, Soto C, et al. Normothermic ex vivo perfusion provides superior preservation and enables viability assessment of hearts from DCD donors. Am J Transplant. 2015;15:371–380.

[206] Brüggenwirth IMA, de Meijer VE, Porte RJ, Martins PN. Viability criteria assessment during liver machine perfusion. Nat Biotechnol. 2020;38:1260–1262.

[207] Bhogal RH, Mirza DF, Afford SC, Mergental H. Biomarkers of liver injury during transplantation in an era of machine perfusion. Int J Mol Sci. 2020;21(5):1578.

[208] Ardehali A, Esmailian F, Deng M, Soltesz E, Hsich E, Naka Y, et al. Ex-vivo perfusion of donor hearts for human heart transplantation (PROCEED II): a prospective open-label multicentre randomised non-inferiority trial. Lancet. 2015;385:2577–2584.

[209] Furukori M, Matsuno N, Meng LT, Shonaka T, Nishikawa Y, Imai K, et al. Subnormothermic machine perfusion preservation with rewarming for donation after cardiac death liver grafts in pigs. Transplant Proc. 2016;48:1239–1243.

[210] Selzner M, Goldaracena N, Echeverri J, Kaths JM, Linares I, Selzner N, Serrick C, Marquez M, Sapisochin G, Renner EL, et al. Normothermic ex vivo liver perfusion using Steen solution as perfusate for human liver transplantation: first North American results. Liver Transpl. 2016;22:1501–1508.

[211] Orman MA, Berthiaume F, Androulakis IP, Ierapetritou MG. Advanced stoichiometric analysis of metabolic networks of mammalian systems. Biomed Eng. 2011;39(6):511–534.

[212] Kauffman KJ, Prakash P, Edwards JS. Advances in flux balance analysis. Curr Opin Biotechnol. 2003;14:491–496.

[213] Llaneras F, Pico J. Stoichiometric modelling of cell metabolism. J Biosci Bioeng. 2008;105(1):1–11.

[214] Orman MA, Mattick J, Androulakis IP, Berthiaume F, Ierapetritou MG. Stoichiometry based steady-state hepatic flux analysis: computational and experimental aspects. Metabolites. 2012;2:268–291.

[215] Kaths JM, Spetzler VN, Goldaracena N, Echeverri J, Louis KS, Foltys DB, et al. Normothermic ex vivo kidney perfusion for the preservation of kidney grafts prior to transplantation. J Vis Exp. 2015;101:e52804.

[216] Sunjaya AF, Sunjaya AP. Combating donor organ shortage: Organ Care System prolonging organ storage time and improving the outcome of heart transplantations. Cardiovasc Ther. 2019;2019:4926094.

[217] Rigo F, De Stefano N, Navarro-Tableros V, David E, Rizza G, Catalano G, et al. Extracellular vesicles from human liver stem cells reduce injury in an ex vivo normothermic hypoxic rat liver perfusion model. Transplantation. 2018;102(5):205–210.

[218] Caenegem OV, Beauloyea C, Bertrand L, Horman S, Lepropre S, Sparavier G, et al. Hypothermic continuous machine perfusion enables preservation of energy charge and functional recovery of heart grafts in an ex vivo model of donation following circulatory death. Eur J Cardiothorac Surg. 2015;49:1348–1353.

[219] Tolboom H, Olejnikova V, Reser D, Rosser B, Wilhelm MJ, Gassmann M, et al. Moderate hypothermia during ex vivo machine perfusion promotes recovery of hearts donated after cardiocirculatory death. Eur J Cardiothorac Surg. 2015;49(1):25–31.

[220] El-Rhalibi A, Wilson C, Nasralla D. Artificial intelligence in photography of normothermic machine perfusion of livers. Br J Surg. 2022;109(Suppl 4):znac242.023.

[221] Calleja Lozano R, Hervás Martínez C, Briceño Delgado FJ. Crossroads in liver transplantation: is artificial intelligence the key to donor–recipient matching? Medicina. 2022;58(12):1743.

[222] Doyle HR, Dvorchik I, Mitchell S, Marino IR, Ebert FH, McMichael J, Fung JJ. Predicting outcomes after liver transplantation: a connectionist approach. Ann Surg. 1994;219:408–415.

[223] Deo RC. Machine learning in medicine. Circulation. 2015;132:1920–1930.

[224] Stanfield CL. Principles of Human Physiology. 4th ed. Benjamin Cummings; 2011.

[225] Bubin E, Gorstein F, Rubin R, Schwarting R, Strayer D. Rubin's Pathology: Clinicopathologic Foundations of Medicine. 4th ed. Lippincott Williams & Wilkins; 2005.

[226] Wu MY, Yiang GT, Liao WT, Tsai APY, Cheng YL, Cheng PW, Li CY, Li CJ. Current mechanistic concepts in ischemia and reperfusion injury. Cell Physiol Biochem. 2018;46:1650–1667.

[227] Frascari I. Sistemi endorfinergici e modulazione di segnali molecolari e profili trascrizionali coinvolti in processi di protezione e autoriparazione del miocardio danneggiato. Dottorato di ricerca in Scienze Mediche Specialistiche, Alma Mater Studiorum – Università di Bologna, Ciclo XXV; 2013.

[228] Lorenzelli F. Principi di saturimetria e di funzionamento del pulsossimetro. Scuola di Ingegneria e Architettura, Laurea in Ingegneria Biomedica, Alma Mater Studiorum – Università di Bologna; A.A. 2016/2017.

[229] Cowled P, Fitridge R. Pathophysiology of reperfusion injury. In: Fitridge R, Thompson M, editors. Mechanisms of Vascular Disease: A Reference Book for Vascular Specialists. Adelaide (AU): University of Adelaide Press; 2011.

[230] Gilbo N, Catalano G, Salizzoni M, Romagnoli R. Liver graft preconditioning, preservation and reconditioning. Digest Liver Dis. 2016;48:1265–1274.

[231] Panisello-Roselló A, Lopez A, Folch-Puy E, Carbonell T, Rolo A, Palmeira C, Adam R, Net M, Roselló-Catafau J. Role of aldehyde dehydrogenase 2 in ischemia reperfusion injury: an update. World J Gastroenterol. 2018;24:2984–2994.

[232] van Golen RF, van Gulik TM, Heger M. The sterile immune response during hepatic ischemia/reperfusion. Cytokine Growth Factor Rev. 2012;23:69–84.

[233] Dubbeld J, Hoekstra H, Farid W, Ringers J, Porte RJ, Metselaar HJ, et al. Similar liver transplantation survival with selected cardiac death donors and brain death donors. Br J Surg. 2010;97:744–753.

[234] He X, Guo Z, Zhao Q, et al. The first case of ischemia-free organ transplantation in humans: a proof of concept. Am J Transplant. 2018;18(3):737–744.

[235] Czigany Z, Lurje I, Schmelzle M, Schöning W, Öllinger R, Raschzok N, Sauer IM, Tacke F, Strnad P, Trautwein C, Neumann UP, Fronek J, Mehrabi A, Pratschke J, Schlegel A, Lurje G. Ischemia-reperfusion injury in marginal liver grafts and the role of hypothermic machine perfusion: molecular mechanisms and clinical implications. J Clin Med. 2020;9(3):846. doi:10.3390/jcm9030846

[236] Konishi T, Lentsch AB. Hepatic ischemia/reperfusion: mechanisms of tissue injury, repair, and regeneration. Gene Expr. 2017;17:277–287.

[237] Zaouali MA, Ben Abdennebi H, Padrissa-Altés S, Mahfoudh-Boussaid A, Roselló-Catafau J. Pharmacological strategies against cold ischemia reperfusion injury. Expert Opin Pharmacother. 2010;11:537–555. doi:10.1517/14656560903547836

[238] Zaouali MA, Ben Abdennebi H, Padrissa-Altés S, Alfany-Fernandez I, Rimola A, Roselló-Catafau J. How Institut Georges Lopez preservation solution protects nonsteatotic and steatotic livers against ischemia-reperfusion injury. Transplant Proc. 2011;43:77–79. doi:10.1016/j.transproceed.2010.12.026

[239] Cursio R, Gugenheim J. Ischemia-reperfusion injury and ischemic-type biliary lesions following liver transplantation. J Transpl. 2012;2012:164329.

[240] Kalogeris T, Baines CP, Krenz M, Korthuis RJ. Cell biology of ischemia/reperfusion injury. Int Rev Cell Mol Biol. 2012;298:229–317. doi:10.1016/B978-0-12-394309-5.00006-7

[241] Jaeschke H. Mechanisms of reperfusion injury after warm ischemia of the liver. J Hepatobiliary Pancreat Surg. 1998;5:402–408.

[242] Fondevila C, Busuttil RW, Kupiec-Weglinski JW. Hepatic ischemia/reperfusion injury – a fresh look. Exp Mol Pathol. 2003;74:86–93.

[243] Jaeschke H. Molecular mechanisms of hepatic ischemia-reperfusion injury and preconditioning. Am J Physiol Gastrointest Liver Physiol. 2003;284:G15–G26.

[244] Rampes S, Ma D. Hepatic ischemia-reperfusion injury in liver transplant setting: mechanisms and protective strategies. J Biomed Res. 2019;33(4):221–234. doi:10.7555/JBR.32.20180087

[245] Zhai Y, Petrowsky H, Hong JC, Busuttil RW, Kupiec-Weglinski JW. Ischaemia-reperfusion injury in liver transplantation—from bench to bedside. Nat Rev Gastroenterol Hepatol. 2013;10(2):79–89. doi:10.1038/nrgastro.2012.225

[246] Mao XL, Cai Y, Chen YH, Wang Y, Jiang XX, Ye LP, Li SW. Novel targets and therapeutic strategies to protect against hepatic ischemia reperfusion injury. Front Med. 2022;8:757336. doi:10.3389/fmed.2021.757336

[247] Brunner SM, Junger H, Ruemmele P, et al. Bile duct damage after cold storage of deceased donor livers predicts biliary complications after liver transplantation. J Hepatol. 2013;58:1133–1139.

[248] Hansen T, Hollemann D, Pitton MB, et al. Histological examination and evaluation of donor bile ducts received during orthotopic liver transplantation – a morphological clue to ischemic-type biliary lesion? Virchows Arch. 2012;461:41–48.

[249] Brüggenwirth IMA, Burlage LC, Porte RJ, Martins PN. Is single portal vein perfusion the best approach for machine preservation of liver grafts? J Hepatol. 2016;64(5):1194–1195.

[250] Karimian N, Weeder PD, Bomfati F, Gouw AS, Porte RJ. Preservation injury of the distal extrahepatic bile duct of donor livers is representative for injury of the intrahepatic bile ducts. J Hepatol. 2015;63:284–287.

[251] Brüggenwirth IMA, Moore C, Mahboub P, Thijssen MF, E X, Leuvenink HGD, Mandrekar P, Wang X, Kowalik TF, Porte RJ, Martins PN. A comparative study of single and dual perfusion during end-ischemic subnormothermic liver machine preservation. Transplant Direct. 2018;4(11):e400.

[252] Lautt WW. Hepatic Circulation: Physiology and Pathophysiology. 1st ed. San Rafael: Morgan & Claypool Life Sciences; 2009.

[253] Hou J, Liavåg OMI, Færden IH, et al. Utilization of dielectric properties for assessment of liver ischemia-reperfusion injury in vivo and during machine perfusion. Sci Rep. 2022;12:11183.

[254] Low G, et al. Imaging of vascular complications and their consequences following transplantation in the abdomen. Radiographics. 2013;33:633–652.

[255] Nishida S, Nakamura N, Kadono J, Komokata T, et al. Intrahepatic biliary strictures after liver transplantation. J Hepatobiliary Pancreat Surg. 2006;13:511–516.

[256] Sezai A, Shiono M, Orime Y, et al. Major organ function under mechanical support: comparative studies of pulsatile and nonpulsatile circulation. Artif Organs. 1999;23:280–285.

[257] Cheng A, Williamitis CA, Slaughter MS. Comparison of continuous-flow and pulsatile-flow left ventricular assist devices: is there an advantage to pulsatility? Ann Cardiothorac Surg. 2014;3(6):573–581. doi:10.3978/j.issn.2225-319X.2014.08.24

[258] Baba A, Dobsak P, Saito I, et al. Microcirculation of the bulbar conjunctiva in the goat implanted with a total artificial heart: effects of pulsatile and nonpulsatile flow. ASAIO J. 2004;50:321–327.

[259] Lee JJ, Tyml K, Menkis AH, et al. Evaluation of pulsatile and nonpulsatile flow in capillaries of goat skeletal muscle using intravital microscopy. Microvasc Res. 1994;48:316–327.

[260] von Horn C, Minor T. Isolated kidney perfusion: the influence of pulsatile flow. Scand J Clin Lab Invest. 2018;78:131–135.

[261] Timsit MO, Tullius SG. Hypothermic kidney preservation: a remembrance of the past in the future? Curr Opin Organ Transplant. 2011;16:162–168.

[262] Jia JJ, Zhang J, Li JH, Chen XD, Jiang L, Zhou YF, He N, Xie HY, Zhou L, Zheng SS. Influence of perfusate on liver viability during hypothermic machine perfusion. World J Gastroenterol. 2015;21(29):8848–8857.

[263] Kramer RS, Morton JR, Groom RC, Robaczewski DL. Coronary artery bypass grafting. In: Vasan RS, Sawyer DB, editors. Encyclopedia of Cardiovascular Research and Medicine. Elsevier; 2018. p. 700–729. doi:10.1016/B978-0-12-809657-4.99754-0

[264] Nassar A, Liu Q, Farias K, et al. Ex vivo normothermic machine perfusion is safe, simple, and reliable: results from a large animal model. Surg Innov. 2015;22(1):61–69.

[265] Gilbo N, Wylin T, Heedfeld V, Jochmans I, Pirenne J, Friend P, Monbaliu D. Porcine liver normothermic machine perfusion: methodological framework and potential pitfalls. Transplant Direct. 2021;8(1):e1276.

[266] Bruinsma BG, Berendsen TA, Izamis ML, Yarmush ML, Uygun K. Determination and extension of the limits to static cold storage using subnormothermic machine perfusion. Int J Artif Organs. 2013;36(11):775–780. doi:10.5301/ijao.5000250

[267] Magbagbeola M, Doyle K, Rai ZL, Lindenroth L, Dwyer G, Stilli A, Davidson BR, Stoyanov D. Evaluation of a novel organ perfusion research platform. Annu Int Conf IEEE Eng Med Biol Soc. 2022;2022:2565–2568. doi:10.1109/EMBC48229.2022.9871028

[268] Imber CJ, St Peter SD, Lopez de Cenarruzabeitia I, Pigott D, James T, Taylor R, McGuire J, Hughes D, Butler A, Rees M, Friend PJ. Advantages of normothermic perfusion over cold storage in liver preservation. Transplantation. 2002;73(5):701–709.

[269] Riveros S, Marino C, Ochoa G, Morales E, Soto D, Alegría L, et al. Implementation and design of customized ex vivo machine perfusion: analysis of its first results. Artif Organs. 2022;46:210–218. doi:10.1111/aor.14060

[270] Kafagy D, Gitano-Briggs H. Axial flow artificial heart blood pumps: a brief review. Trends Biomater Artif Organs. 2013;27(3):124–130.

[271] Ritchi AC. Extracorporeal artificial organs. In: Ratner BD, Hoffman AS, Schoen FJ, Lemons JE, editors. Biomaterials Science: An Introduction to Materials. 3rd ed. Amsterdam: Academic Press; 2013. p. 827–841.

[272] Watson C, Kosmoliaptsis V, Pley C, et al. Observations on the ex situ perfusion of livers for transplantation. Am J Transplant. 2018;18:2005–2020.

[273] Ghinolfi D, Rreka E, Pezzati D, Filipponi F, De Simone P. Perfusion machines and hepatocellular carcinoma: a good match between a marginal organ and an advanced disease? Transl Gastroenterol Hepatol. 2017;2:87.

[274] Watson CJE, Kosmoliaptsis V, Randle LV, Gimson AE, Brais R, Klinck JR, et al. Normothermic perfusion in the assessment and preservation of declined livers before transplantation: hyperoxia and vasoplegia—important lessons from the first 12 cases. Transplantation. 2017;101:1084–1098.

[275] de Vries Y, Matton APM, Nijsten MWN, et al. Pretransplant sequential hypo- and normothermic machine perfusion of suboptimal livers donated after circulatory death using a hemoglobin-based oxygen carrier perfusion solution. Am J Transplant. 2019;19:1202–1211.

[276] Laing RW, Bhogal RH, Wallace L, et al. The use of an acellular oxygen carrier in a human liver model of normothermic machine perfusion. Transplantation. 2017;101(11):2746–2756.

[277] Buttari B, Profumo E, Rigano R. Crosstalk between red blood cells and the immune system and its impact on atherosclerosis. Biomed Res Int. 2015;2015:616834.

[278] Gage F, Leeser DB, Porterfield NK, Graybill JC, Gillern S, Hawksworth JS, et al. Room temperature pulsatile perfusion of renal allografts with Lifor compared with hypothermic machine pump solution. Transpl Proc. 2009;41:3571–3574.

[279] Guo M, Lu C, Gao Y, Zhang H, Chen D, Li Y. Lifor solution: an alternative preservation solution in small bowel transplantation. Gastroenterol Res Pract. 2016;2016:3925751. doi:10.1155/2016/3925751

[280] Stowe DF, Camara AKS, Heisner JS, Aldakkak M, Harder DR. Ten-hour preservation of guinea pig isolated hearts perfused at low flow with air-saturated Lifor solution at 26°C: comparison to ViaSpan solution. Am J Physiol Heart Circ Physiol. 2007;293(1):H895–H901. doi:10.1152/ajpheart.00149.2007

[281] Mergental H, Stephenson BTF, Laing RW, Kirkham AJ, Neil DAH, Wallace LL, et al. Development of clinical criteria for functional assessment to predict primary nonfunction of high-risk livers using normothermic machine perfusion. Liver Transpl. 2018;24:1453–1469. doi:10.1002/lt.25291

[282] – [nota vuota, saltata]

[283] Stowe DF, Camara AKS, Heisner JS, Aldakkak M, Harder DR. Low-flow perfusion of guinea pig isolated hearts with 26°C air-saturated Lifor solution for 20 hours preserves function and metabolism. J Heart Lung Transplant. 2008;27(9):1008–1015. doi:10.1016/j.healun.2008.05.028

[284] Regner KR, Nilakantan V, Ryan RP, et al. Protective effect of Lifor solution in experimental renal ischemia-reperfusion injury. J Surg Res. 2010;164(2):e291–e297. doi:10.1016/j.jss.2010.08.033

[285] Karakoyun R, Romano A, Nordström J, Ericzon BG, Nowak G. Type of preservation solution, UW or HTK, has an impact on the incidence of biliary stricture following liver transplantation: a retrospective study. J Transplant. 2019;2019:8150736.

[286] Xu X, Zhu YF, Lv T, Zheng JL, Li Y, Zhang BH, Jiang L, Yang JY. Histidine-tryptophan-ketoglutarate solution versus University of Wisconsin solution in adult-to-adult living donor liver transplantation: a propensity score matching analysis from mainland China. Medicine (Baltimore). 2020;99(51):e23584.

[287] Minor T, Efferz P, Fox M, et al. Controlled oxygenated rewarming of cold stored liver grafts by thermally graduated machine perfusion prior to reperfusion. Am J Transplant. 2013;13:1450–1460. doi:10.1111/ajt.12235

[288] Belzer FO, D'Alessandro AM, Hoffmann RM, Knechtle SJ, Reed A, Pirsch JD, Kalayoglu M, Sollinger HW. The use of UW solution in clinical transplantation: a 4-year experience. Ann Surg. 1992;215(6):579–583; discussion 584–585. doi:10.1097/00000658-199206000-00004

[289] Cameron AM, Barandiaran Cornejo JF. Organ preservation review: history of organ preservation. Curr Opin Organ Transplant. 2015;20:146–151.

[290] Jamieson RW, Friend PJ. Organ reperfusion and preservation. Front Biosci. 2008;13:221–235.

[291] Gibelin H, Eugene M, Hebrard W, et al. Comparison of Euro-Collins and University of Wisconsin solutions in the isolated perfused rat liver model: evaluation by proton nuclear magnetic resonance spectroscopy. Transplant Proc. 2000;32:2792.

[292] Bejaoui M, Pantazi E, Folch-Puy E, Baptista PM, García-Gil A, Adam R, Roselló-Catafau J. Emerging concepts in liver graft preservation. World J Gastroenterol. 2015;21(2):396–407.

[293] Southard JH, Belzer FO. Organ preservation. Annu Rev Med. 1995;46:235–247.

[294] Wahlberg JA, Southard JH, Belzer FO. Development of a cold storage solution for pancreas preservation. Cryobiology. 1986;23:477–482.

[295] Chen Y, Shi J, Xia TC, Xu R, He X, Xia Y. Preservation solutions for kidney transplantation: history, advances and mechanisms. Cell Transplant. 2019;28(12):1472–1489. doi:10.1177/0963689719872699

[296] Tripathy S, Das SK. Strategies for organ preservation: current prospective and challenges. Cell Biol Int. 2023;1–19. doi:10.1002/cbin.11984

[297] Southard JH, van Gulik TM, Ametani MS, Vreugdenhil PK, Lindell SL, Pienaar BL, Belzer FO. Important components of the UW solution. Transplantation. 1990;49(2):251–257. doi:10.1097/00007890-199002000-00004

[298] O'Callaghan J, Leuvenink HGD, Friend PJ, Ploeg RJ. Chapter 9: kidney preservation. In: Morris PJ, Knechtle SJ, editors. Kidney Transplantation: Principles and Practice. 7th ed. W.B. Saunders; 2014. p. 130–141. doi:10.1016/B978-1-4557-4096-3.00009-X

[299] Petrowsky H, Clavien PA. Chapter 44: principles of liver preservation. In: Busuttil RW, Klintmalm GBG, editors. Transplantation of the Liver. 3rd ed. Philadelphia: W.B. Saunders; 2015. p. 582–599.

[300] Miyoshi S, Shimokawa S, Schreinemakers H, Date H, Weder W, Harper B, Cooper JD. Comparison of the University of Wisconsin preservation solution and other crystalloid perfusates in a 30-hour rabbit lung preservation model. J Thorac Cardiovasc Surg. 1992;103(1).

[301] Cartier R, Hollmann C, Dagenais F, Buluran J, Pellerin M, Leclerc Y. Effects of University of Wisconsin solution on endothelium-dependent coronary artery relaxation in the rat. Ann Thorac Surg. 1993;55(1):50–55; discussion 56. doi:10.1016/0003-4975(93)90472-T

[302] Voigt MR, DeLario GT. Perspectives on abdominal organ preservation solutions: a comparative literature review. Prog Transplant. 2013;23:383–391.

[303] Feng XN, Xu X, Zheng SS. Current status and perspective of liver preservation solutions. Hepatobiliary Pancreat Dis Int. 2006;5(4):490–494.

[304] Marvin RS. The accuracy of measurements of viscosity of liquids. J Res Natl Bur Stand A Phys Chem. 1971;75A(6):535–540. doi:10.6028/jres.075A.041

[305] Berstad DA, Knapstad B, Lamvik M, Skjølsvik PA, Tørklep K, Øye HA. Accurate measurements of the viscosity of water in the temperature range 19.5–25.5°C. Physica A. 1988;151:246–280. doi:10.1016/0378-4371(88)90015-5

[306] Korson L, Drost-Hansen W, Millero FJ. Viscosity of water at various temperatures. J Phys Chem. 1969;73(1):34–39. doi:10.1021/j100721a006

[307] Wei L, Hata K, Doorschodt BM, Büttner R, Minor T, Tolba RH. Experimental small bowel preservation using Polysol: a new alternative to University of Wisconsin solution, Celsior and histidine-tryptophan-ketoglutarate solution? World J Gastroenterol. 2007;13:3684–3691.

[308] Ringe B, Braun F, Moritz M, Zeldin G, Soriano H, Meyers W. Safety and efficacy of living donor liver preservation with HTK solution. Transplant Proc. 2005;37:316–319.

[309] Zhao X, Koshiba T, Nakamura T, Tsuruyama T, Li Y, Bando T, Wada H, Tanaka K. ET-Kyoto solution plus dibutyryl cyclic adenosine monophosphate is superior to University of Wisconsin solution in rat liver preservation. Cell Transplant. 2008;17:99–109.

[310] Morariu AM, Van der Plaats A, Van Oeveren W, Hart NAT, Leuvenik HGD, Graaff R, Ploegh RJ, Rakhorst G. Hyperaggregating effect of hydroxyethyl starch components and University of Wisconsin solution on human red blood cells: a risk of impaired graft perfusion in organ procurement? Transplantation. 2003;76:37–43.

[311] Stewart ZA, Cameron AM, Singer AL, et al. Histidine-tryptophan-ketoglutarate (HTK) is associated with reduced graft survival in deceased donor livers, especially those donated after cardiac death. Am J Transplant. 2009;9:286–293.

[312] Meine MH, Zanotelli ML, Neumann J, et al. Randomized clinical assay for hepatic grafts preservation with University of Wisconsin or histidine-tryptophan-ketoglutarate solutions in liver transplantation. Transplant Proc. 2006;38:1872–1875.

[313] Chan SC, Liu CL, Lo CM, et al. Applicability of histidine-tryptophan-ketoglutarate solution in right lobe adult-to-adult live donor liver transplantation. Liver Transpl. 2004;10:1415–1421.

[314] Mangus RS, Fridell JA, Vianna RM, et al. Comparison of histidine-tryptophan-ketoglutarate solution and University of Wisconsin solution in extended criteria liver donors. Liver Transpl. 2008;14:365–373.

[315] Sahmeddini MA, Khosravi MB. Severe acute hyperkalemia during pre-anhepatic stage in cadaveric orthotopic liver transplantation. Iran J Med Sci. 2012;37(3):208–210.

[316] Zhang L, Xue FS, Tian M, et al. Elevated effluent potassium concentrations predict the development of postreperfusion hyperkalemia in deceased liver transplantation: a retrospective cohort study. BMC Anesthesiol. 2022;22:161. doi:10.1186/s12871-022-01699-1

[317] Boteon YL, Hessheimer AJ, Bruggenwirth IMA, Boteon APCS, Padilla M, de Meijer VE, Domínguez-Gil B, Porte RJ, Perera MTPR, Martins PN. The economic impact of machine perfusion technology in liver transplantation. Artif Organs. 2022;46:191–200.

[318] Bellamy CA, Nicely B, Mattice BJ, Teaster R. Comparative analysis of clinical efficacy and cost between University of Wisconsin solution and histidine-tryptophan-ketoglutarate. Prog Transplant. 2008;18(3):166–171; quiz 172. doi:10.1177/152692480801800304

[319] Schneeberger S, Biebl M, Steurer W, Hesse UJ, Troisi R, Langrehr JM, et al. A prospective randomized multicenter trial comparing histidine-tryptophane-ketoglutarate versus University of Wisconsin perfusion solution in clinical pancreas transplantation. Transpl Int. 2009;22:217–224.

[320] Moray G, Sevmis S, Karakayali FY, Gorur SK, Haberal M. Comparison of histidine-tryptophan-ketoglutarate and University of Wisconsin in living-donor liver transplantation. Transplant Proc. 2006;38:3572–3575.

[321] Hata K, Tolba RH, Wei L, Doorschodt BM, Büttner R, Yamamoto Y, Minor T. Impact of Polysol, a newly developed preservation solution, on cold storage of steatotic rat livers. Liver Transpl. 2007;13:114–121.

[322] Bessems M, Doorschodt BM, Kolkert JLP, Vetelainen RL, van Vliet AK, Vreeling H, et al. Preservation of steatotic livers: a comparison between cold storage and machine perfusion preservation. Liver Transplant. 2007;13(4):497–504.

[323] Schreinemachers MCJM, Doorschodt BM, Florquin S, van den Bergh Weerman MA, Reitsma JB, Lai W, Sitzia M, Minor TM, Tolba RH, van Gulik T. Improved preservation and microcirculation with POLYSOL after transplantation in a porcine kidney autotransplantation model. Nephrol Dial Transplant. 2009;24:816–824.

[324] Yagi S, Doorschodt BM, Afify M, Klinge U, Kobayashi E, Uemoto S, Tolba RH. Improved preservation and microcirculation with POLYSOL after partial liver transplantation in rats. J Surg Res. 2011;167:E375–E383.

[325] Kalenski J, Mancina E, Paschenda P, Beckers C, Bleilevens C, Tothova L, Boor P, Doorschodt BM, Tolba RH. Improved preservation of warm ischemia-damaged porcine kidneys after cold storage in Ecosol, a novel preservation solution. Ann Transplant. 2015;20:233–242.

[326] Menasche P, Termignon JL, Pradier F, Grousset C, Mouas C, Alberici G, Weiss M, Piwnica A, Bloch G. Experimental evaluation of Celsior, a new heart preservation solution. Eur J Cardiothorac Surg. 1994;8(4):207–213.

[327] Mohr A, Brockmann JG, Becker F. HTK-N: modified histidine-tryptophan-ketoglutarate solution—a promising new tool in solid organ preservation. Int J Mol Sci. 2020;21(18):6468. doi:10.3390/ijms21186468

[328] Bretschneider HJ, Hübner G, Knoll D, et al. Myocardial resistance and tolerance to ischemia: physiological and biochemical basis. J Cardiovasc Surg (Torino). 1975;16:241–260.

[329] Bretschneider HJ. Myocardial protection. Thorac Cardiovasc Surg. 1980;28:295.

[330] Pokorny H, Rasoul-Rockenschaub S, Langer F, Windhager T, Rosenstingl A, Lange R, Königsrainer A, Ringe B, Mühlbacher F, Steininger R. Histidine-tryptophan-ketoglutarate solution for organ preservation in human liver transplantation—a prospective multi-centre observation study. Transpl Int. 2004;17(5):256–260.

[331] Lamesch P, Raygrotzki S, Kehrer G, Gubernatis G, Bretschneider HJ, Pichlmayr R. Preservation of the liver with HTK solution. Transplant Proc. 1990;22(2):518.

[332] Gubernatis G, Pichlmayr R, Lamesch P, et al. HTK-solution (Bretschneider) for human liver transplantation: first clinical experiences. Langenbecks Arch Chir. 1990;375(2):66.

[333] Hatano E, Tanaka A, Shinohara H, et al. Superiority of HTK solution to UW solution for tissue oxygenation in living related liver transplantation. Transplant Proc. 1996;28(3):1880.

[334] Erhard J, Lange R, Scherer R, et al. Comparison of histidine–tryptophan–ketoglutarate (HTK) solution versus University of Wisconsin (UW) solution for organ preservation in human liver transplantation: a prospective, randomized study. Transpl Int. 1994;7(3):177.

[335] Mangus RS, Tector AJ, Agarwal A, Vianna R, Murdock P, Fridell JA. Comparison of histidine-tryptophan-ketoglutarate solution (HTK) and University of Wisconsin solution (UW) in adult liver transplantation. Liver Transpl. 2006;12:226–230.

[336] Tolba RH, Akbar S, Müller A, Glatzel U, Minor T. Experimental liver preservation with Celsior: a novel alternative to University of Wisconsin and histidine-tryptophan-alpha-ketoglutarate solutions? Eur Surg Res. 2000;32(3):142–147. doi:10.1159/000008755

[337] Parsons RF, Guarrera JV. Preservation solutions for static cold storage of abdominal allografts: which is best? Curr Opin Organ Transplant. 2014;19(2):100–107.

[338] Ben Abdennebi H, Steghens JP, Margonari J, Ramella-Virieux S, Barbieux A, Boillot O. High-Na+, low-K+ UW cold storage solution reduces reperfusion injuries of the rat liver graft. Transpl Int. 1998;11:223–230.

[339] Rodrigues MG, Castro PMV, Almeida TC, Danziere FR, Sergi Filho FA, Sempertegui BEZ, Branez JR, Mota LT, Miranda MP, Santos RG, Genzini T. Impact of cold ischemia time on the function of liver grafts preserved with Custodiol. Transplant Proc. 2021;53:661–664.

[340] Garcia-Gil FA, Serrano MT, Fuentes-Broto L, et al. Celsior versus University of Wisconsin preserving solutions for liver transplantation: post-reperfusion syndrome and outcome of a 5-year prospective randomized controlled study. World J Surg. 2011;35:1598–1607.

[341] Feng L, Zhao N, Yao X, et al. Histidine-tryptophan-ketoglutarate solution vs. University of Wisconsin solution for liver transplantation: a systematic review. Liver Transpl. 2007;13:1125–1136.

[342] Rayya F, Harms J, Martin AP, et al. Comparison of histidine-tryptophan-ketoglutarate solution and University of Wisconsin solution in adult liver transplantation. Transplant Proc. 2008;40:891–894.

[343] Gulsen MT, Girotra M, Cengiz-Seval G, et al. HTK preservative solution is associated with increased biliary complications among patients receiving DCD liver transplants: a single-center experience. Ann Transplant. 2013;18:69–75.

[344] de Boer JD, Strelniece A, van Rosmalen M, et al. The effect of histidine-tryptophan-ketoglutarate solution and University of Wisconsin solution: an analysis of the Eurotransplant registry. Transplantation. 2018;102:1870–1877.

[345] Adam R, Delvart V, Karam V, et al. Compared efficacy of preservation solutions in liver transplantation: a long-term graft outcome study from the European liver transplant registry. Am J Transplant. 2015;15:395–406.

[346] Guarrera JV, Karim NA. Liver preservation: is there anything new yet? Curr Opin Organ Transplant. 2008;13:148–154.

[347] Cavallari A, Cillo U, Nardo B, et al. A multicenter pilot prospective study comparing Celsior and University of Wisconsin preserving solutions for use in liver transplantation. Liver Transpl. 2003;9:814–821.

[348] Gurusamy KS, Gonzalez HD, Davidson BR. Current protective strategies in liver surgery. World J Gastroenterol. 2010;16(48):6098–6103.

[349] den Butter G, Saunder A, Marsh DC, et al. Comparison of solutions for preservation of the rabbit liver as tested by isolated perfusion. Transpl Int. 1995;8:466–471.

[350] Avolio AW, Agnes S, Nure E, Maria G, Barbarino R, Pepe G, Castagneto M. Comparative evaluation of two perfusion solutions for liver preservation and transplantation. Transplant Proc. 2006;38(4):1066–1067.

[351] Minor T, Olschewski P, Tolba RH, Akbar S, Kocálková M, Dombrowski F. Liver preservation with HTK: salutary effect of hypothermic aerobiosis by either gaseous oxygen or machine perfusion. Clin Transplant. 2002;16(3):206–211.

[352] Olschewski P, Tolba R, Akbar S, Minor T. Use of HTK solution for hypothermic machine perfusion: an alternative for the preservation of less than optimal donor livers?—An experimental study in rats. Transplant Proc. 2003;35(2):767.

[353] Janßen H, Janßen PHE, Broelsch CE. UW is superior to Celsior and HTK in the protection of human liver endothelial cells against preservation injury. Liver Transpl. 2004;10(12):1514–1523.

[354] Nardo B, Bertelli R, Montalti R. Preliminary results of a clinical randomized study comparing Celsior and HTK solutions in liver preservation for transplantation. Transplant Proc. 2005;37:320–322.

[355] Lema Zuluaga GL, Serna Agudelo RE, Zuleta Tobón JJ. Preservation solutions for liver transplantation in adults: Celsior versus Custodiol: a systematic review and meta-analysis with an indirect comparison of randomized trials. Transplant Proc. 2013;45(1):25–32.

[356] Bessems M, Doorschodt BM, Dinant S, de Graaf W, van Gulik TM. Machine perfusion preservation of the pig liver using a new preservation solution, polysol. Transplant Proc. 2006;38(5):1238–1242.

[357] Marecki H, Bozorgzadeh A, Porte RJ, Leuvenink HG, Uygun K, Martins PN. Liver ex situ machine perfusion preservation: a review of the methodology and results of large animal studies and clinical trials. Liver Transpl. 2017;23(5).

[358] Bardallo RG, Company-Marin I, Folch-Puy E, Roselló-Catafau J, Panisello-Roselló A, Carbonell T. PEG35 and glutathione improve mitochondrial function and reduce oxidative stress in cold fatty liver graft preservation. Antioxidants. 2022;11:158.

[359] Ben Mosbah I, Roselló-Catafau J, Franco-Gou R, Abdennebi HB, Saidane D, Ramella-Virieux S, Boillot O, Peralta C. Preservation of steatotic livers in IGL-1 solution. Liver Transpl. 2006;12:1215–1223.

[360] Zaouali MA, Bejaoui M, Calvo M, Folch-Puy E, Pantazi E, Pasut G, Rimola A, Abdennebi HB, Adam R, Roselló-Catafau J. Polyethylene glycol rinse solution: an effective way to prevent ischemia-reperfusion injury. World J Gastroenterol. 2015;20:16203–16214.

[361] Hessheimer AJ, Polak W, Antoine C, Dondero Pozzo F, Maluf D, Monbaliu D, et al. Regulations and procurement surgery in DCD liver transplantation: expert consensus guidance from the International Liver Transplantation Society. Transplantation. 2021;105:945–951.

[362] BridgetoLife. Belzer MPS UW Machine Perfusion Solution. Available from:

https://bridgetolife.com/belzer-mps-uw-machine-perfusion-solution/ [accessed 08/02/2023].

[363] U.S. FDA. K192408 summary. Available from:

https://www.accessdata.fda.gov/cdrh_docs/pdf19/K192408.pdf [accessed 08/02/2023].

[364] Pasut G, Panisello A, Folch-Puy E, Lopez A, Castro-Benítez C, Calvo M, Carbonell T, García-Gil A, Adam R, Roselló-Catafau J. Polyethylene glycols: an effective strategy for limiting liver ischemia reperfusion injury. World J Gastroenterol. 2016;22:6501–6508.

[365] Vallant N, Wolfhagen N, Sandhu B, Hamaoui K, Cook T, Pusey C, Papalois V. A comparison of pulsatile hypothermic and normothermic ex vivo machine perfusion in a porcine kidney model. Transplantation. 2021;105(8):1760–1770.

[366] Liu Q, Vekemans K, Iania L, Komuta M, Parkkinen J, Heedfeld V, Wylin T, Monbaliu D, Pirenne J, van Pelt J. Assessing warm ischemic injury of pig livers at hypothermic machine perfusion. J Surg Res. 2014;186(1):379–389.

[367] Selten J, Schlegel A, de Jonge J, Dutkowski P. Hypo- and normothermic perfusion of the liver: which way to go? Best Pract Res Clin Gastroenterol. 2017;31(2):171–179.

[368] Leber B, Schlechter S, Weber J, et al. Experimental long-term sub-normothermic machine perfusion for non-allocable human liver grafts: first data towards feasibility. Eur Surg. 2022;54:150–155.

[369] van Leeuwen OB, de Vries Y, de Meijer VE, Porte RJ. Hypothermic machine perfusion before viability testing of previously discarded human livers. Nat Commun. 2021;12:1008. doi:10.1038/s41467-021-21182-8

[370] Kaths JM, Cen JY, Chun YM, et al. Continuous normothermic ex vivo kidney perfusion is superior to brief normothermic perfusion following static cold storage in donation after circulatory death pig kidney transplantation. Am J Transplant. 2017;17:957–969.

[371] Reddy SP, Bhattacharjya S, Maniakin N, et al. Preservation of porcine non-heart-beating donor livers by sequential cold storage and warm perfusion. Transplantation. 2004;77:1328–1332.

[372] Hoyer DP, Mathé Z, Gallinat A, et al. Controlled oxygenated rewarming of cold stored livers prior to transplantation: first clinical application of a new concept. Transplantation. 2016;100:147–152.

[373] de Vries Y, et al. Transplantation of high-risk donor livers after resuscitation and viability assessment using a combined protocol of oxygenated hypothermic, rewarming and normothermic machine perfusion: study protocol for a prospective, single-arm study (DHOPE-COR-NMP trial). BMJ Open. 2019;9:e028596. doi:10.1136/bmjopen-2018-028596

[374] von Horn C, Baba HA, Hannaert P, Hauet T, Leuvenink H, Paul A, et al. Controlled oxygenated rewarming up to normothermia for pretransplant reconditioning of liver grafts. Clin Transplant. 2017;31(11).

[375] Jain S, Lee CY, Baicu S, Duncan H, Xu H, Jones JW, Clemens MG, Brassi J, Taylor IMJ, Brockbank KGM. Hepatic function in hypothermically stored porcine livers: comparison of hypothermic machine perfusion vs cold storage. Transplant Proc. 2005;37:340–341.

[376] Schlegel A, Kalisvaart M, Muiesan P. Machine perfusion in liver transplantation: an essential treatment or just an expensive toy? Minerva Anestesiol. 2018;84(2):236–245.

[377] Boteon YL, Laing RW, Schlegel A, et al. The impact on the bioenergetic status and oxidative-mediated tissue injury of a combined protocol of hypothermic and normothermic machine perfusion using an acellular haemoglobin-based oxygen carrier: the cold-to-warm machine perfusion of the liver. PLoS One. 2019;14(10):e0224066.

[378] Chouchani ET, Pell VR, Gaude E, Aksentijević D, Sundier SY, Robb EL, et al. Ischaemic accumulation of succinate controls reperfusion injury through mitochondrial ROS. Nature. 2014;515(7527):431–435.

[379] Ündar A, Wang S, Özyüksel A, Rossano JW. Pediatric devices. In: Mechanical Circulatory and Respiratory Support. 2018:271–297. doi:10.1016/b978-0-12-810491-0.00009-6

[380] Clowes GH, Hopkins AL, Neville WE. An artificial lung dependent on diffusion of oxygen and carbon dioxide through plastic membranes. J Thorac Cardiovasc Surg. 1956;32:630.

[381] Arensman RM, Short BL, Stephens D. Extracorporeal membrane oxygenation. In: Assisted Ventilation of the Neonate. 2017:434–445.e1. doi:10.1016/b978-0-323-39006-4.00040-5

[382] Kammermeyer K. Silicone rubber as a selective barrier. Ind Eng Chem. 1957;49:1685.

[383] Melchior RW, Sutton SW, Harris W, Dalton HJ. Evolution of membrane oxygenator technology for utilization during pediatric cardiopulmonary bypass. Pediatr Health Med Ther. 2016;7:45–56. doi:10.2147/PHMT.S35070

[384] Lim MW. The history of extracorporeal oxygenators. Anaesthesia. 2006;61:984–995. doi:10.1111/j.1365-2044.2006.04781.x

[385] Cohn LH. Fifty years of open-heart surgery. Circulation. 2003;107:2168–2170.

doi:10.1161/01.CIR.0000071746.50876.E2

[386] Haines N, Wang S, Myers JL, Undar A. Comparison of two types of neonatal extracorporeal life support systems with pulsatile and nonpulsatile flow. Artif Organs. 2009;33:958–966.

[387] Yoshida K, Nakamura S, Sakamoto H, Kondo M, Chouno T, Ikegami Y, Shirakigawa N, Mizumoto H, Yamashita Y, Baba H, Ijima H. Normothermic machine perfusion system satisfying oxygen demand of liver could maintain liver function more than subnormothermic machine perfusion. J Biosci Bioeng. 2021;131:107–113.

[388] Murphy GS, Hessel EA, Groom RC. Optimal perfusion during cardiopulmonary bypass: an evidence-based approach. Anesth Analg. 2009;108(5).

[389] Nagase K, Kohori F, Sakai K. Oxygen transfer performance of a membrane oxygenator composed of crossed and parallel hollow fibers. Biochem Eng J. 2005;24(2):105–113. doi:10.1016/j.bej.2005.02.003

[390] Teber O, Altinay AD, Naziri Mehrabani SA, Tasdemir RS, Zeytuncu B, Genceli EA, Dulekgurgen E, Pekkan K, Koyuncu I. Polymeric hollow fiber membrane oxygenators as artificial lungs: a review. Biochem Eng J. 2022;180:108340. doi:10.1016/j.bej.2022.108340

[391] Fondevila C, Hessheimer AJ, Maathuis MH, Munoz J, Taura P, Calatayud D, et al. Hypothermic oxygenated machine perfusion in porcine donation after circulatory determination of death liver transplant. Transplantation. 2012;94:22–29.

[392] Van Der Plaats A, Maathuis MH, Hart NA, et al. The Groningen hypothermic liver perfusion pump: functional evaluation of a new machine perfusion system. Ann Biomed Eng. 2006;34:1924–1934.

[393] Banan B, Watson R, Xu M, Lin Y, Chapman W. Development of a normothermic extracorporeal liver perfusion system toward improving viability and function of human extended criteria donor livers. Liver Transpl. 2016;22:979–993. doi:10.1002/lt.24451

[394] Tingle SJ, Ibrahim I, Thompson ER, Bates L, Sivaharan A, Bury Y, Figuereido R, Wilson C. Methemoglobinemia can complicate normothermic machine perfusion of human livers. Front Surg. 2021;8:634777. doi:10.3389/fsurg.2021.634777

[395] Eshmuminov D, Leoni F, Schneider MA, Becker D, Muller X, Onder C, Hefti M, Schuler MJ, Dutkowski P, Graf R, von Rohr PR, Clavien PA, Bautista Borrego L. Perfusion settings and additives in liver normothermic machine perfusion with red blood cells as oxygen carrier: a systematic review of human and porcine perfusion protocols. Transpl Int. 2018;31:956–969.

[396] Kaminski J, Delpech PO, Kaaki-Hosni S, Promeyrat X, Hauet T, Hannaert P. Oxygen consumption by warm ischemia-injured porcine kidneys in hypothermic static and machine preservation. J Surg Res. 2019;242:78–86.

[397] Xu H, Berendsen T, Kim K, Soto-Gutierrez A, Bertheium F, Yarmush ML, et al. Excorporeal normothermic machine perfusion resuscitates pig DCD livers with extended warm ischemia. J Surg Res. 2012;173:e83–e88.

[398] Jain S, Xu H, Duncan H, Jones JW Jr, Zhang JX, Clemens MG, Lee CY. Ex-vivo study of flow dynamics and endothelial cell structure during extended hypothermic machine perfusion preservation of livers. Cryobiology. 2004;48:322–332.

[399] Debbaut C, et al. From vascular corrosion cast to electrical analog model for the study of human liver hemodynamics and perfusion. IEEE Trans Biomed Eng. 2011;58(1):25–35.

[400] Lascaris B, Thorne AM, Lisman T, Nijsten MWN, Porte RJ, de Meijer VE. American Journal of Physiology-Gastrointestinal and Liver Physiology. 2022;322(2):G183–G200.

[401] Post IC, Dirkes MC, Heger M, Bezemer R, van ’t Leven J, van Gulik TM. Optimal flow and pressure management in machine perfusion systems for organ preservation. Ann Biomed Eng. 2012 Dec;40(12):2698–707. doi:10.1007/s10439-012-0601-9.

[402] Higashi Y, Homma J, Sekine H, et al. External pressure dynamics promote kidney viability and perfusate filtration during ex vivo kidney perfusion. Sci Rep. 2022;12:21564. doi:10.1038/s41598-022-26147-5.

[403] Jochmans I, et al. The prognostic value of renal resistance during hypothermic machine perfusion of deceased donor kidneys. Am J Transplant. 2011;11:2214–20.

[404] Bruinsma B, Sridharan G, Weeder P, et al. Metabolic profiling during ex vivo machine perfusion of the human liver. Sci Rep. 2016;6:22415. doi:10.1038/srep22415.

[405] Melendez HV, Rela M, Murphy G, Heaton N. Assessment of graft function before liver transplantation: quest for the lost ark? Transplantation. 2000;70(4):560–5.

[406] Ceresa CDL, Nasralla D, Watson CJE, Butler AJ, Coussios CC, Crick K, et al. Transient cold storage prior to normothermic liver perfusion may facilitate adoption of a novel technology. Liver Transpl. 2019;25:1503–13. doi:10.1002/lt.25584.

[407] Bral M, Dajani K, Leon Izquierdo D, Bigam D, Kneteman N, Ceresa CDL, Friend PJ, Shapiro AMJ. A back-to-base experience of human normothermic ex situ liver perfusion: does the chill kill? Liver Transpl. 2019;25:848–58. doi:10.1002/lt.25464.

[408] Henry SD, Guarrera JV. Protective effects of hypothermic ex vivo perfusion on ischemia/reperfusion injury and transplant outcomes. Transplant Rev (Orlando). 2012 Apr;26(2):163–75.

[409] Liu Q, Vekemans K, van Pelt J, et al. Discriminate liver warm ischemic injury during hypothermic machine perfusion by proton magnetic resonance spectroscopy: a study in a porcine model. Transplant Proc. 2009;41:3383–6.

[410] Quintini C, Del Prete L, Simioni A, Del Angel L, Diago Uso T, D'Amico G, et al. Transplantation of declined livers after normothermic perfusion. Surgery. 2022 Mar;171(3):747–56.

[411] Liu Q, Hassan A, Pezzati D, Soliman B, Lomaglio L, Grady P, et al. Ex-situ liver machine perfusion: the impact of fresh frozen plasma. Liver Transpl. 2020. 26(2):p 215-226.

[412] Organ Assist. Evidence-based machine perfusion technology. Available at: https://www.organ-assist.nl/evidence-based-machine-perfusion-technology/.

[413] Rossini N. Liver in a machine perfusion: a new scenario for diagnostic imaging techniques [Master's thesis]. Ancona: Università Politecnica delle Marche; 2020.

[414] Quillin RC 3rd, Guarrera JV. Hypothermic machine perfusion in liver transplantation. Liver Transpl. 2018 Feb;24(2):276–81. doi:10.1002/lt.25004.

[415] Markmann J, Abouljoud M, Ghobrial M, Bhati C, Pelletier S, Magliocca J, et al. Superior post-transplant clinical outcomes using portable normothermic perfusion and assessment with the Organ Care System (OCS) Liver System: 1-year outcomes of the OCS Liver Protect randomized controlled trial [abstract]. Am J Transplant. 2021;21(suppl 3).

[416] TransMedics Inc. Organ Care System (OCS™) Liver User Guide. 2015–2021. Available at: https://www.fda.gov/media/150708/download.

[417] Ravaioli M, et al. Strategies to restore adenosine triphosphate (ATP) level after more than 20 hours of cold ischemia time in human marginal kidney grafts. Ann Transplant. 2018;23:34–44.

[418] Giannone FA, Treré D, Domenicali M, Grattagliano I, Baracca A, Sgarbi G, et al. An innovative hyperbaric hypothermic machine perfusion protects the liver from experimental preservation injury. Scientific World Journal. 2012;2012:1–9.

[419] Salehi S, Tran K, Grayson WL. Advances in perfusion systems for solid organ preservation. Yale J Biol Med. 2018 Sep;91(3):301–12.

[420] Organ Recovery Systems. LifePort Liver Transporter. Available at: https://www.organ-recovery.com/lifeport-liver-transporter/. Accessed 2023 Jan 12.

[421] Debbaut C, Monbaliu DRL, Segers P. Validation and calibration of an electrical analog model of human liver perfusion based on hypothermic machine perfusion experiments. Int J Artif Organs. 2014;37(6):486–98.

[422] Ravaioli M, Maroni L, Angeletti A, Fallani G, De Pace V, Germinario G, et al. Hypothermic oxygenated perfusion versus static cold storage for expanded criteria donors in liver and kidney transplantation: protocol for a single-center randomized controlled trial. JMIR Res Protoc. 2020 Mar 19;9(3):e13922. doi:10.2196/13922.

[423] Boettcher W, Merkle F, Weitkemper HH. History of extracorporeal circulation: the conceptional and developmental period. J Extra Corpor Technol. 2003 Sep;35(3):172–83. [424] Zimmermann J, Carter AW. Cost–utility analysis of normothermic and hypothermic ex-situ machine perfusion in liver transplantation. Br J Surg. 2022;109:e31–e32. [425] Raigani S, De Vries RJ, Carroll C, Chen YW, Chang DC, Shroff SG, et al. Viability testing of discarded livers with normothermic machine perfusion: alleviating the organ shortage outweighs the cost. Clin Transplant. 2020;34(11):e14069.

[426] Javanbakht M, Mashayekhi A, Trevor M, Branagan-Harris M, Atkinson J. Cost-utility analysis of normothermic liver perfusion with the OrganOx metra compared to static cold storage in the United Kingdom. J Med Econ. 2020 Nov;23(11):1284–92.

[427] Quintini C, Martins PN, Shah S, et al. Implementing an innovated preservation technology: the American Society of Transplant Surgeons' (ASTS) Standards Committee white paper on ex situ liver machine perfusion. Am J Transplant. 2018;18(8):1865–74. [428] Webb AN, Izquierdo DL, Eurich DT, Shapiro AMJ, Bigam DL. The actual operative costs of liver transplantation and normothermic machine perfusion in a Canadian setting. Pharmacoecon Open. 2021;5:311–8.

[429] Webb AN, Lester ELW, Mark A, Shapiro J, Eurich DT, Bigam DL. Cost-utility analysis of normothermic machine perfusion compared to static cold storage in liver transplantation in the Canadian setting. Am J Transplant. 2022;22:541–51.

[430] Groen H, Moers C, Smits JM, Treckmann J, Monbaliu D, Rahmel A, et al. Cost-effectiveness of hypothermic machine preservation versus static cold storage in renal transplantation. Am J Transplant. 2012;12:1824–30.

"Ignoranti quem portum petat nullus suus ventus est"
(Seneca, from Epistulae morales ad Lucilium, Epistula 71; 1975, pp. 458-459)

Chapter III

Optical Spectroscopic Detection of Mitochondrial Biomarkers (FMN and NADH) for Hypothermic Oxygenated Machine Perfusion: A Comparative Study in Different Perfusion Media

1. Introduction

As we saw in the previous chapter II, organ transplantation is a critical treatment for patients with end-stage organ failure, and maintaining graft viability during the ischemic period is paramount for successful outcomes. In recent years, machine perfusion has emerged as an advanced method for organ preservation, offering the potential for the continuous monitoring of graft quality through the analysis of biomarkers in perfusion solutions [1]. In the previous chapter II, especially in the paragraph titled "*Metabolites as biomarkers in the perfusate*" we understood that while conventional parameters such as lactate, pH, and liver enzymes (ALT, AST, LDH) provide valuable but indirect information regarding metabolic status [2, 3, 4], there is a growing interest in using mitochondrial-derived biomarkers—specifically, flavin mononucleotide (FMN) and nicotinamide adenine dinucleotide (NADH)—as direct indicators of ischemia-reperfusion injury (IRI), shown in **Figure 1.1**, and mitochondrial dysfunction [5, 6, 7, 8, 9, 10].

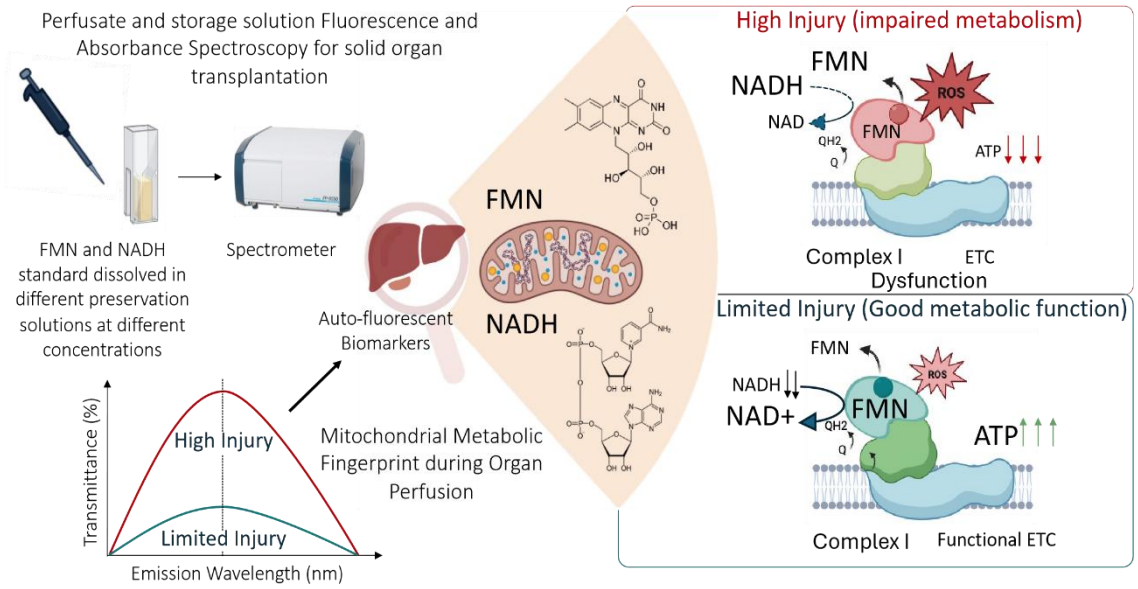

Figure 1.1. Overview of the underlying mechanism of FMN release and NADH accumulation and real-time spectroscopy for organ assessment.

Prior studies have demonstrated the potential of the real-time fluorescence detection of FMN and NADH during organ perfusion [5, 7, 11]. However, a critical review of the literature reveals several limitations:

- Incomplete calibration details: Many works do not report the calibration curves or experimental parameters (e.g., integration times, instrument settings) necessary to reproduce and compare their results.
- Limited detection methods: Most studies rely solely on fluorescence measurements—even though only FMN typically exhibits a robust fluorescence response—while neglecting absorbance techniques, which may be more suitable for quantifying NADH, particularly at high concentrations where nonlinear effects and signal saturation occur.
- Mismatch between calibration and measurement conditions: In several instances, the calibration medium differs from the perfusion medium used in actual settings, which can compromise the reliability of the optical readout.
- Inconsistent methodology across studies: Varied excitation/emission wavelengths and different spectrometers are currently used, making cross-comparisons challenging. For instance, while some studies use 450 nm excitation for FMN detection, others deploy suboptimal wavelengths (e.g., 405 nm or 485 nm) without justifying their choice, leading to potentially longer integration times and added complexity in sensor design.

Table 1.1 provides a comparative overview between the main studies in literature and our work,

Ref.	Type of Analyte	Type of Method	Detection Method	Effects of Media Composition	Calibration Medium/Perfusion Medium	Calibration Curve	Reference Excitation/Emission Wavelengths	Spectrometer Used	Type of Study	LOQ and LOD
[5]	FMN	Fluorescence	Direct on perfusion line	Not reported	Not reported/Belzer	Not reported	Exc: 450 nm; Em: 500–600 nm	Portable	Clinical	Not reported in clinical context
[6]	FMN/NADH	Fluorescence	Direct on perfusion line/Perfusate Sampling	Not reported	Not reported/Belzer	Not reported	FMN-Exc: 450 nm; Em: 500–600 nm NADH-Exc: 360 nm Em: 465 nm	Portable	Preclinical	Not reported in pre-clinical context
[7]	FMN	Fluorescence	Perfusate Sampling	Not reported	Saline/Belzer	Not reported	Exc: 450 nm; Em: 525 nm	Microplate reader	Clinical	Not reported in clinical context
[9]	FMN	Fluorescence	Perfusate Sampling	Not reported	Not reported/Belzer	Yes	Exc: 485 nm; Em: 528 nm	Microplate reader	Preclinical	Not reported in preclinical context
[10]	FMN	Fluorescence	Perfusate Sampling	Not reported	Belzer/Belzer	Yes	Exc: 450 nm; Em: 500–600 nm	Microplate reader	Clinical	Reported for calibration: 0.00356 ng mL^{-1}
[11]	FMN/NADH	Fluorescence	Direct on perfusion line	Not reported	Belzer/Belzer	Yes	FMN-Exc: 405 nm; Em: 530 nm NADH-Exc: 385 nm Em: 460 nm	Portable	Clinical	Reported for calibration: 2.01 ng mL^{-1}
[12]	FMN/NADH	Fluorescence	Perfusate Sampling	Not reported	Not reported	Not Reported	Not Reported	Not reported	Preclinical	Not reported in pre-clinical context
[13]	Only FMN	Fluorescence	Perfusate Sampling	Not reported	Belzer/Belzer	Yes	Exc: 450 nm; Em: 525 nm	Microplate reader	Clinical	Reported for calibration: 7.9 ng mL^{-1}
Our study	Yes	Fluorescence/ Absorption	Preparation in laboratory of perfusion solution simulating perfusate	Yes	Fully described	Yes	Exc: 300–500 nm. Em: 400–600 nm	Benchtop	Methodologic	Reported for FMN calibration: 120 ng mL^{-1}

Table 1.1 Comparative summary of clinical and preclinical studies reporting the detection and analysis of FMN and NADH, with an emphasis on contrasting findings with our study. The comparison includes: (a) the spectrometric detection technique; (b) the detection method utilized; (c) the influence of perfusion solutions on the measurements; (d) the consistency between the calibration medium and the organ perfusion medium; (e) the presence of a reported calibration curve; (f) the study typology; (g) Limits of Detection and Quantification (LOD/LOQ): represent the minimum concentration level that the instrument can accurately detect and quantify.

highlighting differences in detection methods, experimental conditions, and validation parameters.

In light of these challenges, our chapter presents a comprehensive spectroscopic investigation of FMN and NADH in various perfusion media that are routinely used—or intended for future use—in organ perfusion. Specifically, we examine both fluorescence and absorbance modalities across a wide range of concentrations and in diverse media formulations. Our work systematically evaluates:

- The linearity and detection limits of calibration curves,
- The influence of excitation wavelength on signal strength and specificity,
- The impact of media composition on spectral profiles, and
- The reproducibility and robustness of the optical measurements.

The objective of this doctoral thesis is the application of innovative technologies for the detection of the FMN biomarker and, potentially, NADH during perfusion. The study of spectrophotometric properties of FMN and NADH in a perfusion medium is essential to develop the theoretical foundation necessary for the development of real-time optical biosensors. In doing so, it provides key insights for sensor designers, such as the importance of performing media-matched calibration, choosing optimal excitation wavelengths to reduce integration time, and combining fluorescence with absorbance detection to overcome limitations in quantifying NADH. These contributions directly respond to the current gaps in the literature, as summarized in recent studies [5, 7, 9, 10, 14].

The remainder of the chapter II is organized as follows: Section 2 describes the experimental materials, methods, and instrumentation; Section 3 presents our results along with a detailed comparison with the existing literature; and Section 4 concludes with a discussion of the implications for future sensor development and potential clinical applications.

2. Material and Methods

We have used a conventional bench spectrophotometer and a bench spectrofluorometer. Since perfusion can involve liver, kidneys, lungs, and heart, we focused on the perfusion solutions used in such cases, namely Belzer MPS®, Celsior®, Custodiol® HTK, and IGL-1®. Experiments have been performed using riboflavin 5′-monophosphate sodium salt hydrate powder with purity ≥ 70% and NADH disodium salt grade II (purity at 98%, both from Sigma Aldrich, St. Louis, MO, USA). The two compounds were stored at −20 °C and 5 °C, respectively. Belzer MPS (Machine Perfusion Solution), Celsior, Custodiol, and IGL-1 solutions were prepared according to the recipes provided by the manufacturers and available in the literature [15]. Compositions of perfusion solutions are reported in following **Tables 2.1 – 4**.

CONSTITUENT	AMOUNT/1000 ML
Adenine (free base)	0.68 g
Calcium Chloride (dihydrate)	0.068 g
Dextrose (+)	1.80 g
Glutathione (reduced)	0.92 g
HEPES (free acid)	2.38 g
Hydroxyethyl Starch	50.0 g
Magnesium Gluconate	1.13 g
Mannitol	5.4 g
Potassium Phosphate (monobasic)	3.4 g
Ribose, D(-)	0.75 g
Sodium Gluconate	17.45 g
Sodium Hydroxide	0.70 g
Water To 1000 mL Volume	-

Table 2.1. Components of Belzer MPS® UW.

CONSTITUENT	AMOUNT/1000 ML
Sodium Chloride	0.8766 g
Potassium Chloride	0.6710 g
Potassium hydrogen 2-Ketoglutarate	0.1842 g
Magnesium Chloride 6 H_20	0.8132 g
Histidine HCI H_20	3.7733 g
Histidine	27.9289 g
Tryptophan	0.4085 g
Mannitol	5.4651 g
Calcium Chloride	0.0022 g
Water To 1000 mL Volume	-

Table 2.2. Components of Custodiol®.

CONSTITUENT	AMOUNT/1000 ML
Glutathione	0.921 g
Mannitol	10.930 g
Lactobionic acid	28.664 g
Glutamic acid	2.942 g
Sodium hydroxide	4.000 g
Calcium chloride dihydrate	0.037 g
Potassium chloride	1.118 g
Magnesium chloride hexahydrate	2.642 g
Histidine	4.650 g
Water To 1000 mL Volume	-

Table 2.3. Components of Celsior®.

CONSTITUENT	AMOUNT/1000 ML
Lactobionic acid	35,8 g
Adenosine	1,336 g
Allopurinol	0,136 g
Glutathione	0,922 g
Polyethylene glycol (PEG 35000)	1 g
Potassium dihydrogen phosphate	3,402 g
Raffinose pentahydrate	17,84 g
Magnesium sulfate heptahydrate	1,232 g
Sodium Hydroxide: qs pH: 7.4	-
Water To 1000 mL Volume	-

Table 2.4. Components of IGL-1®.

Initially, 50 grams of hydroxyethyl starch were weighed and dissolved in 500 mL of water heated to a temperature range of 38-42 °C in a 1000 mL glass beaker. Given the propensity of hydroxyethyl starch to form aggregates that are difficult to dissolve, heating the water was essential to facilitate dissolution. The solution was vigorously mixed, and aggregates were manually broken up using a glass rod to ensure complete dissolution. Additionally, an ultrasonic bath (Bandelin Sonorex) was employed to further aid in the dissolution of sugars and salts. Subsequently, each component was individually weighed and added to the solution. The resulting mixture was then transferred to a 1000 mL Type A volumetric flask. The pH of the solution was measured using a pH meter (pHep5, HI98128 Hanna Instruments) and adjusted by adding sodium hydroxide. Finally, water was added to reach a total volume of 1000 mL.

The preparation of the other solutions was less demanding as they did not contain critical components like hydroxyethyl starch. However, our objective was to study the spectrophotometric behavior of the components rather than their clinical applications. Consequently, we did not ensure the sterility of the perfusion solution. To inhibit the growth of bacteria and mold, the solution was prepared and stored in a refrigerator at 5 °C for a few hours before being used for sample preparation and measurements. An ultrasonic bath (Bandelin Sonorex) was employed when necessary to aid in the dissolution of sugars and salts. The procedure involved dissolving all components in 500 mL of water heated to 35-39 °C. The solution was then transferred into a 1000 mL volumetric flask, with additional water added to reach the meniscus level.

Stock solutions containing FMN and NADH were also prepared according to usual weighing and dissolution procedures. All the chemicals involved in the preparation of the stock and perfusion solutions were purchased from Sigma Aldrich.

Stock solutions of flavin mononucleotide (FMN) were prepared by accurately weighing 60 mg of FMN powder using a Metter AE 163 microbalance. Due to the hygroscopic nature of FMN, the powder was pre-dried by heating at 45 °C for 15 minutes to ensure precision in measurement. This drying and weighing process was repeated until a constant weight was achieved. The dried FMN powder was then transferred to a 1000 ml Type A volumetric flask and dissolved in a 0.9% saline solution (B. Braun Melsungen AG, Germany). The flask was immediately covered with foil and stored in a dark refrigerator at 5 °C. To ensure thorough dissolution, the solution was mixed continuously for a minimum of 5 hours. The final concentration of the FMN solution was 0.06 mg mL^{-1}.

For the preparation of NADH solution, 500 mg of NADH powder, which is non-hygroscopic, was weighed without the need for drying. The powder was placed in a 50 ml Type A volumetric flask, and saline solution was added to the meniscus level. This resulted in a final NADH concentration of 10 mg mL^{-1}.

The solution temperature was measured using a digital thermometer RS PRO RS 1720 (RS Components Ltd. Birchington Road, Corby, Northants, NN17 9RS, UK). Analytical samples were prepared utilizing a 50 mL volumetric flask (type A) and 100 µL of FMN collected with an ErgoOne® Starlab micropipette. FMN concentration ranged between 0.12 µg mL^{-1} and 0.96 µg mL^{-1}. Similarly, the NADH concentration was adjusted in the range between 20 µg mL^{-1} and 180 µg mL^{-1}. The range of FMN and NADH concentrations under study was selected with the aim of developing a calibration curve suitable for quantifying these analytes in the perfusion fluid during hypothermic organ perfusion. Calibration curves for both absorption and fluorescence measurements were constructed by performing three independent replicates for each concentration point. For each analyte (FMN and NADH), absorbance–concentration and fluorescence–concentration relationships were recorded in triplicate. The resulting calibration curve corresponds to the average of the three individual linear fits obtained from these replicates. The choice of this range was based on the expected concentrations of FMN and NADH that might be released by the organ during the perfusion process [7,10,11,13,14,16]. Light sources were suitably shielded to avoid FMN and NADH degradation processes induced by irradiation during all the handling procedures. Samples were stored in a cool place, protected from light.

To prevent contamination of the previous solution during spectrophotometric measurements, a meticulous cuvette washing protocol was implemented. Since highly diluted solutions were used, it was essential to avoid any cross-contamination between samples. After each measurement, the cuvette was washed with a portion of the solution being analyzed, which was then discarded. This washing procedure ensured the elimination of any residual contamination, thereby enhancing the reliability of the results. The use of 50 mL flasks provided an ample quantity of sample solution for effective cuvette washing after each measurement. For sample injection into the cuvette, a different glass or plastic Pasteur pipette was utilized for each sample. Additionally, the quartz cuvette was thoroughly cleaned and transparent by first washing it with water, followed by acetone or isopropyl alcohol to remove any water traces, and finally drying it with a common hairdryer. This comprehensive cleaning procedure is schematically depicted in Figure SI1.1. The software of the Jasco spectrophotometer and spectrofluorometer allows for data export in CSV format. After

exporting, the data was imported and analyzed using Excel, Python 3.11 in Spyder environment, version 5.4.3 and OriginPro® 2018 for visualization and spectral analysis.

Prior to performing spectrometric measurements, the cuvette was rinsed by flushing it three times with the same sample solution taken from the volumetric flask (**Figure 2.1**). On the fourth rinse, the cuvette was filled with the sample solution for the actual measurement. This procedure ensured that no contamination from previous samples affected the results. Each washing portion was discarded after use, maintaining the integrity of the measurements.

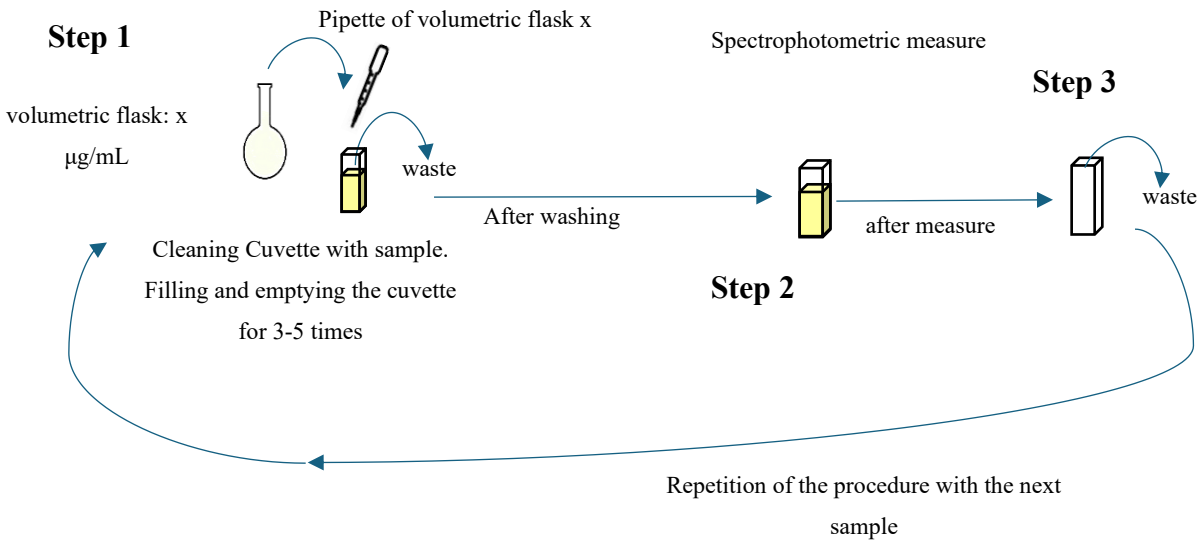

Figure 2.1. Schematization of measurement procedure

The absorption UV-Vis spectra were collected with a Jasco benchtop V-750 double beam UV-Visible spectrophotometer. The parameters configured in the spectrophotometer are provided in the **Table 2.5**.

Measurement range	200 – 800 nm
Data Interval	0.5 nm
Bandwidth	2.0 nm
Response	0.06 nm
Scan mode	Continuous
Scan speed	400 nm/min

Table 2.5. Characteristics of the V-750 Double Beam UV-Visible Spectrophotometer Jasco

Measurements were carried out in the spectral range of 200–800 nm using two Hellma® high-performance quartz glasses, with a path length of 10 × 10 mm and a chamber volume of 3.5 mL. Fluorescence was studied using a Jasco FP-8550 spectrofluorometer (28600 Mary's Ct, Easton, MD 21601, USA) equipped with a Hellma® fluorescence cuvette made of high-performance quartz glass. Contamination was avoided by suitably cleaning the cuvettes and rinsing them with sample solutions. Glass or plastic Pasteur pipettes were used to inject samples into the cuvette. All the collected spectra have been compared with those collected from corresponding saline solutions of FMN and NADH with NaCl 0.9%. The collected data and figure were analyzed and processed using Python 3.8 in Spyder 4.2.

3. Results and Discussion

3.1 Absorption Spectra of FMN and NADH in Saline Solution in Different Conditions of Temperatures and pH

The absorbance and fluorescence spectrophotometry of FMN and NADH under different conditions has been extensively studied [17,18]. FMN absorbs in the blue visible light range between 320 nm and 500 nm due to its extended conjugated structure and the presence of alternating double bonds within the isoalloxazine ring. When the double bonds of the nitrogen atoms at positions 1 and 5 within the isoalloxazine ring system are irradiated with blue light, π bond electrons are excited to higher energy π* states. Notably, nitrogen atoms at positions 1 and 5 also serve as the redox centers of FMN. Upon the reduction of the molecule to the structures FMNH and FMNH2, the double bonds become saturated. Saturation results in the loss of absorption in the blue region and the consequent loss of the yellow color typical of flavin molecules. The absorption spectra of FMN and NADH with a concentration of 0.60 μg mL^{-1} and 180 μg mL^{-1}, respectively, in saline solution at 5 °C, 20 °C, and 38 °C are shown in **Figure 3.1.1**.

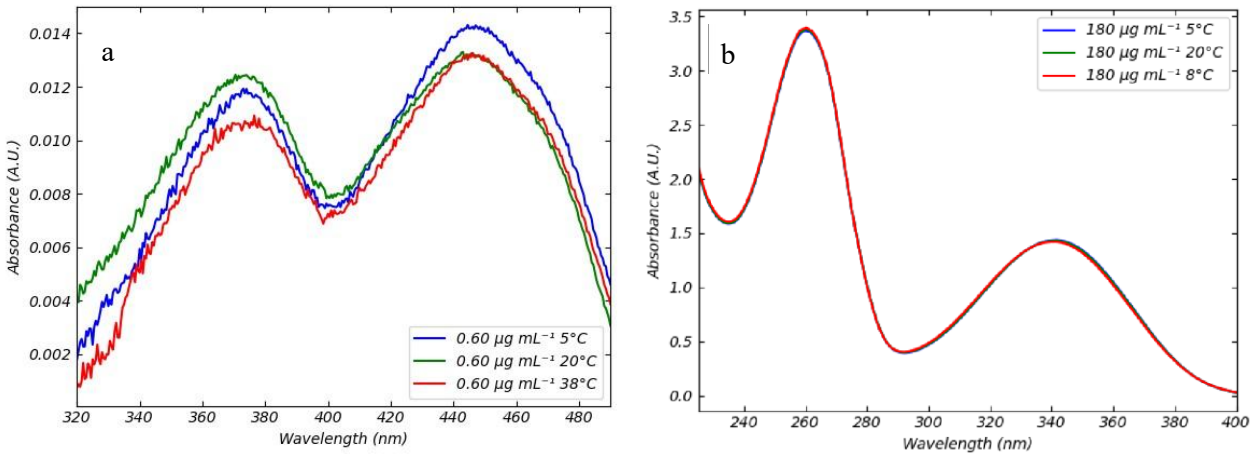

Figure 3.1.1. UV-Vis's absorption spectra (a) FMN in saline solution at 5 ◦C (blue), 20 ◦C (green), and 38 ◦C (red). Data were obtained using a FMN concentration of 0.60 µg mL^{-1}. (b) NADH at different temperatures at concentration of 180 µg mL^{-1}.

The curves of FMN exhibit two maxima, respectively, at 373 nm and 445 nm. NADH has an absorbance behavior similar to FMN. The absorption spectra of NADH displays two maxima, in the UV region, at 260 nm and 340 nm. The peak at 260 nm is due to the adenine chromophore, whereas absorbance at 340 nm is related to the dihydronicotinamide moiety. In the temperature range explored (5–38 °C) no variation in the peaks' positions has been observed for both coenzymes. It follows that FMN and NADH absorbance can be profitably detected under the hypothermic (5–10 °C), subnormothermic (20–25 °C), and normothermic (38 °C) conditions generally utilized for the machine perfusion of organs [19], using a calibration line referred for example at room temperature. Based on such evidence, we observe that temperature does not affect the spectrophotometric behavior of FMN and NADH. In **Figure 3.1.2** we report calibration experiments at 20 °C.

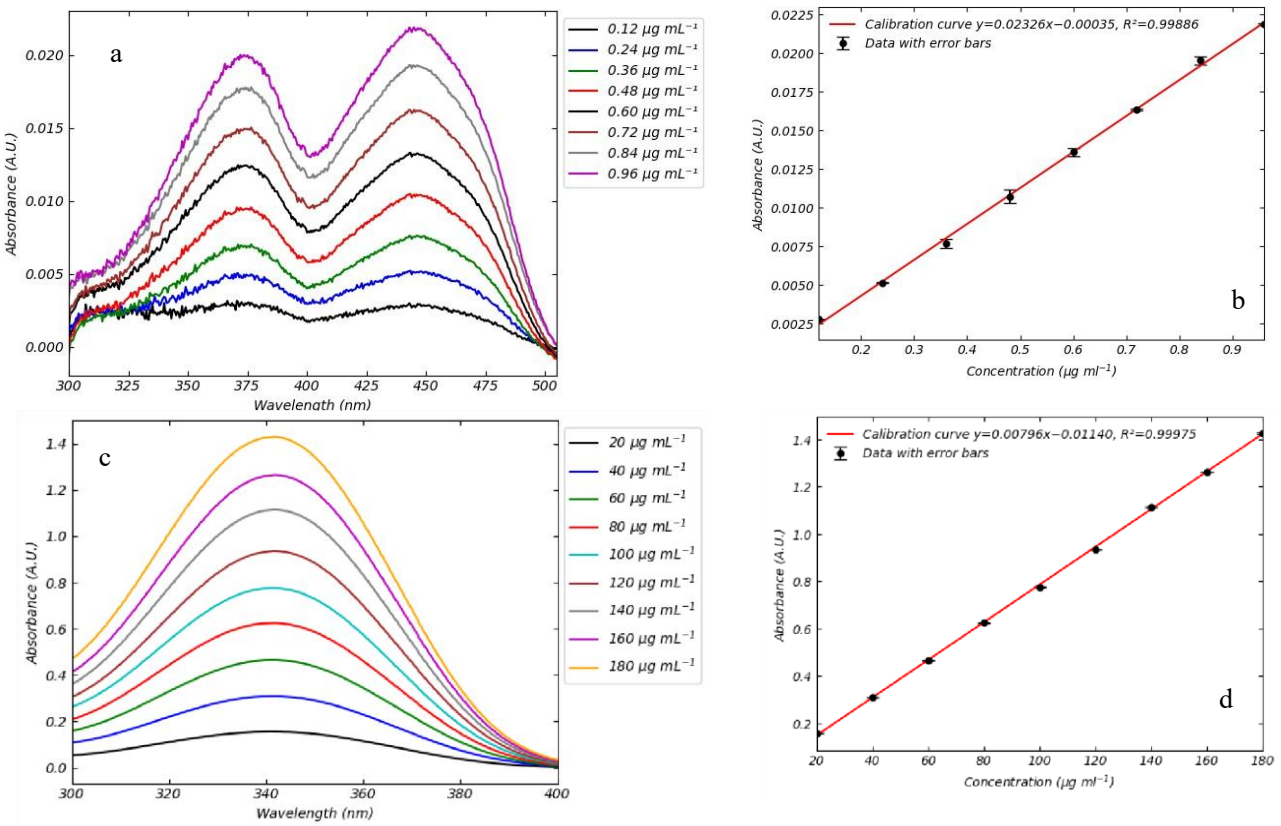

Figure 3.1.2. Absorption spectra of the coenzymes at different concentrations. Full absorption spectra of FMN and NADH in saline water in the 300 nm–400 nm range (**a**,**c**). Absorbance as a function of FMN and NADH concentration in saline solution. Data were collected using a wavelength of 445 nm and 340 nm for FMN and NADH, respectively (**b**,**d**). The best fitted line is also shown, and the corresponding error bar values are reported in **Table 3.1.1**.

Concentration (μg·mL^{-1})	Absorbance (Mean, A.U.)	Standard Error (A.U.)
0.12	0.002777	1.70×10^{-5}
0.24	0.005138	2.63×10^{-5}
0.36	0.007682	2.69×10^{-4}
0.48	0.010725	4.20×10^{-4}
0.60	0.013587	2.67×10^{-4}
0.72	0.016343	7.40×10^{-5}
0.84	0.019524	2.52×10^{-4}
0.96	0.021873	6.51×10^{-5}
20	0.155279	4.08×10^{-4}
40	0.307527	6.66×10^{-4}
60	0.465341	9.87×10^{-4}
80	0.624495	1.39×10^{-3}
100	0.775295	1.63×10^{-3}
120	0.934276	8.05×10^{-4}
140	1.114413	6.18×10^{-4}
160	1.262550	4.58×10^{-4}
180	1.426020	3.07×10^{-3}

Table 3.1.1 Standard errors for absorbance values used in FMN and NADH calibration curve (n = 3).

For the FMN spectra, we determined the Limit of Detection (LOD) and the Limit of Quantification (LOQ). The LOD represents the minimum detectable signal, corresponding to the lowest concentration at which the signal can be reliably distinguished from noise. The LOQ, on the other hand, is the minimum concentration at which the analyte can be quantified with acceptable accuracy and precision. In our case, using our laboratory instrumentation, the LOD was determined to be 0.003 A.U., and the LOQ was 0.12 μg mL^{-1}. At the LOQ concentration, the maximum absorption at the peak wavelength was approximately 0.003, a value close to the instrumental detection limit. Concentrations below 0.12 μg mL^{-1} could not be reliably detected with the current setup. In fact, below the signal corresponding to the concentration of 0.12 μg mL^{-1}, it is not possible to distinguish between a true signal and the natural noise of the device. Generally, NADH concentrations in perfusate are higher than those in FMN [10,11,14]. Minimum concentrations of NADH are around 10 to 20 micrograms per milliliter, so there is no need LOD or LOQ for NADH, as it is already readily detectable in its naturally occurring concentration in the perfusate.

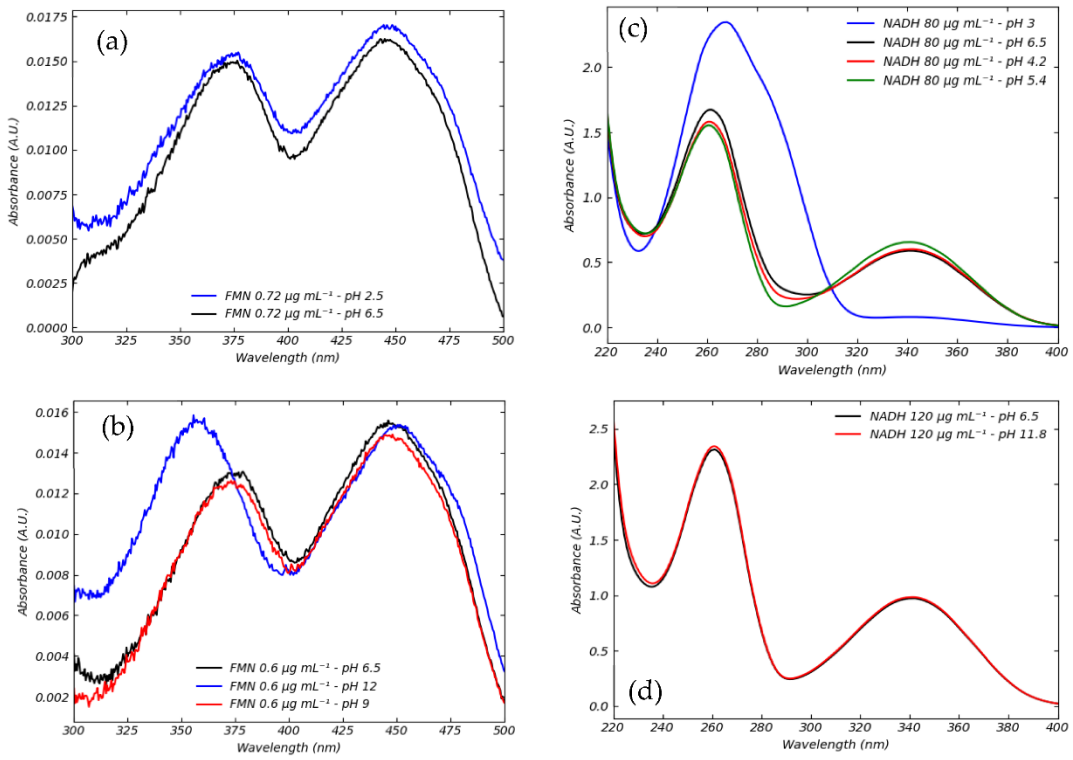

Figure 3.1.3. The effect of pH on FMN and NADH absorption spectrum. (a) The effect of pH acidic at 2.5 (blue) on spectra of FMN at 0.72 μg mL^{-1} compared to spectra at 6.5 (black). (b) The effect of pH basic at 9 (red) and at 12 (blue) on spectra of FMN at and 0.60 μg mL^{-1} compared to spectra at 6.5 (black). The effect of pH on NADH spectrum. (c) The effect of acidic pH at 3 (blue), 4.2 (red), and 5.4 (green) compared to spectrum at 6.5 (black) at concentration of 80 μg mL^{-1}. (d) The effect of basic pH at 12 (red) compared to spectrum at 6.5 (black) at concentration of 120 μg mL^{-1}.

We also investigated the effect of pH on the absorbance spectra of FMN and NADH. Although the perfusate pH during hypothermic machine perfusion typically ranges between 6.5 and 7.5 [20], we extended our analysis to a broader pH range (**Figure 3.1.3**) to better characterize the spectroscopic behavior of these coenzymes under extreme conditions.

In saline solution, FMN remains spectrally stable in acidic environments (down to pH 2.5), showing no significant deviation from spectra acquired at physiological pH. Under strongly basic conditions (up to pH 12), however, FMN exhibits a characteristic blue shift, consistent with known pH-dependent spectral effects in flavins.

Conversely, NADH is highly stable in alkaline conditions (up to pH 12), while it undergoes degradation in acidic environments (pH 3–5), as evidenced by the disappearance of its distinctive absorbance peak at 340 nm.

Although such extreme pH values are not encountered during clinical machine perfusion, this extended analysis was performed to provide a comprehensive, phenomenological understanding of how pH affects the spectral properties of FMN and NADH. This knowledge may prove useful in evaluating sample stability or detecting abnormal conditions during perfusion protocols.

Furthermore, since we have seen that neither temperature nor pH change under physiological conditions affects absorption spectra, we can infer that temperature (5–38 °C) and the range of physiological pH change does not affect fluorescence spectra.

3.2 Absorption and fluorescence of Standard Perfusion Solutions

The quantitative evaluation of FMN and NADH concentrations during the machine perfusion of organs requires discrimination between the possible contributions to absorption and fluorescence coming from the analytes themselves and the perfusion solutions. For this reason, we measured the absorption spectra of the four standard perfusion solutions we selected. The curves are shown in **Figure 3.2.1**.

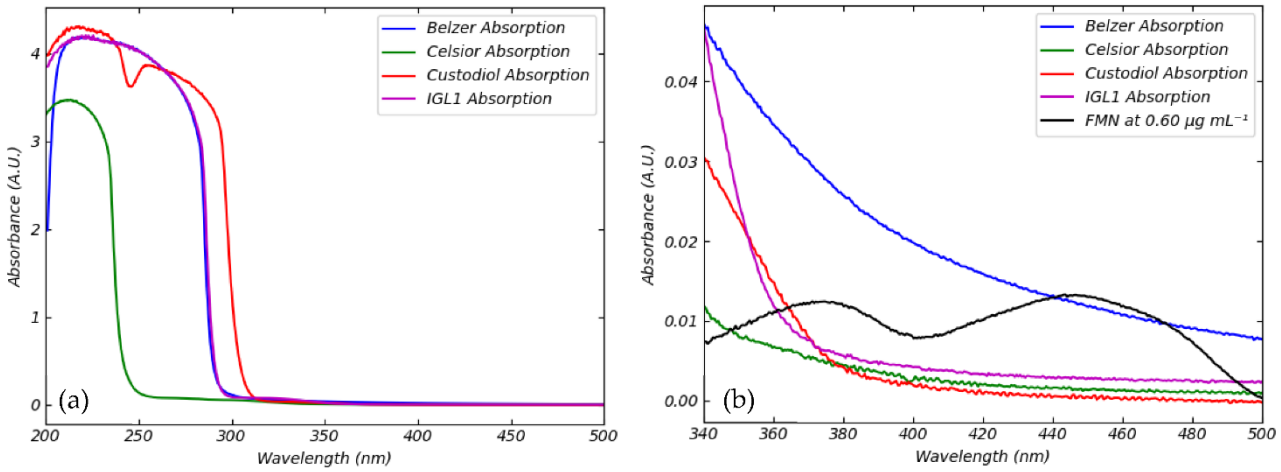

Figure 3.2.1. Absorption of perfusion media. (a) Absorption spectra of Belzer MPS (blue), Celsior (green), Custodiol (red), and IGL-1 (magenta) perfusion solutions. Plots show, in more detail, absorbance in the blue spectral region. (b) Absorption spectra of FMN at concentration of 0.60 μg mL^{-1} (black) compared to Belzer MPS (blue), Celsior (green), Custodiol (red), and IGL-1 (magenta) perfusion solutions.

The four standard preservation solutions exhibit similar spectral behavior. The Belzer MPS, Custodiol, and IGL-1 solutions absorb strongly in the UV region, especially at wavelengths shorter than 300 nm, whereas Celsior medium absorbs substantially at wavelengths below 250 nm. All these aqueous solutions are primarily composed of sugars, organic and inorganic salts, amino acids, nitrogenous bases, starches, and buffering agents. The observed differences in absorption can be ascribed to compositional and concentration factors.

Figure 3.2.1a shows the absorbance of preservation solutions in the ultraviolet and blue spectral region approximately between 200 and 500 nm. **Figure 3.2.1b** presents a detailed comparative analysis of absorption spectra from various perfusion solutions, including the region where FMN absorbs. **Figure 3.2.1b** provides a magnified view of the absorption spectra of different perfusion media in the spectral region where FMN exhibits its characteristic absorption profile. The image compares the absorption spectra of various perfusion media with the absorption spectrum of a reference FMN solution in water at a concentration of 0.60 μg mL^{-1}. The analysis reveals that the Belzer MPS solution exhibits notably higher absorbance compared to other perfusion solutions in the 340–500 nm spectral range.

Further analysis shows the perfusion media studied in these experiments absorb in the blue region (440-490 nm) to varying extents. Belzer solution exhibits higher absorbance than Celsior and Custodiol solutions, indicating that Belzer interferes with FMN more significantly at the studied FMN

concentration. Consequently, it is expected that the fluorescence intensity for the same excitation wavelength will be higher in Belzer solution compared to the other media.

The absorption of the perfusion media increases significantly in the near-ultraviolet region, especially below 350 nm. These aqueous solutions are primarily composed of sugars, organic and inorganic salts, amino acids, nitrogenous bases, starches, and buffering agents. With increased excitation energy intensity, a greater number of chemical bonds can be excited. In the ultraviolet region, photon energy is sufficiently high to cause electronic transitions of electrons in many chemical bonds within the molecules, resulting in increased absorbance in this region. Photon energy in the visible light range is generally lower and insufficient to excite electrons in many types of chemical bonds of molecules dissolved in the solution. As a result, fewer bonds are excited, leading to lower recorded absorbance. In contrast, the absorbances of Celsior and Custodiol solutions are almost negligible compared with the Belzer MPS. IGL-1 shows a similar behavior to Custodiol. **Figure 3.2.2** clearly demonstrates these phenomena.

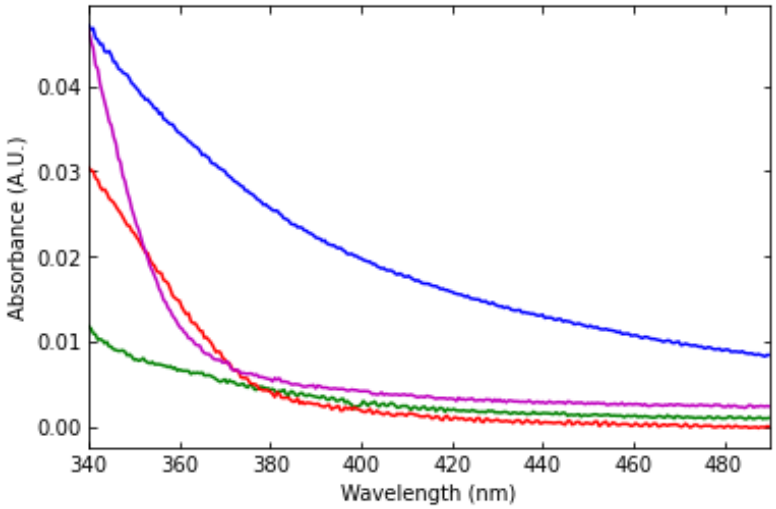

Figure 3.2.2. Absorption of perfusion in near ultraviolet and blue region

The high total absorbance is also due to the high concentration of various solutes in the solution; indeed, the total solute concentration is 84.678 g L^{-1}in Belzer, 55.956 g L^{-1} in Celsior, and 40.123 g L^{-1} in Custodiol.

In **Figure 3.2.3**, 3D and 2D plots of the spectra of the perfusion media are presented. An excitation range of 300-490 nm, corresponding to the absorption range of FMN, was selected to investigate potential emissions in the yellow region (500-600 nm) and determine their intensity.

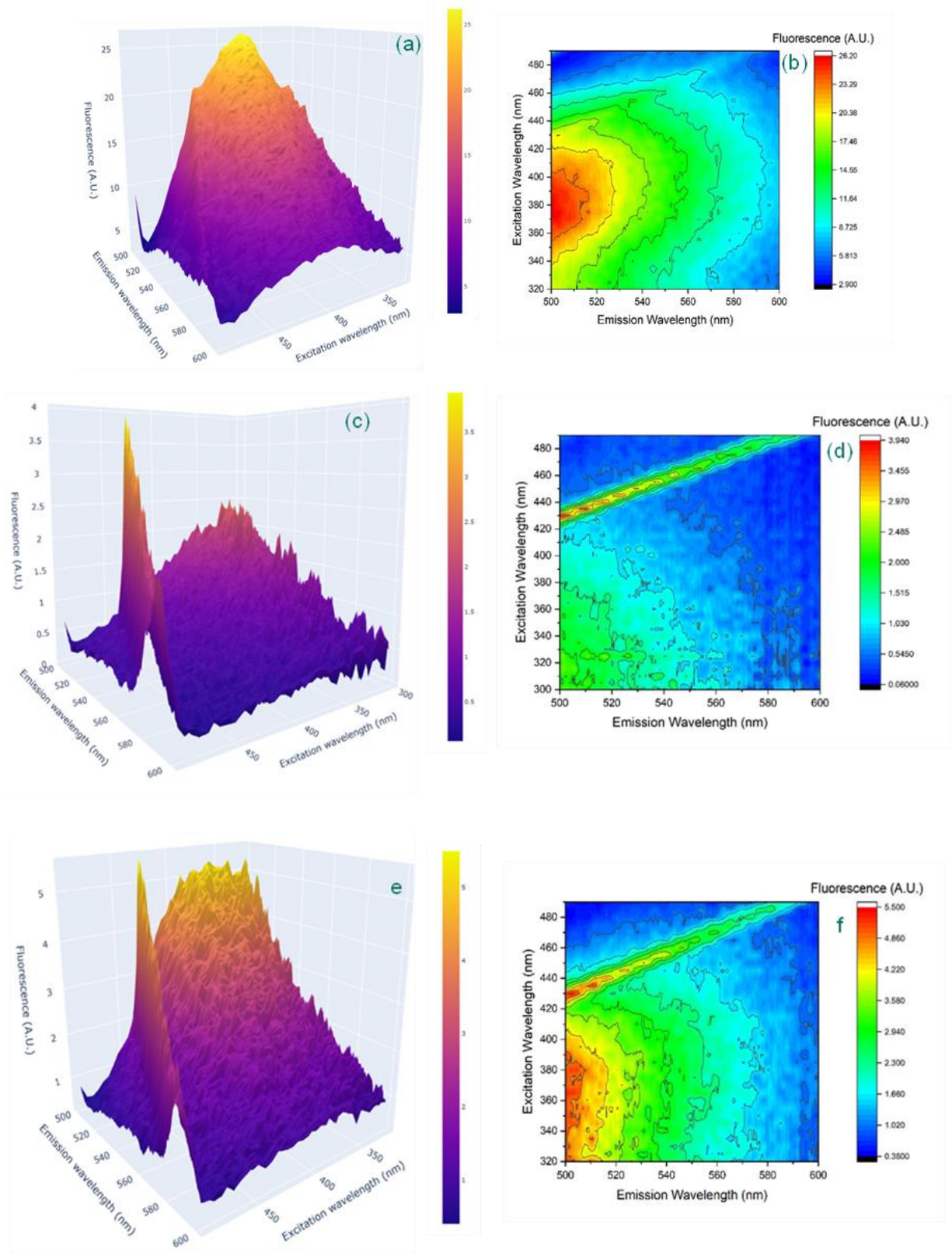

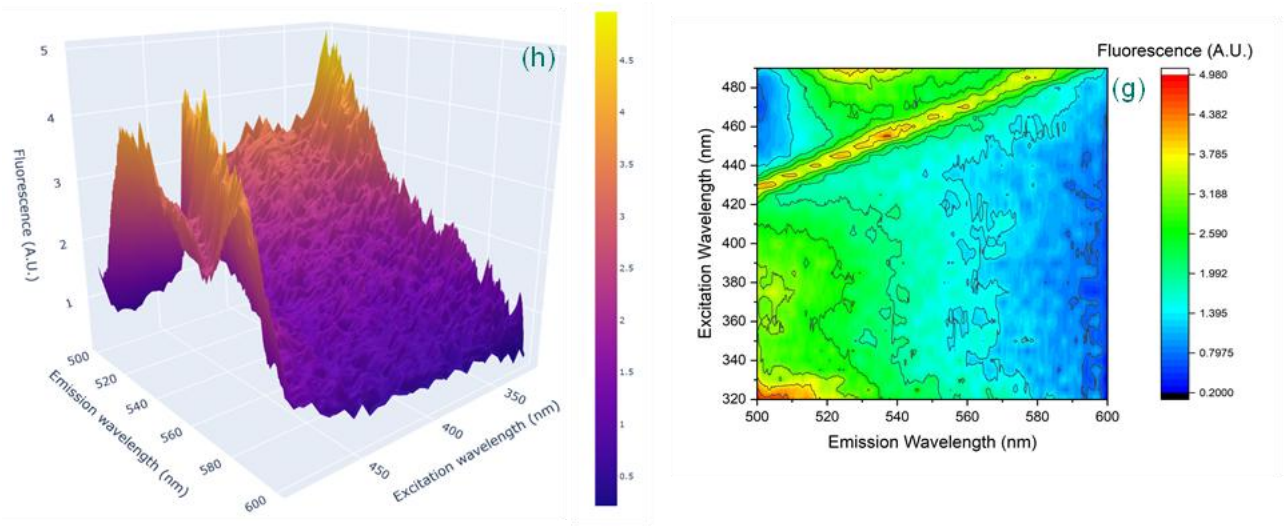

Figure 3.2.3. 3D and 2D fluorescence spectra of perfusion media, (a, b) Belzer. (c, d) Celsior. (e, f) Custodiol. (h, g) IGL1.

It is evident that the emission of the Belzer solution at 500-600 nm is 5-10 times higher than that of Celsior and Custodiol. Notably, a considerable diagonal elevation is observed in both Celsior and Custodiol, likely due to their similar compositions. However, the overall emission of Celsior and Custodiol remains very low.

When FMN, as well as NADH, was diluted in various perfusion solutions, we observed that the shapes of the absorption spectra were identical to those in saline solution. Aside from baseline corrections, the absorption values of FMN in saline solution were consistent with the light absorption values recorded in other perfusion solutions as depicted in **Figure 3.2.4**.

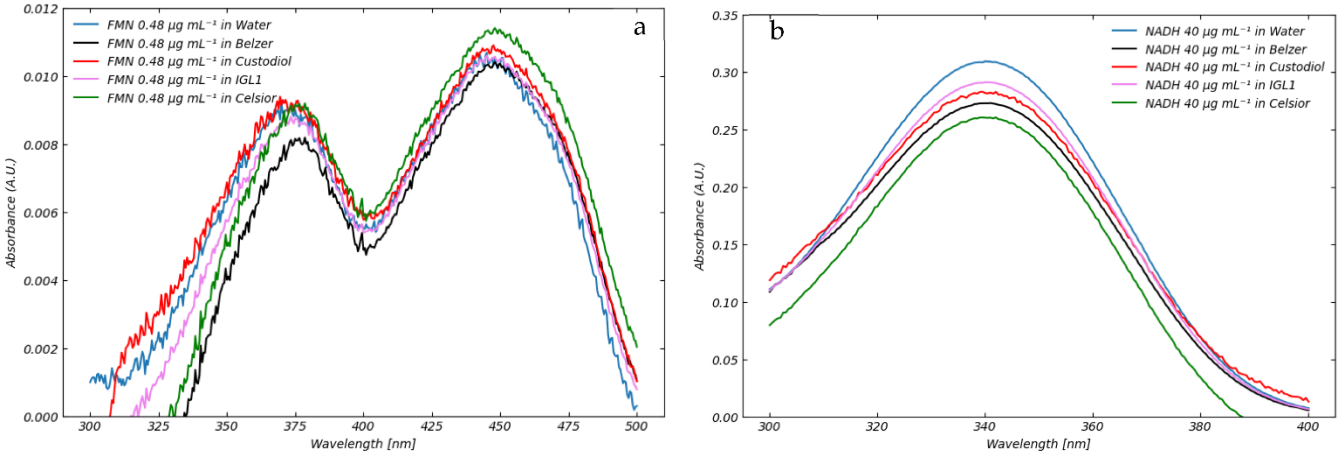

Figure 3.2.4. Absorption spectra of FMN (a) and NADH (b).

Figure 3.2.4 provides preliminary yet meaningful evidence supporting the chemical stability of FMN and NADH in the tested perfusion media. The absorption spectra exhibit consistent peak shapes and intensities across all solutions—Belzer MPS®, Celsior®, Custodiol® HTK, and IGL-1®—when compared to the reference spectrum in water. The absence of spectral deviations, such as peak shifts, flattening, or intensity loss, suggests that no significant chemical degradation or interaction occurs between FMN or NADH and the constituents of the perfusion fluids.

To further support this observation, additional measurements were performed after allowing the FMN solutions to equilibrate in each perfusate for one hour at room temperature. The resulting spectra remained unchanged, indicating that any potential reactive phenomena are either absent or proceed at a rate negligible within the timescale relevant to machine perfusion protocols.

This comparative spectral analysis is crucial for understanding how the choice of perfusion medium can influence FMN measurements in clinical settings.

3.3 Fluorescence of FMN and NADH in Standard Perfusion Solutions

Fluorescence of FMN and NADH in saline solution is well documented [21, 22]. FMN and NADH exhibit their fluorescence respectively in the regions between 500 nm and 600 nm and between 400 and 600 nm. The heat-map fluorescence spectrum of FMN in saline solution at a concentration of 0.36 µg mL^{-1} is shown in **Figure 3.3.1**a.

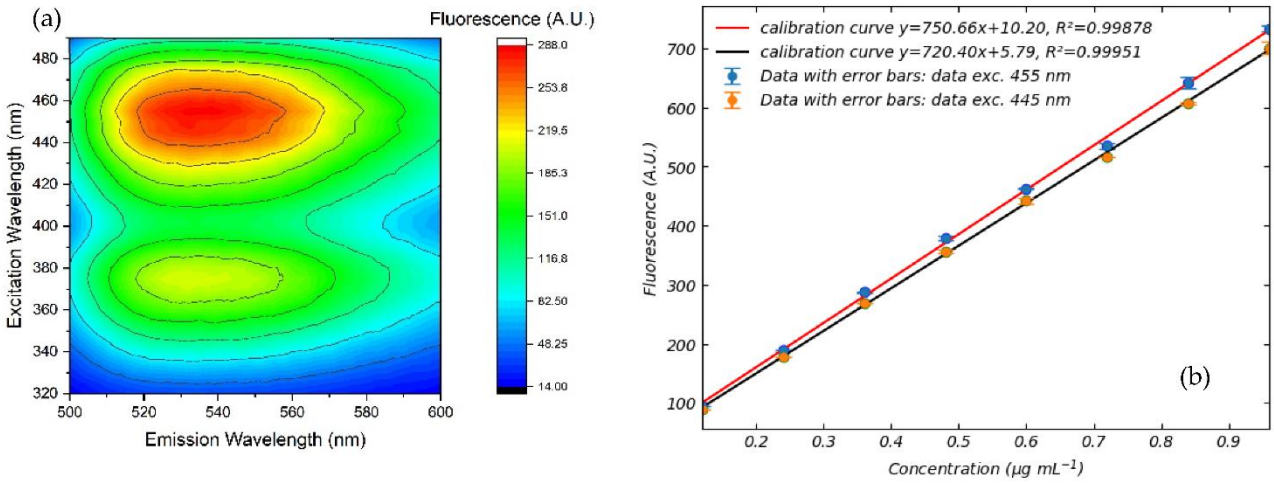

Figure 3.3.1. (a) Fluorescence spectra of FMN in saline solution at a concentration of 0.36 µg mL−1. (b) Calibration curves obtained using an excitation wavelength of 445 nm (black) and 455 nm for emission at 538 nm. Best fitting lines are also shown, and the corresponding error bar values are reported in **Table 3.3.1**.

	Exc. 445 nm		Exc. 455 nm	
Concentration ($\mu g \cdot mL^{-1}$)	Fluorescence (Mean A.U.)	Standard Error (A.U.)	Fluorescence (Mean A.U.)	Standard Error (A.U.)
0.12	94.4921	0.4302	88.7749	0.2351
0.24	189.2913	0.6099	177.7753	0.1832
0.36	287.3993	1.5043	268.9927	0.5976
0.48	379.3207	3.5497	356.0967	3.0412
0.60	462.7110	1.0385	441.9740	4.2942
0.72	535.1927	4.4261	516.2127	0.2915
0.84	642.2623	10.0139	607.7856	1.9467
0.96	733.7770	4.5954	700.7743	10.7981

Table 3.3.1. Fluorescence values and Standard Error (a) induced by 455 nm excitation, (b) induced by 445 nm excitation.

FMN exhibits significant fluorescence in the 520–560 nm range, with a maximum peak at approximately 538 nm. The emission resulting from an excitation wavelength of 455 nm is more intense compared to an excitation wavelength of 445 nm. Although this slight shift in excitation wavelength is normal in the presence of an absorption at 445 nm, it results in the two distinct calibration curves shown in **Figure 3.3.1b**. Data suggest that the sensitivity is highest when FMN fluorescence is excited at a wavelength of 455 nm. Consequently, we used this wavelength in subsequent experiments to evaluate the fluorescence of FMN in standard perfusion solutions. In this regard, it is worth noting that different excitation wavelengths are reported in the literature as well as that different emission wavelengths have been taken as reference for the quantitative or qualitative evaluation of FMN. The use of different excitation and emission wavelengths can raise significant difficulties in the comparison of clinical measurements obtained using different wavelengths [5 – 15]. For instance, the excitation light intensity, integral time, and other parameters being the same, the light emission at 538 nm due to excitation at 455 nm is almost twice as high as with excitation at 485 nm. It follows that induced emission from 485 nm can be obtained only if the light intensity or integral time are increased. In turn, this can give rise to uncertainties in measurement and control. For example, increasing the integral time can significantly burden data processing on normal devices. These practical aspects also need to be taken into serious consideration for in-line perfusion measurement.

The fluorescence of FMN in saline solution, as well as in Belzer MPS, Celsior, Custodiol, and IGL-1 perfusion solutions, along with the interference caused by these perfusion media, is illustrated in **Figure 3.3.2**.

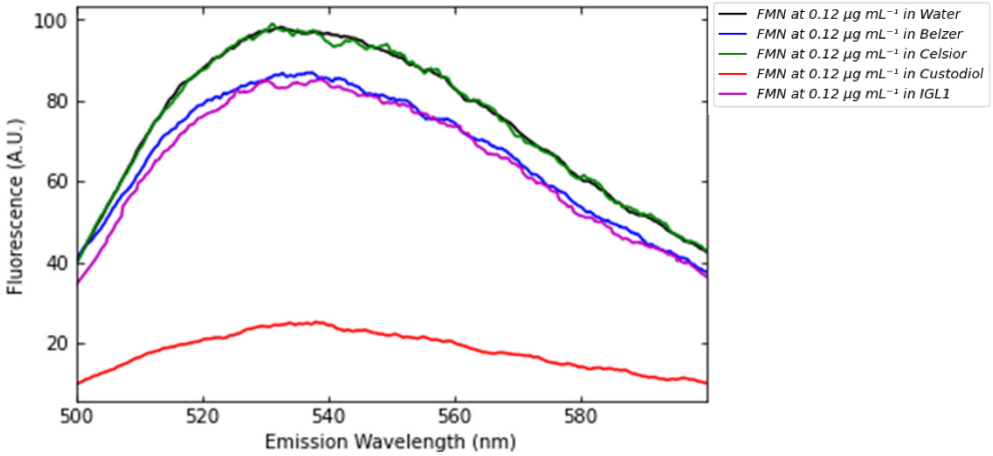

Figure 3.3.2. Fluorescence of FMN in saline solution (black), Belzer MPS (blue), Celsior (green), Custodiol (red), and IGL-1 (magenta) solutions at a concentration of 0.12 µg mL^{-1}.

The key observation is that the intensity of FMN fluorescence is affected by the composition of the perfusion solution and that the shape of the fluorescence spectra of FMN remains consistent across different perfusion media. This variation could be attributed to potential interactions between FMN and the compounds in the perfusion solutions, which may alter FMN's electronic structure. This suggests that FMN does not undergo chemical reactions with other species present in the perfusion solutions as demonstrated by **Figure 3.3.2**. This conclusion is supported by the fact that the shapes of the spectra remain consistent across all perfusion media. As shown in **Figure 3.2.1**, different perfusion solutions exhibit varying capacities to absorb light in the 400–490 nm range. For instance, the Belzer solution absorbs light in the blue region, whereas water and Celsior do not, allowing all available photons to be absorbed by FMN. In contrast, when FMN is dissolved in perfusion solutions, such as Belzer, a portion of the photons is absorbed by the medium itself, reducing the number of photons available to excite FMN. This decrease in excitation photons results in reduced FMN emission. However, in other media like IGL-1 and Custodiol, the reduction in FMN fluorescence may not solely result from photon absorption but could also be influenced by solvent effects, as indicated by the emission spectra shown above. While the effects of solvents on flavins are well-documented in the literature [23], there is a notable absence of comprehensive studies specifically addressing FMN interactions in these types of media. Further investigation is warranted to elucidate the precise

mechanisms underlying these observed phenomena and their implications for analytical applications. Consequently, the varying fluorescence of FMN in different perfusion media generates different calibration curves (**Figure 3.3.3**): the fluorescence emission of FMN in Belzer MPS solution is significantly lower than the one in Celsior or saline solutions. Interestingly, we observe that FMN in Custodiol solution exhibits significantly lower fluorescence compared to Belzer MPS solution, despite the negligible absorption of Custodiol in the 440–470 nm range. Furthermore, FMN in IGL-1 solution also shows emission similar to that of Belzer MPS, even though the absorption of IGL-1 in the blue region is slightly higher than that of Celsior and Custodiol.

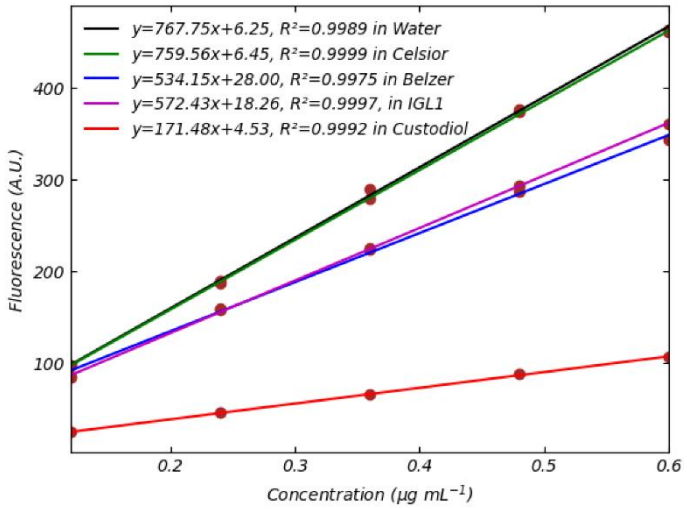

Figure 3.3.3. Calibration curves in fluorescence of FMN dissolved in saline solution (black), Belzer MPS (blue), Celsior (green), Custodiol (red), IGL-1 (magenta) solutions. Data were obtained using an excitation wavelength of 455 nm. Best-fitted lines are shown.

Data in **Figure 3.3.3** clearly show that the saline solution and Celsior solutions give rise to almost identical spectral behavior, with no interference with FMN. It follows that the saline solution of FMN can be used to calibrate the spectrophotometer if the Celsior solution is used as the perfusate. Conversely, such a solution is not viable in the case of Belzer-, IGL1-, or Custodiol-based perfusate. In general, similarities in the spectral behavior of calibration medium and perfusate, such as saline solution and Celsior, allow for reducing error bars in the concentration estimates.

Looking more closely at FMN spectrophotometry, it appears that depending on the excitation wavelengths, FMN's spectra exhibit varying emission intensities. **Figures 3.3.4** present the 3D and 2D emission spectra of FMN at different excitation wavelengths in saline water.

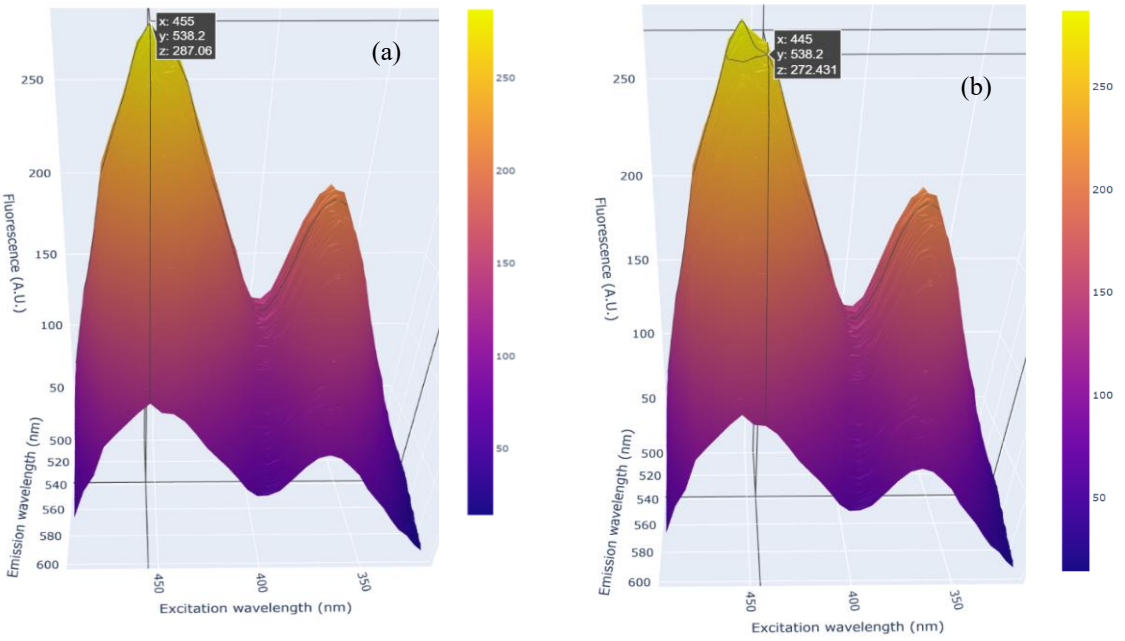

Figure 3.3.4. Indication of emission value for excitation at 455 nm (a) and 445 (b) of FMN

The maximum fluorescence peak obtained at around 538 nm by exciting at 455 nm is higher than the emission induced by excitation at 445 nm. This slight shift in excitation wavelength is expected, considering that FMN absorbs with a peak at 445 nm. Specifically, the emission peak at 538 nm measures 287 A.U. for excitation at 455 nm, compared to 272 A.U. for excitation at 445 nm. Although this minor difference may seem negligible, it could result in two distinct calibration curves. The spectra of FMN in water at higher concentrations maintain the same shape. **Figures 3.3.5** show the fluorescence spectra of FMN due to excitation at 455 nm and 445 nm at varying concentrations..

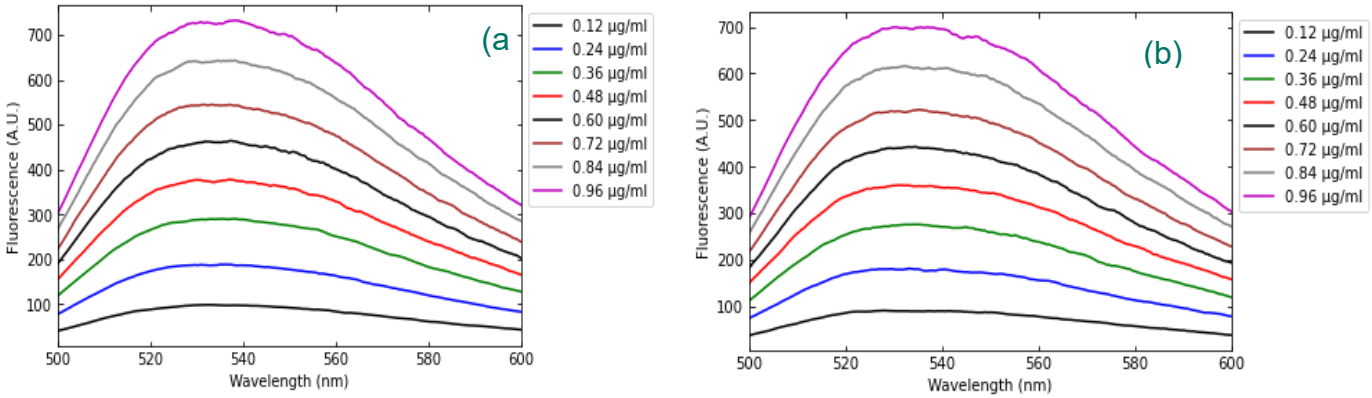

Figure 3.3.5. Spectra of FMN for excitation at 455 nm (a) and at 445 nm (b).

It is evident that the calibration curves differ based on the excitation wavelength. **Figures 3.3.6** illustrates how the emissions change for a minimal concentration of 0.12 μg mL^{-1} at different excitation wavelengths.

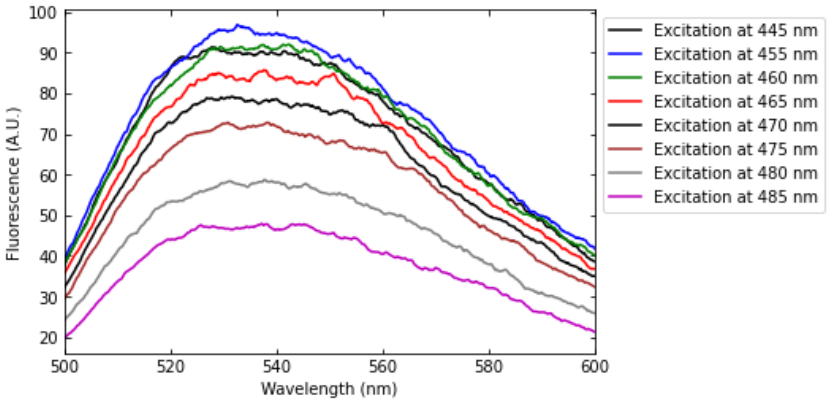

Figure 3.3.6. Spectra of FMN for different excitation wavelengths at the concentration of 0.12 μg mL^{-1}

In **Figures 3.3.7** are plotted spectra of FMN in perfusion media. It appears that FMN does not interact with components for all concentration range studied.

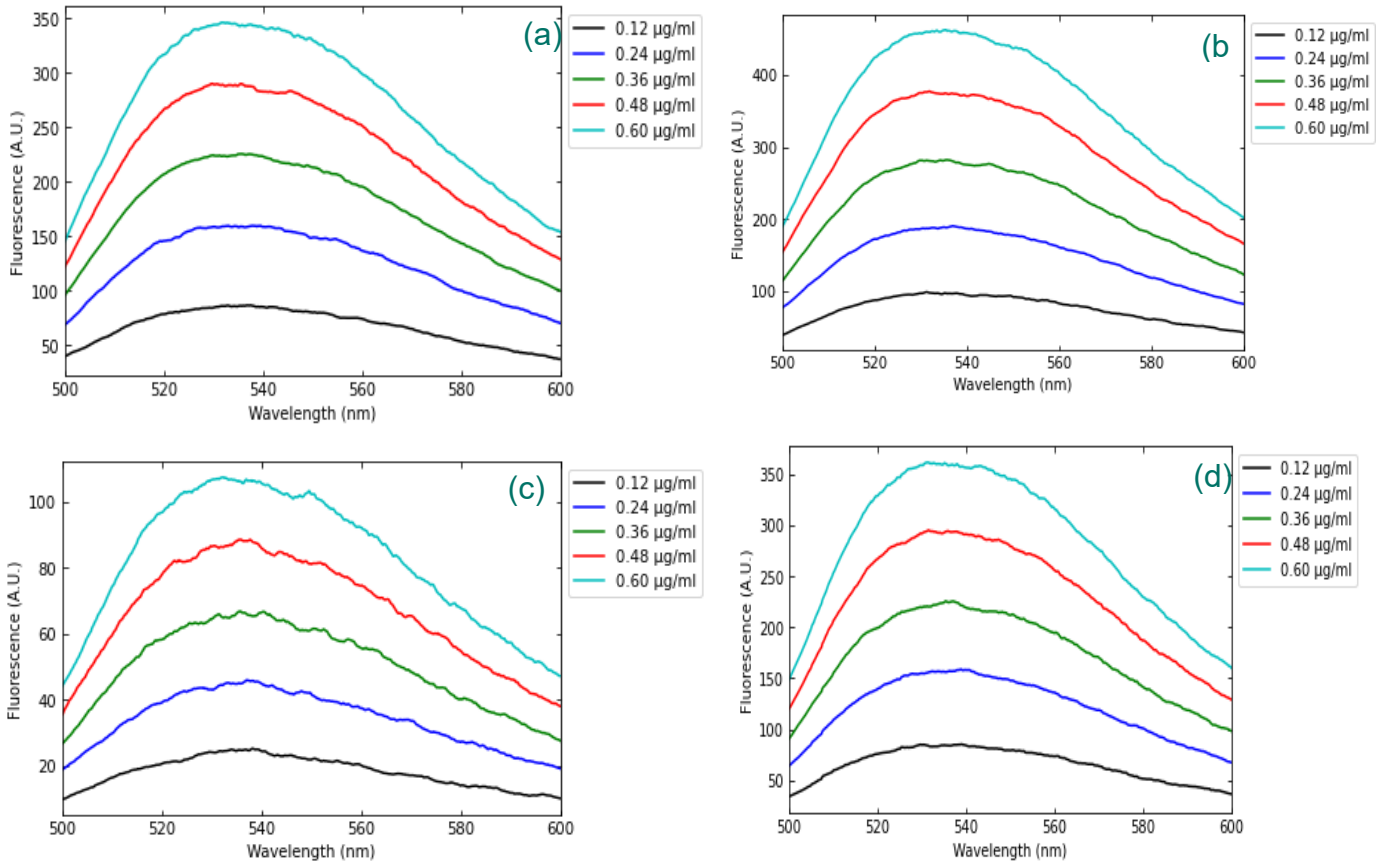

Figure 3.3.7. Fluorescence spectra of FMN in different perfusion solutions. (a) In Belzer. (b) In Celsior. (c) In Custodiol. (d) In IGL1.

However, the composition of the perfusion solution affects FMN fluorescence. As shown in **Figure 3.2.2**, perfusion solutions have different capabilities to absorb light in the 400-490 nm range. Belzer solution absorbs light in the blue region. In water and Celsior, all available photons are absorbed by FMN because these solutions do not absorb photons in the blue region. Conversely, in the FMN-perfusion solution mixture, a portion of the photons is absorbed by the medium itself (as shown in **Figure 3.3.7a** for the Belzer-FMN mixture), leaving fewer photons available to excite FMN. Consequently, this reduction in the quantity of photons available to excite FMN leads to decreased FMN emission. However, the reduction of FMN fluorescence in other media like IGL1 and Custodiol could be due to the effects of the solvents, as reflected in the emission spectra represented above.

Table 3.3.2 reports the fluorescence values of FMN at 538 nm for excitation at 455 nm, both in saline solution (reference values) and in Belzer MPS solution.

Concentration of FMN µg mL^{-1}	FMN Fluorescence in Saline Solution (A.U.)	FMN Fluorescence in Belzer MPS (A.U.)
0.1	83.025	81.415
0.2	159.8	134.83
0.3	236.575	188.245
0.4	313.35	241.66
0.5	390.125	295.075
0.6	466.9	348.49
0.7	543.675	401.905
0.8	620.45	455.32
0.9	697.225	508.735
1	774	562.15
1.1	850.775	615.565
1.2	927.55	668.98

Table 3.3.2. Fluorescence emission values of FMN in saline solution and in Belzer MPS for different concentrations.

Although the fluorescence of FMN in Belzer MPS is lower than in saline solution, the data clearly show that the fluorescence signal is still acceptable. It is observed that the fluorescence of FMN at a concentration of 0.1 μg mL^{-1} is identical in both saline solution and Belzer MPS. However, a divergence in values is noted at concentrations of 0.3 μg mL^{-1} and 0.5 μg mL^{-1}, where the fluorescence of FMN in Belzer is 20% and 25% lower, respectively, compared to that in saline solution. At a concentration of 1.2 μg mL^{-1}, it is predicted that the fluorescence of FMN in Belzer MPS will be 27% lower. Nevertheless, this value remains appreciable, especially when compared to the low fluorescence observed in Custodiol solution. These data clearly demonstrate that FMN is as easily detectable in Belzer MPS as in saline solution. Similar observations are still valid of IGL-1 solutions, although the last one is less used during hypothermic machine perfusion.

In **Table 3.3.3a** and **3.3.3b** we report the standard deviation of errors bars shown in **Figures 3.3.3** and **Figures 3.3.9**.

Concentration (μg/mL)	Saline sol. Error	Belzer Error	Celsior Error	Custodiol Error	IGL1 Error
0.12	3.567	0.910	0.989	0.683	1.286
0.24	1.582	1.720	0.988	0.292	0.767
0.36	4.119	1.907	2.587	1.953	1.159
0.48	2.310	1.767	1.183	0.145	2.358
0.60	0.397	2.889	3.658	0.803	1.792

Table 3.3.3a. Standard deviations of the replicate measurements shown in Figures 3.3.3.

Concentration (μg/mL)	Std Dev at 340 nm	Std Dev at 360 nm
20	1.839	4.341
40	8.115	4.596
60	8.091	3.030
80	12.992	4.214
100	4.863	6.663
120	3.977	6.742
140	0.942	5.575
160	4.493	8.530
180	2.683	13.902
200	9.861	17.203

Table 3.3.3b. Standard deviations of the replicate measurements shown in **Figure 3.3.9**

NADH has a fluorescence emission that ranges from 400 nm to 600 nm, and the experiments focused on the fluorescence induced at different excitation wavelengths. One representative fluorescence spectrum is shown in **Figure 3.3.8**.

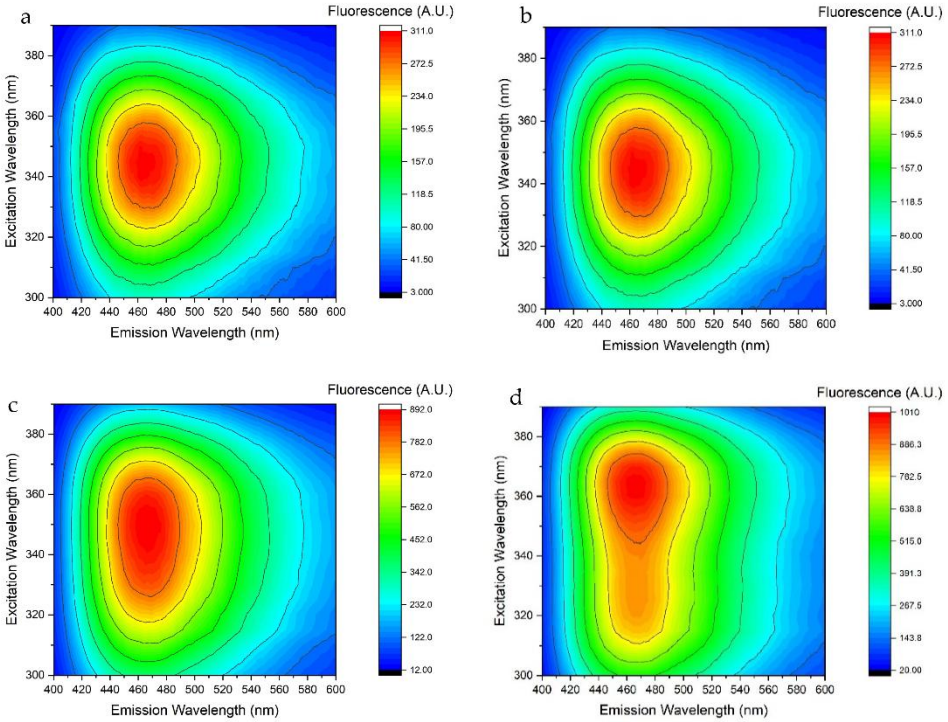

Figure 3.3.8. Fluorescence spectra of NADH in water at different concentration. (a) 20 μg mL^{-1}, (b) 100 μg mL^{-1}, (c) 140 μg mL^{-1}, (d) 200 μg mL^{-1}.

Unlike FMN, the fluorescence spectrum of NADH exhibits greater complexity, as the shape of the spectrum is affected by both the excitation wavelength and the concentration. It is observed that as the concentration of NADH increases, the spectrum changes shape; in particular, for low concentrations, the excitation that generates the greatest fluorescence is at 340 nm, while for other concentrations the optimal wavelength to generate the maximum fluorescence is at 365 nm. This complicates the choice of the optimal excitation wavelength. A second peak in the deep ultraviolet region becomes evident at higher concentrations. Concentration affects not only the shape of the spectrum but also the calibration curve by generating a signal saturation effect as shown in **Figure 3.3.9**.

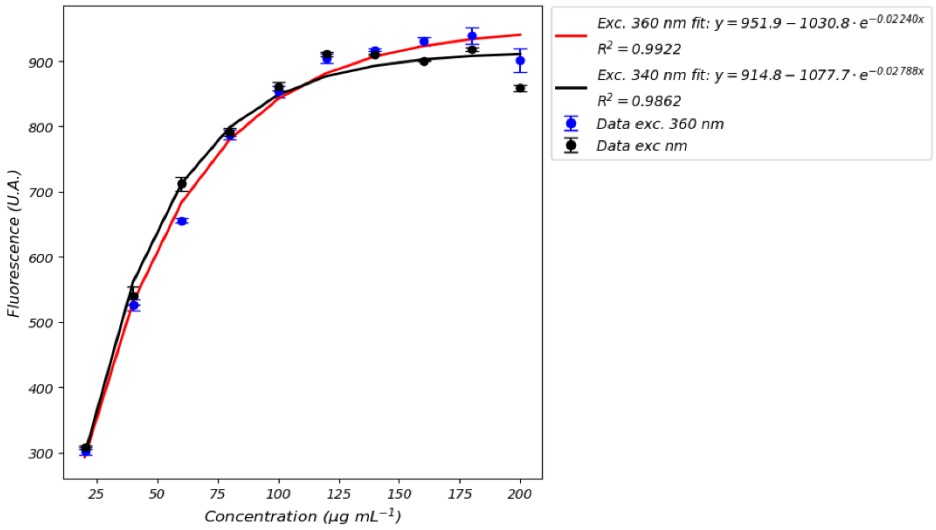

Figure 3.3.9. Calibration curves obtained using an excitation wavelength of 340 nm (black) and 360 nm (red). Emission values are referred to 465 nm. Error bars values are reported in Table 3.3.3b.

Although the curves are well defined, saturation effects appear at relatively high concentrations, around 100 μg mL^{-1}, in every media. As a consequence, we observe non-linear calibration curves. This implies that, above 100 μg mL^{-1}, the fluorescence signal is always the same and it is not possible to distinguish between different concentrations, making it impossible to accurately quantify NADH. Although concentrations normally found in perfusion media are below 70–80 μg mL^{-1}, values above 100 micrograms could be recorded in some situations, especially in perfusate of livers. Detection by fluorescence would present an important limitation in that, in such situations, it would not be possible to be certain of the measured concentration.

As with FMN fluorescence, NADH fluorescence from Celsior and Custodiol media are comparable with the one from saline solution solutions. However, dissolved NADH can attain concentrations as high as approximately 100 times those of FMN. Therefore, although Celsior and Custodiol perfusion solutions absorb in the UV region, NADH can exhibit higher absorbance. In contrast, pure Belzer MPS has a higher absorbance than the Belzer solutions containing NADH, which reduces NADH fluorescence. Despite IGL-1 having similar behavior of Custodiol in absorption, NADH spectra in IGL-1 is the same as in Belzer MPS. As shown in **Figure 3.3.10**,

fluorescence curves in different media almost perfectly overlap. Therefore, NADH does not interact chemically with the other components of the perfusion solutions.

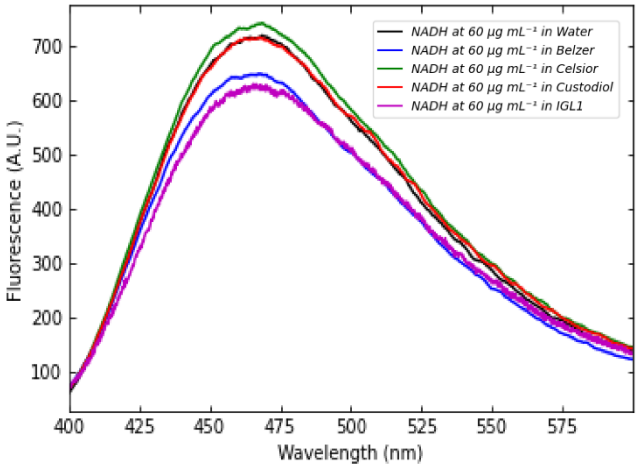

Figure 3.3.10. Fluorescence of NADH in saline solution (black), Belzer MPS (blue), Celsior (green), Custodiol (red), and IGL-1 (magenta) solutions at a concentration of 60 μg mL^{-1} excited at 345 nm.

It has been already observed that its fluorescence shape changes based on concentration. At higher concentrations, a second peak appears in the deep ultraviolet region, as shown in **Figure 3.3.11**. To provide a precise comparison, **Table 3.3.4** reports values of NADH emission for different excitation wavelengths at various concentrations.

	20 μg/ml	100 μg/ml	160 μg/ml	200 μg/ml
Emission at 465 nm for 340 nm of excitation	**306.306 A.U.**	869.509 A.U.	904.822 A.U.	864.662 A.U.
Emission at 465 nm for 350 nm of excitation	301.281 A.U.	**890.695 A.U.**	946.755 A.U.	921.188 A.U.
Emission at 465 nm for 360 nm of excitation	261.818 A.U.	854.245 A.U.	**963.966 A.U.**	995.762 A.U.
Emission at 465 nm for 365 nm of excitation	226.643 A.U.	791.363 A.U.	933.061 A.U.	**1007.91 A.U.**

Table 3.3.4. Values of emissions for different excitation wavelength in various concentrations.

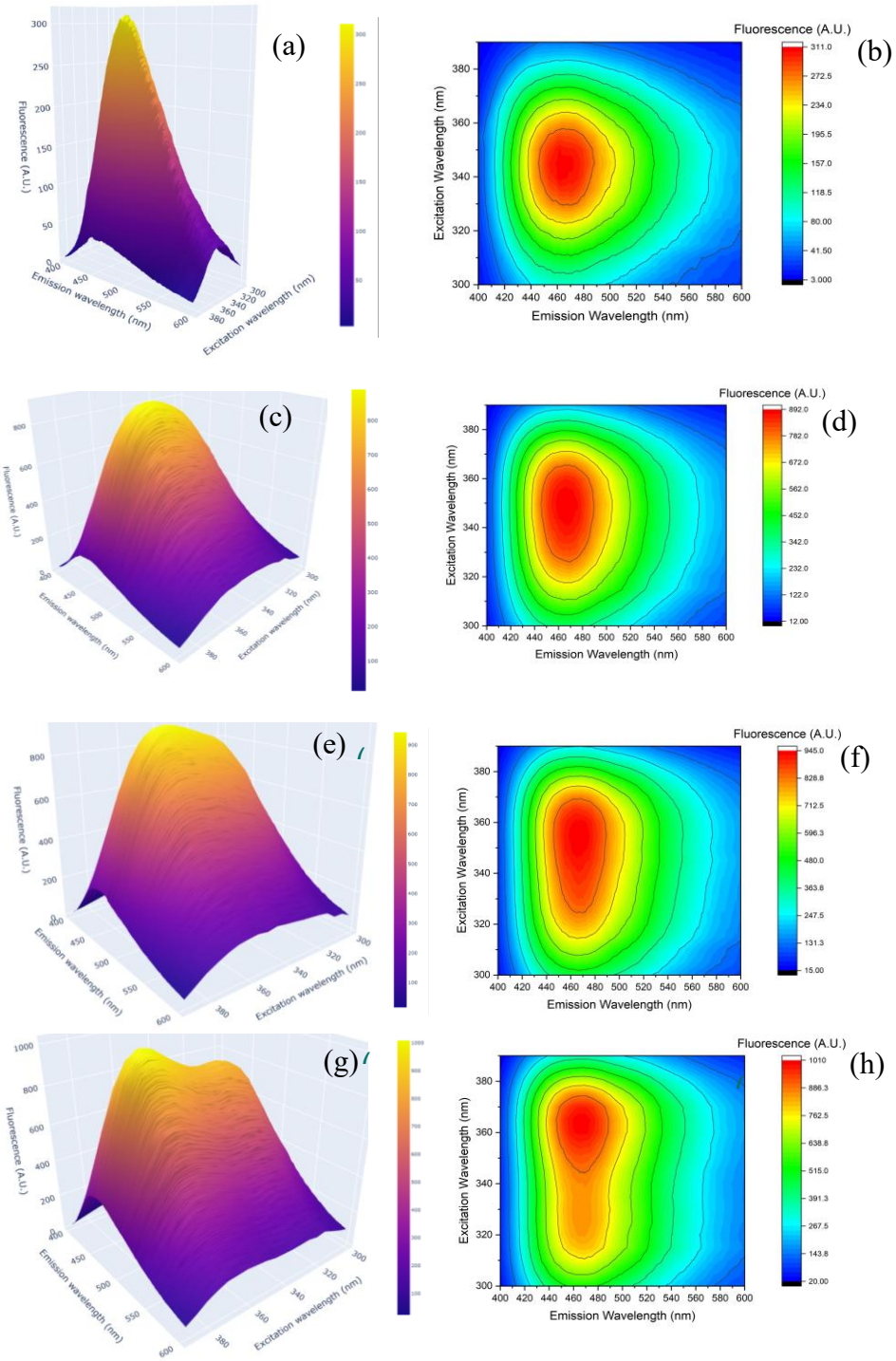

Figure 3.3.11. 3D and 2D fluorescence spectra of NADH in water at different concentration. (a, b) 20 μg mL^{-1}. (c, d) 100 μg mL^{-1}. (e, f) 140 μg mL^{-1}. (h, g) 200 μg mL^{-1}.

It's clear that increasing concentration causes a shift in emission peak at 465 nm. This peculiarity makes it challenging the choice of optimal excitation wavelength.

Based on the results presented so far, the spectral behavior of perfusion solutions containing both FMN and NADH at different concentrations was investigated separately. Specifically, we measured fluorescence starting from an FMN concentration of 0.12 μg mL^{-1} and a NADH concentration of 20 μg mL^{-1}. The two concentrations were increased simultaneously. A few representative three-dimensional fluorescence spectra for FMN + NADH saline solution solutions are shown in **Figure 3.3.12**. Fluorescence was exciting using a wavelength in the range between 300 nm and 390 nm in order to induce NADH emission in wavelength interval from 400 nm to 600 nm.

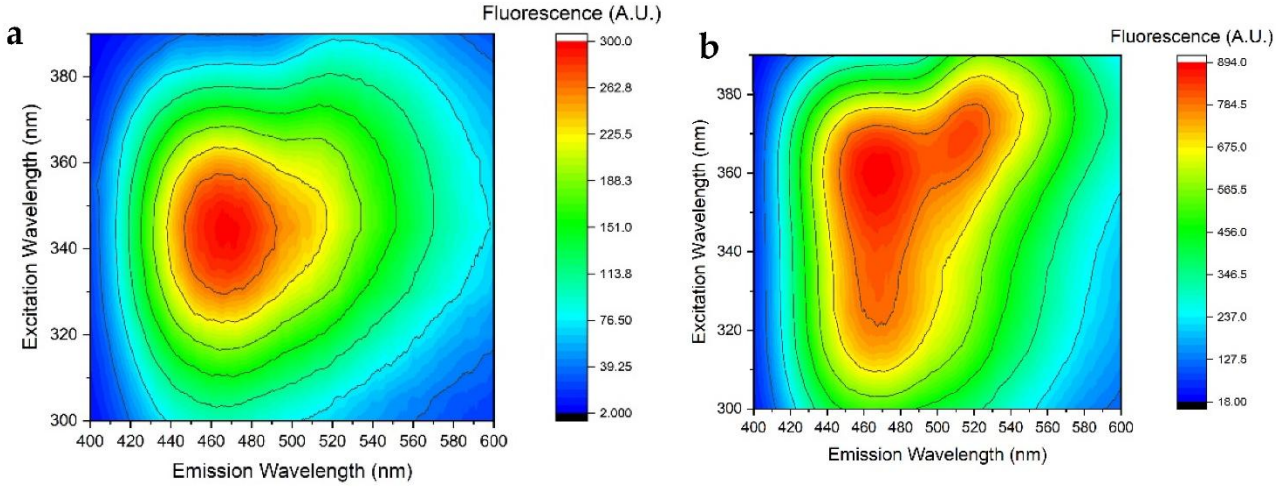

Figure 3.3.12. Fluorescence spectra of FMN + NADH saline solution solutions at FMN and NADH concentrations, respectively, equal to (**a**) 0.12 μg mL^{-1} and 20 μg mL^{-1} and (**b**) 1.08 μg mL^{-1} and 180 μg mL^{-1}.

FMN and NADH share the UV absorption region between 320 nm and 390 nm. It can be seen from **Figure 3.3.13a** that, the FMN concentration being about 100 times lower than NADH, FMN poorly contributes to fluorescence. As the FMN concentration increases, a shoulder and then a peak become evident in the region between 500 nm and 530 nm due to excitation at wavelengths between 360 nm and 370 nm (**Figure 3.3.13b**). This can be explained by the excitation of FMN from NADH emission. Indeed, NADH emits light in the blue region where FMN absorbs. The increase in NADH concentration, and the associated increase in the NADH emission in the blue region, induces the excitation of FMN, eventually causing the growth of the peak in the yellow region. We have exclusively represented the behavior and interactions between FMN and NADH in physiological solution. The decision not to include interactions between FMN and NADH in other solutions (Belzer MPS, Celsior, Custodiol, IGL-1) was made because the interactions observable in water remain the same in other liquid media, with the only difference being lower intensities, as already highlighted in **Figure 3.3.2** and **Figure 3.3.10**.

To study the 3D spectra of FMN and NADH in perfusion solutions, their concentrations were analyzed within the same range as when studied individually, varying both FMN and NADH. From a clinical perspective, the relationship between FMN and NADH release is not well understood and requires further investigation. In this study, fluorescence was evaluated starting from an FMN concentration of 0.12 μg mL^{-1} and an NADH concentration of 20 μg mL^{-1}, increasing both simultaneously. The concentration matrix, shown in **Table 3.3.5**, represents all possible combinations of FMN and NADH concentrations. The spectrophotometric analysis focused along the diagonal of the concentration matrix, considering it less useful to examine other ratios, as simultaneous variation of NADH and FMN in the perfusate is deemed more plausible.

FMN; NADH										
	0.12;20	0.24;20	0.36;20	0.48;20	0.60;20	0.72;20	0.84;20	0.96;20	1.08;20	1.20;20
	0.12;40	**0.24;40**	0.36;40	0.48;40	0.60;40	0.72;40	0.84;40	0.96;40	1.08;40	1.20;40
	0.12;60	0.24;60	**0.36;60**	0.48;60	0.60;60	0.72;60	0.84;60	0.96;60	1.08;60	1.20;60
	0.12;80	0.24;80	0.36;80	**0.48;80**	0.60;80	0.72;80	0.84;80	0.96;80	1.08;80	1.20;80
	0.12;100	0.24;100	0.36;100	0.48;100	**0.60;100**	0.72;100	0.84;100	0.96;100	1.08;100	1.20;100
	0.12;120	0.24;120	0.36;120	0.48;120	0.60;120	**0.72;120**	0.84;120	0.96;120	1.08;120	1.20;120
	0.12;140	0.24;140	0.36;140	0.48;140	0.60;140	0.72;140	**0.84;140**	0.96;140	1.08;140	1.20;140
	0.12;160	0.24;160	0.36;160	0.48;160	0.60;160	0.72;160	0.84;160	**0.96;160**	1.08;160	1.20;160
	0.12;180	0.24;180	0.36;180	0.48;180	0.60;180	0.72;180	0.84;180	0.96;180	**1.08;180**	1.20;180
	0.12;200	0.24;200	0.36;200	0.48;200	0.60;200	0.72;200	0.84;200	0.96;200	1.08;200	**1.20;200**

Table 3.3.5. Concentration matrix. Along with raw FMN concentration varies, along with the column the NADH concentration varies..

Given that the FMN concentration is approximately 100 times lower than the NADH concentration, FMN fluorescence contributes weakly but detectably to the 3D spectra. As the concentration of FMN in the FMN+NADH mixture increases, the influence of FMN fluorescence becomes more pronounced due to its absorption in ultraviolet light, particularly in the 340-380 nm range. From **Figure 3.3.13** and particularly from **Figure 3.3.14**, a notable peak arises in the 500-530 nm region due to excitation at 340-360 nm. This suggests the possibility of mutual excitation between NADH and FMN.

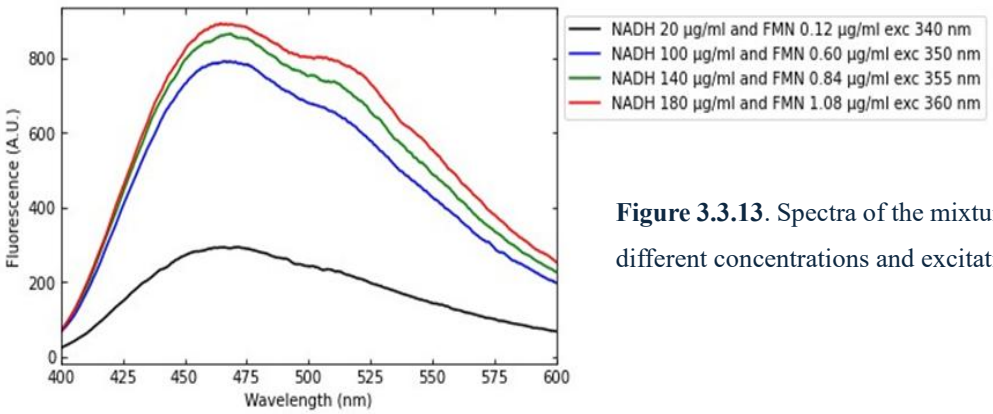

Figure 3.3.13. Spectra of the mixture NADH+FMN in water for different concentrations and excitation wavelengths.

NADH emits light in the blue region, where FMN absorbs. Due to the higher concentration of NADH, the light emission of NADH in the blue region upon excitation at 360-370 nm could have excited FMN, causing the peak in the yellow region to rise. This hypothesis is supported by the higher concentration of NADH relative to FMN. It is plausible that a significant portion of photons are

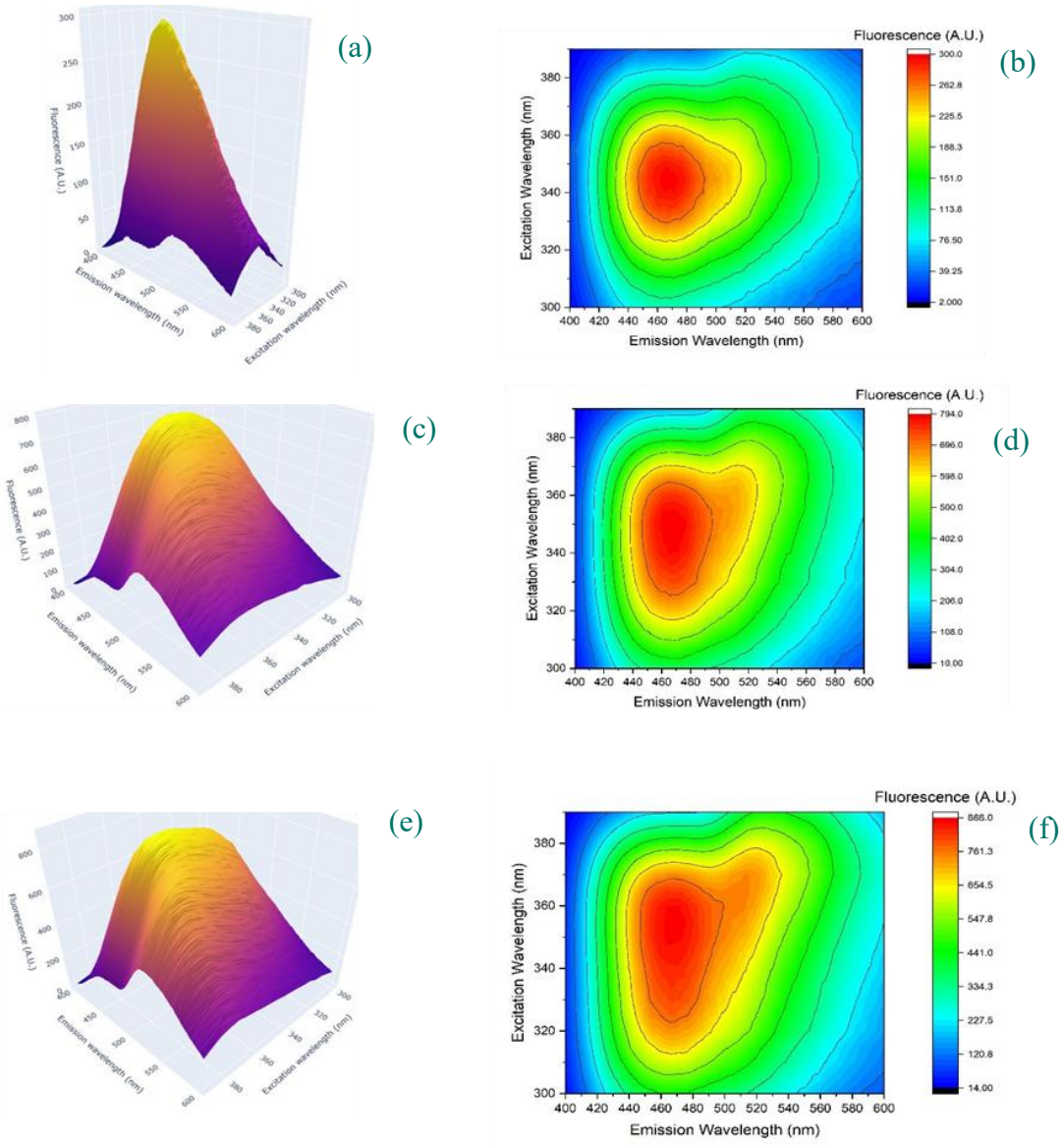

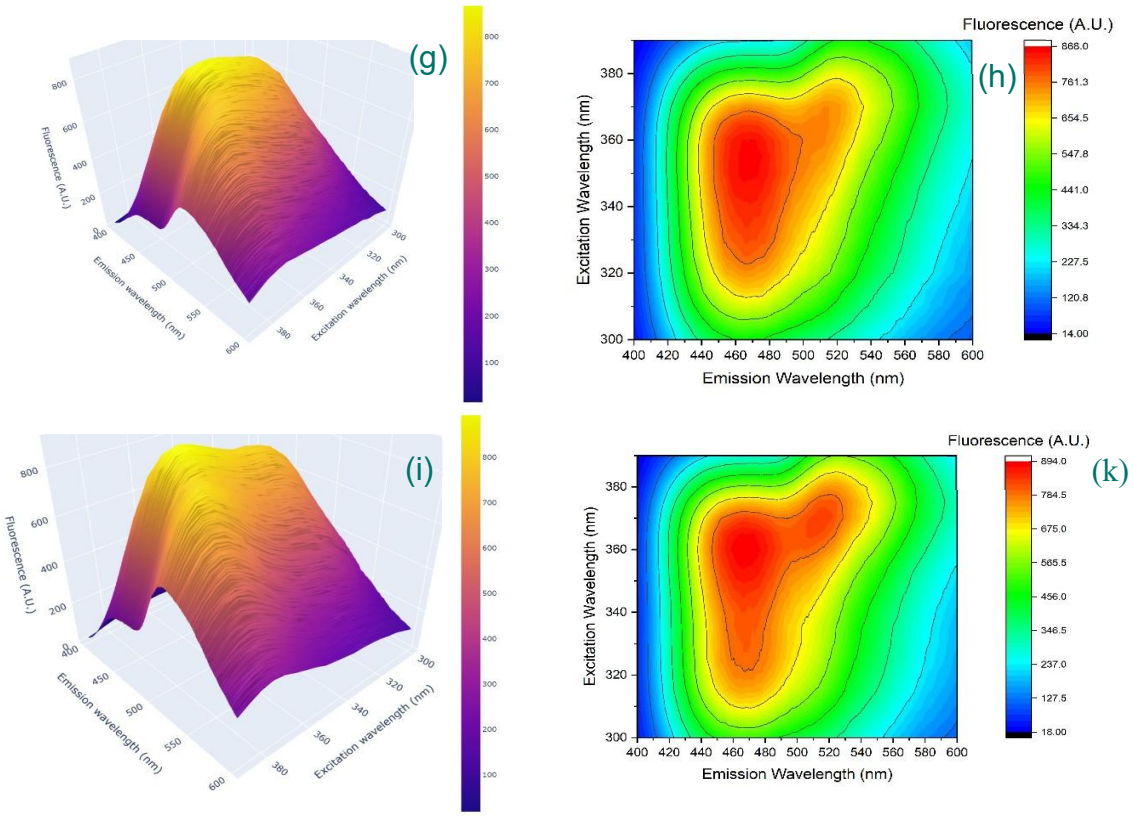

Figure 3.3.14. 3D and 2D fluorescence spectra of FMN+NADH mixture in water at different concentration for excitation in range 300-390 nm and fluorescence in range 400-600 nm

absorbed by NADH molecules, with FMN emission resulting from NADH fluorescence. **Figure 3.3.14** present 3D and 2D heat map spectra at the same concentration to reinforce this explanation.

Figure 3.3.14d, **Figure 3.3.14f**, and **Figure 3.3.14h** confirm that the fluorescence generated by FMN is primarily due to the emission by NADH. Specifically **Figure 3.3.14a**, which plots the spectrum of 0.12 μg mL^{-1} FMN and 20 μg mL^{-1} NADH, appears very similar to the NADH spectrum depicted in **Figure 3.3.11a**. As the concentration of NADH increases, the capability of exciting FMN through NADH emission also increases. However, exciting the FMN+NADH mixture in the 340-360 nm range allows for the observation of NADH fluorescence at 465 nm without significant interference from FMN fluorescence.

After discussing the mutual interference effects between FMN and NADH in fluorescence signals, we now focus on the absorption spectrum of a solution containing both coenzymes. As shown in **Figure 3.1.1a,b**, FMN and NADH share a common absorption range between approximately 300 and 400 nm, making it challenging to distinguish their individual contributions in this spectral region.

In **Figure 3.3.15**, we present the absorption spectrum of a mixture consisting of FMN at the highest concentration studied (0.96 µg mL^{-1}) and NADH at the lowest (20 µg mL^{-1}), with the goal of maximizing the potential interference of FMN on the NADH signal. This test aims to assess how much FMN might affect the quantitative estimation of NADH when absorption spectroscopy is used as the detection method.

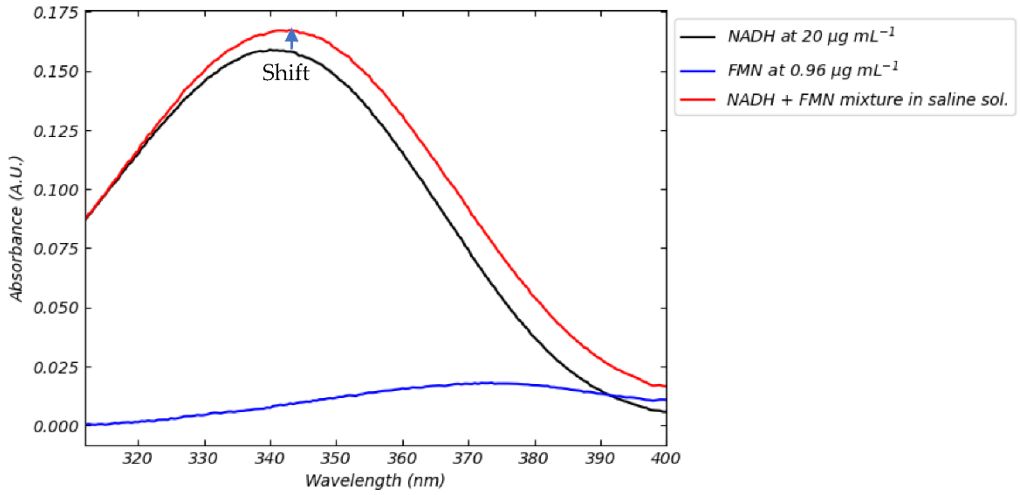

Figure 3.3.15. Absorption spectrum of the FMN+ NADH mixture and the effect of the potential interference of FMN.

The results show that FMN interference is minimal under this specific concentration combination. Applying the NADH calibration curve (**Figure 3.1.2d**) to the mixture's spectrum yields an estimated NADH concentration of approximately 21 µg mL^{-1}, slightly overestimated but still close to the true value. This demonstrates that, despite the spectral overlap, absorption spectroscopy can provide a reasonably accurate estimation of NADH, especially when NADH is present in significantly higher concentrations than FMN.

However, it is important to note that the accuracy of this estimation depends on the relative concentrations of the two coenzymes. In cases where FMN is more concentrated or NADH is present at lower levels, the uncertainty in the measurement may increase. From a clinical perspective, it is therefore essential to determine whether such uncertainty remains within acceptable limits for monitoring or diagnostic purposes.

Our approach thus offers a practical evaluation of the reliability of absorption spectroscopy for NADH quantification in the presence of FMN, contributing to a more informed assessment of its applicability in real-world clinical scenarios.

4. Contribution to the Development of Sensing Technologies

Our work also provides a crucial foundation for developing portable devices and automatic spectral recognition systems. The evolution of perfusion monitoring has been driven by the need for real-time, non-invasive sensing technologies. The Zurich Group's portable perfusion-line-integrated device (2019, 2023) marked a breakthrough in FMN/NADH detection, yet fundamental challenges remain for clinical translation: uncharacterized medium-dependent fluorescence effects and unoptimized excitation parameters for portable systems.

Three key limitations emerge from literature:

1. Methodological inconsistencies: Studies like those by Müller et al. (2019) and Wang et al. (2020) [**5**, **7**] lack critical details (calibration curves, integration times) essential for replicating sensing protocols.
2. Device optimization gaps: Huwyler et al.'s [**11**] device focused on a narrow NADH range, missing the saturation effect we observed >100 µg mL^{-1} (**Figure 3.3.9**)—a critical threshold for sensor dynamic range design.
3. Validation shortcomings: Sousa Da Silva/van de Leemkolk [**9**, **10**] omitted instrumentation details, compromising their utility as references for sensor calibration.

Direct Implications for Optical Sensor Development

Our findings provide actionable insights into sensing systems:

1. Medium-specific calibration (**Figure 3.3.2**, **Figure 3.3.3**, **Figure 3.3.8, Figure 3.3.9** and **Figure 3.3.10**) proves that perfusion solution composition dramatically affects fluorescence, requiring on-device calibration profiles for clinical accuracy.
2. Excitation wavelength flexibility (**Figure 3.3.3**, **Figure 3.3.8** and **Figure 3.3.9**) suggests future devices should incorporate adjustable LEDs (340–450 nm) to accommodate varying analyte concentrations.
3. FMN–NADH fluorescence interaction (**Figure 3.3.12**) demands embedded spectral deconvolution algorithms to prevent crosstalk in multi-analyte detection.
4. Acknowledging that the detection by fluorescence of NADH has a limitation due to signal saturation effect (**Figure 3.3.9**).
5. The implementation of machine learning algorithms capable of recognizing the coenzyme signal from other signals and consequently calculating the corresponding concentration.

Our work addresses these gaps while providing a roadmap for next-generation optical sensor development. Optical data is the mandatory first step in developing devices since no sensor can be designed without these preliminary results.

5. Summary of the chapter and recommendations

We extensively investigated the spectrophotometry of FMN and NADH in standard perfusion solutions to construct calibration curves for quantitative evaluation during machine perfusion. We propose a simple, accurate, and precise calibration method applicable to both benchtop and inline spectrophotometers. This approach is adaptable to various perfusion liquids, including Steen® and Perfadex®, and enables cost estimation related to calibration procedures.

Our findings show that FMN and NADH maintain consistent absorption and fluorescence spectra regardless of the perfusion solution used. Neither pH nor temperature significantly affect their spectral behavior. However, interactions with certain perfusion fluids, such as Belzer MPS, IGL-1, and Custodiol, can reduce fluorescence—especially for FMN—without involving chemical reactions. In contrast, Celsior behaves similarly to saline solution and does not interfere with fluorescence intensity. These observations emphasize the need to perform calibration in the same perfusion medium used for clinical applications.

Based on the results obtained, the use of fluorescence spectroscopy with monochromatic excitation is recommended for the selective detection of FMN. Specifically, excitation at 455 nm proves to be highly specific for FMN, as NADH does not absorb at this wavelength. This allows for the acquisition of a clean fluorescence spectrum free from interference. In contrast, the absorption spectra of FMN and NADH may exhibit substantial overlap in the 300–410 nm range, depending on their relative concentrations. In our experimental results, this overlap was limited, and the estimation of NADH concentration remained within an acceptable range. However, in different scenarios—particularly when FMN concentrations are higher and NADH concentrations lower—the interference could increase, potentially affecting quantification accuracy. From a clinical perspective, it is often more important to monitor the overall trend of biomarker levels over time than to obtain an exact absolute value. Nonetheless, determining the clinically acceptable margin of uncertainty remains an important topic for future investigation and validation. However, the application of machine learning algorithms for classification and regression, properly trained on spectra from mixtures of FMN and NADH at varying concentrations, can effectively support the discrimination of their respective spectral contributions. This is particularly relevant given that FMN is typically present at lower concentrations than NADH.

Therefore, we suggest using fluorescence for FMN quantification and absorption for NADH quantification. If fluorescence is also to be used for NADH detection, we recommend employing optical filters that block spectral components beyond 480 nm, in order to isolate the fluorescence of NADH (which peaks at 465 nm) and prevent overlap with FMN fluorescence.

Finally, the adoption of a sequential excitation strategy represents an additional measure to minimize interference and ensure accurate and differentiated detection of the two biomarkers.

FMN's fluorescence calibration curve remains linear and robust, even in the presence of moderate interferents, making it suitable for both hypothermic and normothermic perfusion. NADH, however, loses fluorescence linearity above 100 μg mL^{-1} and is only relevant during hypothermic perfusion. Interfering substances, such as blood or additives (e.g., antibiotics, albumin, vasodilators), must be considered, and future research should assess their effect on biomarker quantification.

Our method is instrument-specific but broadly transferable to other systems. This study lays the groundwork for innovative device design and real-time monitoring using machine and deep learning algorithms. Techniques such as k-NN, SVM, and neural networks can classify biomarker spectra, estimate concentrations, and detect the presence of interferents. For example, a model trained on FMN data in Belzer MPS could monitor perfusion in real-time, aiding clinical decisions.

From a spectrophotometric perspective, the optimal perfusion solution mimics saline and avoids interactions with FMN and NADH. We recommend designing new solutions that do not absorb in the 400–500 nm range and do not alter biomarker fluorescence. Among those tested, Belzer MPS and IGL-1 performed best, particularly for FMN and NADH fluorescence.

This chapter should be viewed not only as a study on FMN and NADH spectrophotometry but as a guide for developing or refining devices for machine perfusion. It answers key questions about the best detection techniques, excitation wavelengths, calibration protocols, and the integration of machine learning. For existing setups or new devices, this framework offers a reference for the future development of devices and standardization.

References

[1] Schlegel A, Muller X, Kalisvaart M, Muellhaupt B, Perera MTPR, Isaac JR, Clavien P-A, Muiesan P, Dutkowski P. Outcomes of DCD liver transplantation using organs treated by hypothermic oxygenated perfusion before implantation. J Hepatol. 2019;70:50–57.

[2] Quintini C, Del Prete L, Simioni A, Del Angel L, Uso TD, D'Amico G, Hashimoto K, Aucejo F, Fujiki M, Eghtesad B, et al. Transplantation of declined livers after normothermic perfusion. Surgery. 2022;171:747–756.

[3] Guzzi F, Knight SR, Ploeg RJ, Hunter JP. A systematic review to identify whether perfusate biomarkers produced during hypothermic machine perfusion can predict graft outcomes in kidney transplantation. Transpl Int. 2020;33:590–602.

[4] Bhogal RH, Mirza DF, Afford SC, Mergental H. Biomarkers of liver injury during transplantation in an era of machine perfusion. Int J Mol Sci. 2020;21:1578.

[5] Müller X, Schlegel A, Kron P, Eshmuminov D, Würdinger M, Meierhofer D, Clavien P-A, Dutkowski P. Novel real-time prediction of liver graft function during hypothermic oxygenated machine perfusion before liver transplantation. Ann Surg. 2019;270:783–790.

[6] Schlegel A, Müller X, Mueller M, Stepanova A, Kron P, de Rougemont O, Muiesan P, Clavien P-A, Galkin A, Meierhofer D, et al. Hypothermic oxygenated perfusion protects from mitochondrial injury before liver transplantation. eBioMedicine. 2020;60:103014.

[7] Wang L, Thompson E, Bates L, Pither TL, Hosgood SA, Nicholson ML, Watson CJE, Wilson C, Fisher AJ, Ali S, et al. Flavin mononucleotide as a biomarker of organ quality—A pilot study. Transplant Direct. 2020;6:e600.

[8] Panconesi R, Carvalho MF, Eden J, Fazi M, Ansari F, Mancina L, Navari N, Da Silva RX, Dondossola D, Borrego LB, et al. Mitochondrial injury during normothermic regional perfusion (NRP) and hypothermic oxygenated perfusion (HOPE) in a rodent model of DCD liver transplantation. eBioMedicine. 2023;98:104861.

[9] Sousa Da Silva RX, Darius T, Mancina L, Eden J, Wernlé K, Ghoneima AS, Barlow AD, Clavien P-A, Dutkowski P, Kron P. Real-time assessment of kidney allografts during HOPE using flavin mononucleotide (FMN)—A preclinical study. Front Transplant. 2023;2:1132673.

[10] Van de Leemkolk FE, Lo Faro ML, Shaheed S, Mulvey JF, Huurman VAL, Alwayn IPJ, Putter H, Jochmans I, Lindeman JHN, Ploeg RJ, et al. The role of flavin mononucleotide (FMN) as a potentially clinically relevant biomarker to predict the quality of kidney grafts during hypothermic (oxygenated) machine perfusion. PLoS ONE. 2023;18:e0287713.

[11] Huwyler F, Eden J, Binz J, Cunningham L, Sousa Da Silva RX, Clavien PA, Dutkowski P, Tibbitt MW, Hefti M. A spectrofluorometric method for real-time graft assessment and patient monitoring. Adv Sci. 2023;10:2301537.

[12] Darius T, Vergauwen M, Maistriaux L, Evrard R, Schlegel A, Mueller M, O'Neil D, Southam A, Aydin S, Devresse A, et al. Intermittent surface oxygenation results in similar mitochondrial protection and maintenance of aerobic metabolism as compared to continuous oxygenation during hypothermic machine kidney machine perfusion. J Clin Med. 2023;12:3731.

[13] Dingfelder J, Kollmann D, Rauter L, Pereyra D, Kacar S, Weijler AM, Zadeh TS, Tortopis C, Silberhumer G, Salat A, et al. Validation of mitochondrial FMN as a predictor for early allograft dysfunction and patient survival measured during hypothermic oxygenated perfusion. Liver Transpl. 2025;31:476–488.

[14] Sun K, Jiao C, Panconesi R, Satish S, Karakaya OF, De Goeij FH, Diwan T, Ali K, Cadinu LA, Cazzaniga B, et al. Quantifying flavin mononucleotide: An internationally validated methodological approach for enhanced decision making in organ transplantation. eBioMedicine. 2025;116:105761.

[15] Antunović M, Aleksić D. Preparation and testing of solutions for organ perfusion and preservation in transplantation. Vojnosanit Pregl. 2008;65:596–600.

[16] Panayotova G, Paterno F, Galan M, Simonishvili S, Qin Y, McCarty M, Brown L, Amin A, Lunsford KE, Guarrera JV. Hypothermic oxygenated machine perfusion preserves cholangiocyte homeostasis and protects against biliary complications post liver transplantation: Preliminary results from a single center. J Am Coll Surg. 2021;233:S267–S268.

[17] Edwards AM. Structure and general properties of flavins. In: Weber S, Schleicher E, eds. Flavins and Flavoproteins. Methods in Molecular Biology. New York: Humana Press; 2014. p. 3–13.

[18] Hull R, Conger P, Hoobler R. Conformation of NADH studied by fluorescence excitation transfer spectroscopy. Biophys Chem. 2001;90:9–16.

[19] De Vries Y, Berendsen TA, Fujiyoshi M, van den Berg AP, Blokzijl H, de Boer MT, van der Heide F, de Kleine RH, van Leeuwen OB, Matton AP, et al. Transplantation of high-risk donor livers after resuscitation and viability assessment using a combined protocol of oxygenated hypothermic, rewarming and normothermic machine perfusion: Study protocol for a prospective, single-arm study (DHOPE-COR-NMP). BMJ Open. 2019;9:e028596.

[20] Van Beekum CJ, Vilz TO, Glowka TR, von Websky MW, Kalff JC, Manekeller S. Normothermic machine perfusion (NMP) of the liver—Current status and future perspectives. Ann Transplant. 2021;26:e931664.

[21] Ghisla S, Massey V, Lhoste JM, Mayhew SG. Fluorescence and optical characteristics of reduced flavines and flavoproteins. Biochemistry. 1974;13:589–597.

[22] Gorbunova IA, Sasin ME, Yachkov DV, Volkov DA, Vedyaykin AD, Nikiforov AA, Vasyutinskii OS. Two-photon excited fluorescence of NADH-alcohol dehydrogenase complex in a mixture with bacterial enzymes. Biomolecules. 2023;13:256.

[23] Kotaki A, Yagi K. Fluorescence properties of flavins in various solvents. J Biochem. 1970;68:509–516.

Dimidium facti, qui coepit, habet
Horace, Epistulae (I, 2, 40)

Chapter IV

A New Online Prototype for Continuous Real-Time Monitoring of FMN

1. Introduction

In **Chapter III**, we explored the application of well-established technologies, such as benchtop spectrophotometers, to investigate the spectrophotometric properties of FMN and NADH in different perfusion media. In this section, we outlined the fundamental criteria required to construct reliable and reproducible calibration curves, as well as the challenges arising from the mutual interaction between FMN and NADH, two molecules whose coexistence can significantly influence measurement outcomes.

Beyond highlighting technical limitations, we also provided practical recommendations that may prove valuable for the development of devices designed to detect biomarkers during organ perfusion. These considerations led us to propose a **potential measurement protocol** conceived for application in a real clinical setting. The proposed protocol is characterized by its operational simplicity, does not require highly specialized expertise, and is cost-effective. Nevertheless, it must be noted that, to date, it has not yet been tested in an actual clinical environment. Despite this limitation, its methodological rigor and robustness make it a strong candidate for future implementation.

Alternative protocols have been described in the literature. Notably, Sun et al. (2025) [1] introduced a method developed and validated at the *Cleveland Clinic*, which has already proven to be reliable in real clinical practice. Other studies have also reported comparable strategies, albeit with operational differences. For instance, Wang et al. (2020) [2] described the collection of perfusate

during perfusion followed by freezing for subsequent analyses. Other authors prosed different criteria [3 – 6]. Similarly, Cadinu et al. (2025) [7], as well as Sun et al., presented protocols involving the collection of perfusate regardless of whether the perfusion was performed under normothermic or hypothermic conditions.

These approaches can be defined as **“offline”** methods, since FMN quantification by spectrophotometry takes place after sample collection. Although these techniques are relatively fast compared with other analytical approaches, they nevertheless require the intervention of a healthcare professional, thus introducing inherent complexities and risks: sampling, potential contamination, the use of a benchtop spectrophotometer or a Micro Plate Reader, and subsequent management of the specimen (freezing or disposal). In other words, the “offline” method provides only a punctual measurement limited to the time of sampling, comparable to taking a photograph of a flowing river: the observation represents only the portion of liquid collected at that precise moment, without capturing the continuity of the process.

Conversely, we define as **“online”** those techniques that enable biomarker detection directly within the circulating perfusion medium, without the need for sampling [8, 9]. The advantages of an “online” approach are considerable: FMN can be monitored in real time, thereby eliminating the issues associated with sample handling; measurements can be performed either at regular intervals or continuously, on a moment-by-moment basis; and, importantly, the quantification process can be entirely delegated to the measuring device, further reducing operator workload.

Table 1.1 provides a classification framework for the measurement methods discussed, allowing a clear distinction between the characteristics and limitations of the different “offline” and “online” approaches.

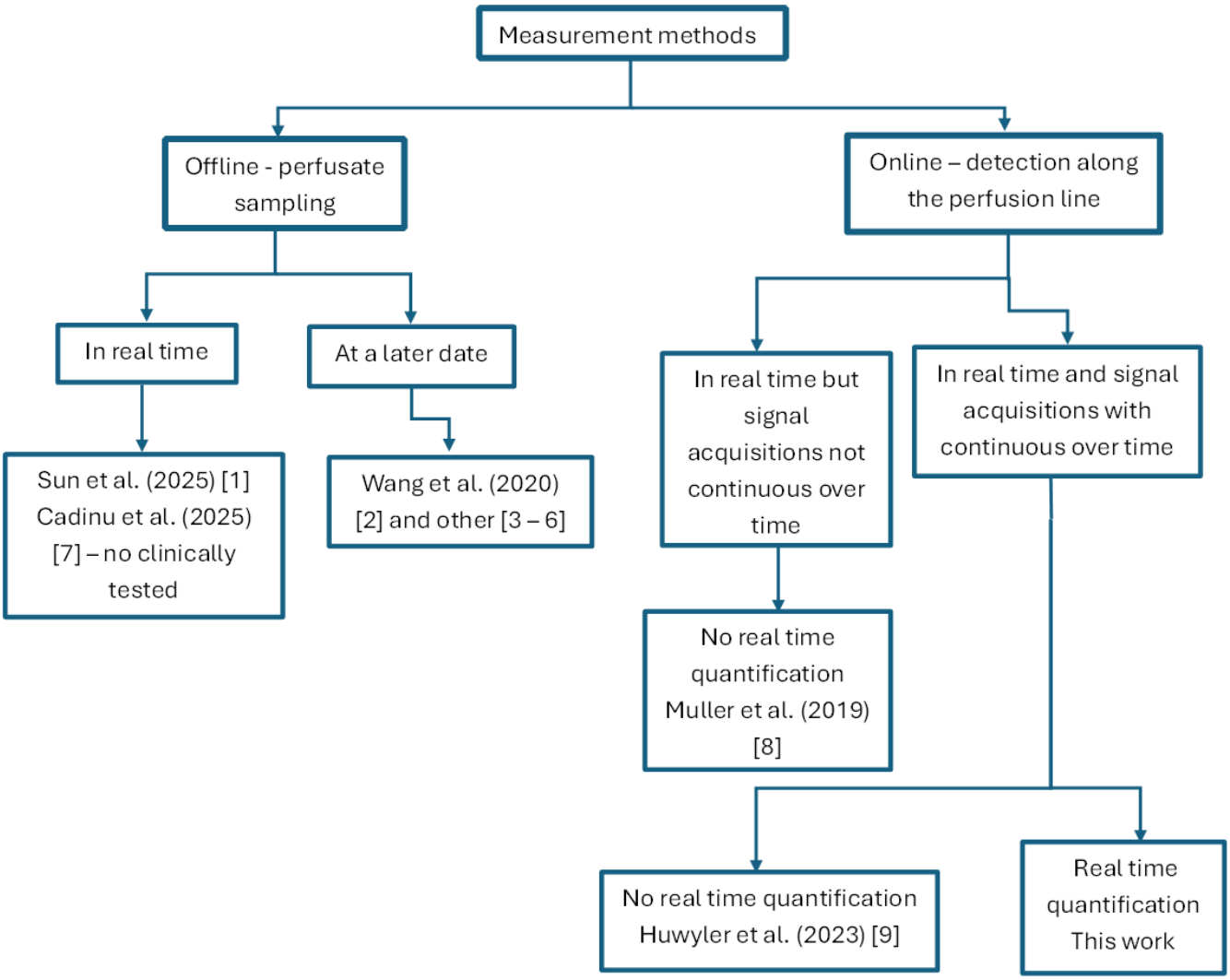

Table 1.1. Classification of current FMN detection methods using spectrophotometry.

The main innovation presented in this thesis is the use of a device capable of detecting and quantifying in real time the biomarker FMN within a perfusion medium. Although the device could potentially also be applied to the quantification of NADH, in the present work we focused exclusively on FMN.

It is important to clarify that this device is a prototype developed and assembled by *Medica Spa* (Via Degli Artigiani, 7 41036 - Medolla (MO) - ITALY). However, the intellectual property rights are held by a third party that is not involved as a stakeholder in this thesis project. Since this is an experimental prototype and has not yet been patented, no technical information will be disclosed in order to ensure confidentiality and to prevent possible legal actions. In this chapter, only a brief and general description of the device will be provided, with the sole purpose of giving an overview of its operating principle.

2. General description and operating principle

The device, similarly to others already reported in the literature, is a **stand-alone prototype** consisting of a spectrophotometric measurement unit and an optical measurement unit. Internally, it incorporates suitable electrical, electronic, and optical architectures that enable power supply, fluorescence signal processing, and information transmission. The device can be connected to a *Raspberry Pi*, where it is operated through a dedicated custom software developed in Qt and written in C++.

Figure 2.1 shows a photograph of the prototype, enclosed within a protective casing.

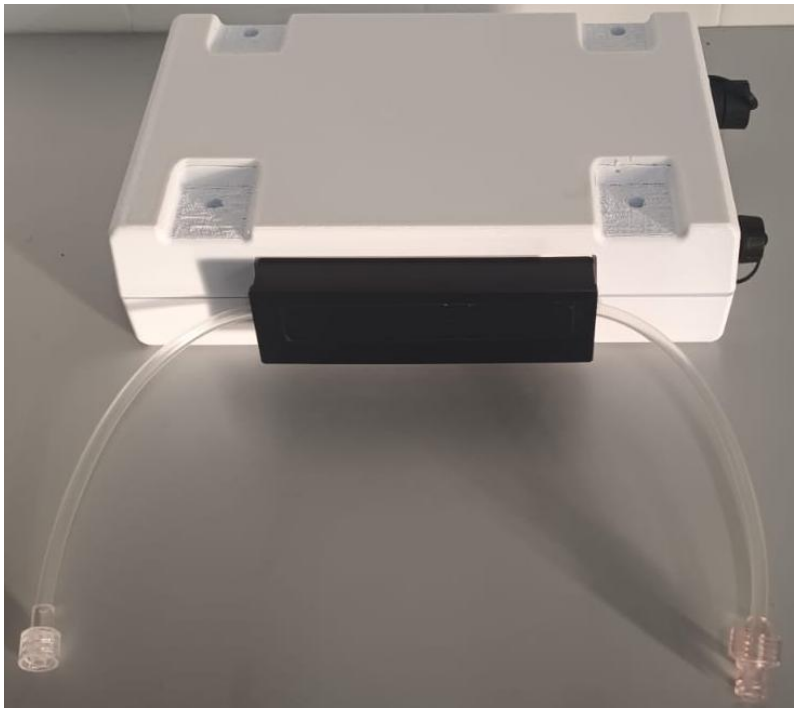

Figure 2.1. photo of the box containing the device.

It can be observed that within the integrated optical unit there is a custom-designed cuvette, specifically developed for this device, through which the perfusate can flow. This cuvette is then incorporated into an organ perfusion circuit. The device processes the fluorescence signal and displays the FMN spectrum on a dedicated screen. A block diagram of the prototype's operating principle is shown in **Figure 2.2**.

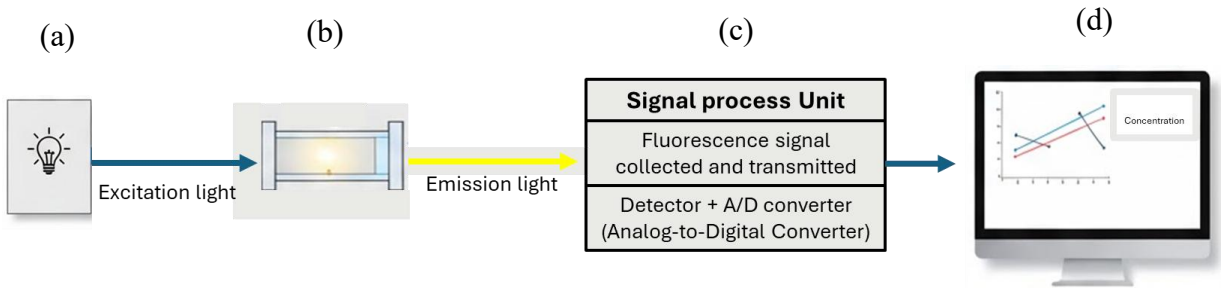

Figure 2.2. Prototype operating principle. (a) Illumination source. (b) Optical unit containing the cuvette through which the perfusion fluid continuously flows. (c) The emitted fluorescence signal is collected and transmitted via an optical fiber, then converted into a digital signal and sent to the processing unit. (d) The fluorescence spectrum is displayed and analyzed on a computer screen running the prototype's dedicated software application, with automatic calculation of the concentration and plotting of the concentration–time graph. In a future perspective, the system may be further expanded to include the calculation of trend derivatives and the integration of statistical models for predicting post-transplant outcome based on the FMN trend and other physiological parameters (see Chapter 6, Section 5).

A similar schematic of the working principle is reported in reference [8].

Figure 2.3 shows a typical fluorescence signal of FMN.

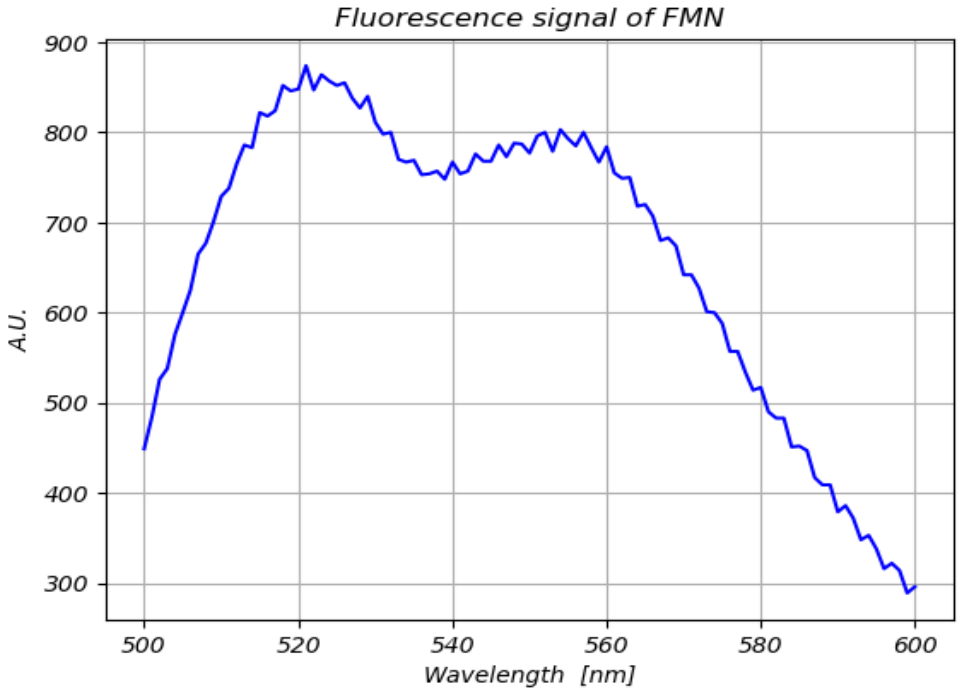

Figure 2.3. An example of FMN fluorescence spectrum.

When comparing the spectrum presented in **Figure 2.3** with the FMN spectrum shown in **Figure 3.3.2 of Chapter III**, it can be noted that the spectrum recorded by the prototype exhibits two peaks, whereas the spectrum obtained with a benchtop spectrophotometer displays only a single peak. The shape of this fluorescence spectrum is likely attributable to the partial reabsorption of a section of the spectrum itself (self-absorption effect), which generates its characteristic double-peak structure. Nevertheless, this does not represent a limitation, since the spectrum reported in **Figure 2.3** is characteristic of FMN alone and cannot be attributed to any other molecule when it's detected with this prototype.

3. Calibration method of the prototype

The most critical aspect of the prototype is its calibration. A simple yet highly efficient technique has been developed to construct calibration curves.

The starting point is the preparation of a stock solution of 59.4 mg mL^{-1}, as described in **Chapter III**. The concentration range proposed for this device is 11.88 ng mL^{-1} to 237 ng mL^{-1}. Unlike the microgram-level range reported in **Chapter III**, here the values are at the nanogram scale. The reason is that this prototype, by setting an appropriate integration time, is able to reliably detect FMN concentrations as low as 5 ng mL^{-1}. This value represents the Limit of Quantification (LOQ), whereas the minimum detectable signal at this concentration corresponds to the Limit of Detection (LOD). In Figure 3.A we show the LOD and LOQ of this prototype for a specific (no disclosable integration time).

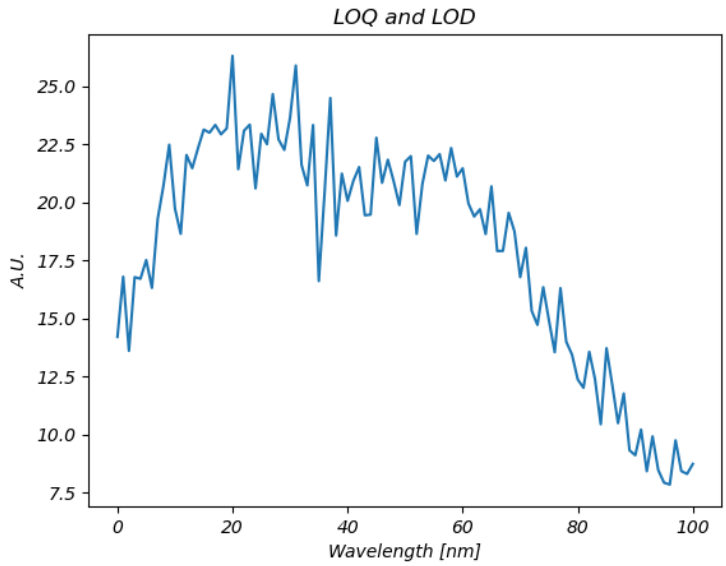

Figure 3.A. LOQ and LOD.

For calibration, the following laboratory equipment is required: a beaker, a calibrated volumetric flask, and a calibrated micropipette. The procedure begins by pouring 500 mL of Belzer UW perfusion solution into the volumetric flask, taking great care to align precisely with the meniscus level. Since the concentrations involved are extremely small, high precision in volume measurement is essential. The use of a Class A volumetric flask is strongly recommended, whereas less accurate instruments such as Falcon tubes or non-calibrated containers should be avoided.

It should be noted that several manufacturers produce the Belzer perfusion solution. Consequently, it is possible that Belzer UW solutions supplied by different companies might exhibit slightly different spectrophotometric properties. Such variations could be sufficient to generate distinct calibration curves. In this study, the Belzer perfusion solution from Bridge to Life was used to establish the calibration curve. It is reasonable to hypothesize that a solution distributed by another supplier might have produced a different calibration response. Only a more comprehensive methodological and statistical analysis could confirm or refute this assumption.

Once the perfusion volume has been measured, it is transferred into a beaker. The beaker is then placed on a magnetic stirrer, and a stir bar is added to ensure homogeneous mixing of the solution. To prevent FMN degradation by light exposure, the beaker should be carefully covered on all sides, including the liquid surface, with aluminum foil. While FMN remains relatively stable under normal ambient light, the calibration procedure requires several hours; therefore, shielding the solution from light eliminates a potential confounding variable. Covering the beaker with foil also prevents dust contamination.

Figure 3.1. Arrangement of suction and delivery cannulas in the perfusion fluid.

After connecting the perfusion pump, turning on the device with the cuvette in place, and immersing both the inlet and outlet cannulas—as illustrated in **Figure 3.1**—the liquid circulation can be initiated. The device is capable of recording fluorescence signals at a frequency of one measurement per second, though it is also possible to specify longer acquisition intervals (e.g., every 10 or 30 seconds).

Figure 3.2 shows the configuration of the calibration equipment.

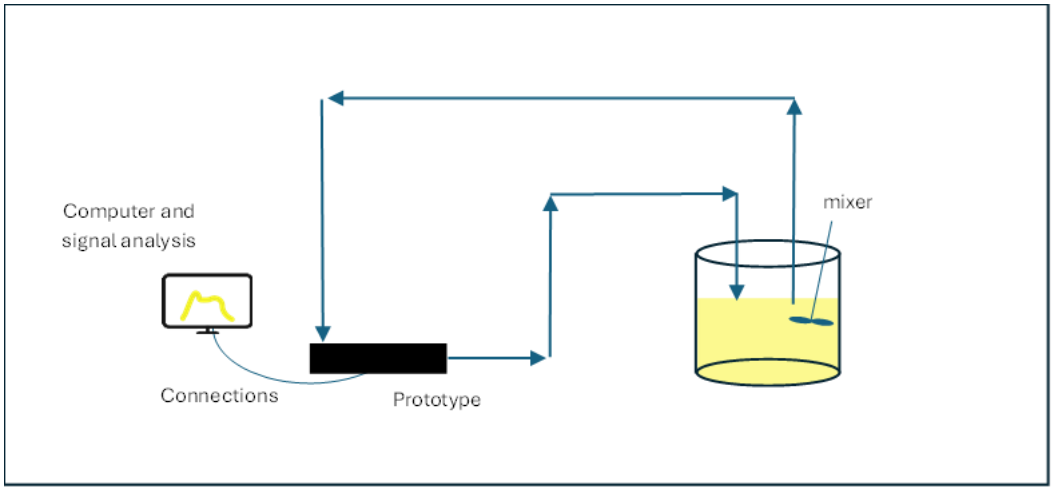

Figure 3.2. Experimental configuration of device calibration.

The software generates a CSV file in real time, storing fluorescence records for each wavelength. This file can subsequently be used for further analysis.

Once the liquid circulation has been initiated and the mixer activated, the calibration procedure can begin. A volume of 100 µL of stock solution is withdrawn and injected into the circulating and stirred liquid. Within a few minutes (depending on the selected flow rate and the total perfusion volume), the FMN fluorescence signal corresponding to a concentration of 11.88 ng mL^{-1} becomes detectable. The concentration value in the circulating medium is calculated according to the dilution formula:

$$c_1 V_1 = c_2 V_2 \tag{3.1}$$

In this case, $c_1 = 0.0594 \frac{mg}{ml}; V_1 = 0.1\ ml;\ V_2 = 500\ ml$

$$c_2 = \frac{c_1 V_1}{V_2} = \frac{0.0594\ {}^{mg}/_{ml} * 0.1\ ml}{500\ ml} = 0.00001188 \frac{mg}{ml} = 0.01188\ \frac{\mu g}{ml} = 11.88 \frac{ng}{ml} \qquad (3.2)$$

A waiting period of approximately 5–10 minutes is required to achieve signal stabilization. The fluorescence signal depends exclusively on the spatial distribution of FMN: when the stock solution is injected, FMN molecules begin to diffuse through the medium following a concentration gradient. By mixing the liquid with a magnetic stirrer, the concentration becomes uniform not only throughout the entire circulating volume but also over time. Once a steady state is reached—that is, when the FMN signal fluctuates around a stable mean value—this value can be considered the reference point for calibration.

The importance of proper mixing is illustrated in **Figures 3.3** and **3.4**.

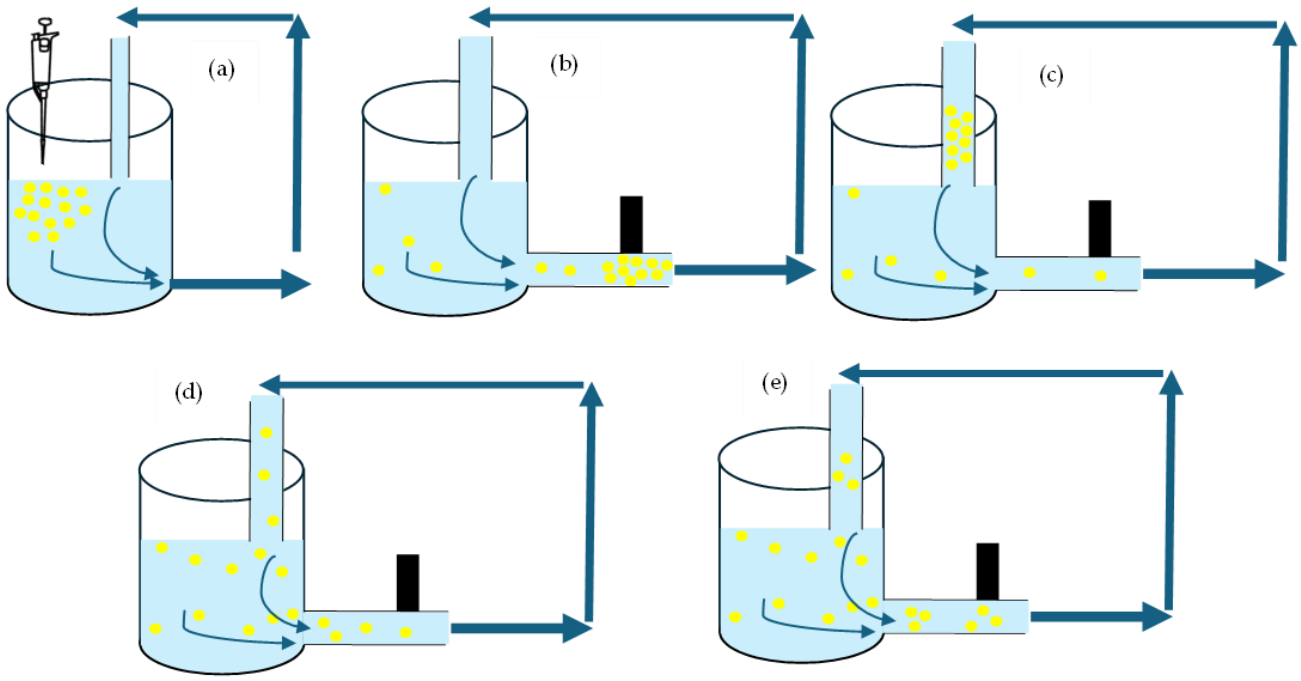

Figure 3.3. Schematic representation of fluid dynamics and the transition from analyte injection to steady state without mixing. (a) At the time of injection, the liquid remains largely stationary, except in regions affected by inlet and outlet flows. The injected bolus of analyte gradually expands due to diffusion along the concentration gradient. The duration of this process depends on the selected flow rate. (b) As the bolus expands, it encounters the suction flow and is largely drawn out. During the first stage, a substantial portion of the analyte is rapidly aspirated, generating a signal peak corresponding to the locally high concentration. (c) Once the initial bolus with high local concentration has passed, a subsequent bolus with lower concentration follows, resulting in a marked decrease in fluorescence signal. (d) Continuous suction and recirculation progressively mix the fluid, leading to a slow and gradual increase in the signal. (e) Eventually, the liquid reaches a fully mixed state, where all fluid portions exhibit the same concentration.

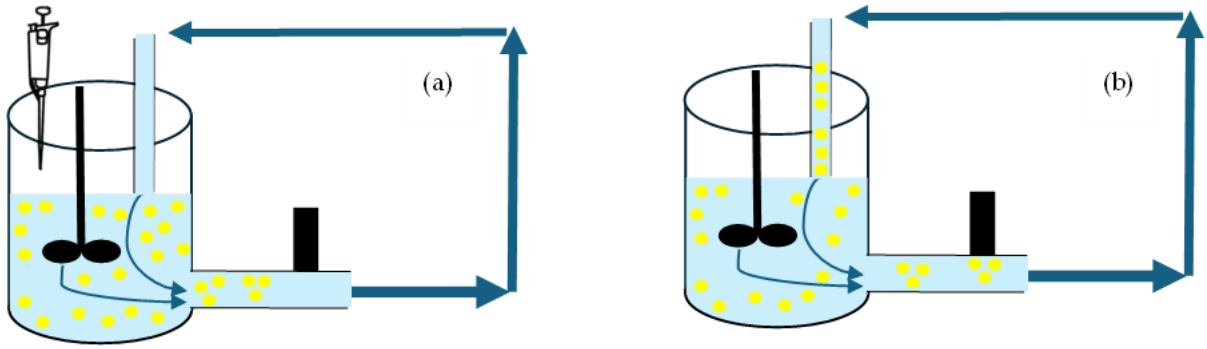

Figure 3.4. Schematic representation of fluid dynamics and the transition from analyte injection to steady state **with mixing**. (a) The agitation of the liquid ensures that, immediately after injection of the bolus containing the stock solution, rapid and complete mixing occurs. (b) The near-instantaneous homogenization allows a stable and steady signal to be established from the very beginning.

Figures 3.5a and **b** show the area under the FMN spectrum curve over time.

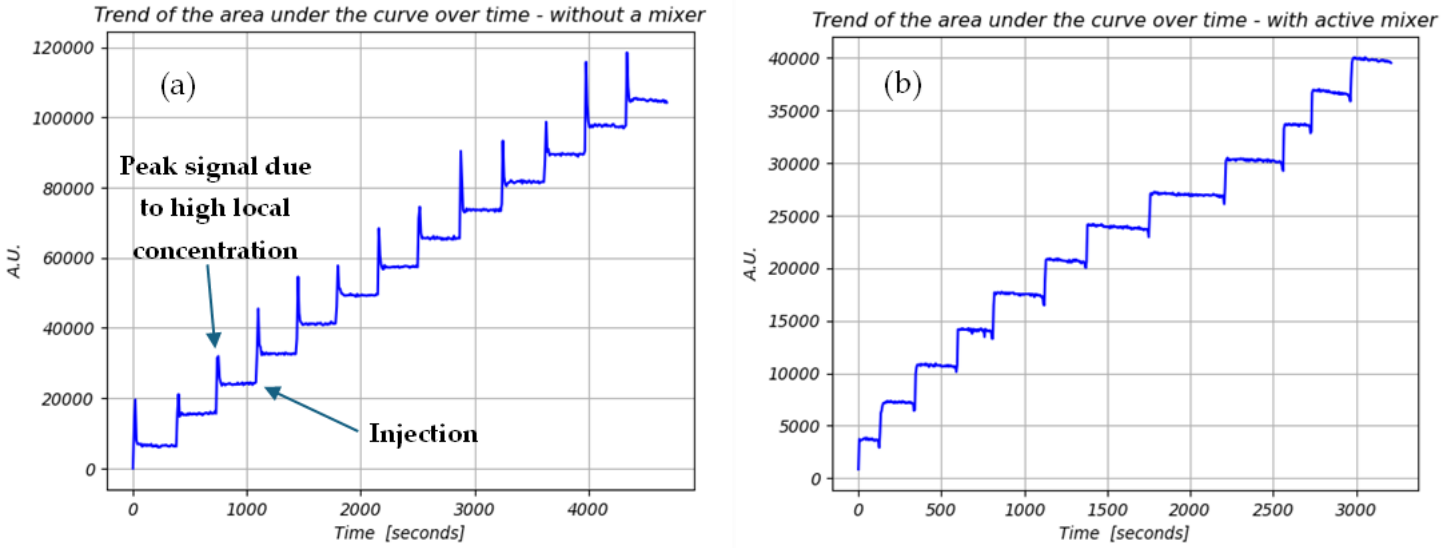

Figure 3.5. Fluid dynamics effects on calibration method. (a) Area under the curve of the entire spectrum over time without mixing. As shown in Figure 3.3, a sharp increase in signal is followed by a rapid decline and subsequent stabilization, as a result of the fluid dynamics within the system. (b) Area under the curve of the entire spectrum over time with active mixing.

Figures 3.5a and **b** clearly illustrate the impact of fluid dynamics on the calibration process. In both cases, a stepwise increase can be observed: when the amount of analyte injected remains constant

over time, the concentration increases in a discrete step-like manner. An effective calibration should display a signal evolution similar to that shown in **Figures 3.5a** and **b**. Indeed, if the injected concentration is constant (as ensured by accurate preparation of the stock solution), then the signal also increases consistently with each injection.

$$c_2 = 0.00001188\frac{mg}{ml} + \frac{0.0594\ {}^{mg}/_{ml} * 0.1\ ml}{500.1\ ml} = 0.00001188\frac{mg}{ml} + 0.00001188\frac{mg}{ml} = 23.76\frac{ng}{ml} \quad (3.3)$$

Once the system reaches steady state, the same volume of stock solution is added again, raising the concentration to 23.76 ng mL^{-1}. After waiting approximately ten minutes, another injection of the same stock volume can be performed. The resulting concentration is calculated according to the formula (3.1) and the procedure was repeated up to get the calibration concentration range depicted in **Table 3.1**.

Each concentration is associated with a specific FMN spectrum, as shown in **Figure 3.6** below.

N° pipetting	Concentration [ng/ml]
1	11.88
2	23.76
3	35.64
4	47.52
5	59.4
6	71.28
7	83.16
8	95.04
9	106.92
10	118.8
11	130.68
12	142.56
13	154.44
14	166.32
15	178.2
16	190.08
17	201.96
18	213.84
19	225.72
20	237.6

Table 3.1. Calibration concentration range list.

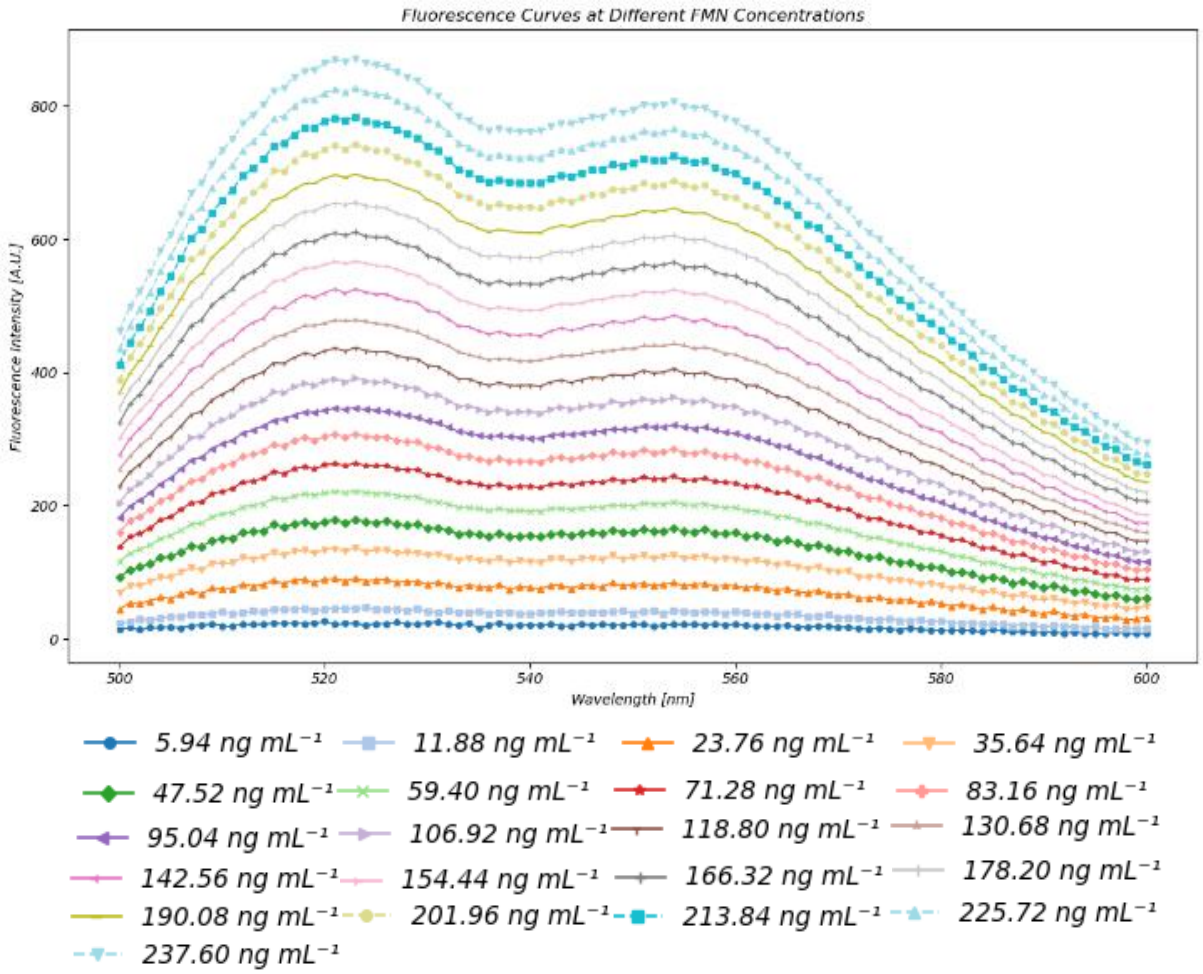

Figure 3.6. FMN fluorescence spectra as concentration varies.

It can be observed that, as the concentration increases, the fluorescence spectrum also grows in intensity and exhibits well-defined features. This dataset constitutes the **training set** that will be used to quantify FMN concentration.

By considering a specific wavelength, for example the peak at **523 nm**, and correlating the fluorescence signal with the corresponding concentration across all concentrations, the so-called **calibration curve** is obtained. An example is shown in **Figure 3.7**.

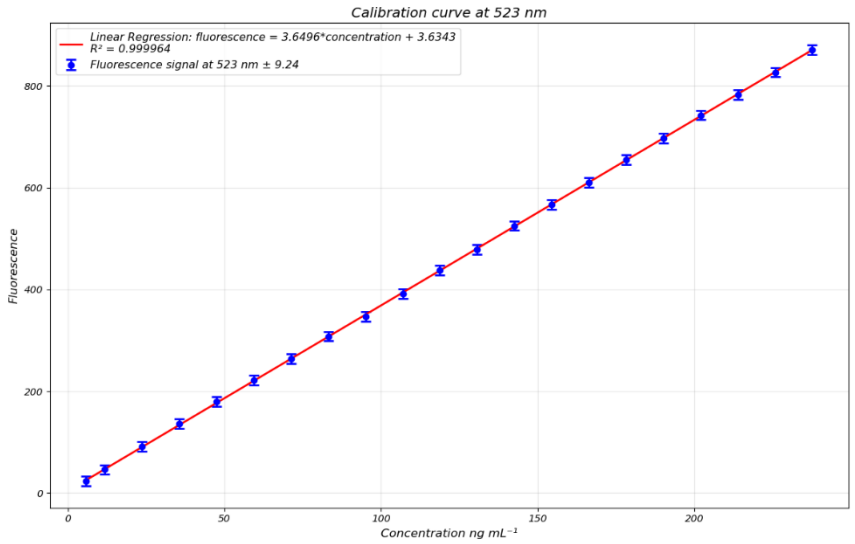

Figure 3.7. FMN calibration curve for wavelength of 523 nm.

Figure 3.7 presents the calibration curve for the wavelength of 523 nm. The data points are perfectly aligned along a straight line, with negligible measurement noise. Moreover, the intercept is very close to zero, indicating excellent linearity. In principle, a calibration curve can be determined for every wavelength between 500 nm and 600 nm, yielding up to **101 calibration curves**. Some examples of calibration curves at different wavelengths are illustrated in **Figure 3.8**.

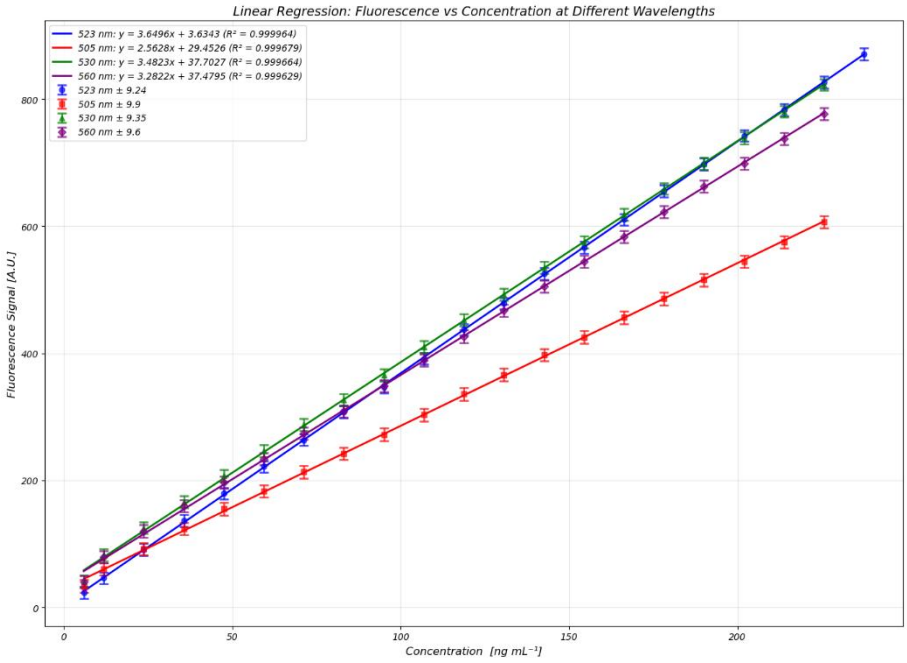

Figure 3.8. FMN calibration curves for different wavelengths

The dataset shown in **Figure 3.6** and the 101 calibration curves will be used in the regression algorithm explained in the following sections.

4. Study of the replicability of the measure

In this section, the reproducibility of fluorescence measurements for samples with identical concentrations will be analyzed in detail. The objective is to assess the instrument's ability to replicate measurements under perfectly identical experimental conditions and to estimate the associated experimental error. To this end, all acquisition parameters are kept constant: the same stock solution, identical volumes withdrawn and diluted to obtain samples of equal concentration, the same circulation flow rate, and identical spectral parameters (integration time, optical fiber, illumination source, and excitation wavelength).

The calibration procedure was repeated multiple times, naturally producing slightly different spectra and calibration curves. The main question is: how different are these data in practice? This section aims to address this question.

In scientific research, experimental error is always present; it is impossible to obtain data completely free of variations. However, by conducting a rigorous and careful experimental campaign, it is possible to minimize such errors, so that any observed differences between measurements can be attributed solely to experimental variability rather than technical or procedural mistakes.

The measurement protocol was executed 14 times, resulting in a total of 14 independent experimental datasets and, consequently, 14 calibration curves. The prototype performs fluorescence scans, and the data recording interval was set to 5 seconds. Therefore, a fluorescence array is saved every 5 seconds. Considering that the acquisition time between consecutive concentrations is approximately 5–10 minutes, each acquisition produces between 60 and 120 fluorescence records. Since 14 experimental campaigns were conducted, for each concentration we have a total of 840–1680 fluorescence samples.

To clarify the procedure: on day 1, the calibration protocol was applied, and a certain number of fluorescence records were recorded for each concentration. On day 2 and day 3, the same measurement procedure was repeated, and so on, up to 14 different days. In this way, 14 independent experimental datasets were obtained. **Table 4.1** presents the fluorescence records corresponding to a

concentration of 106.96 ng mL^{-1} at the wavelength of 523 nm during a single data acquisition test on the day 1.

Time [s]	Fluorescence signal at 560 nm [A.U.]		
2635	297	2750	302
2640	294	2755	315
2645	312	2760	290
2650	310	2765	288
2655	308	2770	294
2660	294	2775	301
2665	305	2780	302
2670	298	2785	293
2675	299	2790	284
2680	292	2795	303
2685	302	2800	296
2690	311	2805	308
2695	293	2810	306
2700	295	2815	311
2705	288	2820	293
2710	299	2825	305
2715	301	2830	307
2720	302	2835	289
2725	303	2840	291
2730	307	2845	299
2735	292	2850	288
2740	306	2855	295
2745	298	2860	302
2750	302		

Table 4.1. Fluorescence signal values recorded at 560 nm for the concentration of 95.04 ng mL^{-1} during a single trial.

Table 4.1 presents the fluorescence values recorded over time at a constant concentration in a single trial. As can be seen, the values fluctuate around a mean, as expected for experimental measurements. Since the circulating concentration remains constant, except for any variations due to the fluid dynamics of the flow, the fluorescence value associated with that concentration and a specific wavelength should also remain constant, except for small oscillations related to fluid dynamic fluctuations.

This section is aimed to illustrate an analysis to evaluate the reproducibility of the measurements and to characterize the statistical distribution of the obtained data. Under ideal experimental conditions, where the only sources of variability are random in nature, we expect to observe a Gaussian distribution of the results. Deviation from this theoretical model represents a sensitive indicator of the presence of systematic error sources or uncontrolled phenomena influencing the measurement process.

To identify and quantify these potential anomalies, we implemented an analytical approach structured across three complementary levels: basic descriptive statistical analysis, an in-depth study of the distributional shape, and the evaluation of data robustness with respect to anomalous values. This integrated strategy allows us to discriminate between variability intrinsic to the phenomenon under examination and alterations induced by undesired external factors. In the study of the distribution, we introduce the Kernel Density Estimation (KDE). This represents a fundamental non-parametric technique for estimating the probability density function of a random variable. Unlike parametric approaches that presuppose a specific distributional shape, KDE allows the data to "speak for themselves," revealing their intrinsic structure without predefined mathematical constraints.

The comparison with the theoretical Gaussian distribution constitutes a pillar of exploratory statistical analysis. This systematic comparison serves to validate or refute the assumption of normality that underlies many parametric statistical tests. The Gaussian distribution represents the theoretical reference model against which to evaluate the empirical behavior of the data. When we observe significant discrepancies between the KDE and the Gaussian curve, it probably means that our data might obey more complex dynamics than those captured by the simple normal model. In our case, these are either attributable to the instrument's difficulty in replicating measurements or, more probably, to variability among the prepared samples.

The simultaneous visualization of the mean and median provides valuable information about the distribution's symmetry. In a perfectly symmetric distribution, these two indices of central tendency coincide; their divergence, however, signals the presence of asymmetries. The mean, although widely used, is sensitively influenced by extreme values, whereas the median maintains its robustness even in the presence of outliers. This dual representation allows us to consciously choose the most appropriate measure to describe the center of the distribution.

The identification of the point of maximum divergence between the KDE and the Gaussian distribution holds particular diagnostic importance. This critical point indicates the region of the sample space where the empirical behavior deviates most significantly from theoretical expectations.

This information is not limited to signaling non-normality but localizes its origin, suggesting possible underlying causes: it could be due to heavier distributional tails, localized asymmetries, or even evidence of multimodality.

Finally, the peak of the KDE represents the empirical mode of the distribution—the most probable or frequently observed value. In many practical applications, especially when the distribution exhibits significant asymmetries, the KDE peak provides an estimate of the "true value" that is more representative than the arithmetic mean. This information is particularly valuable when the measurement process is affected by noise or systematic biases that distort the sample distribution.

Basic Statistics	Parameter	95.04 ng/mL
	Mean	299.33
	Median	301.0
	Standard Deviation	7.72
	Coefficient of Variation	2.58%
	Range	31
	95% Confidence Interval	(297.11, 301.54)
Distribution Analysis	Skewness	-0.158
	Kurtosis	-0.762
	Maximum Divergence (x)	297.4
Distribution Divergence Analysis (Real vs Gaussian)	Total Divergence Area	0.1879
	KDE Peak	303.0
	Interpretation	Moderate deviations
	Shapiro–Wilk Statistic	0.974
	Shapiro–Wilk p-value	0.342
Robustness Analysis	IQR	12.0
	Lower Limit	275.0
	Upper Limit	323.0
	Outliers Detected	None
Dataset Info	Number of Scans	49

Table 4.2. Analysis of the measurement quality and repeatability of the fluorescence signal at 560 nm constant concentration of 95.04 ng mL^{-1}. Data from Table 4.1.

Table 4.2 reports the results of statistical analyses conducted on the data from Table 4.1, providing a summary of the variations and the precision of the signal.

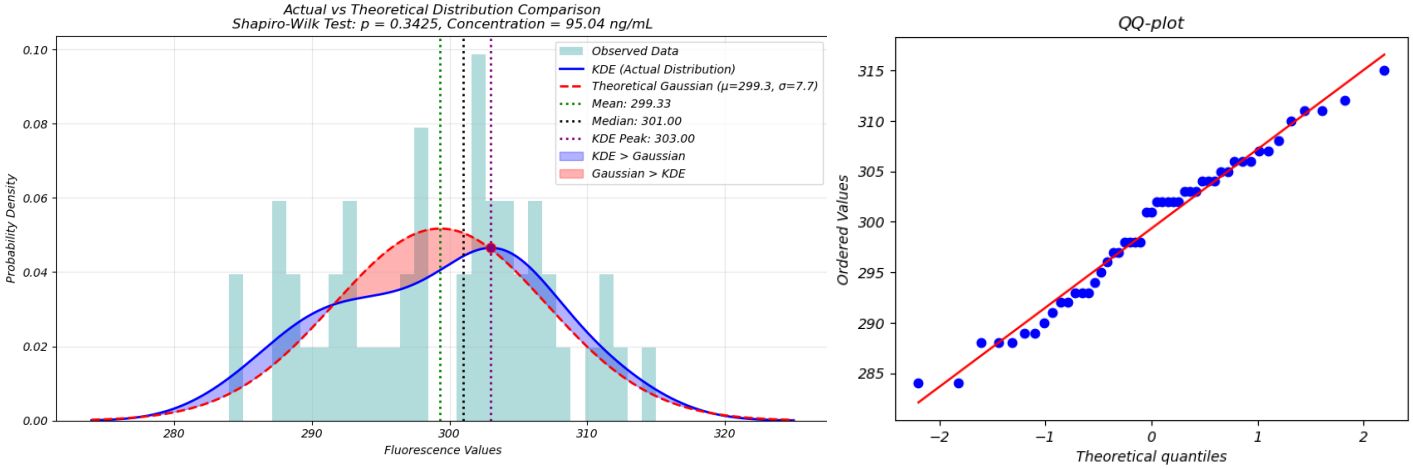

Figure 4.1. (a) Histogram with KDE curve and theoretical gaussian distributions. (b) QQ-plot. Analysis of fluorescence signal at with 560 nm constant concentration of 95.04 ng mL^{-1}. Data from Table 4.1.

In **Figure 4.1**, the histogram of the data, the corresponding Kernel Density Estimate (KDE) curve, theoretical gaussian distribution, and the QQ-plot are presented. These tools allow the assessment of the fluorescence value distribution and the evaluation of any deviations from normality.

The **QQ-plot** (Quantile-Quantile plot), **Figure 4.1b**, compares the distribution of the experimental data with a theoretical distribution, typically the normal distribution.

- The x-axis shows the expected quantiles of the theoretical distribution (e.g., those of a standard normal).
- The y-axis shows the corresponding quantiles from the experimental data.

If the data follow the theoretical distribution, the points align along a 45° diagonal line.

- Points closely following the diagonal → the data are consistent with the theoretical distribution.
- Systematic deviations from the diagonal → the data show particular characteristics (e.g., skewness, heavy tails).

The comprehensive statistical analysis of fluorescence measurements at 560 nm reveals a well-characterized experimental system with notable distributional properties. The dataset demonstrates excellent measurement precision, as evidenced by a coefficient of variation of 2.58%, indicating highly reproducible fluorescence readings across 49 independent scans. The absence of detected outliers further confirms the cleanliness and reliability of the acquired data, while the narrow 95%

confidence interval spanning only ±2.21 units around the mean provides strong statistical support for the measurement stability.

The distribution analysis uncovers a subtle yet meaningful asymmetric pattern in the data structure. A consistent progression is observed from the arithmetic mean of 299.33 through the median of 301.0 to the KDE peak of 303.0, indicating a light left-tailed distribution. This systematic shift suggests the presence of occasional lower-value measurements that slightly depress the arithmetic mean relative to the more representative central tendency measures. The maximum divergence between the empirical KDE and theoretical Gaussian distributions occurs at 297.4, precisely in the region where actual measurements demonstrate systematically lower values compared to normal distribution expectations.

Despite the Shapiro-Wilk test yielding a non-significant p-value of 0.342, which traditionally would not reject the null hypothesis of normality, the kernel density estimation reveals substantial deviations from perfect Gaussian behavior. The total divergence area of 0.1879 qualifies as moderate, indicating that while the distribution approximates normality, it possesses distinct characteristics that merit consideration in analytical interpretation. The interquartile range of 12.0 units confirms a compact data distribution with well-contained variability.

For the estimation of the true fluorescence value, the KDE peak of 303.0 emerges as the most representative metric, as it reflects the most frequently observed measurement value unaffected by distributional asymmetries. The median of 301.0 provides a robust alternative estimate, while the arithmetic mean of 299.33 appears slightly depressed due to the influence of the left-tail values. The systematic discrepancy between these central tendency measures suggests either minor measurement underestimation in certain observations or inherent variability in sample preparation that introduces slight distributional skewness.

In summary, the fluorescence emission at 560 nm demonstrates excellent experimental precision with a characteristic distribution that favors values slightly higher than those indicated by conventional arithmetic mean calculations. The KDE-derived peak value of 303.0 provides the most accurate representation of the typical system behavior, supported by the comprehensive distributional analysis and robustness metrics.

This type of statistical analysis was performed for each sampled wavelength and for every concentration. For the purpose of explaining the analytical method used in this thesis, we have chosen to present in the main text only the results concerning the fluorescence emitted at one specific

wavelength for a given concentration. The complete fluorescence data for various wavelengths and their corresponding concentrations are instead reported in **Appendix A**.

This type of analysis was repeated for measurements at different concentrations and wavelengths, both within the *same* experimental campaign and across subsequent campaigns, yielding very similar results. **Table 4.3** summarizes the statistical analysis results of the concentration 106.92 ng mL^{-1} at the wavelength of 523 nm in different trials (14 trial per day).

In other words, the following table reports the statistical analysis of the fluorescence data measured at 523 nm, corresponding to a concentration of 106.92 ng mL^{-1}, acquired over 14 different days under the same experimental conditions.

Basic Statistics	Parameter	Day 1	Day 2	Day 3	Day 4	Day 5	Day 6	Day 7
	Mean	386.25	394.72	391.86	392.24	395.65	397.74	376.51
	Median	386.0	395.0	389.0	393.0	398.0	398.0	377.0
	Standard Deviation	7.27	6.16	7.05	4.13	6.93	5.64	5.37
	Coefficient of Variation (%)	1.88	1.56	1.8	1.05	1.75	1.42	1.43
	Range	32	33	26	16	26	29	26
	95% Confidence Interval	(384.04, 388.46)	(392.83, 396.62)	(389.18, 394.54)	(390.36, 394.12)	(393.10, 398.19)	(396.20, 399.28)	(374.72, 378.30)
Distribution Analysis	Skewness	0.4296	-0.1691	1.0639	-0.2577	-0.423	-0.5552	-1.219
	Kurtosis	0.044	1.289	0.13	-0.234	-0.526	1.106	2.613
	Shapiro-Wilk Statistic	0.976	0.973	0.872	0.984	0.952	0.952	0.917
	Shapiro-Wilk p-value	0.49	0.411	0.002	0.968	0.174	0.031	0.009
Distribution Divergence Analysis (Actual vs Theoretical Gaussian)	Maximum Divergence (x)	392.0	399.7	396.2	390.3	393.6	398.3	382.4
	Total Divergence Area	0.1251	0.1112	0.3552	0.1431	0.2001	0.1581	0.1591
	KDE Peak	386.0	394.2	388.5	393.1	398.9	394.9	377.5
	Interpretation	Moderate	Moderate	Significant	Moderate	Moderate	Moderate	Moderate
Robustness Analysis	IQR	9.5	7.0	7.0	5.0	10.0	8.0	6.0
	Lower Limit	366.5	380.5	376.5	382.5	375.0	382.0	365.0
	Upper Limit	404.5	408.5	404.5	402.5	415.0	414.0	389.0
	Outliers Detected	None	[376, 409]	[406, 409]	None	None	[380]	[358]
	Number of Scans	44	43	29	21	31	54	37

Table 4.3. Analysis of the measurement quality and repeatability of the fluorescence signal at 523 nm at concentration of 106.92 ng mL^{-1} collected in different trials.

Basic Statistics	Parameter	Day 8	Day 9	Day 10	Day 11	Day 12	Day 13	Day 14
	Mean	417.46	394.88	366.27	381.85	377.33	385.88	393.51
	Median	416.5	394.0	368.0	381.5	377.0	386.0	395.0
	Standard Deviation	5.29	6.06	8.95	4.19	5.09	6.93	8.88
	Coefficient of Variation (%)	1.27	1.53	2.44	1.1	1.35	1.8	2.26
	Range	21	25	41	16	19	32	36
	95% Confidence Interval	(415.33, 419.60)	(393.16, 396.60)	(363.29, 369.25)	(380.64, 383.07)	(375.91, 378.75)	(383.75, 388.02)	(391.11, 395.91)
Distribution Analysis	Skewness	0.4567	0.4041	-1.498	0.2485	0.2908	0.465	-0.0606
	Kurtosis	0.139	-0.258	2.372	-0.749	-0.615	0.462	-0.804
	Shapiro-Wilk Statistic	0.954	0.961	0.859	0.96	0.938	0.972	0.976
	Shapiro-Wilk p-value	0.28	0.102	0.0	0.099	0.01	0.365	0.347
Distribution Divergence Analysis (Actual vs Theoretical Gaussian)	Maximum Divergence (x)	420.7	398.6	359.1	383.8	381.2	393.5	392.7
	Total Divergence Area	0.169	0.1819	0.331	0.1981	0.1965	0.1148	0.1804
	KDE Peak	415.9	393.3	369.3	380.1	376.9	386.6	398.3
	Interpretation	Moderate	Moderate	Significant	Moderate	Moderate	Moderate	Moderate
Robustness Analysis	IQR	6.5	7.75	8.0	5.25	4.5	8.5	13.0
	Lower Limit	404.5	379.38	352.0	370.88	368.0	368.25	367.5
	Upper Limit	430.5	410.38	384.0	391.88	386.0	402.25	419.5
	Outliers Detected	None	None	[345, 348, 338, 351]	None	[387, 387]	[404]	None
	Number of Scans	26	50	37	48	52	43	55

Table 4.3. Continued. Analysis of the measurement quality and repeatability of the fluorescence signal at 523 nm at concentration of 106.92 ng mL^{-1} collected in different trials.

The analysis of data collected over fourteen consecutive measurement days provides meaningful insights into the stability of the experimental system and the consistency of the results obtained over time. Descriptive statistics, **Table 4.3**, show mean values ranging between 366 and 417, indicating an overall modest variability. A one-way ANOVA test was implemented to assess the variability among the experimental days conducted under identical conditions. The purpose was to determine whether, from a purely statistical standpoint, the differences observed among the experimental data could be attributed solely to experimental error or whether other factors might also contribute. The result of the one-way ANOVA, with an F statistic of 14.959 and an extremely low p-value (1.295×10^{-16}), clearly indicates that the differences between daily means cannot be ascribed solely to experimental

noise or random variability. Statistically, the rejection of the null hypothesis suggests the presence of systematic effects, albeit of small magnitude, that influence the results in a repeatable manner.

This evidence is fully consistent with the findings from the descriptive analysis: the day-to-day variations are limited but sufficiently consistent to be detected by a sensitive test such as ANOVA. Considering that the experimental conditions were nominally identical, the origin of such differences is likely linked to secondary factors, including sample preparation procedures, minor variations in manual handling, or uncontrolled fluctuations in the operational conditions.

This conclusion does not represent a limitation but rather emphasizes the sensitivity and reliability of the measuring system. The instrument is indeed capable of discriminating very small differences resulting from marginal variations in experimental parameters, thereby demonstrating a coherent and sensitive response to calibration conditions. From an experimental perspective, this confirms that the unexplained component of variability does not originate from the instrument itself but rather from external factors of manual or procedural nature.

Within the context of measurement protocol validation, the ANOVA result can thus be interpreted as a positive indicator of the system's precision, which is sufficiently stable to detect even minor differences arising from sample handling. Consequently, the entire set of analyses confirms the robustness of the experimental setup while simultaneously highlighting the importance of maintaining strict control over operational procedures to ensure maximum data reproducibility.

The proximity between mean and median values suggests a generally symmetric distribution, free from systematic deviations. The standard deviation, ranging between 4 and 9 units, together with coefficients of variation between 1% and 2.5%, indicates high repeatability of the measurements, confirming that the system maintains stable behavior under the tested operating conditions. The ranges and 95% confidence intervals are similarly narrow, with amplitudes of only a few percentage points, supporting the conclusion of limited dispersion and high instrumental precision.

From a statistical distribution perspective, the skewness and kurtosis parameters show values generally close to those expected for a Gaussian distribution. Only a few days present more pronounced deviations, particularly days 7 and 10, which exhibit slight negative skewness and kurtosis values exceeding 2, indicating flatter or heavier-tailed distributions. The Shapiro–Wilk test confirms this overall tendency: most days show p-values greater than 0.05, consistent with normality, while a few isolated days display statistically significant deviations. These deviations, however, do not appear to be systematic and do not compromise the overall evaluation of system stability.

The comprehensive analysis of distribution patterns across the 14-day measurement campaign reveals significant insights into the behavior of the fluorescence measurement system and its deviations from theoretical normality. The Kernel Density Estimation (KDE) peaks, representing the most probable measurement values, demonstrate notable variations throughout the experimental period, ranging from 369.3 on Day 10 to 415.9 on Day 8. This substantial spread of 46.6 units between extreme KDE peaks indicates considerable day-to-day variability in the system's most frequent output values, suggesting potential instrumental drift or environmental influences affecting measurement consistency.

The divergence analysis between empirical KDE distributions and theoretical Gaussian models uncovers a consistent pattern of moderate deviations across most experimental days. Only two days (Day 3 and Day 10) exhibited significant deviations from normality, with total divergence areas of 0.3552 and 0.3310 respectively. Day 3 displayed particularly pronounced skewness (1.0639) with maximum divergence occurring at 396.2, indicating a right-tailed distribution where actual measurements consistently exceeded Gaussian expectations in the upper range. Conversely, Day 10 showed extreme negative skewness (-1.4980) with maximum divergence at 359.1, revealing a heavy left-tailed distribution where measurements fell substantially below normal distribution predictions.

The relationship between KDE peaks and traditional central tendency measures provides crucial information about distribution symmetry. On Days 1, 4, 11, 12, and 13, the KDE peaks closely aligned with both mean and median values, indicating approximately symmetric distributions despite moderate statistical deviations from perfect normality. However, Days 5 and 14 demonstrated notable disparities where KDE peaks (398.9 and 398.3 respectively) significantly exceeded their corresponding means (395.65 and 393.51), suggesting distributions skewed toward higher values with the most frequent measurements clustering above the arithmetic average.

The maximum divergence locations offer diagnostic insights into specific regions where empirical distributions deviate from theoretical expectations. Days 2, 3, 6, 8, and 9 all showed maximum divergences in the upper measurement ranges (399.7, 396.2, 398.3, 420.7, and 398.6 respectively), indicating consistent patterns where the system produced more high-value measurements than predicted by Gaussian models. This pattern suggests possible saturation effects, instrumental ceiling behaviors, or systematic overestimation in certain measurement conditions.

The Shapiro-Wilk test results present an interesting contrast to the KDE-based divergence analysis. While several days (1, 2, 4, 5, 8, 9, 11, 13, 14) showed non-significant p-values (>0.05) suggesting normality acceptance, the KDE analysis revealed moderate divergences (0.1112-0.2001)

in all these cases. This discrepancy highlights the superior sensitivity of KDE analysis in detecting distributional abnormalities that may escape detection by traditional normality tests, particularly for smaller sample sizes where statistical power is limited.

The temporal pattern of distribution characteristics shows no clear progression or deterioration over the 14-day period, indicating that the observed deviations represent inherent system properties rather than time-dependent degradation. The coexistence of acceptable Shapiro-Wilk p-values with consistent KDE-Gaussian divergences suggests that while the measurement system generally approximates normal behavior, it possesses distinct distributional fingerprints that merit consideration in data interpretation and uncertainty estimation.

In summary, the KDE-based analysis provides a more nuanced understanding of measurement distributions than traditional parametric approaches, revealing systematic patterns of deviation that inform both instrumental characterization and appropriate statistical treatment of the data. The consistent moderate divergences observed across most experimental days recommend the use of robust statistical methods and careful consideration of distribution-specific characteristics in subsequent data analysis and interpretation.

The robustness analysis performed through the assessment of the interquartile range and the identification of outliers, provides further confirmation. The IQR values remain generally low, between 4.5 and 13, consistent with the limited variability observed previously. The identified outliers are few and isolated, distributed without recurring temporal patterns, and primarily concentrated on days that already displayed slight asymmetries. Their presence does not significantly affect data distribution nor suggest instrumental drift or systematic errors.

Overall, the behavior of the statistical parameters across the fourteen days demonstrates a remarkable internal consistency. The stability of the means and the low intra- and inter-day variability indicate that the measuring system, under the applied operating conditions, exhibits excellent repeatability and robustness. The minor deviations from normality observed in a few cases can be attributed to random fluctuations or minimal variations in experimental conditions, but they do not compromise the overall reliability of the protocol. Taken together, the analysis confirms that both the experimental setup and the instrument used ensure stable and reproducible performance over time, fully satisfying the requirements for measurement validation. In **Appendix A** we report actual vs theoretical distribution of data referred to 106.92 ng mL^{-1} collected in different trials.

In **Figure 4.2** and in **Table 4.4** a comprehensive analysis was conducted by aggregating the entire data set, including all scans from the 14 experimental tests. This inclusive approach also incorporated

measurements from sessions that had previously shown deviations from the Gaussian distribution, thus allowing for an overall assessment of the stability of the measurement system and the reproducibility of the results over the entire duration of the study.

Basic Statistics	Parameter	Value
	Mean	391.57
	Median	392.00
	Standard Deviation	9.25
	Coefficient of Variation	2.36%
	Range	61
	95% Confidence Interval	(390.82, 392.31)
Distribution Analysis	Skewness	-0.4585
	Kurtosis	0.442
	Maximum Divergence (x)	400.3
	Total Divergence Area	0.1148
Distribution Divergence Analysis (Actual vs Theoretical Gaussian)	KDE Peak	394.0
	Interpretation	Moderate deviations from normality
	Shapiro–Wilk Statistic	0.986
	Shapiro–Wilk p-value	0.000
Robustness Analysis	IQR	13.00
	Lower Limit	365.50
	Upper Limit	417.50
	Outliers Detected	[358, 360, 363, 353]
	Number of Scans	596

Table 4.4. Statistical analysis of fluorescence signal emitted at 523 nm at concentration of 106.92 ng mL^{-1} aggregating the entire data set.

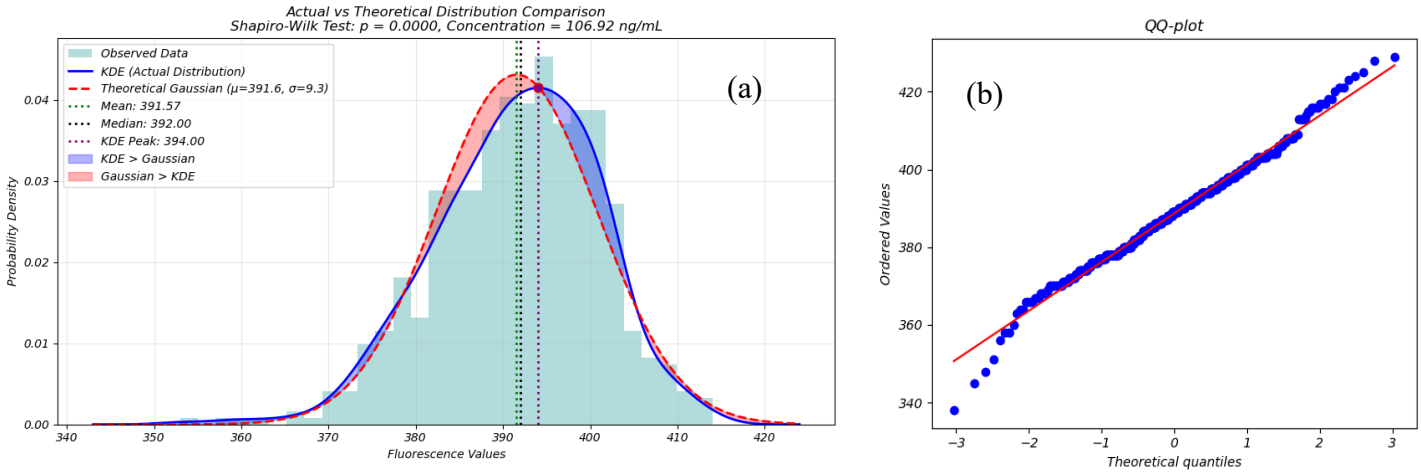

Figure 4.2. (a) Histogram of fluorescence signal emitted at 523 nm at concentration of 106.92 ng mL^{-1} aggregating the entire data set with KDE curve and theoretical gaussian distributions. (b) QQ-plot.

The measurement system demonstrates satisfactory analytical precision, as evidenced by the coefficient of variation of 2.36%. This value, though not excellent, falls within acceptable ranges for fluorescence techniques, indicating good reproducibility of the measurements. The extremely narrow 95% confidence interval (390.82 - 392.31), with a width of only 1.49 units, confirms the high reliability of the mean estimate despite the relatively high standard deviation of 9.25 units. The consistency between the mean (391.57) and the median (392.00) suggests a substantial stability of the distribution's center.

The distributional analysis reveals a complex profile characterized by moderate negative asymmetry (skewness = -0.4585) and slight leptokurtosis (kurtosis = 0.442). The Kernel Density Estimation identifies a peak at 394.0, positioned significantly higher than the arithmetic mean, indicating that the most frequent values are concentrated in the upper region of the distribution. The divergence from the Gaussian ideal, quantified as a total area of 0.1148, classifies the behavior as moderately non-normal, with maximum divergence localized at 400.3 units.

The system demonstrates good overall robustness, with an interquartile range of 13.0 units containing the central 50% of observations. However, the identification of four outliers concentrated at the lower extreme (358, 360, 363, 353) signals the presence of uncontrolled sources of variability that occasionally produce anomalous measurements. The wide range of 61 units between minimum and maximum values confirms the existence of significant dispersion, though confined to extreme cases.

The combination of a highly significant Shapiro-Wilk p-value (0.000) with moderate divergence from normality represents an apparent paradox, resolvable by considering the high sample size (596 scans). This large dataset provides the statistical test with sufficient power to detect minimal deviations, even if clinically or experimentally insignificant. The localization of the maximum divergence in the upper region (400.3) suggests a possible instrumental saturation effect or the presence of a sub-population of measurements with different dynamics.

The KDE peak at 394.0 emerges as the most representative estimate of the true value, being less influenced by distributional asymmetry than the arithmetic mean. The median of 392.00 constitutes a valid, conservative alternative. The evidence of systematic deviations from normality, though moderate, recommends the use of robust statistical methods for subsequent inferential analyses and the correct characterization of measurement uncertainty. The high sample size nonetheless guarantees the applicability of the central limit theorem for inferential purposes, while the presence of outliers

suggests the need to investigate the experimental conditions generating anomalous values at the lower extreme of the distribution.

This type of analysis was performed not only for the concentration of 106.92 ng mL^{-1} but also for other concentrations and wavelengths. However, providing a comprehensive report of all analyses is not feasible. In total, 101 wavelengths and 20 concentrations were considered, which would theoretically result in 101 × 20 = 2,020 combinations to be analyzed for each experimental run. Since 14 runs were conducted, the total number of required analyses would amount to 2,020 × 14 = 28,280. Additional analyses performed at different wavelengths and concentrations are presented in **Appendix A**.

The calibration curve was constructed according to the following procedure. As an illustrative example, let us consider the 523 nm wavelength. For this wavelength, the average fluorescence signal for each concentration (ranging from 11.88 to 237.6 ng mL^{-1}) was calculated by aggregating data from all 14 experimental trials. This identical protocol was systematically applied to each of the investigated wavelengths. In **Table 4.5** we report the summary of the statistical analysis of the fluorescence signals measured at the same wavelength for all the concentrations examined and in **Table 4.6** we report the values of the calibration curve considering the fluorescence emitted at 523 nm. Since the median is considered the most robust indicator for estimating the true fluorescence value in the aggregated set of repeated measurements, we used the median as the estimate of the true fluorescence value associated with each concentration. This calibration curve corresponds, in detail, to the one shown in **Figure 3.7**.

This procedure can be applied, as previously mentioned, to every other wavelength. Appendix A also illustrates several distributions of the fluorescence data, taken from **Table 4.4**, relating to different concentrations and wavelengths.

Basic Statistics	Parameter	11.88 ng/mL	23.76 ng/mL	35.64 ng/mL	47.52 ng/mL	59.40 ng/mL
	Mean	46.09	91.15	136.34	179.31	221.8
	Median	46.0	91.0	137.0	180.0	222.0
	Standard Deviation	7.78	7.61	7.74	7.92	8.47
	Coefficient of Variation (%)	16.89	8.34	5.68	4.41	3.82
	Range	42	50	44	47	46
	95% Confidence Interval	(45.47, 46.70)	(90.56, 91.75)	(135.68, 137.00)	(178.60, 180.01)	(221.09, 222.51)
Distribution Analysis	Skewness	0.2086	0.1934	-0.2655	-0.213	-0.1944
	Kurtosis	-0.373	-0.059	-0.238	-0.067	-0.364
	Maximum Divergence (x)	48.1	84.6	136.7	188.3	215.7
	Shapiro-Wilk Statistic	0.992	0.995	0.992	0.994	0.992
	Shapiro-Wilk p-value	0.001	0.051	0.005	0.074	0.007
Distribution Divergence Analysis (Actual vs Theoretical Gaussian)	Total Divergence Area	0.103	0.0731	0.113	0.0718	0.1015
	KDE Peak	43.9	91.0	140.0	179.9	221.9
	Interpretation	Moderate	Almost Normal	Moderate	Almost Normal	Moderate
Robustness Analysis	IQR	11.0	10.0	11.0	11.0	12.0
	Lower Limit	23.5	71.0	114.5	157.5	198.0
	Upper Limit	67.5	111.0	158.5	201.5	246.0
	Outliers Detected	None	[69, 119]	[114, 112]	[156, 202, 155]	None
Dataset Info	Number of Scans	623	639	530	483	549

Basic Statistics	Parameter	71.28 ng/mL	83.16 ng/mL	95.04 ng/mL	106.92 ng/mL	118.80 ng/mL
	Mean	263.73	307.8	346.83	391.57	437.45
	Median	264.0	308.0	348.0	392.0	438.0
	Standard Deviation	8.13	8.82	8.99	9.25	7.56
	Coefficient of Variation (%)	3.08	2.87	2.59	2.36	1.73
	Range	44	49	69	61	41
	95% Confidence Interval	(263.03, 264.42)	(307.04, 308.56)	(346.12, 347.54)	(390.82, 392.31)	(436.76, 438.14)
Distribution Analysis	Skewness	-0.2024	-0.3588	-0.3171	-0.4585	-0.2954
	Kurtosis	-0.205	-0.193	0.245	0.442	-0.02
	Shapiro-Wilk Statistic	0.992	0.987	0.985	0.986	0.99
	Shapiro-Wilk p-value	0.005	0.0	0.0	0.0	0.003
Distribution Divergence Analysis (Actual vs Theoretical Gaussian)	Maximum Divergence (x)	258.5	300.7	342.2	400.3	442.6
	Total Divergence Area	0.102	0.1305	0.1507	0.1148	0.1076
	KDE Peak	265.1	309.5	350.6	394.0	440.4
	Interpretation	Moderate	Moderate	Moderate	Moderate	Moderate
Robustness Analysis	IQR	11.0	12.0	12.0	13.0	9.0
	Lower Limit	241.5	284.0	323.0	365.5	419.5
	Upper Limit	285.5	332.0	371.0	417.5	455.5
	Outliers Detected	[286]	[283]	[321, 316, 385]	[358, 360, 363, 353]	[419, 415, 416, 417, 418, 456]
Dataset Info	Number of Scans	530	520	617	596	464

Table 4.5. Statistical analysis of fluorescence signal emitted at 523 nm of every concentration aggregating the entire data set.

Basic Statistics	Parameter	130.68 ng/mL	142.56 ng/mL	154.44 ng/mL	166.32 ng/mL	178.20 ng/mL
	Mean	478.58	525.28	566.58	610.68	655.25
	Median	480.0	526.0	567.0	611.0	655.5
	Standard Deviation	9.64	9.12	7.79	10.6	9.93
	Coefficient of Variation (%)	2.01	1.74	1.37	1.74	1.52
	Range	49	53	45	52	54
	95% Confidence Interval	(477.71, 479.44)	(524.58, 525.98)	(565.94, 567.23)	(609.78, 611.58)	(654.34, 656.16)
Distribution Analysis	Skewness	-0.4454	-0.1978	0.0159	-0.059	-0.0376
	Kurtosis	-0.105	-0.227	-0.284	-0.641	-0.475
	Shapiro-Wilk Statistic	0.978	0.994	0.996	0.99	0.995
	Shapiro-Wilk p-value	0.0	0.012	0.157	0.001	0.137
Distribution Divergence Analysis (Actual vs Theoretical Gaussian)	Maximum Divergence (x)	469.9	534.6	565.6	613.8	653.9
	Total Divergence Area	0.1905	0.0951	0.0752	0.127	0.0944
	KDE Peak	481.5	526.3	568.2	609.0	656.9
	Interpretation	Moderate	Almost Normal	Almost Normal	Moderate	Almost Normal
Robustness Analysis	IQR	12.0	13.0	11.0	16.0	14.0
	Lower Limit	455.0	499.5	544.5	579.0	627.0
	Upper Limit	503.0	551.5	588.5	643.0	683.0
	Outliers Detected	[454, 454, 454, 453, 454]	[497]	[590]	None	None
Dataset Info	Number of Scans	485	649	565	541	460

Basic Statistics	Parameter	190.08 ng/mL	201.96 ng/mL	213.84 ng/mL	225.72 ng/mL	237.60 ng/mL
	Mean	697.61	742.57	783.37	826.88	871.08
	Median	697.0	742.0	784.0	828.0	871.0
	Standard Deviation	10.26	10.54	10.85	12.59	11.28
	Coefficient of Variation (%)	1.47	1.42	1.38	1.52	1.3
	Range	51	68	55	94	69
	95% Confidence Interval	(696.70, 698.53)	(741.62, 743.52)	(782.37, 784.38)	(825.73, 828.02)	(870.39, 871.78)
Distribution Analysis	Skewness	0.3016	-0.2672	0.0788	-0.0499	-0.0063
	Kurtosis	-0.581	0.052	-0.481	0.119	-0.516
	Shapiro-Wilk Statistic	0.983	0.988	0.992	0.989	0.992
	Shapiro-Wilk p-value	0.0	0.001	0.017	0.001	0.0
Distribution Divergence Analysis (Actual vs Theoretical Gaussian)	Maximum Divergence (x)	702.5	744.1	780.4	825.0	871.4
	Total Divergence Area	0.1722	0.1422	0.1131	0.1427	0.1477
	KDE Peak	694.4	738.1	786.7	833.1	863.5
	Interpretation	Moderate	Moderate	Moderate	Moderate	Moderate
Robustness Analysis	IQR	15.0	16.0	16.0	18.0	18.0
	Lower Limit	667.5	711.0	751.0	791.0	835.0
	Upper Limit	727.5	775.0	815.0	863.0	907.0
	Outliers Detected	None	[700, 710]	None	[788, 882]	[832]
Dataset Info	Number of Scans	484	474	452	467	1009

Table 4.5. Continued. Statistical analysis of fluorescence signal emitted at 523 nm of every concentration aggregating the entire data set.

The comprehensive analysis of fluorescence data across the concentration range of 11.88 to 237.6 ng mL^{-1} reveals several significant aspects concerning measurement quality and the statistical characteristics of the analytical system. The statistical analysis of fluorescence measurements across the concentration range from 11.88 to 237.60 ng mL^{-1} reveals a system with excellent analytical characteristics suitable for reliable calibration curve construction. A marked improvement in measurement precision is observed with increasing concentration, as evidenced by the coefficient of variation decreasing progressively from 16.89% at the lowest concentration to 1.30% at the highest concentration. This thirteen-fold enhancement in precision demonstrates the system's superior performance at higher concentrations where fluorescence signals are more intense and less susceptible to background noise interference.

The central tendency measures exhibit remarkable stability throughout the concentration series, with near-perfect agreement between mean and median values across all levels. This consistency indicates substantially symmetric distributions despite formal statistical tests detecting moderate deviations from perfect normality. The arithmetic means demonstrate excellent linear progression from 46.09 to 871.08 across the dynamic range, covering approximately a 19-fold increase that provides a solid foundation for calibration curve fitting.

Distributional characteristics show predominantly moderate deviations from Gaussian normality, with only two concentrations (23.76 and 47.52 ng mL^{-1}) approaching near-normal distributions. The prevalence of negative skewness across most concentrations suggests a slight tendency toward values lower than the distribution center. Kernel Density Estimation peaks show excellent alignment with arithmetic means, particularly at intermediate concentrations, confirming that distributions maintain substantial symmetry around central values despite statistical deviations from perfect normality.

System robustness appears generally good, with interquartile ranges remaining relatively stable across concentrations. However, an increase in outlier frequency is noted at higher concentrations, particularly evident at 118.80 ng mL^{-1} with ten anomalous values, potentially indicating saturation phenomena or instrumental limitations. The concentrations 142.56, 154.44, and 178.20 ng mL^{-1} demonstrate near-normal distributional stability with divergence areas below 0.10, with 154.44 ng mL^{-1} combining excellent normality (Shapiro-Wilk p-value 0.157) with the best precision (1.37% CV) in the entire dataset.

Divergence patterns reveal interesting concentration-dependent behaviors, with maximum deviations occurring in lower regions at low concentrations and shifting to upper regions at high concentrations, suggesting different variability mechanisms across the concentration spectrum. The

highest concentration (237.60 ng mL^{-1}) benefits from the most extensive dataset (1009 scans) and demonstrates exceptional precision (1.30% CV) despite a single outlier, confirming system robustness even at the upper measurement limits.

All concentrations benefit from high replicate numbers (452 to 1009 scans), ensuring statistical solidity, while exceptionally narrow confidence intervals, particularly at higher concentrations with widths often below two units, indicate high estimation reliability. For calibration curve construction, 154.44 ng mL^{-1} emerges as the optimal point combining precision and distributional normality, while 237.60 ng mL^{-1} provides the most precise measurement and 154.44 ng mL^{-1} along with 178.20 ng mL^{-1} offer the most normal distributions. The system demonstrates excellent characteristics for reliable calibration curve development, showing linear response, improved precision at higher concentrations, and sufficient distributional normality for standard analytical applications

Therefore, the fluorescence measurement system demonstrates satisfactory analytical characteristics throughout the studied concentration range, with precision that significantly improves at higher concentrations. The deviations from statistical normality do not compromise the reliability of central estimates, supporting the use of these data for constructing robust calibration curves, although the application of appropriate statistical methods is recommended to handle the observed non-normal distributions.

The plots of the actual distributions and the theoretical Gaussian distributions, along with the QQ plots, are reported in **Appendix A**.

We will now examine how the calibration curves were constructed. The selection of the median as the estimator of the true value represents a methodological choice based on both statistical and practical considerations. In experimental contexts where data distributions exhibit deviations from Gaussian normality, the median offers superior robustness compared to the arithmetic mean, being substantially insensitive to the presence of outliers and distributional asymmetries. This characteristic proves particularly important in our case, where the analysis of empirical distributions has highlighted consistent deviations from normality while maintaining a fundamentally symmetric structure.

The decision not to use the peak of the Kernel Density Estimation as the primary estimator stems from considerations regarding the method's stability and reproducibility. Although the KDE peak provides an accurate estimate of the mode of the empirical distribution, its determination depends on smoothing parameters that introduce an element of subjectivity into the analysis. The median, in contrast, represents an intrinsically defined and reproducible measure that does not require

the specification of additional parameters, thereby ensuring greater comparability across different experiments and researchers.

The substantial equivalence observed between the median values and the KDE peaks across the different concentrations confirms the adequacy of the median as an estimator of the distribution's central value. This convergence between two methodologically distinct approaches further validates the choice of the median, demonstrating that it effectively captures the central tendency of the data without the potential instabilities associated with kernel density estimation. Furthermore, the median enjoys broader recognition within the scientific community for applications of this type, facilitating the interpretation and communication of results in interdisciplinary contexts.

The use of the median also preserves consistency with robust statistical methods that are particularly indicated when working with experimental data affected by multiple sources of variability. While KDE provides valuable information about the distributional shape and deviations from normality, the median remains the preferable tool for the point estimation of the true value by virtue of its stability, reproducibility, and solid theoretical foundation in robust statistical inference.

Concentration	Median [A.U.]
11.88 ng/mL	46.00
23.76 ng/mL	91.00
35.64 ng/mL	137.00
47.52 ng/mL	180.00
59.40 ng/mL	222.00
71.28 ng/mL	264.00
83.16 ng/mL	308.00
95.04 ng/mL	348.00
106.92 ng/mL	392.00
118.80 ng/mL	438.00
130.68 ng/mL	480.00
142.56 ng/mL	526.00
154.44 ng/mL	567.00
166.32 ng/mL	611.00
178.20 ng/mL	655.50
190.08 ng/mL	697.00
201.96 ng/mL	742.00
213.84 ng/mL	784.00
225.72 ng/mL	828.00
237.60 ng/mL	871.00

Table 4.6. Median data of fluorescence at 523 nm for every concentration.

Table 4.6 reports the median values of the fluorescence emitted at 523 nm for each concentration. This same analysis was performed for each wavelength. In this thesis, we only show how we constructed the calibration curve for one wavelength. However, as seen in the previous data, the considerations made for the concentrations and wavelengths shown here are also valid for other concentrations and wavelengths.

As can be observed, excellent reproducibility can be achieved at all concentrations and wavelengths. Having confirmed the instrument's high reproducibility, we proceed to describe the machine learning classification algorithm.

5. Description of the Machine Learning Algorithm

One of the most innovative aspects of this work is the implementation, within the custom software of the prototype, of a subroutine capable of identifying the FMN spectrum at any concentration and accurately quantifying its concentration, limited to the concentration range considered during training. Specifically, two distinct subroutines were developed: one dedicated to identification and one to regression.

The first subroutine represents a sequence of instructions designed to analyze the FMN spectrum, allowing it to be distinguished from spectra of other substances present in the sample. The main advantage of this procedure is that it does not require training data: it is not a conventional classification algorithm but rather a *lazy learning algorithm*. In other words, if the analyzed spectrum satisfies certain characteristic requirements unique to the FMN spectrum, it is possible to identify the presence of FMN with certainty. This subroutine constitutes one of the strengths of the prototype; however, in accordance with confidentiality agreements, the details of its operation cannot be publicly disclosed.

The second subroutine is based on a true machine learning algorithm and requires the definition of a training and test dataset to evaluate performance. In the actual device, a neural network was implemented, whose specifications remain confidential. For the purposes of this thesis, as a demonstrative example, the **XGBoost** (eXtreme Gradient Boosting) algorithm was employed. The official online documentation for this model is available at this link:

https://xgboost.readthedocs.io/en/latest/

XGBoost is an open-source machine learning library, developed by Tianqi Chen at the University of Washington, which utilizes gradient-boosted decision trees. It is a *supervised learning* algorithm

known for its high speed, efficiency, and ability to scale effectively on large datasets. The methodology underlying XGBoost involves combining multiple *weak learners*, represented by individual decision trees, into a *strong learner* by aggregating the residuals from previous models.

Decision trees are a fundamental tool for classification or regression tasks in machine learning. They adopt a hierarchical structure in which each internal node represents a decision function, each branch corresponds to a data-splitting rule, and each leaf represents a model outcome. However, because decision trees are prone to overfitting, *ensemble learning* techniques, such as boosting, are often employed to obtain more robust models.

Boosting combines multiple weak learners—models with slightly better performance than random guessing—into a strong learner. Each weak learner is sequentially trained to correct the errors of previous models, and after numerous iterations, the weak learners are combined into a final strong learner. Both random forests and boosting algorithms are ensemble learning techniques that use multiple trees to improve predictive performance; random forests are based on *bagging* (bootstrap aggregation), training each tree independently and combining predictions, whereas boosting adopts an additive approach, with sequential trees correcting the errors of predecessors.

Gradient boosting, implemented in XGBoost, begins with a weak learner that makes initial predictions (*base learner*). Subsequently, new trees are added additively, based on the errors of the base learner. The algorithm calculates residuals—the difference between predicted and actual values—and uses them to update the model through a loss function. In machine learning practice, loss functions measure model performance: gradient descent is used to minimize this function, thereby improving predictive accuracy. Common examples of loss functions include mean squared error or mean absolute error for regression tasks, cross-entropy loss for classification tasks, or custom loss functions developed for specific use cases.

Advanced features of XGBoost compared to standard gradient boosting implementations in scikit-learn include:

- Parallel and distributed computation: XGBoost stores data in blocks that can be distributed across multiple machines or stored in external memory (*out-of-core processing*). It is possible to train distributed models on clusters, significantly speeding up computation.
- Cache-aware prefetching: reduces execution time for large datasets, enabling processing up to ten times faster than other frameworks on a single machine.

- Built-in regularization: XGBoost includes L1/L2 penalties in the learning objective, improving model generalization compared to traditional scikit-learn gradient boosting.
- Missing value handling: the algorithm recognizes sparsity and automatically learns the optimal direction for dealing with missing data.

Operational Logic of XGBoost

The operational workflow for using XGBoost consists of several steps:

1. Data splitting and DMatrix conversion: After preliminary exploratory data analysis, the data are divided into training and test sets and converted into the *DMatrix* format, XGBoost's internal structure optimized for memory efficiency and training speed.
2. Model creation and evaluation: An XGBoost model instance is created, and the objective function is set via the *objective* hyperparameter (e.g., "multi:softmax" for multiclass classification, "binary:logistic" for binary classification). The model is trained on the training set and tested on the test set, evaluating performance using metrics such as accuracy, precision, recall, or F1-score. The confusion matrix can be used to visualize true positives, true negatives, false positives, and false negatives.
3. Hyperparameter tuning: This involves optimizing the algorithm's hyperparameters through grid search and cross-validation, iterating over different combinations to maximize predictive performance.

The primary hyperparameters used for gradient-boosted trees in XGBoost are:

- Learning rate (η): Determines the speed at which the model learns from each iteration. Lower values slow learning and reduce overfitting risk, whereas higher values accelerate learning but may increase overfitting. Default = 0.36.
- n_estimators: Number of trees to build in the ensemble. Influences model complexity and generalization ability.
- Gamma: Controls the minimum loss reduction required to make a further split on a leaf node. Higher values increase model complexity and overfitting risk; lower values favor simplicity. Default = 0.
- Max_depth: Maximum depth of each decision tree. Higher values increase model complexity and the risk of overfitting. Default = 6.

This configuration allows for a robust and efficient model capable of accurately recognizing the FMN spectrum based on the training data while maintaining excellent generalization for previously unseen data.

6. Training and implementation of the algorithm

Once the spectrum is correctly identified as FMN, the next step is to calculate the corresponding concentration based on the training dataset. To achieve this, it is first necessary to train the XGBoost model.

Initially, the data are prepared. As previously discussed in paragraph 3, and illustrated in **Figures 3.7** and **3.8**, calibration curves can theoretically be generated for each wavelength. Since the prototype produces a fluorescence array ranging from 500 to 600 nm with a 1 nm step, a vector of 101 wavelengths is obtained. Considering a range of 20 concentrations, it is therefore possible to generate a 101×20 matrix. An example of such a training matrix is shown in **Table 6.1**.

Wavelength [nm]	**11.88 ng/ml**	**23.76 ng/ml**	**35.64 ng/ml**	**47.52 ng/ml**	**59.4 ng/ml**	**71.28 ng/ml**	**…**	**201.96 ng/ml**	**213.84 ng/ml**	**225.72 ng/ml**	**237.6 ng/ml**
500	23.5	44.5	68.8	92.3	116.3	137.9	…	388.4	412.9	435.5	462.0
501	25.4	53.9	80.2	103.8	128.4	153.0	…	422.6	445.7	470.7	498.1
502	29.8	52.9	79.7	107.7	134.4	158.2	…	443.1	467.8	494.5	522.3
503	27.7	57.2	85.7	112.6	140.8	167.0	…	466.8	492.7	520.2	550.6
…	…	…	…	…	…	…	…	…	…	…	…
597	15.9	33.3	50.0	66.0	80.7	96.2	…	269.6	284.6	301.2	319.2
598	16.1	28.4	44.6	61.1	76.5	90.3	…	258.4	273.2	289.4	306.6
599	15.8	29.3	45.5	59.0	74.4	89.1	…	248.7	265.8	281.1	298.5
600	15.2	32.3	48.3	62.0	75.0	90.0	…	248.2	262.3	277.4	294.4

Table 6.1. Training data matrix.

This matrix, together with the corresponding concentration vector, is directly passed to the XGBoost function. In Python, the training procedure is implemented as follows:

```
xgboost = xgb.XGBRegressor(n_estimators=100, random_state=42)

xgboost.fit(X, y)
```

Here, X represents the matrix shown in **Table 6.1** without the concentration label, while y is the vector of corresponding concentrations. The hyperparameters were kept at their default values, as the model performance was already satisfactory without additional tuning.

To evaluate the reliability of the training, new fluorescence data at known concentrations—never encountered by the model during training—were provided as a test set. Fluorescence signals recorded in the range from 11.88 ng mL^{-1} to 237.6 ng mL^{-1} were used as the test set with the following Python command:

```
predictions_xgboost = xgboost.predict(X_test)
```

where X_test represents the fluorescence vector for which the corresponding concentration is to be estimated. Since the actual concentration is known to the experimenters but unknown to the model, a close match between the predicted and actual concentration indicates that the model is correctly trained and reliable.

Figure 6.1 schematically illustrates the program logic, showing the workflow from spectrum acquisition to concentration estimation using XGBoost.

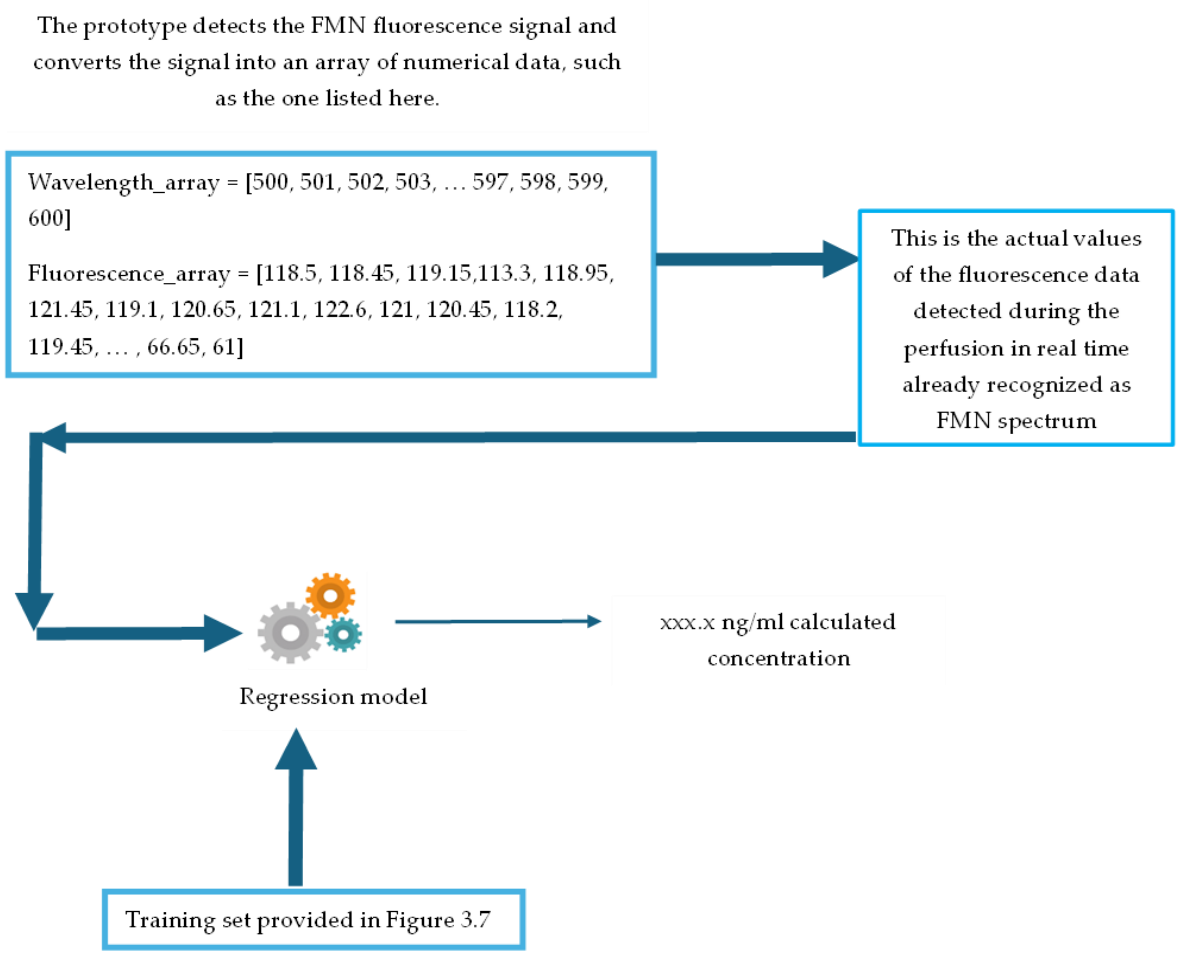

Figure 6.1. Working principle of the regression program.

The ultimate goal of this work is to develop a system capable of autonomously calculating and verifying FMN concentration with high precision. Once the concentration is determined, it is essential to have a tool that allows the algorithm to assess whether the calculated value accurately represents the true concentration. For this purpose, calibration curves are employed. As previously discussed, it is possible to generate 101 calibration curves, one for each wavelength. The general formula for calculating the calibration curve is:

$$Fluorescence\ (A.U.)(at\ wavelength\ \lambda) = concentration\left(\frac{ng}{mL}\right) \cdot slope(at\ wavelength\ \lambda) + intercept(at\ wavelength\ \lambda \quad (6.1)$$

By performing a linear regression of the equation above for each wavelength, the slope and intercept values are obtained for each curve. Knowing these parameters and having computed the concentration using the XGBoost model, it is possible to generate the expected fluorescence values at each wavelength, thus obtaining a synthetic FMN spectrum.

This synthetic spectrum can then be compared with the experimentally measured spectrum. The greater the similarity between the two spectra, the higher the likelihood that the calculated concentration is correct. To quantify the degree of similarity between the two spectra, five complementary statistical metrics were employed:

1. Coefficient of determination (R^2) – measures the proportion of variance explained between the predicted and actual spectrum.
2. Root Mean Square Error (RMSE) – provides an estimate of the mean absolute deviation, penalizing larger errors more heavily.
3. Pearson's correlation coefficient (r) – assesses the linear relationship between the two curves, indicating how closely the data follow a common trend.
4. Kolmogorov-Smirnov (KS) test – compares the cumulative distributions to identify statistically significant differences between the curves.
5. Mean Absolute Percent Error (MAPE) – quantifies the relative error with respect to the true spectral intensity, making the analysis comparable across different scales.

Additionally, the Spectral Angle Mapper (SAM) was used, a statistical metric that compares the shape similarity between two spectra interpreted as vectors in a multidimensional space (where each

dimension corresponds to a wavelength). Unlike metrics such as MSE or R^2, which evaluate absolute differences or linear correlations, SAM measures the angle between the vectors, providing an indication of the overall spectral shape similarity. Based on these metrics, it is possible to determine whether the concentration calculated by the trained XGBoost model is reliable. In **Figure 6.2**, both the actual FMN spectra at different concentrations and the synthetic FMN spectra generated from the

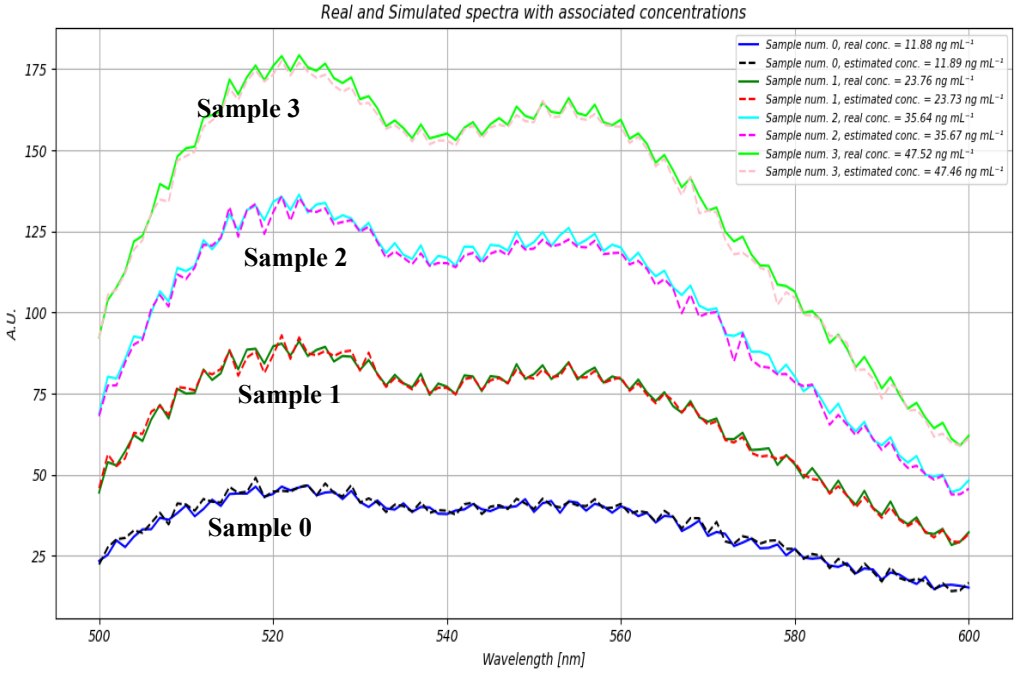

Figure 6.2. Machine learning model training performance.

Metric	11.88 ng·mL^{-1}	23.76 ng·mL^{-1}	35.64 ng·mL^{-1}	47.52 ng·mL^{-1}	Interpretation
R^2	0.97	0.99	0.99	0.99	Model explains >97% variance
RMSE	1.42	1.27	2.15	2.07	Low absolute error (<2.2 ng·mL^{-1})
Pearson	0.98	0.99	0.99	0.99	Near-perfect correlation ($p \approx 0$)
KS p-value	0.70	0.97	0.82	0.91	No significant difference between distributions ($p > 0.05$)
MAPE	3.81%	1.59%	1.80%	1.39%	Relative error <4% (acceptable for clinical applications)
SAM	2.08°	1.02°	0.84°	0.56°	Nearly identical spectral shape (<5°)
Δ Conc	0.0063	0.0291	0.0340	0.0646	Excellent accuracy, within the acceptable margin of error for clinical applications

Table 6.2. Statistical analysis of machine learning model performance.

calibration curves are shown. In **Table 6.2**, the results of the statistical analysis comparing the spectra are reported.

The XGBoost model was tested using fluorescence records corresponding to the same concentrations as those in the training set, but obtained from experimental campaigns that were not included in the model training. The differences between the actual and predicted concentrations were found to be negligible, all below 0.07 ng mL^{-1}, confirming the high precision of the model. The R^2 values consistently exceeded 0.97, indicating that the variability of the real spectra is almost entirely explained by the predicted spectra. RMSE values, ranging from 1.27 to 2.15, reflect minimal absolute errors in the spectral signal. The Pearson correlation coefficient exceeded 0.98 in all cases, with extremely low ppp-values, highlighting a highly significant correspondence between the real and simulated spectra. The Kolmogorov–Smirnov test yielded high ppp-values (above 0.7) and D statistics below 0.1, supporting the conclusion that any differences between the distributions are random rather than systematic. The MAPE remained below 4% in all cases, indicating a very low mean percentage error, consistent with high-quality experimental measurements. Finally, the spectral similarity analysis based on SAM further confirmed the excellent agreement between the real and predicted spectra.

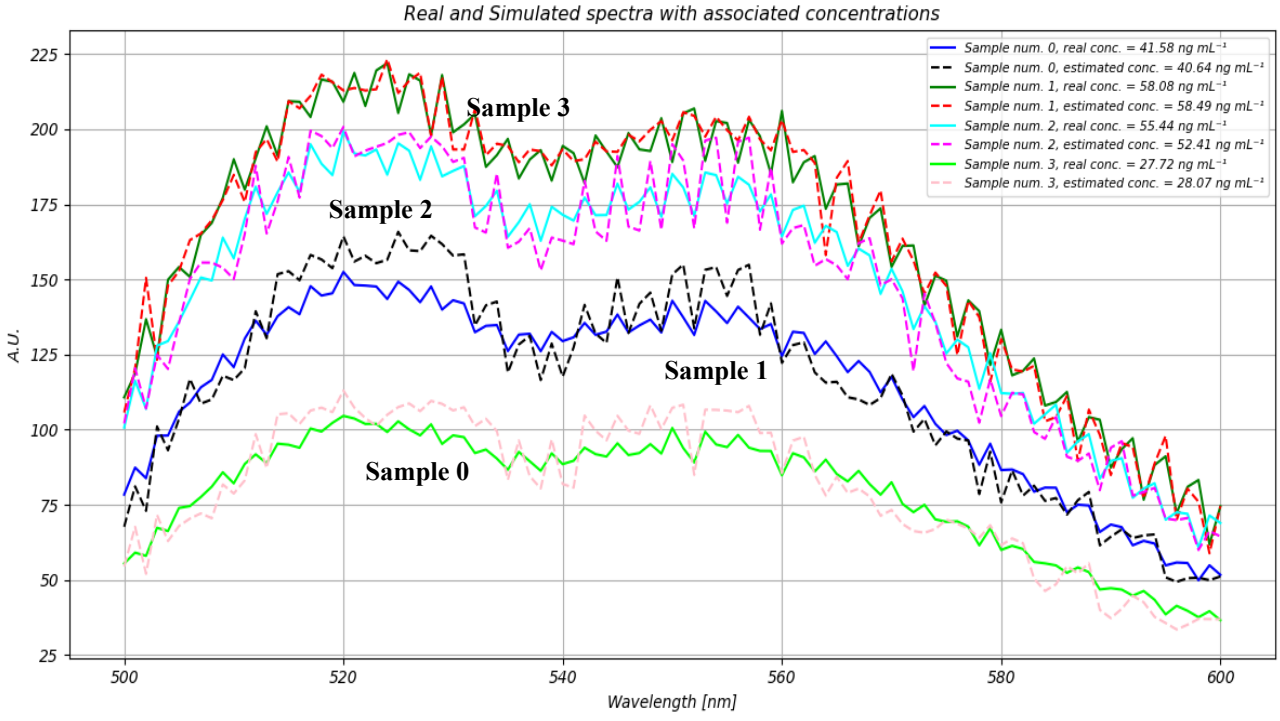

Figure 6.3. Performance testing with concentrations different from those used in training.

In conclusion, when test data similar to the training set are provided, the model yields fully satisfactory results. However, this represents only a validation and is not sufficient to fully assess robustness. Additional solutions were prepared with concentrations intermediate or distant from those in the training set to further evaluate the model's robustness. The corresponding results are presented in **Figure 6.3** and **Table 6.3**.

Metric	41.58 ng·mL^{-1}	58.08 ng·mL^{-1}	55.44 ng·mL^{-1}	27.72 ng·mL^{-1}	Interpretation
R^2	0.91	0.98	0.96	0.87	Satisfactory explanation of variance R^2>0.87.
RMSE	8.49	4.62	6.81	6.80	Higher RMSE but still acceptable.
Pearson	0.97	0.99	0.98	0.97	Good correlation (r > 0.97 in all cases (p≈0)).
KS p-value	0.0065	0.708	0.055	0.00238	Significant differences at 27.72/41.58 ng mL^{-1} (p < 0.05).
MAPE	5.86%	2.30%	3.88%	7.46%	Relative error <8% (acceptable for clinical applications).
SAM	3.86°	1.53°	2.53°	4.41°	Acceptable spectral shape (SAM <5°)
Δ Conc	0.94	0.41	3.03	0.35	Within the acceptable margin of error for clinical applications

Table 6.3. Metric performance between actual and simulated spectra based on calculated concentration.

Figure 6.3 shows that the algorithm provides reliable estimates of concentration even for values not used during training, as demonstrated by the strong similarity between the predicted and measured spectra.

In the first series, the predicted concentrations were remarkably accurate, with absolute errors consistently below 0.07 ng·mL^{-1} and MAPE values below 4%. Spectral agreement was excellent, as confirmed by R^2 values consistently above 0.97, RMSE values between 1.27 and 2.15, and Pearson correlation coefficients exceeding 0.98 with highly significant p-values. The KS tests indicated no significant differences ($p > 0.7$), and the spectral angle measurements confirmed nearly identical spectral shapes.

The second validation series, while still showing good overall agreement, presented slightly higher errors in some cases. For two of the four tested concentrations (41.58 and 27.72 ng·mL^{-1}), the absolute concentration errors reached 0.94 and 0.35 ng·mL^{-1}, respectively, with RMSE values above 6.8 and lower R^2 values (0.9136 and 0.8767), indicating a less accurate fit. KS tests for these two cases also indicated statistically significant differences between the predicted and actual spectra ($p < 0.01$), and the MAPE increased to 5.86% and 7.46%. Nevertheless, for the other two cases (58.08 and 55.44 ng·mL^{-1}), performance metrics remained very good, with R^2>0.96, low RMSE, and spectral angle errors below 3°.

The slightly lower performance observed in the second dataset can be attributed to the fact that the XGBoost regression model was trained on fluorescence signal intervals corresponding to concentrations of 11.88 ng mL^{-1}. In contrast, the intermediate concentrations used in the second series fell within the ranges 23.76–35.64 ng·mL^{-1} and 47.52–59.4 ng·mL^{-1}. As expected, the further a test sample is from the training points, the greater the uncertainty in the regression. Therefore, reducing the calibration step size, for example from 11.88 to 5.95 ng·mL^{-1}, would likely improve prediction accuracy.

Although performance in this second group appears slightly lower, from a clinical perspective the absolute FMN value is less critical than the overall trend. Practically, clinicians are primarily interested in the initial slope (i.e., the first derivative) of the FMN concentration curve over time and, in some cases, in the final concentration after a defined perfusion period. Consequently, even a margin of error of up to ±10 ng·mL^{-1} is considered acceptable. It is important to note that the observed errors remain well below this threshold.

Overall, both validation series confirm the robustness of the system, demonstrating high predictive accuracy and good spectral agreement. The first dataset exhibited near-perfect agreement, while the second revealed some sensitivity to specific concentrations, but still within acceptable limits for experimental use.

In the following chapter, the application of the instrument under hypothermic perfusion conditions of animal and human organs will be investigated.

7. Choice of the calibration line criterion: single-wavelength fluorescence or spectral integral?

In the literature, some studies [8, 9] report calibration lines defined on the basis of the area under the entire spectrum at a given concentration. This approach represents a legitimate alternative to the method described in this chapter. However, the author argues that it may present significant limitations, particularly in the presence of potential interferents in the perfusion medium.

Figure 7.1a shows the spectrum of FMN with its corresponding area at a defined concentration, whereas **Figure 7.1b** illustrates the spectrum of a mixture containing FMN and an unknown interferent.

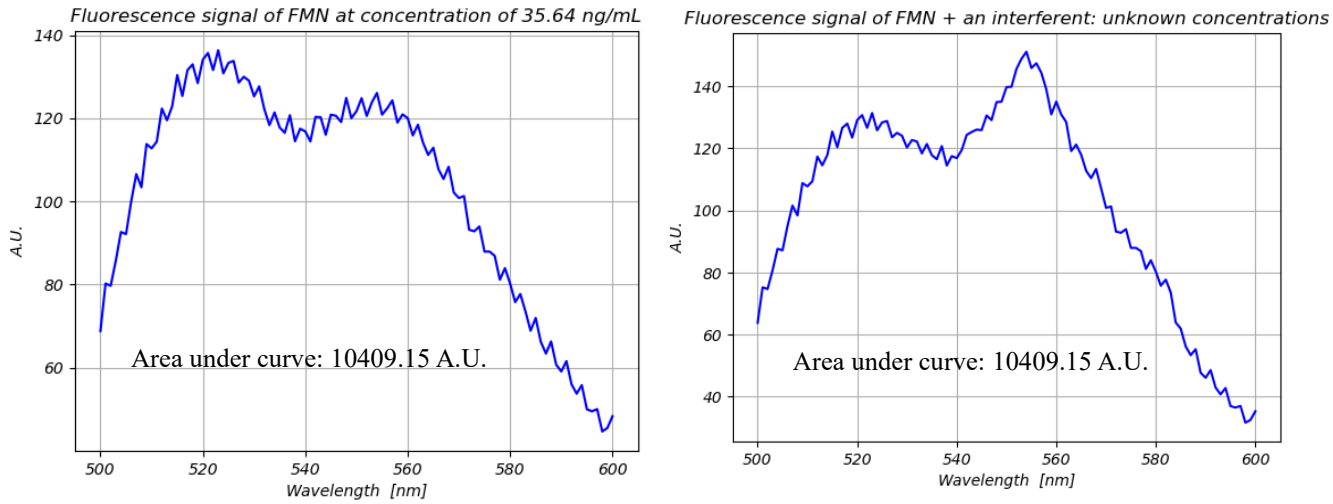

Figure 7. Comparison of two FMN spectra with and without interferent. (a) pure FMN spectrum. (b) FMN + interferent.

In both cases, the total area under the curve is the same (10409.15 A.U.). Assuming a calibration line of the form:

$$Area_{under\ curve} = concentration \cdot slope + intercept \qquad (7.1)$$

The instrument would yield the same estimated concentration in both cases. However, in the spectrum of **Figure 7.1b**, the total area results from the sum of the FMN and the interferent contributions. Consequently, the actual FMN concentration is inevitably overestimated.

This example highlights that the area-based calibration approach is reliable only under the strict assumption of an interference-free medium. In real experimental conditions, where this assumption is rarely guaranteed, it is preferable to adopt more robust methods, such as the machine learning approaches described in this chapter, which allow spectral contributions to be discriminated and the concentration to be estimated with greater accuracy.

8. Chapter summary

For clarity, **Figure 8.1** summarizes the logical workflow followed throughout this study.

The work was organized into the following main phases:

1. Instrument calibration.

   Samples were prepared with concentrations ranging from 11.88 to 237.6 ng/mL. For each concentration, the fluorescence spectrum was acquired and used to construct the calibration curve. The entire procedure was repeated 14 times, resulting in 14 independent calibration curves.

2. Reproducibility assessment.

   The instrument's ability to provide consistent measurements under identical experimental conditions was evaluated. The results demonstrated excellent reproducibility within the same experimental campaign. However, when comparing data collected on different days, a higher variability was observed, mainly due to the difficulty of reproducing exactly the same concentrations — that is, the operator-related error.

3. Recognition algorithm implementation.

   Once the calibration curve was obtained, a recognition algorithm was developed to analyze the spectrum and provide a binary output:

   - 0: the spectrum does not correspond to FMN
   - 1: the spectrum corresponds to FMN.

This algorithm is based on a logical sequence of conditional checks rather than a full machine learning classification model.

When the conditions characteristic of FMN spectra are met, the concentration estimation is performed using a regression algorithm such as XGBoost (although other regression methods could also be applied).

4. Model verification.

   Using the calibration curves, the theoretical fluorescence signal is recalculated and compared with the experimental spectrum. The overlap between the two spectra confirms the reliability of the estimated concentration.

   This method can also be used to identify possible interferences in the FMN spectrum, as illustrated in **Figure 7**. However, if a reliable recognition algorithm is already in place, this additional analysis may not be necessary.

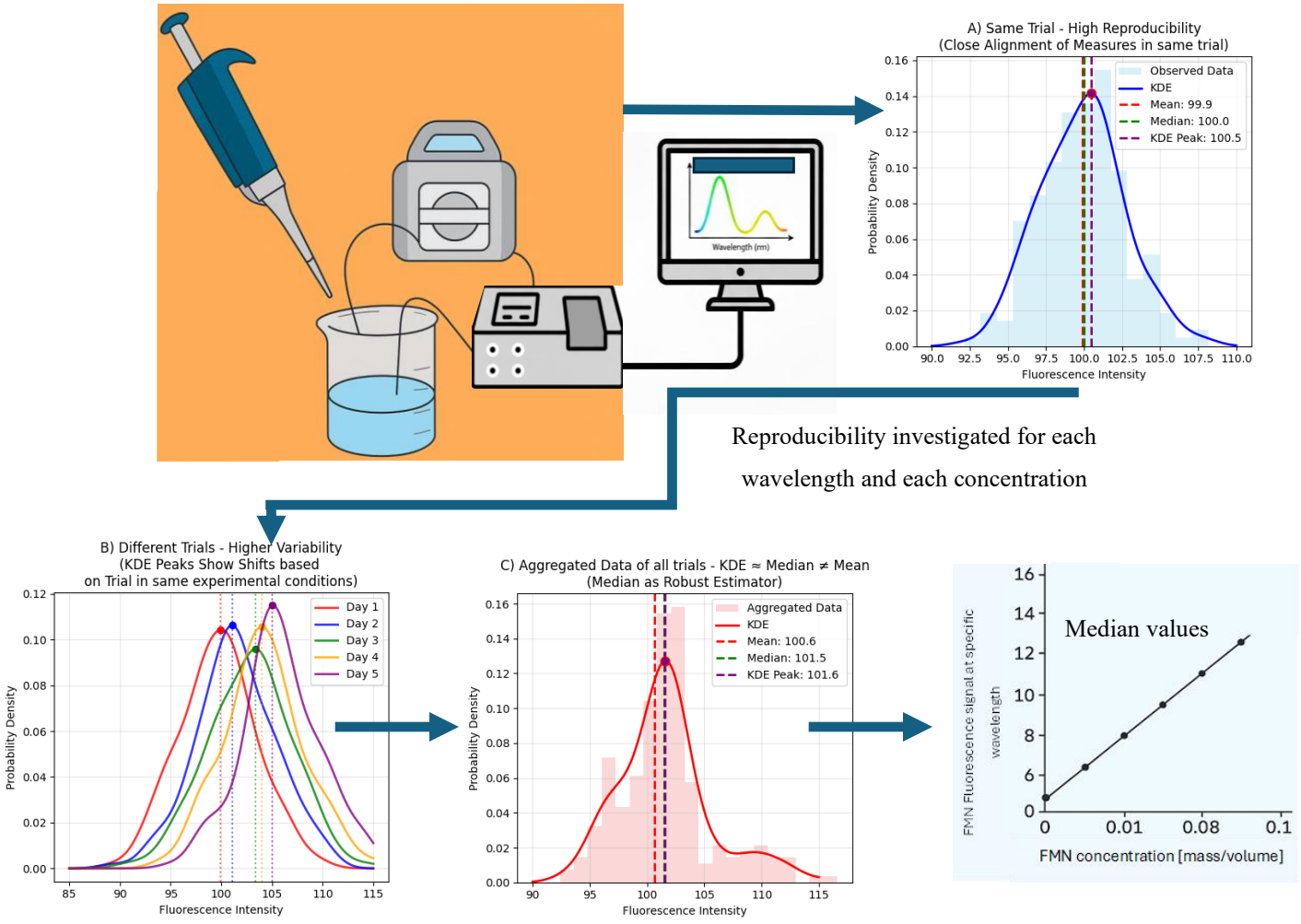

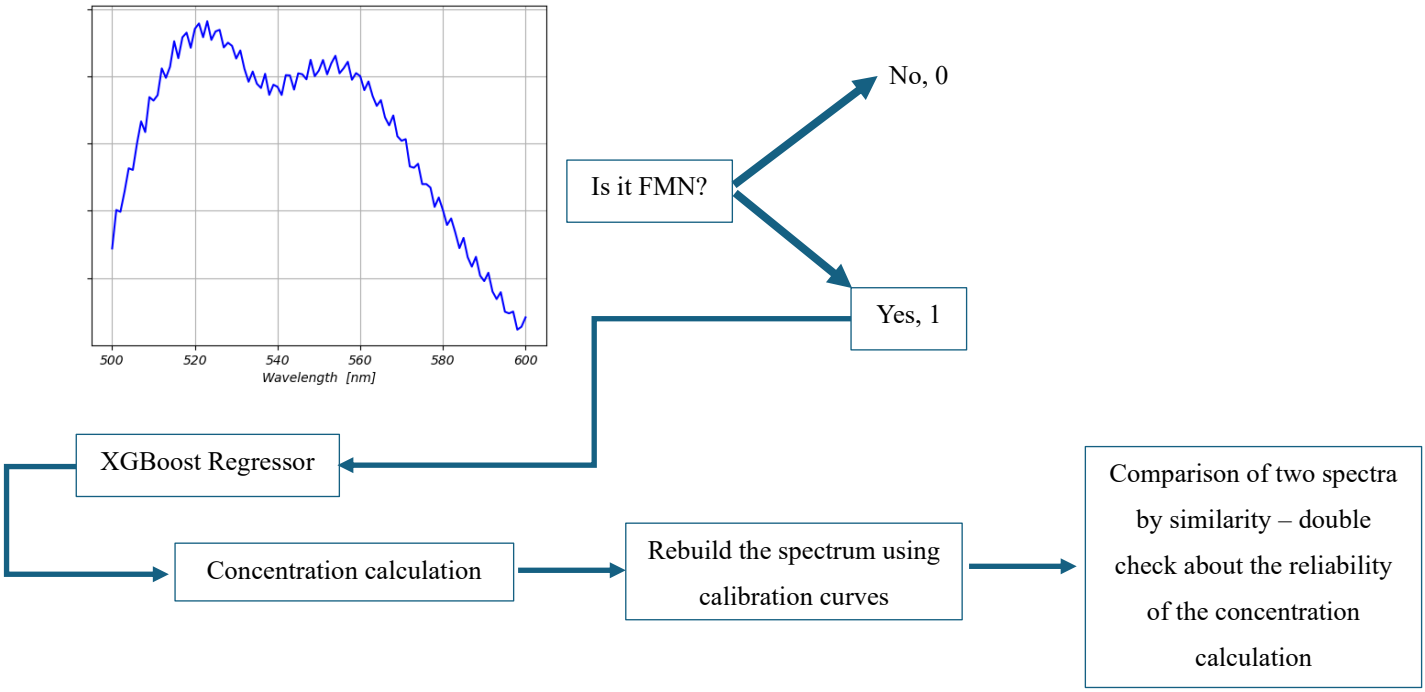

Figure 8.1 Logical workflow of characterization of the prototype.

References

[1] Sun, K., Jiaoa, C., Panconesi, R., Satish, S., Karakaya, O. F., De Goeijc, F. H. C.,·Diwan, T., Ali, K., Cadinu, L. A., Cazzaniga, B., Liu, Q.,·Miyazaki, Y., Pita, A., Khalil, M., Kim, J. K., Hussein, A., Müller, P. C.,·Aucejo, F.,·Kwon, D. H. C., Fernandes, E., Esfeh, J. M., Cywinski, J., Fujiki, M., Sun, L.,·Pinna, A., Dutkowski, P., Wehrle, C. J., Fairchild, R. L., Meierhofer, D., De Jonge, J., Miller, C., Hashimoto, K.,·Schlegel, A. Quantifying Flavin mononucleotide: an internationally validated methodological approach for enhanced decision making in organ transplantation. eBiomedicine, 116, 105761, 2025. https://doi.org/10.1016/j.ebiom.2025.105761.

[2] Wang L, Thompson E, Bates L, Pither TL, Hosgood SA, Nicholson ML, Watson CJE, Wilson C, Fisher AJ, Ali S, et al. Flavin mononucleotide as a biomarker of organ quality—A pilot study. Transplant Direct. 2020;6:e600.

[3] Sousa Da Silva RX, Darius T, Mancina L, Eden J, Wernlé K, Ghoneima AS, Barlow AD, Clavien PA, Dutkowski P, Kron P. Real-time assessment of kidney allografts during HOPE using flavin mononucleotide (FMN) - a preclinical study. Front Transplant. 2023 Feb 28;2:1132673. doi: 10.3389/frtra.2023.1132673.

[4] Van de Leemkolk FE, Lo Faro ML, Shaheed S, Mulvey JF, Huurman VAL, Alwayn IPJ, Putter H, Jochmans I, Lindeman JHN, Ploeg RJ, et al. The role of flavin mononucleotide (FMN) as a potentially clinically relevant biomarker to predict the quality of kidney grafts during hypothermic (oxygenated) machine perfusion. PLoS ONE. 2023;18:e0287713.

[5] Horné F, Drefs M, Schirren MJ, Koch DT, Cepele G, Jacobi SJ, et al. Hypothermic oxygenated machine perfusion (HOPE) prior to liver transplantation mitigates post-reperfusion syndrome and perioperative electrolyte shifts. J Clin Med. 2022;11(24):7381.

[6] Eden J, Thorne AM, Bodewes SB, Patrono D, Roggio D, Breuer E, Lonati C, Dondossola D, Panayotova G, Boteon APCS, Walsh D, Carvalho MF, Schurink IJ, Ansari F, Kollmann D, Germinario G, Rivas Garrido EA, Benitez J, Rebolledo R, Cescon M, Ravaioli M, Berlakovich GA, De Jonge J, Uluk D, Lurje I, Lurje G, Boteon YL, Guarrera JV, Romagnoli R, Galkin A, Meierhofer D, Porte RJ, Clavien PA, Schlegel A, de Meijer VE, Dutkowski P. Assessment of liver graft quality during hypothermic oxygenated perfusion: The first international validation study. J Hepatol. 2025 Mar;82(3):523-534. doi: 10.1016/j.jhep.2024.08.030.

[7] Cadinu, L.A.; Sun, K.; Jiao, C.; Panconesi, R.; Satish, S.; Yildirim, F.S.; Karakaya, O.F.; Wehrle, C.J.; Crasta, G.S.; Fernandes, F.W.; et al. Optical Spectroscopic Detection of Mitochondrial Biomarkers (FMN and NADH) for Hypothermic Oxygenated Machine Perfusion: A Comparative Study in Different Perfusion Media. Sensors 2025, 25, 4031, https://doi.org/10.3390/s25134031.

[8] Huwyler F, Eden J, Binz J, Cunningham L, Sousa Da Silva RX, Clavien PA, Dutkowski P, Tibbitt MW, Hefti M. A spectrofluorometric method for real-time graft assessment and patient monitoring. Adv Sci. 2023;10:2301537.

[9] Muller X, Schlegel A, Kron P, Eshmuminov D, Wurdinger M, Meierhofer D, Clavien PA, Dutkowski P. Novel real-time prediction of liver graft function during hypothermic oxygenated machine perfusion before liver transplantation. *Ann Surg.* 2019; 270(5): 783-790.

"Aut inveniam viam aut faciam"
Attributed to Hannibal (247 – between 183 and 181 BC)

Chapter V

Preclinical and Clinical Validation of the Prototype for FMN Monitoring

1. Introduction

In the previous chapter, we described in detail the functioning of the device and assessed its performance, demonstrating its ability to autonomously analyze spectra and calculate concentration based on the detected signal. In this chapter, we present the results obtained from the use of the device during organ perfusion, focusing in particular on the analysis of FMN concentration trends. Further examination of the device's reliability will not be necessary, as this has already been addressed in the preceding chapter.

Although two examples of *online* real-time FMN monitoring have been reported in the literature [1, 2], this work introduces for the first time the use of a device capable of measuring FMN concentration in real time through an integrated program that autonomously recognizes its concentration.

The chapter is structured as follows: in the first section, we present the results related to kidney perfusion. We will provide a general commentary on the FMN signals obtained from human organs (liver, heart, lung, intestine, and pancreas), both through the method introduced by Sun et al. [3] and by means of the prototype. As part of the PhD program, a research period was carried out at the Cleveland Clinic, where studies were conducted on human organs provided by the institution. This research involved both the use of the prototype for real-time FMN detection and the analysis of samples collected using the method introduced by Sun et al. [3]. Unfortunately, formal authorization for the disclosure of the collected or analyzed data has not been granted; therefore, results will only be discussed qualitatively, without reporting specific details. In addition, we contributed as co-authors to the development of a novel predictive model that integrates traditional risk factors with viability

markers [4]. This work has been published in the form of an abstract in a peer-reviewed journal, while the extended manuscript is currently in preparation. Consequently, no information on its validation will be disclosed, and the discussion will be limited to the modeling aspects.

2. Porcine kidney perfusion

As a first preclinical test, the device was evaluated during the perfusion of porcine kidneys. This experiment was designed to assess the device's ability to detect FMN under conditions of hypothermic organ perfusion. The choice of porcine kidneys was motivated by practical considerations: they can be readily obtained at low cost from slaughterhouses, as they are not regarded as commercially valuable cuts of meat, and their removal from the carcass does not present significant technical challenges. Furthermore, several studies [6 – 8] are available in the literature to compare our results.

2.1. Organs procurement

The animals were slaughtered in compliance with current Italian and European regulations on animal welfare, ethics, and food safety. The kidneys were obtained from pigs raised for meat consumption and commercial distribution, and were therefore considered suitable from a hygienic and sanitary perspective. The organs were retrieved approximately 30 minutes after death and preserved in a storage solution at 4 °C, kept on ice. The total ischemia time, including transport and cannulation, was approximately 2–3 hours. In total, three porcine kidneys were tested.

2.2. Preparation of the kidneys

Cannulation was performed at the level of the renal artery using an appropriately sized catheter. Prior to the start of perfusion, a physiological saline solution was injected through the catheter with a syringe in order to flush out any residual blood. **Figure 2.2.1** shows a representative image of a cannulated kidney.

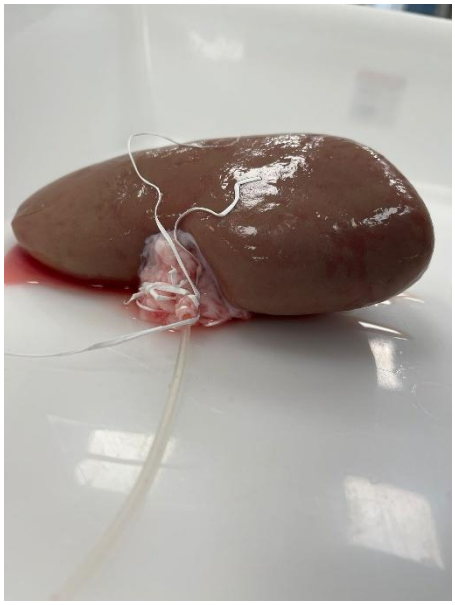

Figure 2.2.1. Cannulation of a kidney through the renal artery.

One liter of 0.9% NaCl saline solution was injected with the dual purpose of removing potential ischemic by-products from the tissues and, most importantly, flushing out residual traces of blood which, if present at high concentrations, may cause scattering and interfere with signal quality.

2.3. Setup of the Hypothermic Machine Perfusion

Perfusion setup (**Figure 2.3.1**) was performed using a complete apparatus consisting of a peristaltic pump, employed to circulate one liter of Belzer perfusion solution (Bridge-to-Life®), an oxygenator, a cannula circuit derived from a perfusion system, a blood filter, two bubble-trap chambers, two temperature and oxygen sensors positioned before and after the oxygenator, an insulated tank, and several ice packs to maintain the perfusion solution at the desired temperature.

Figure 2.3.1. Perfusion setup for the kidneys: (a) perfusion machine (Bridge-to-Life®), (b) oxygenator, (c) bubble-trap chambers, (d) oxygen and temperature sensors, (e) tank containing the perfusate, (f) kidney.

The perfusion flow rate was set at 60 mL/min to avoid excessive pressure on the arterial cannulation. Temperature and oxygenation were monitored using a Delta Ohm HD2109 (accuracy ±0.1 °C). Overall, hypothermic perfusion at 4–5 °C lasted 3.3 hours for the first two kidneys and 5.5 hours for the third kidney.

2.4. FMN levels detected in HOPE

As mentioned in previous Chapter, the prototype can generate a CSV file containing fluorescence data recorded during the perfusion. We decided to set the save time every 5 seconds. The software generated a CSV file containing an array of 101 elements representing fluorescence intensity between 500 nm – 600 nm, with a step of 1 nm. At the end of the perfusion, the file was analyzed to extract the vector of concentrations calculated throughout the process. During the perfusion, no interfering signals by other chemical species were observed, confirming that the excitation wavelength of 450 nm is optimal: none of the substances present in the system showed significant absorption at this

wavelength. Moreover, FMN did not induce secondary fluorescence in other molecules potentially dissolved in the perfusion fluid. However, it is important to specify that during hypothermic perfusion, intended as a method for organ preservation while awaiting transplantation, it is generally not necessary to add substances to the perfusion solution; therefore, no interferents are present. If, for clinical reasons, an interferent were to be introduced into the perfusate, its presence could potentially interfere with the fluorescence signal depending on its absorption/emission spectrum and the excitation wavelength. However, in the context of this study, this situation does not occur.

Figure 2.4.1 shows the FMN concentration trend estimated by the algorithm during the perfusion.

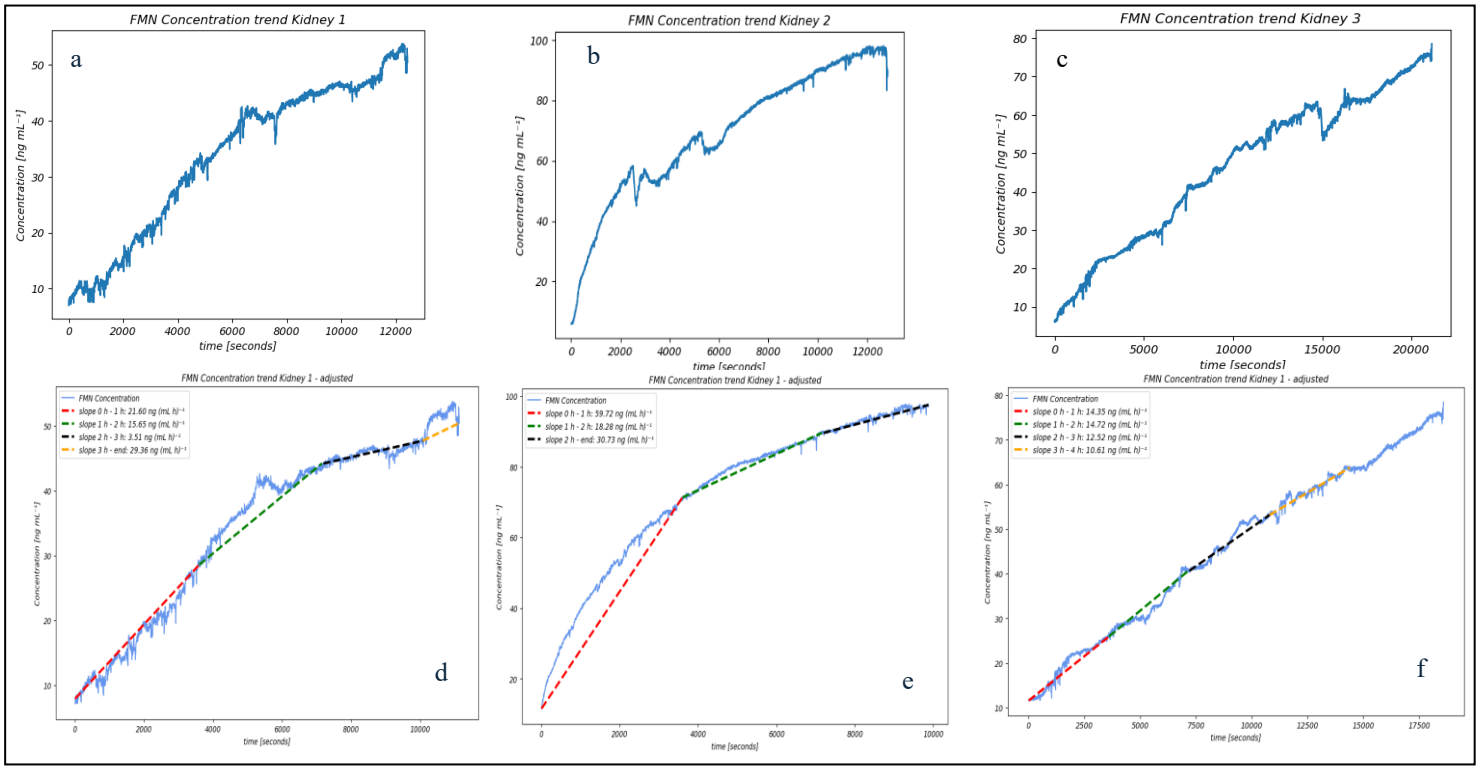

Figure 2.4.1. FMN concentration trend released by the kidneys. (a–c) Time-course concentration profiles for kidney 1, kidney 2, and kidney 3, respectively, with noise from external interferences removed. The approximate average release rate is shown, calculated between the beginning and end of perfusion. (d–f) Same trends for kidney 1, kidney 2, and kidney 3, highlighting the initial release phase. Kidney 3 is the only one that has been perfused for more than 3 hours. However, we calculated the growth rate up to 4 hours because from the clinical point of view, 4 hours of hypothermic perfusion is sufficient to have evaluate the quality of the organ.

In all three cases analyzed, a nonlinear increase in concentration with an initial delay was observed. This behavior is plausible, as the release of FMN from mitochondria damaged by ischemia-reperfusion injury is likely a capacitive process involving complex physiological mechanisms. Additionally, the three trends differ from one another, which is expected since each organ originated from a donor with a unique clinical history. Nevertheless, the concentration ranges reached are similar across the three cases.

The delay in signal onset is primarily determined by the time required for the perfusion fluid to fully oxygenate and permeate the organ tissues. Given that this is a hypothermic perfusion, time is needed for the fluid to dilate blood vessels constricted by the cold. On average, the first signal appeared after approximately 30–40 minutes. This delay may itself serve as an additional indicator of ischemic damage.

A particularly relevant aspect is the presence of transient drops in concentration. These fluctuations are attributed to the spatiotemporal distribution of FMN within the perfusion fluid. It should be noted that the organ was immersed in the same perfusion fluid used for circulation. External manipulations—such as massaging the organ to promote perfusion—caused volume variations that in turn led to changes in the measured concentration. These interferences introduce noise into the system and should be minimized as much as possible.

In **Figure. 2.4.1d**, **2.4.1d** and **2.4.1f** the effects of external interferences were removed to better analyze the release dynamics. In Figure **2.4.1d** and **2.4.1e**, an initial rapid increase in concentration followed by a gradual reduction in growth rate tending toward a plateau can be observed. Although perfusion was not prolonged enough to clearly reach this plateau, we anticipate that it would eventually occur. Conversely, **Figure 2.4.1c** shows an almost linear trend.

Table 2.4.1 presents the average slope, and final concentration value. These parameters—particularly the average slope (average growth rate) and the final concentration—could potentially serve as useful predictors of post-transplant outcomes in future clinical applications. The average slope is a quantity representing the average rate of concentration increase over a given time interval and indicates how much the concentration increases (or decreases) on average per unit of time. It's calculated according to the following formula:

$$slope = \frac{c(t_1) - c(t_0)}{t_1 - t_0} \tag{2.4.1}$$

It is particularly useful for comparing the initial release dynamics across different samples or organs, estimating the release speed of a substance under controlled conditions, and potentially

serving as a predictive parameter in clinical models—such as in transplantation—if found to correlate with specific clinical outcomes.

It is important to note that this is a rough estimate, valid only when the concentration trend is sufficiently linear between the two points considered. In our case, for example, **Figure 2.4.1f** shows an almost linear trend, which justifies the use of this approximation. However, in cases where the trend is highly nonlinear, the average derivative may not adequately reflect the actual release dynamics. In such situations, it is preferable to compute the instantaneous derivative, i.e., the derivative of the interpolating function or model at a specific time point. For this reason, in the following paragraph, we introduce a simplified model aimed at more accurately describing the observed trend.

	Average Growth Rate	Initial value of concentration	Final value of concentration	Δ Conc.
Kidney 1	17.53 ng (mL h)$^{-1}$	6.99 ng mL^{-1}	50.48 ng mL^{-1}	43.49 ng mL^{-1}
Kidney 2	36.24 ng (mL h)$^{-1}$	6.04 ng mL^{-1}	89.31 ng mL^{-1}	83.27 ng mL^{-1}
Kidney 3	13.05 ng (mL h)$^{-1}$	6.27 ng mL^{-1}	78.52 ng mL^{-1}	72.25 ng mL^{-1}

Table 2.4.1. Parameter values characterizing the trend with possible clinical application.

As previously discussed, each kidney originates from a different donor, and thus carries its own biological and clinical history. Although all samples share the same initial baseline concentration, the final concentration values vary considerably. Additionally, both the trajectory and the rate at which these final values are reached differ across samples. The average slope—representing the mean release rate—and the final concentration may serve as clinically relevant parameters, potentially providing predictive value for post-transplant outcomes.

Although other techniques have been developed to detect FMN from tissues and cells [5], detection of the two coenzymes from liquid perfusate samples by fluorescence or absorption remains the simplest and most widely used technique in clinical practice [3], [6 – 8]. The concentrations we detected are consistent with those reported by other authors [6] (15–90 ng mL^{-1}), although they are lower than those found in other studies, which report values around 100-500 ng mL^{-1} [7, 8].

Prior to our work, the only reported real-time measurement approach was carried out by the group in Zurich [1]. However, their method was limited to monitoring the FMN fluorescence signal without

providing a real-time estimation of its concentration. Moreover, they did not address the optimization of the excitation wavelength and relied solely on constructing a calibration curve based on the area under the fluorescence spectrum. This method poses a significant risk in the presence of interfering substances that also absorb light at 450 nm and emit in the yellow spectral region. In such cases, it becomes challenging to distinguish FMN from the interfering compound, introducing substantial uncertainty into the measurement.

Our setup not only enables real-time quantification of FMN but also introduces an engineering-based perspective to the problem. This includes modeling the release mechanisms using advanced mathematical tools. **Table 2.4.2** presents a comparison between our approach and previous studies reported in the literature.

	Type of study	Calibration curve	Real-time measurement	LOD and LOQ	Real time calculation	Capability to distinguish interference
[1]	Clinical	Reported	Yes	Yes	No	Not discussed
[2]	Clinical	Not reported	Yes	No	No	Not discussed
[3]	Clinical	Reported	No	No	No	Not discussed
[6]	Clinical	Reported	No	Yes	No	Not discussed
[7]	Clinical	Reported	No	Yes	No	Not discussed
[8]	Clinical	Not reported	No	No	No	Not discussed
[9]	Pre-clinical	Reported	No	Yes	No	Discussed
[10]	Clinical	Not reported	No	No	No	Not discussed
[11]	Clinical	Not reported	No	No	No	Not discussed
[12]	Clinical	Not reported	No	No	No	Not discussed
Our Study	Pre-clinical	Reported	Yes	Yes, but not disclosable	Yes	Yes

Table 2.4.2. Comparison between key points of different studies in FMN real time detection

An important advantage of real-time calculation of FMN concentration is the ability to predict the outcome of the operation even before transplantation [2]. In fact, knowing parameters such as ischemia time, admission to intensive care, the presence of cholangitis or thrombosis, and the age and weight of the donor and recipient, it is possible to predict the outcome of the transplant [4]. Not only can the concentration itself be predictive, but the rate at which FMN increases or decreases can also be considered an important parameter for predicting the outcome of the transplant.

3. Release of FMN in Human Organs

During the PhD program, we conducted a research period at the Cleveland Clinic in Cleveland, Ohio (USA). In this context, we tested the prototype on perfusion fluids used for the preservation of human organs not suitable for transplantation and analyzed data related to FMN and NADH obtained from perfusate samples. Furthermore, we had access to and analyzed samples collected from transplanted organs, particularly livers.

However, we did not obtain the authorization required for the dissemination of experimental data. For this reason, the clinical and preclinical data on which we worked are not reported in this thesis. Nevertheless, some general considerations can be provided. The organs studied included liver, small intestine (jejunum and ileum), pancreas, lungs, and heart subjected to hypothermic perfusion, while livers were also investigated under normothermic perfusion conditions.

Consistent with our previous findings on kidneys, the FMN signal observed in human organs displayed a noisy profile, influenced by external factors such as fluid mixing, tissue sampling, residual blood, and other experimental variables. Importantly, each organ exhibited a specific and unique FMN release pattern. It is therefore extremely challenging, if not impossible, to propose a universal mathematical model that could a priori describe FMN dynamics in all organs.

Each organ originated from a donor with a unique clinical and personal history, including metabolism, stress exposure, environmental conditions, and genetic background. Our analyses revealed no clear correlation between FMN dynamics and macroscopic variables such as age, sex, body weight, presence or absence of comorbidities, cause of death, or ischemia time. Since FMN is localized in the mitochondria, its release appears to result from complex processes potentially linked to non-quantifiable factors such as lifestyle, stress, and mitochondrial activity, rather than to simple measurable parameters.

In fact, every organ analyzed displayed a distinctive FMN profile, which could not be grouped or clustered according to conventional clinical parameters. Based on these observations, one may cautiously hypothesize—subject strictly to clinical validation—that FMN release is more strongly related to mitochondrial metabolism and activity, as well as to the specific mechanisms through which ischemia-reperfusion injury affects the mitochondria.

This hypothesis, presented here solely for exploratory purposes, must not under any circumstances be interpreted as a medical conclusion. The comprehensive explanation of FMN release mechanisms lies beyond the scope of this thesis and remains the responsibility of medical experts in the field.

4. Modelling FMN Release

4.1. Theoretical Framework

To outline a theoretical framework for a possible model of FMN release into the perfusion fluid, we will provide a simplified description of the release process.

Flavin mononucleotide (FMN) is a cofactor located in Complex I of the mitochondrial respiratory chain and plays a key role in cellular respiration. When an organ is explanted and preserved while awaiting transplantation, it undergoes a period of ischemia, a condition characterized by oxygen deprivation and the consequent production of free radicals. This leads progressively to cellular dysfunction and, in severe cases, to cell death.

During subsequent machine perfusion, the so-called ischemia-reperfusion injury (IRI) occurs. Abundant reoxygenation promotes the formation of reactive oxygen species (ROS), which damage cellular structures, including mitochondria and Complex I. In this context, FMN dissociates from Complex I, crosses the mitochondrial and cellular membranes, dissolves in the intracellular compartment, and finally enters the perfusion fluid, where it can be detected through fluorescence. Over the course of perfusion, which may last up to 24 hours, FMN concentration reflects the dynamics of cellular injury: it increases in the early phases and then stabilizes as cells progressively recover their function. The ultimate fate of the released FMN remains uncertain: some studies suggest partial reuptake, while others exclude it.

The process can be schematized in the following main phases:

1. **Ischemia**: oxygen deprivation and free radical formation.
2. **Reperfusion**: ROS production through the reaction of oxygen with free radicals.
3. **Cellular damage**: degradation of cellular structures and Complex I.
4. **FMN dissociation**: release of the cofactor from Complex I.
5. **Transfer into the perfusion medium**: FMN diffusion and convection across damaged membranes.
6. **Detection**: FMN dissolved in the medium is measurable through fluorescence.
7. **Stabilization**: as cells recover, FMN release ceases.

From a conceptual standpoint, FMN release can be interpreted as the interaction of two fundamental dynamics:

- a **dissociation reaction**, in which the cofactor separates from Complex I;
- a **transport process**, involving diffusion and forced convection across membranes and fluids.

The following treatment does not aim to provide an exhaustive description of the biological complexity of FMN release but instead proposes a simplified theoretical framework designed to:

- break down the process into elementary mechanisms,
- provide an initial conceptual approximation,
- offer interpretative tools useful to open new research perspectives.

To address this problem, two distinct approaches can be employed. The first is a deterministic approach, based on the use of material balance equations, formulated at either a macroscopic or microscopic level, with the aim of quantitatively describing the mechanisms of the phenomenon. The second is a "black box" approach, in which the intrinsic nature of the process is not investigated, focusing instead on establishing direct correlations between inputs and outputs.

To this end, we adopt a model borrowed from chemical engineering: the batch reactor with first-order kinetics. Despite its limitations, this approach enables the analysis of a complex biological phenomenon through well-established interpretative tools from other disciplines.

4.2 Macroscopic modeling

Let us consider a useful simplification to describe the system. We define the entire circulating volume of perfusion fluid—including that which flows through the organ as well as that contained in the cannulas and the reservoir—as our control volume. In this formulation, the system does not exchange matter with the external environment: there are no fluid inflows or outflows, no tissue sampling, and we neglect any potential perfusate withdrawals. This assumption is consistent with clinical practice.

Within this framework, the only exchange of matter occurs with the organ. The organ can therefore be regarded as a black box, that is, as a process unit which, over time, either releases or consumes a given substance—in this case FMN. We further assume that the perfusion fluid is perfectly mixed. Although this condition is not strictly satisfied in practice, as demonstrated by

experimental evidence, it is adopted here as a simplifying assumption. Under these assumptions, the system can be assimilated to the behavior of a batch reactor.

Let's consider a generic schematic of machine perfusion depicted in **Figure 4.2.1**.

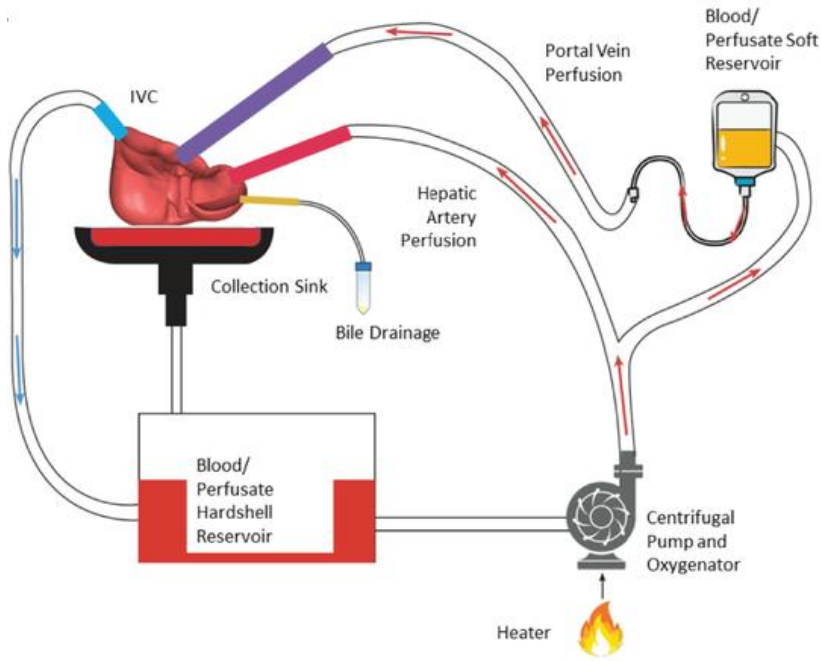

Figure 4.2.1. General schematic of machine perfusion, from [13]. This figure is reprinted with the Creative Commons Attribution License (CC BY)

Definition of Batch reactor

A **batch reactor**, **Figure 4.2.2**, can be defined as a closed system in which a chemical reaction takes place under controlled conditions. The key characteristic of this type of reactor is that, once the process begins, no mass enters or leaves the system: the reactants and products remain confined within the reactor volume throughout the entire duration of the reaction.

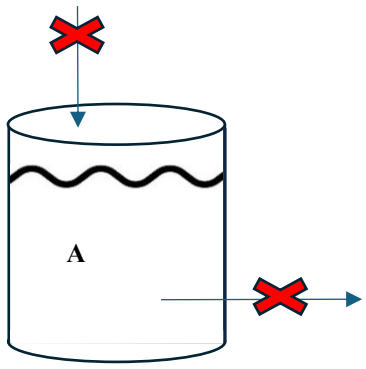

Figure 4.2.2. General schematic of batch reactor.

A simple example is a system containing a single reactant, denoted as $\boldsymbol{A}$. Under suitable conditions (e.g., appropriate temperature or catalytic environment), $\boldsymbol{A}$ undergoes a transformation into a product, $\boldsymbol{B}$, according to the stoichiometric scheme:

$$\boldsymbol{A \rightarrow B}$$

This representation, known as the stoichiometric equation, provides a formal description of the transformation by defining the relationship between reactants and products. In this specific case, one mole of $\boldsymbol{A}$ yields one mole of $\boldsymbol{B}$.

The evolution of the reaction is governed by the rate law, which relates the speed of the transformation to the concentration of the reactant(s). In the simplest case, the reaction follows a first-order rate law, where the reaction rate is directly proportional to the concentration of $\boldsymbol{A}$:

$$r = kc_A \tag{1}$$

Here, r represents the rate of the reaction, $\boldsymbol{c_A}$ is the concentration of reactant $\boldsymbol{A}$, and $\boldsymbol{k}$ is the kinetic constant. By convention, the rate of disappearance of $\boldsymbol{A}$ and the rate of appearance of $\boldsymbol{B}$ are expressed as:

The reaction rate of species $\boldsymbol{A}$ is related to the reaction-rate law r through the stoichiometric coefficient of species $\boldsymbol{A}$:

$$r_A = \nu_A r \tag{2}$$

Similarly, the reaction rate of species $\boldsymbol{B}$ is linked to the overall reaction rate r through the stoichiometric coefficient of species $\boldsymbol{B}$:

$$r_B = \nu_B r \tag{3}$$

Here, $\boldsymbol{\nu_A}$ and $\boldsymbol{\nu_B}$ are the stoichiometric coefficients defined by the stoichiometric law. In this specific case, they are ν_A=−1 and ν_B=+1, as we are describing a scenario where each mole of $\boldsymbol{A}$ generates one mole of $\boldsymbol{B}$. So,

$$r_A = -kc_A \tag{4}$$

$$r_B = kc_A \tag{5}$$

At this point in the discussion, it is necessary to consider the concept of a **mass balance**, **Figure 4.2.3**. This principle is grounded in the law of conservation of matter: mass cannot be created or destroyed, only transformed or redistributed. A mass balance thus provides a rigorous framework to account for the fate of a substance within a defined system.

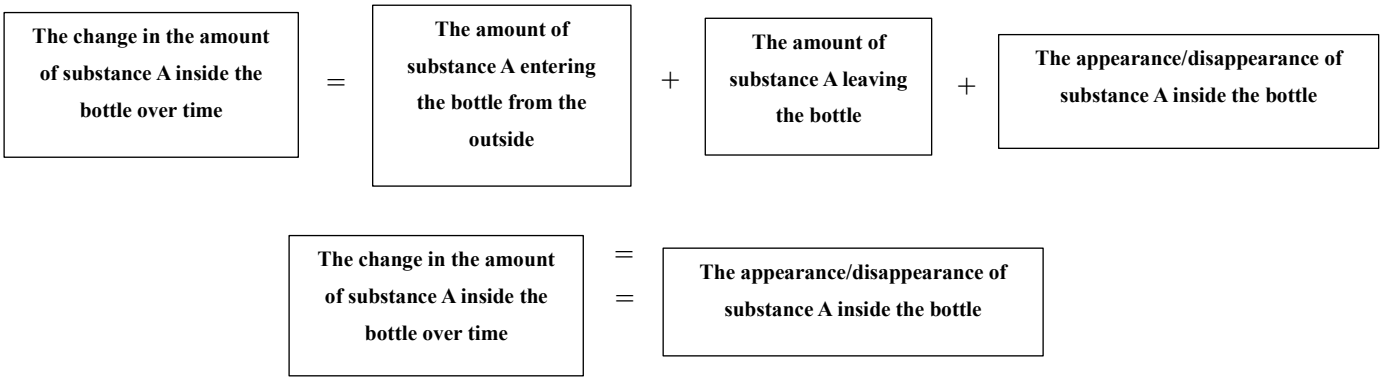

Figure 4.2.3. General concept of the material balance.

In the illustrative case of a closed water bottle, no material enters or leaves the system. Consequently, the only factor influencing the temporal variation of substance A is the chemical reaction occurring inside the bottle. Put differently, the system is isolated with respect to mass exchange, and the observed changes in $\boldsymbol{A}$ arise exclusively from its chemical transformation. Under these assumptions, the general mass balance equation can be simplified accordingly:

$$\frac{dn_A}{dt} = R_A \tag{6}$$

where $\boldsymbol{n_A}$ represents the amount of substance A (expressed in moles) and R_A denotes the rate of production or consumption due to the reaction.

This equation highlights that the variation in the amount of $\boldsymbol{A}$ is solely attributable to its consumption (or generation) via the chemical reaction, while all other contributions (inflows and outflows) remain absent.

To quantify this variation, it is necessary introduce a fundamental mathematical tool: the derivative. The derivative expresses the instantaneous rate of change of a quantity with respect to time (or space). In this context, it captures the velocity at which $\boldsymbol{A}$ is consumed and B is produced as the reaction progresses. An intuitive analogy is the speedometer of a car, which indicates how fast the vehicle is moving at a given instant. Similarly, the derivative of $\boldsymbol{n_A}$ with respect to time provides the rate at which substance $\boldsymbol{A}$ is being transformed.

Thus, the mass balance—coupled with the concept of the derivative—offers a concise yet powerful description of the reaction dynamics within the system.

Since the number of moles of $\boldsymbol{A}$ is equal to $\boldsymbol{n_A = c_A V}$ and considering that the volume is constant over time during the perfusion, we have:

$$V\frac{dc_A}{dt} = R_A \rightarrow \frac{dc_A}{dt} = \frac{R_A}{V} = r_A \tag{7}$$

When the rate term r_A is already expressed per unit volume (as is common in chemical kinetics), the balance reduces to the compact form:

$$\frac{dc_A}{dt} = r_A \tag{8}$$

This equation tells that the rate of change of the concentration of A ($\frac{dc_A}{dt}$) is equal to the reaction rate for A (r_A).

Since it is known that r_A is directly proportional to the concentration of A, we can write:

$$\frac{dc_A}{dt} = -kc_A \qquad\qquad t = 0 \;\; c_A = c_A^0 \tag{9}$$

Here, $\boldsymbol{k}$ denotes the kinetic constant, while the negative sign indicates that the concentration of species $\boldsymbol{A}$ decreases over time as a consequence of the reaction. In other words, this equation formalizes the progressive consumption of $\boldsymbol{A}$ as it is transformed into $\boldsymbol{B}$. A useful analogy is that of an hourglass: the quantity of sand in the upper chamber (species $\boldsymbol{A}$) continuously diminishes as it flows downward, symbolizing its conversion into another form.

It is possible to say the same thing for substance B:

$$\frac{dc_B}{dt} = kc_A \tag{10}$$

Since the reaction $\boldsymbol{A \rightarrow B}$ involves a direct stoichiometric conversion, we can write the conservation of mass as:

$$c_A + c_B = c_A^0 \tag{11}$$

where $\boldsymbol{c_A^0}$ is the initial concentration of $\boldsymbol{A}$ in the reactor.

From this relationship, we can express c_A as a function of c_B:

$$c_A = c_A^0 - c_B \tag{12}$$

Substituting this into the equation, we get

$$\frac{dc_B}{dt} = k(c_A^0 - c_B) \tag{13}$$

Thus, two mathematical expressions are obtained:

$$\frac{dc_A}{dt} = -kc_A \qquad t = 0 \;\; c_A = c_A^0 \tag{14}$$

$$\frac{dc_B}{dt} = k(c_A^0 - c_B) \qquad t = 0 \;\; c_B = 0 \tag{15}$$

They are two first-order ordinary differential equations that describe how quantities evolve over time. Such equations are fundamental tools in science and chemical engineering, as they provide a framework to model processes governed by rates of change—ranging from chemical reactions and heat transfer, to bacterial population growth, the motion of objects, and even the release of FMN from damaged mitochondria.

Fortunately, in this case an analytical solution is available, which greatly simplifies the interpretation of the system. The solutions are:

$$c_A(t) = c_A^0 e^{-kt} \tag{16}$$

$$c_B(t) = c_A^0(1 - e^{-kt}) \tag{17}$$

These expressions convey clear physical meaning. At time t=0, the system contains only species $\boldsymbol{A}$ $c_A(at\ t = 0) = c_A^0, c_B(at\ t = 0) = 0$. As the reaction begins, the consumption of $\boldsymbol{A}$ is initially rapid, due to its high concentration. With the progression of time, the concentration of $\boldsymbol{A}$ decreases, leading to a progressive reduction in the reaction rate. Eventually, at sufficiently long times ($t \to t_{end}$), species $\boldsymbol{A}$ is entirely consumed, and the concentration of $\boldsymbol{B}$ reaches the initial concentration of $\boldsymbol{A}$ $c_A(at\ t = t_{end}) = 0, c_B(at\ t = t_{end}) = c_A^0$.

A useful analogy is that of transferring water from one container to another: at the beginning, the flow is fast because the first container is full, but as it empties, the flow slows until all the water has been transferred.

This simple yet powerful model provides the conceptual basis of a batch reactor, which remains a valuable framework for investigating complex phenomena. In the present work, it will serve as the starting point to describe and understand the mechanisms underlying FMN release.

Preconditions for Developing the Model

At first consideration, the decision to adopt a simplified analytical model to describe a biologically complex process such as FMN release may appear questionable. The two phenomena—one mathematical, the other physiological—seem to belong to fundamentally different domains. Nevertheless, the analogy merits rigorous examination.

An analysis of the FMN concentration–time profiles obtained during kidney perfusion in the present study, when compared with analogous data reported in the scientific literature [1, 14–16], reveals a consistent and reproducible trend. The temporal evolution of FMN concentration closely aligns with the analytical solution of a first-order differential equation, as previously described. This correspondence suggests that, despite its simplicity, the model captures key kinetic features underlying the observed release dynamics.

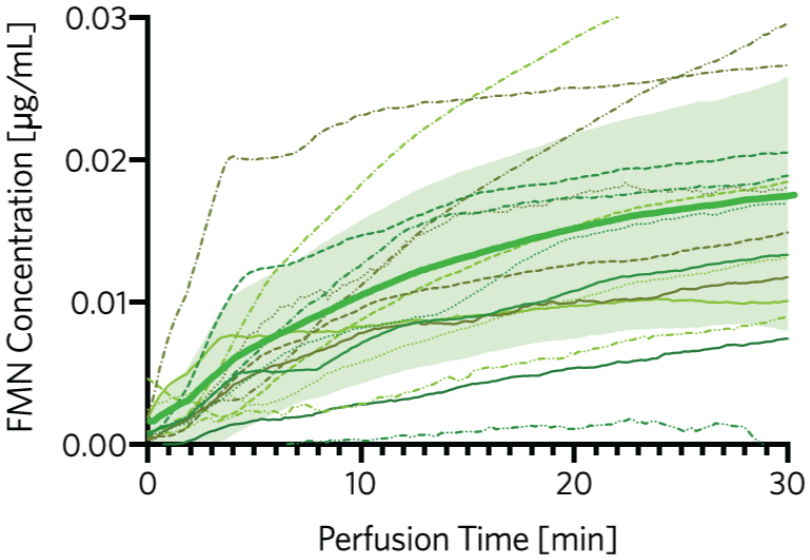

Figure 4.2.4. Illustration of the various trends of FMN release over time during perfusion, from [1]. This Figure is reprinted with Creative Commons CC BY license.

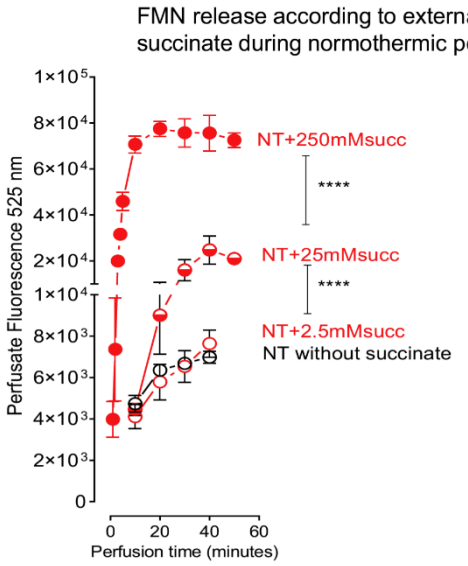

Figure 4.2.6. Release of FMN increased in accordance with the amount of administered succinate, from [15]. This Figure is reprinted with Creative Commons Attribution-NonCommercial-No Derivatives License (CC BY NC ND).

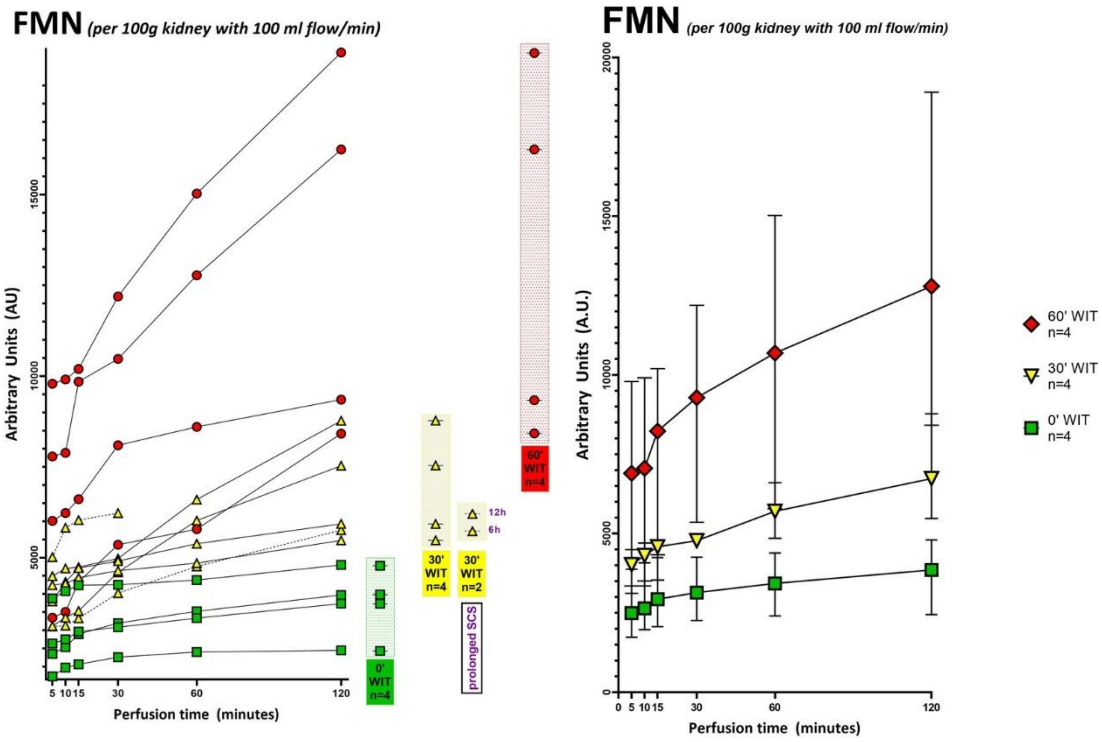

Figure 4.2.5. Illustration of the various trends of FMN release over time during perfusion, from [14]. This Figure is used with Creative Commons Attribution License (CC BY).

It's possible to observe that trends we have reported are consistent with those described by other authors [1, 14 – 16].

This observation led to the working hypothesis that FMN release may be approximated by a first-order process, and thus described by the same type of mathematical model typically used for chemical reactions in a batch reactor. Naturally, FMN release from mitochondria during ischemia–reperfusion injury is not a chemical reaction in the strict sense. Nonetheless, it can be conveniently represented as if it were one:

$$FMN_{mitochondria} \rightarrow FMN_{perfusate}$$

Here, FMN stored within mitochondria plays the role of the reactant (species ***A***), which is progressively "consumed" as it is released into the perfusate, where it accumulates as the "product" (species B). While this formulation is clearly metaphorical, the resemblance between the kinetics of release and the solution of a first-order model justifies its adoption as an analytical tool.

Moreover, the analogy can be extended beyond mere curve fitting. In chemical kinetics, reaction rates depend on factors such as temperature, concentration, and activation energy. Similarly, FMN release is modulated by parameters including ischemia time, organ viability, perfusion method, and preservation protocol. In both contexts, such variables accelerate or decelerate the dynamics of the process.

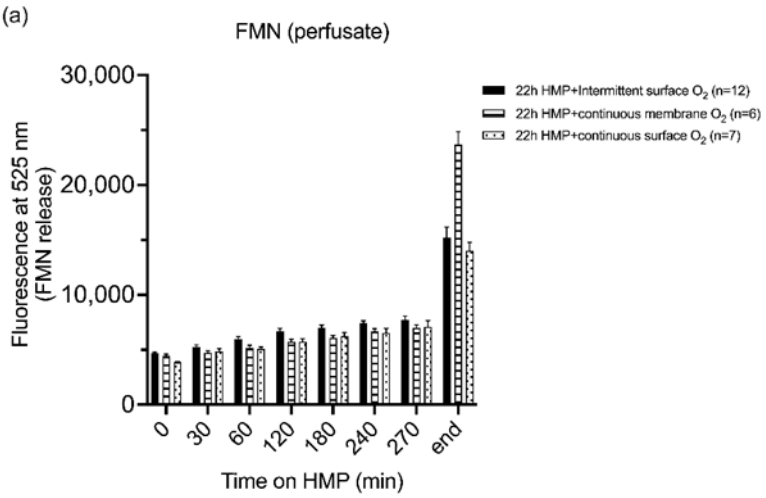

Figure 4.2.7. Illustration of the various trends of FMN release over time during perfusion. Unfortunately, the authors showed the FMN values for the first few hours but not the complete trend for the entire perfusion. But already looking at the trends we can see that they are consistent with those reported by other authors, from [16].

It is important, however, to clarify a key assumption underpinning this model. By definition, a first-order kinetic model converges asymptotically to a steady-state value determined by the kinetic constant ***k*** (here referred to as the *FMN release constant*), **Figure 4.2.8**. The question is whether this assumption holds true in the context of organ perfusion.

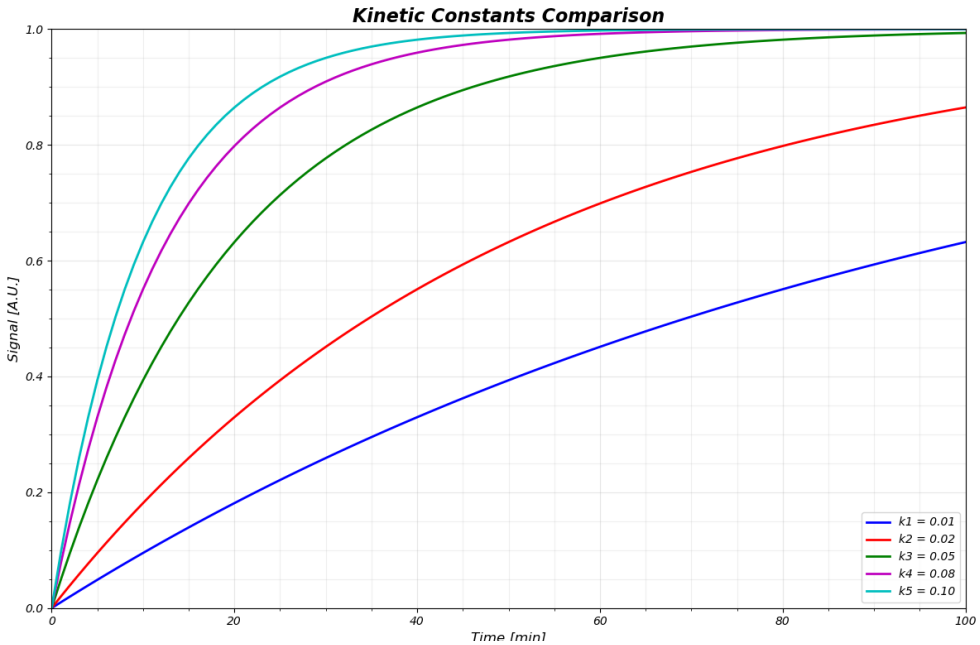

Figure 4.2.8. Effects of the kinetic constant. The model for different values of k (k is the kinetic constant that gives us an idea of the time it takes to reach the steady-state value, i.e., how fast the reaction goes, in this case, how fast is the release of FMN either due to ischemia-reperfusion injury or from perfusion efficiency (vascular resistances, good channeling of fluid inside the blood vessels and other factors).

During hypothermic oxygenated perfusion, the organ is expected to reach a state of stabilization, both functionally and metabolically, where FMN release diminishes and circulating FMN concentration approaches a plateau. This would indeed correspond to the asymptotic behavior predicted by the model. The assumption is valid provided that FMN is not subsequently removed from the perfusate by competing processes such as reabsorption into tissues (e.g., adipose or structural components) or photochemical degradation.

From a theoretical standpoint, therefore, a steady-state concentration could be reached irrespective of the initial ischemic damage. Whether this assumption reflects biological reality, however, requires confirmation by clinical experts.

Modelling

Having established the necessary premises, we can now proceed to the construction of the model. To achieve this, it is essential to introduce a series of simplifying assumptions, which act as boundary conditions that allow us to isolate the main phenomenon of interest while neglecting secondary effects. Specifically, we assume that:

- During perfusion, no additional FMN is introduced into the system and no perfusate is withdrawn.
- The FMN present in the circulating fluid is not degraded by ambient light nor oxidized by dissolved oxygen.
- FMN is not adsorbed or sequestered by the organ's tissues, including adipose tissue, connective structures, or other support material. Consequently, all FMN detected spectroscopically in the perfusate originates exclusively from mitochondria damaged by ischemia.

Under these assumptions, the system becomes analytically tractable: the FMN measured in the perfusate corresponds directly to that released by mitochondria as a consequence of ischemia.

To characterize the extent of ischemic injury, we introduce a dimensionless parameter, denoted as $\boldsymbol{\alpha}$, referred to as the ischemic damage index. This index quantifies the proportion of damaged mitochondria relative to the total mitochondrial population in the organ at the time of retrieval. Formally, it can be defined in two equivalent ways:

$$\alpha = \frac{Number\ of\ Damaged\ Mitochondira}{Total\ number\ of\ Mitochondria} \tag{18}$$

or, expressed in terms of FMN content:

$$\alpha = \frac{Amount\ of\ FMN\ in\ Damaged\ Mitochondira\ [expressed\ in\ ng]}{Total\ Amount\ of\ FMN\ in\ all\ Mitochondira\ [expressed\ in\ ng]} \tag{19}$$

From a practical standpoint, $\boldsymbol{\alpha}$ = 0 indicates an organ with no ischemic injury (all mitochondria intact), whereas $\boldsymbol{\alpha}$ = 1corresponds to complete mitochondrial damage, i.e., a non-viable organ unsuitable for transplantation. Although this definition is necessarily a simplification, it provides an intuitive and useful framework for quantifying ischemic severity.

The temporal evolution of $\boldsymbol{\alpha}$ during ischemia is of particular interest. Initially, $\boldsymbol{\alpha}$ = 0, and it increases progressively as ischemic time elapses. The rate of increase depends on donor-specific factors such as age, comorbidities, and lifestyle. For example, a healthy donor may exhibit a slower increase in $\boldsymbol{\alpha}$, whereas in donors with risk factors (e.g., smoking, alcohol or drug use, or metabolic disease), the rate of increase is expected to be higher. Conceptually, possible trajectories influenced by values of $\boldsymbol{\alpha}$ during ischemia are illustrated in **Figure 4.2.9**.

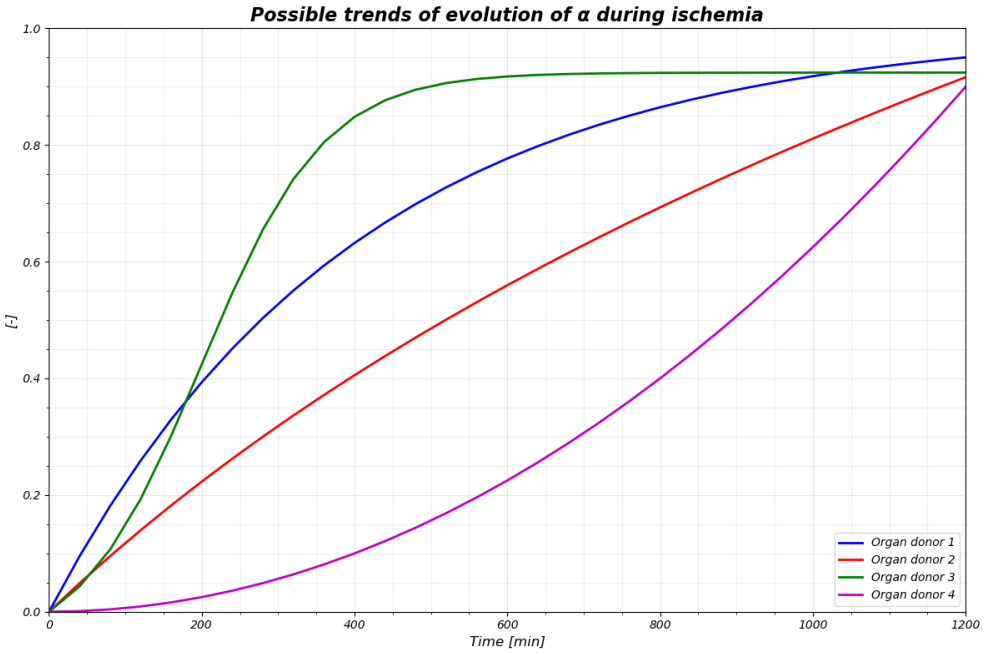

Figure 4.2.9. Schematic representation of possible ischemic damage progression **α** as a function of ischemia time for different donor health conditions.

It should be emphasized that these curves are purely hypothetical and serve only to pose the fundamental question: what is the actual trend of the ischemic damage index over time? While the exact dynamics require experimental validation, we can reasonably assume that α does not increase indefinitely. Instead, it approaches a maximum value at the onset of hypothermic oxygenated perfusion (HOPE).

The initiation of HOPE stabilizes the organ by supplying oxygen, thereby mitigating ischemia-reperfusion injury and partially restoring mitochondrial function. Accordingly, for modeling purposes, we assume that α increases only during the ischemic interval (from static cold storage until the initiation of perfusion) and subsequently remains constant once perfusion begins.

This formulation enables a simplified but effective description of the system: at the onset of perfusion, only a fraction of the mitochondria is irreversibly damaged, meaning that only part of the total FMN is available for release into the perfusate, while the remainder remains confined within intact mitochondria.

Let $m_{FMN,damaged}$ denote the mass of FMN releasable during perfusion, and $m_{FMN,total}$ the total mitochondrial FMN content of the organ (associated with complex I). By definition:

$$m_{FMN,damaged} = \alpha \cdot m_{FMN,total} \tag{20}$$

At the end of the ischemic interval, when hypothermic perfusion is initiated, mitochondria that sustained irreversible damage during ischemia begin releasing FMN into the circulating perfusate. As illustrated schematically in **Figure 4.2.10**, the value of **α** at this point determines the maximum fraction of FMN that can be released: since **α** < 1, only a portion of the total mitochondrial FMN becomes available for detection.

Figure 2. Schematic representation of the ischemic damage index α reaching its maximum at the end of ischemia and remaining constant during hypothermic perfusion.

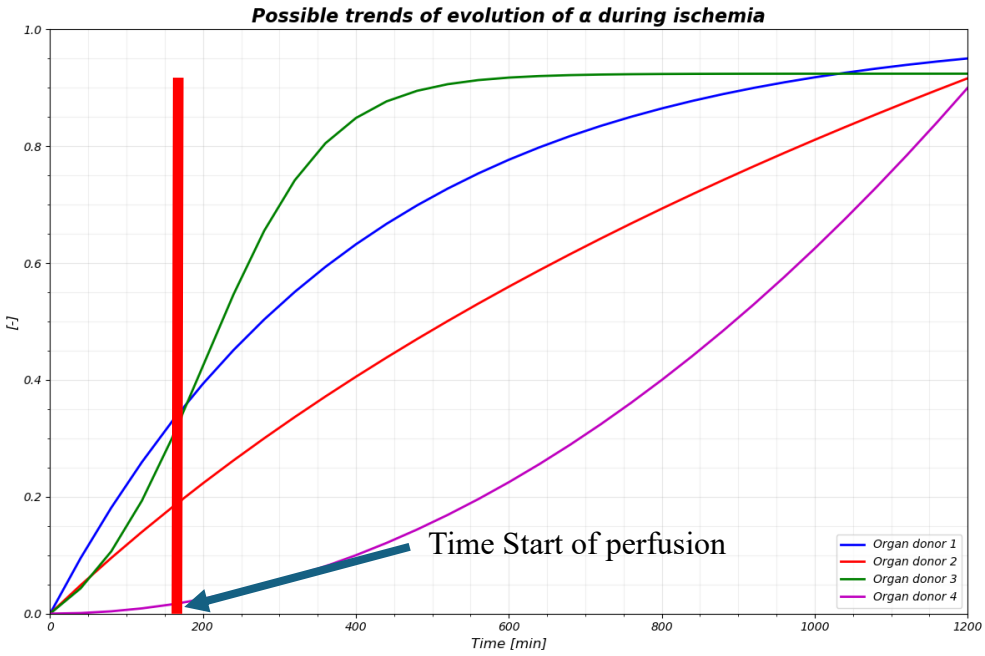

Figure 4.2.10. Schematic representation of the ischemic damage index α reaching its maximum at the end of ischemia and remaining constant during hypothermic perfusion.

Considering to write the mass balance for FMN during perfusion, it is possible to say that the total amount of releasable FMN (i.e., the FMN present in damaged mitochondria) is equal to the sum of

the FMN still inside the damaged mitochondria and the FMN already released into the perfusate, **Figure 4.2.11**:

$$m_{FMN,damaged} = m_{FMN,mitochondria}(t) + m_{FMN,perfusate}(t) \quad (21)$$

- $m_{FMN,damaged}$: is the total amount of FMN present in damaged mitochondria and available to be **released**. In other words, is the quantity of FMN releasable. This quantity is **constant over time**.
- $m_{FMN,mitochondria}(t)$: is the amount of FMN still inside the damaged mitochondria, which will be gradually released during perfusion. This quantity **decreases over time**.
- $m_{FMN,perfusate}(t)$: is the amount of FMN that has already been released into the perfusate. This quantity **increases over time**.

The sum $m_{FMN,mitochondria}(t) + m_{FMN,perfusate}(t)$ remains constant because it represents the total amount of releasable FMN. In other words, the mass balance equation:

$$m_{FMN,damaged} = m_{FMN,mitochondria}(t) + m_{FMN,perfusate}(t) \quad (22)$$

Have to be considered always hold true.

The eq. (22) accounts for both the FMN still inside the organ and the FMN that has been released into the perfusion liquid.

Considering the eq. (21),

$$\alpha \cdot m_{FMN,total} = m_{FMN,mitochondria}(t) + m_{FMN,perfusate}(t) \quad (23)$$

The "term" $\alpha \cdot m_{FMN,total}$ is a number.

At time t=0, we can say that $m_{FMN,damaged} = m_{FMN,mitochondria}(t = 0)$, because at the very start of perfusion, all the releasable FMN is still inside the damaged mitochondria, and none has yet entered the perfusate. As time passes, $m_{FMN,mitochondria}(t)$ decreases because the damaged mitochondria release FMN, while $m_{FMN,perfusate}(t)$ increases as FMN moves into the perfusion liquid. However, the total amount of releasable FMN, $m_{FMN,damaged}$ remains constant over time. In fact, don't forget that $m_{FMN,damaged}$ is the number of damaged mitochondria.

Now, let's picture the system perfusion circuit + organ as a batch reactor, like in **Figure 4.2.11**: in which there is reaction of the type $A \rightarrow B$, where FMN is transferred from the mitochondria to the perfusate.

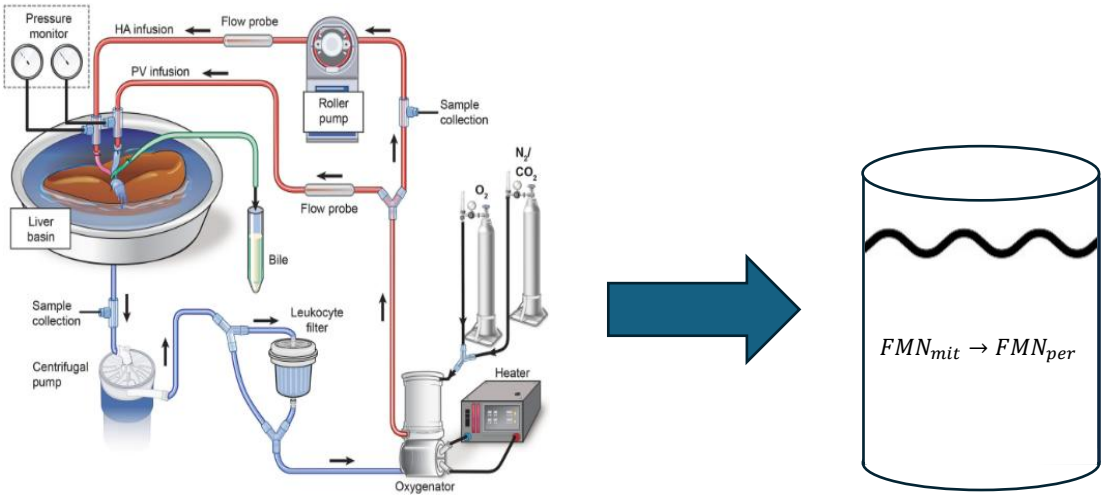

Figure 4.2.11. Representation of the machine perfusion like a batch reactor. This Figure, from [17], is reprinted with License Number 6126541351069.

Now, let's write the material balance for mitochondrial FMN and FMN dissolved in perfusate.

For FMN in the mitochondria:

$$\frac{dm_{FMN,mitochondria}}{dt} = -k \cdot m_{FMN,mitochondria} \tag{24}$$

This equation tells us that the rate of change of FMN in the mitochondria over time is proportional to the speed at which it is being transferred to the perfusate. The constant k, in chemical reaction is the kinetic constant, here plays the role of transfer rate constant, depends on factors like the severity of ischemia and other variables such as the donor's medical history, the organ's condition, and more. Solving this equation we can observe the variations of FMN contained in the mitochondria.

For FMN in the perfusate:

$$\frac{dm_{FMN,perfusate}}{dt} = k \cdot m_{FMN,mitochondria} \tag{25}$$

This equation describes how the amount of FMN in the perfusate increases over time, depending on the FMN still available in the damaged mitochondria. Just like in a first-order reaction,

the rate of transfer is determined by the constant k and the amount of FMN remaining in the mitochondria.

If we take the equation (23) and rewrite it as:

$$m_{FMN,mitochondria}(t) = \alpha \cdot m_{FMN,total} - m_{FMN,perfusate}(t) \tag{26}$$

then substitute it into the mass balance equation:

$$\frac{dm_{FMN,perfusate}}{dt} = k \cdot \left(\alpha \cdot m_{FMN,total} - m_{FMN,perfusate}(t)\right) \tag{27}$$

we arrive at an equation we can solve, as the term $\alpha \cdot m_{FMN,total}$ is a constant starting from the moment perfusion begins.

By solving this differential equation with the initial conditions $m_{FMN,perfusate}(t = 0) = 0$, we get the following expression:

$$m_{FMN,perfusate}(t) = \alpha \cdot m_{FMN,total} \cdot (1 - e^{-k \cdot t}) \tag{28}$$

Examination of the meaning of this model

In simple terms, it shows that if ischemic damage is severe (with α close to 1), the final amount of FMN in the perfusate at the end of perfusion will be very high—almost equal to the total FMN initially present in the organ. This means that nearly all the mitochondria are damaged, and almost all the FMN ends up being released.

Conversely, if $\boldsymbol{\alpha}$ is close to zero, the amount of FMN in the perfusate will be very low, since only a small fraction of mitochondria are damaged.

And what about the role of $\boldsymbol{k}$?

The constant $\boldsymbol{k}$ represents the reaction rate. In chemical kinetics, the product $\boldsymbol{k \cdot t}$ is often viewed as a "time constant" that determines how fast a process approaches equilibrium. In this context:

- A **larger** $\boldsymbol{k}$ means the system reaches steady state more quickly—less FMN needs to be released, since fewer mitochondria are damaged.
- A **smaller** $\boldsymbol{k}$ means more mitochondria are damaged, so a larger amount of FMN is released, and the system takes longer to reach steady state.

An example of the explanation is shown in **Figure 4.2.12** using our experimental data.

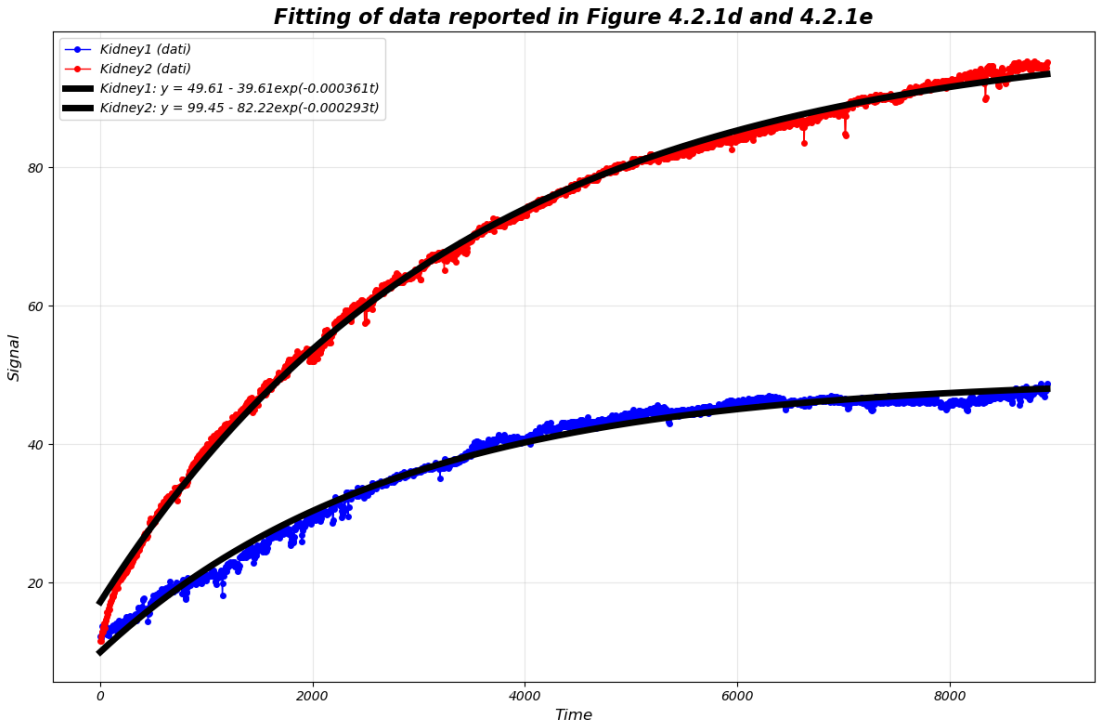

Figure 4.2.12. Fitting of data of experimental results using the batch reactor model.

The following is an analysis about this explanation and if it holds up by comparing it with our experimental data and those from other authors [1, 14]. The comparison of the FMN curves obtained from our experience. The blue curve represents a kidney that underwent 2 hours of ischemia, while the red curve corresponds to a kidney with about 5 hours of ischemia.

According to the model, a longer ischemia time increases $\boldsymbol{\alpha}$ because the fraction of damaged mitochondria is higher. But that's not all: a longer ischemia time also causes a decrease in $\boldsymbol{k}$.

The introduction of the parameter $\boldsymbol{\alpha}$ gives the model a more realistic physical meaning: it predicts an **asymptotic trend**, where after a certain number of hours of perfusion, the organ reaches an equilibrium state. Of course, whether this assumption holds true in practice must ultimately be verified (or refuted) by physicians and clinicians through real-world perfusion studies.

Comparison between model and experimental evidence

To assess the plausibility of the proposed first-order release model, we compared its behavior with experimentally observed FMN concentration–time profiles. Specifically, we examined two kidney perfusion traces recorded during our experience: the blue trace corresponds to a kidney exposed to ≈2 hours of ischemia, while the red trace corresponds to a kidney exposed to ≈5 hours of

ischemia. We also compared these curves with the data reported by Sousa da Silva et al. (2023) [14], which employ a comparable preclinical porcine model.

Two consistent trends emerge from both my data and the literature:

- **Effect of ischemic duration on $\boldsymbol{\alpha}$ and $\boldsymbol{k}$.** Longer ischemia is associated with a larger ischemic-damage index $\boldsymbol{\alpha}$ (a greater fraction of mitochondria damaged) and with a smaller kinetic constant $\boldsymbol{k}$. In the dataset examined, the kidney with prolonged ischemia (red trace) exhibits a lower estimated $\boldsymbol{k}$ and a higher $\boldsymbol{\alpha}$ than the kidney with shorter ischemia (blue trace). Sousa da Silva et al. report analogous behaviour: short ischemia times correspond to high $\boldsymbol{k}$ and low $\boldsymbol{\alpha}$, whereas prolonged ischemia correlates with low $\boldsymbol{k}$ and high $\boldsymbol{\alpha}$.
- **Qualitative agreement with first-order kinetics.** The concentration–time profiles frequently display the monotonic, asymptotic shape expected from a first-order release process, supporting the use of a first-order approximation as a first step of analysis.

It must be emphasized that, for the present analysis, we have assumed ischemia duration is the dominant determinant of $\boldsymbol{\alpha}$ and $\boldsymbol{k}$. This is a simplifying hypothesis: in practice, multiple covariates (donor comorbidities, organ-specific properties, preservation conditions, perfusion protocol, temperature, etc.) also affect $\boldsymbol{\alpha}$ and $\boldsymbol{k}$. Nevertheless, within the limited scope of the present preliminary dataset, the ischemia-time dependence provides a useful and interpretable first approximation.

About the validity and utility of the kinetic analogy

Is it appropriate to apply a kinetic model, borrowed from chemical engineering, to clinical perfusion data? The honest answer is: **not uncritically**. The first-order batch analogy is overly simple to capture the full biophysical complexity of ischemia-reperfusion and mitochondrial FMN dynamics. Nevertheless, two considerations justify its use as an initial modelling strategy:

- **Phenomenological similarity.** The empirical concentration–time profiles frequently resemble the analytical solution of a first-order model, which motivates the hypothesis that a first-order approximation may capture dominant dynamics over the measurement timescales.
- **Interpretability.** Parameters such as $\boldsymbol{\alpha}$ (damage fraction) and $\boldsymbol{k}$ (effective release constant) provide physically interpretable summary metrics that can be correlated with experimental conditions and clinical covariates.

Thus, the first-order model should be viewed as a **semi-empirical, hypothesis-generating tool** rather than a definitive mechanistic description. It is a pragmatic starting point: relatively simple to fit and interpret, and therefore useful for identifying regimes or outliers that require more detailed study.

Towards more realistic models: the packed-bed analogy and spatial dynamics

A richer representation of the organ–perfusate interaction can be obtained by relaxing the well-mixed assumption and incorporating spatial heterogeneity. An instructive analogy comes from chemical engineering: the **packed-bed adsorption column**. In that system, a solvent flows through a packed porous medium where an adsorbent captures a solute; downstream, the adsorbent can be regenerated by a different fluid. If one regards the vasculature and parenchymal microstructure as an intricate porous network, the perfusion process shows formal similarities: the perfusate pervades complex pathways, and FMN is released from local tissue volumes into the flowing fluid.

Adopting this view leads naturally to a local (microscopic) mass balance of the form (representative, not exhaustive):

$$\frac{1}{\varepsilon}\frac{\partial c_A}{\partial t} = -\frac{\partial (c_A u)}{\partial z} - \frac{\partial (N_A)}{\partial z} + \frac{(1-\varepsilon)}{\varepsilon}\rho_s k_s \cdot \frac{\partial q_A}{\partial t} \tag{29}$$

where $\frac{\partial c_A}{\partial t}$ is the fluid concentration of FMN along a spatial coordinate z, ε is porosity (fractional fluid volume), u is the interstitial velocity, $\frac{\partial (N_A)}{\partial z}$ is the diffusive flux, ρ_s and k_s are solid-phase density and kinetic parameters, and q_A denotes the FMN bound or contained in the solid (tissue) phase. Equation (29) is a partial differential equation that captures coupled advection, dispersion/diffusion, and exchange between solid and fluid phases. With suitable boundary and initial conditions, it can describe both spatial and temporal evolution of FMN within the organ.

Equation (29) is more realistic than a spatially lumped batch model because it accounts for:

- axial transport (advection) along vascular pathways,
- local dispersion/diffusion between microvascular compartments and tissue,
- sorption/desorption or release kinetics from the solid (cellular) phase.

However, this increased realism comes at a computational cost: solution of Equation (29) typically requires numerical methods and substantial parameterization (geometry, permeability, dispersion coefficients, tissue exchange kinetics), which in turn demand extensive experimental data.

To provide a theoretical and simplified framework for quantifying the term $\frac{\partial q_A}{\partial t}$ and assigning it a physical meaning, we attempt to schematize the FMN release process through a conceptual model that necessarily approximates the underlying biological and physico-chemical mechanisms. As engineers, it is essential to begin with a simplified model of the phenomenon in order to identify its key features and thereby establish a foundation for more advanced and accurate descriptions of complex processes.

The release of FMN during ischemia-reperfusion can be conceptually described through the following sequence of steps:

1. **Ischemic phase** – oxygen deprivation leads to the generation of free radicals.
2. **Perfusion phase** – the introduction of the perfusion fluid ensures oxygen availability throughout the vasculature. Oxygen reacts with free radicals, generating reactive oxygen species (ROS).
3. **ROS-induced damage** – ROS attack and compromise cellular structures, including Complex I of the mitochondria.
4. **FMN dissociation and migration** – once detached, FMN crosses mitochondrial and cellular membranes and dissolves in the circulating perfusion fluid.
5. **Fluorescence detection** – dissolved FMN is detected via spectroscopic fluorescence techniques.
6. **Cessation of release** – after a certain time, cells begin to recover and stop releasing FMN. It is assumed that the released FMN remains dissolved in the perfusion medium and that any potential reabsorption by cells is negligible.

From this perspective, two distinct processes govern the transfer of FMN from Complex I to the perfusion fluid:

- **Enzymatic dissociation**: FMN detaches from Complex I, a process that can be conceptualized as a reaction step in which the cofactor dissociates from its enzymatic site.
- **Mass transfer**: FMN subsequently migrates across mitochondrial and cellular membranes into the perfusion fluid. Due to ischemia-reperfusion injury, the membranes are compromised, allowing diffusion of FMN. Although FMN is larger than glucose, it remains significantly smaller than lipids, proteins, or enzymes, making its diffusion across damaged membranes

physically plausible. This process can be modeled as a combination of molecular diffusion through membranes, diffusion in liquid layers, and forced convection.

To formalize this concept, we schematize the interior of the organ by focusing on a single representative cell (**Figure 4.2.13**).

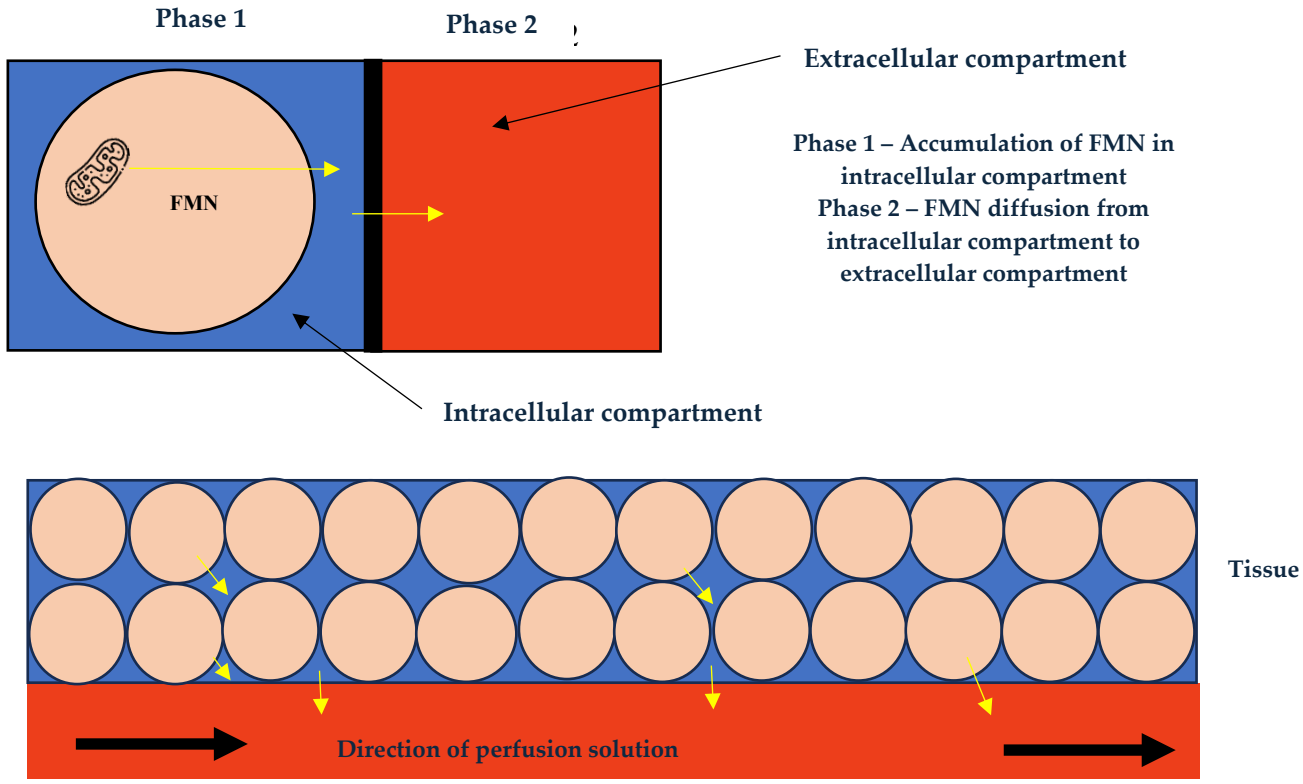

Figure 4.2.13. Schematic representation of FMN release at the microscopic scale.

While macroscopic modeling approaches treat the organ as a "black box," this microscopic perspective magnifies the process at the cellular level. We idealize the cell as a spherical unit, assuming that the organ consists of billions of identical cells behaving homogeneously and synchronously. This is, of course, a strong simplification, but it provides a practical starting point.

From **Figure 4.2.13**, we distinguish two compartments and phases:

- **Intracellular compartment**: FMN accumulates following dissociation from mitochondria.
- **Extracellular compartment**: FMN crosses the cell membrane and enters the perfusion fluid.

We thus define a two-compartment model:

1. **Material balance on intracellular FMN**:

$$\frac{dc_{FMN,i}}{dt} = k_1 f(t) - k_2\left(c_{FMN,i} - c_{FMN,e}\right) \tag{30}$$

where:

- $k_1 f(t)$represents FMN generation through enzymatic dissociation, with k_1 as the dissociation constant. At present, the precise kinetic law is unknown; it might resemble Michaelis–Menten kinetics, but no specific studies are available.
- $k_2\left(c_{FMN,i} - c_{FMN,e}\right)$ models FMN transport across the cell membrane according to film theory, where the flux is proportional to a mass transfer coefficient k_2, with units of [1/time]) and the concentration gradient between intracellular and extracellular compartments.

2. **Material balance on extracellular FMN (perfusion fluid)**:

$$\frac{dc_{FMN,e}}{dt} = k_2\left(c_{FMN,i} - c_{FMN,e}\right) \tag{31}$$

To these two differential equations we have to write the initial conditions $c_{FMN,i}(0) = 0; c_{FMN,e}(0) = 0$.

The quantity $\frac{dc_{FMN,e}}{dt}$ is attributable to $\frac{\partial q_A}{\partial t}$, which we mentioned earlier.

This formulation highlights the interplay between the two processes. Solving the system of differential equations would enable us to identify the controlling mechanism:

- If **enzymatic dissociation** is rate-limiting, it would indicate relatively intact mitochondrial function and thus limited ischemic damage.
- Conversely, if **mass transfer** is rate-limiting, this would imply rapid dissociation but significant membrane disruption, corresponding to severe cellular damage.

This compartmentalized framework provides a first-order approximation of the microscopic dynamics of FMN release, complementing the macroscopic "black box" approach and enabling a deeper exploration of the mechanisms underlying ischemia-reperfusion injury.

Macroscopic vs microscopic approaches

It is useful to contrast the two levels of description:

- **Macroscopic (global) balance** — e.g., the batch formulation — treats the entire perfusate volume as a single well-mixed compartment and yields ordinary differential equations for mean concentration. This approach is low-dimensional, easy to fit to data, and useful for extracting global parameters (e.g. effective $\boldsymbol{k}$, $\boldsymbol{\alpha}$). It is appropriate when spatial gradients are small or when one only requires an empirical predictive model of bulk behaviour.
- **Microscopic (local) balance** — e.g., Equation (29) — resolves concentration as a function of space and time. It captures transport heterogeneity, local depletion zones, and tissue–fluid exchange kinetics. This approach is necessary when spatial non-uniformity is relevant (e.g., incomplete perfusion, regional necrosis) or when one must infer local tissue parameters.

Selecting the appropriate modelling scale depends on the scientific objective and the available data. The macroscopic model is an expedient first step; the microscopic framework can be pursued when richer datasets and resources permit.

Outlook and research pathway

The present study has adopted a simple semi-empirical kinetic model as a first approximation. The advantages are clear: interpretability, low data requirements, and the ability to rapidly test hypotheses against measured FMN curves. The limitations are equally clear: the model neglects spatial heterogeneity, competing removal mechanisms (re-uptake, adsorption, photodegradation), and the full biochemistry of mitochondrial damage.

A possible research pathway is therefore:

- **Continue with the macroscopic approach** to characterize cohorts, estimate $\boldsymbol{\alpha}$ and $\boldsymbol{k}$ under controlled conditions, and identify systematic dependencies (e.g., ischemia time, temperature, donor risk factors).
- **Collect richer data** (spatially resolved sampling, imaging, or higher-frequency temporal data) to enable parameter estimation for local models such as Equation (29).
- **Develop and validate a hybrid model** that couples a macroscopic perfusate compartment with one or more tissue sub compartments (or a reduced-order spatial discretization of Equation (29)), thereby balancing realism and identifiability.
- **Incorporate clinical validation** through multi-centre datasets and interdisciplinary collaboration with clinicians to assess predictive value for transplant outcomes.

In this paragraph, we have attempted to construct an initial mathematical model to interpret the release of FMN from an organ—specifically the kidney—during hypothermic perfusion. We relied on the analogy of a batch reactor, employing an approach based on several simplifications to represent

the phenomenon. Naturally, such a simplified framework is prone to errors and cannot be regarded as a definitive model or as one immediately applicable in clinical practice. Nevertheless, it may serve as a starting point for the development of more accurate models, potentially inspired by alternative methodologies from chemical engineering, to describe FMN release associated with ischemia-reperfusion injury during HOPE.

The main objective of this paragraph was to demonstrate that, when supported by experimental data, an engineering approach can provide meaningful insights and establish a foundation for future developments. The path remains open and may be further explored if considered of interest. During our experience at the Cleveland Clinic, this topic emerged as a potential line of investigation alongside other ongoing projects.

This document has provided a useful contribution and, above all, has offered clarity rather than confusion. The simplified representation of the perfusion process as a "container of Belzer solution" where FMN is released—treated analogously to a batch reactor—may appear reductive, yet it exemplifies how chemical engineers attempt to distill complex biological processes into a tractable set of equations.

It is essential to emphasize the limitations of this approach and recognize that further knowledge is required to achieve a deeper understanding of these mechanisms. Nonetheless, the author is convinced that each incremental step—even if preliminary—can contribute to building a more robust and useful framework for the future.

5. A Novel Risk Score Using Flavin Mononucleotide (FMN) for Predicting Graft Loss After Liver Transplantation with Normothermic Machine Perfusion[1]

So far, we have examined how FMN release can be detected and modeled. A highly relevant clinical aspect concerns the ability of FMN levels measured during *machine perfusion* to predict post-transplant outcomes before the transplant itself, through the use of predictive scoring models. Satish et al. [4] published an abstract describing an initial predictive model that integrates viability markers.

[1] This paragraph is reproduced and adapted from reference [4] with License Number 6126550205774.

In this context, a new predictive model has been developed that combines traditional risk factors with viability markers. The abstract is part of a broader study, currently under preparation as a full scientific article; therefore, no additional information can be disclosed beyond what has already been published.

The proposed model integrates eight traditional risk factors—portal vein thrombosis, pre-transplant ICU admission, primary sclerosing cholangitis, re-transplantation, labMELD, recipient age, recipient BMI, and cold ischemia time—with the FMN concentration measured after 4 hours of normothermic perfusion. It should be emphasized that, although many other parameters could be considered, this work focused only on the most significant ones. Notably, FMN becomes relevant only when evaluated in conjunction with other clinical factors.

As reported by Satish et al. [4], risk analysis was conducted on 200 patients undergoing *normothermic machine perfusion* (NMP) at their institution, generating a new score through multivariable logistic regression with bootstrapping. The Framingham methodology was employed to construct a point-based system to predict 12-month graft survival.

Main results:

- Cold ischemia time and FMN levels at 4 hours of NMP were used to define donor risk (range 0–15).
- The above-listed traditional risk factors were used to define recipient risk (range 0–17).
- The model showed high predictive performance on 234 cases for overall graft survival (AUROC = 0.82) and recipient survival (AUROC = 0.77), with excellent predictive capacity for death-censored graft survival (AUROC = 0.96).
- Other commonly used scores (BAR, DRI, SOFT, MEAF) showed only marginal predictive capacity within the NMP-treated cohort.
- Recipients with a score >6 had significantly lower 1-year graft survival ($p < 0.0001$) and a higher incidence of post-transplant complications, particularly biliary complications.
- Low-risk recipients (≤6 points) experienced significantly impaired graft survival when livers with high donor risk (>3 points) were used.

In **Table 5.1** and in **Figure 5.1** are reported the scores used by the model and results, from [4].

Variable	Categories	W_{ij}	W_{ref}	Coefficient (b)	$b*(W_{ij}-W_{ref})$	B	Points
Cold ischemia time (CIT)	≤ 10 hours	6	6	0.059938	0		0
	> 10 hour	12			0.359628		3
FMN concentration (µg/ml)	≤ 1.25	0.5	0.5	0.840089	0		0
at 4-hours of NMP	1.25 < FMN ≤ 1.75	1.5			0.840089		6
	> 1.75	2.5			1.680178		12
Portal vein thrombosis	No	0	0	0.657611	0		0
(yes/no)	Yes	1			0.657611		5
Pre-transplant ICU	No	0		0.567672	0	0.141681	0
admission (yes/no)	Yes	1			0.567672		4
Primary Sclerosing	No	0	0	0.312369	0		0
Cholangitis (yes/ no)	Yes	1			0.312369		2
Retransplantation (yes/no)	No	0	0	0.288724	0		0
	Yes	1			0.288724		2
LabMELD (points)	≤ 30	20	20	0.019605	0		0
	> 30	40			0.3921		3
Log (recipient age/recipient	≤ 0.3	0.1	0.1	0.283362	0		0
BMI)	> 0.3	0.6			0.141681		1
Total							**0 - 32**

Table 5.1. Development of point-based score based on multivariate logistic regression model

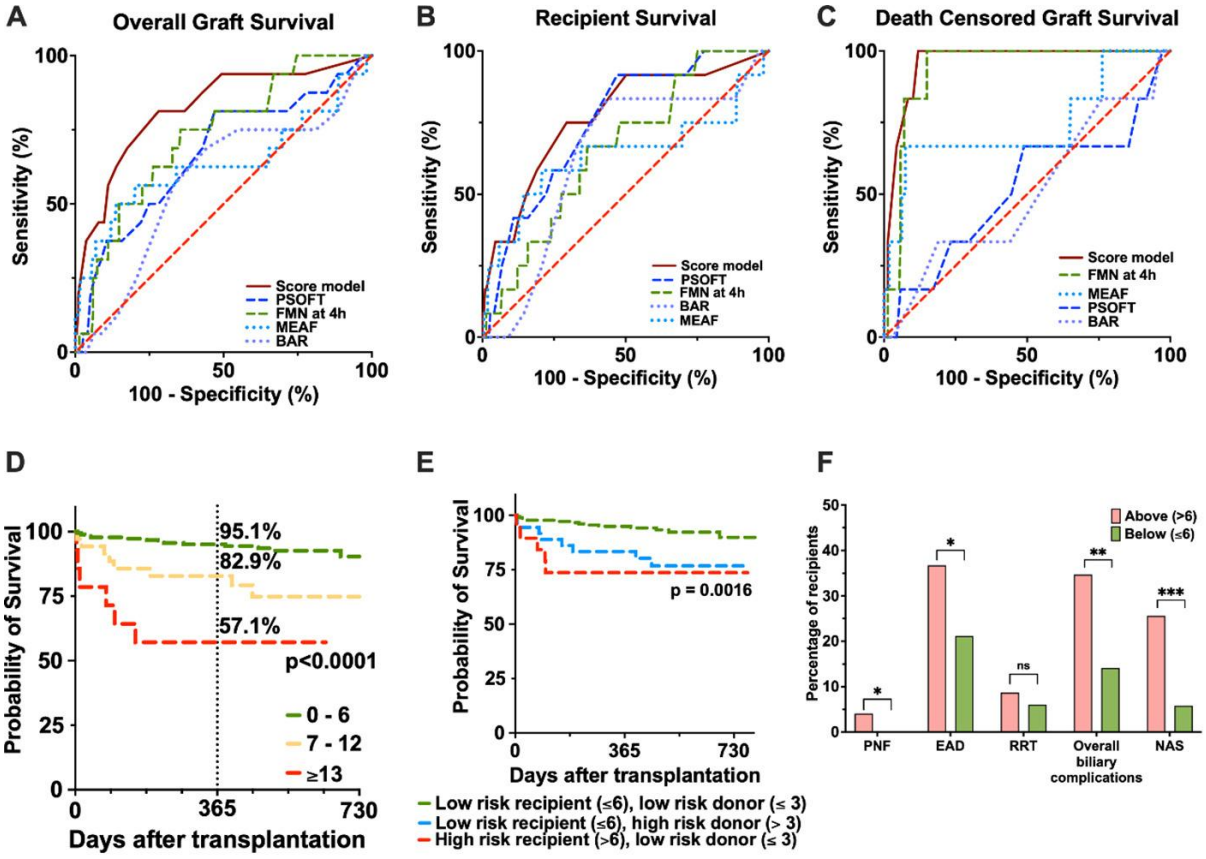

Figure 5.1. Receiver operating curves (ROC) for overall graft survival (A), recipient survival (B) and death censored graft survival (C) for FMN score model and other risk assessment scores (MEAF, BAR, PSOFT). D) Kaplan Meier Survival Curve by FMN score model points. E) Kaplan Meier Survival Curves for recipient survival stratified by risk of recipient and donor according to FMN score model, F) Incidence of post operative complications within recipients with FMN score model > 6 points. Abbreviations: BAR: balance of risk score, EAD: early allograft dysfunction, FMN: flavin mono-nucleotide, MEAF: model for early allograft function, NAS: non-anastomotic strictures PNF: primary non function, PSOFT – pre-allocation survival outcomes after transplant, RRT: renal replacement therapy

This new model, which incorporates mitochondrial injury measured through FMN, therefore demonstrates excellent discriminative capacity for predicting graft survival and other post-transplant outcomes. Clinically, AUROC values close to 1 denote outstanding discriminative performance, underlining the robustness of this model. Compared with existing predictive tools (BAR, DRI, SOFT), the inclusion of FMN represents a clear improvement: it brings a biochemical parameter into a multiparametric predictive framework, showing how engineering-based modeling of a molecular biomarker can be translated into clinical practice.

This section also aligns with the earlier chapters on mathematical modeling of FMN release, showing consistency between the theoretical approach (equations) and clinical applications (risk prediction). Looking ahead, machine learning approaches could further integrate FMN with other biomarkers, potentially refining prediction accuracy and enabling real-time, adaptive decision-support tools for clinicians.

Further internal and external validation studies are currently ongoing to consolidate its clinical applicability.

6. Effects of External interferences on FMN detection

This section discusses the main interfering factors identified during FMN fluorescence measurements and their potential impact on signal intensity. The identified sources of interference include: ambient light, oxygenation level, reabsorption effects, residual blood, presence of additives, organ handling, and perfusion volume. The latter cannot be regarded as a true interferent, since it is an intrinsic variable of the perfusion protocol; however, because the perfusion volume affects the dilution of FMN and thus the signal intensity, it can be considered an indirect influencing factor.6.1

6.1 Ambient Light

It is well established that ambient light can cause FMN degradation [18–21]. The manufacturer itself recommends storing FMN powder protected from sunlight [22]. We confirmed this effect experimentally. A stock solution of FMN (0.06 mg mL^{-1}), initially characterized by an intense yellow coloration, was placed in a plastic cuvette, sealed to prevent air exchange, and exposed to standard room lighting. After approximately two weeks, the color visibly faded, indicating partial degradation. Although UV–visible absorption spectra were not recorded, the visual evidence was conclusive.

Nevertheless, FMN degradation at high concentrations proceeds relatively slowly. To minimize any potential photodegradation effects during calibration, both the sample containers and the perfusion liquids were kept in the dark. During prototype tests performed with both animal and human organs under standard LED room illumination, no significant decrease in FMN signal intensity was observed. Photodegradation would, in fact, require exposure times much longer than those typical of calibration or perfusion experiments (2–4 hours). In summary, ambient light can induce FMN degradation, but its effects become relevant only after prolonged and continuous exposure lasting several days.

6.2 Oxygenation

L'ossigeno ha un potere ossidante. Teoricamente l'ossigeno dovrebbe ossidare l'FMN degradandolo eppure non abbiamo notato fenomeni di questo genere. Probabilmente la quantità di ossigeno disciolta nel sangue o in un liquido di perfusione non è sufficientemente alta da ossidare l'FMN. Se un ossidazione avviene, possiamo considerarla molto limitata al punto da trascurarla.

6.3 FMN Reabsorption by the Organ

Several studies have suggested that flavin mononucleotide (FMN) may undergo reabsorption by tissues [23–26], although its exact fate during organ perfusion remains uncertain. It is not yet clear whether cellular repair processes during perfusion can occur rapidly enough to allow the reuptake of FMN previously released from damaged mitochondria. During the experiments conducted at the Cleveland Clinic, perfused organs using blood-based solutions often exhibited FMN concentration profiles characterized by an initial rise followed by a gradual decline. This recurring trend prompted questions regarding the underlying cause of the FMN decrease over time.

The author proposes the following reasoning. In blood, oxygen is bound and transported by red blood cells, resulting in a very low amount of freely dissolved oxygen compared to acellular perfusion solutions. In acellular media, although free oxygen is present, its concentration is limited by Henry's law; therefore, oxygen is unlikely to be the main factor responsible for FMN reduction. The perfusion circuit itself adds another layer of complexity. It consists of several components — including a reservoir, filters, and an oxygenator — where mixing is never perfectly homogeneous. As a result, samples collected at different points in the circuit may exhibit varying concentrations. As demonstrated in Chapter IV, even in simplified experimental setups (a single tube and a beaker), the

presence of a mixer significantly influences system dynamics. It is thus plausible that, in a real perfusion circuit, localized accumulations or concentration gradients may develop over time.

Furthermore, the inherent turbidity of blood greatly limits the penetration of ambient light; hence, even during prolonged perfusion experiments (up to 48 hours), the effect of light on FMN degradation can be considered negligible. Based on these considerations, the author hypothesizes that the observed decrease in FMN concentration may be partially related to tissue reabsorption, either localized or diffuse throughout the organ. This hypothesis aligns with established evidence that both hypothermic and normothermic perfusion promote the recovery of mitochondrial activity and restore organ functionality [27–29].

Although the author does not claim clinical expertise, it is conceivable that FMN reuptake could represent an indirect marker of tissue metabolic recovery. Nonetheless, this remains an open area of research, and future studies will be necessary to elucidate this mechanism in greater detail.

6.4 Presence of Residual Blood During Hypothermic Perfusion

Before initiating hypothermic perfusion, the organ is thoroughly rinsed and flushed to remove any residual blood. It is then perfused with a static preservation solution to eliminate remnants generated by ischemic processes and to promote vasodilation, thereby facilitating continuous perfusion.

Although the presence of residual blood during hypothermic perfusion is not considered essential, the author strongly recommends performing a complete washing of the organ to ensure the removal of all blood traces. If residual blood remains, it mixes with the perfusion solution, creating a complex fluid that, for reasons not yet fully understood, induces scattering in the FMN fluorescence signal. This phenomenon was observed only when using the prototype system.

While the exact cause remains uncertain, experimental observations confirmed that the presence of residual blood can distort the FMN signal, preventing stable and accurate measurements. The author proposed a technological solution to mitigate this interference, but its details cannot be disclosed for confidentiality reasons.

6.5 Presence of Additives

During both normothermic and hypothermic perfusion, specific additives may be introduced into the perfusion solution. A recent study [30] suggested the addition of quercetin for clinical purposes.

Quercetin, like FMN, absorbs light at 450 nm and emits fluorescence in the same spectral range (500–600 nm), with a peak around 560 nm.

Because the fluorescence spectrum of quercetin perfectly overlaps with that of FMN, a high concentration of quercetin can completely mask the FMN signal. In theory, quercetin should be progressively absorbed by the organ during perfusion; however, if this does not occur and its concentration remains high in circulation, FMN detection becomes impossible with the tested prototype. This represents an operational limitation of the instrument.

Therefore, it is essential to accurately characterize the UV-visible and fluorescence spectra of all components present in the perfusion solution to identify potential interferents and understand their interaction mechanisms. Although Fernandes et al. [30] recommend the addition of quercetin for its clinical benefits, this practice may hinder FMN detection.

6.6 Organ Handling

As demonstrated in this chapter, the FMN signal often exhibits significant noise, which can be influenced by several factors. One likely source is the physical manipulation of the organ—such as tissue sampling, cannula adjustment, or suturing procedures—which can introduce temporary fluctuations in the fluorescence signal. An additional aspect to consider during organ handling concerns the maintenance of temperature during perfusion.

In normothermic perfusion, the desired temperature is maintained by means of an electric resistor that heats the perfusion solution. In contrast, in hypothermic perfusion, the low temperature is ensured by the use of ice. To perform hypothermic perfusion, a metal tray is typically used, in which the organ is placed and immersed in the perfusion solution. The procedure involves filling the tray with ice, covering it with a sterile plastic bag, then filling the bag with the perfusion solution and submerging the organ.

However, the use of a metal tray presents a significant drawback. The main heat exchange does not occur along the perfusion lines, which are made of polymeric materials and are therefore poor thermal conductors, but rather within the tray itself. Since metal is an excellent conductor of heat, it provides no thermal insulation.

From a theoretical standpoint, it would therefore be preferable to use a plastic tray or, alternatively, to thermally insulate the container.

Good thermal insulation would allow the temperature to remain low for a longer period, reducing the frequency of replacing the water formed by melted ice and, consequently, the amount of new ice required.

Experimental observations have also shown that each time water is removed and ice is added, disturbances occur in the perfusion volume, which are reflected in fluctuations of the detected signal. Indeed, abrupt movements of the perfusion volume alter the spatial distribution of FMN concentration, causing undesired variations in the recorded signal.

From an engineering perspective, an alternative solution could be the use of a Peltier cell to actively cool the perfusion fluid.

This represents an interesting technical challenge, as it would enable precise control of the system temperature; however, it also has the disadvantage of increasing both the cost and the complexity of the perfusion process.

Therefore, in practical terms, the most efficient and sustainable approach remains the use of ice within a well-insulated container, which effectively maintains low temperatures while minimizing both operational costs and system complexity.

6.7 Volume of Perfusion Solution

The amount of perfusion solution used during the procedure does not represent an experimental interferent but rather an essential component of the clinical protocol. However, the selected volume plays a crucial role, as it determines the degree of dilution of metabolites released by the organ. For instance, perfusing a liver with 1 liter of solution may yield an FMN concentration of x, whereas using 2 liters results in a lower concentration $y < x$ due to increased dilution. Therefore, defining a standardized perfusion volume is fundamental to ensure the comparability of results across different clinical centers. If clinical center X consistently uses 1 liter of solution, obtaining concentrations x_1, x_2, etc., while center Y uses 2 liters and obtains y_1, y_2, etc., the two datasets cannot be directly compared, as they are derived from non-uniform experimental protocols.

Table 6.1 summarizes the perfusion volumes reported in selected clinical studies. As shown, some studies employ 3 liters, others 4 liters, and in several cases the total volume is not even specified. This lack of standardization highlights the need for a unified approach to achieve reproducible and comparable results.

Source	Organ	Litres of perfusate
[1]	Livers	3 litres of Belzer MPS
[2]	Livers	3 litres of Belzer MPS
[6]	Livers	Not reported
[11]	Livers	Not reported
[31]	Livers	4 litres of Belzer MPS
[32]	Livers	3 litres of Belzer MPS
[33]	Livers	Not reported
[34]	Livers	Not reported
[35]	Livers	3 litres of Vasosol
[36]	Livers	Not reported

Table 6.1. Comparison of liters of perfusion solutions used in machine perfusion.

The chosen volume also depends on the organ's weight (in kilograms). To establish a uniform criterion, it is necessary to determine the average amount of FMN released per kilogram of organ (liver, kidney, intestine, etc.). Knowing this value, together with the ratio of perfusion volume per kilogram of organ, would enable the definition of a standardized guideline for selecting the optimal perfusion volume, thereby ensuring data comparability across clinical centers.

To reduce the disruptive effects of potential interferents that may perturb the perfusion volume and composition, the following approach could be implemented (**Figure 6.1**):

1. Addition of a Mixing System

Incorporating a mixer within the perfusate reservoir could ensure continuous and thorough mixing of FMN, leading to a homogeneous concentration throughout the system. Proper mixing would minimize fluctuations caused by external disturbances such as organ manipulation or flow variations.

A simple yet effective solution would involve placing the perfusate in a glass beaker equipped with a magnetic stir bar positioned on a magnetic stirrer. This setup guarantees uniform FMN distribution and reduces concentration gradients that could otherwise affect fluorescence measurements.

2. Separation Between Perfusate and Immersion Fluid

Instead of immersing the organ directly in the circulating perfusate, a dual-circuit approach could be adopted. In this configuration, both the artery and vein of the organ are cannulated: the perfusate enters through the arterial cannula, exits through the venous cannula, and is collected in a separate container where it can be continuously mixed and refrigerated.

Meanwhile, the organ itself could be immersed in a distinct preservation fluid, physically separated from the perfusate circuit.

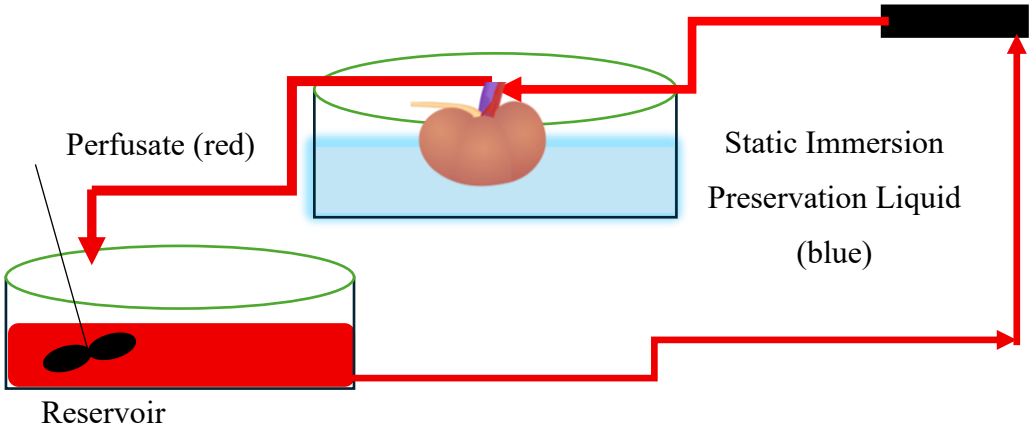

Figure 6.1. A strategy to mitigate external interferences.

Advantages of the Proposed System

- Homogeneous FMN Concentration
- Continuous magnetic stirring within the perfusate reservoir ensures that FMN remains evenly distributed at all times, leading to stable and reproducible fluorescence measurements.
- Reduced Retention and Dispersion of FMN
- By preventing the organ from being directly immersed in the perfusate, potential retention of FMN within the tissue—possibly due to a “sponge effect”—can be minimized. Although this mechanism remains hypothetical, separating the two liquids would eliminate the risk of FMN absorption or dispersion into the immersion fluid.
- Stability During Handling and Measurement
- Maintaining FMN entirely within the closed perfusion loop would prevent concentration variations when the organ is manipulated. This results in a more reliable and stable monitoring system, ensuring that any detected fluorescence variations are due to physiological factors rather than mechanical or dilutional effects.

- Simplified Perfusate Recovery and Reuse
- Since the perfusate is collected in a dedicated container, it can be easily recovered, analyzed, or reused, improving both experimental control and cost efficiency.

References

[1] Huwyler F, Eden J, Binz J, Cunningham L, Sousa Da Silva RX, Clavien P-A, et al. A Spectrofluorometric Method for Real-Time Graft Assessment and Patient Monitoring. Adv Sci. 2023;10(23):2301537. doi:10.1002/advs.202301537.

[2] Muller X, Schlegel A, Kron P, Eshmuminov D, Würdinger M, Meierhofer D, Clavien PA, Dutkowski P. Novel Real-time Prediction of Liver Graft Function During Hypothermic Oxygenated Machine Perfusion Before Liver Transplantation. Ann Surg. 2019 Nov;270(5):783-790. doi: 10.1097/SLA.0000000000003513.

[3] Sun, K., Jiao, C., Panconesi, R., Satish, S., Karakaya, O. F., De Goeijc, F. H. C.,·Diwan, T., Ali, K., Cadinu, L. A., Cazzaniga, B., Liu, Q.,·Miyazaki, Y., Pita, A., Khalil, M., Kim, J. K., Hussein, A., Müller, P. C.,·Aucejo, F.,·Kwon, D. H. C., Fernandes, E., Esfeh, J. M., Cywinski, J., Fujiki, M., Sun, L.,·Pinna, A., Dutkowski, P., Wehrle, C. J., Fairchild, R. L., Meierhofer, D., De Jonge, J., Miller, C., Hashimoto, K.,·Schlegel, A. Quantifying Flavin mononucleotide: an internationally validated methodological approach for enhanced decision making in organ transplantation. eBiomedicine, 116, 105761, 2025.

[4] Satish S., Cadinu L., Nadeem M., Sun K., Jiao C., Ali K., Karakaya O., Crasta G., Yildirim S., Walsh F., Aucejo F., Kwon D., Kim J., Pita A., Khalil M., Fujiki M., Wehrle C., Miller C., Hashimoto K., Schlegel A. A Novel Risk Score Using Flavin Mononucleotide (FMN) for Predicting Graft Loss After Liver Transplantation with Normothermic Machine Perfusion. American Journal of Transplantation. Volume 25, Issue 8, Supplement 1, S215, August 2025. 10.1016/j.ajt.2025.07.472.

[5] S. Kalinina, C. Freymueller, N. Naskar, B. von Einem, K. Reess, R. Sroka, et al. Bioenergetic Alterations of Metabolic Redox Coenzymes as NADH, FAD and FMN by Means of Fluorescence Lifetime Imaging Techniques. Int J Mol Sci. 2021 May 31;22(11):5952. doi: 10.3390/ijms22115952.

[6] Van de Leemkolk FE, Lo Faro ML, Shaheed S, Mulvey JF, Huurman VAL, Alwayn IPJ, Putter H, Jochmans I, Lindeman JHN, Ploeg RJ, et al. The role of flavin mononucleotide (FMN) as a potentially clinically relevant biomarker to predict the quality of kidney grafts during hypothermic (oxygenated) machine perfusion. PLoS ONE. 2023;18:e0287713.

[7] Sousa Da Silva RX, Darius T, Mancina L, Eden J, Wernlé K, Ghoneima AS, Barlow AD, Clavien P-A, Dutkowski P, Kron P. Real-time assessment of kidney allografts during HOPE using flavin mononucleotide (FMN)—A preclinical study. Front Transplant. 2023;2:1132673.

[8] Wang L, Thompson E, Bates L, Pither TL, Hosgood SA, Nicholson ML, Watson CJE, Wilson C, Fisher AJ, Ali S, et al. Flavin mononucleotide as a biomarker of organ quality—A pilot study. Transplant Direct. 2020;6:e600.

[9] Cadinu, L.A.; Sun, K.; Jiao, C.; Panconesi, R.; Satish, S.; Yildirim, F.S.; Karakaya, O.F.; Wehrle, C.J.; Crasta, G.S.; Fernandes, F.W.; et al. Optical Spectroscopic Detection of Mitochondrial Biomarkers (FMN and NADH) for Hypothermic Oxygenated Machine Perfusion: A Comparative Study in Different Perfusion Media. Sensors 2025, 25, 4031, https://doi.org/10.3390/s25134031.

[10] Darius T, Vergauwen M, Smith T, Gerin I, Joris V, Mueller M, Aydin S, Muller X, Schlegel A, Nath J, Ludwig C, Dessy C, Many MC, Bommer G, Dutkowski P, Gianello P, Mourad M. Brief O_2 uploading during continuous hypothermic machine perfusion is simple yet effective oxygenation method to improve initial kidney function in a porcine autotransplant model. Am J Transplant. 2020 Aug;20(8):2030-2043. doi: 10.1111/ajt.15800.

[11] Dingfelder J, Kollmann D, Rauter L, Pereyra D, Kacar S, Weijler AM, Saffarian Zadeh T, Tortopis C, Silberhumer G, Salat A, Soliman T, Berlakovich G, Györi GP. Validation of mitochondrial FMN as a predictor for early allograft dysfunction and patient survival measured during hypothermic oxygenated perfusion. Liver Transpl. 2025 Apr 1;31(4):476-488. doi: 10.1097/LVT.0000000000000512.

[12] Ali, K., Cazzaniga, B., Liu, Q., Miyazaki, Y., Tuul, M., Raj, R., Hussein, A., Wehrle, C., Zhang, M., Calderon, E., Kusakabe, J., Shanmugarajah, K., Wakam, G., Khalil, M., Pita, A., Aucejo, F., Kwon, CD., Kim, J., Fujiki, M., Miller, C., et al. Machine Perfusion or Straight to Transplant? Predictive Value of Flavin Mononucleotide Levels in Flush Solution of Human Liver Allograft. Ann Surg. 2024 Oct 25. doi: 10.1097/SLA.0000000000006576.

[13] Lee ACH, Edobor A, Lysandrou M, Mirle V, Sadek A, Johnston L, Piech R, Rose R, Hart J, Amundsen B, Jendrisak M, Millis JM, Donington J, Madariaga ML, Barth RN, di Sabato D, Shanmugarajah K and Fung J. The Effect of Normothermic Machine Perfusion on the Immune Profile of Donor Liver. *Front. Immunol* 2022. 13:788935. doi: 10.3389/fimmu.2022.788935

[14] Sousa Da Silva RX, Darius T, Mancina L, Eden J, Wernlé K, Ghoneima AS, Barlow AD, Clavien PA, Dutkowski P, Kron P. Real-time assessment of kidney allografts during HOPE using flavin mononucleotide (FMN) - a preclinical study. Front Transplant. 2023 Feb 28;2:1132673. doi: 10.3389/frtra.2023.1132673.

[15] Schlegel A, Muller X, Mueller M, Stepanova A, Kron P, de Rougemont O, Muiesan P, Clavien PA, Galkin A, Meierhofer D, Dutkowski P. Hypothermic oxygenated perfusion protects from mitochondrial injury before liver transplantation. EBioMedicine. 2020 Oct;60:103014. doi: 10.1016/j.ebiom.2020.103014. Epub 2020 Sep 24.

[16] Darius T, Vergauwen M, Maistriaux L, Evrard R, Schlegel A, Mueller M, O'Neil D, Southam A, Aydin S, Devresse A, De Meyer M, Gianello P, Ludwig C, Dutkowski P, Mourad M. Intermittent Surface Oxygenation Results in Similar Mitochondrial Protection and Maintenance of Aerobic Metabolism as Compared to Continuous Oxygenation during Hypothermic Machine Kidney Machine Perfusion. J Clin Med. 2023 May 29;12(11):3731. doi: 10.3390/jcm12113731.

[17] Blum MF, Liu Q, Soliman B, Vagefi PA. Machine Perfusion of Organs. In: Nadig S, Wertheim J, editors. Technological Advances in Organ Transplantation. Cham: Springer; 2017. p. 11-30. https://doi.org/10.1007/978-3-319-62142-5_2.

[18] Holzer W, Shirdel J, Zirak P, Penzkofer A, Hegemann P, Deutzmann R, et al. Photo-induced degradation of some flavins in aqueous solution. **Chem Phys**. 2005;308(1–2):69–78. doi:10.1016/j.chemphys.2004.08.006.

[19] Smith EC, Metzler DE. The photochemical degradation of riboflavin. **J Am Chem Soc**. 1963;85:3367.

[20] Moore WM, Spence JT, Reymond FA, Colson SD. Photochemistry of Riboflavin. I. The Hydrogen Transfer Process in the Anaerobic Photobleaching of Flavins. **J Am Chem Soc**. 1963;85:3367. doi:10.1021/ja00904a013.

[21] Hemmerich P, Veeger C, Wood HCS. Fortschritte in Chemie und Molekularbiologie der Flavine und Flavocoenzyme. **Angew Chem**. 1965;77:699. doi:10.1002/ange.19650771604.

[22] Sigma Aldrich. Riboflavin Sodium Phosphate Hydrate. Product code: 77623-50G-F www.sigmaaldrich.com/US/en/sds/sial/77623?userType=anonymous

[23] Rouslin W, Ranganathan S. Impaired function of mitochondrial electron transfer complex I in canine myocardial ischemia: Loss of flavin mononucleotide. J Mol Cell Cardiol. 1983;15(8):537-42. doi:10.1016/0022-2828(83)90329-2.

[24] Holt PJ, Efremov RG, Nakamaru-Ogiso E, Sazanov LA. Reversible FMN dissociation from *Escherichia coli* respiratory complex I. Biochim Biophys Acta Bioenerg. 2016;1857(11):1777-85. doi:10.1016/j.bbabio.2016.08.008.

[25] Ten V, Galkin A. Mechanism of mitochondrial complex I damage in brain ischemia/reperfusion injury. A hypothesis. *Mol Cell Neurosci*. 2019;100:103408. doi:10.1016/j.mcn.2019.103408.

[26] Yoval-Sánchez B, Guerrero I, Chen Q, Sosunov S, Ansari F, Siragusa M, Konrad C, Niatsetskaya Z, Stepanova A, Starkov AA, Khruschev S, Magrane J, Nikitina AA, Bereshchenko O, Zhou P, Zhou L, Szibor M, Wittig I, Manfredi G, Gross SS, Ten V, Galkin A. Rescuing Ischemic Brain Injury by Rewiring Mitochondrial Electron Flow. bioRxiv [Preprint]. 2025 Sep 22:2025.05.19.650489.

[27] Jeddou H, Tzedakis S, Chaouch MA, Sulpice L, Samson M, Boudjema K. Viability Assessment During Normothermic Machine Liver Perfusion: A Literature Review. *Liver Int*. 2025;45:e16244.

[28] Parente A, Osei-Bordom DC, Ronca V, Perera MTPR, Mirza D. Organ Restoration With Normothermic Machine Perfusion and Immune Reaction. Front Immunol. 2020 Oct 19;11:565616. doi: 10.3389/fimmu.2020.565616.

[29] López-Martínez S, Simón C, Santamaria X. Normothermic Machine Perfusion Systems: Where Do We Go From Here? Transplantation. 2024 Jan 1;108(1):22-44. doi: 10.1097/TP.0000000000004573.

[30] Fernandes FW, Yildirim FS, Horie H, Karakaya OF, Jiao C, Crasta GS, Eshraghi N, Takase K, Diwan T, Batista de Oliveira L, et al. Beyond Static Cold Storage: Toward the Next Generation of Tailored Organ Preservation Solutions. *International Journal of Molecular Sciences*. 2025; 26(19):9515. https://doi.org/10.3390/ijms26199515.

[31] van Rijn R, Schurink IJ, de Vries Y, van den Berg AP, Cortes Cerisuelo M, Darwish Murad S, Erdmann JI, Gilbo N, de Haas RJ, Heaton N, van Hoek B, Huurman VAL, Jochmans I, van Leeuwen OB, de Meijer VE, Monbaliu D, Polak WG, Slangen JJG, Troisi RI, Vanlander A, de Jonge J, Porte RJ. Hypothermic machine perfusion in liver transplantation — a randomized trial. N Engl J Med. 2021;384:1391–1401.

[32] Schlegel A, Mueller M, Muller X, Eden J, Panconesi R, von Felten S, et al. A multicenter randomized-controlled trial of hypothermic oxygenated perfusion (HOPE) for human liver grafts before transplantation. *J Hepatol*. 2023;78:783-793. doi:10.1016/j.jhep.2022.12.030.

[33] Nastase AG, Vasilescu AM, Trofin AM, Zabara M, Cadar R, Vasiluta C, Vlad N, Ciuntu BM, Lupascu Ursulescu C, Muzica C, et al. Hypothermic Machine Perfusion Is Associated with Improved Short-Term Outcomes in Liver Transplantation: A Retrospective Cohort Study. *Life*. 2025; 15(7):1112. https://doi.org/10.3390/life15071112

[34] Brüggenwirth IMA, Mueller M, Lantinga VA, Camagni S, De Carlis R, De Carlis L, Colledan M, Dondossola D, Drefs M, Eden J, Ghinolfi D, Koliogiannis D, Lurje G, Manzia TM, Monbaliu D, Muiesan P, Patrono D, Pratschke J, Romagnoli R, Rayar M, Roma F, Schlegel A, Dutkowski P, Porte RJ, de Meijer VE. Prolonged preservation by hypothermic machine perfusion facilitates logistics in liver transplantation: A European observational cohort study. Am J Transplant. 2022 Jul;22(7):1842-1851. doi: 10.1111/ajt.17037.

[35] Panayotova GG, Lunsford KE, Quillin RC 3rd, Rana A, Agopian VG, Lee-Riddle GS, et al. Portable hypothermic oxygenated machine perfusion for organ preservation in liver transplantation: A randomized, open-label, clinical trial. *Hepatology*. 2024;79(5):1033-1047. doi:10.1097/HEP.0000000000000715.

[36] Ravaioli M, De Pace V, Angeletti A, et al. Hypothermic Oxygenated New Machine Perfusion System in Liver and Kidney Transplantation of Extended Criteria Donors:First Italian Clinical Trial. *Sci Rep*. 2020;10:6063. doi:10.1038/s41598-020-62979-9.

Conclusions

The increase and aging of the global population, combined with the progressive rise in life expectancy and the growing incidence of obesity and other chronic diseases, are leading to a significant rise in the demand for transplantable organs. However, the current availability of donors is insufficient to meet this demand, resulting in a profound imbalance between supply and demand on a global scale. This situation translates into increasingly long waiting lists, a high mortality rate among patients awaiting transplantation, and, unfortunately, a rise in illegal practices related to organ trafficking.

The current gold-standard method for organ preservation is static cold storage (SCS). This technique, widely used in clinical practice, consists of immersing the organ in a preservation saline solution that helps maintain the stability of the cellular and tissue environment. The addition of ice lowers the temperature, thereby slowing down metabolic processes and reducing damage caused by the absence of oxygen and nutrients. Cooling effectively decreases the rate of biochemical reactions responsible for ischemic injury, temporarily preserving the structural and functional integrity of the organ.

In recent years, however, machine perfusion has been re-evaluated and increasingly adopted as an alternative preservation method. Initially developed as a research tool for studying organs *ex situ*, this technique has demonstrated clear advantages over traditional SCS. Numerous studies have shown that organs subjected to perfusion — whether hypothermic, normothermic, or in combined modes — exhibit superior functional performance and higher post-transplant survival rates compared to those preserved exclusively by SCS.

In Chapter II, an in-depth and comprehensive review of the literature on machine perfusion was conducted, with the aim of outlining the current state of the art and identifying the main directions of development in this field. The medical community's interest in this technology is now extremely broad, as evidenced by the large number of scientific papers, reviews, and conferences devoted exclusively to the topic.

Machine perfusion has reached a remarkable level of technological maturity. A wide variety of devices are now available, designed for the perfusion of different organs and operating under hypothermic, normothermic, or combined conditions. The intensity of research and development activity is reflected in the presence of multiple commercial versions from the same manufacturer, as well as the continuous introduction of new models to the market.

The current trend is the development of increasingly autonomous and integrated systems, capable of automatically monitoring and regulating key perfusion parameters such as dissolved oxygen, flow rate, CO_2 and glucose concentration, pH, and the presence of relevant biomarkers. Looking ahead, artificial intelligence is expected to play a pivotal role in the automatic control of perfusion processes and in the prediction of post-transplant outcomes, paving the way for machines capable of dynamically adapting perfusion conditions in real time according to the characteristics of the organ being treated.

The analysis of the literature also highlights a strong and growing interest in the development of new perfusion and static preservation solutions, as well as in the optimization of existing ones. However, several critical questions remain open, particularly regarding the definition of the optimal perfusion parameters — including perfusion duration, oxygenation levels, perfusate volume, and pumping modality (centrifugal or pulsatile).

Furthermore, the identification of the ideal perfusion protocol — not only for the liver but also for other transplantable organs — remains an active topic of debate. Despite the large body of scientific literature available, many questions still lack a definitive answer. Considering these aspects is essential, as they can guide biomedical engineers and clinicians in the development of more targeted and personalized strategies for organ preservation and viability assessment.

The main advantage of machine perfusion, particularly normothermic perfusion, lies in its ability to evaluate organ functionality in real time before transplantation. This represents a substantial advancement in transplant medicine, as it enables clinicians to make a more reliable assessment of organ viability and to predict post-transplant outcomes with greater accuracy. Within this context, the need to establish objective evaluation criteria has become increasingly evident — specifically, the identification of metabolic biomarkers capable of reflecting both the functional and mitochondrial status of the tissue.

Ischemia-reperfusion injury (I/R), an unavoidable event during the donation and transplantation process, remains one of the major causes of organ dysfunction. This type of injury particularly affects the mitochondria, leading to both structural and functional alterations of Complex

I within the respiratory chain. One of the consequences of such mitochondrial damage is the release of flavin mononucleotide (FMN) into the perfusion medium, an event that has been shown to correlate strongly with mitochondrial vitality and, consequently, with the overall functional integrity of the organ.

Several studies have confirmed that the concentration of FMN in the perfusate serves as an early and reliable biomarker of mitochondrial injury, with elevated levels being associated with a higher risk of post-transplant dysfunction. In parallel, NADH has also gained increasing attention, as it is a key coenzyme involved in cellular respiration and energy metabolism.

Both molecules — FMN and NADH — are now recognized as critical parameters for assessing mitochondrial viability and functionality during machine perfusion, paving the way for the development of innovative quantitative real-time monitoring methodologies aimed at improving organ evaluation and preservation prior to transplantation.

It therefore emerges the need to develop a simple, rapid, and cost-effective method for detecting FMN and NADH in the perfusion medium during *machine perfusion*. Currently, in several clinical centers worldwide, these molecules are monitored by sampling the perfusate and analyzing it using bench-top spectrophotometers, through fluorescence, UV-Visible absorption, or microplate reader techniques. Such analyses can be performed either during perfusion or after transplantation.

Some researchers have already tested real-time FMN detection directly in the perfusion liquid, without sampling, by monitoring the fluorescence signal and correlating it with concentration. However, these approaches allowed only a qualitative assessment of the fluorescence signal rather than an accurate quantification of FMN concentration.

This doctoral thesis aims to address this limitation by testing and improving an existing stand-alone device capable of detecting fluorescence and quantifying in real time the FMN concentration in the perfusate.

To achieve this goal, Chapter III presents an in-depth and comprehensive spectrophotometric analysis of FMN (including NADH).

Our study represents a fundamental first step aimed at characterizing the absorption and fluorescence spectroscopy of FMN and NADH in various clinically relevant perfusion media, under controlled laboratory conditions. No human or animal organs were used at this initial stage, in order to isolate and thoroughly understand the spectroscopic behavior of the mitochondrial biomarkers in

the different media. Each perfusion solution has a distinct chemical composition, and our priority was to investigate the spectrophotometric behavior of the two analytes when dissolved in different media.

We fully agree that validation of the method in a real clinical setting—through the analysis of perfusate samples from actual organ perfusion—is a crucial step to demonstrate its full applicability. However, such validation requires resources and an experimental design that go beyond the scope of this preliminary work, and would deserve a dedicated follow-up study, possibly in collaboration with clinical centers.

Moreover, we are aware that substances such as bilirubin, creatinine, hemoglobin, cells, tissue fragments, and phenolic compounds (e.g., quercetin) may potentially interfere with spectroscopic measurements. However, the aim of the present study was to systematically analyze the optical response of FMN and NADH in perfusion media in the absence of such interferents, in order to establish a solid and reproducible reference model.

A thorough investigation into the effect of interferents would require a detailed and extensive analysis, which we believe is more appropriate for an independent study, given the complexity and number of variables involved.

Although this study does not present a ready-to-use real-time monitoring device, we are convinced that it lays essential theoretical and practical foundations for the development of such a system, especially for applications in organ perfusion prior to transplantation, and could be useful for the scientific community working in the field.

To illustrate this point clearly, let us consider a practical example: suppose we aim to develop an optical sensor to detect FMN and NADH in the perfusate of an organ preservation system. The first question would be: which optical technique should we use—fluorescence or absorbance? Chapter III provides an evidence-based answer.

Figures 3.3.12 and **3.3.13** of Chapter III show that fluorescence is a highly effective method for detecting FMN, as it exhibits linear behavior and can be excited at 450–455 nm with minimal interference from NADH. Conversely, fluorescence is less suitable for NADH, as it presents saturation effects at concentrations above ~100 μg mL^{-1}, regardless of excitation wavelength. Absorbance, on the other hand, shows a linear response for NADH even at higher concentrations. This leads to a crucial design recommendation: a dual-mode optical system should be implemented, enabling both absorbance and fluorescence detection. Given the geometric differences in optimal optical path design (90° for fluorescence, 180° for absorbance), this has non-trivial implications for sensor layout.

As noted by Müller et al. (2019) and Huwyler et al. (2023) cited in Chapter III, a first-generation real-time detection system has already been developed. However, in their work, fluorescence was calibrated for NADH without exploring the saturation effect at high concentrations, possibly because their calibration range was narrower than ours. Had they tested concentrations above 100–150 μg mL^{-1}, especially in liver perfusion (where NADH can exceed 200 μg mL^{-1}), signal saturation would likely have emerged as a limiting factor. This is not just a theoretical concern—it underscores the need to rely on absorbance for NADH detection in specific clinical contexts.

A second critical point is the choice of excitation wavelengths. Our results from Chapter III (**Figures 3.3.1** and **3.3.9**) clearly show that optimal excitation occurs at 455 nm for FMN and 340 nm for NADH. This is a key consideration when selecting light sources, especially if LED or laser diodes are to be used. Using non-optimal wavelengths—as done in some literature studies (e.g., 405 nm or 485 nm for FMN)—would require longer integration times to achieve the same signal quality. Furthermore, optimizing the excitation wavelength not only improves the selectivity and signal quality, but also directly reduces the required integration time. This is a key parameter for achieving high-frequency, real-time monitoring without overloading the processing capabilities of portable and cost-effective acquisition systems.

In our ongoing hardware development (not mentioned in this manuscript), we have encountered this exact trade-off: extending the integration time to compensate for suboptimal excitation is not feasible with the microcontroller-based architecture we are using. Therefore, our current hardware design is based on the specific theoretical findings reported in this manuscript.

We also highlight another novel and important aspect: spectral shape analysis. While Müller et al. and Huwyler et al. rely on the area under the curve (AUC) for quantification, this approach can be problematic. If other substances in the perfusate absorb at similar wavelengths or emit overlapping fluorescence, the AUC alone cannot distinguish their contributions. This becomes especially relevant if exogenous substances (e.g., antioxidants, flavonoids, other flavins) are introduced during perfusion. For this reason, we propose the future development of machine learning models capable of resolving overlapping spectra and performing classification/regression based on full-spectrum data. While of our presented in Chapter III does not implement those algorithms, it provides a theoretical justification for why such approaches will be essential in future sensor development.

In Chapter IV we introduced a real-time sensor prototype inspired by the results presented here. Without this preliminary characterization of spectral behavior, excitation/emission interactions, and concentration-dependent effects, it would have been extremely difficult to make informed

engineering choices or to avoid the limitations seen in previous designs. We would respectfully point out that a thorough phenomenological understanding must precede technical implementation. Unfortunately, due to industrial secrecy, non-disclosure agreements and IP protection concerns, we are currently unable to disclose hardware details. Therefore, our work presented in Chapter III forms the scientific basis of the device now under development.

The presentation of the prototype in Chapter IV is intentionally concise, as it serves solely to illustrate the operating principle and basic logic of the system. This limitation is necessary because the device is the property of a third party, and therefore certain technical aspects cannot be disclosed. The doctoral research conducted on this prototype was primarily focused on two key directions. The first goal was the development of a scientifically rigorous and robust calibration method to ensure the reliability of the measurements. To this end, a thorough analysis was carried out on factors that may appear secondary but have a significant influence on the final results, such as fluid dynamic effects within the optical system. In addition, the measurement repeatability and the impact of experimental variance were carefully investigated to assess the stability and accuracy of the device. This phase was essential for determining the reliability of the measurements and for understanding whether fluctuations could compromise the overall quality of the acquired data. A spectral identification criterion was also developed, enabling the prototype to autonomously analyze and recognize fluorescence spectra with high accuracy, without the need for any training examples. This represents a significant advantage over traditional machine learning classification algorithms, which generally require large training datasets to operate effectively. In our case, the classification relies on a deterministic sequence of criteria that ensures reliable spectral identification even in the absence of pre-trained models.

The most innovative aspect of this PhD work concerns the implementation of well-established machine learning algorithms, such as XGBoost (although neural networks or Random Forest models could also be employed effectively), for the real-time quantification of FMN concentration. This approach enables the device to autonomously compute the FMN concentration during measurement, without the need for human supervision.

The innovation lies not only in the autonomous computation but also in the built-in validation mechanism of the estimated result. By combining calibration curves with spectral reconstruction, the system compares the theoretical spectrum corresponding to the estimated concentration with the experimentally measured one. This allows the device to verify whether the computed concentration is consistent and reliable. As a result, the device can autonomously recognize potential measurement

inconsistencies, representing a significant step toward a fully automated and self-validating analysis system.

Naturally, some limitations were also identified. The calibration range used during testing was limited to 11.88–237 ng mL^{-1}, which should ideally be extended beyond 500 ng mL^{-1} to cover a broader concentration interval. Furthermore, the presence of optical interferents, particularly trace amounts of blood, can compromise spectral measurements due to absorption and scattering effects. Although, in theory, hypothermic machine perfusion should ensure that the organ is fully washed and free of blood, in clinical practice this condition is not always met. For this reason, it is recommended to perform a thorough organ wash and to include blood filters in the perfusion circuit, in order to minimize residual blood contamination and thus improve the accuracy and reliability of the fluorescence-based measurement. Furthermore, the optimal performance of the device was demonstrated, confirming its suitability for potential clinical application. An important limitation of the prototype is that, for confidential reasons, it was not possible to test its performance in the detection of NADH.

In Chapter V, we presented the temporal evolution of FMN release, both in animal and human organs. However, data from human samples were not disclosed, as authorization for publication was not granted. A particularly relevant finding from this analysis is that each organ exhibited a unique FMN release pattern over time. The observed FMN trends appeared to be organ-specific and independent of external macroscopic variables such as ischemia time, cause of death, age, weight, sex, or the presence of underlying diseases. Instead, they seem to be driven by intrinsic metabolic factors that remain largely unexplored. This observation currently makes it impossible to establish a deterministic or predictive mathematical model capable of accurately describing the time evolution of FMN concentration based on the initial perfusion measurements. The FMN dynamics appear to follow nonlinear and unpredictable behaviors that do not conform to simple kinetic assumptions. Nonetheless, a deterministic modeling approach was explored in this study as a conceptual exercise aimed at providing an approximate interpretation of FMN release. We are fully aware of the limitations of this method, which proves effective only in certain conditions. More advanced approaches, particularly statistical or black-box models based on machine learning techniques, could offer more accurate descriptions of such complex phenomena. However, our intent was to lay the groundwork for future studies by proposing a preliminary and physically interpretable model of FMN dynamics. Finally, we demonstrated that FMN concentration can serve as an informative parameter for predicting post-transplant outcomes when integrated into score-based evaluation models. This

finding reinforces the role of FMN as a clinically relevant metabolic biomarker, potentially useful for improving organ assessment during machine perfusion.

Future Directions

Based on the findings of this work, several research directions are proposed for future development:

- **Expand the spectrophotometric characterization of FMN and NADH**, systematically evaluating the influence of potential interferents in the perfusion medium such as bilirubin, creatinine, quercetin, antibiotics, and anticoagulants.
- **Implement more robust and generalizable machine learning algorithms** to improve the accuracy and reliability of FMN and NADH concentration estimation, even in the presence of instrumental noise or biological variability.
- **Develop advanced classification models** capable of distinguishing NADH fluorescence from other molecules emitting within the same spectral range, thereby enhancing analytical specificity.
- **Enhance the use of real-time and online monitoring devices**, improving their sensitivity, stability, and adaptability to complex clinical conditions.
- **Continue investigating new modeling strategies for FMN and NADH release**, combining deterministic, physics-based models with statistical and machine learning approaches to better describe the underlying kinetics.
- **Develop and test novel mathematical methods** to predict FMN release profiles during prolonged perfusion times, aiming to identify potential functional relationships between FMN and other measurable parameters.
- **Integrate score-based predictive models directly into perfusion devices**, combining both FMN and NADH concentrations to anticipate post-transplant outcomes in real time during organ perfusion.

Making projections about the future evolution of the transplantation field is extremely challenging.

As of 2025, looking back over the past decade, remarkable progress has been achieved, and it is reasonable to expect that even more innovative developments will emerge in the near future.

Machine perfusion is already being used not only for organ preservation but also for organ regeneration. Consider, for example, a portion of a donor liver damaged by disease: it can be explanted and kept viable through an extracorporeal perfusion system. A computer automatically monitors and regulates the liver perfusion using a solution containing oxygenated blood and nutrients, while clinicians apply regenerative therapies. Once its function has been restored, the organ can be re-transplanted.

In this context, real-time monitoring of biomarkers such as FMN, NADH, and others is essential to assess the organ's viability and guide therapeutic interventions. Similarly, one can envision applications in the cultivation of artificial tissues and organs, where continuous perfusion and biomarker monitoring through spectrometric techniques—such as those employed in this thesis—will likely play a central role. It is conceivable that, in the not-so-distant future, computer-controlled systems could automatically repair or cultivate tissues and organs, relying on spectrophotometric analyses to detect, quantify, and monitor in real time the organ's functional status and stage of regeneration.

In conclusion, this doctoral work establishes both theoretical and experimental foundations for the development of new-generation monitoring systems for organ perfusion. By combining spectrophotometric characterization, algorithmic innovation, and experimental validation, it contributes to bridging the gap between engineering and transplantation medicine. Future developments integrating multi-parametric sensing and artificial intelligence will likely transform machine perfusion from a static preservation technique into a truly smart and adaptive platform for organ assessment and optimization prior to transplantation.

Appendix A

Table 1 presents data of fluorescence for concentrations of 59.4 ng mL^{-1} at 530 nm, 83.16 ng mL^{-1} at 570 nm, and 142.56 ng mL^{-1} at 590 nm and 154.44 ng mL^{-1} at 585 nm considering all data from aggregated trials. **Figures 1a-h** , and show the data distributions and corresponding QQ-plots.

Basic Statistics	Parameter	59.4 ng/mL at 530 nm	83.16 ng/mL at 570 nm	142.56 ng/mL at 590 nm	154.44 ng/mL at 585 nm
	Mean	207.44	228.18	227.88	288.49
	Median	207.0	228.0	226.0	288.0
	Standard Deviation	7.87	8.97	11.21	11.03
	Coefficient of Variation	3.79%	3.93%	4.92%	3.82%
	Range	42	48	64	56
	95% Confidence Interval	(206.78, 208.09)	(227.41, 228.96)	(227.02, 228.75)	(287.58, 289.40)
Distribution Analysis	Skewness	-0.0501	0.1243	0.4503	0.2034
	Kurtosis	-0.428	-0.212	-0.255	-0.721
	Maximum Divergence (x)	208.0	228.0	230.7	292.2
Distribution Divergence Analysis (Real vs Gaussian)	Total Divergence Area	0.0965	0.0848	0.1937	0.1891
	KDE Peak	206.1	231.3	222.5	282.6
	Interpretation	Almost normal	Almost normal	Moderate deviations	Moderate deviations
	Shapiro–Wilk Statistic	0.994	0.995	0.98	0.983
	Shapiro–Wilk p-value	0.041	0.059	0.00	0.00
Robustness Analysis	IQR	11.0	12.0	15.0	17.0
	Lower Limit	185.5	204.0	197.5	254.50
	Upper Limit	229.5	252.0	257.5	322.5
	Outliers Detected	None	[254]	[263, 259, 261, 259]	None
Dataset Info	Number of Scans	549	520	649	565

Table 1. Analysis of the measurement quality and repeatability of the fluorescence signal at different wavelengths and concentrations.

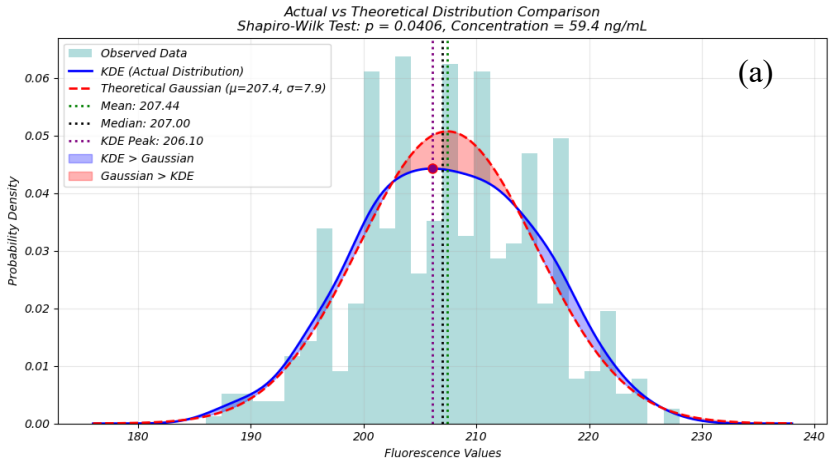
Actual vs Theoretical Distribution Comparison
Shapiro-Wilk Test: p = 0.0406, Concentration = 59.4 ng/mL
(a)
Observed Data
KDE (Actual Distribution)
Theoretical Gaussian (μ=207.4, σ=7.9)
Mean: 207.44
Median: 207.00
KDE Peak: 206.10
KDE > Gaussian
Gaussian > KDE
Probability Density
Fluorescence Values

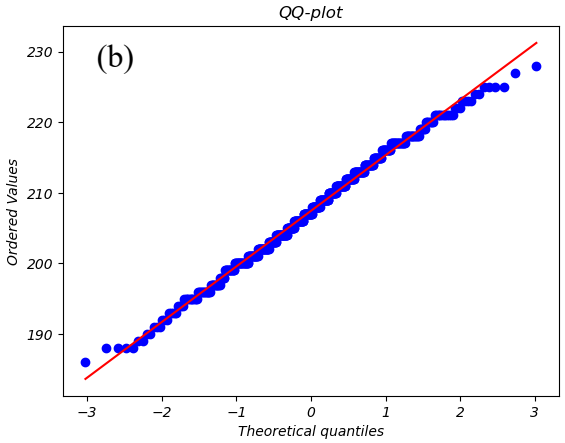
QQ-plot
(b)
Ordered Values
Theoretical quantiles

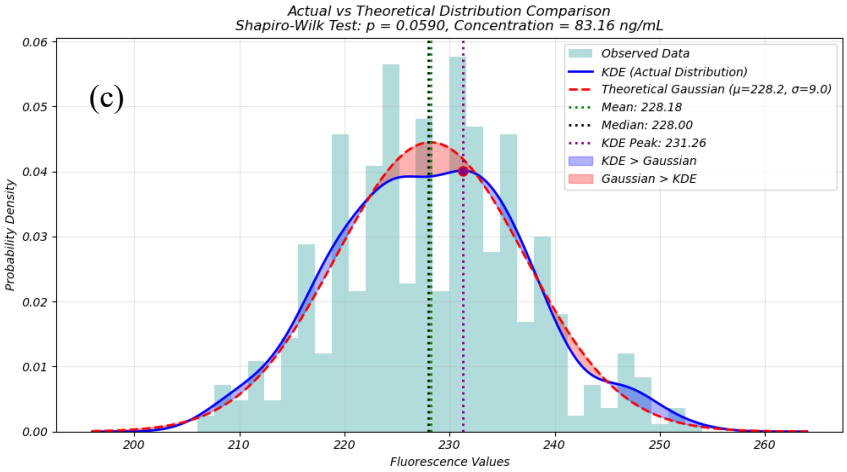
Actual vs Theoretical Distribution Comparison
Shapiro-Wilk Test: p = 0.0590, Concentration = 83.16 ng/mL
(c)
Observed Data
KDE (Actual Distribution)
Theoretical Gaussian (μ=228.2, σ=9.0)
Mean: 228.18
Median: 228.00
KDE Peak: 231.26
KDE > Gaussian
Gaussian > KDE
Probability Density
Fluorescence Values

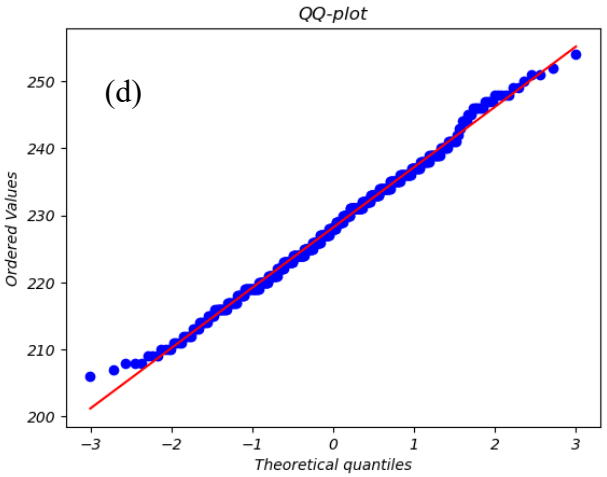
QQ-plot
(d)
Ordered Values
Theoretical quantiles

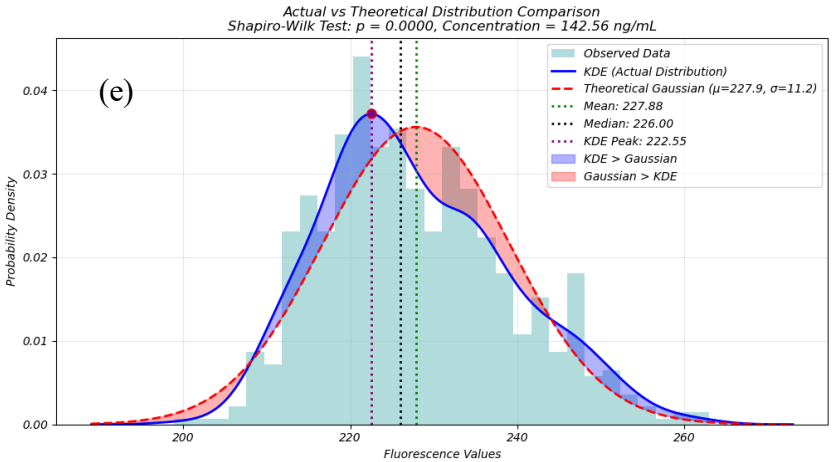
Actual vs Theoretical Distribution Comparison
Shapiro-Wilk Test: p = 0.0000, Concentration = 142.56 ng/mL
(e)
Observed Data
KDE (Actual Distribution)
Theoretical Gaussian (μ=227.9, σ=11.2)
Mean: 227.88
Median: 226.00
KDE Peak: 222.55
KDE > Gaussian
Gaussian > KDE
Probability Density
Fluorescence Values

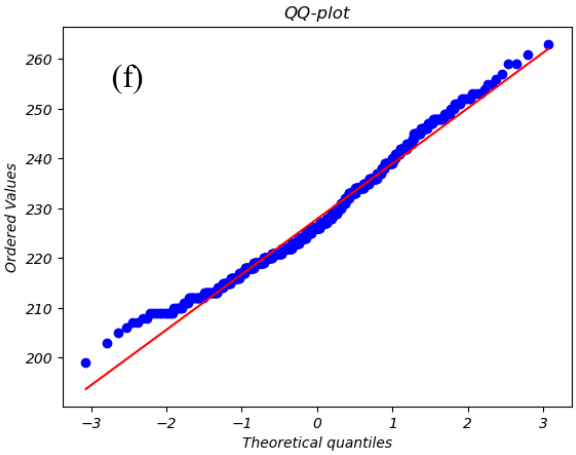
QQ-plot
(f)
Ordered Values
Theoretical quantiles

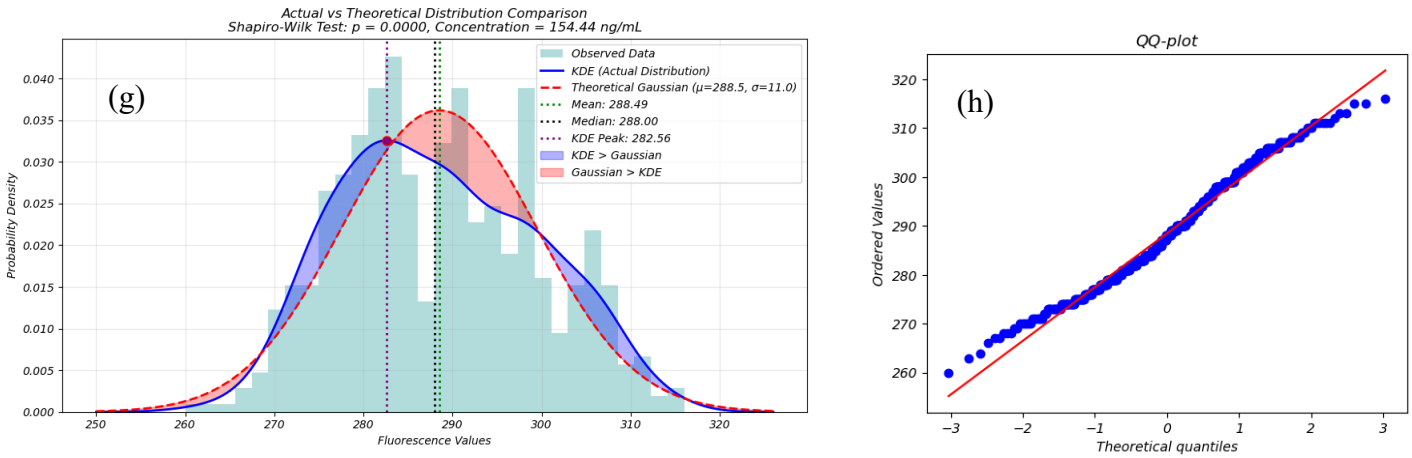

Figure 1. Data for the concentration of 59.4 ng mL^{-1} at 530 nm, 83.16 ng mL^{-1} at 570 nm, and 142.56 ng mL^{-1} at 590 nm and 154.44 ng mL^{-1} at 585 nm.

For the concentration of 59.40 ng mL^{-1} at 530 nm, the measurements exhibit good stability, with a mean of 207.44 and a low standard deviation (7.87), corresponding to a coefficient of variation of 3.79%. The confidence interval is relatively narrow, indicating high precision of the estimates. However, the Shapiro-Wilk test shows a slight deviation from normality ($p = 0.041$), suggesting that the data distribution is not perfectly Gaussian. Robustness analysis indicates a small IQR (11.00) and no outliers, confirming that the data are concentrated around the mean value and that the instrument performed stably.

For the concentration of 83.16 ng mL^{-1} at 570 nm, the mean (228.18) and standard deviation (8.97) again indicate high precision, with a coefficient of variation of 3.93%, similar to the previous case. Here, the Shapiro-Wilk test does not indicate deviations from normality ($p = 0.059$), so the data can be considered normally distributed. Robustness analysis shows a slightly wider IQR (12.00) and a single outlier (254), which does not compromise the overall measurement stability.

For the concentration of 142.56 ng mL^{-1} at 590 nm, the mean (227.88) is associated with a higher standard deviation (11.21) and a coefficient of variation of 4.92%, indicating slightly lower precision compared to the previous cases. The confidence interval remains narrow, but the Shapiro-Wilk test reveals a significant deviation from normality ($p < 0.001$), suggesting that the data distribution is not perfectly Gaussian. Robustness analysis indicates a wider IQR (15.00) and several outliers (263, 259, 261, 259), reflecting greater fluctuations at this concentration. By filtering the data and removing outliers, the distribution is expected to approximate a Gaussian. This discrepancy is attributable to

operator-induced experimental error, not the instrument, as similar anomalies would have appeared for other wavelengths and concentrations otherwise.

Figures 2a-ab show data distribution of fluorescence emitted at 523 nm for the concentration of 106.92 ng mL^{-1} in different trials.

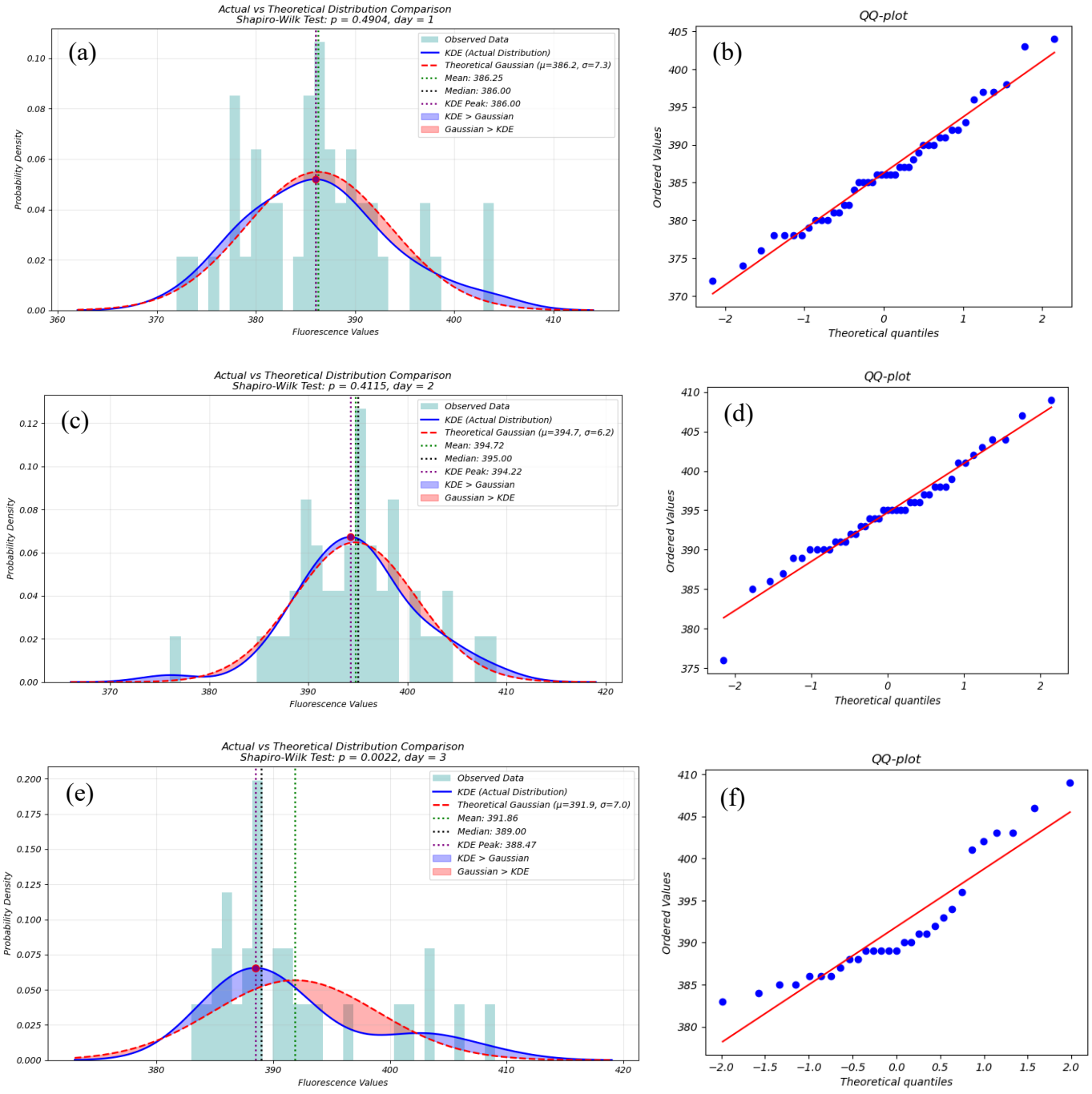

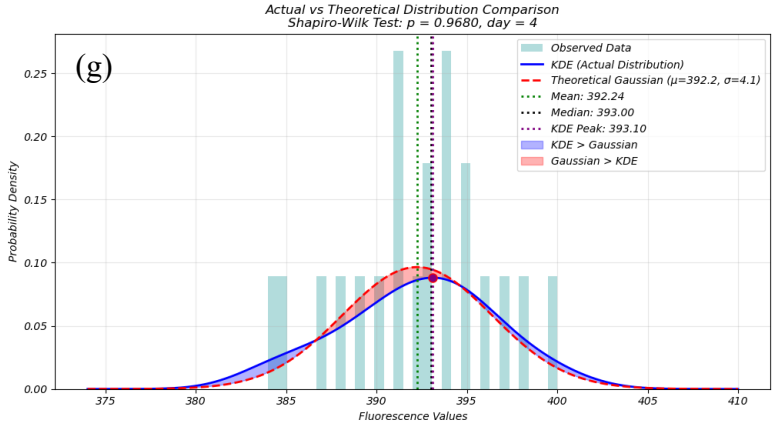
Actual vs Theoretical Distribution Comparison
Shapiro-Wilk Test: p = 0.9680, day = 4
(g)
Observed Data
KDE (Actual Distribution)
Theoretical Gaussian (μ=392.2, σ=4.1)
Mean: 392.24
Median: 393.00
KDE Peak: 393.10
KDE > Gaussian
Gaussian > KDE
Probability Density
Fluorescence Values

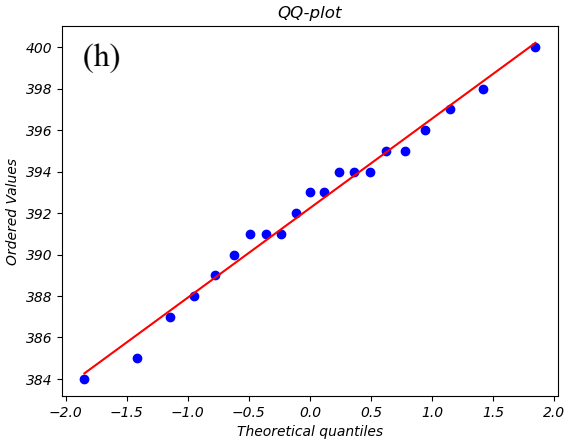
QQ-plot
(h)
Ordered Values
Theoretical quantiles

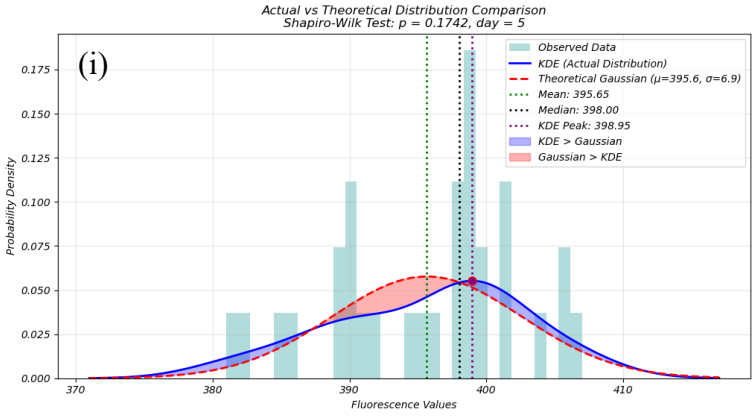
Actual vs Theoretical Distribution Comparison
Shapiro-Wilk Test: p = 0.1742, day = 5
(i)
Observed Data
KDE (Actual Distribution)
Theoretical Gaussian (μ=395.6, σ=6.9)
Mean: 395.65
Median: 398.00
KDE Peak: 398.95
KDE > Gaussian
Gaussian > KDE
Probability Density
Fluorescence Values

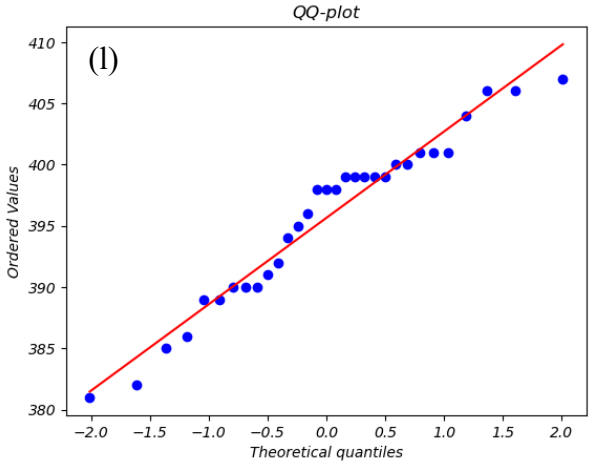
QQ-plot
(l)
Ordered Values
Theoretical quantiles

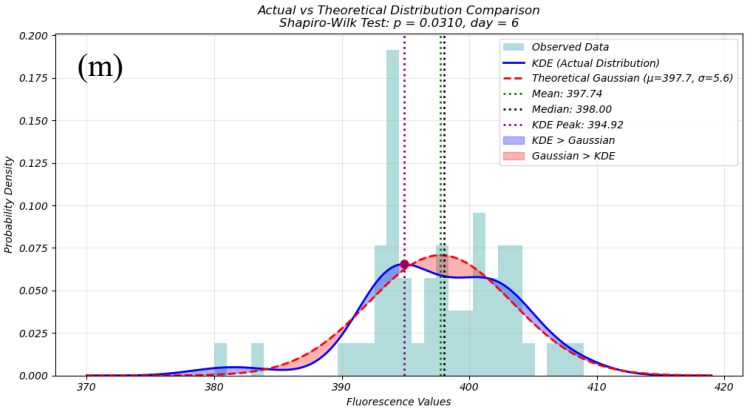
Actual vs Theoretical Distribution Comparison
Shapiro-Wilk Test: p = 0.0310, day = 6
(m)
Observed Data
KDE (Actual Distribution)
Theoretical Gaussian (μ=397.7, σ=5.6)
Mean: 397.74
Median: 398.00
KDE Peak: 394.92
KDE > Gaussian
Gaussian > KDE
Probability Density
Fluorescence Values

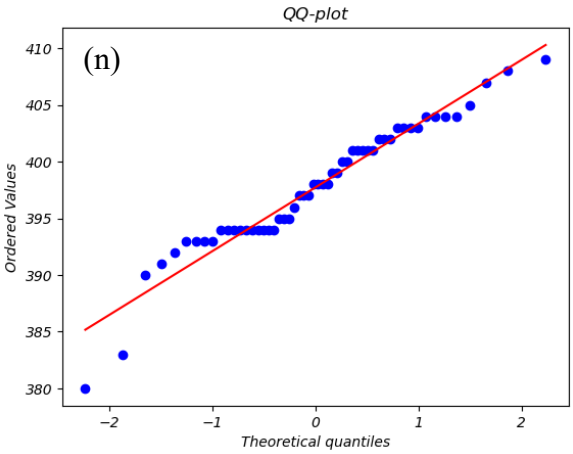
QQ-plot
(n)
Ordered Values
Theoretical quantiles

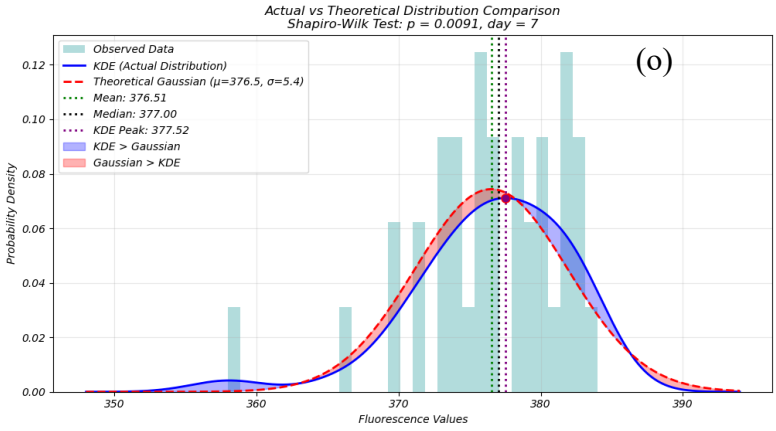
Actual vs Theoretical Distribution Comparison
Shapiro-Wilk Test: p = 0.0091, day = 7
(o)
Observed Data
KDE (Actual Distribution)
Theoretical Gaussian (μ=376.5, σ=5.4)
Mean: 376.51
Median: 377.00
KDE Peak: 377.52
KDE > Gaussian
Gaussian > KDE
Probability Density
Fluorescence Values

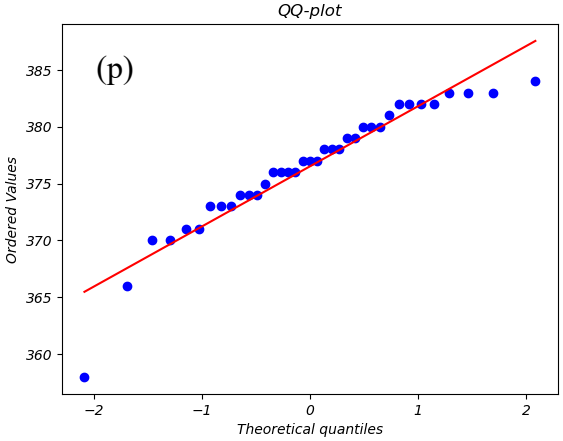
QQ-plot
(p)
Ordered Values
Theoretical quantiles

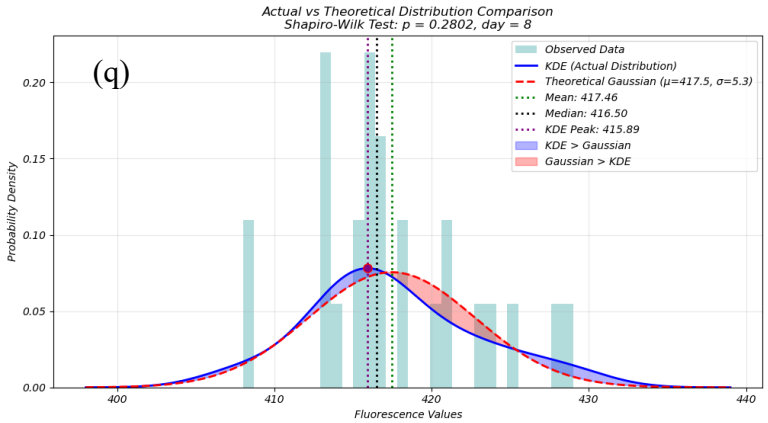
Actual vs Theoretical Distribution Comparison
Shapiro-Wilk Test: p = 0.2802, day = 8
(q)
Observed Data
KDE (Actual Distribution)
Theoretical Gaussian (μ=417.5, σ=5.3)
Mean: 417.46
Median: 416.50
KDE Peak: 415.89
KDE > Gaussian
Gaussian > KDE
Probability Density
Fluorescence Values

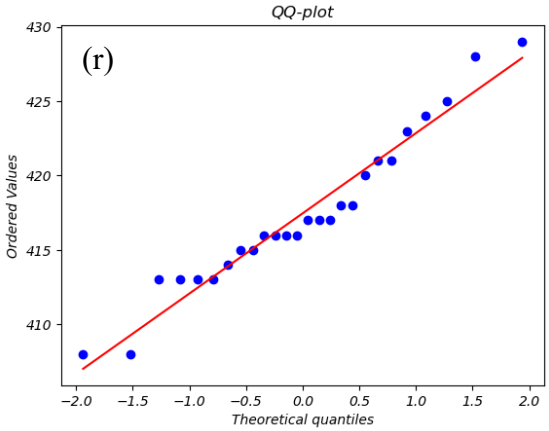
QQ-plot
(r)
Ordered Values
Theoretical quantiles

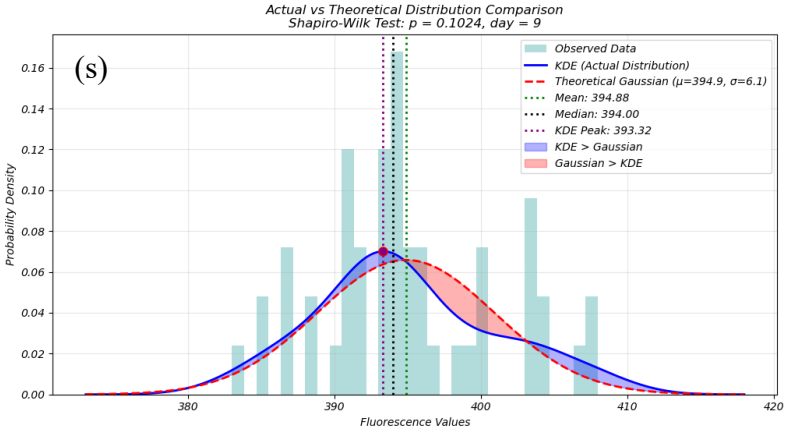
Actual vs Theoretical Distribution Comparison
Shapiro-Wilk Test: p = 0.1024, day = 9
(s)
Observed Data
KDE (Actual Distribution)
Theoretical Gaussian (μ=394.9, σ=6.1)
Mean: 394.88
Median: 394.00
KDE Peak: 393.32
KDE > Gaussian
Gaussian > KDE
Probability Density
Fluorescence Values

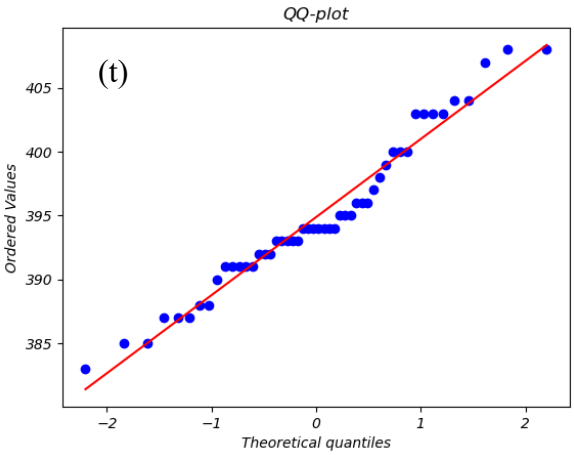
QQ-plot
(t)
Ordered Values
Theoretical quantiles

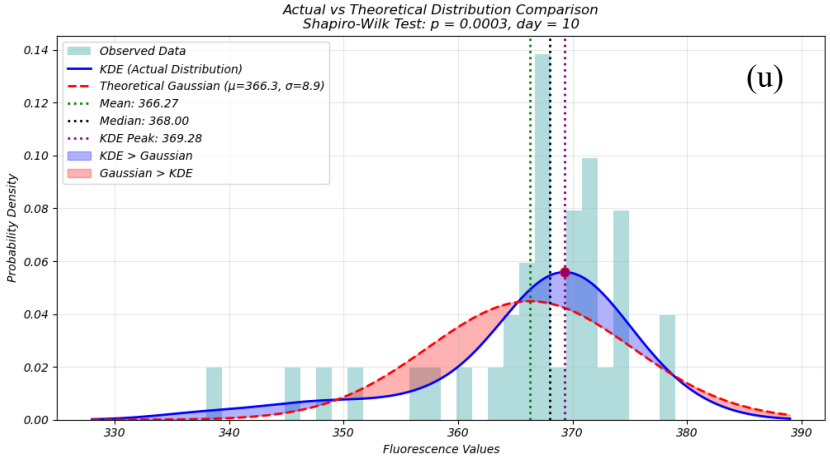
Actual vs Theoretical Distribution Comparison
Shapiro-Wilk Test: p = 0.0003, day = 10
(u)
Observed Data
KDE (Actual Distribution)
Theoretical Gaussian (μ=366.3, σ=8.9)
Mean: 366.27
Median: 368.00
KDE Peak: 369.28
KDE > Gaussian
Gaussian > KDE
Probability Density
Fluorescence Values

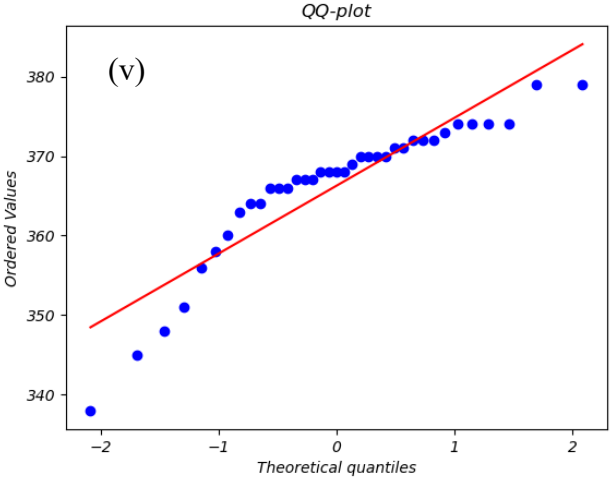
QQ-plot
(v)
Ordered Values
Theoretical quantiles

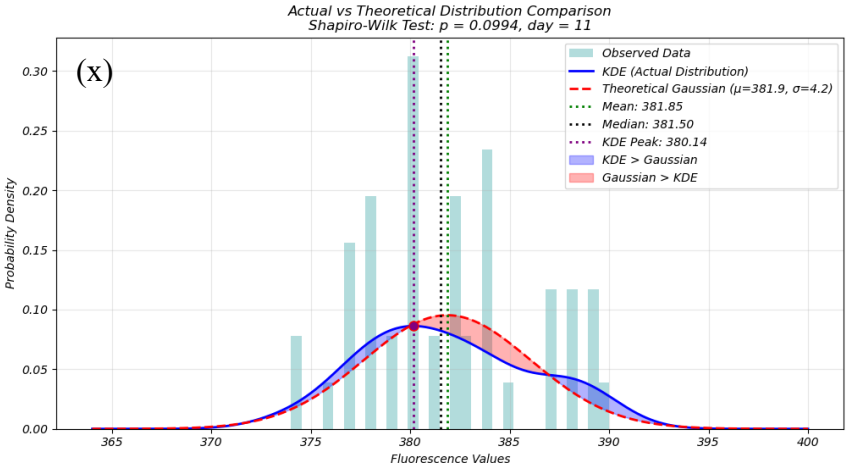
Actual vs Theoretical Distribution Comparison
Shapiro-Wilk Test: p = 0.0994, day = 11
(x)
Observed Data
KDE (Actual Distribution)
Theoretical Gaussian (μ=381.9, σ=4.2)
Mean: 381.85
Median: 381.50
KDE Peak: 380.14
KDE > Gaussian
Gaussian > KDE
Probability Density
Fluorescence Values

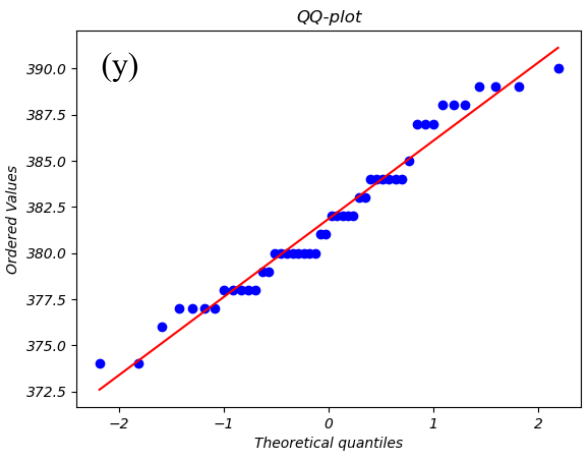
QQ-plot
(y)
Ordered Values
Theoretical quantiles

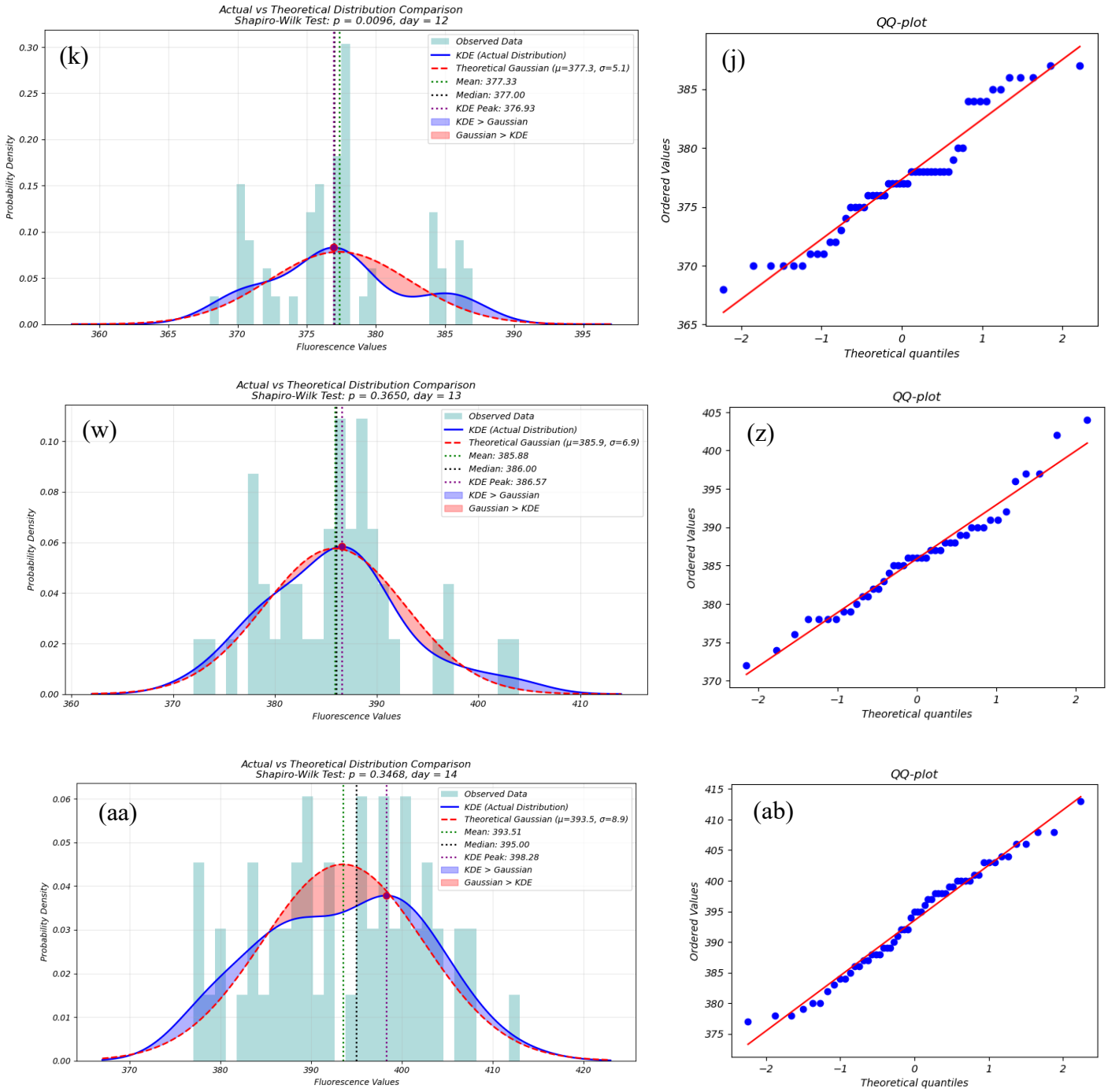

Figure 2. Data for the concentration of 106.92 ng mL^{-1} at 523 nm of 14 trial. Comparison of real and theoretical distribution and QQ plot.

Table 2 show data analysis for the concentration of 71.28 ng mL^{-1} in different trials and **Figures 3a-ab** show data distributions of fluorescence emitted at 548 nm. **Figure 4** and **Table 3** report data of aggregated data of the fluorescence emitted at 548 nm of 71.28 ng mL^{-1}.

The statistical analysis of the fluorescence emission at 548 nm for the concentration of 71.28 ng mL^{-1}, acquired over 14 experimental days, reveals a globally consistent picture that allows significant considerations to be drawn regarding the stability of the measurement system and the sensitivity of the experimental protocol.

The daily mean values range between approximately 212 and 268 A.U., with variations that, although limited to a few percentage points, are nonetheless statistically significant. The coefficient of variation, always below 3.5%, indicates good intra-day repeatability, suggesting that the instrument ensures high precision under identical measurement conditions. Similarly, the small standard deviations and narrow confidence intervals reflect low data dispersion within each group.

The Shapiro–Wilk test shows that most of the daily distributions can be considered approximately normal, with p-values generally greater than 0.05. Exceptions are observed on certain days (particularly the second, fourth, sixth, and eighth), where the test indicates significant deviations from normality, likely due to the presence of outliers or slight asymmetry in the data distribution. This observation is consistent with the skewness and kurtosis values, which in some cases deviate from zero or one, though without indicating systematic or substantial distortions.

The robustness analysis generally confirms the absence of severe outliers, with few exceptions (for instance, on days 4, 6, 7, and 8), where a small number of values fall outside the interquartile range limits. However, these occurrences appear to stem more from operational variations or random fluctuations in sample preparation rather than from instrumental instability.

From an inferential standpoint, the one-way ANOVA yielded an F-statistic of 14.959 with a p-value of 1.295×10^{-16}, leading to the rejection of the null hypothesis. This result indicates that the differences among daily means cannot be attributed solely to experimental error, but rather reflect, with high probability, the influence of additional factors. It is plausible that such factors are related to minor inconsistencies in sample preparation, slight manual errors by the operator, or uncontrolled variations in environmental conditions (such as temperature or exposure time).

In summary, the analysis demonstrates that the measurement system and experimental protocol are overall solid and reproducible, yet highly sensitive to even minimal operational variations. Such sensitivity, while representing a limitation in terms of absolute inter-day reproducibility, at the same

time confirms the instrument's high capability to detect real differences in the fluorescence signal, underscoring its precision and overall reliability.

Basic Statistics	Parameter	Day 1	Day 2	Day 3	Day 4	Day 5	Day 6	Day 7
	Mean	241.84	258.38	223.15	218.9	241.33	212.17	244.72
	Median	242.0	260.0	223.5	219.5	242.0	213.0	245.0
	Standard Deviation	6.12	5.59	6.02	5.67	8.01	6.71	6.41
	Coefficient of Variation (%)	2.53	2.16	2.7	2.59	3.32	3.16	2.62
	Range	26	25	24	22	33	23	27
	95% Confidence Interval	(239.60, 244.08)	(256.74, 260.02)	(220.72, 225.59)	(217.29, 220.51)	(238.86, 243.79)	(209.27, 215.08)	(242.08, 247.36)
Distribution Analysis	Skewness	0.2109	-0.4693	-0.3866	0.2195	-0.524	0.7046	0.5837
	Kurtosis	-0.049	-0.035	-0.344	-0.174	-0.24	-0.292	0.852
	Maximum Divergence (x)	245.5	254.6	222.4	224.2	237.0	217.5	242.3
	Total Divergence Area	0.1744	0.2687	0.1671	0.223	0.178	0.2329	0.1335
Distribution Divergence Analysis (Actual vs Theoretical Gaussian)	KDE Peak	239.8	260.6	225.5	219.1	243.7	209.4	246.1
	Interpretation	Moderate	Moderate	Moderate	Moderate	Moderate	Moderate	Moderate
	Shapiro-Wilk Statistic	0.966	0.923	0.97	0.926	0.967	0.912	0.951
	Shapiro-Wilk p-value	0.417	0.004	0.63	0.004	0.248	0.046	0.262
Robustness Analysis	IQR	7.0	6.5	8.0	3.75	11.0	7.0	9.0
	Lower Limit	227.5	245.75	207.0	210.62	220.5	196.5	225.5
	Upper Limit	255.5	271.75	239.0	225.62	264.5	224.5	261.5
	Outliers Detected	None	[272]	None	[226, 228, 210, 231, 230, 209]	None	[225, 226]	[262]
Dataset Info	Number of Scans	31	47	26	50	43	23	25

Basic Statistics	Day 8	Day 9	Day 10	Day 11	Day 12	Day 13	Day 14
	229.18	247.26	238.38	267.66	236.2	249.85	226.99
	230.0	248.0	236.5	268.0	236.0	251.0	227.0
	2.74	8.17	7.95	7.65	7.44	7.93	7.9
	1.2	3.3	3.34	2.86	3.15	3.17	3.48
	16 (228.48, 229.88)	32 (244.74, 249.77)	32 (235.51, 241.24)	30 (265.55, 269.77)	30 (233.64, 238.76)	33 (247.28, 252.42)	42 (225.09, 228.88)
Distribution Analysis	0.8383	-0.1585	0.2526	-0.0511	-0.0568	0.0316	-0.0602
	3.096	-0.585	-0.319	-0.58	-0.375	-0.656	0.166
	230.2	248.4	243.0	263.5	236.2	248.7	222.8
	0.1793	0.1435	0.1981	0.1561	0.1147	0.1871	0.0764
Distribution Divergence Analysis (Actual vs Theoretical Gaussian)	230.0	245.8	235.4	269.0	236.3	254.2	226.9
	Moderate	Moderate	Moderate	Moderate	Moderate	Moderate	Almost Normal
	0.886	0.979	0.955	0.969	0.98	0.971	0.995
	0.0	0.621	0.203	0.18	0.768	0.397	0.993
Robustness Analysis	2.0	11.0	9.25	10.0	9.5	12.5	11.0
	225.0	225.5	219.12	247.0	217.25	223.75	204.5
	233.0	269.5	256.12	287.0	255.25	273.75	248.5
	[240, 234, 224]	None	None	None	None	None	None
Dataset Info	61	43	32	53	35	39	69

Table 2. Data for the concentration of 71.28 ng mL^{-1} at 548 nm of 14 trials. Comparison of real and theoretical distribution and QQ plot.

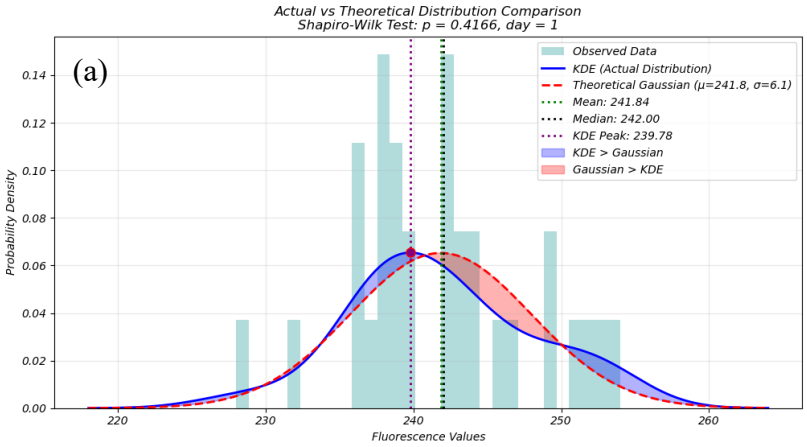
Actual vs Theoretical Distribution Comparison
Shapiro-Wilk Test: p = 0.4166, day = 1
(a)
Observed Data
KDE (Actual Distribution)
Theoretical Gaussian (μ=241.8, σ=6.1)
Mean: 241.84
Median: 242.00
KDE Peak: 239.78
KDE > Gaussian
Gaussian > KDE
Probability Density
Fluorescence Values

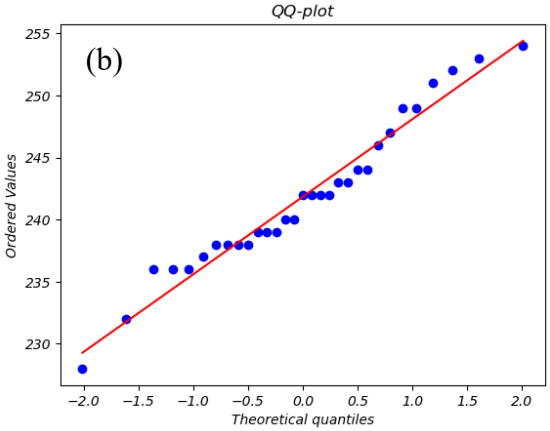
QQ-plot
(b)
Ordered Values
Theoretical quantiles

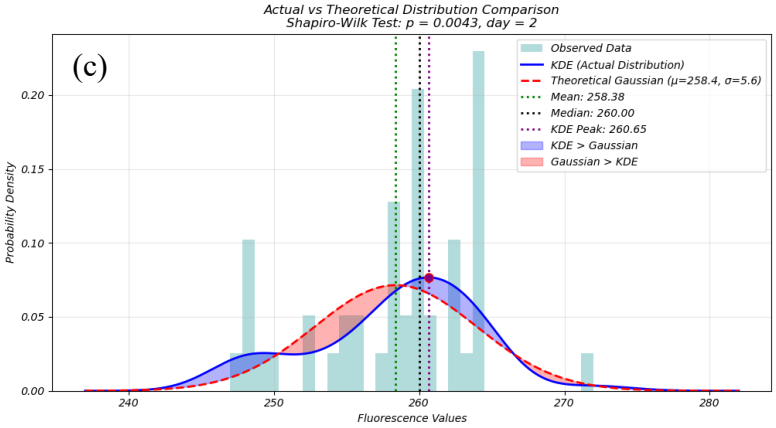
Actual vs Theoretical Distribution Comparison
Shapiro-Wilk Test: p = 0.0043, day = 2
(c)
Observed Data
KDE (Actual Distribution)
Theoretical Gaussian (μ=258.4, σ=5.6)
Mean: 258.38
Median: 260.00
KDE Peak: 260.65
KDE > Gaussian
Gaussian > KDE
Probability Density
Fluorescence Values

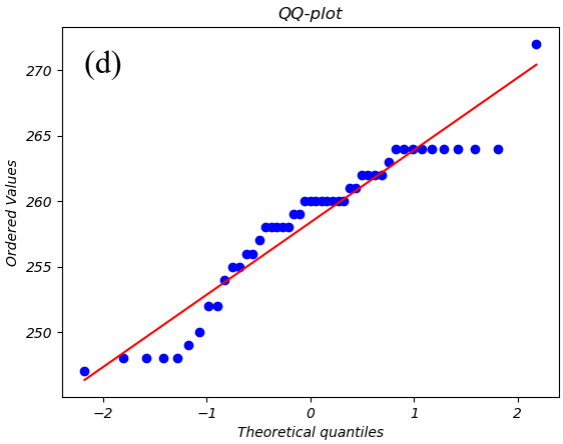
QQ-plot
(d)
Ordered Values
Theoretical quantiles

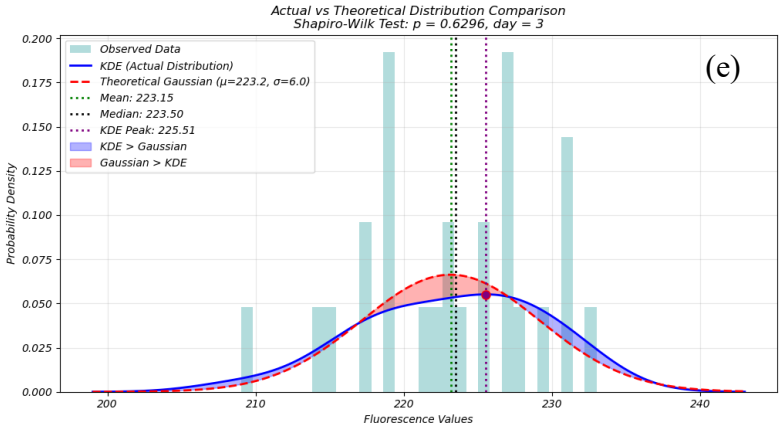
Actual vs Theoretical Distribution Comparison
Shapiro-Wilk Test: p = 0.6296, day = 3
(e)
Observed Data
KDE (Actual Distribution)
Theoretical Gaussian (μ=223.2, σ=6.0)
Mean: 223.15
Median: 223.50
KDE Peak: 225.51
KDE > Gaussian
Gaussian > KDE
Probability Density
Fluorescence Values

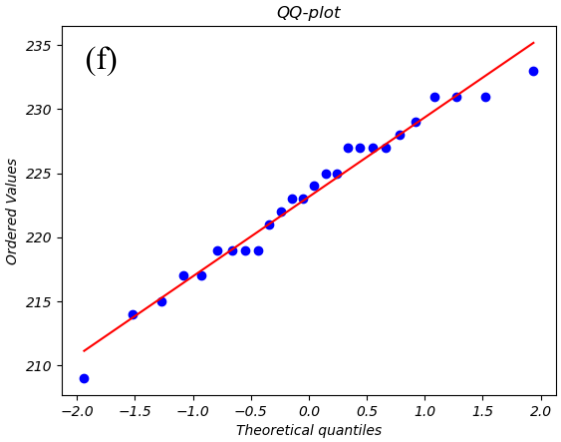
QQ-plot
(f)
Ordered Values
Theoretical quantiles

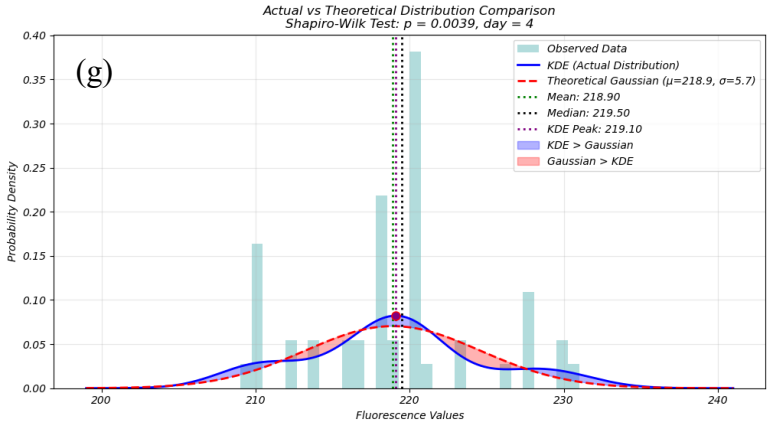
Actual vs Theoretical Distribution Comparison
Shapiro-Wilk Test: p = 0.0039, day = 4
(g)
Observed Data
KDE (Actual Distribution)
Theoretical Gaussian (μ=218.9, σ=5.7)
Mean: 218.90
Median: 219.50
KDE Peak: 219.10
KDE > Gaussian
Gaussian > KDE
Probability Density
Fluorescence Values

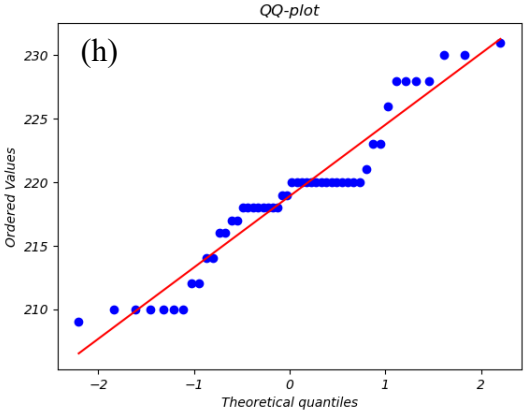
QQ-plot
(h)
Ordered Values
Theoretical quantiles

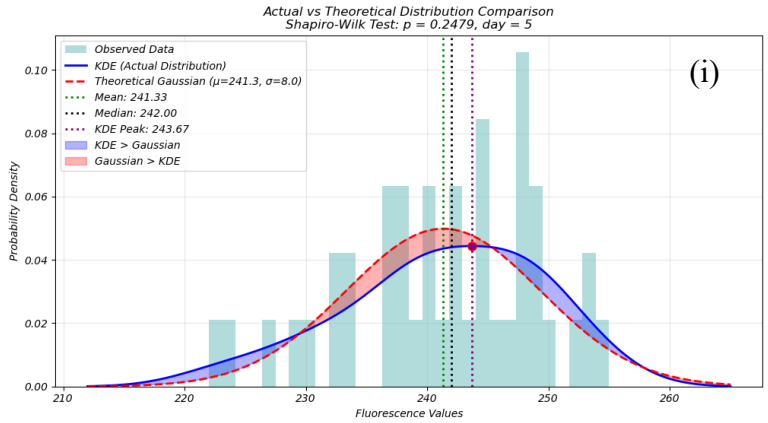
Actual vs Theoretical Distribution Comparison
Shapiro-Wilk Test: p = 0.2479, day = 5
(i)
Observed Data
KDE (Actual Distribution)
Theoretical Gaussian (μ=241.3, σ=8.0)
Mean: 241.33
Median: 242.00
KDE Peak: 243.67
KDE > Gaussian
Gaussian > KDE
Probability Density
Fluorescence Values

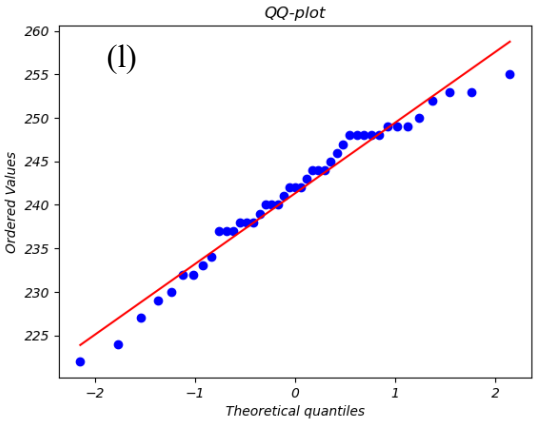
QQ-plot
(l)
Ordered Values
Theoretical quantiles

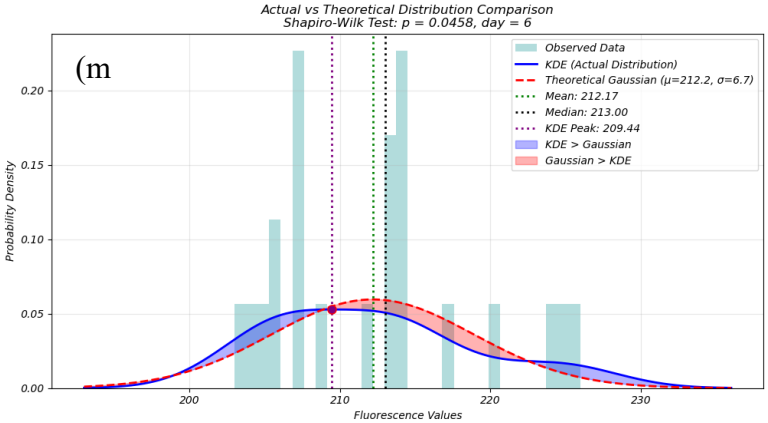
Actual vs Theoretical Distribution Comparison
Shapiro-Wilk Test: p = 0.0458, day = 6
(m)
Observed Data
KDE (Actual Distribution)
Theoretical Gaussian (μ=212.2, σ=6.7)
Mean: 212.17
Median: 213.00
KDE Peak: 209.44
KDE > Gaussian
Gaussian > KDE
Probability Density
Fluorescence Values

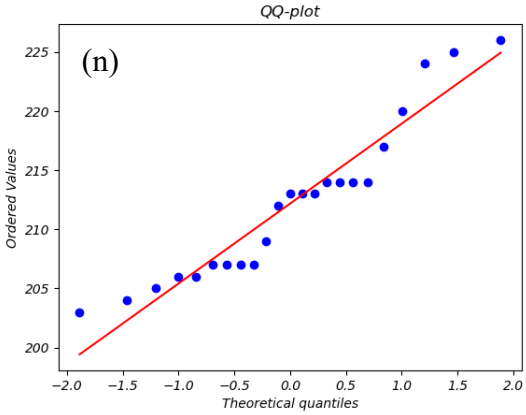
QQ-plot
(n)
Ordered Values
Theoretical quantiles

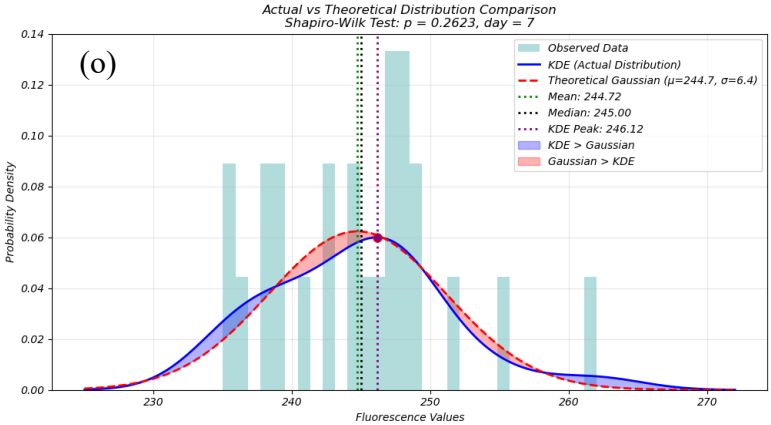
Actual vs Theoretical Distribution Comparison
Shapiro-Wilk Test: p = 0.2623, day = 7
(o)
Observed Data
KDE (Actual Distribution)
Theoretical Gaussian (μ=244.7, σ=6.4)
Mean: 244.72
Median: 245.00
KDE Peak: 246.12
KDE > Gaussian
Gaussian > KDE
Probability Density
Fluorescence Values

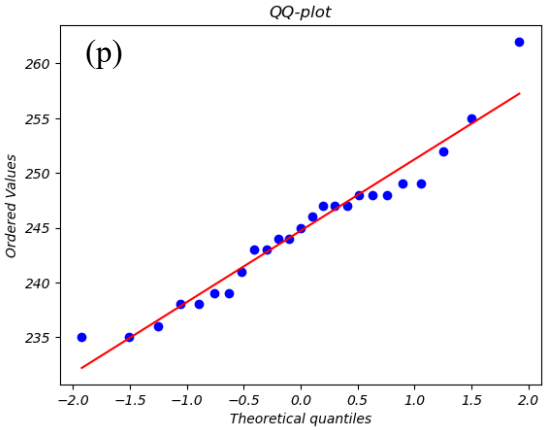
QQ-plot
(p)
Ordered Values
Theoretical quantiles

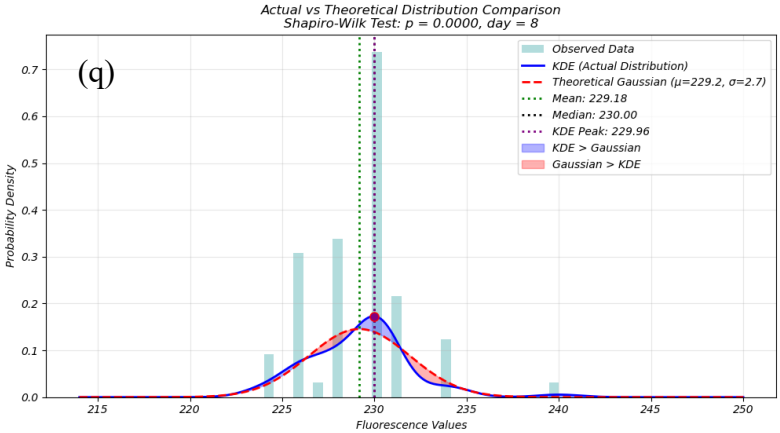
Actual vs Theoretical Distribution Comparison
Shapiro-Wilk Test: p = 0.0000, day = 8
(q)
Observed Data
KDE (Actual Distribution)
Theoretical Gaussian (μ=229.2, σ=2.7)
Mean: 229.18
Median: 230.00
KDE Peak: 229.96
KDE > Gaussian
Gaussian > KDE
Probability Density
Fluorescence Values

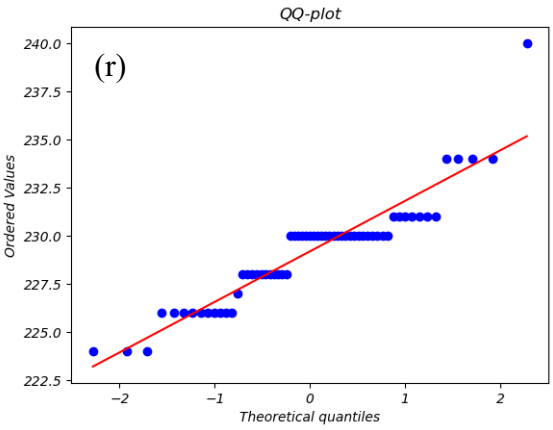
QQ-plot
(r)
Ordered Values
Theoretical quantiles

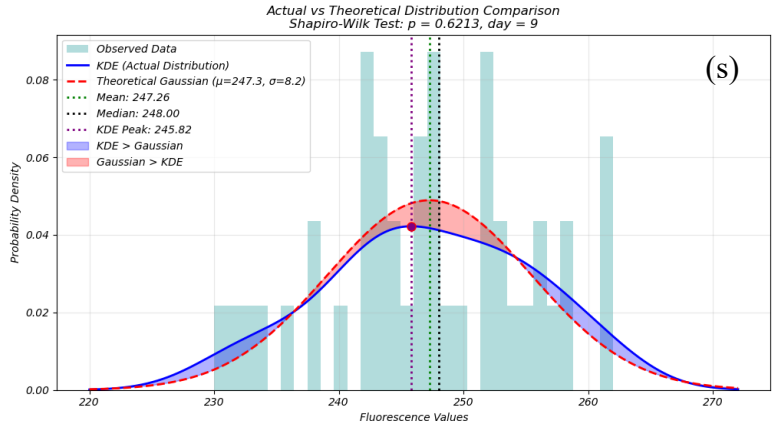
Actual vs Theoretical Distribution Comparison
Shapiro-Wilk Test: p = 0.6213, day = 9
(s)
Observed Data
KDE (Actual Distribution)
Theoretical Gaussian (μ=247.3, σ=8.2)
Mean: 247.26
Median: 248.00
KDE Peak: 245.82
KDE > Gaussian
Gaussian > KDE
Probability Density
Fluorescence Values

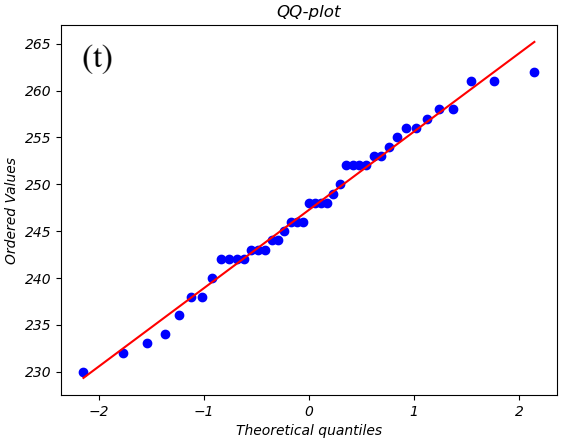
QQ-plot
(t)
Ordered Values
Theoretical quantiles

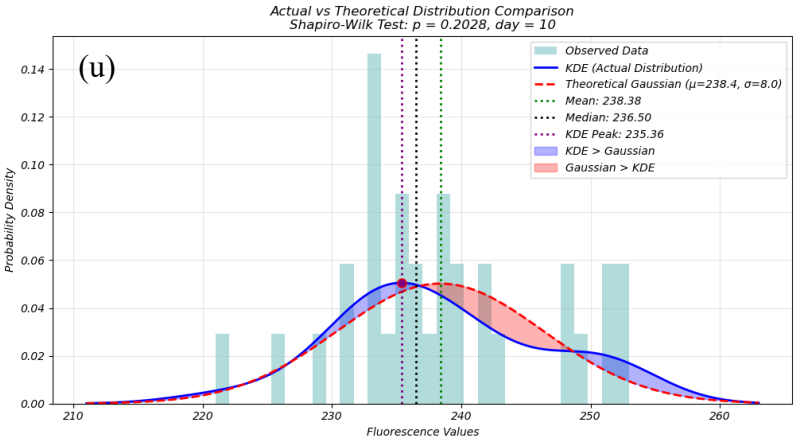
Actual vs Theoretical Distribution Comparison
Shapiro-Wilk Test: p = 0.2028, day = 10
(u)
Observed Data
KDE (Actual Distribution)
Theoretical Gaussian (μ=238.4, σ=8.0)
Mean: 238.38
Median: 236.50
KDE Peak: 235.36
KDE > Gaussian
Gaussian > KDE
Probability Density
Fluorescence Values

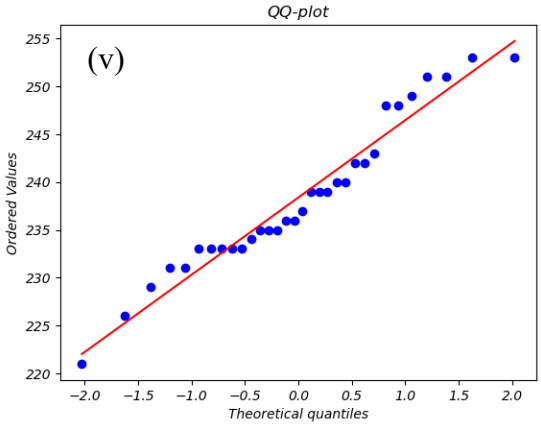
QQ-plot
(v)
Ordered Values
Theoretical quantiles

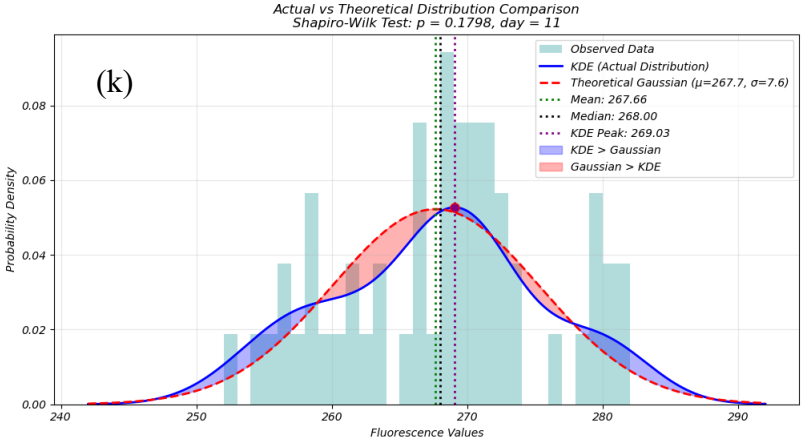
Actual vs Theoretical Distribution Comparison
Shapiro-Wilk Test: p = 0.1798, day = 11
(k)
Observed Data
KDE (Actual Distribution)
Theoretical Gaussian (μ=267.7, σ=7.6)
Mean: 267.66
Median: 268.00
KDE Peak: 269.03
KDE > Gaussian
Gaussian > KDE
Probability Density
Fluorescence Values

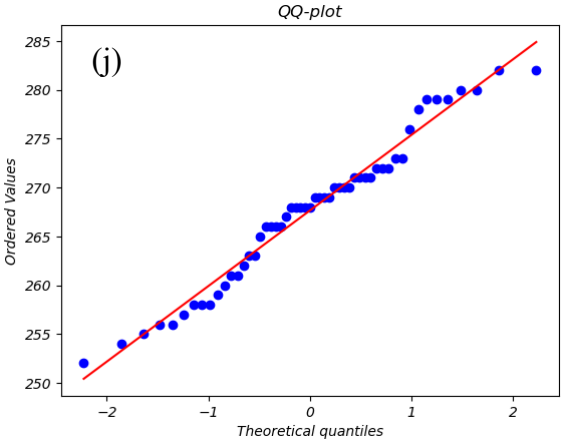
QQ-plot
(j)
Ordered Values
Theoretical quantiles

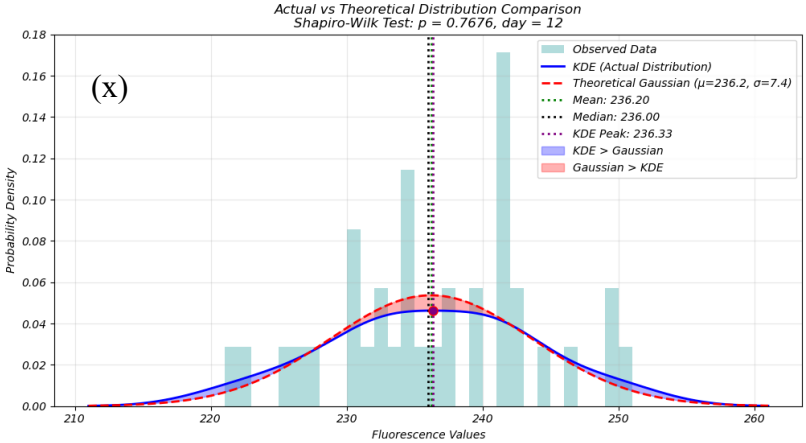
Actual vs Theoretical Distribution Comparison
Shapiro-Wilk Test: p = 0.7676, day = 12
(x)
Observed Data
KDE (Actual Distribution)
Theoretical Gaussian (μ=236.2, σ=7.4)
Mean: 236.20
Median: 236.00
KDE Peak: 236.33
KDE > Gaussian
Gaussian > KDE
Probability Density
Fluorescence Values

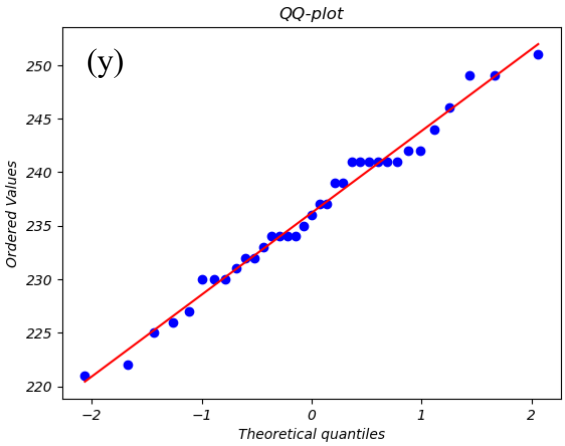
QQ-plot
(y)
Ordered Values
Theoretical quantiles

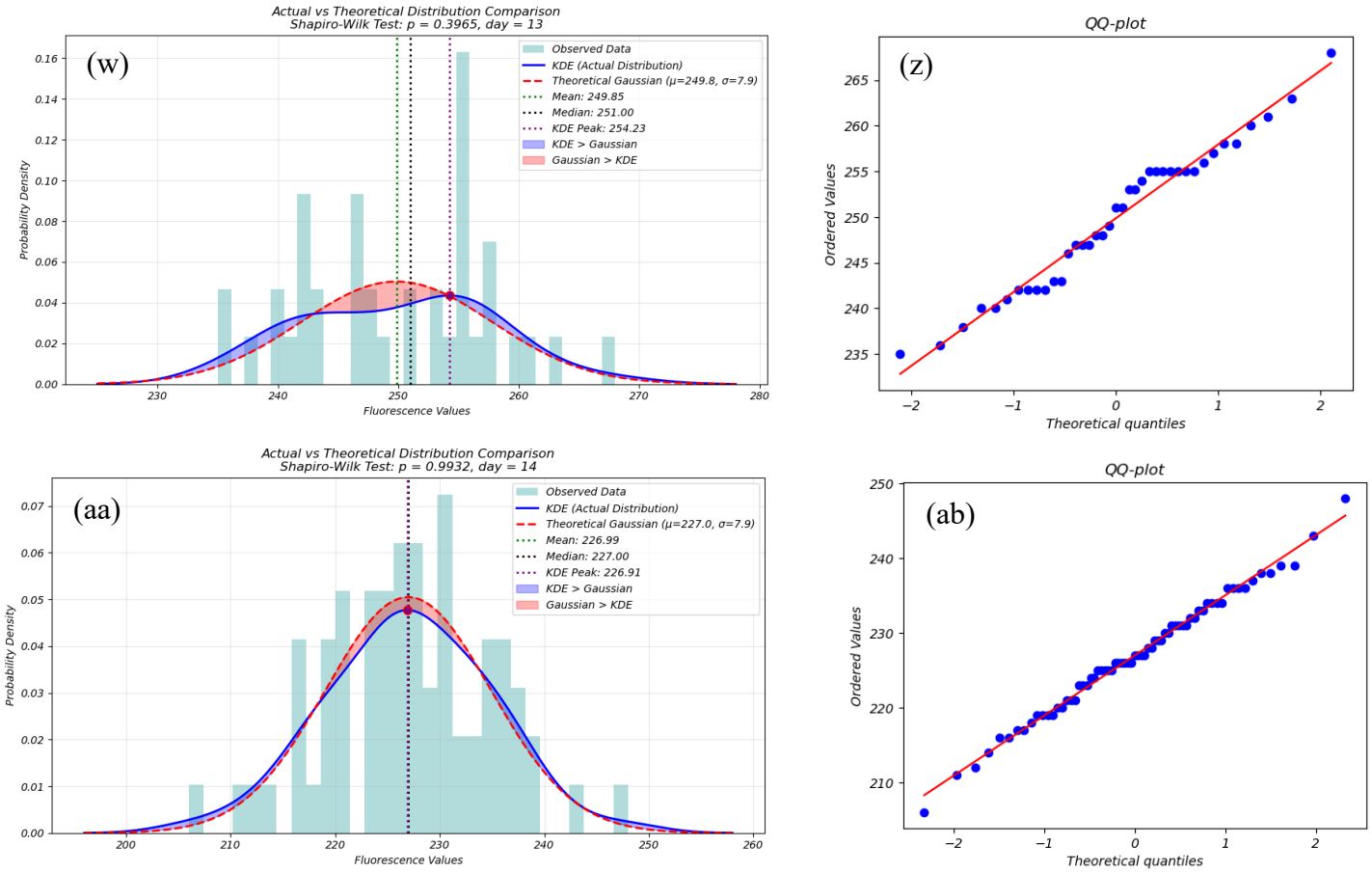

Figure 3. Data for the concentration of 71.28 ng mL^{-1} at 548 nm of 14 trials. Comparison of real and theoretical distribution and QQ plot.

Basic Statistics	Parameter	Value
	Mean	238.93
	Median	238.00
	Standard Deviation	16.45
	Coefficient of Variation	6.89%
	Range	79
	95% Confidence Interval	(237.58, 240.27)
Distribution Analysis	Skewness	0.2728
	Kurtosis	-0.508
	Shapiro–Wilk Statistic	0.986
	Shapiro–Wilk p-value	0.000
Distribution Divergence Analysis (Actual vs Theoretical Gaussian)	Maximum Divergence (x)	242.9
	Total Divergence Area	0.1569
	KDE Peak	230.5
	Interpretation	Moderate deviations from normality
Robustness Analysis	IQR	24.00
	Lower Limit	191.00
	Upper Limit	287.00
	Outliers Detected	None
Dataset Info	Number of Scans	577

Table 3. Data for the concentration of 71.28 ng mL^{-1} at 548 nm of aggregated trials.

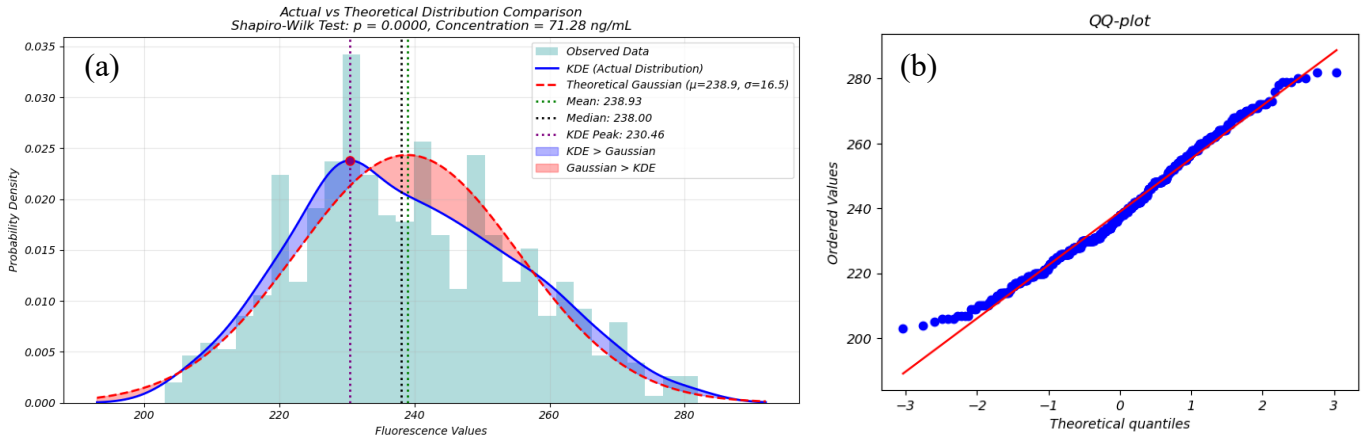

Figure 4. Data for the concentration of 71.28 ng mL^{-1} at 548 nm of aggregated trials. (a) Comparison of real and theoretical distribution and (b) QQ plot.

In **Figure 5.1-40** we report the actual and theoretical distribution of fluorescence signal at 523 nm for all concentrations with aggregated data of every trial.

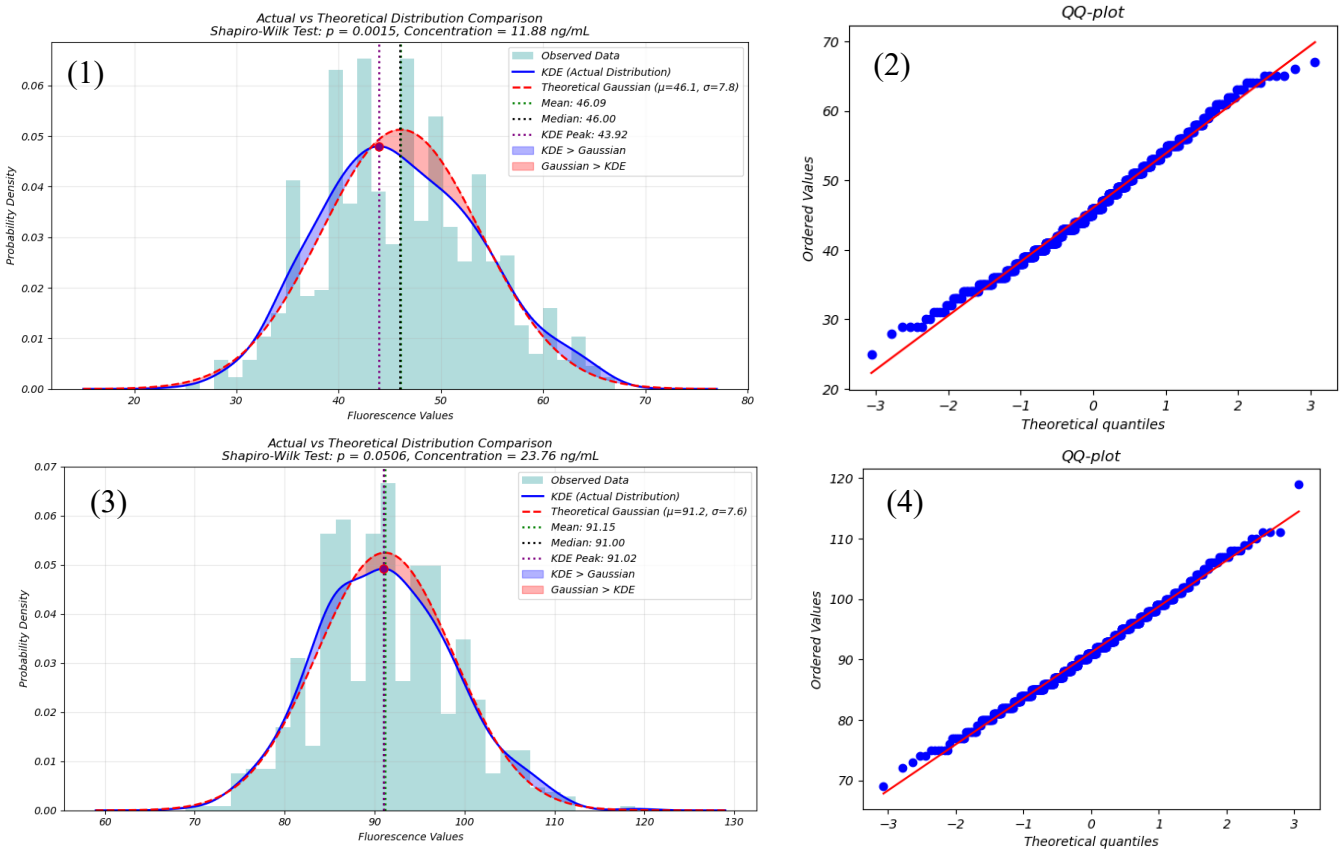

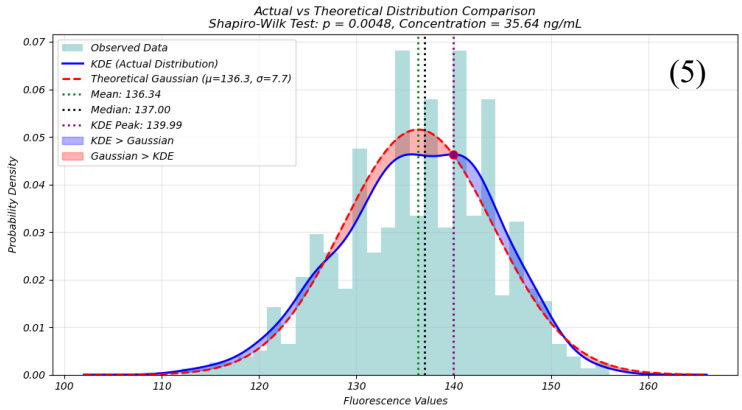
Actual vs Theoretical Distribution Comparison
Shapiro-Wilk Test: p = 0.0048, Concentration = 35.64 ng/mL
(5)
Observed Data
KDE (Actual Distribution)
Theoretical Gaussian (μ=136.3, σ=7.7)
Mean: 136.34
Median: 137.00
KDE Peak: 139.99
KDE > Gaussian
Gaussian > KDE
Probability Density
Fluorescence Values

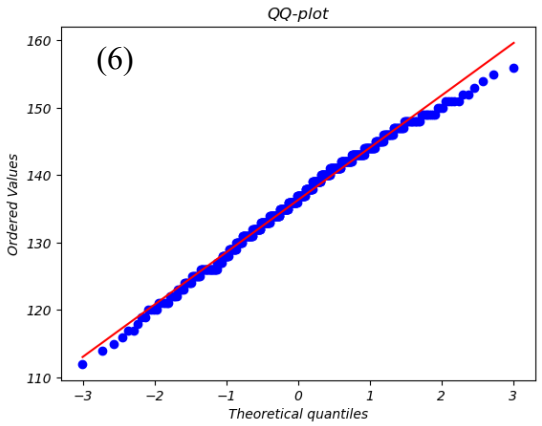
QQ-plot
(6)
Ordered Values
Theoretical quantiles

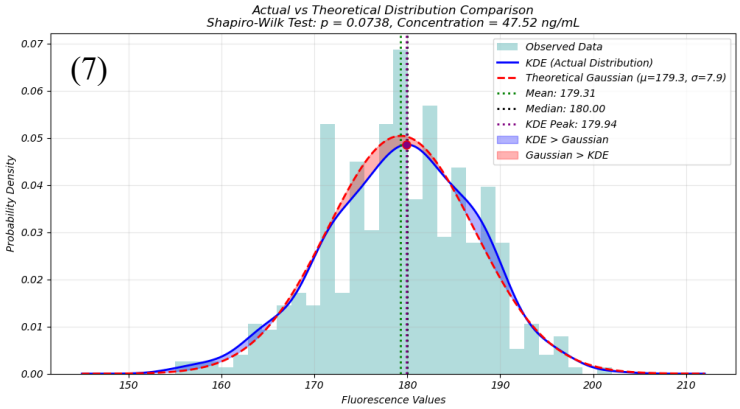
Actual vs Theoretical Distribution Comparison
Shapiro-Wilk Test: p = 0.0738, Concentration = 47.52 ng/mL
(7)
Observed Data
KDE (Actual Distribution)
Theoretical Gaussian (μ=179.3, σ=7.9)
Mean: 179.31
Median: 180.00
KDE Peak: 179.94
KDE > Gaussian
Gaussian > KDE
Probability Density
Fluorescence Values

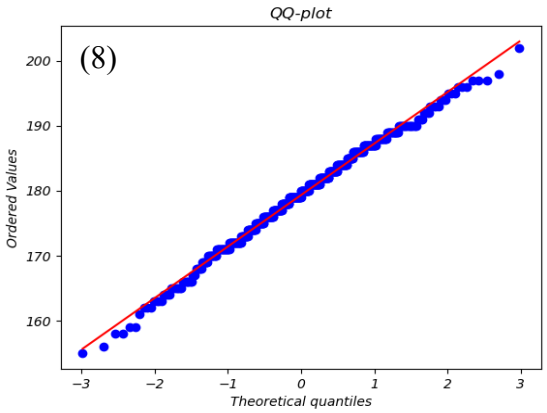
QQ-plot
(8)
Ordered Values
Theoretical quantiles

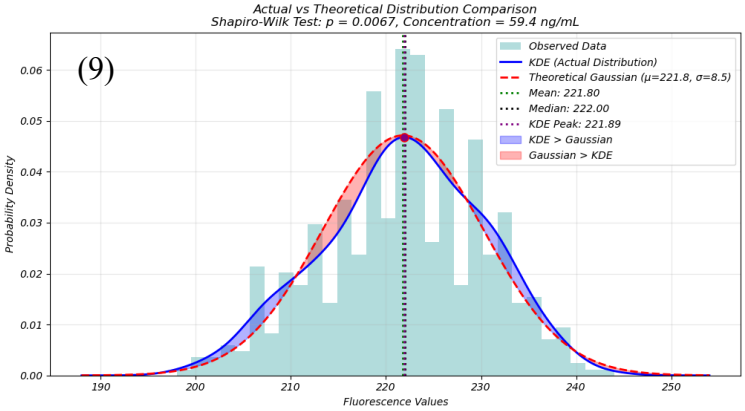
Actual vs Theoretical Distribution Comparison
Shapiro-Wilk Test: p = 0.0067, Concentration = 59.4 ng/mL
(9)
Observed Data
KDE (Actual Distribution)
Theoretical Gaussian (μ=221.8, σ=8.5)
Mean: 221.80
Median: 222.00
KDE Peak: 221.89
KDE > Gaussian
Gaussian > KDE
Probability Density
Fluorescence Values

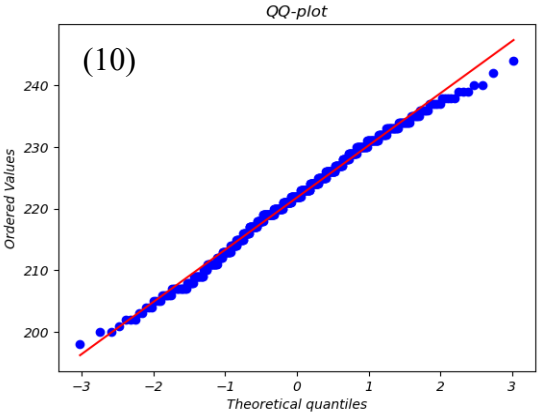
QQ-plot
(10)
Ordered Values
Theoretical quantiles

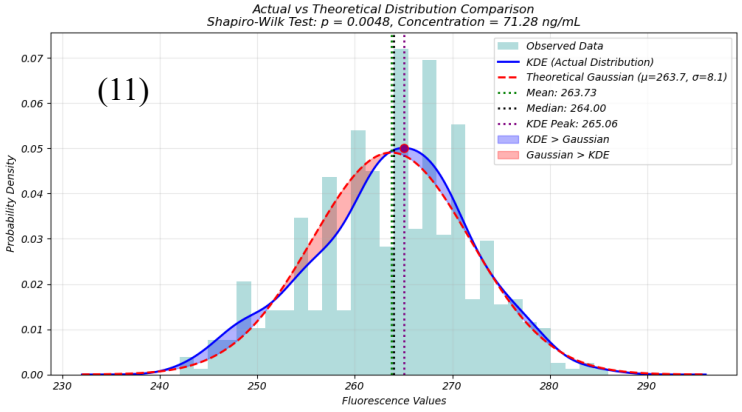
Actual vs Theoretical Distribution Comparison
Shapiro-Wilk Test: p = 0.0048, Concentration = 71.28 ng/mL
(11)
Observed Data
KDE (Actual Distribution)
Theoretical Gaussian (μ=263.7, σ=8.1)
Mean: 263.73
Median: 264.00
KDE Peak: 265.06
KDE > Gaussian
Gaussian > KDE
Probability Density
Fluorescence Values

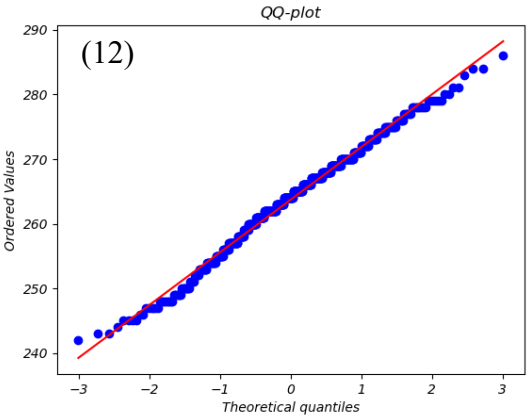
QQ-plot
(12)
Ordered Values
Theoretical quantiles

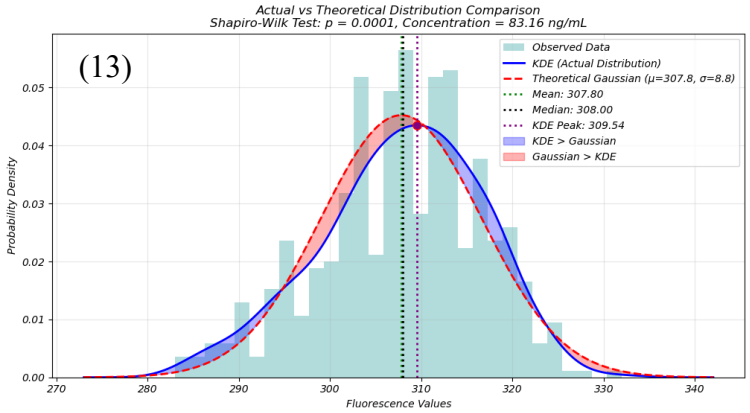
Actual vs Theoretical Distribution Comparison
Shapiro-Wilk Test: p = 0.0001, Concentration = 83.16 ng/mL
(13)
Observed Data
KDE (Actual Distribution)
Theoretical Gaussian (μ=307.8, σ=8.8)
Mean: 307.80
Median: 308.00
KDE Peak: 309.54
KDE > Gaussian
Gaussian > KDE
Probability Density
Fluorescence Values

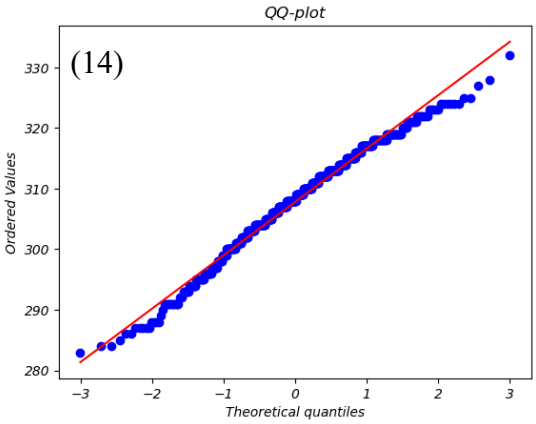
QQ-plot
(14)
Ordered Values
Theoretical quantiles

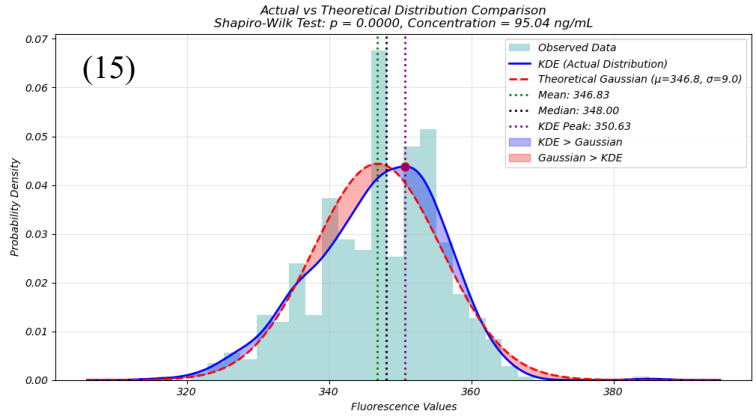
Actual vs Theoretical Distribution Comparison
Shapiro-Wilk Test: p = 0.0000, Concentration = 95.04 ng/mL
(15)
Observed Data
KDE (Actual Distribution)
Theoretical Gaussian (μ=346.8, σ=9.0)
Mean: 346.83
Median: 348.00
KDE Peak: 350.63
KDE > Gaussian
Gaussian > KDE
Probability Density
Fluorescence Values

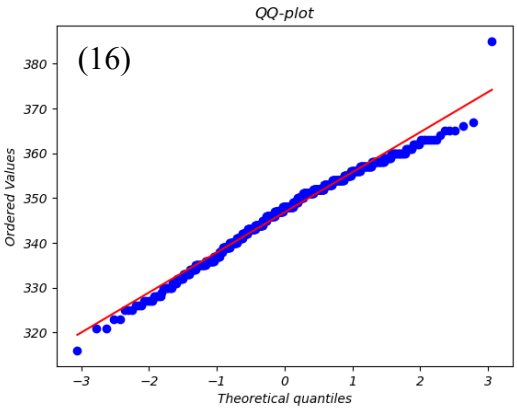
QQ-plot
(16)
Ordered Values
Theoretical quantiles

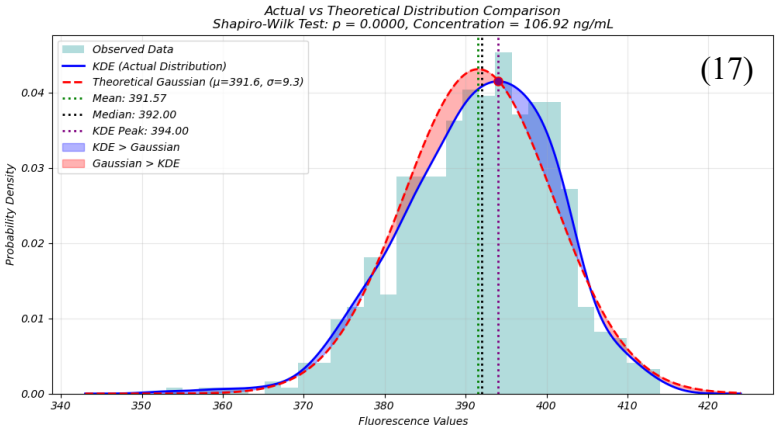
Actual vs Theoretical Distribution Comparison
Shapiro-Wilk Test: p = 0.0000, Concentration = 106.92 ng/mL
(17)
Observed Data
KDE (Actual Distribution)
Theoretical Gaussian (μ=391.6, σ=9.3)
Mean: 391.57
Median: 392.00
KDE Peak: 394.00
KDE > Gaussian
Gaussian > KDE
Probability Density
Fluorescence Values

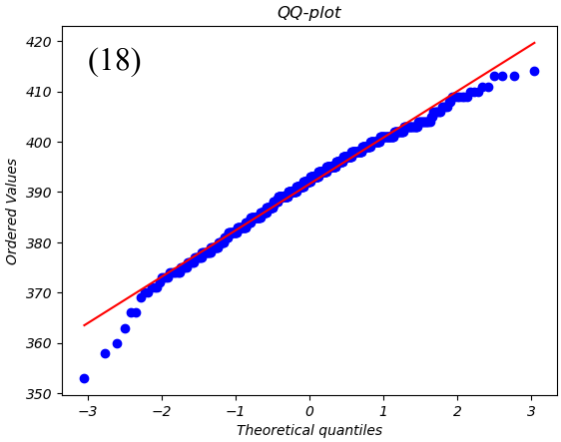
QQ-plot
(18)
Ordered Values
Theoretical quantiles

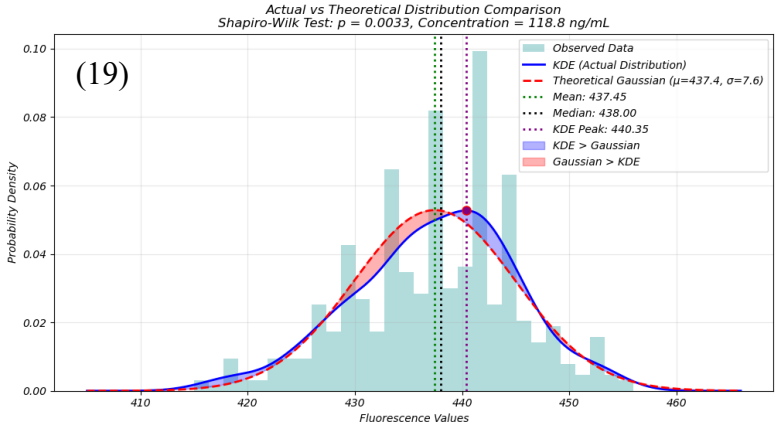
Actual vs Theoretical Distribution Comparison
Shapiro-Wilk Test: p = 0.0033, Concentration = 118.8 ng/mL
(19)
Observed Data
KDE (Actual Distribution)
Theoretical Gaussian (μ=437.4, σ=7.6)
Mean: 437.45
Median: 438.00
KDE Peak: 440.35
KDE > Gaussian
Gaussian > KDE
Probability Density
Fluorescence Values

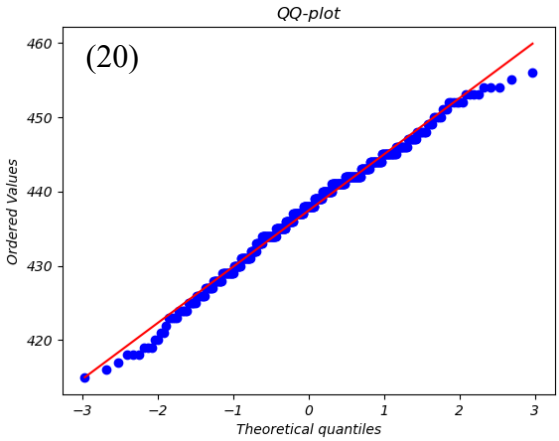
QQ-plot
(20)
Ordered Values
Theoretical quantiles

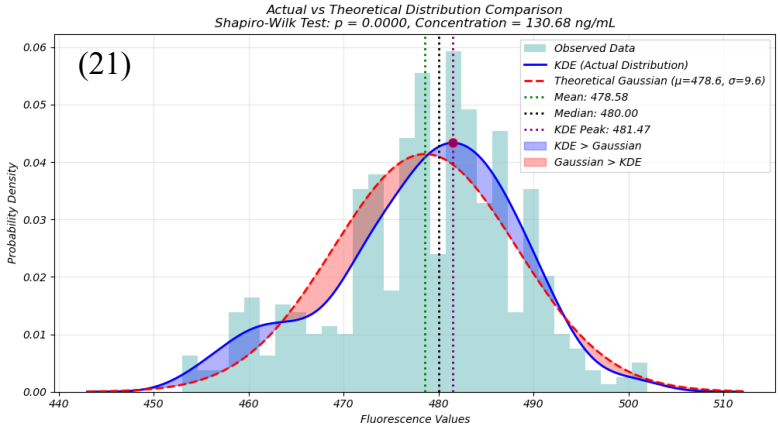
Actual vs Theoretical Distribution Comparison
Shapiro-Wilk Test: p = 0.0000, Concentration = 130.68 ng/mL
(21)
Observed Data
KDE (Actual Distribution)
Theoretical Gaussian (μ=478.6, σ=9.6)
Mean: 478.58
Median: 480.00
KDE Peak: 481.47
KDE > Gaussian
Gaussian > KDE
Probability Density
Fluorescence Values

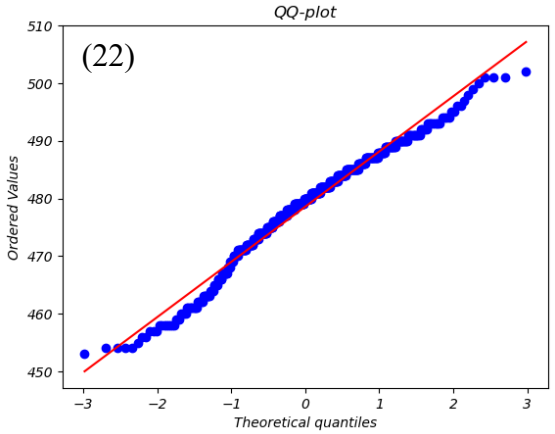
QQ-plot
(22)
Ordered Values
Theoretical quantiles

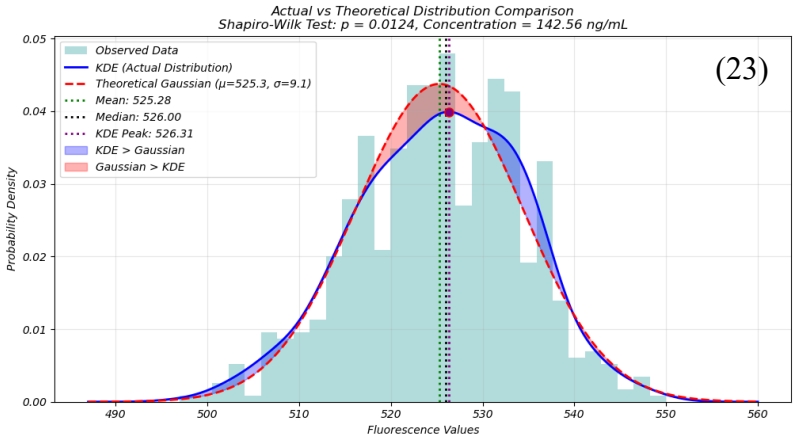
Actual vs Theoretical Distribution Comparison
Shapiro-Wilk Test: p = 0.0124, Concentration = 142.56 ng/mL
(23)
Observed Data
KDE (Actual Distribution)
Theoretical Gaussian (μ=525.3, σ=9.1)
Mean: 525.28
Median: 526.00
KDE Peak: 526.31
KDE > Gaussian
Gaussian > KDE
Probability Density
Fluorescence Values

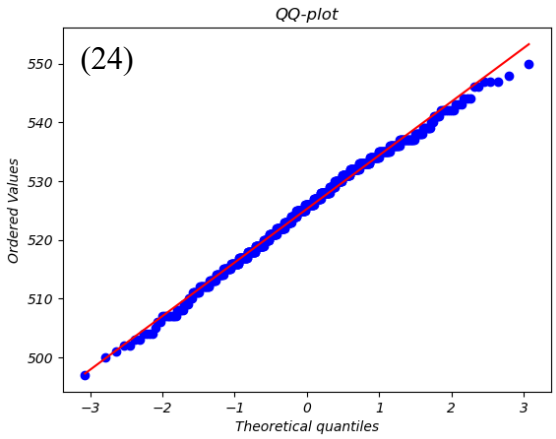
QQ-plot
(24)
Ordered Values
Theoretical quantiles

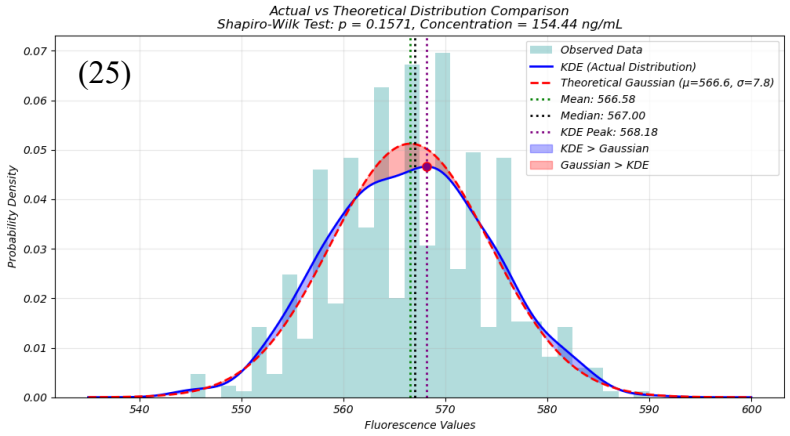
Actual vs Theoretical Distribution Comparison
Shapiro-Wilk Test: p = 0.1571, Concentration = 154.44 ng/mL
(25)
Observed Data
KDE (Actual Distribution)
Theoretical Gaussian (μ=566.6, σ=7.8)
Mean: 566.58
Median: 567.00
KDE Peak: 568.18
KDE > Gaussian
Gaussian > KDE
Probability Density
Fluorescence Values

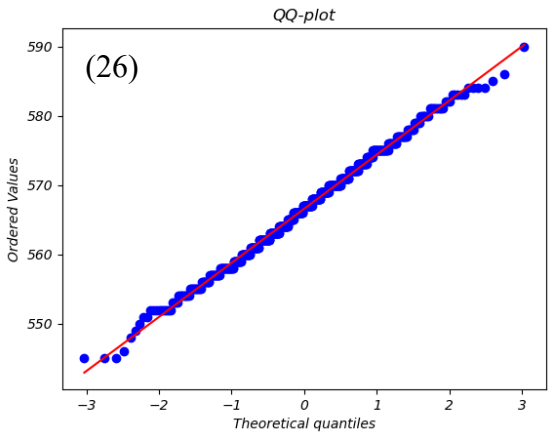
QQ-plot
(26)
Ordered Values
Theoretical quantiles

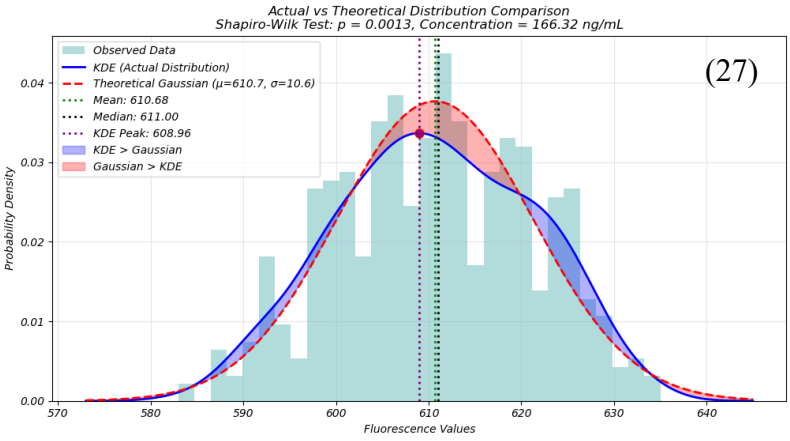
Actual vs Theoretical Distribution Comparison
Shapiro-Wilk Test: p = 0.0013, Concentration = 166.32 ng/mL
(27)
Observed Data
KDE (Actual Distribution)
Theoretical Gaussian (μ=610.7, σ=10.6)
Mean: 610.68
Median: 611.00
KDE Peak: 608.96
KDE > Gaussian
Gaussian > KDE
Probability Density
Fluorescence Values

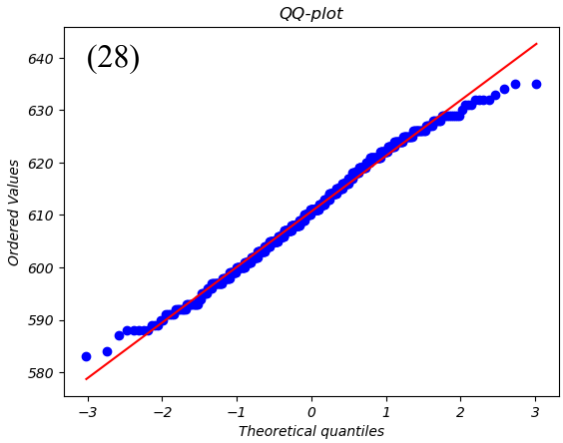
QQ-plot
(28)
Ordered Values
Theoretical quantiles

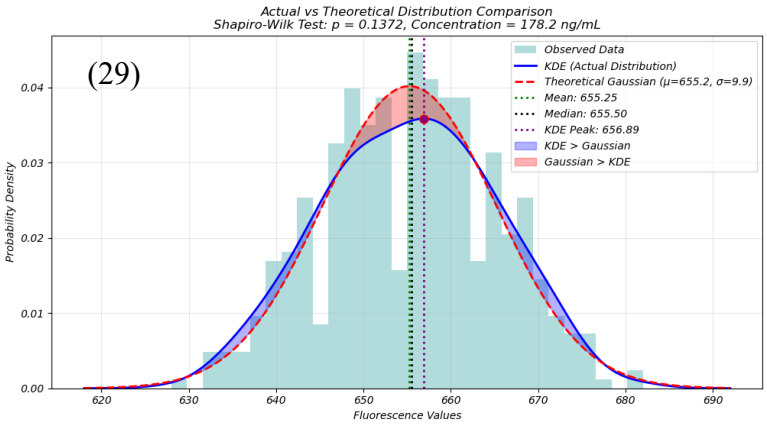
Actual vs Theoretical Distribution Comparison
Shapiro-Wilk Test: p = 0.1372, Concentration = 178.2 ng/mL
(29)
Observed Data
KDE (Actual Distribution)
Theoretical Gaussian (μ=655.2, σ=9.9)
Mean: 655.25
Median: 655.50
KDE Peak: 656.89
KDE > Gaussian
Gaussian > KDE
Probability Density
Fluorescence Values

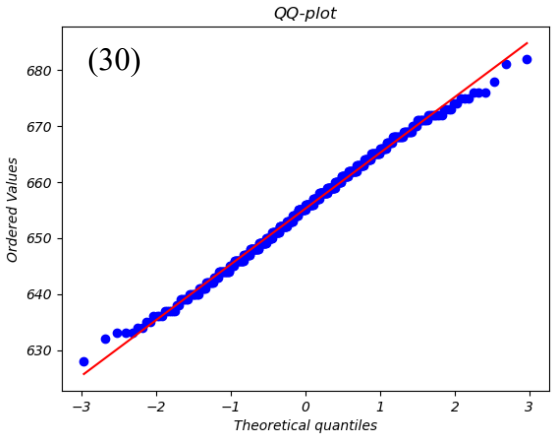
QQ-plot
(30)
Ordered Values
Theoretical quantiles

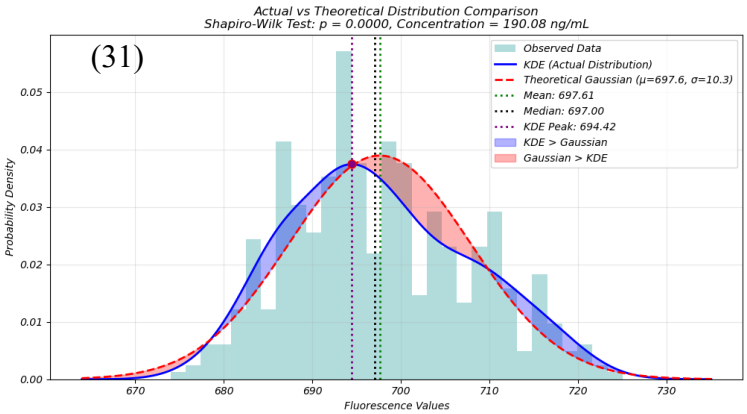
Actual vs Theoretical Distribution Comparison
Shapiro-Wilk Test: p = 0.0000, Concentration = 190.08 ng/mL
(31)
Observed Data
KDE (Actual Distribution)
Theoretical Gaussian (μ=697.6, σ=10.3)
Mean: 697.61
Median: 697.00
KDE Peak: 694.42
KDE > Gaussian
Gaussian > KDE
Probability Density
Fluorescence Values

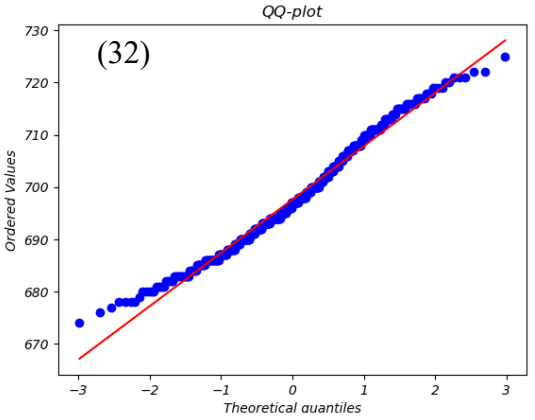
QQ-plot
(32)
Ordered Values
Theoretical quantiles

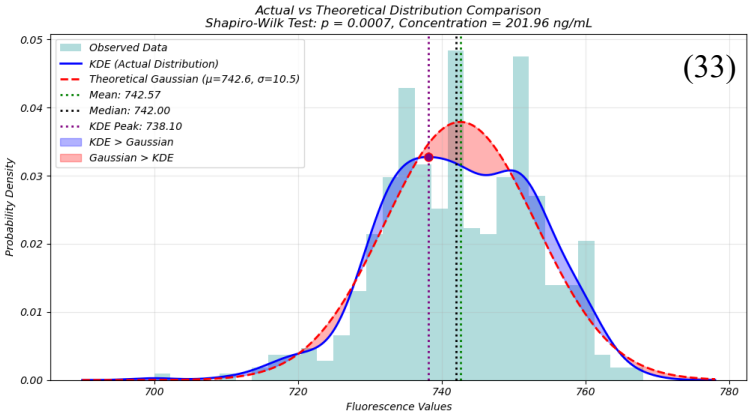
Actual vs Theoretical Distribution Comparison
Shapiro-Wilk Test: p = 0.0007, Concentration = 201.96 ng/mL
(33)
Observed Data
KDE (Actual Distribution)
Theoretical Gaussian (μ=742.6, σ=10.5)
Mean: 742.57
Median: 742.00
KDE Peak: 738.10
KDE > Gaussian
Gaussian > KDE
Probability Density
Fluorescence Values

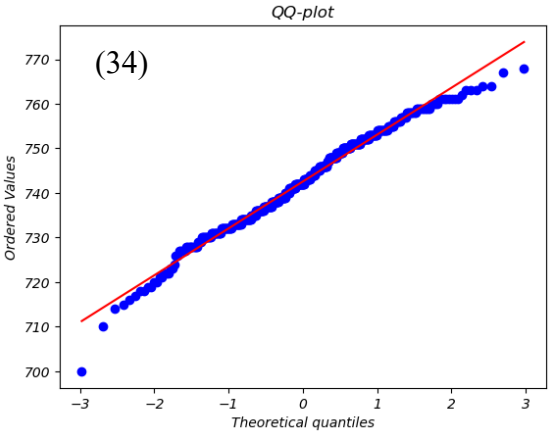
QQ-plot
(34)
Ordered Values
Theoretical quantiles

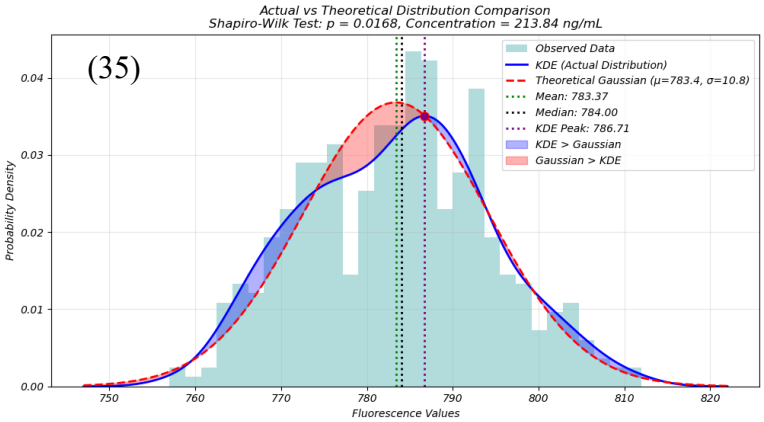
Actual vs Theoretical Distribution Comparison
Shapiro-Wilk Test: p = 0.0168, Concentration = 213.84 ng/mL
(35)
Observed Data
KDE (Actual Distribution)
Theoretical Gaussian (μ=783.4, σ=10.8)
Mean: 783.37
Median: 784.00
KDE Peak: 786.71
KDE > Gaussian
Gaussian > KDE
Probability Density
Fluorescence Values

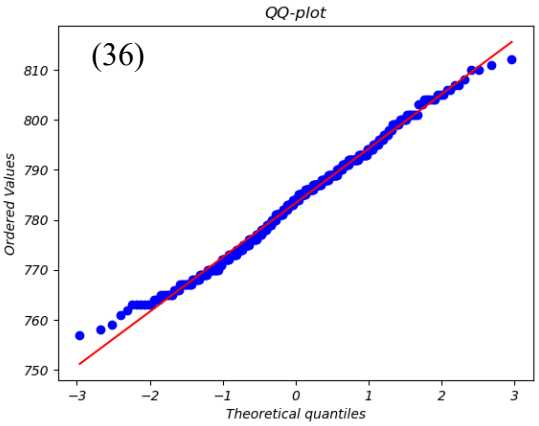
QQ-plot
(36)
Ordered Values
Theoretical quantiles

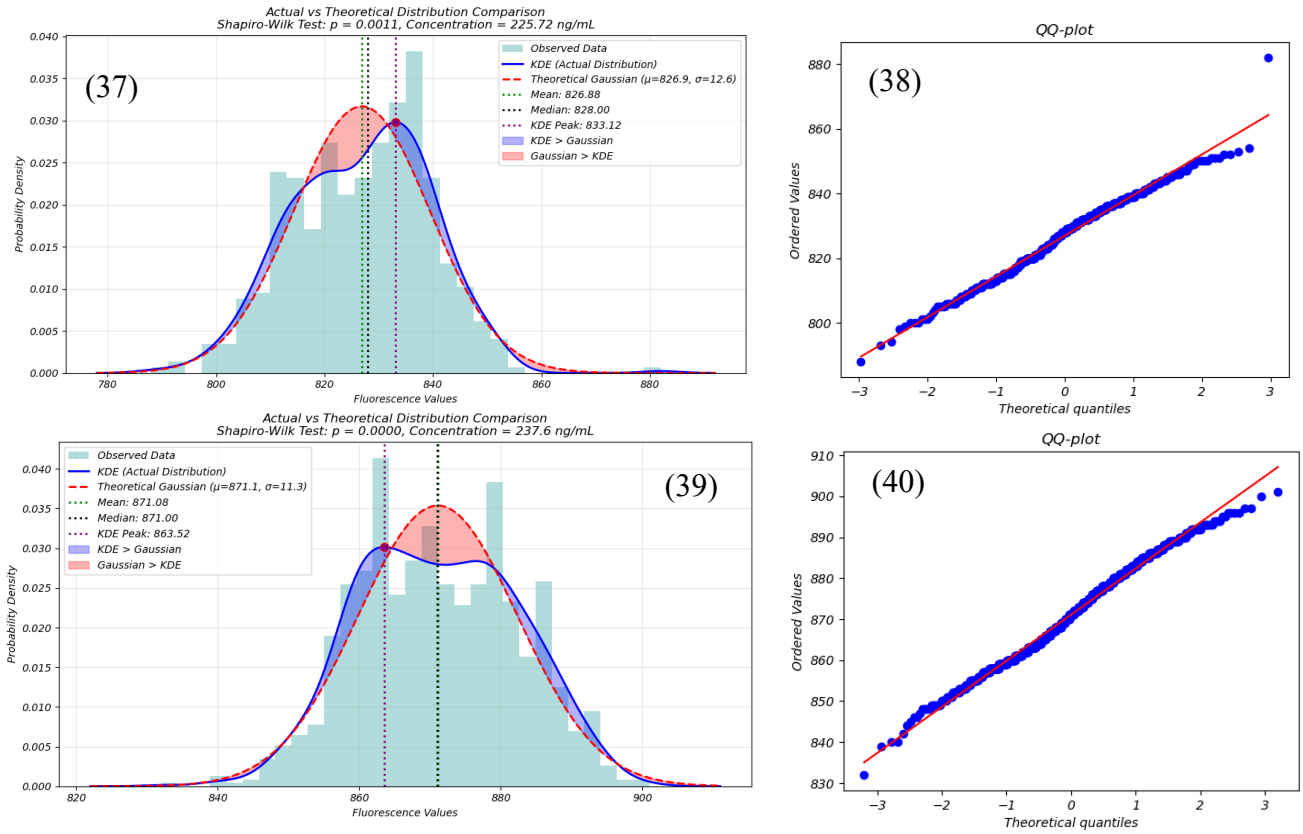

Figure 5.1-40. Data of fluorescence signal for the all concentrations at 523 nm of aggregated trials. (a) Comparison of real and theoretical distribution and (b) QQ plot.

Acknowledgment

There are many people who, in one way or another, have influenced my journey, and here I would like to thank you all.

The first person I wish to thank is my longtime best friend, **Francesco**. You have been a true and sincere friend, and you have shown it on every occasion. I would have liked to write more heartfelt words, though I know you'd say it's not necessary. So I simply say, with all my heart, thank you once again.

I would like to thank **Mauricio Flores Carvalho**, as he was one of the most influential people throughout my Ph.D. I am deeply grateful to Mauricio for his extensive professionalism, expertise, and valuable suggestions provided during my research. I also wish to thank him for making essential research materials available and for his personal support. Moreover, he showed great kindness by hosting me in his home in Cleveland during my stay. Thank you so much, Mauricio — you are someone who has taught me a great deal, and I am truly grateful.

I would also like to thank **Andrea Schlegel**. It was an immense honor to meet her in person and to have had the great opportunity to collaborate. Thanks to her, I had the wonderful chance to work at the prestigious **Cleveland Clinic** and to experience an extraordinary period in the United States. For me, Andrea Schlegel has been an inspiring role model, and I feel very lucky to have met her. If this Ph.D. has achieved important success, it is thanks to Andrea and Mauricio — for their fundamental and irreplaceable support when I arrived in Cleveland, and for having given me the opportunity to live a truly world-class research experience. Thank you both — I will always carry with me these beautiful memories of you as exceptional people.

I would like to express my deepest gratitude to **Medica S.p.A.** for the support and collaboration provided throughout my Ph.D. journey. The company's contribution has been fundamental to the success of this work and to my stay in Mirandola and Medolla.

A special thank you goes to my **industrial supervisor Davide Bagnoli** of Medica S.p.A., who accompanied me throughout the entire journey with extraordinary availability, professionalism, and patience. I am deeply grateful for his trust and continuous support over these three years.

I fondly remember the time spent at **Medica S.p.A.** in Bologna, Mirandola, and Medolla — a rich and stimulating experience made unforgettable by the extraordinary people I had the privilege to meet. I would like to especially thank **Riccardo Molinari** and **Francesco Fregni** for their constant availability and invaluable help in solving technical issues.

My heartfelt thanks also go to **Letizia Bocchi** for welcoming me into her laboratory and to her wonderful team — **Davide, Chiara, Elena, Maria,** and **Olta**. It has been a true pleasure to meet you and to share with you this experience of personal and professional growth. You are fantastic people who have made my time there full of wonderful memories. Thank you so much.

I would also like to thank all the **staff at Medica S.p.A.** — **Marco, Andrea, Nicola**, and many others — who made it possible to carry out the experimental tests with the organs, always showing competence and great collaboration.

I would like to thank **Giuseppe Palumbo** of the **Medica** S.p.A. My gratitude also goes to all the **Sarmed staff** for their support and collaboration.

I am immensely grateful to the company **Sarmed** S.r.l. for the fundamental **financial support** provided to my PhD research program. This crucial contribution was instrumental in the completion of this thesis and my doctoral studies.

A heartfelt thank you to **Prof. Pier Carlo Ricci**, who hosted me in his laboratory at the Department of Physics of the University. His help was essential and irreplaceable for the success of this Ph.D. I am sincerely grateful for his professionalism, kindness, patience, and for the valuable advice that significantly contributed to the quality of this research. My thanks also extend to his **colleagues** and his PhD student **Sahar**, for their warm welcome and hospitality within the department.

My heartfelt thanks go to my Austrian friend**, Florentina**, with whom I shared so many fun moments in Cleveland. You are a wonderful person, and I am truly happy to have met you. Thank you for all the times you kept me company and made my days brighter.

I would like to thank **James and Sharon** for welcoming me into their home during my stay in Cleveland. I will never forget the happy moments I spent there, feeling as if I were in my own home. I will always cherish my American life experience — it taught me to love the United States by living with real Americans. I fondly remember the times spent playing with **Pip** and **Cookie**, and especially **Apollo**, James's German Shepherd, who I played with every day and adored. I would also like to thank **James's son, James Jr.**, for kindly hosting me at his home in **Las Vegas**, giving me a truly unique experience. Thank you so much, my friends!

I also wish to thank all those who helped me with the **English language** and introduced me to American culture. It is thanks to the time they dedicated to me that I was able to improve my English and carry out my research experience in the United States.

A special thank-you goes to my **dear friend Mary from Iowa**. She is my best American friend, and I sincerely thank her and her husband for welcoming me into their home and showing me the beauty of Iowa — its vast fields and wonderful people. Mary was always close to me during my time in the United States. Thank you so much!

My warm thanks also go to my kind friends **Pam and Steven**, who hosted me at their home in **Arizona**, making me fall in love with the vast and scorching deserts, the breathtaking landscapes, and the delicious Mexican food. Arizona is my favorite state, and I am so grateful to you for showing me such beautiful places and sharing wonderful moments together.

I would like to thank **my friend Susan** and her husband for hosting me in their home in **North Carolina**, allowing me to experience a completely different side of the U.S. Thank you, Susan, for your warmth and hospitality — I truly enjoyed my time at your home. I am also grateful to you for all the time you dedicated to helping me improve my English.

My gratitude also goes to **my dear friend Joy** from **Minnesota**, whom I had the great pleasure of meeting in Cleveland. Joy was the first American I met, and she helped me greatly in improving my English. She has been incredibly kind and treated me like a true friend, even during my difficult moments. Thank you so much, Joy!

I would also like to thank **my friend Deborah**, who helped me a lot with my English even though I, unfortunately, didn't get the chance to meet her when I went to **Denver, Colorado**. Thank you for all our lovely conversations.

I also thank **my friend Mary from Australia**, with whom I shared many great conversations that helped me further improve my English — thank you so much!

Finally, I wish to thank **my dearest friend Mattia**, who has been a constant presence since our high school days. Even throughout these three years of Ph.D., he has always shown care, encouragement during difficult moments, and companionship during the good ones. Thank you so much, Mattia.

I would also like to thank **my friends Giovanni and Cristian**, with whom I've shared a lasting friendship since our undergraduate years.

A special thank you goes to my godfather, **Don Stefano**, for his constant presence and guiding wisdom. I am truly grateful.

I would also like to sincerely thank **Fausto** and **Daniela**, who have always been incredibly kind to me and genuinely interested in what I do. They have known me for many years and, in a way, have watched me grow up. I hold them in deep esteem not only for their kindness, but also for their great love and dedication in caring for cats — a gesture that reflects their sensitivity and generosity. They are truly wonderful people, and I want to thank them wholeheartedly for their kindness and for everything they have done for me.

I would also like to thank my aunt **Paola**, my uncle **Mauro**, and **Federico** and **Matilde**. They have always been kind and pleasant with me. My aunt has always shown me great affection, and I have always appreciated Mauro for his cheerful and friendly spirit. I am also very happy for Federico and Matilde, and I wish them all the best in everything they do.

The PhD journey was, as often happens, an intense and demanding experience, but it was made bearable by the presence of precious colleagues.

A due acknowledgement goes to **Nasri**, dear colleague and accomplice in this 'adventure/misfortune'. Together we faced and overcame countless obstacles. Your presence and constant support were fundamental throughout this long journey. I am grateful for the friendship that developed during these years.

I also thank **Gabriele** for choosing to tackle his Bachelor's thesis on the same subject as my research. I hold a beautiful memory of the time spent working together and of the challenges that, with commitment, we were able to overcome in collaboration.

A big thanks to **Paolo** and **Ciro**, two familiar faces I will never forget: my high school classmates. Bumping into you again on this journey, after so many years, has been incredible. Thank you for sharing this time with me; you made me relive, with a smile, the wonderful memories of that period. It was just as much a pleasure as it was back then!

I would also like to thank **Dr. Andrea Schlegel's entire team**, and especially **Chunbao**, for his kindness and gesture of friendship.

I would also like to thank the new colleagues I met during this concluding phase of my PhD. Thank you to **Claudia**, **Roberto**, and **Mattia**. I greatly appreciate the interest you showed by regularly asking me how the thesis writing was progressing. It was a small but significant moral support.

I would like to thank **my parents**, who have always loved me and supported every choice I've made. I'm not sure if this PhD will truly be useful in the end but I know for certain that your love will never fail me. My mother has always believed in me, even more than I have believed in myself. She taught me to dream big, to

be ambitious, and to never stop moving forward — to look at the world with curiosity and strive to understand how it truly works. She is a woman of great culture, and since I was a child, she has instilled in me the value of knowledge, intellect, and education as essential tools for building one's own future. She has always encouraged me to study not merely to achieve a goal, but to grow as a person and find my place in the world. I will always carry her teachings with me, as they are the most precious compass guiding both my journey and the person I have become. My father has always supported me, and whenever I faced great difficulties, he was there for me — he never abandoned me nor turned his back on me. He has always been proud and happy for my achievements, and I know that he always will be. I love you both, and I thank you for believing in me even when I doubted myself. I would also like to remember my brother, **Antonio**, who passed away many years ago when he was still very young. He will continue to live forever in our hearts and memories.

A special thank you goes to **Tania**, who has shown me love and patience throughout this entire journey. She encouraged me not to give up during the hardest moments, when I was often on the verge of quitting my PhD. She has always been by my side, in the way only someone who truly loves you can be. I don't know what the future holds — life is unpredictable — but I do know that since the day I met you, you have been the most important person in my life. I hope that one day you will remember more of what brought us together than what pulled us apart. Words aren't enough to express my deepest gratitude and affection, but I still want to say thank you, from the bottom of my heart.

I would also like to thank **Mauro**, Tania's father, and Mauro's friend, **Raffaele** for his generosity and for helping me several times with my car, and **Veronica**, Tania's sister, for her kindness. On a personal note, I would like to express my heartfelt thanks to **Sonia**, Tania's friend, for her kindness shown towards me and for her valuable suggestion to visit New Orleans. I am also grateful to her cousin, **Valentina**, for her constant availability. Finally, a very special thank you to **Tania's entire family** for their warmth support.

Lastly, I want to remember my cat, **Perlina**. I know she will never be able to read these words, but I still want to thank her. She gave me pure, unconditional love and endless comfort, quietly keeping me company through the long hours of work. Every time I sat at the computer, she would jump onto the desk and lie next to me, simply to be close. Whenever I lie down or go to bed, she immediately runs over and curls up on top of me, always seeking affection. If I could, I would spend much more time with her. I love my cat Perlina deeply, and I feel truly fortunate to have her in my life. Her presence has been a priceless source of serenity, warmth, and companionship throughout this challenging journey.

I would like to thank my supervisor, **Prof. Massimo Barbaro**, for his constant support, guidance during the most challenging moments, and for making this wonderful research journey possible.

Finally, my thanks go to the **Doctoral Board of the Ph.D. Program in Electronic and Computer Engineering** for organizing a training experience of the highest scientific and human value.

Funding statement

This doctoral thesis was produced while attending the PhD Programme in Electronic and Computer Engineering at the University of Cagliari (Cycle XXXVIII), with the support of a scholarship co-funded under the Ministerial Decree No. 352 of 9 April 2022, pursuant to the National Recovery and Resilience Plan (NRRP) — funded by the European Union — NextGenerationEU — Mission 4 “Education and Research”, Component 2 “From Research to Business”, Investment 3.3, and by Sarmed Srl. Sarmed Srl is a company belonging to the Medica Group Spa. The research activities were partially carried out at the Cleveland Clinic, Cleveland, OH, USA, during a predoctoral fellowship period supported by the same scholarship.